



LUND UNIVERSITY

The role of sugar sensing and pathway selection on D-xylose utilization by *Saccharomyces cerevisiae*

Tufvegren, Celina

2020

Document Version:

Publisher's PDF, also known as Version of record

[Link to publication](#)

Citation for published version (APA):

Tufvegren, C. (2020). *The role of sugar sensing and pathway selection on D-xylose utilization by Saccharomyces cerevisiae*. [Doctoral Thesis (compilation)]. Lund University.

Total number of authors:

1

General rights

Unless other specific re-use rights are stated the following general rights apply:

Copyright and moral rights for the publications made accessible in the public portal are retained by the authors and/or other copyright owners and it is a condition of accessing publications that users recognise and abide by the legal requirements associated with these rights.

- Users may download and print one copy of any publication from the public portal for the purpose of private study or research.
- You may not further distribute the material or use it for any profit-making activity or commercial gain
- You may freely distribute the URL identifying the publication in the public portal

Read more about Creative commons licenses: <https://creativecommons.org/licenses/>

Take down policy

If you believe that this document breaches copyright please contact us providing details, and we will remove access to the work immediately and investigate your claim.

LUND UNIVERSITY

PO Box 117
221 00 Lund
+46 46-222 00 00

The role of sugar sensing and pathway selection on D-xylose utilization by *Saccharomyces cerevisiae*

CELINA BORGSTRÖM TUFVEGREN | APPLIED MICROBIOLOGY | LUND UNIVERSITY



The role of sugar sensing and pathway selection on D-xylose utilization by *Saccharomyces cerevisiae*

Celina Borgström Tufvegren



LUND
UNIVERSITY

DOCTORAL DISSERTATION

which, by due permission of the Faculty of Engineering, Lund University, Sweden, will be publically defended on January 22nd 2021 at 10:00 a.m. in Lecture Hall K:A, Kemicentrum, Naturvetarvägen 12-18, Lund, for the Degree of Doctor of Philosophy.


Faculty opponent

Prof. Antonius van Maris

Department of Industrial Biotechnology, School of Engineering Sciences in Chemistry, Biotechnology and Health, KTH Royal Institute of Technology, Stockholm, Sweden

Organization LUND UNIVERSITY Applied Microbiology P.O. Box 124 SE-22100 Lund, Sweden	Document name Doctoral dissertation	
Author Celina Borgström Tufvegren	Date of issue 22 nd of January, 2021 Sponsoring organization Swedish Energy Agency, Swedish Research Council and EU projects BioREFINE-2G.	
Title The role of sugar sensing and pathway selection on D-xylose utilization by <i>Saccharomyces cerevisiae</i>		
Abstract <p>Biorefineries have the potential to partially or entirely replace petrochemistry for the production of our daily bulk and fine chemicals. However, this replacement can only be sustainable and cost-effective if the raw material used is cheap, renewable and does not compete with the food and feed industry. One raw material meeting these criteria is lignocellulose from agricultural and forestry waste streams. Lignocellulosic hydrolysates are rich in hexose sugars such as D-glucose and pentose sugars such as D-xylose. The industrial workhorse <i>Saccharomyces cerevisiae</i> readily ferments D-glucose into value-added products such as bioethanol and metabolic engineering has enabled the utilization of D-xylose, albeit not with the same efficiency as for D-glucose. The aim of the present thesis has been to investigate two approaches for improving D-xylose utilization in <i>S. cerevisiae</i>: introduction of a new pathway for D-xylose oxidation and exploration of the signaling response to D-xylose, including their engineering.</p> <p>The oxidative Weimberg pathway from the native bacterial host <i>Caulobacter crescentus</i> was introduced into <i>S. cerevisiae</i>. Out of the five enzymes of the pathway, one (XylC) was found to be highly active, leading to the accumulation of toxic D-xylonate, one (XylB) exhibited intermediate activity, two (XylD and XylX) had low activity and one (XylA) was not produced at all in the <i>S. cerevisiae</i> host. The issues observed were resolved by omitting XylC, substituting XylA with KsaD from <i>Corynebacterium glutamicum</i>, deregulating iron homeostasis to increase activity of XylD and introducing a total of 4 copies of the genes encoding the lower pathway (<i>xylD-xylX-ksaD</i>). The resulting strain assimilated 60 % of the available D-xylose through the Weimberg pathway, producing biomass and carbon dioxide, with D-xylonate being the main by-product. In parallel, the Weimberg pathway was studied in <i>C. crescentus</i>, showing that this pathway was expressed and active, using both D-xylose and the structurally related pentose sugar L-arabinose.</p> <p>The signaling response towards D-xylose was explored using a set of biosensors, coupling the expression of D-glucose-responsive promoters to a green fluorescent protein and measuring fluorescence with flow cytometry. D-Xylose was found to exert a weak effect on extracellular sensors in wild-type <i>S. cerevisiae</i> but the sugar was sensed in strains capable of D-xylose utilization, although with a response resembling the one observed with low levels of D-glucose. These results indicated that the D-xylose signal is mainly dependent on the intracellular metabolites formed during assimilation. Measurements of a panel of intracellular metabolites identified correlations with the sugar signaling response, independently of whether the metabolites stemmed from D-glucose or D-xylose. The correlation was also maintained in a <i>pgi1Δ</i> strain exhibiting a severe blockage in glycolysis.</p> <p>Engineering of the signaling response within the present thesis included evaluation of deletion mutants found to improve D-xylose utilization. In addition to confirming the increased D-xylose consumption, D-xylose was observed to cause a high D-glucose response within some signaling pathways. Furthermore, the catalytic and regulatory protein hexokinase 2 was engineered for D-xylose tolerance, resulting in a 64 % increase in catalytic activity in the presence of D-xylose, compared to the wild-type enzyme.</p> <p>In conclusion, the present thesis demonstrates novel methods of assaying and interpreting the D-xylose signaling response, and describes the first successful introduction of the Weimberg pathway in a eukaryote. Additionally, several potential targets for further engineering of metabolic and signaling pathways are identified and discussed.</p>		
Key words: <i>Saccharomyces cerevisiae</i> , D-xylose, sugar sensing, sugar signaling, biosensors, Weimberg pathway, Hxk2p, sugar phosphates, <i>Caulobacter crescentus</i>		
Classification system and/or index terms (if any)		
Supplementary bibliographical information	Language English	
ISBN, print: 978-91-7422-774-1		ISBN, digital: 978-91-7422-775-8
Recipient's notes	Number of pages 114	Price
Security classification		

I, the undersigned, being the copyright owner of the abstract of the above-mentioned dissertation, hereby grant to all reference sources permission to publish and disseminate the abstract of the above-mentioned dissertation.

Signature 

Date 2020-12-02

The role of sugar sensing and pathway
selection on D-xylose utilization by
Saccharomyces cerevisiae

Celina Borgström Tufvegren



LUND
UNIVERSITY

Cover art: “Stilleben” by Celina Borgström Tufvegren and Joakim Tufvegren

Copyright pp i-93 Celina Borgström Tufvegren

Paper I © the Authors 2018

Paper II © the Authors 2019

Paper III © the Authors 2016

Paper IV © FEMS 2018

Paper V © the Authors (Unpublished manuscript)

Paper VI © the Authors 2013

Paper VII © the Authors 2019

Lund University
Department of Chemistry
Center for Applied Life Sciences
Division of Applied Microbiology

ISBN 978-91-7422-774-1 (print)
ISBN 978-91-7422-775-8 (digital)

Printed in Sweden by Media-Tryck, Lund University
Lund 2020



Media-Tryck is a Nordic Swan Ecolabel
certified provider of printed material.
Read more about our environmental
work at www.mediatryck.lu.se

MADE IN SWEDEN 

*For those who come after. May our shoulders be
wide enough for you to stand comfortably.*

Contents

Contents	vi
Populärvetenskaplig sammanfattning.....	viii
Popular scientific summary	xi
Abstract.....	xv
List of publications	xvii
My Contribution to the papers	xix
Abbreviations.....	xx
Introduction	1
Towards a sustainable world	1
Biomass as a feedstock.....	2
<i>Saccharomyces cerevisiae</i>	3
Broadening the product spectrum	4
Aims and outline of this thesis	5
Glucose catabolism and sensing in <i>S. cerevisiae</i>.....	7
Metabolic response to D-glucose in <i>S. cerevisiae</i>	7
D-glucose sensing pathways in <i>S. cerevisiae</i>	9
Initial D-glucose sensing through the Snf3p/Rgt2p transmembrane receptor pathway regulates sugar transport into the cell.....	9
Fast and sustained cAMP/PKA signaling is achieved by combining extra- and intracellular sugar sensing	13
The SNF1/Mig1p pathway fine-tunes the response to D-glucose concentration and ATP levels through balancing of Snf1p kinase/Glc7p phosphatase kinetics	18
All D-glucose signaling pathways converge for the regulation of gene expression through transcription factors.....	21
Response to established <i>versus</i> new carbon sources.....	24
D-Xylose pathways in natural microorganisms and engineered <i>S. cerevisiae</i>	25

Natural D-xylose utilization.....	25
D-Xylose transport.....	26
D-Xylose assimilation pathways	27
Diversity of D-xylose utilizers in nature	30
D-Xylose utilization by <i>S. cerevisiae</i>	31
Wild-type <i>S. cerevisiae</i>	31
Transporter engineering.....	32
Engineering <i>S. cerevisiae</i> for growth on D-xylose via glycolysis ..	34
Engineering D-xylose utilization that bypasses glycolysis	37
Pathway analysis.....	41
Role of sensing in D-xylose utilization in natural organisms and engineered <i>S. cerevisiae</i>	45
Sensing and response to D-xylose in natural D-xylose-utilizing species .	45
<i>Escherichia coli</i>	45
<i>Caulobacter crescentus</i>	48
<i>Scheffersomyces stipitis</i>	50
Sensing and response to D-xylose in natural and engineered <i>S. cerevisiae</i>	52
Response to redox imbalances are the most obvious features of D-xylose fermentation.....	52
Is D-xylose sensed as a carbon source by <i>S. cerevisiae</i> ?.....	53
Mechanisms for D-xylose sensing	53
Engineering the sensing and signaling components in recombinant <i>S. cerevisiae</i>	60
Engineering of the Snf3p/Rgt2p pathway	60
Engineering of the SNF1/Mig1p pathway	60
Engineering of the cAMP/PKA pathway.....	61
Conclusions and outlook.....	65
Signaling response to D-xylose	65
Engineering of the signaling response to D-xylose.....	66
Assimilatory pathways.....	66
Outlook	67
Acknowledgements	70
References	73

Populärvetenskaplig sammanfattning

Global uppvärmning och resursbrist kommer troligen bestå som orosmoln och påverka våra liv under hela 2000-talet, om vi inte handlar beslutsamt. Effektivt agerande kräver hushållande och nya lösningar, som kan uppnås via samarbete och forskning. Den forskning som presenteras här ämnar bidra till den globala kunskapen kring hållbarhet genom att öppna upp för biobaserade sätt att producera bränslen och andra kemikalier som traditionellt sett tillverkas från fossila råvaror.

Jästen *Saccharomyces cerevisiae* har varit en av de viktigaste godartade mikroorganismerna under hela mänsklighetens historia. Sedan civilisationens födelse har jästen använts för att konservera och förädla mat. De främsta produkterna var då bröd, öl och vin, men på senare tid har även drivmedlet bioetanol lagts till listan. *S. cerevisiae* använder biomassa istället för fossila råvaror vid tillverkning av användbara produkter, och bidrar därmed till att minska koldioxidutsläpp och resursbrister. Men det finns alltid utrymme för förbättringar. Hexoser, sockermolekyler med sex kol som erhålles från bearbetning av exempelvis majs och sockerrör, bryts lätt ned av *S. cerevisiae*. Mer komplex biomassa, som återfinns i t.ex. avfall från jord- och skogsbruk, innehåller även socker med fem kol, såsom xylos, och dessa lämnas orörda av *S. cerevisiae*. Eftersom upp till 30 % av hållbar biomassa består av xylos så är en jäst som kan använda detta socker i industrin av högsta vikt. I enlighet med detta har nya metabola vägar för användning av xylos introducerats på genteknisk väg. Men trots att två nya vägar har tillförts och optimerats för *S. cerevisiae* så använder jästen fortfarande xylos betydligt långsammare än glukos. En anledning till detta uppförande är att jästen inte tros känna igen xylos som en källa till kol och energi. I mikroorganismer fungerar förnimmelse av näringsämnen på ett liknande sätt som doft och smak hos djur. När vi luktar eller smakar god mat så gör våra kroppar sig redo att smälta den: det vattnas i munnen och magen knorrar. På samma sätt behöver jästens matsmältnings-system, dess metabolism, aktiveras innan den kan ta upp xylos effektivt. Studierna som presenteras här ämnar svara på frågan om xylos kan kännas igen som en användbar kolkälla av *S. cerevisiae*, och i så fall, vilka mekanismer som används.

Ett av verktygen som använts i mina studier är biosensorer: färggranna proteiner som kan designas till att tillverkas när jästen uppfattar specifika

signaler. Mängden färg inuti kan sedan mätas och tolkas som en signaleringsrespons på det specifika stimuli. Med hjälp av biosensorer som känner av socker i omgivningen kunde jag bekräfta att ursprunglig jäst inte känner av xylos alls. Istället tror jästen att den svälter. Efter introduktion av en av de ovannämnda metaboliska vägarna för xylos ändrades dock signalen. Jästen tolkade nu höga nivåer av xylos som låga nivåer av glukos. Denna förändring antydde att även om xylos i sig inte gjorde det, så kunde eventuellt de molekyler som bildas när xylos bryts ned uppfattas av *S. cerevisiae*. Vissa av dessa molekyler, även kallade metaboliter, bildas både när glukos och xylos bryts ned, vilket skulle kunna förklara att användning av xylos tolkas som glukos av jästen.

Utforskandet av metaboliternas effekt på jästens förmågor fortsatte i denna studie då jag designade en jäst att producera metaboliter i proportioner som är annorlunda mot de naturliga, och sedan jämförde de resulterande koncentrationerna av metaboliterna med biosensorernas signaleringsrespons mot xylos eller glukos. På detta vis kunde jag identifiera flera samband mellan metabolit och signal. En ökad koncentration av exempelvis metaboliten glukos 6-fosfat, tolkades som en signal av höga halter av glukos, medan det motsatta förhållandet observerades av för, till exempel, xylulos 5-fosfat. Som namnen antyder är dessa metaboliter starkt kopplade till metabolism av glukos respektive xylos. Från dessa resultat drog jag slutsatsen att effektivt nyttjande av xylos kräver modifiering av signaleringsmekanismerna i *S. cerevisiae*. Detta kan ske genom förändring av proteinerna som bygger upp signaleringsnätverket, eller av koncentrationerna av dess nyckelmetaboliter. Den förstnämnda strategin utforskades ytterligare genom att titta på signaleringssvaret mot ett antal genetiska modifieringar som förbättrade xylosanvändningen. Jag fann att vissa av modifieringarna orsakade en respons som liknade den sedd då höga halter av glukos användes. Detta hade dock ett pris; jästen var nu också överkänslig mot stress, och växte dåligt.

En ny metabolisk väg för xylos introducerades i jäst, med mål att generera en ny typ av metaboliter. Vägen, döpt efter Dr. Ralph Weimberg, togs från bakterien *Caulobacter crescentus* och tillfördes och anpassades för att fungera i jäst. För att förstå Weimberg-vägen bättre studerades först tillväxten och sockerupptaget i *C. crescentus*. Sedan skapades en jäst som använder xylos via Weimberg-vägen genom att öka antalet kopior av vissa gener medan andra gener togs bort. Den resulterande jästen kan nu användas för att studera signaleringsresponsen mot nya metaboliter. Den öppnar också upp möjligheter att producera andra kemikalier än etanol.

Slutligen riktades uppmärksamhet mot hexokinas 2, ett protein med koppling till både glukos och xylos. Hexokinas 2 omvandlar glukos till glukos 6-fosfat, en metabolit av vikt för signalering. Xylose dämpar dock aktiviteten hos hexokinas 2, och sänker därmed produktionen av glukos 6-fosfat. Så jag modifierade hexokinas 2 till att vara mindre känslig mot xylos, för att underlätta upptag av både glukos och xylos.

Sammanfattningsvis representerar dessa studier ett betydande ansats att förstå och förbättra användningen av xylos hos *S. cerevisiae*, genom att förstå och förbättra hur jästen känner av och reagerar på detta socker. Detta gjordes med målet att få ut mer av koldioxid-neutral och hållbar biomassa och för att kunna producera kemikalier som vanligtvis härrör från fossila råvaror.

Popular scientific summary

Global warming and resource scarcity will likely remain key issues, significantly affecting life on Earth throughout the 21st century, if left unresolved. Effective alleviation is contingent on conservation and novel solutions, achieved through collaboration and research. The research presented here contributes to increasing our global knowledge towards sustainability by opening up for bio-based ways to produce fuels and other chemicals that are conventionally produced from fossil resources

The yeast *Saccharomyces cerevisiae* has been one of the most important benevolent microorganisms throughout the history of mankind. Ever since the birth of human civilizations this yeast has been used to preserve and increase the nutritional value of food. The main products were then bread, beer and wine, and in modern times the fuel bioethanol has been added to the list. *S. cerevisiae* uses biomass rather than fossil fuels to produce valuable compounds, alleviating both carbon dioxide emissions and resource scarcity. However, there is always room for improvement. Hexose sugars, i.e. sugars having six carbons that are obtained by breaking down e.g. corn and sugarcane are easily digested by *S. cerevisiae*. More complex biomass, such as agricultural and forestry waste stream, also contain five carbon sugars, such as xylose, that are left untouched by the yeast. As up to 30 % of sustainable biomass can be broken down to xylose, a yeast that can utilize this sugar to produce valuable compounds industrially is essential. Consequently, genetic engineering has been able to introduce new pathways for xylose utilization in *S. cerevisiae*. However, although two pathways for xylose utilization have been introduced and optimized for *S. cerevisiae*, xylose is still not used at the same rate as glucose. One of the reasons behind this behavior xylose is not thought to be recognized by the yeast as a source for carbon and energy. In microorganisms, nutrient sensing functions in a way similar to how taste and smell work for mammals. When we smell or taste delicious food, our body gets ready to digest it: our mouths water and our stomachs growl. The yeast also needs an active digestive system to take up xylose efficiently. The question of whether *S. cerevisiae* is able to sense xylose as a digestible sugar, and if so, by which mechanism(s), is the subject of the work presented here.

One of the tools used in this work is biosensors: colorful proteins that can be engineered to be produced when the yeast senses specific signals. The amount of color inside the yeast can then be measured and interpreted as a signaling response to that specific stimulus Using biosensors that report on the sensing of

sugars in the environment, I was able to confirm that xylose is not sensed in unmodified *S. cerevisiae*. Instead, the yeast feels that it is starving. However, when one of the xylose utilization pathways mentioned above was introduced, the sensing changed. The yeast now interpreted a high level of xylose as a low level of glucose. This change hinted that while xylose itself is not sensed, compounds formed during metabolism of xylose could be. Some of these compounds, called metabolites, are formed during utilization of both glucose and xylose, which could explain why yeast interprets xylose as glucose.

The effect of the metabolites on sensing was further studied in the present work. I created a yeast engineered to skew the concentrations of these metabolites substantially, and correlated these concentrations with the sensing response when utilizing xylose or glucose. This allowed me to identify several relationships between some of the metabolites and the sensing response. For example, increased concentration of the metabolite glucose 6-phosphate correlated with sensing of high levels of glucose, while the opposite relationship was observed with xylulose 5-phosphate. As their names imply, these metabolites are strongly associated with glucose and xylose utilization, respectively. From this, I concluded that efficient xylose utilization would require engineering of the sensing mechanisms of *S. cerevisiae*. This could be done through modification of either the proteins that make up the sensing network, or the levels of key intracellular metabolites. The former strategy was studied by looking at the sensing response to genetic modifications that increased xylose utilization. I found that some of the modifications caused a sensing state similar to that when high levels of glucose were utilized. However, this increased sensing came at a price; the yeast was now overly sensitive to stress and did not grow well.

A new pathway for utilization of xylose was also introduced in yeast in order to generate different types of intracellular metabolites. The so-called Weimberg pathway was adopted from the bacterium *Caulobacter crescentus* and modified to function within the yeast. To help understand the pathway the growth and sugar uptake of the original *C. crescentus* was first studied. Then a yeast that could use xylose was obtained by adding genes in multiple copies while deleting others. This yeast can now be used to investigate the sensing response to new metabolites while opening up for the production of other end-products than ethanol.

Finally, hexokinase 2, a protein with connection to both glucose and xylose was addressed. Hexokinase 2 converts glucose to glucose 6-phosphate, an important sensing metabolite. However, xylose reduces the activity of hexokinase and lowers the production of glucose 6-phosphate. So I engineered hexokinase 2 to be less affected by xylose, to facilitate the utilization of both glucose and xylose.

In conclusion, this work represents a considerable effort to understand and improve xylose utilization in the yeast *S. cerevisiae*, by understanding and improving the way yeast senses this sugar. This was done with the aim to get

more out of carbon-neutral sustainable biomass and to produce compounds that are traditionally made from fossil resources.

Abstract

Biorefineries have the potential to partially or entirely replace petrochemistry for the production of our daily bulk and fine chemicals. However, this replacement can only be sustainable and cost-effective if the raw material used is cheap, renewable and does not compete with the food and feed industry. One raw material meeting these criteria is lignocellulose from agricultural and forestry waste streams. Lignocellulosic hydrolysates are rich in hexose sugars such as D-glucose and pentose sugars such as D-xylose. The industrial workhorse *Saccharomyces cerevisiae* readily ferments D-glucose into value-added products such as bioethanol and metabolic engineering has enabled the utilization of D-xylose, albeit not with the same efficiency as for D-glucose.

The aim of the present thesis has been to investigate two approaches for improving D-xylose utilization in *S. cerevisiae*: introduction of a new pathway for D-xylose oxidation and exploration of the signaling response to D-xylose, including their engineering.

The oxidative Weimberg pathway from the native bacterial host *Caulobacter crescentus* was introduced into *S. cerevisiae*. Out of the five enzymes of the pathway, one (XylC) was found to be highly active, leading to the accumulation of toxic D-xylonate, one (XylB) exhibited intermediate activity, two (XylD and XylX) had low activity and one (XylA) was not produced at all in the *S. cerevisiae* host. The issues observed were resolved by omitting XylC, substituting XylA with KsaD from *Corynebacterium glutamicum*, deregulating iron homeostasis to increase activity of XylD and introducing a total of 4 copies of the genes encoding the lower pathway (*xylD-xylX-ksaD*). The resulting strain assimilated 60 % of the available D-xylose through the Weimberg pathway, producing biomass and carbon dioxide, with D-xylonate being the main by-product. In parallel, the Weimberg pathway was studied in *C. crescentus*, showing that this pathway was expressed and active, using both D-xylose and the structurally related pentose sugar L-arabinose.

The signaling response towards D-xylose was explored using a set of biosensors, coupling the expression of D-glucose-responsive promoters to a green fluorescent protein and measuring fluorescence with flow cytometry. D-Xylose was found to exert a weak effect on extracellular sensors in wild-type *S. cerevisiae* but the sugar was sensed in strains capable of D-xylose utilization, although with a response resembling the one observed with low levels of D-glucose. These results indicated that the D-xylose signal is mainly dependent

on the intracellular metabolites formed during assimilation. Measurements of a panel of intracellular metabolites identified correlations with the sugar signaling response, independently of whether the metabolites stemmed from D-glucose or D-xylose. The correlation was also maintained in a *pgi1*Δ strain exhibiting a severe blockage in glycolysis.

Engineering of the signaling response within the present thesis included evaluation of deletion mutants found to improve D-xylose utilization. In addition to confirming the increased D-xylose consumption, D-xylose was observed to cause a high D-glucose response within some signaling pathways. Furthermore, the catalytic and regulatory protein hexokinase 2 was engineered for D-xylose tolerance, resulting in a 64 % increase in catalytic activity in the presence of D-xylose, compared to the wild-type enzyme.

In conclusion, the present thesis demonstrates novel methods of assaying and interpreting the D-xylose signaling response, and describes the first successful introduction of the Weimberg pathway in a eukaryote. Additionally, several potential targets for further engineering of metabolic and signaling pathways are identified and discussed.

List of publications

This thesis is based on the following publications and manuscripts, which will be referred to by Roman numerals:

- I. Characterization of the Weimberg pathway in *Caulobacter crescentus***
Almqvist H, Jonsdottir Glaser S, Tufvegren C, Wasserstrom L & Lidén G (2018) Fermentation MDPI 4(2):44. doi:10.3390/fermentation4020044.
- II. Identification of modifications procuring growth on xylose in recombinant *Saccharomyces cerevisiae* strains carrying the Weimberg pathway**
Borgström C*, Wasserstrom L*, Almqvist H*, Broberg K, Klein B, Noack S, Lidén G & Gorwa-Grauslund MF (2019) Metabolic Engineering 55:1-11. doi:10.1016/j.ymben.2019.05.010. (*: Shared first author)
- III. Real-time monitoring of the sugar sensing in *Saccharomyces cerevisiae* indicates endogenous mechanisms for xylose signaling**
Brink DP*, Borgström C*, Tueros FG & Gorwa-Grauslund MF (2016) Microb Cell Fact 15: 183. doi:10.1186/s12934-016-0580-x. (*: Shared first author)
- IV. Assessing the effect of D-xylose on the sugar signaling pathways of *Saccharomyces cerevisiae* in strains engineered for xylose transport and assimilation**
Osiro KO, Brink DP, Borgström C, Wasserstrom L, Carlquist M & Gorwa-Grauslund MF (2018) FEMS Yeast Research 18:fox096. doi:10.1093/femsyr/fox096.
- V. Using phosphoglucose isomerase-deficient *Saccharomyces cerevisiae* to further understand the role of glycolytic intermediates in strains engineered for D-xylose utilisation**
Borgström C, Rogova O, Osiro KO, Lundberg E, Spégel P, Gorwa-Grauslund MF. Manuscript.

- VI. Engineering yeast hexokinase 2 for improved tolerance toward xylose-induced inactivation**
Bergdahl B, Sandström AG, Borgström C, Boonyawan T, van Niel EW & Gorwa-Grauslund MF. (2013) PLoS ONE 8: e75055.
doi:10.1371/journal.pone.0075055.
- VII. Exploring the xylose paradox in *Saccharomyces cerevisiae* through *in vivo* sugar signalomics of targeted deletants**
Osiro KO, Borgström C, Brink DP, Fjölnisdóttir BL & Gorwa-Grauslund MF (2019) Microb Cell Fact 18: 88.
doi:10.1186/s12934-019-1141-x.
- .

My Contribution to the papers

- Paper I** I performed enzymatic measurements, contributed to the analysis of data and revised the manuscript
- Paper II** I participated in the design of the study. I performed strain constructions, shake flask cultures, preparation of cells for proteomics, enzymatic assays and adaptive laboratory evolution. I was involved in the analysis of results and in decisions on how to proceed based on those results. I co-drafted the manuscript.
- Paper III** I designed the biosensor strains and the initial cloning strategy, and I carried out part of the molecular biology experiments. I co-supervised Felipe Gonzalo Tueros in performing the growth and flow cytometry experiments. I wrote custom scripts for data analysis, contributed significantly to the discussion of the data and finalized the manuscript.
- Paper IV** I contributed to the design of the experiments, performed analysis of the flow cytometry data and contributed to the discussion in the manuscript.
- Paper V** I designed the study and supervised Ester Lundberg for strain construction, enzymatic measurements and growth assessments. I performed flow cytometry and preparation of intracellular extracts for metabolite analysis. I led discussions of results and wrote the manuscript.
- Paper VI** I was involved in the strain constructions, Hxk2p library selection and enzymatic measurements. I contributed to the data analysis and revised the manuscript.
- Paper VII** I co-designed the study and performed the aerobic shake flask cultures and flow cytometry. I contributed to the analysis of data and to the discussion in the manuscript.

Abbreviations

α KG	α -Ketoglutarate
α KGSA	α -Ketoglutarate semialdehyde
ABC	ATP-binding cassette
Adh	Alcohol dehydrogenase
ADP	Adenosine diphosphate
ATP	Adenosine triphosphate
cAMP	Cyclic adenosine monophosphate
CAP	Catabolite activator protein
CDW	Cell dry weight
DHAP	Dihydroxyacetone phosphate
DNA	Deoxyribonucleic acid
EU	European Union
F1,6bP	Fructose-1,6-bisphosphate
G3P	Glyceraldehyde-3-phosphate
G6P	Glucose-6-phosphate
GAP	GTPase-activating protein
GEF	Guanine nucleotide exchange factor
GDP	Guanosine diphosphate
GPCR	G-protein-coupled receptor
GTP	Guanosine triphosphate
HDX	5-hydroxy-2,4-dioxoxylonate
D-KDX	D-2-keto-3-deoxyxylonate
KGSADH	α -Ketoglutarate semialdehyde dehydrogenase
K_M	Michaelis-Menten constant

KsaD	α -Ketoglutarate semialdehyde dehydrogenase
NAD	Nicotinamide adenine dinucleotide, oxidized form
NADH	Nicotinamide adenine dinucleotide, reduced form
NADP	Nicotinamide adenine dinucleotide phosphate, oxidized form
NADPH	Nicotinamide adenine dinucleotide phosphate, reduced form
PKA	Protein Kinase A
PPP	Pentose phosphate pathway
RNA	Ribonucleic acid
R _{sel}	Cofactor selectivity ratio
SDG	Sustainable development goal
TCA	Tricarboxylic acid
TF	Transcription factor
V _{max}	Maximal catalytic activity
XDH	Xylose dehydrogenase
XI	Xylose isomerase
XK	Xylulokinase
XR	Xylitol reductase
XylA	α -Ketoglutarate semialdehyde dehydrogenase
XylB	Xylose dehydrogenase
XylC	Xylonolactonase
XylD	Xylonate dehydratase
XylX	2-Keto-3-deoxyxylonate dehydratase

Introduction

Towards a sustainable world

In 2015 the United Nations (UN) established *17 Sustainable Development Goals (SDGs)* with the aim of improving living standards and environmental conditions worldwide. These goals include, among others, measures to combat poverty, hunger and inequality, to improve education, and to ensure clean water and fair judiciary procedures, by the year 2030 (UN General Assembly, 2015). Four of these SDGs focus on the responsible production of materials (SDG 12) and energy (SDG 7), the amelioration of resource scarcity and climate change (SDG 13), and the infrastructure and technological innovation (SDG 9) required for this sustainable development. However, environmental and resource sustainability should be seen as an integral part of overall goal fulfillment. The frequency of natural disasters such as droughts, floods, hurricanes and wildfires, is anticipated to increase as a result of climate change. This will be accompanied by secondary consequences including crop failure and conflicts resulting from resource scarcity, and even emergence of pathogens capable of causing pandemics, through cramped living quarters and close contact with wildlife. These concerning conditions would definitely complicate the eradication of hunger, disease and poverty. In addition, establishment of due process, safety and consistent education for the hundreds of millions of environmental migrants projected by the year 2050 (Brown, 2008) would become a highly complicated task.

Consequently, great efforts have been exerted in pursuit of novel alternatives to the petrochemical industry. In 2018 renewable sources, including geothermal, ambient heat, solar, wind, hydropower and energy from biomass, amassed to 34 % of the primary energy production in the European Union (EU) (Eurostat, 2020). The transport sector is the largest energy consumer in the EU, corresponding to 31 % of the total energy consumption in 2018, most of which is utilized through combustion engines. While the majority of renewable sources are applicable to production of electricity or heat, only biomass-derived energy carriers can be used within the current infrastructure of the transport sector. The major biofuels are bioethanol from sugar fermentation, biodiesel from transesterification of fatty acids, and biogas from anaerobic digestion. Additionally, biomass can be converted industrially to compounds able to replace

petrochemistry, such as bioplastics. The sustainability of this alternative, however, depends on the source of the biomass feedstock.

Biomass as a feedstock

Plant material contains a complex polymer called lignocellulose, consisting of cellulose, hemicellulose and lignin. Cellulose is a linear polymer of D-glucose molecules, while hemicellulose is a branched polymer combining D-glucose with other sugars such as D-xylose, D-galactose and L-arabinose, and lignin is an amorphous complex polymer of crosslinked phenolic compounds (Willey et al., 2017).

Different parts of a plant contain different ratios of these lignocellulosic constituents (Table 1.1). For example, in fruits, vegetables and grains the main carbohydrate is cellulose (up to 37 % by dry weight), which is hydrolyzed to simple hexoses during ripening. Some hemicellulose and lignin are found in fruits and vegetables, comprising what is nutritionally called dietary fiber, i.e. carbohydrates that are not digestible in themselves, but aid in digestion through physical means. Plant constituents requiring higher structural stability and recalcitrance, such as leaves and stems, typically contain higher ratios of hemicellulose and lignin.

Table 1.1. Composition of various plant components and feedstock, in percentage of dry weight

	Free sugars	Cellulose	Hemicellulose	Lignin	Reference
Mango	16-17 ^a		0.85-1.1		Maldonado-Celis et al. (2019)
Mulberry	37 ^a		15		Sun et al. (2012)
Broccoli	13		30		Butnariu and Butu (2015)
Cabbage	41		32		Butnariu and Butu (2015)
Corn	75		7.3		Tacer-Caba et al. (2015)
Brown rice	76		3.4		Tacer-Caba et al. (2015)
Sugarcane	28-62		41-67		Legendre (1988)
Corn stover	-	40	25	17	Saha (2003)
Rice straw	-	35	25	12	Saha (2003)
Sugarcane bagasse	-	40	24	25	Saha (2003)
Switchgrass	-	45	30	12	Saha (2003)
Oak leaves	-	17-24	12-17	15-17	Castro-Díez et al. (1997)
Softwood	-	41	23-31	27-33	Kirk (1973)
Hardwood	-	42-51	23-38	19-24	Kirk (1973)

^aCellulose is progressively degraded to monomeric sugars during the ripening of fruits and vegetables.

The cellulose and derived simple sugars found in ripe fruits, vegetables and grains are easily degraded or converted into value-added products through microbial fermentation, for example, bioethanol, biogas, bio-hydrogen and bioplastics. However, fruits, vegetables and grains are also vital in food and feed production, and subverting streams of edible lignocellulose could significantly

increase their price, especially in developing countries (Tenenbaum, 2008). This so-called “food *versus* fuel” dilemma could potentially put the UN’s SDG 13 for climate action at odds with SDG 2 of zero hunger, unless other raw materials can be found for the sustainable production of fuel and other products.

The inedible parts of plants are cheap and abundant, but due to their complexity and recalcitrance they require more extensive pretreatment than do fruits, vegetables and grains. Polymeric cellulose and hemicellulose can be converted into simple sugars through pretreatment at high temperature and pressure, followed by hydrolysis, either enzymatically or using acids. Depending on the kind of pretreatment and hydrolysis, different compounds will be formed that may inhibit the fermentation process. For example, hemicellulose hydrolysis leads to inhibitory concentrations of acetic acid. Biomass pretreatment also generates monomeric phenolics from the lignin polymer, such as vanillin, furfural and hydroxymethylfurfural, which have been shown to inhibit microbial fermentation (Jönsson and Martín, 2016).

To overcome the problems resulting from pretreatment and hydrolysis, the subsequent microbial fermentation should ideally be carried out by a robust microorganism. High tolerance to low pH, weak acids and phenolic inhibitors found in pretreated hydrolysates is desirable, as is the capacity of the cells to grow on and ferment all available sugars with high yield and productivity.

Saccharomyces cerevisiae

The budding yeast *S. cerevisiae* was domesticated by early civilizations up to 9000 years ago (McGovern et al., 2004). Since then, new yeast strains have been selected for desirable properties, resulting in a species that consumes a range of simple sugars very quickly, and ferments them efficiently into ethanol. In addition, *S. cerevisiae* is very robust and tolerant, to both high ethanol concentrations and industrial conditions such as low pH and the presence of inhibitors. This yeast is also known as baker’s or brewer’s yeast, and has traditionally been utilized for the production of bread, beer, wine, and other alcoholic beverages. Due to its industrial robustness and its well-developed genetic engineering toolbox, *S. cerevisiae* has more recently been the subject of interest for the production of fuels and specialty chemicals. Bioethanol production from simple glucose-rich feedstock such as sugarcane and corn syrup is known as *first generation bioethanol*, and is a well-established process. *Second generation bioethanol*, however, utilizes the wide variety of sugars found in lignocellulosic biomass, and is a substantially less well-developed process (Naik et al., 2010).

Wild-type *S. cerevisiae* cannot utilize the five-carbon sugar D-xylose found at high levels in lignocellulosic hydrolysates. Over the past two decades, recombinant strains able to ferment D-xylose to ethanol have been constructed through

genetic engineering, but the consumption rates and productivities are far lower than those achieved on D-glucose. Moreover, if the substrate contains mixtures of D-glucose and D-xylose, as is the case in many hydrolysates, D-xylose utilization will only start when the D-glucose is almost depleted ($< 2 \text{ g L}^{-1}$) (Krahulec et al., 2010), highlighting the need for further strain improvement. One of the suggested engineering targets is the sugar signaling network of *S. cerevisiae*, which is suspected to not naturally recognize D-xylose.

Broadening the product spectrum

While bioethanol has long been seen as the trailblazer of sustainable fuels, this is not its only application. Ethanol is commonly used as a solvent in the chemical industry, but it can also be used to produce renewable polyethylene. Polyethylene is the most common conventional plastic used in the world, and is normally produced from fossil ethylene. Replacing this non-renewable ethylene with sustainably produced ethanol within the same chemical process is called drop-in (Figure 1.1), and is one suggested strategy to reduce our dependence on fossil resources (Taylor et al., 2015). Other drop-in compounds formed by recombinant *S. cerevisiae* include long-chain alkanes, which can be used instead of gasoline or diesel (Zhou et al., 2016), and succinic acid, a surfactant and platform chemical (Sandström et al., 2014). It is also possible to produce novel alternative building blocks, such as the biopolymer polylactic acid, used for the production of biobased plastics (Table 1.2).

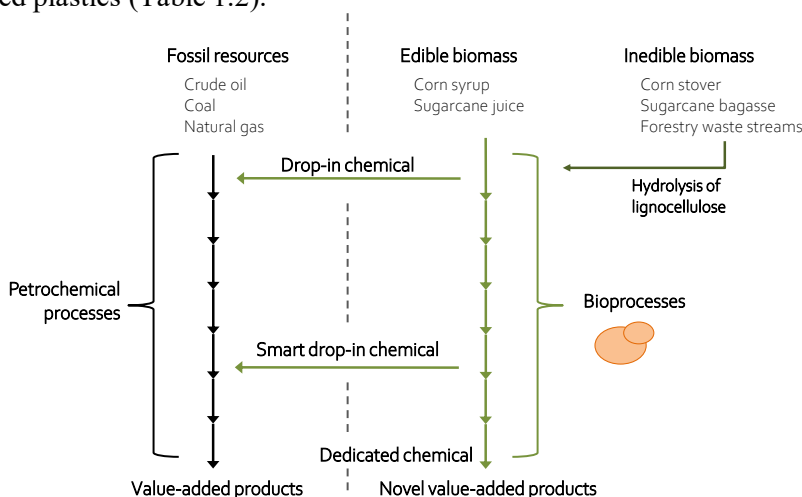


Figure 1.1. Valorization of biomass through integration in the chemical industry. Compounds produced from edible (first generation) or inedible (second generation) biomass can be dropped into traditional petrochemical processes to reduce the carbon footprint of the overall process; the later the entry into the petrochemical pipeline, the smarter the drop-in.

Table 1.2. Examples of compounds produced from biomass, by e.g. *S. cerevisiae*, that can replace fossil-based equivalents in the chemical industry (drop-in compounds) or that have no petrochemical counterpart (dedicated compound). Price, value and volume of each market are given for biomass or fossil resources as raw material, for the year 2013. Adapted from Taylor et al. (2015).

Compound	Application	Price (\$ kg ⁻¹)		Volume (10 ⁶ kg year ⁻¹)		Value (10 ⁶ \$ year ⁻¹)	
		Bio	Fossil	Bio	Fossil	Bio	Fossil
Drop-in compounds							
Ethanol	Solvent, platform chemical	0.815	0.932	71,310	5,367	58,141	5,000
Polyethylene	Plastics	1.2-2.6	1.7	200	88,000	240-520	150,000
Succinic acid	Pharmaceuticals, surfactants	2.94	2.08	38	38	112	79
Adipic acid	Nylon	1.5 ^a	1.85	0.45 ^a	27	0.67 ^a	50
Dedicated compounds							
Lactic acid	Pharmaceuticals, cosmetics	1.45	n.a.	472	n.a.	684	n.a.
Polylactic acid	Plastics	2.0-2.2	1.8 ^b	120	73,000 ^b	252	130,000 ^b
Farnesene	Adhesives, resins	5.58	n.a.	12.2	n.a.	68	n.a.

^a Projected by industry

^b Based on non-identical fossil alternatives

n.a.: Not applicable.

For each new bioprocess, a pathway from substrate to product must be selected, introduced into the microbial host and optimized for the industrial application. Pathway selection can be influenced by the characteristics of the original host organism, the expected intermediates formed, subcellular localization of the enzymes, cellular transport of substrate, intermediates and product, and the signaling response to flux through the pathway. By exploring natural biodiversity or *de novo* enzyme design, new catalytic activities can be discovered, further broadening the spectrum of possible product compounds.

Aims and outline of this thesis

The work presented within this thesis was carried out with the ambition to enable improved D-xylose consumption and ethanol production in *S. cerevisiae*, by i) investigating the signaling response to D-xylose, using the D-glucose signaling network as a benchmark, and ii) broadening the spectrum of achievable products and intermediates from D-xylose by introducing a new pathway to *S. cerevisiae*, the Weimberg pathway.

The D-glucose signaling network in yeast is among the best studied regulatory systems in eukaryotes. In the present thesis this network is divided into three main pathways that are described and contrasted in Chapter 2. To date, five metabolic pathways for D-xylose utilization have been described. Chapter 3 discusses characteristics of each pathway, as well as the engineering strategies employed for their introduction into *S. cerevisiae*. In Chapter 4 the aim is to apply the knowledge gained regarding sensing and signaling of D-glucose on the behavior

exhibited by *S. cerevisiae* utilizing D-xylose through engineered assimilation pathways.

Glucose catabolism and sensing in *S. cerevisiae*

Metabolic response to D-glucose in *S. cerevisiae*

S. cerevisiae assimilates D-glucose through the Embden-Meyerhof-Parnas pathway (also known as glycolysis), producing two pyruvate intermediates, two ATP and two NADH molecules per sugar molecule (Figure 2.1). The fate of pyruvate is determined by the sensed level of D-glucose. When D-glucose levels are high (over $\sim 18 \text{ g L}^{-1}$), the metabolism is routed towards fermentation, and pyruvate is reduced to ethanol, re-oxidizing the NADH produced during glycolysis. When D-glucose levels decrease, however, respiration is initiated and pyruvate is channeled through acetyl-CoA into the mitochondrial tricarboxylic acid (TCA) cycle for the production of carbon dioxide and biomass precursors (Willey et al., 2017). Due to a mitochondrial inner NADH dehydrogenase not generally seen in eukaryotes, respiration in *S. cerevisiae* cannot reach the theoretical upper limit of 36 ATP per glucose molecule (Bakker et al., 2001). Instead, the maximum yield of energy carriers in this yeast is about 16 ATP per glucose molecule.

When the metabolic mode is determined by the concentrations of available carbon sources this is referred to as the *Crabtree effect* (de Deken, 1966). The Crabtree effect is found in several fungal species within the *Saccharomyces*, *Schizosaccharomyces*, *Debaryomyces* and *Brettanomyces* genera. Other yeast species, such as *Candida utilis*, *Kluyveromyces lactis* and *Scheffersomyces stipitis* are so-called *Crabtree-negative* (de Deken, 1966; Merico et al., 2009; Passoth et al., 1996). In these species the metabolism is primarily dictated instead by the oxygen availability; respiration occurring during high aeration and fermentation when oxygen is limited.

From an evolutionary perspective, the Crabtree effect provides yeast with a dual competitive advantage over other species (Dashko et al., 2014). In nature, *S. cerevisiae* is often found on decomposing fruits, which are rich in sugars, and thus provide a good substrate for many microorganisms. In this environment, sugar fermentation enables the rapid uptake of most of the D-glucose from the fruits and the release of ethanol, which inhibits the growth of most microorganisms, whereas *S. cerevisiae* has naturally developed a relatively high

tolerance to ethanol. Once D-glucose is depleted and most competition has been removed, *S. cerevisiae* can re-assimilate the ethanol produced for growth via respiration and gluconeogenesis, which channels the carbon back towards glucose for the production of NADPH used in anabolic reactions via the pentose phosphate pathway (PPP) (Figure 2.1). Under anaerobicity, however, ethanol cannot be respired, and remains unmetabolized together with its latent energy content.

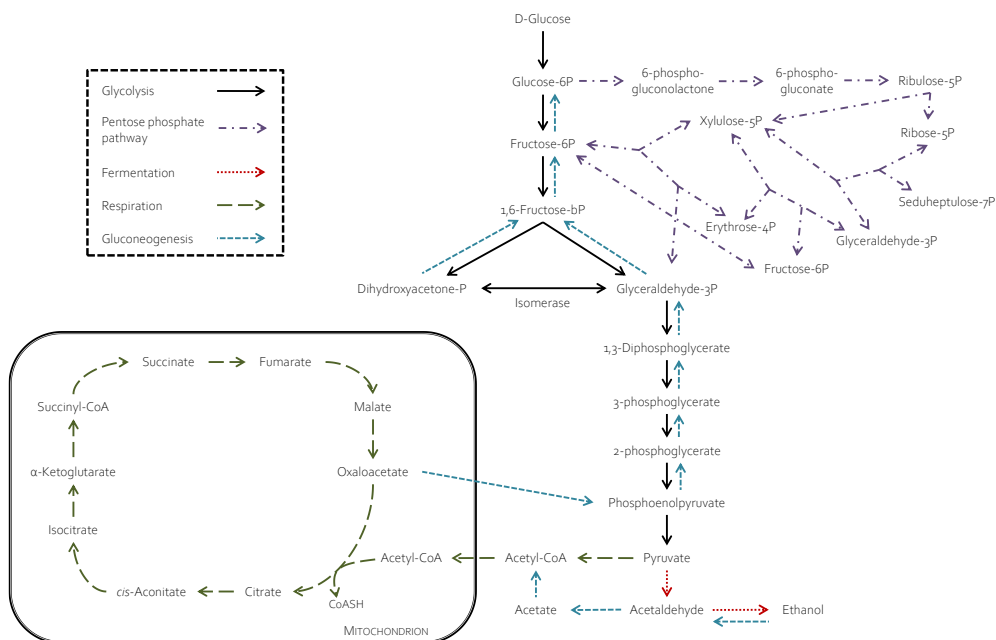


Figure 2.1. Central carbon metabolism in the yeast *S. cerevisiae*. The glycolytic Embden-Meyerhof-Parnas pathway, the pentose phosphate pathway, ethanolic pyruvate fermentation and gluconeogenesis occur in the cytosol, while the TCA cycle takes place in the mitochondria. Cofactors are omitted in favor of clarity.

Aerobic fermentation and inhibition of respiration have also been observed in many mammalian tumors. In fact, the phenomenon was first described in cancer, where the Crabtree effect was observed as a short-term shift in metabolism from respiration to aerobic fermentation in these growths (Warburg et al., 1927; Crabtree, 1929). The mechanisms behind aerobic fermentation in yeast and cancer cells are similar, and several important components of the yeast sugar signaling network have oncogene homologs in mammalian cells (Diaz-Ruiz et al., 2011; Vara-Ciruelos et al., 2019).

D-glucose sensing pathways in *S. cerevisiae*

In addition to regulating fermentation and respiration, D-glucose also influences the repression and inactivation of gluconeogenesis, as well as the pathways required for the assimilation of other carbon sources. The latter is called *catabolite repression*, or in this specific case, *glucose repression*. *S. cerevisiae* has thus developed several partially redundant and interacting pathways to signal the presence and level of D-glucose. The purpose of this is to ensure that all the enzymes needed for glycolysis are produced and active, while the genes involved in TCA, gluconeogenesis and utilization of other carbon sources are repressed and/or the corresponding proteins inactivated during growth on D-glucose; the response being reversed upon D-glucose depletion. Although the signaling network is complex, three mostly independent, but crosstalking pathways have been identified: namely, the Snf3p/Rgt2p pathway, the SNF1/Mig1p pathway and the cAMP/PKA pathway (Figure 2.2). These pathways, described in further detail below, sense either extracellular D-glucose or its metabolized intermediates, and are able to discern between different levels of D-glucose. Each signaling pathway can be divided into three parts: (i) presence of D-glucose recognized by the pathway, (ii) molecular modifications of the proteins within the pathway, and (iii) gene repression/induction or enzyme activation/inactivation of the targets of the pathway.

The two first parts are described below for each pathway. As gene regulation is highly dependent on crosstalk between the pathways, the third part is discussed later in the context of global D-glucose sensing.

Initial D-glucose sensing through the Snf3p/Rgt2p transmembrane receptor pathway regulates sugar transport into the cell

Mechanism of signal transduction

The *Snf3p/Rgt2p pathway* senses extracellular D-glucose and is responsible for the expression of hexose transporters allowing D-glucose to enter the cell (Figure 2.3). Binding of D-glucose to the Snf3p and Rgt2p transmembrane receptors leads to a conformational change in their C-terminal cytosolic tails. The cytosolic tail differs in length and in conserved regions between the two sensors. A conserved 25-amino-acid sequence appears once in the Rgt2p tail and twice in the Snf3p tail (Özcan et al., 1996). This sequence is thought to confer strength in D-glucose signaling since Rgt2p only senses high levels of extracellular D-glucose, whereas Snf3p recognizes both high and low D-glucose concentrations. When D-glucose levels are low ($\sim 1 \text{ g L}^{-1}$), only low-capacity, high-affinity hexose transporter genes such as *HXT2* and *HXT4* are induced, dependent on the Snf3p receptor. At higher D-glucose concentrations ($\sim 35 \text{ g L}^{-1}$)

however, higher-capacity, low-affinity transporter genes such as *HXT1* are induced (Özcan et al., 1998; Lutfiyya et al., 1998).

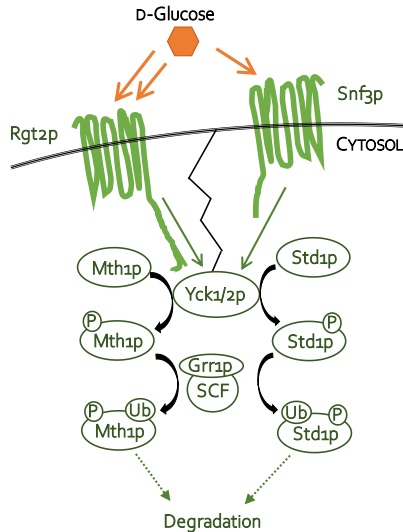


Figure 2.3. Sensing of D-glucose (orange hexagon) by the Snf3p/Rgt2p pathway leads to post-translational modifications and, ultimately, degradation of the transcriptional repressors Mth1p and Std1p. See text for details.

The conformational changes in the cytosolic tails of Rgt2p and Snf3p enable the transmission of the D-glucose signal to the cytosol through the interaction with the cell-membrane-anchored casein kinases Yck1/2p, as well as the transcriptional repressors Mth1p and Std1p, activating the former pair and bringing the latter pair closer to the cell membrane to be phosphorylated by the kinases (Moriya and Johnston, 2004). The phosphorylated Mth1p and Std1p are then ubiquitinated by the SCF^{Grr1p} complex. This complex consists of the three proteins (Skp1p, Cdc53p/cullin and Rbx1p/Roc1p) conferring ubiquitin-ligase activity, together with Grr1p protein, which is an F-box protein associated with the ubiquitination target, thereby determining the specificity of the complex. Grr1p is responsible for the ubiquitination of Mth1p and Std1p upon D-glucose addition, interacting with its targets via its leucine-rich repeat domains (Hsiung et al., 2001). The ubiquitination of Mth1p and Std1p leads to their degradation, no longer allowing them to repress their genetic targets, detailed below (Moriya and Johnston, 2004).

Cellular response to pathway signaling

The genes that are directly affected by the Snf3p/Rgt2p pathway encode hexose transporters, specifically Hxt1/2/4/6p, but also the pathway protein Std1p itself, Mig2/3p, which are all gene repressors, as well as and some relatively uncharacterized ORFs: *YGL157W*, *YKR075C*, *YOR062C* and *YNL234W* (Kaniak et al., 2004). Mig2p and Mig3p bind to mostly the same DNA sequences as the important D-glucose repressor Mig1p, whose activity is strictly controlled by the

SNF1/Mig1p pathway (as described below) through regulation of its phosphorylation state (Lutfiyya and Johnston, 1996). The homologs Mig2p and Mig3p are, however, not under the same control, but appear to be regulated at the transcriptional level by the Snf3p/Rgt2p pathway only (Kaniak et al., 2004). The D-glucose induction of *STD1* seems to convey negative feedback to the Snf3p/Rgt2p pathway (Moriya and Johnston, 2004), while there is some pathway crosstalk, with the Mth1p repressor itself being D-glucose-repressed through the SNF1/Mig1p pathway (Kaniak et al., 2004). Among the less-well-characterized genes that are D-glucose-induced through the Snf3p/Rgt2p pathway, several have potential regulatory functions. For example, Ykr075 and Yor062 show similarities with the Reg1p regulatory protein vital for Glc7p phosphatase activity in the SNF1/Mig1p pathway, while Ygl157 might have some oxidoreductase activity, and Ynl234 contains a heme-binding group. The *YNL234W* gene might also be regulated by other mechanisms since it has been shown to react to cellular stress (Sartori et al., 1999).

Mutants within the pathway

snf3Δ rgt2Δ mutants exhibit severe growth defects on 18 g L⁻¹ D-glucose (Özcan et al., 1998), due to a lack of D-glucose-dependent induction of genes encoding hexose transporters. At lower D-glucose concentrations there is basal expression of sugar transporters not induced by the Snf3p/Rgt2p pathway, such as Gal2p, and some hexose transporters (e.g. Hxt3p and Hxt5p), allowing for growth under these conditions. At higher D-glucose concentrations, however, the genes encoding these transporters are D-glucose repressed, disabling D-glucose transport into the cell and inhibiting growth. Overexpression of a hexose transporter gene such as *HXT1* alleviates the detrimental effect of high D-glucose levels on the growth of these deletion mutants, but it does not restore D-glucose signaling through the Snf3p/Rgt2p pathway (Özcan et al., 1998).

Both Rgt2p and Snf3p contain twelve transmembrane domains. There is a cytoplasmic region between the fourth and fifth domains, which is conserved in many hexose transporters and sensors found in nature, including several *S. cerevisiae* sugar transporters, for example, xylE from *E. coli* and human GLUT1 (Celenza et al., 1988; Colas et al., 2016). When the highly conserved arginine residue within this region (at positions 231 and 229 for Rgt2p and Snf3p, respectively) is replaced by lysine, constitutive expression of both *HXT1* and *HXT2* is observed in the absence of D-glucose (Özcan et al., 1996), highlighting the key role of these regions in sugar signaling. In the Rgt2p^{R231K} mutant, *HXT1* is expressed even on glycerol medium, which is normally considered a non-inducing condition; the expression of this gene is further induced by increasing the D-glucose concentration, a phenomenon that is even more evident in a *snf3Δ* background (Özcan et al., 1996). Both Rgt2p^{R231K} and Snf3p^{R229K} mutants cause relatively high expression of *HXT2* on glycerol, which is only marginally inducible with the addition of a low concentration of D-glucose (~1 g L⁻¹).

The C-terminal cytoplasmic tails of Rgt2p and Snf3p are also crucial for D-glucose signaling; removing the tail in a mutant strain leads to loss of D-glucose sensing, equivalent to a null mutant. However, upon removal of the tail from the constitutively active Rgt2p^{R231K} and Snf3^{R229K} mutants, the receptors return to their D-glucose-sensing states. Moreover, attaching the tail of Snf3p to either Hxt1p or Hxt2p transforms the transporters into D-glucose-sensitive signaling entities (Özcan et al., 1998). These findings strongly implicate the cytoplasmic tails as the signal transduction domains of Snf3p/Rgt2p. The transmembrane domains, on the other hand, determine ligand specificity and would be the suggested engineering targets to enable sensing of ligands that are currently not recognized.

Fast and sustained cAMP/PKA signaling is achieved by combining extra- and intracellular sugar sensing

Mechanism of signal transduction

The cAMP/PKA pathway senses extracellular D-glucose and its internalized metabolites through the transmembrane receptor protein Gpr1p and the Ras1/2p proteins (presumably via Ira1/2p), respectively (Figure 2.4). Gpr1p is a G-protein-coupled receptor (GPCR) that is responsive to relatively high concentrations of D-glucose (with a half maximal effective concentration of 3.6 g L⁻¹) or low concentrations of sucrose (half maximal effective concentration of 0.17 g L⁻¹). Gpr1p is unresponsive to galactose and fructose, but inhibited by mannose (Lemaire et al., 2004).

G-proteins are heterotrimeric complexes consisting of an α -, a β - and a γ -unit (Bos et al., 2007). The activity of a G-protein is regulated by the energy state of the guanine nucleotide associated with it. The G-protein is activated by replacing a bound GDP with a GTP, accomplished by guanine nucleotide exchange factors (GEFs), and it is inactivated by the hydrolysis of GTP to GDP by the G-protein itself upon stimulation by GTPase-activating proteins (GAPs) (Bos et al., 2007).

Interactions between Gpr1p and its activating sugars likely cause a conformational change in both the transmembrane domains and in the cytoplasmic domains, as in other GPCRs. This conformational change allows Gpr1p to interact with Gpa2p, which acts as the α -unit of a corresponding G-protein complex (Kobilka, 2007). No conventional β - or γ -subunits have been found to make up a G-protein complex together with Gpa2p. Instead, Gpa2p interacts with Gbp1p and Gbp2p (also known as Krh2p and Krh1p, respectively) that both mimic the β -subunit of a G-protein (Harashima and Heitman, 2002). When sensing D-glucose the Gpr1p receptor activates Gpa2p by acting as a GEF (Xue et al., 1998). GTP-bound, activated Gpa2p can then interact with membrane-anchored adenylate cyclase (Cyr1p), which in turn becomes activated and catalyzes the

ATP to cAMP reaction, causing a spike in intracellular cAMP levels within minutes (Kraakman et al., 1999).

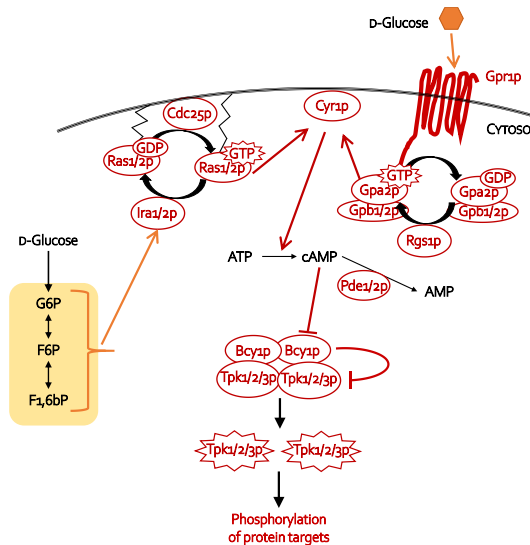


Figure 2.4. In the cAMP/PKA pathway, D-glucose, or its metabolites, is sensed and the signal is transduced via cAMP to PKA, which phosphorylates its protein targets. See text for details.

In analogy with Gpr1p/Gpa2p, the Ras1/2p proteins are also considered to be G-proteins, binding GDP in their inactivated form and GTP in the active state. For Ras1/2p the GEF is Cdc25p and, to some extent, Sdc25p, while the latent endogenous GTPase-activity is stimulated by Ira2p and Ira1p (Colombo et al., 2004). Again, the presence of D-glucose changes the GTP/GDP ratio towards GTP-bound activation of Ras1/2p, causing interaction with Cyr1p and activating the cyclase activity. Whereas Gpa2p comes into proximity with Cyr1p through association with the transmembrane Gpr1p, Ras1/2p are anchored by a post-translational farnesylation and interacts with a cyclase-associated protein for rapid translocation; the bound GTP is then essential for interaction with, and the activation of, Cyr1p (Shima et al., 2000).

The exact mechanism behind Gpr1p/Gpa2p and Ras1/2p activity and, by extension, cAMP accumulation, has long been debated. It was first proposed that Gpr1p/Gpa2p activity required D-glucose phosphorylation (Beullens et al., 1988), but activity was later reported in purified membranes (assumed to contain both Gpr1p/Gpa2p and Cyr1p) upon stimulation by D-glucose (Pardo et al., 1991). This activity was also achieved in strains deficient in D-glucose-phosphorylation capacity, as well as when D-glucose analogs incapable of phosphorylation (e.g. 6-deoxy-glucose) were used. This implies that the ligands of Gpr1p are the unmodified sugar D-glucose (or sucrose). The fact that sucrose, a disaccharide that cannot be taken up by *S. cerevisiae* without first being hydrolyzed to two D-glucose molecules using invertase, is still sensed through Gpr1p/Gpa2p in an

invertase-deficient strain also indicates that sensing takes place in the extracellular space (Lemaire et al., 2004).

Whereas Gpr1p/Gpa2p signaling is specific to D-glucose (and sucrose), Ras1/2p respond to more general intracellular acidification. In viable cells, the cytosol maintains a neutral pH over time, but can be transiently acidified by the addition of, for example, D-glucose, which is rapidly converted into the weak acid glucose 6-phosphate (G6P) ($pK_a=1.4$), or 2,4-dinitrophenol, which depolarizes cellular membranes. Both these methods of intracellular acidification have been shown to result in an increase in the bound GTP:GDP ratio in Ras1/2p and a subsequent spike in cAMP (Colombo et al., 1998). The exact mechanism by which acidification activates Ras1/2p is not known; however, as all protein functions are more or less dependent on pH, it seems probable that activation is caused by a change in activity of the GEFs (Cdc25p and Sdc25p), the GAPs (Ira1/2p) or Ras1/2p themselves.

In addition to intracellular acidification, Ras1/2p is also activated by fructose-1,6-bisphosphate (F1,6bP) and, to lesser extents, by dihydroxyacetone-3-phosphate (DHAP) and glyceraldehyde-3-phosphate (G3P). In this case, the mechanism seems to involve activation of the GEF Cdc25p, as F1,6bP was shown to bind to the homologous human GEF Sos1 (Peeters et al., 2017). Increased levels of these metabolites require active flux through glycolysis, which depends on glucose transport and phosphorylation (Ramos et al., 1989).

Gpr1p and Gpa2p are both required for fast accumulation of cAMP upon D-glucose addition to cells grown on non-fermentable carbon sources (Kraakman et al., 1999). However, this arm of the pathway does not sense D-glucose concentrations below $4\text{--}20\text{ g L}^{-1}$; whereas Ras1/2p can detect D-glucose at concentrations as low as $0.2\text{--}2\text{ g L}^{-1}$ (Colombo et al., 1998; Colombo et al., 2004; Kraakman et al., 1999; Ramos et al., 1989). The sensing of low glucose concentrations is thought to almost certainly take place through intracellular acidification, as it occurs before any F1,6bP has had time to accumulate. The pathway is down-regulated through the GAP activity on Gpa2p and Ras1/2p, by Rgs1p and Ira1/2p, respectively, as well as the breaking down of cAMP to AMP by the phosphodiesterases Pde1p and Pde2p (Nikawa et al., 1987; Versele et al., 1999; Wilson and Tatchell, 1988).

cAMP is a powerful secondary signaling metabolite whose function in the pathway is to counteract the inhibitory action exerted by Bcy1p on the Tpk1/2/3p subunit of Protein Kinase A (PKA). In its inactive form, PKA is a protein complex made up of two regulatory Bcy1p subunits and two catalytic subunits consisting of Tpk1p, Tpk2p or Tpk3p. Upon stimulation by cAMP the Tpk1p subunit is autophosphorylated, leading to dissociation from the regulatory Bcy1p subunits, allowing PKA to exert its catalytic function, which is to phosphorylate various protein targets (Hixson and Krebs, 1980; Toda et al., 1987). Autophosphorylation has been shown to occur on serine-179 of Tpk1p (Solari et al., 2014) and multiple sequence alignment using clustalOmega (Sievers and

Higgins, 2018) shows analogous regions in Tpk2/3p, suggesting similar autophosphorylation and Bcy1p dissociation mechanisms also for Tpk2p and Tpk3p. However, two-dimensional gel studies showed that only Tpk1p and Tpk3p increased their phosphorylation state upon D-glucose addition, so the conditions leading to autophosphorylation could differ between the three homologs (Solari et al., 2014). The mechanism, by which the spike in cAMP levels induces autophosphorylation in Tpk1p, and possibly Tpk3p, remains to be elucidated.

Cellular response to pathway signaling

The phosphorylation carried out by activated PKA affects the activity of a number of enzymes involved in gluconeogenesis and carbohydrate storage. Examples of the former are fructose-1,6-bisphosphatase (Fbp1p) (Gancedo et al., 1983) and isocitrate lyase (Icl1) (Ordiz et al., 1996), which are down-regulated through phosphorylation-induced inactivation and degradation, while the latter is represented by glycogen branching enzyme (Glc3p) (Smith et al., 1998) as well as trehalose-6P synthase and phosphatase (Tps1p and Tps2p) (Apweiler et al., 2012), which are involved in glycogen accumulation and trehalose synthesis, respectively, and are repressed by PKA on the transcriptional level. Moreover, activated PKA increases the flux through glycolysis by activating 6-phosphofructo-2-kinase (Pfk26p) (Francois et al., 1984) and neutral trehalase (Nth1p) (Ortiz et al., 1983) by direct phosphorylation and pyruvate decarboxylase (Pdc1p) (Belinchon and Gancedo, 2007) by up-regulating its transcription. Activated PKA also leads to a reduction in heat and general stress tolerance, mainly through repression of several stress regulated element (STRE) genes (Kobayashi and McEntee, 1993; Marchler et al., 1993).

PKA also affects the transcriptional machinery, for example, by inactivating the repressive function of Rgt1p through phosphorylation (Kim and Johnston, 2006), repressing the negative regulator of cell growth *YAK1* and increasing RNA turnover of the ribosome 60S subunit proteins Rpl3p and Rpl24p (Yin et al., 2003).

Mutants within the pathway

Differences have been observed in the signaling phenotype through the cAMP/PKA pathway in standard laboratory strains of *S. cerevisiae* (Vanhalewyn et al., 1999). This is caused by a single amino acid substitution in position 1876 of Cyr1p. The vast majority of laboratory strains, such as W303 and S288C, as well as the industrial strain Ethanol Red (Vanhalewyn et al., 1999; Daran-Lapujade et al., 2003; Wallace-Salinas et al., 2015) have a lysine in this position, which leads to the “normal” signaling response described above. However, CEN.PK-derived strains that are often used in applied research, display a methionine in position 1876 (Vanhalewyn et al., 1999). This substitution yields a signaling pathway that is no longer inducible by D-glucose or intracellular

acidification. Instead, the cells maintain a basal level of cAMP after D-glucose addition, which then increases when entering the stationary phase. The mutation has also been shown to confer increased resistance to heat stress, which might explain why the CEN.PK background has been popular in industrial application. However, when studying the sugar signaling of *S. cerevisiae*, strains with “normal” pathways, such as W303, are usually preferred.

Deletion mutants abolishing all signaling through the cAMP/PKA pathway, such as the *tpk1*Δ *tpk2*Δ *tpk3*Δ triple mutant, are not viable (Hartley et al., 1994). This is due to the loss of transcriptional control over the *YAK1* gene whose overexpression causes cell cycle arrest. The growth defects in a cAMP/PKA pathway null mutant can be alleviated through deletion of *YAK1* or its transcriptional activators *MSN2* and *MSN4*. Although the transcriptional profiles of PKA null strains differ slightly depending on the suppressor mutant used, some trends can be discerned (Livias et al., 2011). For example, PKA deficiency is associated with a reduction in D-glucose induction of the genes involved in amino acid synthesis and ribosome biosynthesis, as well as a loss of D-glucose repression of genes involved in stress response, trehalose synthesis and vacuolar proteins.

Mutations in *RAS2* and *GPA2* resulting in substitutions from the wild-type glycine residues in position 19 or 132, respectively, to a valine residues have been found to yield constitutively activated PKA phenotypes: i.e., low accumulation of trehalose and glycogen and a decrease in tolerance to heat and general stress, while growth and substrate consumption were not affected in cells growing on D-glucose in rich media (Colombo et al., 2004; Kraakman et al., 1999). The *Gpa2p*^{G132V} also restored the cAMP peak deficiency observed in a *gpr1*Δ mutant (Kraakman et al., 1999). In higher eukaryotes, *RAS* is a potential oncogene, and mutations in any of the three human *ras* genes H-Ras, K-Ras and N-Ras are found in a large variety of cancers (Bos, 1989). The incidence of Ras mutants in different carcinomas is highly tissue dependent, with a frequency of up to 84 % in adenocarcinomas of the pancreas. Of the mutational sites identified, the glycine-12 position is the most prevalent, and although substitution with aspartic acid is the most commonly found, G12V mutations have also been observed (Hobbs et al., 2016). This substitution, among others, renders the Ras protein active, regardless of external stimuli, leading to the deregulated cell growth and proliferation associated with carcinomas.

The SNF1/Mig1p pathway fine-tunes the response to D-glucose concentration and ATP levels through balancing of Snf1p kinase/Glc7p phosphatase kinetics

Mechanism of signal transduction

The response of the third signaling pathway, the *SNF1/Mig1p pathway*, is dependent on the first step of glycolysis in which D-glucose is phosphorylated to G6P. This reaction is catalyzed by hexo- and glucokinases, with hexokinase 2 (Hxk2p) being the highest contributor at high D-glucose levels (Diderich et al., 2001). D-glucose phosphorylation sends an activating signal to the Reg1p-Glc7p phosphatase complex, by an, as of yet, not conclusively characterized mechanism, which leads to the dephosphorylation of its targets; Hxk2p, Mig1p and the SNF1 complex being the major targets (Figure 2.5) (Sanz et al., 2000; Fernandez-Garcia et al., 2012).

Hxk2p is a bifunctional protein which, in addition to its important role in the first step of glycolysis, also has a prominent gene regulatory function in this glucose-repressive pathway. Dephosphorylation of Hxk2p by the Glc7p phosphatase allows a subpopulation of Hxk2p to be transported from the cytoplasm to the nucleus (Fernandez-Garcia et al., 2012).

SNF1 is a heterotrimeric protein complex consisting of the Snf1p α -unit, the Snf4p γ -unit and any of the three β -units: Sip1p, Sip2p or Gal83p (Yang et al., 1994; Erickson and Johnston, 1993). The kinase activity is carried out by Snf1p, a large (633-amino-acid) protein containing an N-terminal kinase domain (330 amino acids) and a C-terminal regulatory domain (300 amino acids) (Nayak et al., 2006). In the presence of D-glucose, Snf1p is dephosphorylated and the regulatory domain binds to the kinase domain, disturbing interactions with the Snf4p subunit and inactivating the complex. When the D-glucose concentration decreases, the activation signal to Glc7p is weakened, and the balance is shifted towards SNF1 phosphorylation by Sak1p (formerly known as Pak1p), Tos3p or Elm1p (Liu et al., 2011; Hong et al., 2003). Phosphorylation causes a conformational shift, weakening the regulatory-kinase domain interaction, and allowing Snf4p to bind to the regulatory domain. This leaves the kinase domain activated and free to carry out its catalytic function (Celenza and Carlson, 1989; Jiang and Carlson, 1996).

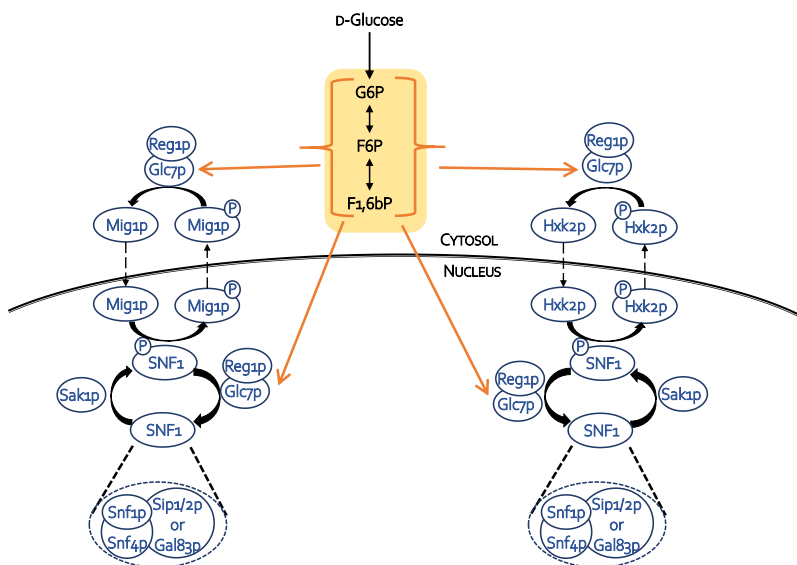


Figure 2.5. Glucose repression is achieved through the SNF1/Mig1p pathway in *S. cerevisiae*. SNF1 is a heterotrimeric protein consisting of the Snf1p kinase, the regulatory Snf4p and Sip1p, Sip2p or Gal83p determining catalytic specificity. Sensing of glycolytic metabolites offsets the Snf1p kinase/Glc7p phosphatase kinetics in favor of Glc7p. This results in dephosphorylation of the transcriptional repressors Mig1p (left) and Hxk2p (right), leading to their nuclear enrichment and subsequent repression of target genes.

Cellular response to pathway signaling

The effects on the most relevant targets of the SNF1/Mig1p pathway, in terms of activity and subcellular localization, are summarized in Figure 2.6. One of the direct effects of SNF1 activation during low D-glucose conditions is the phosphorylation of Reg1p, a regulator of Glc7p activity and specificity. Phosphorylation of Reg1p causes inactivation of Glc7p, leading to phosphorylation and cytosolic localization of Hxk2p and Mig1p (Figure 2.5) (Sanz et al., 2000). Increased level of D-glucose, however, sends a separate, partially activating signal to Glc7p. When this signal is sufficiently strong, i.e. at sufficient D-glucose levels, Glc7p can dephosphorylate Reg1p and fully reactivate itself (Figure 2.6A). The mechanism of the SNF1/Mig1p pathway is thus a kinetic balance between kinase and phosphatase activities. This makes the SNF1/Mig1p pathway the most sensitive to changes in D-glucose concentration, whereas the Snf3p/Rgt2p and the cAMP/PKA pathways mainly sense the presence of D-glucose and, to some extent, its level. Since phosphorylation as a mechanism is both reversible and able to bring about either activation or inactivation depending on the protein target, the SNF1/Mig1p pathway can signal for both the presence and absence of D-glucose.

In the absence of D-glucose, SNF1 is phosphorylated, allowing it to phosphorylate Hxk2p and Mig1p (Hedbacker and Carlson, 2008). The added phosphate group causes dissociation from the chromosomes and a change in subcellular

localization from the nucleus towards the cytosol (Figure 2.6B). The localization SNF1 itself is dependent both on the D-glucose level and on the β -unit of the complex. In conditions with high concentrations of D-glucose, all complexes are localized in the cytosol. When D-glucose levels are low, however, complexes containing Sip1p migrate to vacuoles, while Sip2p associated complexes remain in the cytosol and Gal83p dictates nuclear localization (Figure 2.6C) (Vincent et al., 2001).

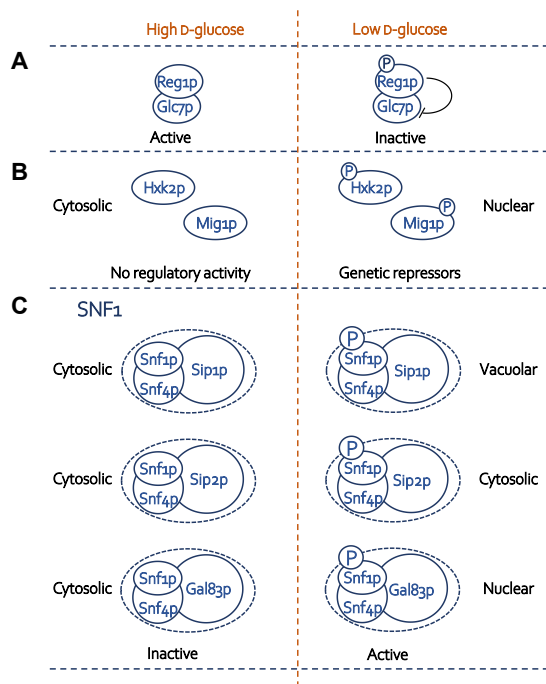


Figure 2.6. Subcellular location and activity level of D-glucose responsive proteins and complexes within the SNF1/Mig1p signaling pathway. A) Glc7p phosphatase and its Reg1p regulator; B) The genetic regulators Hxk2p and Mig1p; and C: The SNF1 complex with Snf1p kinase activity, Snf4p regulator and localization-determining β -units (Sip1/2p and Gal83p). Hammerhead arrows indicate catalytic repression. See the text for details.

The mammalian homolog of SNF1, AMP-activated protein kinase (AMPK), has similar functions to yeast SNF1 but, as its name implies, is controlled by the intracellular AMP/ATP ratio (Sanders et al., 2007). This relation to the endogenous energy state makes AMPK more of a general stress response mediator than SNF1. AMPK has also been implicated in human diseases such as diabetes type 2 and cancer (Winder and Hardie, 1999; Vara-Ciruelos et al., 2019). Although the yeast homolog has not been shown to be activated by AMP, binding of ADP, and to some extent AMP, has been shown to protect SNF1 from dephosphorylation and inactivation by Glc7p (Mayer et al., 2011). The reason for this mechanism could be to sense ATP depletion and re-route metabolism from ATP-consuming anabolism, from gluconeogenesis and breakdown of carbohydrate storage molecules towards ATP production.

Mutants within the pathway

Since the *S. cerevisiae* genome encodes two other D-glucose-phosphorylating enzymes, Hxk1p and Glk1p, both lacking the regulatory function, *hxx2Δ* mutants still grow on D-glucose but show loss of D-glucose repression of, for example, *SUC2* and the *GAL* genes responsible for sucrose and galactose catabolism, respectively (Rose et al., 1991). Likewise, strains deleted for genes encoding the three subunits of the SNF1 complex are viable, but lead to abnormal glucose repression (Chandrashekarappa et al., 2011). Deletion of *GLC7*, however, is deleterious to the yeast cell, possibly due to G₂/M cell cycle arrest (Bloecher and Tatchell, 1999).

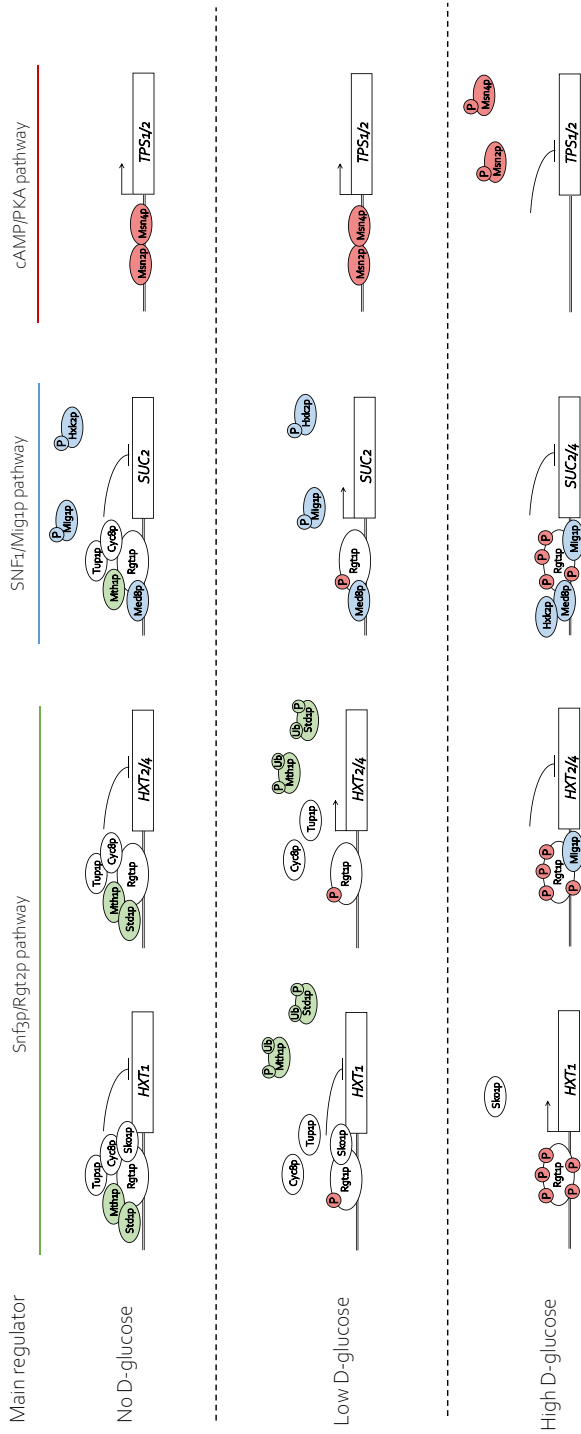
All D-glucose signaling pathways converge for the regulation of gene expression through transcription factors

As described above, sensing of different D-glucose levels produces a signal through three main D-glucose signaling pathways, resulting in the modulation of enzyme activities, as well as the induction or repression of target genes. Control of enzymatic activity is mainly achieved through phosphorylation via the cAMP/PKA pathway. Transcriptional regulation, on the other hand, involves modulation of so-called transcription factors (TFs) and their co-regulators, for which significant crosstalk has been observed between the signaling pathways.

TFs are proteins that bind to DNA and either induce or repress transcription by interacting with RNA polymerase II and/or histones, while a co-regulator is a protein interacting with one or more TFs (Latchman, 1997). In order to exert their effects, TFs and co-regulators need to be (i) active and (ii) present in the nucleus. Binding of signaling ligands or co-regulators can affect activity and help recruit the TFs to their DNA binding site. Their presence in the nucleus is, in general, dependent on the production and degradation kinetics of the TF or the co-regulator, as well as the mechanisms of nuclear import and export. Post-translational modifications such as phosphorylation affect both TF activity and subcellular localization in a reversible manner (Latchman, 1997).

Mth1p, Std1p, Cyc8p and Tup1p are co-repressors that interact with the TF Rgt1p to repress the expression of the *HXT* genes in the absence of D-glucose (Figure 2.7). Sensing of D-glucose through the Snf3p/Rgt2p pathway causes degradation of Mth1p and Std1p, destabilizing the repressor complex (Polish et al., 2005). The loss of interaction with Mth1p and Std1p leaves Rgt1p vulnerable to phosphorylation by PKA, which has been activated by a D-glucose signal through the cAMP/PKA pathway (Kim and Johnston, 2006).

A



B

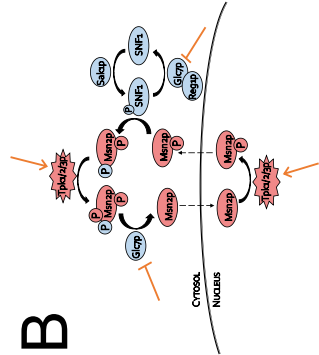


Figure 2.7. A) Mechanisms of gene induction and repression as a result of glucose signaling. Proteins primarily categorized as belonging to the Snf3p/Rgt2p pathway are shown in green, SNF1/Mig1p in blue, and cAMP/PKA in red. TFs and co-regulators not regarded as belonging to any of the pathways are shown in white. Arrows indicate genetic induction and hammerhead repression. See the text for details. B) Illustration of cross-talk between signaling pathways affecting the subcellular location of the TF Msn2p. The SNF1/Mig1p pathway is indicated in blue and cAMP/PKA in red. Orange arrows and hammerheads indicate proteins whose activities are increased or decreased, respectively, by the sensing of high glucose concentrations.

Phosphorylation converts Rgt1p from a transcriptional repressor to an activator. When D-glucose levels are low ($\sim 1 \text{ g L}^{-1}$), PKA activity is also low, and Rgt1p is phosphorylated at only a few sites. This is sufficient for induction of the *HXT2/4* genes, encoding high-affinity hexose transporters. However, the promoter of *HXT1*, encoding a low-affinity transporter, also contains a binding site for the general repressive TF Sko1p (Tomas-Cobos et al., 2004). The activity of this repressor prevents the induction of *HXT1* at low D-glucose concentrations. Higher concentrations of D-glucose, however, lead to hyperphosphorylation of Rgt1p through increased activity of PKA, which in turn enhances the activator strength of the TF, and results in the expression of *HXT1* (Mosley et al., 2003). However, at these high D-glucose concentrations, *HXT2/4* are instead repressed by Mig1/2p (Özcan and Johnston, 1995). The subcellular location of these three TFs is determined by their phosphorylation state. When D-glucose is sensed at high concentrations through the SNF1/Mig1p pathway, Mig1p is dephosphorylated by Glc7p, allowing for nuclear enrichment (Figure 2.6B) (Shashkova et al., 2017). The mechanism determining the phosphorylation state of Mig2p is independent of D-glucose signaling; however, the expression of *MIG2* is induced on D-glucose via the Snf3p/Rgt2p pathway (Kaniak et al., 2004). Inside the nucleus, Mig1/2p interact with promoters of the *HXT2/4* genes to inhibit expression (Westholm et al., 2008).

Msn2/4p are TFs that interact with about 180 STRE-regions throughout the *S. cerevisiae* genome and induce expression of their targets upon sensing of D-glucose depletion and cellular stresses (Treger et al., 1998). Again, the subcellular locations of the TFs are determined by their phosphorylation state. During conditions of no or low D-glucose levels, Msn2p, the better studied of the pair, is dephosphorylated by Glc7p, causing nuclear import and induction of STRE genes, including *TPS1/2* (Figure 2.7B) (Görner et al., 2002). PKA activity increases with increasing D-glucose concentration, and Msn2p is first phosphorylated in serine-288 (de Wever et al., 2005). This residue is part of a nuclear export sequence in Msn2p, and its phosphorylation activates export by interaction with the exportin Msn5p. In the cytoplasm, the nuclear localization signal in Msn2p is hyperphosphorylated by both PKA and the SNF1 complex, inactivating relocation of the TF into the nucleus as long as D-glucose is present in the medium. Once D-glucose is depleted, the phosphatase activity of Glc7p increases, once again overtaking the kinase activities of PKA and SNF1 (Sanz et al., 2000). The regulation of Msn4p is not as well characterized as the paralog Msn2p. The serine-263 and serine-558 sites of Msn4p correspond to the Msn2p serine-288 and serine-582 phosphorylation sites, respectively, but Msn4p lacks a serine-620 equivalent. In general, the functions of Msn2p and Msn4p mostly overlap; however, expression of *MSN4* is Msn2/4p-dependent, while *MSN2* is constitutively induced (Gasch et al., 2000).

Repression of the *SUC2* and *GAL* genes at high D-glucose concentrations is carried out by a repressor complex consisting of the Rgt1p TF, the Med8p co-

activator, the Mig1/2/3p TFs and the Hxk2p co-repressor (Özcan and Johnston, 1996; Vega et al., 2016; de la Cera et al., 2002). Under these conditions Rgt1p is in its activator state, being hyperphosphorylated by PKA, but due to the action of nucleus-enriched Mig1/2/3p and Hxk2p, dephosphorylated by Glc7p through the SNF1/Mig1p pathway, the overall result is repression of the target genes (Polish et al., 2005). At lower D-glucose concentrations, however, the activated SNF1 complex phosphorylates Mig1p and Hxk2p, changing the subcellular location by inducing nuclear export and inhibiting import. The activated Rgt1p TF and Med8p co-activator remain bound to the promoters allowing the induction of *SUC2*. If no D-glucose is sensed, Rgt1p is dephosphorylated, allowing for interactions with Tup1p, Cyc8p, Mth1p and Std1p and reducing the expression of *SUC2* (Polish et al., 2005). The *GAL* genes, encoding the galactose utilization pathway, require separate sensing of D-galactose, in addition to relief of D-glucose repression (Lohr et al., 1995). As long as D-glucose is absent, the *GAL* genes retain their expression as long as there is D-galactose is sensed in the medium.

Response to established *versus* new carbon sources

S. cerevisiae uses a palette of molecular mechanisms to enable sensing of D-glucose and other fermentable sugars over a wide spectrum of concentrations. These mechanisms include conformational changes due to allosteric activation, phosphorylations, degradation of proteins, nucleo-cytosolic shuttling and interaction with produced metabolites or other signaling molecules, such as GTP or cAMP. By balancing these signaling mechanics the yeast is able to interpret and respond to the wide array of conditions found in its natural environment. However, it does not prepare the yeast for a carbon source it has not previously been able to use, such as D-xylose. Introduction of heterologous pathways for D-xylose utilization has been observed to produce new metabolite fluxes and energy states within the yeast. These pathways and the resulting effect on the *S. cerevisiae* signaling mechanics will be discussed in the following chapters.

D-Xylose pathways in natural microorganisms and engineered *S. cerevisiae*

Natural D-xylose utilization

D-Xylose is the second most prevalent sugar in nature. It is found in oligomers such as xylan and hemicellulose which make up plant cell walls. Natural D-xylose-degrading microbes have been isolated from a variety of niches: decaying wood (white and brown rot fungi) and the gut of wood-degrading insects (*Sc. stipitis* and *Spathaspora passalidarum*), as well as nutrient-poor environments such as freshwater (*Caulobacter crescentus*) and hydrothermal vents (*Caldicellulosiruptor* spp.) (Suh et al., 2003; Nguyen et al., 2006; Poindexter, 1964; Sissons et al., 1987). Moreover, xylose-utilizing organisms are part of the human microbiome, including opportunistic pathogens (*Escherichia coli*, *Candida albicans* and *Herbaspirillum huttiense*) (Smith et al., 2007; Beck-Sague and Jarvis, 1993; Ding and Yokota, 2004). Example of representative organisms and their main characteristics regarding D-xylose utilization are summarized in Table 3.1 and reviewed in the following paragraphs.

Table 3.1. Representative organisms naturally utilizing D-xylose, the kingdom they stem from as well as their D-xylose uptake system and pathways used. The aeration condition for observed D-xylose assimilation is also given.

Organism	Kingdom/ Domain	Xylose transport	Pathway	Aerobicity
<i>E. coli</i>	Gram ⁻ bacteria	AP + ABC	XI	Facultative anaerobic
<i>Pseudomonas</i> spp.	Gram ⁻ bacteria	n.d.	Dahms	Aerobic
<i>C. crescentus</i>	Gram ⁻ bacteria	AP	Weimberg	Aerobic
<i>H. huttiense</i>	Gram ⁻ bacteria	n.d.	Route III	Aerobic
<i>Sc. stipitis</i>	Fungi	FD + AP	XR/XDH	Microaerobic
<i>Piromyces</i> sp. E2	Fungi	FD	XI	Facultative anaerobic

Gram⁻: Gram-negative; FD: facilitated diffusion transport; AP: antiporter; ABC: ATP-binding cassette transporter; n.d.: Not determined.

D-Xylose transport

Saccharides such as D-glucose and D-xylose are too large to spontaneously pass through the cellular plasma membrane, and hence their uptake requires specific transmembrane proteins. The transported molecule, the ligand, interacts with the transporter on the extracellular side of the membrane. This interaction causes a conformational change in the transporter, opening up a channel for the ligand to pass through. However, a force is required, i.e. a chemical potential, that enables the translocation of the ligand. Transporters can be categorized by the mechanism used to produce this chemical potential. Several types of transporters for the uptake of D-xylose have been identified, illustrated in Figure 3.1.

In the simplest transport mechanism, *facilitated diffusion* (Figure 3.1A), the driving force for D-xylose uptake is the concentration gradient between the extra- and intracellular spaces (Jeckelmann and Erni, 2020). This system therefore supplies the cell with “free” substrate, but only if it is in excess in the extracellular environment. Facilitated diffusion is used by most pentose-utilizing yeasts to transport xylose (Stambuk et al., 2003; Leandro et al., 2006; Knoshaug et al., 2015).

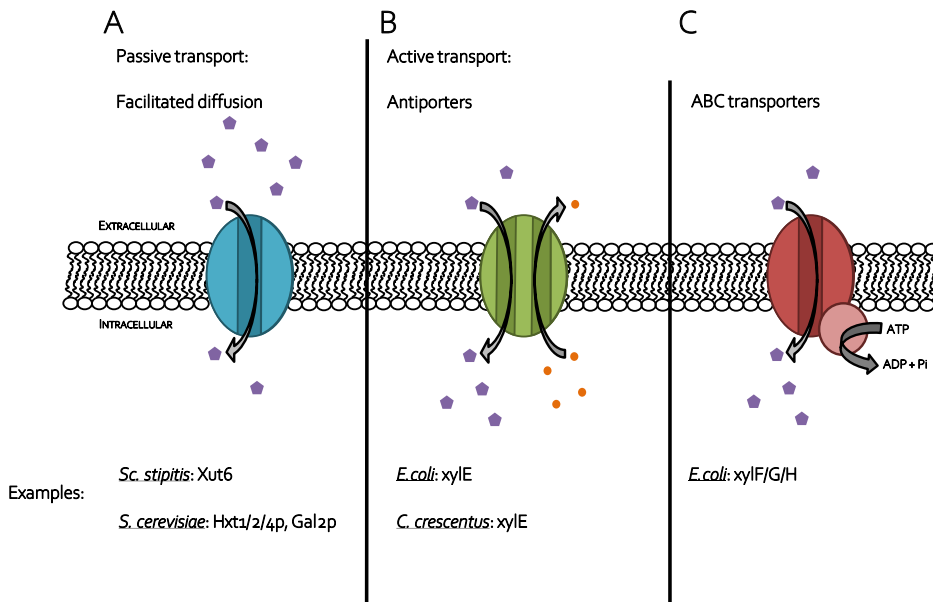


Figure 3.1. Illustration of the types of transmembrane transporters found in nature, and examples of corresponding D-xylose transporters. A) Facilitated diffusion, where the ligand (purple pentagons) concentration gradient determines the direction of transport; B) anti- (or sym-) porters, where primary (purple hexagons) and secondary (orange dots) ligands are transported simultaneously; and C) ABC transporters, where ATP hydrolysis on the intracellular side drives ligand transport.

The other major transport system, *active transport*, is itself divided into two categories. Secondary active transport uses sym- and antiporters that solve the problem of insufficient concentration gradients by transporting a secondary

ligand with a more favorable gradient profile (Figure 3.1B). In the case of symporters, both ligands are translocated in the same direction, while antiporters cause them to move in opposite directions (Jeckelmann and Erni, 2020). In *E. coli* and *C. crescentus*, D-xylose is transported via specific, low-affinity D-xylose/H⁺ symporters, called XylE (Davis and Henderson, 1987; Hottes et al., 2004). Several high-affinity, non-specific, D-xylose or D-glucose/H⁺ symporters have also been identified in xylose-utilizing yeast species such as *Candida intermedia*, *Ca. utilis*, *Sc. stipitis* and *Debaryomyces hansenii* (Kilian and Vanuden, 1988; Kilian et al., 1993; Does and Bisson, 1989; Nobre et al., 1999).

During primary active transport (Figure 3.1C), *ATP-binding cassette (ABC) transporters* catalyze the hydrolysis of ATP on the intracellular side of the membrane to provide the energy required for membrane translocation (Thomas and Tampe, 2020). This mechanism works against concentration gradients and is not dependent on other ligands; however, each import is a considerable ATP investment. Therefore, prokaryotes often express multiple transporters for the same ligand, utilizing different mechanisms depending on the ligand concentration. One example of this is *E. coli*, which combines the low-affinity sugar/H⁺ symporter with a high-affinity ABC transporter, consisting of XylF, XylG and XylH (Sofia et al., 1994). *C. crescentus*, on the other hand, seems to only have a D-xylose/H⁺ symporter (Nobre et al., 1999).

Most of the D-xylose transporters mentioned also interact with other ligands such as D-glucose, D-fructose and L-arabinose, displaying higher affinity for hexoses, and only transporting pentoses after hexose depletion. However, some transporters are D-xylose-specific, such as the active XylFGH ABC transporter of *E. coli* and the passive facilitators in *Sc. stipitis* and *Neurospora crassa* (Ahlem et al., 1982; Du et al., 2010).

D-Xylose assimilation pathways

So far, five different types of microbial pathways for D-xylose assimilation have been identified in nature (Figure 3.2). These pathways can be divided into two groups: those phosphorylating D-xylose and those oxidizing D-xylose.

In the phosphorylating pathways, D-xylose is first converted into xylulose through either isomerization by xylose isomerase (XI), or reduction into xylitol, followed by oxidation to xylulose, by xylose reductase (XR) and xylitol Ndehydrogenase (XDH), respectively. The overall reaction is redox neutral; but, due to differences in the cofactor selectivity of XR and XDH, the oxido-reductive pathway mostly consumes NADPH in the XR reaction, while it produces NADH in the XDH reaction. The two phosphorylating pathways converge at xylulose, which is phosphorylated by xylulose kinase (XK), producing xylulose-5P, a metabolite within the PPP (see Figure 3.2). Xylulose-5P can then be interconverted into important anabolic intermediates such as ribose-5P and erythrose-4P, or enter glycolysis at the fructose-6P and glyceraldehyde-3P nodes.

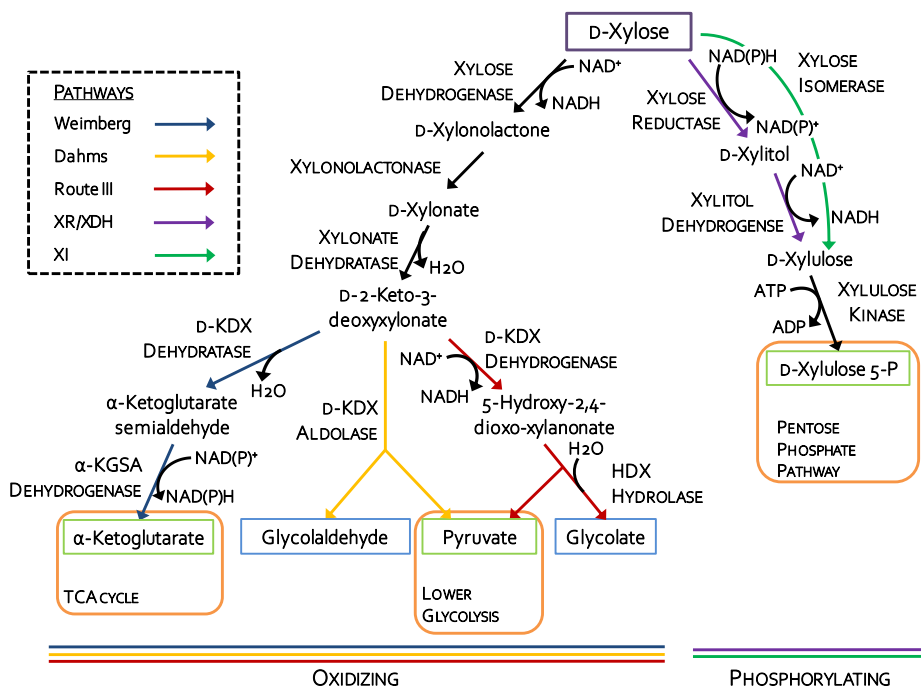


Figure 3.2. D-Xylose assimilation pathways identified in nature. D-Xylose (purple box) is converted into central carbon metabolism constituents (green boxes), in some cases accompanied by the formation of byproducts that require further degradation (blue boxes). Pathway-specific reactions are indicated by colored arrows (see legend), while black arrows denote reactions shared by at least two pathways. Pathway intermediates are given in normal font and the enzymes catalyzing reactions in all capitals. Abbreviations: D-KDX: D-2-keto-3-deoxyxylonate; α -KGSA: α -ketoglutarate semialdehyde; HDX: 5-hydroxy-2,4-dioxo-xylanate.

The three oxidative pathways currently identified in nature start with the same three steps (Figure 3.2). First, D-xylose is oxidized to xylonolactone by xylose dehydrogenase (XylB), after which the lactone ring is opened, either spontaneously or catalyzed by xylonolactonase (XylC), producing D-xylonate. The final common step consists of dehydration by D-xylonate dehydratase (XylD), from which D-2-keto-3-deoxyxylonate (D-KDX) is formed (Weimberg, 1961). In the *Weimberg pathway*, D-KDX is further dehydrated into α -ketoglutaric semialdehyde (α KGSA) by KDX dehydratase (XylX), and oxidized by α KGSA dehydrogenase (KsaD) to α -ketoglutarate (α KG), an intermediate of the TCA cycle. In the *Dahms pathway*, however, D-KDX is cleaved by an aldolase into pyruvate and glycolaldehyde. From there, the pyruvate is shuttled into either the TCA cycle or towards fermentation, while the glycolaldehyde can be either oxidized to glycolate or reduced to ethylene glycol, and then excreted from the cell (Dahms, 1974). In the third oxidative pathway, currently known as *Route III*, D-KDX is oxidized by D-KDX dehydrogenase to 5-hydroxy-2,4-dioxo-xylanate (HDX), which is then hydrolyzed to pyruvate and glycolate by HDX hydrolase. Again, pyruvate is used for either fermentation towards ethanol or

lactic acid, or respiration via the TCA cycle, and glycolate can be excreted (Watanabe et al., 2019).

The pentose sugar L-arabinose is the third most prevalent monosaccharide in agricultural waste hydrolysates (up to 16 % by wet weight), after D-glucose and D-xylose (Okeke and Obi, 1994). Naturally, the larger fraction of the lignocellulosic raw material that can be converted to value-added products, the more economically feasible and sustainable the overall process becomes. Using the same assimilatory pathway for several different substrates and funneling the carbon towards one end product is an interesting potential strategy that could be realized if the pathway enzymes are sufficiently promiscuous. The molecular structures of D-xylose and L-arabinose differ only in the chirality of the C-4 carbon (Figure 3.3), making this pentose pair good candidates for pathway sharing.

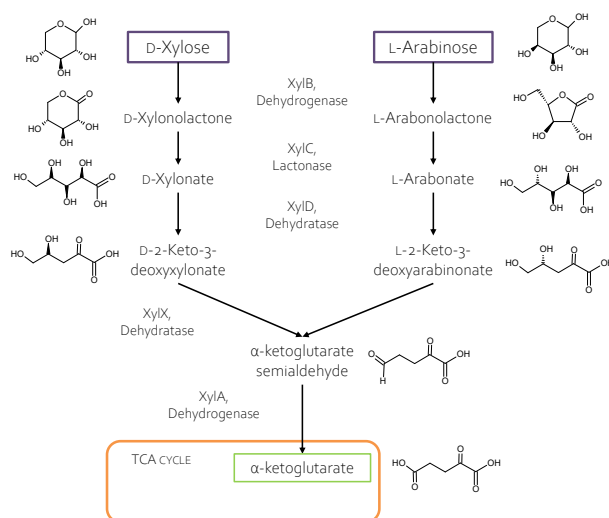


Figure 3.3. Suggested Weimberg pathway for the metabolism of D-xylose (left) and L-arabinose (right) by *C. crescentus*.

L-Arabinose oxidation through the Weimberg pathway was first described in *Pseudomonas fragi* (Weimberg, 1961), and the identity of the genes encoding this pathway has been reported for the soil bacterium *Azospirillum brasiliense* (Watanabe et al., 2006). In order to assess the enzymatic potential for simultaneous D-xylose and L-arabinose utilization through the Weimberg pathway, *C. crescentus* cells were grown on various sugars and the activities of the pathway were assayed *in vitro* (Paper I). As expected, cells pregrown on D-glucose did not display any Weimberg activity (Figure 3.4). Cells grown on either of the pentoses, however, displayed clear activity with all substrates used; D-xylose or L-arabinose as substrate for XylB and D-xylonate for the combined XylDXA reaction. The finding that the enzymes produced in D-xylose-grown cells had affinity and activity for L-arabinose, and vice versa, was interpreted as

a strong indication that the same Weimberg enzymes are used for the metabolism of both pentoses, as illustrated in Figure 3.3.

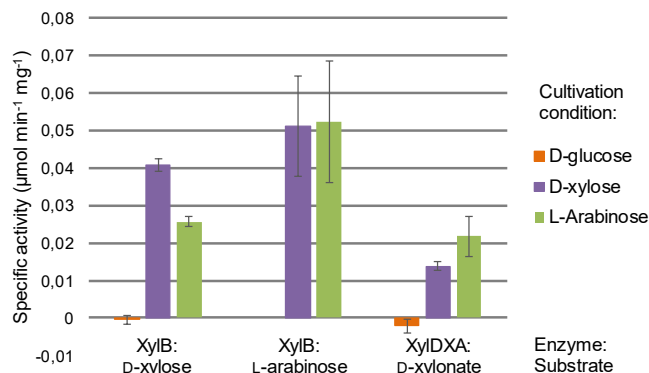


Figure 3.4. Enzyme activity in crude cell-free extracts from *C. crescentus* pregrown on either D-glucose, D-xylose or L-arabinose. XylB was assayed with D-xylose or L-arabinose as substrate and for the combined XylDXA assay D-xylonate was used.

Diversity of D-xylose utilizers in nature

D-Xylose-utilizing eukaryotes, such as the pseudohyphal yeast *Sc. stipitis*, almost exclusively use the XR/XDH pathway (Wohlbach et al., 2011). The XI pathway, on the other hand, has been described in a number of bacteria (e.g. *E. coli*), archaea and plants, and has so far been identified in a handful of fungal species, e.g. *Piromyces* sp. E2 (Kuyper et al., 2003). The Weimberg and Dahms pathways were first described in different *Pseudomonas* species in 1961 and 1974, respectively (Weimberg, 1961; Dahms, 1974). Since then, the Weimberg pathway has been identified in the freshwater bacterium *C. crescentus*, and similar operons have been found in a few other species (Stephens et al., 2007a; Sutter et al., 2017; Wagner et al., 2018; Kohler et al., 2015). The Dahms pathway has, to date, not been described in any further species. However, the pathway can be reconstituted through the combination of individual components found within the bacterial community. For example, XylB and XylC from *C. crescentus* can be combined with D-xylonate dehydratase (YjhG) and D-KDX aldolase (YjhH) from *E. coli* (Cabulong et al., 2018). Route III was not discovered until 2019, and only one bacterial species has been identified so far: the opportunistic pathogen *H. huttiense* (Watanabe et al., 2019).

D-Xylose utilization by *S. cerevisiae*

Wild-type *S. cerevisiae*

Although wild-type *S. cerevisiae* cannot grow on D-xylose, several *S. cerevisiae* strains have been shown to take up D-xylose from the environment (van Zyl et al., 1989), by facilitated diffusion through hexose transporters (Table 3.2). Inside the cell, D-xylose can be reduced to xylitol. At least four NADPH-dependent aldose reductases that reduce D-xylose have been identified in *in vitro* assays (Petrash et al., 2001), and Gre3p has been shown to be the most active *in vivo* (Träff et al., 2002). Further studies of the *S. cerevisiae* genome have led to the identification of two genes encoding XDHs, *XYL2* and *SOR1*, and one gene encoding XKs, *XKS1*. Therefore, it is theoretically possible for the yeast to form biomass from D-xylose through this pathway; however, this was only observed under very specific conditions, with only about 2 % of the carbon assimilated into biomass, and with xylitol as the main product (van Zyl et al., 1989). The bottleneck of the endogenous pathway therefore seems to be the XDH and/or XK activities, either in expression levels, affinity for D-xylose, or cofactor availability. As *in vivo* functionality of both Sor1p and Xks1p has been observed (Harcus et al., 2013; Deng and Ho, 1990), the issue is suspected to mainly be regulatory.

The cryptic D-xylose pathway phenotype exhibited by *S. cerevisiae* is not unique among non-xylose-metabolizing yeasts. In the oleaginous yeast *Yarrowia lipolytica*, overexpression of the endogenous XDH and XK genes was enough to enable growth on D-xylose, as the basal expression levels of the two genes encoding XRs were already sufficient (Rodriguez et al., 2016). In addition, Ryu and colleagues (2016) reported significant activity of *Y. lipolytica* XR using NADH as a cofactor, which could explain the growth observed on D-xylose, especially considering the NADPH requirement for fatty acid production in oleaginous yeasts. Attempts have also been made to boost the potential endogenous D-xylose assimilation pathway in *S. cerevisiae* through breeding and evolution of laboratory strains. After evolution for over four years, isolated clones were found to have increased XR/XDH activity and to be able to grow on D-xylose with a doubling time of about six hours (Attfield and Bell, 2006). However, all the D-xylose was respired and no ethanol was formed.

To conclude, depending on the conditions, D-xylose is taken up by wild-type *S. cerevisiae*, and is either converted into xylitol, a small amount of biomass and carbon dioxide, or remains unmetabolized. However, this yeast has the potential to be engineered for efficient ethanolic fermentation of D-xylose, as will become evident below.

Table 3.2. Genes identified for D-xylose assimilation in the *S. cerevisiae* genome, annotated activity and kinetic properties of the gene products. Primary K_M refers to the affinity for the substrate within the D-xylose assimilatory pathway, and secondary K_M to that of competitive compounds (in the case of transporters) or cofactors (for catalytic enzymes). Maximal velocity (V_{max}) is given for the primary substrate and, when applicable, the secondary, cofactor substrate.

Gene	Activity	V_{max}^a	Primary K_M (g L ⁻¹)	Secondary K_M (g L ⁻¹)	Reference
<i>HXT1</i>	Hexose transport	750 ± 94	D-Xylose: 132 ± 1.2	D-Glucose: 19.3	Saloheimo et al. (2007); Maier et al. (2002)
<i>HXT2</i>	Hexose transport	340 ± 10	D-Xylose: 39.0 ± 19.5	D-Glucose: 0.52	Saloheimo et al. (2007); Maier et al. (2002)
<i>HXT4</i>	Hexose transport	190 ± 23	D-Xylose: 25.5 ± 18.0	D-Glucose: 1.1	Saloheimo et al. (2007); Maier et al. (2002)
<i>HXT7</i>	Hexose transport	67 ± 2.0	D-Xylose: 30.0 ± 1.98	D-Glucose: 0.09 ± 0.02	Farwick et al. (2014)
<i>HXT11</i>	Hexose transport	84.6 ± 2.4	D-Xylose: 12.6 ± 1.50	D-Glucose: 6.02 ± 0.38	Shin et al. (2015)
<i>HXT36</i>	Hexose transport	62.5 ± 5.9	D-Xylose: 16.2	D-Glucose: 1.1	Nijland et al. (2014)
<i>GAL2</i>	Galactose transport	91.3 ± 3.2	D-Xylose: 33.9 ± 2.37	D-Glucose: 0.27 ± 0.04	Farwick et al. (2014)
<i>GRE3</i>	Aldose reductase	10.7 ± 0.4	D-Xylose: 4.19 ± 0.68	NADPH: 0.010 ± 0.0015	Kuhn et al. (1995) Ford and Ellis (2001)
<i>YPR1</i>	Aldose reductase	24.5 ± 5.5	D-Xylose: 5.6	NAD(P)H: n.d.	Petrash et al. (2001) Ford and Ellis (2001)
<i>YJR096W</i>	Aldose reductase	n.d.	D-Xylose: 17.4	NAD(P)H: n.d.	Petrash et al. (2001)
<i>YDL124W</i>	Aldose reductase	n.d.	D-Xylose: N.D.	NAD(P)H: n.d.	Petrash et al. (2001)
<i>XYL2</i>	Xylitol dehydrogenase	1.2-3	Xylitol: 3.8 ± 0.46	NAD ⁺ : 0.16 ± 0.03	Richard et al. (1999)
<i>SOR1</i>	Sorbitol dehydrogenase	n.d.	Xylitol: n.d.	NAD(P) ⁺ : n.d.	Harcus et al. (2013)
<i>XKS1</i>	D-Xylulose kinase	38.4	D-Xylulose: 0.047 ± 0.0015	ATP: 0.786 ± 0.04	Richard et al. (2000)

^a V_{max} measured as nmol min⁻¹ mg⁻¹ dry weight for transporters and as μmol min⁻¹ mg⁻¹ protein for catalytic enzymes.

K_M : substrate Michaelis-Menten constant; n.d.: Not determined.

Transporter engineering

As mentioned above, the *S. cerevisiae* genome encodes several passive sugar transporters. However, the affinity and transport rate of these natural transporters for D-xylose are low, especially relative to that for D-glucose (Table 3.3). This is a particular problem during co-consumption of D-xylose and D-glucose, as D-glucose acts as a competitive inhibitor of D-xylose uptake (Subtil and Boles, 2012). The ideal D-xylose transporter would simultaneously enhance the affinity for the pentose sugar and reduce that for D-glucose. Additionally, any increase in D-xylose transport rate would, of course, also be beneficial to the overall process.

In pursuit of this ambitious goal, several D-xylose-specific transporters have

Table 3.3. Heterologous and/or engineered endogenous transporters for increased D-xylose uptake in *S. cerevisiae*. Maximal velocity (V_{max}) refers to D-xylose as the substrate.

Gene	Activity	Origin	Substitution	V_{max} nmol min ⁻¹ mg ⁻¹ dry weight	D-xylose K_m (mM)	D-glucose K_m (mM)	Reference
<i>HXT7-N370S</i>	Hexose facilitator	<i>S. cerevisiae</i>	N370S	24.1 ± 1.6	25.5 ± 3.9	1.95 ± 0.18	Farwick et al. (2014)
<i>HXT11-N366T</i>	Hexose facilitator	<i>S. cerevisiae</i>	N366T	76.2 ± 4.8	1.00 ± 0.41	35.0 ± 8.6	Shin et al. (2015)
<i>HXT36-N367A</i>	Hexose facilitator	<i>S. cerevisiae</i>	N367I	29.1 ± 0.4	3.74 ± 0.51	30.8 ± 6.8	Nijland et al. (2014)
<i>GAL2-N376F</i>	Galactose facilitator	<i>S. cerevisiae</i>	N376F	37.3 ± 1.3	13.7 ± 1.3	No transport	Farwick et al. (2014)
<i>SUT1</i>	Sugar facilitator	<i>Sc. stipitis</i>	WT	132.0 ± 1.0	21.8 ± 0.15	0.27 ± 0.02	Weierstall et al. (1999)
<i>At5g5920</i>	Sugar facilitator	<i>Arabidopsis thaliana</i>	WT	148 ± 39	24.9 ± 0.9	n.d.	Runquist et al. (2010b)
<i>GXF1</i>	Sugar facilitator	<i>Ca. intermedia</i>	WT	513 ± 12	7.31 ± 0.98	0.36 ± 0.11	Leandro et al. (2006); Runquist et al. (2009)
<i>GXS1</i>	Sugar/H ⁺ symporter	<i>Ca. intermedia</i>	WT	6.5 ± 1.5	0.060 ± 0.015	0.002 ± 0.0007	Leandro et al. (2006)
<i>XPY29 (STL12)</i>	D-xylose facilitator	<i>Sc. stipitis</i>	WT	0.692 ± 0.04	8.40 ± 1.4	No transport	Du et al. (2010)
<i>AN25</i>	D-xylose facilitator	<i>N. crassa</i>	WT	0.612 ± 0.05	26.3 ± 3.21	No transport	Du et al. (2010)

K_m : substrate Michaelis-Menten constant; WT: wild-type amino acid sequence; n.d.: Not determined.

been identified from natural utilizers, and wild-type *S. cerevisiae* transporters have been mutated (Table 3.3).

The genes encoding D-xylose transporters in natural utilizers have been identified either by functionally complementing a sugar-transport-deficient *S. cerevisiae* strain and selecting for growth on D-xylose, or by probing the genomes using DNA sequences of known genes (Leandro et al., 2006; Du et al., 2010). For the adaptation of wild-type transporters, targeted or random mutagenesis has been combined with selection for growth on D-xylose in a transporter-deficient background strain (e.g. Shin et al., 2015). Alternatively, selection for D-xylose preference over D-glucose can be performed in media containing both sugars, in a background strain that grows on D-xylose but has a blockage in upper glycolysis (Farwick et al., 2014; Nijland et al., 2014).

Engineering *S. cerevisiae* for growth on D-xylose via glycolysis

As the potential for D-xylose assimilation by *S. cerevisiae* via the endogenous XR/XDH/XK genes has been shown to be limited, heterologous pathways have been introduced.

The XR/XDH pathway

Among NADPH-dependent XRs identified within D-xylose-utilizing fungal species, the first found to also exhibit activity using NADH came from *Sc. stipitis*, Xyl1 (Table 3.5). This enzyme was combined with the NAD⁺-dependent *Sc. stipitis* XDH, Xyl2, and overexpression of the endogenous XK gene, *XKS1*, to produce the first recombinant *S. cerevisiae* strain to channel D-xylose through lower glycolysis for ethanol formation (Kötter et al., 1990). However, anaerobic growth was not possible on this carbon source, and under aerobic conditions most of the D-xylose was converted into carbon dioxide, indicating that respiration was required to maintain redox balance. The reason for this is that although *Sc. stipitis* Xyl1 can use NADH as a cofactor, its affinity for NADPH is significantly higher (K_M's of 19.0 ± 3.6 and 0.77 ± 0.46 mg L⁻¹ for NADH and NADPH, respectively; Bengtsson et al., 2009). Targeted and random protein engineering and bioprospecting strategies were utilized to identify XR variants with higher selectivity for NADH (Table 3.5). These variants, combined with wild-type *Sc. stipitis* Xyl2, allowed for anaerobic growth and fermentation of D-xylose to ethanol, which could be further improved by downstream pathway engineering. As an alternative, NADP⁺-dependent XDH variants were also designed to create a XR-XDH pathway relying on NADP(H) (Watanabe et al., 2005).

The XI pathway

While the implementation of the XI pathway in *S. cerevisiae* avoids major redox issues, it has its own challenges. As this pathway is mainly found in bacteria, expression in eukaryotes was not guaranteed. Attempts to express the XI genes from e.g. *E. coli*, *Bacillus subtilis* or *Thermoanaerobacterium thermosulfurigenes* (formerly *Clostridium thermosulfurogenes*) in *S. cerevisiae* resulted in the production of non-functional proteins (Amore and Hollenberg, 1989; Sarthy et al., 1987; Moes et al., 1996).

The first recorded successful introduction of a bacterial XI gene was the *Thermus thermophilus xylA* gene (Table 3.6; Walfridsson et al., 1996). However, as the species name implies, this enzyme is adapted to high temperatures, showing maximal activity at 85 °C and only 4 % at 30 °C. Random mutagenesis allowed for the identification of cold-adapted variants which, in addition to slightly increased activity at 30 °C, also exhibited a substantially lower affinity for the inhibitor xylitol (Lönn et al., 2002; Yamanaka, 1969). However, these variants have only been assayed in an *E. coli* host, and their activity in yeast has yet to be determined.

In 2003, Kuyper and colleagues reported on the first fungal species to express a D-xylose isomerase: *Piromyces* sp. E2. Since then, functional XIs have also been identified from the bacterium *Lachnoclostridium phytofermentans* (formerly *Clostridium phytofermentans*) and the fungus *Orpinomyces* sp. (Table 3.6; Brat et al., 2009; Madhavan et al., 2009).

Lower phosphorylative D-xylose pathways

The XR/XDH and XI pathways converge to the native XK converting xylulose to xylulose-5P, which enters the non-oxidative part of the PPP towards glycolysis. As the route introduction was reported to only result in slow aerobic growth on D-xylose, efficient ethanolic fermentation and anaerobic growth required further engineering of the downstream pathway. Accordingly, overexpression of the genes encoding XK, as well as one or more of the enzymes in the non-oxidative PPP – transketolase, transaldolase, ribose 5-phosphate ketol-isomerase and ribulose 5-phosphate epimerase – improved xylose utilization by increasing the flux through the pathways (Walfridsson et al., 1996; Karhumaa et al., 2005). Furthermore, the deletion of *GRE3*, encoding the main endogenous, NADPH-dependent D-xylose reductase, also improved fermentation, primarily by reducing the concentration of xylitol inhibiting XI activity (Träff et al., 2001; Kuyper et al., 2005).

Further metabolic engineering, including copy number modulation, adaptive laboratory evolution, random mutagenesis and *in silico* modelling, was utilized to further increase ethanol yields and anaerobic growth on D-xylose (e.g. Bracher et al., 2019; Lee et al., 2012; Parachin et al., 2011). The highest reported anaerobic growth rate, specific D-xylose consumption rate and ethanol yield through the XR/XDH pathway achieved to date, utilizing Xyl1.2 from

Table 3.4. Genes utilized for the implementation of the XR/XDH pathways in *S. cerevisiae*

Gene	Activity	Origin	Substitution	Substrate	V_{max} (U mg ⁻¹ protein)	K_m substrate (g L ⁻¹)	K_m cofactor (g L ⁻¹)	R_{rel}	Reference
<i>XYL1</i>	D-Xylose reductase	<i>Sc. stipitis</i>	WT	D-Xylose	0.30 ± 0.05 0.21 ± 0.01	9.32 ± 4.16 8.89 ± 1.58	NADPH: 0.0008 NADH: 0.019	0.024 ^a	Bengtsson et al. (2009)
<i>XYL1</i>	D-Xylose reductase	<i>Sc. stipitis</i>	K270R	D-Xylose	2.13 ± 0.24 0.96 ± 0.09	70.3 ± 22.7 21.8 ± 5.54	NADPH: 0.020 NADH: 0.042	0.13 ^a	Bengtsson et al. (2009)
<i>XYL1</i>	D-Xylose reductase	<i>Sc. stipitis</i>	N272D	D-Xylose	2.4 ± 0.1 1.09 ± 0.05	6.0 ± 1.5 5.4 ± 1.2	NADPH: 0.019 NADH: 0.003	5.4 ^a	Runquist et al. (2010a)
<i>XYL1.2</i>	D-Xylose reductase	<i>Sp. passalidarum</i>	WT	D-Xylose	n.d.	7.84 ± 0.57 2.57 ± 0.27	NADPH: 0.024 NADH: 0.011	3.58 ^b	Hou (2012)
<i>XYL2</i>	Xylitol dehydrogenase	<i>Sc. stipitis</i>	WT	Xylitol	n.d.	3.30 ± 0.02 0.099 ± 0.003	NAD ⁺ : 0.253 NADP ⁺ : 127	925 ^b	Watanabe et al. (2005)
<i>XYL2 C4/ARS</i>	Xylitol dehydrogenase	<i>Sc. stipitis</i>	S96C, S99C, Y102C, D207A, I208R, F209S	Xylitol	n.d.	n.d. 16.9 ± 0.76	NAD ⁺ : 15.6 NADP ⁺ : 0.88	0.020 ^b	Watanabe et al. (2005)

K_{M1} : substrate Michaelis-Menten constant; R_{rel} : selectivity ratio between cofactors; WT: wild-type amino acid sequence; n.d.: Not determined.

^a Determined as V_{max}/K_{M1} ratio for NADH over V_{max}/K_{M1} ratio for NADPH.

^b Determined as measured specific enzyme activity for NADH over NADPH or NAD⁺ over NADP⁺, under identical conditions.

Table 3.5. Genes utilized for the implementation of the XI pathways in *S. cerevisiae*

Gene	Activity	Origin	Substitution	V_{max} (U mg ⁻¹ protein)	K_m D-xylose (g L ⁻¹)	K_i xylitol (g L ⁻¹)	Reference
<i>xylA</i>	D-Xylose isomerase	<i>T. thermophilus</i>	WT	85 °C: 1.0 30 °C: 0.04	0.52 ± 0.06 ^a	0.70 ^a	Walfridsson et al. (1996); Lönn et al. (2002)
<i>xylA</i>	D-Xylose isomerase	<i>T. thermophilus</i>	E372G, V379A	75 °C: 100 % 30 °C: 5 %	3.77 ± 0.60 ^a	5.05 ^a	Lönn et al. (2002)
<i>xylA</i>	D-Xylose isomerase	<i>T. thermophilus</i>	F163L, E372	90 °C: 100 % 30 °C: 5 %	13.4 ± 1.3 ^a	179 ^a	Lönn et al. (2002)
<i>xylA</i>	D-Xylose isomerase	<i>Pirionmyces</i> sp. E2	WT	0.053 ± 0.007	13.1 ± 0.98	0.70 ± 0.27	Kuyper et al. (2003); Lee et al. (2012)
<i>xylA</i> *3	D-Xylose isomerase	<i>Pirionmyces</i> sp. E2	E129D, V433I, E15D, E114G, T142S, A177T	0.094 ± 0.006	25.3 ± 1.80	n.d.	Lee et al. (2012)
<i>xylA</i>	D-Xylose isomerase	<i>Orpinomyces</i>	WT	1.90 ± 0.04	n.d.	n.d.	Madhavan et al. (2009)
<i>xylA</i>	D-Xylose isomerase	<i>L. phytofermentans</i>	WT	n.d.	9.90 ± 0.15	2.2 ± 0.17	Brat et al. (2009)

K_{M1} : substrate Michaelis-Menten constant; K_i : inhibitor Michaelis-Menten constant; wild-type amino acid sequence; n.d.: Not determined.

^a Determined at 60 °C in crude extracts from *E. coli* hosts.

Sp. passalidarum, are 0.11 h^{-1} , $0.76 \text{ g (g CDW *h)}^{-1}$ and 0.40 g g^{-1} , respectively; (Cadete et al., 2016). The corresponding XI strain, expressing *Piromyces* XI on a multicopy plasmid and evolved for anaerobic D-xylose assimilation, has yielded similar values: 0.12 h^{-1} , $1.4 \text{ g D-xylose (g CDW*h)}^{-1}$ and $0.41 \text{ g ethanol g}^{-1}$ D-xylose (Kuyper et al., 2005).

Engineering D-xylose utilization that bypasses glycolysis

Interest has recently increased in two D-xylose-utilization pathways that are quite rare in known microbiota: the oxidative Dahms and Weimberg pathways (Fig. 3.2). These pathways were first described in different *Pseudomonas* species in 1974 and 1961, and were successfully introduced into yeast in 2017 and 2019, respectively (Dahms, 1974; Weimberg, 1961; Salusjärvi et al., 2017; Paper II). The delay in introduction compared to the phosphorylative pathways is partly due to the fact that the oxidative pathways do not enter glycolysis, and most or all of the carbon cannot be shuttled into ethanol. Instead, these pathways can be used for the production of small organic acids, such as intermediates of the TCA cycle. As *S. cerevisiae* grows best at slightly acidic pH (pH 5-6) and has a relatively high tolerance to organic acids, it has the potential to be a good production host for these acids from D-xylose.

Upper Dahms and Weimberg pathways

Since the Dahms and Weimberg pathways have only been described in bacteria and archaea, codon-optimization has been required prior to gene introduction into *S. cerevisiae*. The first two (shared) steps of the pathways are performed by XylB and XylC (Fig. 3.2), taken from *C. crescentus*, and high activity has been obtained in *S. cerevisiae* without further modifications; the activity of XylC was actually so high that the yeast displayed growth defects in the presence of D-xylose (Nygard et al., 2014; Wasserstrom et al., 2018). This was assumed to be caused by accumulation of the product D-xylonate, an organic acid with a pKa of 3.66 (Hummel et al., 2010). Since lactone ring opening has been described to occur spontaneously at lower rates, the *xylC* gene was later omitted from engineering strategies (Nygard et al., 2014).

When the Dahms or Weimberg pathway was introduced into *S. cerevisiae*, omitting *xylC*, D-xylonate still accumulated, indicating a bottleneck downstream of this intermediate (Salusjärvi et al., 2017; Wasserstrom et al., 2018). The third common enzyme, XylD was initially suspected to be the limiting step, as biochemical characterization had shown its activity to be highly dependent on iron-sulfur clusters (Andberg et al., 2016), whose loading mechanisms differ significantly between bacteria and eukaryotes. In general, bacteria have one cytosolic loading system, while the main eukaryotic system is mitochondrial, with a minor cytosolic iron-sulfur cluster assembly. The labelling and transport of iron-sulfur cluster-requiring proteins also varies between bacteria and

eukaryotes, and thus these types of proteins are notoriously difficult to activate over domain boundaries (Lill and Muhlenhoff, 2005). The challenge of potential inadequate iron-sulfur loading has been tackled by screening enzymes from other hosts. These enzymes were selected from the two major sources of D-xylonate dehydratase: the IlvD/EDD and the MR/MLE families. The dehydratases within the IlvD/EDD family, to which *C. crescentus* XylD belongs, all contain iron-sulfur clusters, while the MR/MLE enzymes only require magnesium (Mg^{2+}) or manganese (Mn^{2+}) as cofactors (Rahman et al., 2018; Babbitt et al., 1996). On the other hand, dehydratases belonging to the MR/MLE family are often found in extremophilic bacteria and archaea, which could imply additional requirements for full functionality, e.g. high temperatures and/or salt concentrations (Nunn et al., 2010; Johnsen et al., 2009). As substrate promiscuity has been observed for several dehydratases (Kerstens et al., 1971; Kim and Lee, 2006), a few enzymes not primarily described to use D-xylonate have also been screened. Unfortunately, none of the enzymes assayed displayed a higher activity than the original *C. crescentus* XylD, including bacterial genes expressed in *E. coli* and fungal genes expressed in yeast (Wasserstrom et al., 2018; Boer et al., 2019). Instead, the key to expressing a functional iron-sulfur dehydratase was found to lie, at least partly, in the deregulation of the yeast iron metabolism, through deletion of the repressor *FRA2* (also known as *BOL2*): removal of this gene led to a 13-fold increase in D-xylonate dehydratase activity (Salusjärvi et al., 2017). Tagging XylD to the mitochondria, where most of the iron-sulfur assembly takes place, further boosted the activity 27-fold compared to cytosolic XylD (Salusjärvi et al., 2017); however, it is difficult to implement this improvement since the remainder of the pathway is localized in the cytosol, and it is not known whether transport both D-xylonate and the product D-KDX through the mitochondrial membrane is possible.

Table 3.6. Genes utilized for implementation of the Dahms and Weimberg pathways in *S. cerevisiae*

Gene	Activity	Origin	Substrate	<i>S. cerevisiae</i> functionality	Reference
<i>xylB</i>	D-Xylose dehydrogenase	<i>C. crescentus</i>	D-Xylose	Functional w/o modification	Toivari et al. (2012)
<i>xylC</i>	Xylonolactonase	<i>C. crescentus</i>	Xylonolactone	Activity causes lethal D-xylonate levels	Wasserstrom et al. (2018)
<i>xylD</i>	D-Xylonate dehydratase	<i>C. crescentus</i>	D-Xylonate	Activity boosted by <i>FRA2</i> deletion	Salusjärvi et al. (2017)
<i>yjhH</i>	D-KDX aldolase	<i>E. coli</i>	D-KDX	Functional w/o modification	Salusjärvi et al. (2017)
<i>yagE</i>	D-KDX aldolase	<i>E. coli</i>	D-KDX	Functional w/o modification	Salusjärvi et al. (2017)
<i>xylX</i>	D-KDX dehydratase	<i>C. crescentus</i>	D-KDX	Functional w/o modification	Paper II
<i>xylA</i>	α KGSA dehydrogenase	<i>C. crescentus</i>	α KGSA	Not functional in <i>S. cerevisiae</i>	Paper II
<i>ksaD</i>	α KGSA dehydrogenase	<i>Co. glutamicum</i>	α KGSA	Functional w/o modification	Brüsseler et al. (2019)

The Dahms pathway

In the Dahms pathway, only one step remains downstream of XylD, namely splitting of D-KDX into pyruvate and glycolaldehyde (Dahms, 1974) (Figure 3.2). This reaction is similar to the last step in the glycolytic Entner-Doudoroff pathway, where 2-keto-3-deoxy-6-phosphogluconate is cleaved into pyruvate and G3P. Some of the aldolases performing this step have been shown to be promiscuous and also cleave D-KDX, for example, YjhH and YagE from *E. coli* (Liu et al., 2013). In a proof-of-concept study, Salusjärvi and colleagues (2017) expressed a complete Dahms pathway using *C. crescentus* *xylB* and *xylD* and *E. coli* *yjhH* in a laboratory yeast strain with a *fra2Δ* deletion. The resulting strain was able to form 14 mg L⁻¹ ethylene glycol, a product of endogenous aldo-keto reductase activity on glycolaldehyde, from 20 g L⁻¹ D-xylose.

The Weimberg pathway

The successful implementation of the Weimberg pathway (Figure 3.2) in *S. cerevisiae*, achieved through a series of modifications, is described for the first time in the present thesis (Paper II; Figure 3.5). First, the codon-optimized versions of the *C. crescentus* *xylABDX* operon, without *xylC* (Wasserstrom et al., 2018), were combined with the deletion of *FRA2* (cf. above). However, this led to equimolar amounts of D-xylonate being produced from D-xylose. Enzyme activities in the lower Weimberg pathway, measured on crude cell extracts, were basically undetectable, either for the combined XylDXA assay or XylA alone, despite previously confirmed expression of all the pathway genes using reverse-transcript PCR analysis (Wasserstrom et al., 2018); therefore the protein abundances were assessed using untargeted proteomics. It was found that the proteins XylB, XylD and XylX were all present in the recombinant strain, whereas XylA, the last enzyme of the pathway, was not. Whether the absence of XylA was caused by mRNA instability, possibly by splicing, or problems associated with the protein itself, such as misfolding or immediate labelling for destruction, remains to be elucidated. Instead, a functional alternative to XylA was sought for. The *ksaD* gene within the Gram-positive *Corynebacterium glutamicum* also encodes an αKGSA dehydrogenase, which was tested as the predicted secondary structures of KsaD and XylA were very similar, despite having only a 25 % amino acid sequence identity (Brüsseler et al., 2019). Replacing *xylA* with a codon-optimized *ksaD* in the *S. cerevisiae* Weimberg strain (*fra2Δ*, *xylB-xylD-xylX*) yielded a 20-fold increase in αKGSA dehydrogenase activity *in vitro* (Figure 3.6), but the strain still produced only D-xylonate from D-xylose.

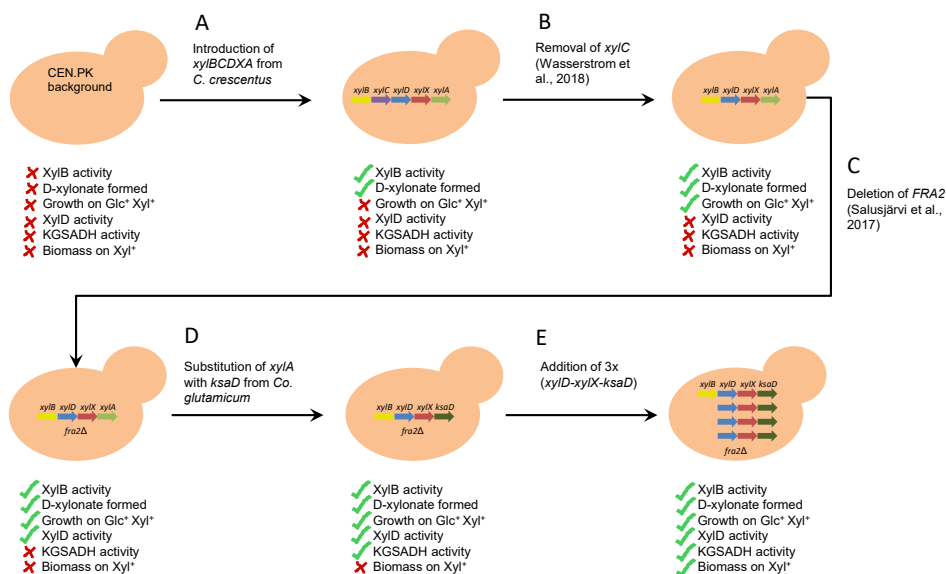


Figure 3.5. Schematic of engineering process for establishing the Weimberg pathway in *S. cerevisiae*, described in Paper II. Engineering steps, genetic modifications and physiological results are shown. The effects of steps B and C were demonstrated by Wasserstrom et al. (2018) and Salusjärvi et al. 2017. KGSADH: α KGSA dehydrogenase.

Biomass formation from D-xylose was finally achieved by increasing the copy number of the lower pathway (*xylD*, *xylX* and *ksaD*) to four integrated copies. The resulting strain (*fra2Δ*, *xylB*, 4x(*xylD-xylX-ksaD*)) was able to convert 60 % of the supplied D-xylose carbon through the Weimberg pathway, measured in terms of the biomass gain and carbon dioxide formed, when grown aerobically on a mixture of D-glucose and D-xylose. All pathway intermediates could be qualitatively identified except D-KDX, while the main byproduct remained D-xylonate (Figure 3.7).

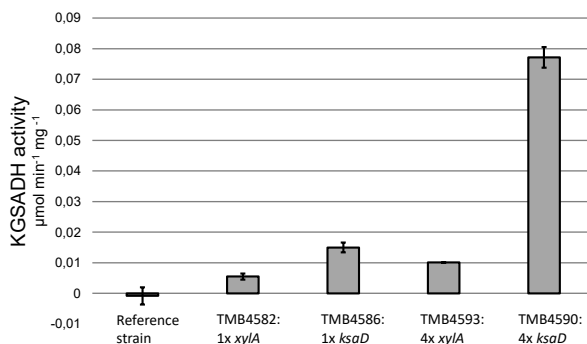


Figure 3.6. *In vitro* α KGSA dehydrogenase (KGSADH) activity of *S. cerevisiae* strains harboring either zero, one or four copies of codon-optimized KGSADH genes from *C. crescentus* (*xylA*) or *Co. glutamicum* (*ksaD*). Adapted from Paper II.

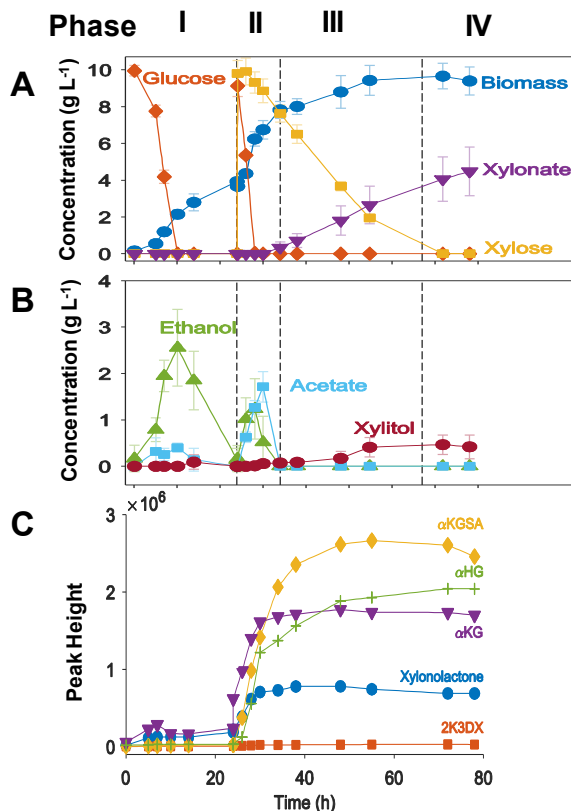


Figure 3.7. Physiological profile of strain TMB4590, in an aerobic bioreactor. A) D-Glucose (orange diamonds), D-xylose (yellow squares), D-xylonate (purple triangles) and biomass (blue dots). B) Ethanol (green triangles), acetate (cyan squares) and xylitol (red dots). C) Xylonolactone (blue dots), D-KDX (orange squares), αKGS (yellow diamonds), αKG (purple triangles) and a natural product of αKG, αHG (green pluses). Adapted from Paper II.

Pathway analysis

The establishment of the XDH/XR and the XI pathways represented a significant step towards the efficient valorization of lignocellulosic waste streams, as this allowed D-xylose to be fermented, via glycolysis, into ethanol by a robust yeast. The introduction of the Dahms and Weimberg pathways now opens up the possibility of D-xylose utilization that bypasses glycolysis altogether, forming products from either the pyruvate or the αKG node (Figure 3.8). Each pathway presents a different set of traits that can be seen as advantages or challenges depending on the conditions and the desired output (Table 3.7).

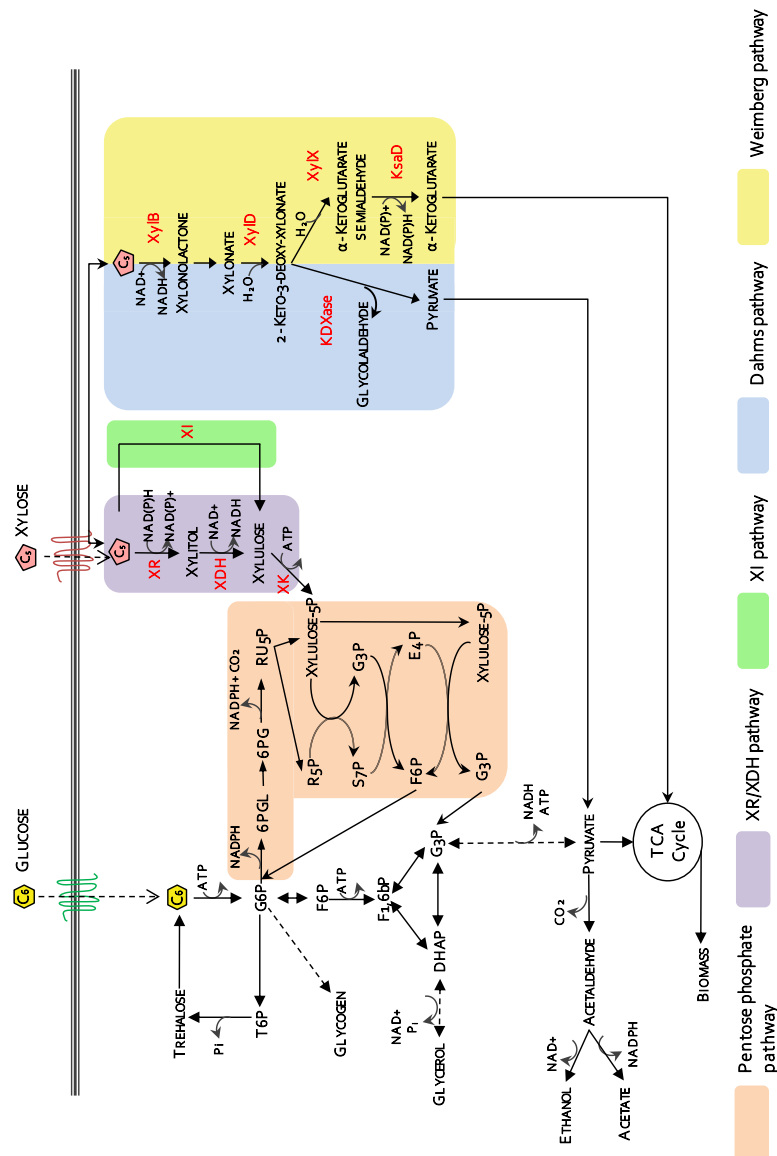


Figure 3.8. Summary of the xylose assimilation pathways that have been successfully introduced into *S. cerevisiae* to date. Enzymes required to channel D-xylose into central carbon metabolism are shown in red. XR: xylose reductase; XDH: xylitol dehydrogenase; XI: xylose isomerase; XK: xylulokinase; XylB: xylose dehydrogenase; XylD: xylonate dehydratase; KDxase: 2-keto-3-deoxy-xylonate aldolase; XylX: 2-keto-3-deoxy-xylonate dehydratase; KsaD: α -ketoglutarate semialdehyde dehydrogenase; G6P: glucose-6-phosphate; T6P: trehalose-6-phosphate; 6PGL: 6-phosphogluconate lactone; 6PG: 6-phosphogluconate; R5P: ribulose-5-phosphate; R5P: ribulose-5-phosphate; S7P: seduheptulose-7-phosphate; G3P: glyceraldehyde-3-phosphate; F6P: fructose-6-phosphate; E4P: erythrose-4-phosphate; F1,6bP: fructose-1,6-bisphosphate; DHAP: dihydroxyacetone phosphate; TCA cycle: tricarboxylic acid cycle; NAD(P)H: nicotinamide adenine dinucleotide (phosphate); ATP: adenosine triphosphate.

Table 3.7. Comparison of D-xylose-utilizing pathways

Pathway	Node	Aerobicity	Optimization target	Main byproduct
XR/XDH	Xylulose 5-P	Anaerobic	Redox	Glycerol, xylitol
XI	Xylulose 5-P	Anaerobic	Gene expression (<i>xyIA</i>)	Glycerol, xylitol
Dahms	Pyruvate	Aerobic	Enzyme activity (<i>XylD</i>)	D-Xylonate
Weimberg	α KG	Aerobic	Enzyme activity (<i>XylD</i>)	D-Xylonate

After alleviation of the redox imbalance through changes in the cofactor specificity of XR, both the XR/XDH and the XI pathways support anaerobic fermentation of D-xylose. The Dahms and Weimberg pathways, on the other hand, are oxidative, and require aeration to maintain the redox balance. Aerobic conditions are more expensive than anaerobic on an industrial scale, so the oxidative pathways would have to provide more valuable products than ethanol in order to be economically feasible.

Ethanol has been the most common model product for the XR/XDH and the XI pathways, whereas the end products formed by the introduction of the Dahms pathway is ethylene glycol or glycolic acid, and flux through the Weimberg pathway was confirmed by biomass formation. However, the potential products that could be formed from D-xylose through these pathways are plentiful and diverse. The XR/XDH, the XI and the Dahms pathway all converge on pyruvate, from which polyhydroxybutarate, 1-hexadecanol, glycolic acid and 2,3-butanediol have been formed (de Las Heras et al., 2016; Guo et al., 2016; Salusjärvi et al., 2017; Kim et al., 2013). The Weimberg pathway, however, leads to the formation of intermediates that can be diverted towards products such as succinate, glutamate, 1,4-butanediol and 1,2,4-butanetriol, which can be used to manufacture nylon, bioplastics, synthetic rubbers and pharmaceuticals. In fact, 1,2,4-butanetriol was recently produced by diverting the carbon flux from D-KDX in *S. cerevisiae* through the introduction of two heterologous genes (Yukawa et al., 2020).

Since the introduction of the XR/XDH and the XI pathways, several rounds of engineering and improvements have been carried out. D-xylose fermentation can now be carried out anaerobically, enzymes have been optimized for eukaryotic expression, and the formation of byproducts such as xylitol and glycerol has been reduced. However, there are still aspects that can be further improved. For example, a fully redox balanced XR/XDH pathway would require an NADH-dependent xylose reductase, which has yet to be discovered in nature or produced through protein engineering. Rapid D-xylose consumption through the XI pathway however, is dependent on stable, high expression of the XI enzyme, achievable by introduction of up to 36 copies of the *xyIA* gene (Verhoeven et al., 2017).

In studies where the XR/XDH and XI pathways have been compared with the same strain background, the XR/XDH pathway was found to confer the highest ethanol productivity, while fermentation via the XI pathway resulted in higher

ethanol yields (Karhumaa et al., 2007; Cunha et al., 2019). Strains harboring the XI pathway were observed to exhibit low D-xylose consumption rates in media containing inhibitors such as acetate and furan aldehydes while expression of the XR/XDH pathway was associated with increased inhibitor tolerance, possibly due to recycling of redox cofactors during furan aldehyde detoxification (Karhumaa et al., 2007). This trait was particularly evident in an industrial strain expressing both pathways simultaneously, where a synergistic effect was observed; higher D-xylose consumption and ethanol yields were achieved from non-detoxified corn cob hydrolysate than in strains carrying only one pathway (Cunha et al., 2019).

As the Dahms and Weimberg pathways were only introduced into *S. cerevisiae* in 2017 and 2019, respectively, little optimization has been achieved. During D-xylose consumption, a strain expressing the Weimberg pathway was found, in the present work, to still accumulate D-xylonate, but not its direct downstream intermediate, D-KDX (Paper II). This indicated that XylD remained a bottleneck and a future target for pathway engineering.

A common denominator for all D-xylose-utilization pathways is that they introduce a new sugar into the substrate range of *S. cerevisiae*. Although heterologous pathway genes are usually associated with promoters that show high expression under many conditions, such as those controlling the expression of glycolytic genes (Chambers et al., 1995), the general metabolic state is dependent on sensing of a carbon source. As discussed in Chapter 2, *S. cerevisiae* tightly regulates and coordinates its metabolic state through carbon source sensing, signal transduction, and the induction or repression of genetic targets. The question of whether or not utilization of the new sugar D-xylose triggers a signaling response in *S. cerevisiae*, what that signal would be, and how it is affected by co-utilization of other carbon sources, will be discussed in Chapter 4.

Role of sensing in D-xylose utilization in natural organisms and engineered *S. cerevisiae*

Regardless of the route of D-xylose utilization, each cell needs to be able to sense the presence of the carbon source and to convey the information necessary to activate the transporters and enzymes required for its assimilation. The diversity of responses among the microbial kingdoms is illustrated in the present chapter by discussing the regulation of native D-xylose metabolism in three representative species utilizing the most studied D-xylose pathways: the ubiquitous bacterium *E. coli*, carrying the D-xylose isomerase pathway, the oligotrophic freshwater bacterium *C. crescentus*, carrying the Weimberg pathway and *Sc. stipitis*, a yeast most commonly found in insect guts, that carries the xylose reductase/xylitol dehydrogenase pathway. These responses towards D-xylose metabolism are compared to that observed in the non-natural utilizer, *S. cerevisiae*, with and without engineering for xylose utilization.

Sensing and response to D-xylose in natural D-xylose-utilizing species

Escherichia coli

Organization of the genes involved in D-xylose utilization

The enzymes required for D-xylose utilization, xylose isomerase and xylulokinase, are encoded in *E. coli* by the *xylAB* operon (Fig. 4.1). Located only 366 bases upstream, but oriented in the opposite direction, is the *xylFGHR* operon, encoding the xylose ABC transporter XylFGH and the transcriptional regulator XylR (Sofia et al., 1994). The gene for a second xylose transporter identified in *E. coli*, an H⁺ symporter called XylE, is located at around 91 centisomes, adjacent to genes encoding maltose transporters (Davis and Henderson, 1987).

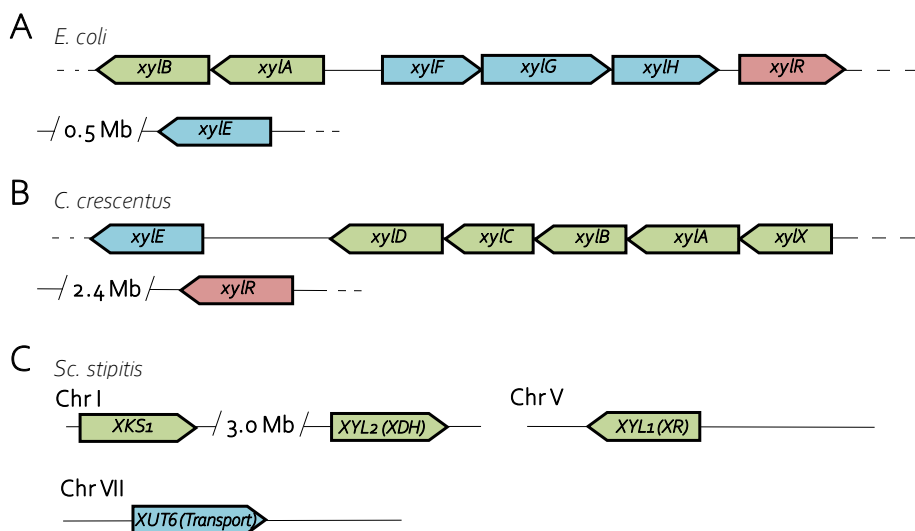


Figure 4.1. Genomic distribution of genes involved in D-xylose utilization in: A) *E. coli*; B) *C. crescentus* and C) *Sc. stipitis*. Genes encoding D-xylose transporters are indicated in blue, catalytic enzymes in green, and regulatory proteins in red.

General response to D-xylose

E. coli grows on D-xylose, both aerobically and anaerobically, but at significantly lower growth rates than on D-glucose (Gonzalez et al., 2017). Transport of D-xylose, through either the XylE antiporter or the XylFGH ABC transporter, consumes more ATP than that of D-glucose and, consequently, fewer energy equivalents are available for biomass formation. Furthermore, D-xylose consumption has been found to be associated with increased amounts of carbon dioxide at the expense of biomass, and during anaerobiosis it is associated with increased production of the electron acceptors ethanol, acetate, formate and succinate. In the central carbon metabolism, D-xylose utilization has been reported to be correlated with high fluxes through both the PPP and glycolysis, whereas the activity of the TCA cycle *versus* fermentation is determined by the aeration conditions (Gonzalez et al., 2017).

Gonzalez and colleagues (2017) further examined the cofactor fluxes via various pathways. Aerobically, D-glucose and D-xylose utilization exhibited similar cofactor fluxes, with slightly lower ATP production during growth on D-xylose; while anaerobically, D-xylose catabolism led to significantly reduced fluxes of NADH/FADH₂, NADPH and ATP, compared to growth on D-glucose. The decreased production of NADH/FADH₂ and ATP arose mainly from a reduction in glycolysis, whereas low NADPH production was caused by both a decrease in oxidative PPP flux and reduced activity of transhydrogenase that interconverts NAD(H) and NADP(H).

Comparisons of transcriptional profiles from *E. coli* under various conditions led to the identification of a set of xylose-dependent genes (Sastry et al., 2019). Specifically, the XylR regulator was found to control the expression levels of 13 genes: the *xyl* operons and genes encoding inner membrane proteins as well as proteins for D-xylose oligosaccharide transport and hydrolysis. Comparing only between carbon sources, however, revealed that D-xylose is seen as a substantially poorer sugar than D-glucose. In addition to the XylR-controlled genes, growth on D-xylose was found to lead to increased expression of genes associated with starvation response, degradation of fatty acids and amino acids and both anaerobic and aerobic respiratory chains, compared to the D-glucose condition (Sastry et al., 2019). Genes related to degradation of alternative carbon sources was further induced on glycerol, but interestingly, no additional induction of the respiratory chain was observed on this carbon source, compared to D-xylose. Furthermore, expression of genes associated with motility and biofilm formation was found to be reduced during growth on D-xylose, in comparison with both D-glucose and glycerol.

Xylose sensing

E. coli is a peritrichously flagellated bacterium and, as such, is capable of chemotaxis. In the presence of a gradient of any of its so-called chemoattractants, usually nutrient sources, *E. coli* moves towards the compound(s). *E. coli* recognizes a large number of chemoattractants, including D-galactose, D-glucose, D-fructose and D-ribose, and at least nine chemoreceptors have been identified for sugars (Adler et al., 1973). D-xylose is also an attractant, but of intermediate strength, and is sensed by the same chemoreceptor as D-galactose. The chemotactic response to D-xylose is lost if D-galactose or D-glucose is present in the environment, as the chemoreceptors appear to have a higher affinity for hexose than for pentose sugars.

The further activation of D-xylose metabolism in *E. coli* is contingent on two requirements: (i) the preferred carbon source D-glucose is not sensed; and (ii) D-xylose is sensed. The catabolite activator protein (CAP) plays a central role in the former. In many bacterial species, adenylate cyclase activity and the subsequent increase in cAMP levels signal the absence of a repressing carbon source, in contrast to, for example, *S. cerevisiae*. High levels of D-glucose inhibit the formation of cAMP and cause CAP to remain inactive. Upon D-glucose depletion, however, cAMP accumulates and binds to CAP, which can then interact with DNA, allowing for the induction of its numerous targets, such as genes involved in gluconeogenesis and the respiratory chain (Brückner and Titgemeyer, 2002; Sastry et al., 2019). However, activation of specific promoters requires additional sensing of the target metabolite. In most D-xylose-utilizing bacteria, D-xylose is sensed by a protein called XylR. Crystallization of the *E. coli* XylR has revealed similarities with the LacI-repressor family: homodimers where each subunit consists of an N-terminal ligand binding domain and a C-

teminal DNA binding domain (Ni et al., 2013). Binding of D-xylose causes conformational change in the C-terminal, enabling interaction with, and induction of, the upstream regions of the XylR target genes. The dimeric nature of XylR allows for simultaneous activation of two adjacent DNA regions, forming a DNA hairpin in between. In fact, this appears to be the case for the *xylAB* and *xylFGHR* operons that separated by only 366 bases but oriented in opposite directions (Figure 4.1A).

Caulobacter crescentus

Organization of the genes involved in D-xylose utilization

In *C. crescentus*, the genes encoding the enzymes involved in the Weimberg pathway are found in the *xylXABCD* operon (Stephens et al., 2007a). In addition, one D-xylose transporter has been identified in the bacterium, a D-xylose/H⁺ symporter encoded by *xylE*, located only five ORFs upstream of the *xylXABCD* operon. In contrast, the operon regulator, *xylR*, is found approximately 2.4 Mb downstream of the *xylXABCD* operon (Figure 4.1B).

General response to D-xylose

The sugar preference of *C. crescentus*, notably its D-xylose utilization compared to other carbon sources, was investigated in the present thesis work through cultivations in shake flasks and bioreactors on media containing varying concentrations of D-glucose, D-xylose, or the structurally related pentose sugar L-arabinose (Paper I). A clear hierarchy was observed between the sugars; D-glucose and D-xylose being assimilated faster than L-arabinose. A significant lag phase was observed before growth began with all the carbon sources and, not surprisingly for a bacterium found in nutrient-poor freshwater, higher sugar concentrations prolonged the lag phase. Growth on D-glucose and D-xylose exhibited similar trends, where 5 and 10 g L⁻¹ resulted in moderate lag phases of around 24 h, whereas at 20 g L⁻¹ the lag phase was increased to around 70 h (Figure 4.2). After growth had begun, however, the D-glucose cultures reached a final optical density of almost double that observed on D-xylose cultivations. As optical density is affected by the cell morphology, which in turn varies with nutrient source, pH and aeration, the shake flask cultures were repeated in bioreactors where biomass and extracellular metabolites were assayed. Higher variation was observed between replicates, and the difference in growth on D-glucose *versus* D-xylose media was not as apparent. However, the yield of extracellular α -ketoglutarate was substantial in the D-xylose cultures; up to 0.4 g g⁻¹ D-xylose. This indicated that the main bottleneck in D-xylose utilization in this species was not in the Weimberg pathway, but downstream, in the TCA cycle. Growth in shake flasks on L-arabinose was even poorer than that on D-xylose, with lag phases between

50 and 100 h, and optical density reaching only a fourth of that obtained on D-xylose.

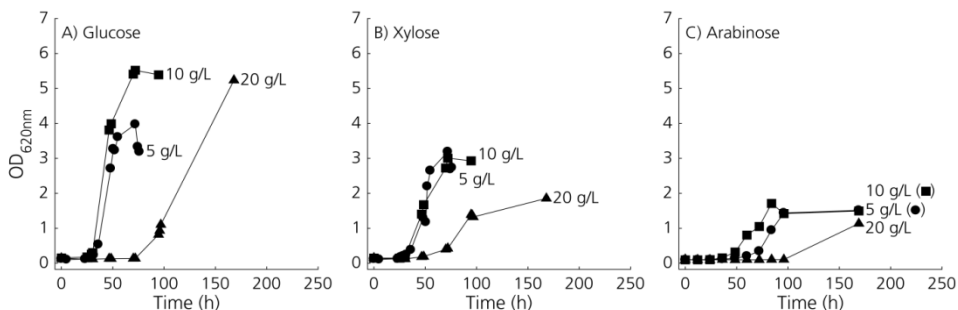


Figure 4.2. Growth, expressed as optical density (OD at 620 nm) of cultures of *C. crescentus* in defined medium supplemented with A) D-glucose, B) D-xylose or C) L-arabinose as substrate. Growth was monitored in three concentrations of substrate: 5 g L⁻¹ (circles), 10 g L⁻¹ (squares) and 20 g L⁻¹ (triangles). Adapted from Paper I.

Transcriptome analysis of *C. crescentus* grown on D-xylose in mineral medium also identified 51 genes that were upregulated compared to growth on D-glucose (Hottes et al., 2004). As expected, these included the *xylXABCD* and *xyIE* operons, but also eight genes encoding polysaccharide-degrading enzymes and secreted proteins, as well as ten genes encoding receptors and transporters. This indicates that in *C. crescentus*, the sensing of D-xylose, but not D-glucose, could signal the presence of lignocellulosic polysaccharides.

Sensing of D-xylose

C. crescentus exhibits an unusual dimorphic life cycle. Non-motile, stalked cells are anchored to surfaces in the aquatic environment, where it replicates through binary fission. The swarmer progeny has a single polar flagellum that is used to find a favorable location to put down a new stalk (Hirsch, 1986). Both chemotaxis and stalk adherence are dependent on the sensing of nutrients through partially overlapping mechanisms (Berne and Brun, 2019). D-Xylose functions as a chemoattractant, together with other sugars such as D-glucose, D-galactose and D-ribose, and amino acids such as alanine, proline and glutamine (Ely et al., 1986). Up to 18 confirmed and putative chemoreceptors have been identified within the *C. crescentus* genome; McpA and McpB appearing to be the most important for sensing of extracellular D-xylose (Berne and Brun, 2019).

Activation of the D-xylose catabolic pathway does not seem to be D-glucose repressed, as the promoter regulating the expression of the *xylXABCD* operon was found to display similar activities on D-glucose/D-xylose mixtures, as on D-xylose alone (Meisenzahl et al., 1997). This, and the fact that *C. crescentus* also utilizes both sugars quite well as carbon and energy sources (Paper I), indicates a lack of D-glucose repression on D-xylose utilization. In contrast, the utilization of lactose and D-galactose is D-glucose repressed, although this is relieved by the addition of an exogenous cell-permeable cAMP analog (Kurn et al., 1977).

The major regulator governing D-xylose utilization in *C. crescentus* appears to be XylR, which, in contrast to *E. coli*, functions as a transcriptional repressor. In the absence of D-xylose, XylR binds to the promoters of the *xyl* operons, inhibiting transcription. When D-xylose is sensed, however, XylR is released and transcription is enabled (Stephens et al., 2007b). Although the XylR mechanism resembles that of the Gram-positive *Bacillus subtilis* (Rodionov et al., 2001), neither the XylR amino acid sequences nor its DNA target motifs are homologous, showing identities of only 12 and 50 %, respectively (Nierman et al., 2001; Kunst et al., 1997; Hottes et al., 2004; Rodionov et al., 2001; Sievers and Higgins, 2018). Instead, the closest homologs of XylR are found in *Nitrospirillum* and *Sphingomonas* species, with identities of 60-80 % (Altschul et al., 1990).

Scheffersomyces stipitis

Organization of genes involved in D-xylose utilization

Eukaryotic mRNA is monocistronic, but genes associated with a specific metabolic process, such as D-galactose assimilation or the biosynthesis of antibiotics, are often located close to each other in so-called functional gene clusters (Jeffries and Van Vleet, 2009). Nevertheless, this does not seem the case in D-xylose utilization, for which the vast majority of yeasts and filamentous fungi use the enzymes xylose reductase, xylitol dehydrogenase and xylulose kinase. In species where the genomic locations of at least two of the genes are known (e.g. *Sc. stipitis*, *Sp. passalidarum*, *Kluyveromyces marxianus*, *Rhodotorula toruloides*, and *Penicillium chrysogenum*), genes are scattered across the chromosomes, as illustrated for *Sc. stipitis* in Figure 4.1C (Jeffries and Van Vleet, 2009; Wohlbach et al., 2011; Lertwattanasakul et al., 2015; Sambles et al., 2017; van den Berg et al., 2008).

General response to D-xylose

Sc. stipitis is Crabtree-negative and, as such, its metabolic regulation is primarily dependent on oxygen availability. Under fully aerobic conditions *Sc. stipitis* respire all its carbon sources, but as the oxygen level decreases, metabolism is rerouted towards fermentation (Passoth et al., 1996). Under microaerobic conditions *Sc. stipitis* grows on and ferments D-glucose and D-xylose at similar growth rates (0.23 and 0.22 h⁻¹, respectively) and with similar ethanol yields (0.40 and 0.39 g g⁻¹, respectively) (du Preez et al., 1986). While D-mannose, D-galactose and D-cellobiose are also efficiently fermented, with slightly lower ethanol yields (0.32-0.36 g g⁻¹), consumption of L-arabinose, L-rhamnose and xylitol is slow and only leads to respiration.

Optimal conditions for the fermentation of D-glucose and D-xylose are around 2 % oxygen. At this minimal aeration, *Sc. stipitis* exhibits the highest ethanolic

fermentation capacity from D-xylose among known native species, producing up to 44 g L⁻¹ ethanol (Slininger et al., 2015). However, both fermentation and cell growth stop under full anaerobicity (Shi and Jeffries, 1998). This precise oxygen requirement for efficient fermentation is the major hurdle in the industrial application of *Sc. stipitis* for ethanol production (van Brunt, 1986).

To distinguish between responses to oxygen level and those to carbon source, Jeffries and van Vleet (2009) performed transcriptomics on *Sc. stipitis* cultures with either D-glucose or D-xylose under aerobic and oxygen-limited conditions. Regardless of the carbon source, oxygen limitation was associated with an increased expression of *PDC1*, encoding the first step branching from glycolysis toward fermentation. Several genes involved in glycolysis were also induced in this condition, possibly to compensate for the reduced ATP yield achieved through fermentation. Increased expression of the XR/XDH pathway and the PPP was seen during growth on D-xylose under both aeration conditions. Only one clear D-glucose-specific induction pattern was observed; that of alcohol dehydrogenase (*Adh*). The *Sc. stipitis* genome contains at least seven *Adh* isoforms, catalyzing the formation of ethanol from acetaldehyde, among other oxidation reactions. Regardless of aeration and carbon source, *Sc. stipitis* was found to express mainly *ADH5* followed by *ADH1*, but under oxygen limitation D-xylose and D-glucose triggered strong expression of *ADH7* and *ADH4*, respectively. It is possible that differences in cofactor specificity between the *Adh* isoforms could compensate for potential redox imbalances created during D-xylose and D-glucose catabolism, which would be especially important under oxygen-limited conditions.

Sensing of D-xylose

The mechanisms behind sugar and oxygen sensing and signaling in *Sc. stipitis* are not well known. As *S. cerevisiae* contains the best studied signaling network among the yeasts, it is frequently used as the standard. Some of the important sugar-signaling proteins in *S. cerevisiae* are conserved in *Sc. stipitis*, such as Snf1p, Snf3p, Grr1p and Mig2p, while others, including Mig1p and Rgt1p, lack homologs in *Sc. stipitis* (Jeffries and Van Vleet, 2009). However, conservation of sequence does not guarantee conservation of function, as single amino acid substitutions or differences in promoter sequence can lead to significant changes in specificity or expression patterns. For example, Snf3p and Sks1p, which are involved in sensing of low D-glucose concentrations in *S. cerevisiae*, have homologs that respond to oxygen limitation in *Sc. stipitis* (Jeffries & van Vleet, 2009; Özcan et al., 1996; Yang & Bisson, 1996) (Özcan et al., 1996; Yang and Bisson, 1996; Jeffries and Van Vleet, 2009). D-Xylose utilization has been shown to be D-glucose repressed in *Sc. stipitis*, but interestingly, the repression was relieved when respiration was limited (Shi et al., 1999).

Sensing and response to D-xylose in natural and engineered *S. cerevisiae*

Response to redox imbalances are the most obvious features of D-xylose fermentation

The physiological response to D-xylose utilization in recombinant *S. cerevisiae* harboring either the XR/XDH or the XI pathway has been studied using transcriptomics, proteomics and metabolic flux analysis. As mentioned in Chapter 3, strains expressing the XR/XDH pathway display signs of redox imbalance due to the cofactor preference of XR to NADPH over NADH and the requirement of XDH for NAD⁺ over NADP⁺. This imbalance is aggravated under anaerobic conditions, where the electron transport chain cannot be utilized for the regeneration of NAD⁺ (Salusjärvi et al., 2003); this can be partially alleviated using XRs with an increased affinity for NADH (Petschacher and Nidetzky, 2008; Runquist et al., 2010a; Cadete et al., 2016) (Runquist et al., 2010; Cadete et al. 2016). Wasylenko and Stephanopoulos (2015) have suggested that, even in XI strains, a limited lower glycolytic flux leads to redox imbalance issues.

Redox imbalances are alleviated by a microorganism through respiration or byproduct formation, the latter reducing process yields and productivities of the desired product. During fermentation of D-glucose and other fermentable sugars, *S. cerevisiae* produces ethanol to regenerate the NAD⁺ consumed in the lower glycolysis. On D-xylose, apart from the accumulation of xylitol due to the lack of the NAD⁺ cofactor for XDH, these strains display increased flux through the oxidative PPP, which increases the NADPH pool, as well as changes in the expression patterns of acetaldehyde and ethanol dehydrogenases (Salusjärvi et al., 2006). For instance, *ALD6*, encoding acetaldehyde dehydrogenase with NADP⁺ specificity is induced during growth on D-xylose, while *ALD2* and *ALD3*, encoding enzymes with a preference for NAD⁺, are repressed (Karhumaa et al., 2009; Salusjärvi et al., 2006). Additionally, *ADH2*, encoding a NAD⁺-dependent cytosolic ethanol dehydrogenase, and *ALD4*, encoding a mitochondrial acetaldehyde dehydrogenase with dual cofactor specificity, display higher expression during aerobic growth on D-xylose than on D-glucose (Salusjärvi et al., 2003). It has been suggested that these two enzymes together shuttle redox equivalents between the cytosol and mitochondria through compartmentalized oxidation of ethanol to acetaldehyde and acetate (Bakker et al., 2001) (Salusjärvi et al., 2006).

Is D-xylose sensed as a carbon source by *S. cerevisiae*?

The responses to D-xylose discussed above could be described as the direct effect of sensing cofactor imbalance caused by suboptimal xylose assimilation. The currently available evidence regarding the response to the pentose sugar itself, and the question of whether recombinant *S. cerevisiae* senses D-xylose as a metabolizable carbon source or not, is ambiguous. On the one hand, some responses to D-xylose cultivations resemble indicators of starvation. For example, growth on D-xylose has been found to induce *ICL2* and *PHO84*, which are constituents of carbon scavenging and phosphate transport that are active in yeast that is starved of carbon or phosphate, respectively (Salusjärvi et al., 2006). On the other hand, D-xylose has been shown to inhibit the derepression of several D-glucose-repressible genes, even in the presence of their inducing carbon sources. For example, Fbp1p and galactokinase have been reported to be expressed and active when D-glucose-repressed cells were incubated with ethanol or galactose, respectively, but when 10 g L⁻¹ D-xylose was added this induction was no longer seen (Belinchon and Gancedo, 2003). The same pattern has been observed for invertase, which is induced by low levels of D-glucose, although higher concentrations of D-xylose were required for full repression. In addition, the adenylate energy charge (calculated as $(ATP + \frac{1}{2} ADP) / (ATP + ADP + AMP)$) remained as high on D-xylose as on D-glucose in recombinant strains growing, about 0.8 (Bergdahl et al., 2012; Wasylenko and Stephanopoulos, 2015). This indicates that the cell might be sensing carbon starvation without energy deficit, an uncommon state for a chemoheterotrophic yeast.

Mechanisms for D-xylose sensing

At least four potential, possibly co-acting, mechanisms can be foreseen to explain the effect of D-xylose on D-xylose-utilizing *S. cerevisiae*:

- (i) D-xylose is recognized as a carbon source through, at least partially, D-xylose-specific sensing pathways;
- (ii) the D-xylose molecule resembles recognizable carbon sources such as D-glucose leading to a similar, but weaker or stronger, sensing response;
- (iii) pathways for D-xylose assimilation create the same intermediates as glycolysis and gluconeogenesis (several of these intermediates are important for intracellular sensing), leading to similar intracellular signaling responses;
- (iv) D-xylose catabolism affects the levels of cofactors such as redox and energy carriers, which can be sensed as a change in cell homeostasis.

Depending on the structure of the signaling pathways, these mechanisms are expected to vary in effect, possibly explaining why clear categorization of the *S. cerevisiae* response to D-xylose has been elusive. No D-xylose-specific signaling pathway has yet been discovered in this yeast. Therefore, the three other mechanisms will be discussed in the context of the three major sugar-signaling pathways described in Chapter 2: the Snf3p/Rgt2p, SNF1/Mig1p and cAMP/PKA pathways. A summary of the observed effects of D-xylose on these pathways is shown in Figure 4.3.

The Snf3p/Rgt2p pathway senses D-xylose with low affinity

D-xylose is structurally similar to several sugars that can be metabolized by wild-type *S. cerevisiae*, for example, D-glucose and D-galactose (Figure 4.4). D-glucose and D-xylose are very similar; the only difference being a methoxy-group on the C-5 carbon. As the Snf3/Rgt2p pathway detects extracellular sugars, this similarity could lead to low-affinity signaling of D-xylose. However, Dietvorst and colleagues (2010) concluded that Snf3p was unresponsive to D-xylose, as the sugar did not cause clear Mth1p degradation in an *rgt2Δ* non-xylose-utilizing strain, as does D-glucose. The SDS-PAGE assay used was, however, only qualitative, making it difficult to detect potential partial signaling. In the present thesis work, sugar signaling routes were coupled to GFP expression from promoters induced by each route, which allowed the potential signaling response to D-xylose to be assayed quantitatively, and on a single-cell level using flow cytometry (Paper III). Most biosensors in non-xylose-utilizing strains were found to be unresponsive to the sugar, while their expected responses to D-glucose and to starvation were observed. For example, the *HXT1p*-biosensor, which is induced by high levels of D-glucose, remained repressed in the presence of D-xylose. Exceptions to this were the biosensors for *HXT2p* and *HXT4p*, which are induced by low concentrations of D-glucose through the Snf3p/Rgt2p signaling pathway. When incubated with D-xylose, two cell populations with different level of fluorescence were recorded in non-xylose-engineered strains. The population with low fluorescence maintained approximately the same fluorescence intensity as during the initial, repressed state, while the higher fluorescence population corresponded to a 4 to 6-fold induction as compared to the initial state. As a preliminary hypothesis it was speculated that the dual populations were caused by a stochastic event that allowed some cells to take up the D-xylose, and that the internalized sugar triggered the induction of the transporters. However, the dual fluorescence

populations remained when a D-xylose-specific transporter was overexpressed in the non-xylose-utilizing biosensor strains (Paper IV). It was not until an XR/XDH pathway was added that *HXT2p* and *HXT4p* exhibited a single induced population on high levels of D-xylose. The partial induction of *HXT2p* in a non-xylose-utilizing strain was also recently reported by Wu and colleagues (2020) using a qPCR assay. Furthermore, they identified Snf3p, the sensor of low D-glucose levels, as being essential for the D-xylose signal.

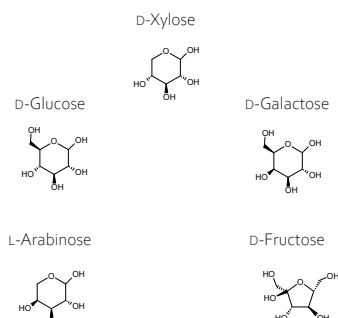


Figure 4.4. Structural comparison of common monosaccharides.

Taken together, these observations indicate that within the Snf3p/Rgt2p pathway D-xylose is mainly sensed extracellularly by Snf3p. Furthermore, it appears that high levels of D-xylose are interpreted as low levels of D-glucose, which is not unreasonable considering their structural similarities. The disappearance of the dual populations in the D-xylose-utilizing strains has not been further studied, but indicates that some intracellular signaling cannot be ruled out. It is possible that D-xylose assimilation produces metabolites that can be sensed by the *S. cerevisiae* sugar signaling network in a way that extracellular D-xylose is not able to. This mechanism will be discussed further below.

D-xylose affects the SNF1/Mig1p pathway directly and indirectly

SUC2 and its gene product invertase, which hydrolyzes extracellular sucrose into one D-glucose and one D-fructose molecule, have long been used as reporters for D-glucose repression. The expression pattern of *SUC2p* is somewhat puzzling, as only low concentrations of D-glucose (~5-0.5 g L⁻¹) induce the gene, while both high D-glucose levels and the absence of D-glucose lead to repression (Özcan et al., 1997). Hxk2p, the SNF1 complex, and at least one of Mig1/2p are required to achieve this repression (Neigeborn and Carlson, 1984; Lutfiyya and Johnston, 1996). Papers III and IV report on the behavior of a *SUC2p* biosensor on D-xylose in wild-type and D-xylose-utilizing *S. cerevisiae*, respectively. In the wild-type strain, D-xylose levels of 25-100 g L⁻¹ did not increase the expression of *SUC2p* significantly, compared to the repressive condition. However, when 5 g L⁻¹ D-glucose was added to 50 g L⁻¹ D-xylose, induction increased by 150 % compared to the condition with D-glucose only. Furthermore, when D-xylose

utilization through the XR/XDH pathway was enabled, both high and low levels of D-xylose induced *SUC2p*, while the inducing effect of the D-glucose and D-xylose mixtures was lost. As induction of *SUC2p* is a response to low D-glucose levels, it could be concluded from the studies presented in Papers III and IV that, in the case of the SNF1/Mig1p pathway, high amounts of D-xylose are interpreted by the cell as low concentrations of D-glucose. This was seen both with and without a D-xylose utilization pathway, although in slightly different ways, indicating effects of both the pentose sugar and its metabolites.

One of the ways in which D-xylose has previously been shown to affect *S. cerevisiae* is through Hxk2p, an enzyme with important functions in glycolysis and the SNF1/Mig1p sugar-signaling pathway. Again, the structural similarities between D-xylose and D-glucose come into play. Hxk2p catalyzes the first phosphorylation step of glycolysis. The reaction is carried out through interaction with D-glucose or D-fructose at the Hxk2p catalytic site, followed by a conformational change enabling the substitution of a hydroxyl group on the C-6 carbon with a phosphate group donated by ATP (Pelaez et al., 2010). It appears that D-xylose is sufficiently similar to D-glucose and D-fructose (Figure 4.4) to bind Hxk2p and induce a conformational change. However, since D-xylose does not have a C-6 carbon, it cannot be phosphorylated; instead, Hxk2p will autophosphorylate at the adjacent amino acid serine-158. This serine is crucial in stabilizing the C-6 hydroxyl group in D-glucose and D-fructose, which means that autophosphorylation renders Hxk2p irreversibly catalytically inactivated (Kuser et al. 2000; Heidrich et al., 1997).

As mentioned in Chapter 2, Hxk2p is a bifunctional protein that also has regulatory functions within the SNF1/Mig1p pathway. In the present thesis, D-xylose was shown to reduce D-glucose repression of the Hxk2p target *SUC2p* in media containing both D-glucose and D-xylose (Paper III). The specific phosphorylation of serine-158 might have an allosteric effect on the regulatory domain of Hxk2p, or the reduced repression might be related to the decrease in catalytic activity. Ma and colleagues (1989) expressed 24 different Hxk2p mutants and found that the residual D-glucose-phosphorylating activity was correlated to the degree of D-glucose repression. It was, however, not possible to determine whether the change in regulatory capacity was due to the mutations also affecting the regulatory domain of Hxk2p, or whether it was the result of reduced G6P concentration or flux.

The SNF1 complex is another main component of the SNF1/Mig1p pathway. The catalytic subunit of the complex, Snf1p, is allosterically regulated by ADP and AMP. When these nucleotides are bound, which is more likely in a low energy state, Snf1p is resistant to Glc7p and remains as active as under low-D-glucose conditions (Chandrashekarappa et al., 2011). As mentioned above, cultivation on D-xylose maintained adenylate energy charges comparable to those on D-glucose (Bergdahl et al., 2012; Wasylenko and Stephanopoulos, 2015),

which could contribute to the low D-glucose signal sensed through the SNF1/Mig1p pathway under these conditions.

Intracellular arm of the cAMP/PKA pathway senses D-xylose assimilation weakly

In the cAMP/PKA signaling pathway the sensing of D-glucose takes place both extra- and intracellularly. Rolland and colleagues (2000) showed that the extracellular sensor, Gpr1p, did not cause a spike in cAMP upon stimulation by D-xylose. This was corroborated in the present work as D-xylose did not change the expression patterns of any of the cAMP/PKA biosensors (*TPS1p*, *TPS2p* and *TEF4p*) in a wild-type background strain (Paper III). However, in strains metabolizing D-xylose through the XR/XDH pathway, 50 g L⁻¹ D-xylose induced these biosensors to a similar extent as under the inducing condition, 1 g L⁻¹ D-glucose (Paper IV). Since the intracellular arm of the cAMP/PKA pathway is known to be regulated by concentrations, rates and/or ratios of key glycolytic intermediates (Ramos et al., 1989; Peeters et al., 2017), an attractive hypothesis is that the slower assimilation of D-xylose results in glycolytic intermediates levels also found under low D-glucose conditions.

Both arms of D-glucose sensing through the cAMP/PKA pathway are dependent on binding of GTP to Ras1/2p and Gpa2p. Interestingly, the level of guanine nucleotide has been shown to be affected by the carbon source. Klimacek and colleagues (2010) demonstrated that wild-type *S. cerevisiae* grown on D-glucose accumulated intracellular GTP and GDP (3 and 0.9 µg g⁻¹ CDW, respectively), at the expense of GMP (0.1 µg g⁻¹ CDW). After a switch to 20 g L⁻¹, however, GTP and GDP rapidly decreased while GMP increased (0, 0.2 and 1.5 µg g⁻¹ CDW). Strains utilizing D-xylose through the XR/XDH pathway exhibited intermediate guanine nucleotide levels of 1.7 µg g⁻¹ CDW for GTP, 0.8-0.9 µg g⁻¹ CDW for GDP and 0.6-0.8 µg g⁻¹ CDW for GMP (Klimacek et al., 2010), indicating another possible partial explanation to high levels of D-xylose being sensed as low levels of D-glucose.

Role of intracellular metabolite levels on the difference in sensing response between D-glucose and D-xylose

Since the intracellular levels of central carbon metabolites are suspected to affect the signaling state of *S. cerevisiae* (e.g. Peeters et al., 2007; Sanz et al., 2000), the present thesis work aimed to establish connections between the extracellular concentration of D-glucose and the expression of a panel of biosensors in wild-type strains (Paper III) (Fig. 4.5A). The expression of the *HXT1p* biosensor, representing the low-affinity, high-capacity hexose transporter, increased steadily with the external D-glucose concentration, while the *SUC2p* and *TPS1p* biosensors, representing extracellular invertase and T6P synthase, respectively, displayed maximum expression at relatively low D-glucose concentrations (1 g L⁻¹) followed by repression at higher concentrations (20 g L⁻¹) (Paper III).

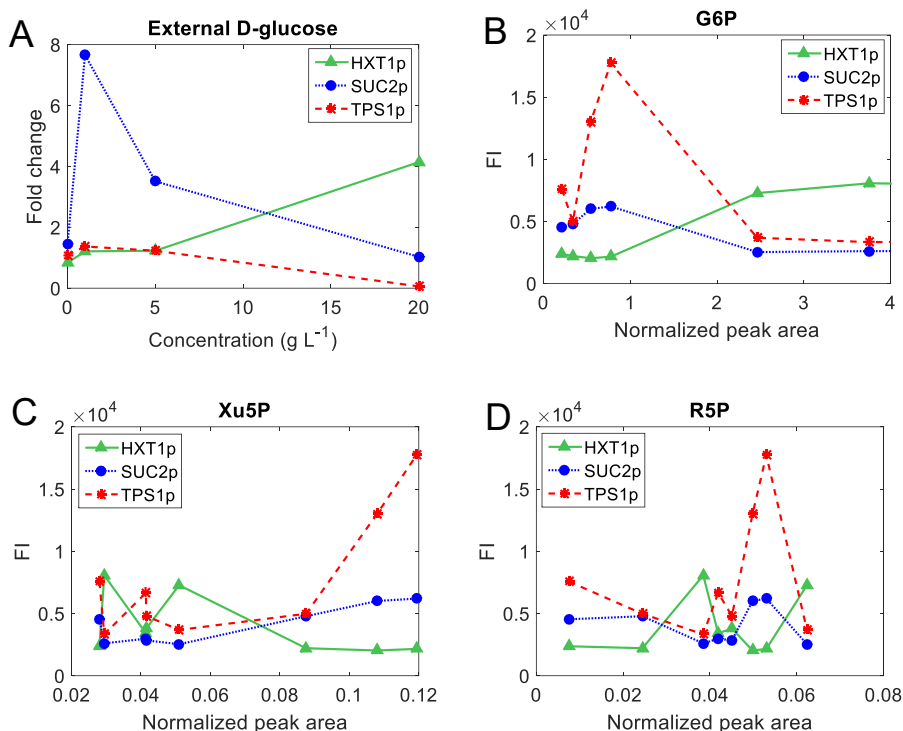


Figure 4.5. Fluorescence intensity (FI) as a function of the corresponding metabolite abundances, obtained from the background strain and deletion strains grown on D-glucose or D-xylose. The *HXT1p*, *SUC2p* and *TPS1p* are presented in green, blue and red, respectively. A) Extracellular D-glucose concentration compared to FI fold change over repressing condition (Paper III); B) Intracellular G6P zoomed in to abundances lower than 4; C) Intracellular xylulose-5-phosphate; D) Intracellular ribulose-5-phosphate (Paper V).

Correlations between intracellular metabolites and the biosensor signaling response on D-xylose were investigated and correlated to the response on D-glucose (Paper V). To achieve a wide variety of metabolite concentrations both sugars were tested in *S. cerevisiae* biosensor strains utilizing D-xylose through the XR/XDH pathway, with and without deletion of the *PGII* gene. *Pgi1p* is the only phosphoglucose isomerase present in *S. cerevisiae*, catalyzing the conversion of G6P into F6P (Figure 2.1). By varying the carbon sources, the *pgi1Δ* strain was manipulated to accumulate certain metabolites at abundances 30-70 times higher than in the background strain.

Several intracellular metabolites exhibited signaling responses similar to those observed for external D-glucose: *SUC2p* and *TPS2p* fluorescence peaks at low metabolite levels and declined at higher levels, while *HXT1p* showed a steady increase with increase metabolite abundance. These metabolites include G6P, glucose-1-phosphate, F1,6bP, trehalose-6-phosphate, 6-phosphogluconate and UDP-glucose and/or UDP-galactose (Figure 4.5B). The opposite behavior, i.e. an

increase in *SUC2p* and *TPS1p* expression with increasing metabolite abundance and a decrease in *HXT1p* expression, was observed for xylulose-5-phosphate, 3-phosphoglycerate, galactose-1-phosphate and seduheptulose-7-phosphate (Figure 4.5C). Other metabolites displayed patterns that were difficult to interpret (ribulose-5-phosphate, dihydroxyacetone phosphate, erythrose-4-phosphate and glyceraldehyde-3-phosphate).

From the observations below, it can be concluded that the low D-glucose signal recorded in D-xylose cultures for recombinant *S. cerevisiae* can, at least in part, be explained by a low flux through the assimilatory pathways. These observations underline the importance of engineering the signaling pathways in order to realize the full potential of D-xylose utilization by *S. cerevisiae*.

Engineering the sensing and signaling components in recombinant *S. cerevisiae*

Engineering of the Snf3p/Rgt2p pathway

Relatively few attempts to engineer the Snf3p/Rgt2p pathway for increased D-xylose utilization have been reported. Instead, engineering of endogenous hexose transporters for increased D-xylose affinity is seen more frequently. Examples include Hxt7p^{F79S}, Hxt36p^{N367A}, Hxt11p^{N376T} and Gal2p^{N376F}, where single amino acid substitutions have significantly increased the affinity for and/or transport rate of D-xylose (Reider Apel et al., 2016; Nijland et al., 2014; Shin et al., 2015; Farwick et al., 2014). Although Snf3p and Rgt2p only show approximately 30 % identity with most hexose transporters in *S. cerevisiae* (Sievers and Higgins, 2018), the substitutions mentioned above occur in highly conserved regions also found in the sensors. Therefore, in the eventuality that engineering an extracellular signaling pathway for D-xylose becomes desirable, these targets would make a good starting point.

Engineering of the SNF1/Mig1p pathway

Zheng and colleagues (2020) recently studied the effect of Hxk2p-mediated D-glucose repression on D-xylose fermentation. By substituting serine-15, whose phosphorylation state determines the subcellular location of Hxk2p, with an alanine that cannot be phosphorylated, the authors produced a constitutively nuclear-localized variant. Using oxygen-limited shake flask cultures, they observed increased growth, D-xylose consumption and ethanol production in the new Hxk2p^{S15A} variant of a strain utilizing D-xylose via the XI pathway, compared to the wild-type protein. Using RNA sequencing, they found that

XKS1, encoding xylulokinase, and genes encoding RNA- and DNA-binding proteins were induced in the Hxk2p^{S15A} strain, while genes involved in respiration and glycerol synthesis were repressed. Based on these findings, the Hxk2p^{S15A} variant is suggested to allow for D-xylose to be interpreted as D-glucose and thereby improving productivity on D-xylose. However, the behavior in larger-scale fermentation as well as in co-cultivation with D-glucose remains to be evaluated.

The effect of D-xylose-triggered Hxk2p autophosphorylation is of even greater relevance cultures on mixtures of D-glucose and D-xylose, as is often the case in industrially interesting substrates (Saha, 2003), where impaired D-glucose repression is compounded by reduced D-glucose phosphorylation rates. This phenomenon was studied in the present work, and an attempt was made to find a D-xylose-insensitive Hxk2p variant (Paper VI). Serine-158 is crucial for catalytic activity and cannot be substituted, therefore, a combinatorial library with substitutions outside of, but close to, the catalytic site was constructed instead. To select improved Hxk2p variants from the library it was assumed that in a strain in which all other D-glucose phosphorylating activity had been removed, a Hxk2p variant less sensitive to D-xylose-triggered autophosphorylation would enable faster growth on mixtures of D-glucose and D-xylose. The clone would therefore survive inside a chemostat when dilution rates were increased, while poorer variants would be washed away. Several clones were isolated in this way, ten of which were sequenced. The most common single substitution found was F159Y. This tyrosine residue is found in the second, non-regulatory *S. cerevisiae* hexokinase homolog, Hxk1p, as well as in the only hexokinase in the D-xylose-utilizing *Sc. stipitis*. Modelling the Hxk2p catalytic site showed that the F159Y introduced an electron-rich area close to the crucial serine-158, suggesting that rather than excluding D-xylose from the active site, this substitution would protect against autophosphorylation by repelling the ATP. To evaluate this new Hxk2p variant, a strain harboring it was grown in a chemostat on various carbon sources. On D-glucose, the catalytic activity of Hxk2p^{F158Y} equaled that of Hxk2p^{WT}, but at steady state on a mixture of D-glucose and D-xylose the new variant exhibited 64 % higher activity than the wild-type. However, other than marginally higher growth and sugar consumption rates in the D-xylose consumption phase, no significant physiological differences were observed in the new variant, indicating that the D-xylose-triggered autophosphorylation of Hxk2p is not the only mechanism regulating the response to D-xylose in mixed media.

Engineering of the cAMP/PKA pathway

Apart from D-glucose sensing, the cAMP/PKA pathway is a general stress regulator, with more global targets than the Snf3p/Rgt2p and SNF1/Mig1p pathways. The pathway has also been identified as a putative engineering target for improving D-xylose consumption. Notably, Sato and colleagues (2016) used

adaptive evolution to enable D-xylose metabolism through the XI pathway. Using reverse engineering, they identified two and four genes whose deletion enabled the yeast to assimilate D-xylose under aerobic and anaerobic conditions, respectively. These genes and the general functions of their encoded proteins are summarized in Table 4.1. One of the identified genes is directly involved in intracellular sugar signaling: *IRA2*, encoding one of two negative regulator homologs (Ira1/2p) of the cAMP/PKA pathway (Colombo et al., 2004).

Table 4.1. Summary of *S. cerevisiae* genes demonstrated to improve D-xylose consumption in strains carrying either the XI or the XR/XDH pathway, during varying levels of aerobicity. Adapted from Sato et al. (2016) and Paper VII.

Gene name	Function of protein	Deletion improves D-xylose consumption	
		XI ^a	XR/XDH ^b
<i>HOG1</i>	Osmotic stress response	A/An	A/n.d.
<i>ISU1</i>	Mitochondrial iron metabolism	A/An	A/n.d.
<i>GRE3</i>	Aldose (e.g. D-xylose) reductase	An	n.d.
<i>IRA2</i>	Negative regulator of cAMP/PKA	An	An

A: Under aerobic conditions; An: Under anaerobic conditions; n.d.: Not determined

^a As determined by Sato et al. (2016).

^b As reported in Paper VII.

Studies were carried out in the present work to determine whether the increased D-xylose consumption exhibited by the *IRA2* deletion, in combination with the other identified modifications, could be replicated in an XR/XDH background strain, and to investigate the D-xylose response in the sugar signaling pathways. The *hog1Δ*, *isu1Δ* and *ira2Δ* genotypes were recreated as single deletions or combinations thereof in D-xylose-utilizing biosensor strain backgrounds (Paper VII). *GRE3* was omitted as its role in the XI pathway is well known, and a significant effect on an XR/XDH background was not foreseen. The deletion strains created were evaluated in terms of D-xylose utilization during aerobic and anaerobic conditions, and their signaling responses to a variety of sugars were assayed.

The highest specific D-xylose consumption rates under aerobic and anaerobic conditions were exhibited by the *isu1Δ* and the *isu1Δ ira2Δ* strains. Interestingly, the combination of *ISU1* and *IRA2* deletions led to significant growth defects, both aerobically and anaerobically, but the strain was able to maintain relatively high D-xylose consumption and ethanol production rates under anaerobic conditions, resulting in specific rates that were three times higher than those of the background strain.

The deletion strains were further evaluated in terms of their signaling response to D-xylose, D-glucose and mixtures thereof. The *isu1Δ ira2Δ* strain stood out again, and it was possible to demonstrate the induction of the low-affinity transporter *HXT1p* in D-xylose-containing media for the first time. This suggested that the Snf3p/Rgt2p pathway had started to interpret D-xylose as high levels of D-glucose. However, the induction of *HXT1p* was also seen in all assayed media, including minimal media without a carbon source, indicating an acquired

constitutive activity of the Snf3p/Rgt2p pathway. A similar pattern was seen for the *TPS1p* biosensor, where constitutive repression indicated a high D-glucose signal through the cAMP/PKA pathway. *SUC2p*, on the other hand, was induced in a carbon-source-dependent manner. *SUC2p* was expressed to a higher degree in the *isu1Δ ira2Δ* strain than in the background strain, in both 50 g L⁻¹ D-xylose and 5 g L⁻¹ D-glucose, indicating that these conditions were interpreted as even lower levels of D-glucose than previously. Similar trends were seen for the *ira2Δ* single-deletion strain, while the *isu1Δ* strain displayed the opposite behavior, i.e. being repressed when the *isu1Δ ira2Δ* strain was induced, and vice versa.

It was shown that the *IRA2* and *ISU1* deletions, which increase specific D-xylose consumption and ethanol production rates under anaerobic conditions, also alter the signaling response to D-xylose, from a uniform low D-glucose signal to a high D-glucose signal for the Snf3p/Rgt2p and cAMP/PKA pathways, in combination with a low D-glucose signal for the SNF1/Mig1p pathway. In addition, the *isu1Δ ira2Δ* strain was associated with an anaerobic growth defect, the cause of which could be reduced ability to progress through the cell cycle and to react to stresses, as has previously been reported for mutants constitutively activating the cAMP/PKA pathway (Park et al., 2005).

Conclusions and outlook

Our ambitions to reduce the consumption of fossil carbon sources depends on the efficient valorization of lignocellulosic biomass into biobased counterparts. *S. cerevisiae* has previously been shown to be an outstanding work-horse and a robust production host. The yeast naturally consumes D-glucose, which is present at up to 70 % in lignocellulosic hydrolysates. Consumption of the second most common sugar, D-xylose, has been enabled but is still not optimized.

The present thesis has aimed to put forward the potential of improving D-xylose utilization in *S. cerevisiae* through engineering of the signaling response to the sugar and by expanding the palette of assimilatory pathways.

Signaling response to D-xylose

The response of *S. cerevisiae* to D-xylose was evaluating using a panel of biosensors reporting on the D-glucose signalling pathways. When applied to wild-type *S. cerevisiae* the majority of the biosensors remained unresponsive. The exception was *HXT2/4p*, encoding high affinity hexose transporters and being inducible on low D-glucose concentrations, where a subpopulation of the yeast was induced on D-xylose (**Paper III**). This indicates that D-xylose is not recognized as a carbon source to the same extent as D-glucose.

After the introduction of the XR/XDH pathway, the biosensor yeast strains exhibited a clearer response to D-xylose. The response to high concentrations of D-xylose was found to be similar to that to low levels of D-glucose (**Paper IV**). This can be interpreted as some, but not all, signaling mechanisms are activated by intracellular sensing of carbon sources.

Further studies of the signaling pathways revealed correlations between intracellular metabolites and the signaling response (**Paper V**). In particular, metabolites such as G6P and F1,6bP displayed similar concentration-response trends to extracellular D-glucose, while xylulose-5-phosphate and seduheptulose-7-phosphate showed the opposite pattern. The correlation was observed regardless of whether the carbon source was D-glucose or D-xylose, or with and without a genetic disruption in glycolysis. Interestingly, growth on D-xylose in a strain engineered to harbor the XR/XDH pathway yielded low levels of glycolytic intermediates and higher levels of metabolites within the PPP; a metabolic state clearly correlated with the low D-glucose signal reported in **Paper V**.

Engineering of the signaling response to D-xylose

A number of genetic targets improving specific D-xylose consumption and ethanol production rates in a *S. cerevisiae* strain harboring the XI pathway (Sato et al., 2016). By selecting a subset of these genes for deletion in the biosensor strains, two questions could be answered: i) Would similar improvements be achieved in an XR/XDH background, and ii) Would there be a change in the signaling state during D-xylose consumption?

Physiological evaluation of the created strains revealed increased specific D-xylose consumption and ethanol production rates, but at the expense of growth (**Paper VII**). The signaling response also showed a switch in D-xylose interpretation from mimicking low D-glucose levels to mimicking high D-glucose levels for two out of three signaling pathways. However, in the most promising *isul* Δ *ira2* Δ strain, the cAMP/PKA pathway was observed to be constitutively active, a feature correlated with lower stress tolerance, which possibly explained the reduced growth.

D-Xylose directly affects the SNF1/Mig1p pathway through action on one of its constituents, Hxk2p. This enzyme, with functions both in the first step of glycolysis and in glucose repression, becomes inactivated through interaction with the D-xylose molecule. An Hxk2p^{F158Y} variant was isolated by preparing an Hxk2p variant library and selecting for reduced D-xylose sensitivity (**Paper VI**). This variant exhibited a 64 % higher catalytic activity than the wild-type under conditions where D-xylose was inactivating the enzyme. These results indicate a promising route for engineering of sugar sensing via Hxk2p.

Assimilatory pathways

Recombinant *S. cerevisiae* was first engineered to ferment D-xylose to ethanol through the phosphorylative XR/XDH and XI pathways at the beginning of the 21st century. Twenty years later, the oxidative Dahms and Weimberg pathways have been added to the assimilatory pathways in *S. cerevisiae*.

To increase understanding of the Weimberg pathway, physiological studies of the freshwater bacterium *C. crescentus* were performed (**Paper I**). It was found that this bacterial species prefers D-glucose over D-xylose and L-arabinose, but it has a relatively low tolerance to high sugar concentrations, consistent with it being a freshwater bacterium. Enzymatic assays revealed that the Weimberg pathway was induced on both D-xylose and L-arabinose, and that both sugars could be utilized through the pathway. This indicates a common pathway for utilization of both pentoses. If this is the case, the higher growth rate on D-xylose observed compared to L-arabinose could be due to variations in either transport of the sugar, or their sensing, leading to different expression levels of the Weimberg operon.

The efficient expression of the Weimberg pathway, described in **Paper II**, utilized three genes from *C. crescentus* together with one gene from *Co. glutamicum*. A strain was created using protein engineering, adaptive laboratory evolution and gene modulation, in which 60 % the D-xylose supplied via the Weimberg pathway could be channeled into biomass and carbon dioxide. The remainder of the D-xylose accumulated as D-xylonate, an intermediate in the pathway. This first description of a functional Weimberg pathway opens up the possibility for production of dicarboxylic acids from D-xylose, by the industrially robust *S. cerevisiae*. Additionally, catalytic activities downstream of the D-xylonate node was identified as potential optimization targets.

Outlook

D-Xylose sensing in strains using phosphorylative pathways

The major difference reported between strains utilizing D-xylose through the XR/XDH and XI pathways is the more severe redox imbalance found in cultures using the XR/XDH pathway (Salusjärvi et al., 2003; Bergdahl et al., 2012). Sugar signaling is not expected to vary significantly between these two D-xylose utilization pathways, as the signals are mainly associated with extracellular D-xylose or intracellular glycolytic intermediates that are present in both pathways. This was corroborated for the cAMP/PKA pathway, where deletion mutants shown by Sato and colleagues (2016) to increase D-xylose utilization were investigated with regard to signaling activity in strains harboring the XR/XDH or XI pathway (Paper VII; Myers et al., 2019). D-xylose was interpreted as a low concentration of D-glucose in the background strain and as a high concentration of D-glucose in the *isu1Δ ira2Δ* strain. However, this strain also displayed severe growth defects (**Paper VII**), suggesting that deregulation of signaling pathways can have unwanted side effects. Instead, engineering a D-xylose-specific signaling response is proposed to increase D-xylose consumption without adverse effects on the general fitness of the yeast.

S. cerevisiae does not naturally sense extracellular D-xylose (**Paper III**). However, engineering of sugar transporters, that are homologous to several sugar sensors, for recognition of D-xylose (e.g. Farwick et al., 2014; Nijland et al., 2014; Shin et al., 2015) suggests that extracellular sensing of this pentose is attainable.

D-Xylose sensing in strains using the oxidative pathways

The Dahms and Weimberg pathways were successfully introduced into *S. cerevisiae* in 2017 and 2018, respectively (Salusjärvi et al., 2017; **Paper II**), and thus the signaling response to D-xylose in these strains has not yet been studied. However, based on existing knowledge of the signaling mechanisms and the metabolic intermediates formed, a number of hypotheses concerning the D-xylose response in strains harboring these pathways are proposed. Extracellular sensing

of D-xylose through the Snf3p/Rgt2p and cAMP/PKA pathways is expected to be similar between all recombinant D-xylose-utilizing strains. Engineering of the Snf3p, Rgt2p and Gpr1p sensors for increase affinity towards D-xylose could therefore increase consumption rates for all pathways. However, neither the Dahms nor the Weimberg pathway can theoretically produce glycolytic intermediates, and flux through these pathways is therefore unlikely to stimulate the SNF1/Mig1p and cAMP/PKA pathways in the same way as for strains harboring the XR/XDH and XI pathways. The major intermediate formed during D-xylose oxidation is D-xylonate, which is a weak acid that could potentially trigger a stress response (Wasserstrom et al., 2018). If this is the case, the *isu1Δ ira2Δ* double deletion that was shown to reduce the stress response and increase ethanol yield from D-xylose in a strain expressing the XR/XDH pathway (**Paper VII**), could present a potential target for signaling engineering of the Dahms and Weimberg pathways.

Pathway engineering should precede signal engineering

Overall, signaling engineering can be a powerful tool to increase flux through a metabolic pathway. It should, however, not be the first tool used. Reduction of potentially toxic intermediates and an established flux through the pathway are required before the signaling response to the pathway can be reliably mapped and engineered. When the signaling network is understood, it can be exploited to produce hypotheses for further pathway engineering.

Capitalizing on biodiversity can aid pathway and signaling engineering

Pathway engineering has, and assumably will continue to require exploration of the biodiversity nature has to offer. The present thesis has cited numerous studies where genes from organisms as diverse as *Sc. stipitis*, *C. crescentus*, *E. coli*, *Sp. passalidarum*, *Co. glutamicum*, *Piromyces* sp. E2, *Orpinomyces* spp., *T. thermophiles* and *L. phytofermentans* have been recruited, with varying success, in the ambition of enabling D-xylose utilization in *S. cerevisiae*. Similar cross-species exploration has, however, yet to be carried out to a comparable extent for the sensing and signaling response to D-xylose. While the D-glucose signaling network of *S. cerevisiae* is undoubtedly the best studied within microbial eukaryotes, exploration of diverse D-xylose utilizers is anticipated to be required to fully understand and effectively engineer D-xylose signaling in *S. cerevisiae*.

To those who came before.
Thank you.

Acknowledgements

To my supervisor and mentor, Marie Gorwa Grauslund: Thank you for everything. Your knowledge, wisdom and emotional strength inspire me. And, after much consideration: 318.

Thank you to my co-supervisors: Anders Sandström and Fredrik Levander. I appreciate being able to work with you and sharing your knowledge during our collaborations.

Basti Bergdahl, thank you for introducing me to the crazy world of research, and to the TMB family.

Thank you to Bärbel Hahn-Hägerdal for advice, support and interesting chats over a cup of coffee.

Peter Rådström, thank you for your unwavering support during both my struggles and my achievements. Thank you for offering compassion when I needed it most, and for providing solution when I couldn't see them myself.

Thank you to Magnus Carlquist, for many fruitful discussions within the signaling project, and for the decisive leadership during this last unpredictable time.

Lisa Wasserstrom, thank you for sharing your knowledge, your positivity in the lab and for being by travel companion to ISSY34 in Argentina.

Anette Ahlberg and Christer Larsson, thank you for administrative and technical support, no matter the time of day nor the complexity of the task.

Thank you to Gunnar Lindahl for encouragement and discussions on weekends and late nights when we were the only people at the department.

During my PhD studies I have been fortunate to work in various group compositions throughout a number of projects projects.

In the signaling project I would like to thank Marie, Karen and Daniel for intense discussions that we sometimes had to record to remember. Thank you for sharing

the moments where we confirmed hypotheses as well as the moments that gave us more questions.

In the Weimberg project, also known as XyloCut, I'm grateful to Marie, Lisa, Gunnar Lidén and Henrik Almqvist as well as Stephan Noak, Jan Marienhagen, Niklas Tenhaef, Christian Brüsseler and Bianca Klein from Forschungszentrum Jülich and Aljoscha Wahl and Jinrui Zhang from TU Delft. Thank you for the open-ended discussions during meeting, where we could both vent frustrations and celebrate successes. A special thank you Niklas, Christian and Andreas Radek for being so welcoming during my stay at Forschungszentrum Jülich. Thank you for the lunches at the Casino and the "Der Ritter Der Kokosnuß" movie night.

Thank you to Marie, Álex Mulet Indrayanti, Radhakrishnan Mahadevan and Kevin Correia within the redox project. Thank you for welcoming me during my short visit to Toronto, and thank you to Álex for daring to come over to Sweden and spending a summer with me in the lab.

I would like to thank the students I have had the chance to work with over the years. Thank you to Gonzalo Tueros, Ester Lundberg, Olivia Eliasson, Viktor Persson and Anna Heiling, for the pleasure of working alongside you, and for the opportunity to learn through teaching.

Thank you to past and present office mates: Nikoleta Zeaki, Alejandro Muñoz de las Heras, Jan Dines Knudsen, Daniel Brink, Diogo Portugal-Nunes, Sandy Chan, Maja Sidstedt, Nikhil Seshagiri Rao, Krishnan Sreenivas. Thank you for a welcoming atmosphere and many, many entertaining discussions.

The greatest thank you of all goes out to my TMB family: Alejandro Muñoz de las Heras, Anders Sandström Anette Ahlberg, Arne Hagman, Basti Bergdahl, Birgit Johansson, Birgitta Rådström, Bärbel Hahn-Hägerdal, Carl-Fredrik Klintner, Catherine J. Paul, Christer Larsson, Daniel Brink, Diogo Portugal-Nunes, Ed van Niel, Eoin Byrne, Fredrik Lund, Gunnar Lindahl, Jan Dines Knudsen, Janine Riechelmann, Javier García Hidalgo, Jenny Schelin, Johannes Hedman, Julia Södergren, Kaisa Karhumaa, Karen Ofuji Osiro, Katharina Leuhrig, Krishnan Sreenivas, Kristjan Pullerits, Linda Jansson, Lisa Wasserstrom, Maja Sidstedt, Malin Sendelius, Magnus Carlquist, Marie Baehr, Marie Gorwa-Grauslund, Nikhil Seshagiri Rao, Nikoleta Zeaki, Nina Muratovska, Nora Weber, Peter Rådström, Raquel Perruca Foncillas, Sandy Chan, Sebastian Jankowski, Sudhanshu Pawar, Tage Rosenqvist, Valeria Wallace Salinas, Violeta Sánchez i Nogué, Venkatachalam Narayan, Yasmine Akel and Yusak Budi. Wow, writing all your names down really took me down memory lane, and I hope reading them did the same for you. To me, TMB is defined by its coffee room and by us, the people who fill it. I will forever cherish both the

light-hearted and the serious conversations I've had with each of you. I am so grateful I got to share my PhD experience with you.

Thank you to my family: Dad, Mom, Samuel, Melinda, Gabriel, Helena, Emanuel, Jenny, Danny and Sophia. After all we have been through together I can honestly say that you are the strongest people I know. I am grateful to you for allowing me to use that strength to build me up.

Joakim, thank you for the support, friendship, and love. You have affected my life in immeasurable ways, and I am forever grateful for meeting you. Also, thanks for the technical support with this thesis.

To Jens, Kerstin, Malin, Maja, Olof, Tor and Alve: Thank you for being my extra family in Skåne.

Thank you to Lena Bliding, for your valuable help in keeping me sane throughout my PhD studies.

Tack till Jolin, Molly och Mio. Ni är den framtid jag kämpar för. Allt jag gör syftar till att göra er värld bättre. / Thank you to Jolin, Molly and Mio. You are the future I fight for. Everything I do is in the hopes of making your world better.

References

- Adler, J., Hazelbauer, G. L., Dahl, M. M., 1973. Chemotaxis toward sugars in *Escherichia coli*. J Bacteriol. 115, 824-47.
- Ahlem, C., Huisman, W., Neslund, G., Dahms, A. S., 1982. Purification and properties of a periplasmic D-xylose-binding protein from *Escherichia coli* K-12. J Biol Chem. 257, 2926-31.
- Altschul, S. F., Gish, W., Miller, W., Myers, E. W., Lipman, D. J., 1990. Basic local alignment search tool. J Mol Biol. 215, 403-10.
- Amore, R., Hollenberg, C. P., 1989. Xylose isomerase from *Actinoplanes missouriensis*: primary structure of the gene and the protein. Nucleic Acids Res. 17, 7515.
- Andberg, M., Aro-Karkkainen, N., Carlson, P., Oja, M., Bozonnet, S., Toivari, M., Hakulinen, N., O'Donohue, M., Penttilä, M., Koivula, A., 2016. Characterization and mutagenesis of two novel iron-sulphur cluster pentonate dehydratases. Applied microbiology and biotechnology. 100, 7549-63.
- Apweiler, E., Sameith, K., Margaritis, T., Brabers, N., van de Pasch, L., Bakker, L. V., van Leenen, D., Holstege, F. C., Kemmeren, P., 2012. Yeast glucose pathways converge on the transcriptional regulation of trehalose biosynthesis. BMC Genomics. 13, 239.
- Attfield, P. V., Bell, P. J., 2006. Use of population genetics to derive nonrecombinant *Saccharomyces cerevisiae* strains that grow using xylose as a sole carbon source. FEMS Yeast Res. 6, 862-8.
- Babbitt, P. C., Hasson, M. S., Wedekind, J. E., Palmer, D. R., Barrett, W. C., Reed, G. H., Rayment, I., Ringe, D., Kenyon, G. L., Gerlt, J. A., 1996. The enolase superfamily: a general strategy for enzyme-catalyzed abstraction of the alpha-protons of carboxylic acids. Biochemistry. 35, 16489-501.
- Bakker, B. M., Overkamp, K. M., van Maris, A. J., Kotter, P., Luttik, M. A., van Dijken, J. P., Pronk, J. T., 2001. Stoichiometry and compartmentation of NADH metabolism in *Saccharomyces cerevisiae*. FEMS Microbiol Rev. 25, 15-37.
- Beck-Sague, C., Jarvis, W. R., 1993. Secular trends in the epidemiology of nosocomial fungal infections in the United States, 1980-1990. National Nosocomial Infections Surveillance System. J Infect Dis. 167, 1247-51.
- Belinchon, M. M., Gancedo, J. M., 2003. Xylose and some non-sugar carbon sources cause catabolite repression in *Saccharomyces cerevisiae*. Arch Microbiol. 180, 293-7.

- Belinchon, M. M., Gancedo, J. M., 2007. Glucose controls multiple processes in *Saccharomyces cerevisiae* through diverse combinations of signaling pathways. *FEMS Yeast Res.* 7, 808-18.
- Bengtsson, O., Hahn-Hägerdal, B., Gorwa-Grauslund, M. F., 2009. Xylose reductase from *Pichia stipitis* with altered coenzyme preference improves ethanolic xylose fermentation by recombinant *Saccharomyces cerevisiae*. *Biotechnol Biofuels.* 2, 9.
- Bergdahl, B., Heer, D., Sauer, U., Hahn-Hägerdal, B., van Niel, E. W., 2012. Dynamic metabolomics differentiates between carbon and energy starvation in recombinant *Saccharomyces cerevisiae* fermenting xylose. *Biotechnol Biofuels.* 5, 34.
- Berne, C., Brun, Y. V., 2019. The Two Chemotaxis Clusters in *Caulobacter crescentus* Play Different Roles in Chemotaxis and Biofilm Regulation. *J Bacteriol.* 201.
- Beullens, M., Mbonyi, K., Geerts, L., Gladines, D., Detremmerie, K., Jans, A. W., Thevelein, J. M., 1988. Studies on the mechanism of the glucose-induced cAMP signal in glycolysis and glucose repression mutants of the yeast *Saccharomyces cerevisiae*. *Eur J Biochem.* 172, 227-31.
- Bloecher, A., Tatchell, K., 1999. Defects in *Saccharomyces cerevisiae* protein phosphatase type I activate the spindle/kinetochore checkpoint. *Genes Dev.* 13, 517-22.
- Boer, H., Andberg, M., Pylkkanen, R., Maaheimo, H., Koivula, A., 2019. *In vitro* reconstitution and characterisation of the oxidative D-xylose pathway for production of organic acids and alcohols. *AMB Express.* 9, 48.
- Bos, J. L., 1989. ras oncogenes in human cancer: a review. *Cancer Res.* 49, 4682-9.
- Bos, J. L., Rehmann, H., Wittinghofer, A., 2007. GEFs and GAPs: critical elements in the control of small G proteins. *Cell.* 129, 865-77.
- Bracher, J. M., Martinez-Rodriguez, O. A., Dekker, W. J. C., Verhoeven, M. D., van Maris, A. J. A., Pronk, J. T., 2019. Reassessment of requirements for anaerobic xylose fermentation by engineered, non-evolved *Saccharomyces cerevisiae* strains. *FEMS Yeast Res.* 19.
- Brat, D., Boles, E., Wiedemann, B., 2009. Functional expression of a bacterial xylose isomerase in *Saccharomyces cerevisiae*. *Appl Environ Microbiol.* 75, 2304-11.
- Brückner, R., Titgemeyer, F., 2002. Carbon catabolite repression in bacteria: choice of the carbon source and autoregulatory limitation of sugar utilization. *Fems Microbiol Lett.* 209, 141-148.
- Brüsseler, C., Späth, A., Sokolowsky, S., Marienhagen, J., 2019. Alone at last! - Heterologous expression of a single gene is sufficient for establishing the five-step Weimberg pathway in *Corynebacterium glutamicum*. *Metab Eng Commun.* 9, e00090.
- Butnariu, M., Butu, A., 2015. Chemical composition of vegetables and their products. In: P., C., B., M., Eds.), *Handbook of Food Chemistry*. Springer, Berlin, Heidelberg, pp. 627-692.

- Cabulong, R. B., Lee, W. K., Banares, A. B., Ramos, K. R. M., Nisola, G. M., Valdehuesa, K. N. G., Chung, W. J., 2018. Engineering *Escherichia coli* for glycolic acid production from D-xylose through the Dahms pathway and glyoxylate bypass. *Appl Microbiol Biotechnol.* 102, 2179-2189.
- Cadete, R. M., de Las Heras, A. M., Sandström, A. G., Ferreira, C., Girio, F., Gorwa-Grauslund, M. F., Rosa, C. A., Fonseca, C., 2016. Exploring xylose metabolism in *Spathaspora* species: XYL1.2 from *Spathaspora passalidarum* as the key for efficient anaerobic xylose fermentation in metabolic engineered *Saccharomyces cerevisiae*. *Biotechnol Biofuels.* 9, 167.
- Castro-Díez, P., Villar-Salvador, P., Pérez-Rontomé, C., Maestro-Martínez, M., Montserrat-Martí, G., 1997. Leaf morphology and leaf chemical composition in three *Quercus* (*Fagaceae*) species along a rainfall gradient in NE Spain. *Trees.* 11, 127-134.
- Celenza, J. L., Carlson, M., 1989. Mutational analysis of the *Saccharomyces cerevisiae* Snf1 protein kinase and evidence for functional interaction with the Snf4 protein. *Mol Cell Biol.* 9, 5034-44.
- Celenza, J. L., Marshall-Carlson, L., Carlson, M., 1988. The yeast *SNF3* gene encodes a glucose transporter homologous to the mammalian protein. *Proc Natl Acad Sci U S A.* 85, 2130-4.
- Chambers, A., Packham, E. A., Graham, I. R., 1995. Control of glycolytic gene expression in the budding yeast (*Saccharomyces cerevisiae*). *Curr Genet.* 29, 1-9.
- Chandrashekarappa, D. G., McCartney, R. R., Schmidt, M. C., 2011. Subunit and domain requirements for adenylate-mediated protection of Snf1 kinase activation loop from dephosphorylation. *The Journal of biological chemistry.* 286, 44532-41.
- Colas, C., Ung, P. M., Schlessinger, A., 2016. Slc transporters: Structure, function, and drug discovery. *MedChemComm.* 7, 1069-1081.
- Colombo, S., Ma, P., Cauwenberg, L., Winderickx, J., Crauwels, M., Teunissen, A., Nauwelaers, D., de Winde, J. H., Gorwa, M. F., Colavizza, D., Thevelein, J. M., 1998. Involvement of distinct G-proteins, Gpa2 and Ras, in glucose- and intracellular acidification-induced cAMP signalling in the yeast *Saccharomyces cerevisiae*. *EMBO J.* 17, 3326-41.
- Colombo, S., Ronchetti, D., Thevelein, J. M., Winderickx, J., Martegani, E., 2004. Activation state of the Ras2 protein and glucose-induced signaling in *Saccharomyces cerevisiae*. *The Journal of biological chemistry.* 279, 46715-22.
- Crabtree, H. G., 1929. Observations on the carbohydrate metabolism of tumours. *Biochem J.* 23, 536-45.
- Cunha, J. T., Soares, P. O., Romani, A., Thevelein, J. M., Domingues, L., 2019. Xylose fermentation efficiency of industrial *Saccharomyces cerevisiae* yeast with separate or combined xylose reductase/xylitol dehydrogenase and xylose isomerase pathways. *Biotechnol Biofuels.* 12, 20.

- Dahms, A. S., 1974. 3-Deoxy-D-pentulosonic acid aldolase and its role in a new pathway of D-xylose degradation. *Biochemical and biophysical research communications*. 60, 1433-1439.
- Daran-Lapujade, P., Daran, J. M., Kötter, P., Petit, T., Piper, M. D., Pronk, J. T., 2003. Comparative genotyping of the *Saccharomyces cerevisiae* laboratory strains S288C and CEN.PK113-7D using oligonucleotide microarrays. *FEMS Yeast Res.* 4, 259-69.
- Dashko, S., Zhou, N., Compagno, C., Piskur, J., 2014. Why, when, and how did yeast evolve alcoholic fermentation? *FEMS Yeast Res.* 14, 826-32.
- Davis, E. O., Henderson, P. J., 1987. The cloning and DNA sequence of the gene *xylE* for xylose-proton symport in *Escherichia coli* K12. *J Biol Chem.* 262, 13928-32.
- de Deken, R. H., 1966. The Crabtree effect: a regulatory system in yeast. *J Gen Microbiol.* 44, 149-56.
- de la Cera, T., Herrero, P., Moreno-Herrero, F., Chaves, R. S., Moreno, F., 2002. Mediator factor Med8p interacts with the hexokinase 2: implication in the glucose signalling pathway of *Saccharomyces cerevisiae*. *J Mol Biol.* 319, 703-14.
- de Las Heras, A. M., Portugal-Nunes, D. J., Rizza, N., Sandström, A. G., Gorwa-Grauslund, M. F., 2016. Anaerobic poly-3-D-hydroxybutyrate production from xylose in recombinant *Saccharomyces cerevisiae* using a NADH-dependent acetoacetyl-CoA reductase. *Microb Cell Fact.* 15, 197.
- de Wever, V., Reiter, W., Ballarini, A., Ammerer, G., Brocard, C., 2005. A dual role for PP1 in shaping the Msn2-dependent transcriptional response to glucose starvation. *EMBO J.* 24, 4115-23.
- Deng, X. X., Ho, N. W., 1990. Xylulokinase activity in various yeasts including *Saccharomyces cerevisiae* containing the cloned xylulokinase gene. *Scientific note. Appl Biochem Biotechnol.* 24-25, 193-9.
- Diaz-Ruiz, R., Rigoulet, M., Devin, A., 2011. The Warburg and Crabtree effects: On the origin of cancer cell energy metabolism and of yeast glucose repression. *Biochim Biophys Acta.* 1807, 568-76.
- Diderich, J. A., Raamsdonk, L. M., Kruckeberg, A. L., Berden, J. A., Van Dam, K., 2001. Physiological properties of *Saccharomyces cerevisiae* from which hexokinase II has been deleted. *Appl Environ Microbiol.* 67, 1587-93.
- Dietvorst, J., Karhumaa, K., Kielland-Brandt, M. C., Brandt, A., 2010. Amino acid residues involved in ligand preference of the Snf3 transporter-like sensor in *Saccharomyces cerevisiae*. *Yeast.* 27, 131-8.
- Ding, L., Yokota, A., 2004. Proposals of *Curvibacter gracilis* gen. nov., sp. nov. and *Herbaspirillum putei* sp. nov. for bacterial strains isolated from well water and reclassification of [*Pseudomonas*] *huttiensis*, [*Pseudomonas*] *lanceolata*, [*Aquaspirillum*] *delicatum* and [*Aquaspirillum*] *autotrophicum* as *Herbaspirillum huttiense* comb. nov., *Curvibacter lanceolatus* comb. nov., *Curvibacter delicatus* comb. nov. and

- Herbaspirillum autotrophicum* comb. nov. Int J Syst Evol Microbiol. 54, 2223-2230.
- Does, A. L., Bisson, L. F., 1989. Characterization of xylose uptake in the yeasts *Pichia heedii* and *Pichia stipitis*. Appl Environ Microbiol. 55, 159-64.
- Du, J., Li, S. J., Zhao, H. M., 2010. Discovery and characterization of novel D-xylose-specific transporters from *Neurospora crassa* and *Pichia stipitis*. Mol Biosyst. 6, 2150-2156.
- du Preez, J. C., Bosch, M., Prior, B. A., 1986. The fermentation of hexose and pentose sugars by *Candida shehatae* and *Pichia stipitis*. Appl Microbiol Biot. 23, 228-233.
- Ely, B., Gerardot, C. J., Fleming, D. L., Gomes, S. L., Frederikse, P., Shapiro, L., 1986. General nonchemotactic mutants of *Caulobacter crescentus*. Genetics. 114, 717-730.
- Erickson, J. R., Johnston, M., 1993. Genetic and molecular characterization of GAL83: its interaction and similarities with other genes involved in glucose repression in *Saccharomyces cerevisiae*. Genetics. 135, 655-64.
- Eurostat, Energy, transport and environment statistics. European Union, 2020.
- Farwick, A., Bruder, S., Schadeweg, V., Oreb, M., Boles, E., 2014. Engineering of yeast hexose transporters to transport D-xylose without inhibition by D-glucose. Proc Natl Acad Sci U S A. 111, 5159-64.
- Fernandez-Garcia, P., Pelaez, R., Herrero, P., Moreno, F., 2012. Phosphorylation of yeast hexokinase 2 regulates its nucleocytoplasmic shuttling. The Journal of biological chemistry. 287, 42151-64.
- Ford, G., Ellis, E. M., 2001. Three aldo-keto reductases of the yeast *Saccharomyces cerevisiae*. Chem Biol Interact. 130-132, 685-98.
- Francois, J., Van Schaftingen, E., Hers, H. G., 1984. The mechanism by which glucose increases fructose 2,6-bisphosphate concentration in *Saccharomyces cerevisiae*. A cyclic-AMP-dependent activation of phosphofructokinase 2. Eur J Biochem. 145, 187-93.
- Gancedo, J. M., Mazon, M. J., Gancedo, C., 1983. Fructose 2,6-bisphosphate activates the cAMP-dependent phosphorylation of yeast fructose-1,6-bisphosphatase in vitro. J Biol Chem. 258, 5998-9.
- Gasch, A. P., Spellman, P. T., Kao, C. M., Carmel-Harel, O., Eisen, M. B., Storz, G., Botstein, D., Brown, P. O., 2000. Genomic expression programs in the response of yeast cells to environmental changes. Mol Biol Cell. 11, 4241-57.
- Gonzalez, J. E., Long, C. P., Antoniewicz, M. R., 2017. Comprehensive analysis of glucose and xylose metabolism in *Escherichia coli* under aerobic and anaerobic conditions by (13)C metabolic flux analysis. Metab Eng. 39, 9-18.
- Guo, W., Sheng, J., Zhao, H., Feng, X., 2016. Metabolic engineering of *Saccharomyces cerevisiae* to produce 1-hexadecanol from xylose. Microb Cell Fact. 15, 24.
- Görner, W., Durchschlag, E., Wolf, J., Brown, E. L., Ammerer, G., Ruis, H., Schuller, C., 2002. Acute glucose starvation activates the nuclear

- localization signal of a stress-specific yeast transcription factor. *EMBO J.* 21, 135-44.
- Harashima, T., Heitman, J., 2002. The G-alpha protein Gpa2 controls yeast differentiation by interacting with kelch repeat proteins that mimic G-beta subunits. *Mol Cell.* 10, 163-73.
- Harcus, D., Dignard, D., Lepine, G., Askew, C., Raymond, M., Whiteway, M., Wu, C., 2013. Comparative xylose metabolism among the ascomycetes *C. albicans*, *S. stipitis* and *S. cerevisiae*. *PLoS One.* 8, e80733.
- Hartley, A. D., Ward, M. P., Garrett, S., 1994. The Yak1 protein kinase of *Saccharomyces cerevisiae* moderates thermotolerance and inhibits growth by an Sch9 protein kinase-independent mechanism. *Genetics.* 136, 465-74.
- Hedbacker, K., Carlson, M., 2008. SNF1/AMPK pathways in yeast. *Front Biosci.* 13, 2408-20.
- Hirsch, P., 1986. Microbial life at extremely low nutrient levels. *Adv Space Res.* 6, 287-98.
- Hixson, C. S., Krebs, E. G., 1980. Characterization of a cyclic AMP-binding protein from bakers' yeast. Identification as a regulatory subunit of cyclic AMP-dependent protein kinase. *J Biol Chem.* 255, 2137-45.
- Hobbs, G. A., Der, C. J., Rossman, K. L., 2016. RAS isoforms and mutations in cancer at a glance. *J Cell Sci.* 129, 1287-92.
- Hong, S. P., Leiper, F. C., Woods, A., Carling, D., Carlson, M., 2003. Activation of yeast Snf1 and mammalian AMP-activated protein kinase by upstream kinases. *Proc Natl Acad Sci U S A.* 100, 8839-43.
- Hottes, A. K., Meewan, M., Yang, D., Arana, N., Romero, P., McAdams, H. H., Stephens, C., 2004. Transcriptional profiling of *Caulobacter crescentus* during growth on complex and minimal media. *J Bacteriol.* 186, 1448-61.
- Hou, X., 2012. Anaerobic xylose fermentation by *Spathaspora passalidarum*. *Appl Microbiol Biotechnol.* 94, 205-14.
- Hsiung, Y. G., Chang, H. C., Pellequer, J. L., La Valle, R., Lanker, S., Wittenberg, C., 2001. F-box protein Grr1 interacts with phosphorylated targets via the cationic surface of its leucine-rich repeat. *Mol Cell Biol.* 21, 2506-20.
- Hummel, M., Leppikallio, M., Heikkinen, S., Niemelä, K., Sixta, H., 2010. Acidity and lactonization of xylonic acid: A nuclear magnetic resonance study. *J Carbohydr Chem.* 29, 416-428.
- Jeckelmann, J. M., Erni, B., 2020. Transporters of glucose and other carbohydrates in bacteria. *Pflugers Arch.* 472, 1129-1153.
- Jeffries, T. W., Van Vleet, J. R. H., 2009. *Pichia stipitis* genomics, transcriptomics, and gene clusters. *Fems Yeast Research.* 9, 793-807.
- Jiang, R., Carlson, M., 1996. Glucose regulates protein interactions within the yeast SNF1 protein kinase complex. *Genes & Development.* 10, 3105-3115.

- Johnsen, U., Dambeck, M., Zaiss, H., Fuhrer, T., Soppa, J., Sauer, U., Schönheit, P., 2009. D-xylose degradation pathway in the halophilic archaeon *Haloferax volcanii*. The Journal of biological chemistry. 284, 27290-303.
- Jönsson, L. J., Martín, C., 2016. Pretreatment of lignocellulose: Formation of inhibitory by-products and strategies for minimizing their effects. Bioresource Technology. 199, 103-112.
- Kaniak, A., Xue, Z., Macool, D., Kim, J. H., Johnston, M., 2004. Regulatory network connecting two glucose signal transduction pathways in *Saccharomyces cerevisiae*. Eukaryot Cell. 3, 221-31.
- Karhumaa, K., Garcia Sanchez, R., Hahn-Hägerdal, B., Gorwa-Grauslund, M. F., 2007. Comparison of the xylose reductase-xylitol dehydrogenase and the xylose isomerase pathways for xylose fermentation by recombinant *Saccharomyces cerevisiae*. Microb Cell Fact. 6, 5.
- Karhumaa, K., Hahn-Hägerdal, B., Gorwa-Grauslund, M. F., 2005. Investigation of limiting metabolic steps in the utilization of xylose by recombinant *Saccharomyces cerevisiae* using metabolic engineering. Yeast. 22, 359-68.
- Karhumaa, K., Pahlman, A. K., Hahn-Hägerdal, B., Levander, F., Gorwa-Grauslund, M. F., 2009. Proteome analysis of the xylose-fermenting mutant yeast strain TMB 3400. Yeast. 26, 371-82.
- Kerstens, K., Khan-Matsubara, J., Nelen, L., de Ley, J., 1971. Purification and properties of D-gluconate dehydratase from *Achromobacter*. Antonie Van Leeuwenhoek. 37, 233-46.
- Kilian, S. G., Prior, B. A., du Preez, J. C., 1993. The kinetics and regulation of M-xylose transport in *Candida utilis*. World J Microbiol Biotechnol. 9, 357-60.
- Kilian, S. G., Vanuden, N., 1988. Transport of xylose and glucose in the xylose-fermenting yeast *Pichia stipitis*. Appl Microbiol Biot. 27, 545-548.
- Kim, J. H., Johnston, M., 2006. Two glucose-sensing pathways converge on Rgt1 to regulate expression of glucose transporter genes in *Saccharomyces cerevisiae*. J Biol Chem. 281, 26144-9.
- Kim, S., Lee, S. B., 2006. Catalytic promiscuity in dihydroxy-acid dehydratase from the thermoacidophilic archaeon *Sulfolobus solfataricus*. J Biochem. 139, 591-6.
- Kim, S. J., Seo, S. O., Jin, Y. S., Seo, J. H., 2013. Production of 2,3-butanediol by engineered *Saccharomyces cerevisiae*. Bioresource Technology. 146, 274-281.
- Kirk, T. K., 1973. The chemistry and biochemistry of decay. In: Nicholas, D. D., (Ed.), Wood deterioration and its prevention by preservative treatments. vol. 1. Syracuse University Press, Syracuse, NY, USA, pp. 149-181.
- Klimacek, M., Krahulec, S., Sauer, U., Nidetzky, B., 2010. Limitations in xylose-fermenting *Saccharomyces cerevisiae*, made evident through comprehensive metabolite profiling and thermodynamic analysis. Appl Environ Microbiol. 76, 7566-74.

- Knoshaug, E. P., Vidgren, V., Magalhaes, F., Jarvis, E. E., Franden, M. A., Zhang, M., Singh, A., 2015. Novel transporters from *Kluyveromyces marxianus* and *Pichia guilliermondii* expressed in *Saccharomyces cerevisiae* enable growth on L-arabinose and D-xylose. *Yeast*. 32, 615-28.
- Kobayashi, N., McEntee, K., 1993. Identification of cis and trans components of a novel heat shock stress regulatory pathway in *Saccharomyces cerevisiae*. *Mol Cell Biol*. 13, 248-56.
- Kobilka, B. K., 2007. G protein coupled receptor structure and activation. *Biochim Biophys Acta*. 1768, 794-807.
- Kohler, K. A., Blank, L. M., Frick, O., Schmid, A., 2015. D-Xylose assimilation via the Weimberg pathway by solvent-tolerant *Pseudomonas taiwanensis* VLB120. *Environ Microbiol*. 17, 156-70.
- Kraakman, L., Lemaire, K., Ma, P., Teunissen, A. W., Donaton, M. C., Van Dijk, P., Winderickx, J., de Winde, J. H., Thevelein, J. M., 1999. A *Saccharomyces cerevisiae* G-protein coupled receptor, Gpr1, is specifically required for glucose activation of the cAMP pathway during the transition to growth on glucose. *Mol Microbiol*. 32, 1002-12.
- Krahulec, S., Petschacher, B., Wallner, M., Longus, K., Klimacek, M., Nidetzky, B., 2010. Fermentation of mixed glucose-xylose substrates by engineered strains of *Saccharomyces cerevisiae*: role of the coenzyme specificity of xylose reductase, and effect of glucose on xylose utilization. *Microb Cell Fact*. 9, 16.
- Kuhn, A., van Zyl, C., van Tonder, A., Prior, B. A., 1995. Purification and partial characterization of an aldo-keto reductase from *Saccharomyces cerevisiae*. *Appl Environ Microbiol*. 61, 1580-5.
- Kunst, F., Ogasawara, N., Moszer, I., Albertini, A. M., Alloni, G., Azevedo, V., Bertero, M. G., Bessieres, P., Bolotin, A., Borchert, S., Borriss, R., Boursier, L., Brans, A., Braun, M., Brignell, S. C., Bron, S., Brouillet, S., Bruschi, C. V., Caldwell, B., Capuano, V., Carter, N. M., Choi, S. K., Cordani, J. J., Connerton, I. F., Cummings, N. J., Daniel, R. A., Denziot, F., Devine, K. M., Dusterhoft, A., Ehrlich, S. D., Emmerson, P. T., Entian, K. D., Errington, J., Fabret, C., Ferrari, E., Foulger, D., Fritz, C., Fujita, M., Fujita, Y., Fuma, S., Galizzi, A., Galleron, N., Ghim, S. Y., Glaser, P., Goffeau, A., Golightly, E. J., Grandi, G., Guiseppi, G., Guy, B. J., Haga, K., Haiech, J., Harwood, C. R., Henaut, A., Hilbert, H., Holsappel, S., Hosono, S., Hullo, M. F., Itaya, M., Jones, L., Joris, B., Karamata, D., Kasahara, Y., Klaerr-Blanchard, M., Klein, C., Kobayashi, Y., Koetter, P., Koningstein, G., Krogh, S., Kumano, M., Kurita, K., Lapidus, A., Lardinois, S., Lauber, J., Lazarevic, V., Lee, S. M., Levine, A., Liu, H., Masuda, S., Mauel, C., Medigue, C., Medina, N., Mellado, R. P., Mizuno, M., Moestl, D., Nakai, S., Noback, M., Noone, D., O'Reilly, M., Ogawa, K., Ogiwara, A., Oudega, B., Park, S. H., Parro, V., Pohl, T. M., Portelle, D., Porwollik, S., Prescott, A. M., Presecan, E., Pujic, P., Purnelle, B., Rapoport, G., Rey, M., Reynolds, S., Rieger, M.,

- Rivolta, C., Rocha, E., Roche, B., Rose, M., Sadaie, Y., Sato, T., Scanlan, E., Schleich, S., Schroeter, R., Scoffone, F., Sekiguchi, J., Sekowska, A., Seror, S. J., Serror, P., Shin, B. S., Soldo, B., Sorokin, A., Tacconi, E., Takagi, T., Takahashi, H., Takemaru, K., Takeuchi, M., Tamakoshi, A., Tanaka, T., Terpstra, P., Togoni, A., Tosato, V., Uchiyama, S., Vandebol, M., Vannier, F., Vassarotti, A., Viari, A., Wambutt, R., Wedler, H., Weitzenegger, T., Winters, P., Wipat, A., Yamamoto, H., Yamane, K., Yasumoto, K., Yata, K., Yoshida, K., Yoshikawa, H. F., Zumstein, E., Yoshikawa, H., Danchin, A., 1997. The complete genome sequence of the gram-positive bacterium *Bacillus subtilis*. *Nature*. 390, 249-56.
- Kurn, N., Shapiro, L., Agabian, N., 1977. Effect of carbon source and the role of cyclic adenosine 3',5'-monophosphate on the *Caulobacter* cell cycle. *J Bacteriol*. 131, 951-9.
- Kuyper, M., Harhangi, H. R., Stave, A. K., Winkler, A. A., Jetten, M. S., de Laat, W. T., den Ridder, J. J., Op den Camp, H. J., van Dijken, J. P., Pronk, J. T., 2003. High-level functional expression of a fungal xylose isomerase: the key to efficient ethanolic fermentation of xylose by *Saccharomyces cerevisiae*? *FEMS Yeast Res*. 4, 69-78.
- Kuyper, M., Hartog, M. M. P., Toirkens, M. J., Almering, M. J. H., Winkler, A. A., van Dijken, J. P., Pronk, J. T., 2005. Metabolic engineering of a xylose-isomerase-expressing *Saccharomyces cerevisiae* strain for rapid anaerobic xylose fermentation. *Fems Yeast Research*. 5, 399-409.
- Kötter, P., Amore, R., Hollenberg, C. P., Ciriacy, M., 1990. Isolation and characterization of the *Pichia stipitis* xylitol dehydrogenase gene, *XYL2*, and construction of a xylose-utilizing *Saccharomyces cerevisiae* transformant. *Curr Genet*. 18, 493-500.
- Latchman, D. S., 1997. Transcription factors: an overview. *Int J Biochem Cell Biol*. 29, 1305-12.
- Leandro, M. J., Goncalves, P., Spencer-Martins, I., 2006. Two glucose/xylose transporter genes from the yeast *Candida intermedia*: first molecular characterization of a yeast xylose-H⁺ symporter. *Biochem J*. 395, 543-9.
- Lee, S. M., Jellison, T., Alper, H. S., 2012. Directed evolution of xylose isomerase for improved xylose catabolism and fermentation in the yeast *Saccharomyces cerevisiae*. *Appl Environ Microb*. 78, 5708-5716.
- Legendre, B. L., 1988. Varietal differences in the chemical composition of sugarcane. In: Clarke, M. A., Godshall, M. A., Eds.), *Sugar Series*. vol. 9. Elsevier BV, Amsterdam, The Netherlands, pp. 176-185.
- Lemaire, K., van de Velde, S., van Dijk, P., Thevelein, J. M., 2004. Glucose and sucrose act as agonist and mannose as antagonist ligands of the G protein-coupled receptor Gpr1 in the yeast *Saccharomyces cerevisiae*. *Mol Cell*. 16, 293-9.
- Lertwattanasakul, N., Kosaka, T., Hosoyama, A., Suzuki, Y., Rodrussamee, N., Matsutani, M., Murata, M., Fujimoto, N., Suprayogi, Tsuchikane, K., Limtong, S., Fujita, N., Yamada, M., 2015. Genetic basis of the highly

- efficient yeast *Kluyveromyces marxianus*: complete genome sequence and transcriptome analyses. *Biotechnol Biofuels*. 8, 47.
- Lill, R., Muhlenhoff, U., 2005. Iron-sulfur-protein biogenesis in eukaryotes. *Trends Biochem Sci*. 30, 133-41.
- Liu, H., Ramos, K. R., Valdehuesa, K. N., Nisola, G. M., Lee, W. K., Chung, W. J., 2013. Biosynthesis of ethylene glycol in *Escherichia coli*. *Applied microbiology and biotechnology*. 97, 3409-17.
- Liu, Y., Xu, X., Carlson, M., 2011. Interaction of SNF1 protein kinase with its activating kinase Sak1. *Eukaryot Cell*. 10, 313-9.
- Livas, D., Almering, M. J., Daran, J. M., Pronk, J. T., Gancedo, J. M., 2011. Transcriptional responses to glucose in *Saccharomyces cerevisiae* strains lacking a functional protein kinase A. *BMC Genomics*. 12, 405.
- Lohr, D., Venkov, P., Zlatanova, J., 1995. Transcriptional regulation in the yeast *GAL* gene family: a complex genetic network. *Faseb J*. 9, 777-87.
- Lutfiyya, L. L., Iyer, V. R., DeRisi, J., DeVit, M. J., Brown, P. O., Johnston, M., 1998. Characterization of three related glucose repressors and genes they regulate in *Saccharomyces cerevisiae*. *Genetics*. 150, 1377-91.
- Lutfiyya, L. L., Johnston, M., 1996. Two zinc-finger-containing repressors are responsible for glucose repression of *SUC2* expression. *Mol Cell Biol*. 16, 4790-7.
- Lönn, A., Gardonyi, M., van Zyl, W., Hahn-Hägerdal, B., Otero, R. C., 2002. Cold adaptation of xylose isomerase from *Thermus thermophilus* through random PCR mutagenesis. Gene cloning and protein characterization. *Eur J Biochem*. 269, 157-63.
- Ma, H., Bloom, L. M., Walsh, C. T., Botstein, D., 1989. The residual enzymatic phosphorylation activity of hexokinase II mutants is correlated with glucose repression in *Saccharomyces cerevisiae*. *Mol Cell Biol*. 9, 5643-9.
- Madhavan, A., Tamalampudi, S., Ushida, K., Kanai, D., Katahira, S., Srivastava, A., Fukuda, H., Bisaria, V. S., Kondo, A., 2009. Xylose isomerase from polycentric fungus *Orpinomyces*: gene sequencing, cloning, and expression in *Saccharomyces cerevisiae* for bioconversion of xylose to ethanol. *Appl Microbiol Biotechnol*. 82, 1067-78.
- Maier, A., Volker, B., Boles, E., Fuhrmann, G. F., 2002. Characterisation of glucose transport in *Saccharomyces cerevisiae* with plasma membrane vesicles (countertransport) and intact cells (initial uptake) with single Hxt1, Hxt2, Hxt3, Hxt4, Hxt6, Hxt7 or Gal2 transporters. *FEMS Yeast Res*. 2, 539-50.
- Maldonado-Celis, M. E., Yahia, E. M., Bedoya, R., Landazuri, P., Loango, N., Aguillon, J., Restrepo, B., Guerrero Ospina, J. C., 2019. Chemical composition of mango (*Mangifera indica* L.) fruit: Nutritional and phytochemical compounds. *Front Plant Sci*. 10, 1073.
- Marchler, G., Schuller, C., Adam, G., Ruis, H., 1993. A *Saccharomyces cerevisiae* UAS element controlled by protein kinase A activates

- transcription in response to a variety of stress conditions. *EMBO J.* 12, 1997-2003.
- Mayer, F. V., Heath, R., Underwood, E., Sanders, M. J., Carmena, D., McCartney, R. R., Leiper, F. C., Xiao, B., Jing, C., Walker, P. A., Haire, L. F., Ogrodowicz, R., Martin, S. R., Schmidt, M. C., Gamblin, S. J., Carling, D., 2011. ADP regulates SNF1, the *Saccharomyces cerevisiae* homolog of AMP-activated protein kinase. *Cell Metab.* 14, 707-14.
- McGovern, P. E., Zhang, J., Tang, J., Zhang, Z., Hall, G. R., Moreau, R. A., Nunez, A., Butrym, E. D., Richards, M. P., Wang, C. S., Cheng, G., Zhao, Z., Wang, C., 2004. Fermented beverages of pre- and proto-historic China. *Proc Natl Acad Sci U S A.* 101, 17593-8.
- Meisenzahl, A. C., Shapiro, L., Jenal, U., 1997. Isolation and characterization of a xylose-dependent promoter from *Caulobacter crescentus*. *J Bacteriol.* 179, 592-600.
- Merico, A., Galafassi, S., Piskur, J., Compagno, C., 2009. The oxygen level determines the fermentation pattern in *Kluyveromyces lactis*. *FEMS Yeast Res.* 9, 749-56.
- Moes, C. J., Pretorius, I. S., van Zyl, W. H., 1996. Cloning and expression of the *Clostridium thermosulfurogenes* D-xylose isomerase gene (*xylA*) in *Saccharomyces cerevisiae*. *Biotechnol Lett.* 18, 269-274.
- Moriya, H., Johnston, M., 2004. Glucose sensing and signaling in *Saccharomyces cerevisiae* through the Rgt2 glucose sensor and casein kinase I. *Proc Natl Acad Sci U S A.* 101, 1572-7.
- Mosley, A. L., Lakshmanan, J., Aryal, B. K., Özcan, S., 2003. Glucose-mediated phosphorylation converts the transcription factor Rgt1 from a repressor to an activator. *J Biol Chem.* 278, 10322-7.
- Myers, K. S., Riley, N. M., MacGilvray, M. E., Sato, T. K., McGee, M., Heilberger, J., Coon, J. J., Gasch, A. P., 2019. Rewired cellular signaling coordinates sugar and hypoxic responses for anaerobic xylose fermentation in yeast. *PLoS Genet.* 15, e1008037.
- Naik, S. N., Goud, V. V., Rout, P. K., Dalai, A. K., 2010. Production of first and second generation biofuels: A comprehensive review. *Renew Sust Energ Rev.* 14, 578-597.
- Nayak, V., Zhao, K., Wyce, A., Schwartz, M. F., Lo, W. S., Berger, S. L., Marmorstein, R., 2006. Structure and dimerization of the kinase domain from yeast Snf1, a member of the Snf1/AMPK protein family. *Structure.* 14, 477-85.
- Neigeborn, L., Carlson, M., 1984. Genes affecting the regulation of *SUC2* gene expression by glucose repression in *Saccharomyces cerevisiae*. *Genetics.* 108, 845-58.
- Nguyen, N. H., Suh, S. O., Marshall, C. J., Blackwell, M., 2006. Morphological and ecological similarities: wood-boring beetles associated with novel xylose-fermenting yeasts, *Spathaspora passalidarum* gen. sp. nov. and *Candida jeffriesii* sp. nov. *Mycol Res.* 110, 1232-41.

- Ni, L., Tonthat, N. K., Chinnam, N., Schumacher, M. A., 2013. Structures of the *Escherichia coli* transcription activator and regulator of diauxie, XylR: an AraC DNA-binding family member with a LacI/GalR ligand-binding domain. *Nucleic Acids Res.* 41, 1998-2008.
- Nierman, W. C., Feldblyum, T. V., Laub, M. T., Paulsen, I. T., Nelson, K. E., Eisen, J. A., Heidelberg, J. F., Alley, M. R., Ohta, N., Maddock, J. R., Potocka, I., Nelson, W. C., Newton, A., Stephens, C., Phadke, N. D., Ely, B., DeBoy, R. T., Dodson, R. J., Durkin, A. S., Gwinn, M. L., Haft, D. H., Kolonay, J. F., Smit, J., Craven, M. B., Khouri, H., Shetty, J., Berry, K., Utterback, T., Tran, K., Wolf, A., Vamathevan, J., Ermolaeva, M., White, O., Salzberg, S. L., Venter, J. C., Shapiro, L., Fraser, C. M., 2001. Complete genome sequence of *Caulobacter crescentus*. *Proc Natl Acad Sci U S A.* 98, 4136-41.
- Nijland, J. G., Shin, H. Y., de Jong, R. M., de Waal, P. P., Klaassen, P., Driessen, A. J., 2014. Engineering of an endogenous hexose transporter into a specific D-xylose transporter facilitates glucose-xylose co-consumption in *Saccharomyces cerevisiae*. *Biotechnol Biofuels.* 7, 168.
- Nikawa, J., Sass, P., Wigler, M., 1987. Cloning and characterization of the low-affinity cyclic AMP phosphodiesterase gene of *Saccharomyces cerevisiae*. *Mol Cell Biol.* 7, 3629-36.
- Nobre, A., Lucas, C., Leao, C., 1999. Transport and utilization of hexoses and pentoses in the halotolerant yeast *Debaryomyces hansenii*. *Appl Environ Microbiol.* 65, 3594-8.
- Nunn, C. E., Johnsen, U., Schonheit, P., Fuhrer, T., Sauer, U., Hough, D. W., Danson, M. J., 2010. Metabolism of pentose sugars in the hyperthermophilic archaea *Sulfolobus solfataricus* and *Sulfolobus acidocaldarius*. *The Journal of biological chemistry.* 285, 33701-9.
- Nygaard, Y., Maaheimo, H., Mojzita, D., Toivari, M., Wiebe, M., Resnekov, O., Gustavo Pesce, C., Ruohonen, L., Penttilä, M., 2014. Single cell and *in vivo* analyses elucidate the effect of xylC lactonase during production of D-xylonate in *Saccharomyces cerevisiae*. *Metab Eng.* 25, 238-47.
- Okeke, B. C., Obi, S. K. C., 1994. Lignocellulose and Sugar Compositions of Some Agro-Waste Materials. *Bioresource Technology.* 47, 283-284.
- Ordiz, I., Herrero, P., Rodicio, R., Moreno, F., 1996. Glucose-induced inactivation of isocitrate lyase in *Saccharomyces cerevisiae* is mediated by the cAMP-dependent protein kinase catalytic subunits Tpk1 and Tpk2. *FEBS Lett.* 385, 43-6.
- Ortiz, C. H., Maia, J. C., Tenan, M. N., Braz-Padiao, G. R., Mattoon, J. R., Panek, A. D., 1983. Regulation of yeast trehalase by a monocyclic, cyclic AMP-dependent phosphorylation-dephosphorylation cascade system. *J Bacteriol.* 153, 644-51.
- Parachin, N. S., Bergdahl, B., van Niel, E. W. J., Gorwa-Grauslund, M. F., 2011. Kinetic modelling reveals current limitations in the production of ethanol from xylose by recombinant *Saccharomyces cerevisiae*. *Metabolic Engineering.* 13, 508-517.

- Pardo, L. A., Sanchez, L. M., Lazo, P. S., Ramos, S., 1991. *In vitro* activation of the *Saccharomyces cerevisiae* Ras/adenylate cyclase system by glucose and some of its analogues. FEBS Lett. 290, 43-8.
- Park, J. I., Grant, C. M., Dawes, I. W., 2005. The high-affinity cAMP phosphodiesterase of *Saccharomyces cerevisiae* is the major determinant of cAMP levels in stationary phase: involvement of different branches of the Ras-cyclic AMP pathway in stress responses. Biochem Biophys Res Commun. 327, 311-9.
- Passoth, V., Zimmermann, M., Klinner, U., 1996. Peculiarities of the regulation of fermentation and respiration in the crabtree-negative, xylose-fermenting yeast *Pichia stipitis*. Appl Biochem Biotechnol. 57-58, 201-12.
- Peeters, K., van Leemputte, F., Fischer, B., Bonini, B. M., Quezada, H., Tsytlonok, M., Haesen, D., Vanthienen, W., Bernardes, N., Gonzalez-Blas, C. B., Janssens, V., Tompa, P., Versees, W., Thevelein, J. M., 2017. Fructose-1,6-bisphosphate couples glycolytic flux to activation of Ras. Nat Commun. 8, 922.
- Pelaez, R., Herrero, P., Moreno, F., 2010. Functional domains of yeast hexokinase 2. Biochem J. 432, 181-90.
- Petrash, J. M., Murthy, B. S., Young, M., Morris, K., Rikimaru, L., Griest, T. A., Harter, T., 2001. Functional genomic studies of aldo-keto reductases. Chem Biol Interact. 130-132, 673-83.
- Petschacher, B., Nidetzky, B., 2008. Altering the coenzyme preference of xylose reductase to favor utilization of NADH enhances ethanol yield from xylose in a metabolically engineered strain of *Saccharomyces cerevisiae*. Microb Cell Fact. 7, 9.
- Poindexter, J. S., 1964. Biological Properties and Classification of the *Caulobacter* Group. Bacteriol Rev. 28, 231-95.
- Polish, J. A., Kim, J. H., Johnston, M., 2005. How the Rgt1 transcription factor of *Saccharomyces cerevisiae* is regulated by glucose. Genetics. 169, 583-94.
- Rahman, M. M., Andberg, M., Koivula, A., Rouvinen, J., Hakulinen, N., 2018. The crystal structure of D-xylose dehydratase reveals functional features of enzymes from the Ilv/ED dehydratase family. Sci Rep. 8, 865.
- Ramos, S., Pardo, L. A., Sanchez, L. M., Lazo, P. S., 1989. Upstream regulation of *Saccharomyces cerevisiae* adenylate cyclase. Biochem Soc Trans. 17, 976-8.
- Reider Apel, A., Ouellet, M., Szmidt-Middleton, H., Keasling, J. D., Mukhopadhyay, A., 2016. Evolved hexose transporter enhances xylose uptake and glucose/xylose co-utilization in *Saccharomyces cerevisiae*. Nature Scientific Reports. 6, 19512.
- Richard, P., Toivari, M. H., Penttilä, M., 1999. Evidence that the gene YLR070c of *Saccharomyces cerevisiae* encodes a xylitol dehydrogenase. FEBS Lett. 457, 135-8.

- Richard, P., Toivari, M. H., Penttilä, M., 2000. The role of xylulokinase in *Saccharomyces cerevisiae* xylulose catabolism. *Fems Microbiol Lett.* 190, 39-43.
- Rodionov, D. A., Mironov, A. A., Gelfand, M. S., 2001. Transcriptional regulation of pentose utilisation systems in the *Bacillus/Clostridium* group of bacteria. *Fems Microbiol Lett.* 205, 305-14.
- Rodriguez, G. M., Hussain, M. S., Gambill, L., Gao, D., Yaguchi, A., Blenner, M., 2016. Engineering xylose utilization in *Yarrowia lipolytica* by understanding its cryptic xylose pathway. *Biotechnol Biofuels.* 9, 149.
- Rolland, F., de Winde, J. H., Lemaire, K., Boles, E., Thevelein, J. M., Winderickx, J., 2000. Glucose-induced cAMP signalling in yeast requires both a G-protein coupled receptor system for extracellular glucose detection and a separable hexose kinase-dependent sensing process. *Mol Microbiol.* 38, 348-58.
- Rose, M., Albig, W., Entian, K.-D., 1991. Glucose repression in *Saccharomyces cerevisiae* is directly associated with hexose phosphorylation by hexokinases PI and PII. *European Journal of Biochemistry.* 199, 511-518.
- Runquist, D., Fonseca, C., Rådström, P., Spencer-Martins, I., Hahn-Hägerdal, B., 2009. Expression of the Gxf1 transporter from *Candida intermedia* improves fermentation performance in recombinant xylose-utilizing *Saccharomyces cerevisiae*. *Appl Microbiol Biotechnol.* 82, 123-30.
- Runquist, D., Hahn-Hägerdal, B., Bettiga, M., 2010a. Increased ethanol productivity in xylose-utilizing *Saccharomyces cerevisiae* via a randomly mutagenized xylose reductase. *Appl Environ Microbiol.* 76, 7796-802.
- Runquist, D., Hahn-Hägerdal, B., Rådström, P., 2010b. Comparison of heterologous xylose transporters in recombinant *Saccharomyces cerevisiae*. *Biotechnol Biofuels.* 3, 5.
- Ryu, S., Hipp, J., Trinh, C. T., 2016. Activating and elucidating metabolism of complex sugars in *Yarrowia lipolytica*. *Appl Environ Microbiol.* 82, 1334-1345.
- Saha, B. C., 2003. Hemicellulose bioconversion. *J Ind Microbiol Biotechnol.* 30, 279-91.
- Saloheimo, A., Rauta, J., Stasyk, O. V., Sibirny, A. A., Penttilä, M., Ruohonen, L., 2007. Xylose transport studies with xylose-utilizing *Saccharomyces cerevisiae* strains expressing heterologous and homologous permeases. *Appl Microbiol Biotechnol.* 74, 1041-52.
- Salusjärvi, L., Pitkänen, J. P., Aristidou, A., Ruohonen, L., Penttilä, M., 2006. Transcription analysis of recombinant *Saccharomyces cerevisiae* reveals novel responses to xylose. *Appl Biochem Biotechnol.* 128, 237-61.
- Salusjärvi, L., Poutanen, M., Pitkänen, J. P., Koivistoinen, H., Aristidou, A., Kalkkinen, N., Ruohonen, L., Penttilä, M., 2003. Proteome analysis of recombinant xylose-fermenting *Saccharomyces cerevisiae*. *Yeast.* 20, 295-314.

- Salusjärvi, L., Toivari, M., Vehkomäki, M. L., Koivistoinen, O., Mojzita, D., Niemela, K., Penttilä, M., Ruohonen, L., 2017. Production of ethylene glycol or glycolic acid from D-xylose in *Saccharomyces cerevisiae*. *Applied microbiology and biotechnology*. 101, 8151-8163.
- Sambles, C., Middelhaufe, S., Soanes, D., Kolak, D., Lux, T., Moore, K., Matouskova, P., Parker, D., Lee, R., Love, J., Aves, S. J., 2017. Genome sequence of the oleaginous yeast *Rhodotorula toruloides* strain CGMCC 2.1609. *Genom Data*. 13, 1-2.
- Sanders, M. J., Grondin, P. O., Hegarty, B. D., Snowden, M. A., Carling, D., 2007. Investigating the mechanism for AMP activation of the AMP-activated protein kinase cascade. *The Biochemical journal*. 403, 139-48.
- Sandström, A. G., Almqvist, H., Portugal-Nunes, D., Neves, D., Liden, G., Gorwa-Grauslund, M. F., 2014. *Saccharomyces cerevisiae*: a potential host for carboxylic acid production from lignocellulosic feedstock? *Applied microbiology and biotechnology*. 98, 7299-318.
- Sanz, P., Alms, G. R., Haystead, T. A., Carlson, M., 2000. Regulatory interactions between the Reg1-Glc7 protein phosphatase and the Snf1 protein kinase. *Mol Cell Biol*. 20, 1321-8.
- Sarthy, A. V., McConaughy, B. L., Lobo, Z., Sundström, J. A., Furlong, C. E., Hall, B. D., 1987. Expression of the *Escherichia coli* xylose isomerase gene in *Saccharomyces cerevisiae*. *Appl Environ Microbiol*. 53, 1996-2000.
- Sartori, G., Aldegheri, L., Mazzotta, G., Lanfranchi, G., Tournu, H., Brown, A. J., Carignani, G., 1999. Characterization of a new hemoprotein in the yeast *Saccharomyces cerevisiae*. *J Biol Chem*. 274, 5032-7.
- Sastry, A. V., Gao, Y., Szubin, R., Hefner, Y., Xu, S., Kim, D., Choudhary, K. S., Yang, L., King, Z. A., Pålsson, B. O., 2019. The *Escherichia coli* transcriptome mostly consists of independently regulated modules. *Nat Commun*. 10, 5536.
- Sato, T. K., Tremaine, M., Parreiras, L. S., Hebert, A. S., Myers, K. S., Higbee, A. J., Sardi, M., McIlwain, S. J., Ong, I. M., Breuer, R. J., Avanesi, R., McGee, M. A., Dickinson, Q., La Reau, A., Xie, D., Tian, M., Reed, J. L., Zhang, Y., Coon, J. J., Hittinger, C. T., Gasch, A. P., Landick, R., 2016. Directed Evolution Reveals Unexpected Epistatic Interactions That Alter Metabolic Regulation and Enable Anaerobic Xylose Use by *Saccharomyces cerevisiae*. *PLoS Genet*. 12, e1006372.
- Shashkova, S., Wollman, A. J. M., Leake, M. C., Hohmann, S., 2017. The yeast Mig1 transcriptional repressor is dephosphorylated by glucose-dependent and -independent mechanisms. *Fems Microbiol Lett*. 364.
- Shi, N. Q., Davis, B., Sherman, F., Cruz, J., Jeffries, T. W., 1999. Disruption of the cytochrome c gene in xylose-utilizing yeast *Pichia stipitis* leads to higher ethanol production. *Yeast*. 15, 1021-1030.
- Shi, N. Q., Jeffries, T. W., 1998. Anaerobic growth and improved fermentation of *Pichia stipitis* bearing a *URA1* gene from *Saccharomyces cerevisiae*. *Appl Microbiol Biotechnol*. 50, 339-45.

- Shima, F., Okada, T., Kido, M., Sen, H., Tanaka, Y., Tamada, M., Hu, C. D., Yamawaki-Kataoka, Y., Kariya, K., Kataoka, T., 2000. Association of yeast adenyl cyclase with cyclase-associated protein CAP forms a second Ras-binding site which mediates its Ras-dependent activation. *Mol Cell Biol.* 20, 26-33.
- Shin, H. Y., Nijland, J. G., de Waal, P. P., de Jong, R. M., Klaassen, P., Driessen, A. J., 2015. An engineered cryptic Hxt11 sugar transporter facilitates glucose-xylose co-consumption in *Saccharomyces cerevisiae*. *Biotechnol Biofuels.* 8, 176.
- Sievers, F., Higgins, D. G., 2018. Clustal Omega for making accurate alignments of many protein sequences. *Protein Sci.* 27, 135-145.
- Sissons, C. H., Sharrock, K. R., Daniel, R. M., Morgan, H. W., 1987. Isolation of cellulolytic anaerobic extreme thermophiles from New Zealand thermal sites. *Appl Environ Microbiol.* 53, 832-8.
- Slininger, P. J., Shea-Anders, M. A., Thompson, S. R., Dien, B. S., Kurtzman, C. P., Balan, V., da Costa Sousa, L., Uppugundla, N., Dale, B. E., Cotta, M. A., 2015. Evolved strains of *Scheffersomyces stipitis* achieving high ethanol productivity on acid- and base-pretreated biomass hydrolyzate at high solids loading. *Biotechnol Biofuels.* 8, 60.
- Smith, A., Ward, M. P., Garrett, S., 1998. Yeast PKA represses Msn2p/Msn4p-dependent gene expression to regulate growth, stress response and glycogen accumulation. *EMBO J.* 17, 3556-64.
- Smith, J. L., Fratafico, P. M., Gunther, N. W., 2007. Extraintestinal pathogenic *Escherichia coli*. *Foodborne Pathog Dis.* 4, 134-63.
- Sofia, H. J., Burland, V., Daniels, D. L., Plunkett, G., 3rd, Blattner, F. R., 1994. Analysis of the *Escherichia coli* genome. V. DNA sequence of the region from 76.0 to 81.5 minutes. *Nucleic Acids Res.* 22, 2576-86.
- Solari, C. A., Tudisca, V., Pugliesi, M., Nadra, A. D., Moreno, S., Portela, P., 2014. Regulation of PKA activity by an autophosphorylation mechanism in *Saccharomyces cerevisiae*. *The Biochemical journal.* 462, 567-79.
- Stambuk, B. U., Franden, M. A., Singh, A., Zhang, M., 2003. D-Xylose transport by *Candida succiphila* and *Kluyveromyces marxianus*. *Appl Biochem Biotechnol.* 105 -108, 255-63.
- Stephens, C., Christen, B., Fuchs, T., Sundaram, V., Watanabe, K., Jenal, U., 2007a. Genetic analysis of a novel pathway for D-xylose metabolism in *Caulobacter crescentus*. *J Bacteriol.* 189, 2181-2185.
- Stephens, C., Christen, B., Watanabe, K., Fuchs, T., Jenal, U., 2007b. Regulation of D-xylose metabolism in *Caulobacter crescentus* by a LacI-type repressor. *J Bacteriol.* 189, 8828-8834.
- Subtil, T., Boles, E., 2012. Competition between pentoses and glucose during uptake and catabolism in recombinant *Saccharomyces cerevisiae*. *Biotechnol Biofuels.* 5, 14.
- Suh, S. O., Marshall, C. J., McHugh, J. V., Blackwell, M., 2003. Wood ingestion by passalid beetles in the presence of xylose-fermenting gut yeasts. *Mol Ecol.* 12, 3137-45.

- Sun, J., Liu, S. F., Zhang, C. S., Yu, L. N., Bi, J., Zhu, F., Yang, Q. L., 2012. Chemical composition and antioxidant activities of *Broussonetia papyrifera* fruits. PLoS One. 7, e32021.
- Sutter, J. M., Johnsen, U., Schonheit, P., 2017. Characterization of a pentonolactonase involved in D-xylose and L-arabinose catabolism in the haloarchaeon *Haloferax volcanii*. Fems Microbiol Lett. 364.
- Tacer-Caba, Z., Nilufer-Erdil, D., Ai, Y., 2015. Chemical composition of cereals and their products. In: P., C., B., M., (Eds.), Handbook of Food Chemistry. Springer, Berlin, Heidelberg, pp. 301-332.
- Taylor, R., Nattrass, L., Alberts, G., Robson, P., Chudziak, C., Bauen, A., Libelli, I. M., Lotti, G., Prussi, M., Nistri, R., Chiaramonti, D., López-Contreras, A. M., Bos, H. L., Eggink, G., Springer, J., Bakker, R., Ree, R. v., From the sugar platform to biofuels and biochemicals : Final report for the european commission directorate-general energy. E4tech/ReCORD/Wageningen UR, 2015.
- Tenenbaum, D. J., 2008. Food vs. fuel: diversion of crops could cause more hunger. Environ Health Perspect. 116, A254-7.
- Thomas, C., Tampe, R., 2020. Structural and mechanistic principles of ABC transporters. Annu Rev Biochem. 89, 605-636.
- Toda, T., Cameron, S., Sass, P., Zoller, M., Scott, J. D., McMullen, B., Hurwitz, M., Krebs, E. G., Wigler, M., 1987. Cloning and characterization of *BCY1*, a locus encoding a regulatory subunit of the cyclic AMP-dependent protein kinase in *Saccharomyces cerevisiae*. Mol Cell Biol. 7, 1371-7.
- Toivari, M., Nygård, Y., Kumpula, E. P., Vehkomäki, M. L., Bencina, M., Valkonen, M., Maaheimo, H., Andberg, M., Koivula, A., Ruohonen, L., Penttilä, M., Wiebe, M. G., 2012. Metabolic engineering of *Saccharomyces cerevisiae* for bioconversion of D-xylose to D-xylonate. Metab Eng. 14, 427-36.
- Tomas-Cobos, L., Casadome, L., Mas, G., Sanz, P., Posas, F., 2004. Expression of the *HXT1* low affinity glucose transporter requires the coordinated activities of the HOG and glucose signalling pathways. J Biol Chem. 279, 22010-9.
- Treger, J. M., Schmitt, A. P., Simon, J. R., McEntee, K., 1998. Transcriptional factor mutations reveal regulatory complexities of heat shock and newly identified stress genes in *Saccharomyces cerevisiae*. J Biol Chem. 273, 26875-9.
- Träff, K., Cordero, R. O., Van Zyl, W., Hahn-Hägerdal, B., 2001. Deletion of the *GRE3* aldose reductase gene and its influence on xylose metabolism in recombinant strains of *Saccharomyces cerevisiae* expressing the *xylA* and *XKS1* genes. Appl Environ Microb. 67, 5668-5674.
- Träff, K. L., Jönsson, L. J., Hahn-Hägerdal, B., 2002. Putative xylose and arabinose reductases in *Saccharomyces cerevisiae*. Yeast. 19, 1233-41.
- UN General Assembly, 2015. Transforming our world: The 2030 agenda for sustainable development.

- van Brunt, J., 1986. Fermentation Economics. *Bio/Technology*. 4, 395-401.
- van den Berg, M. A., Albang, R., Albermann, K., Badger, J. H., Daran, J. M., Driessen, A. J., Garcia-Estrada, C., Fedorova, N. D., Harris, D. M., Heijne, W. H., Joardar, V., Kiel, J. A., Kovalchuk, A., Martin, J. F., Nierman, W. C., Nijland, J. G., Pronk, J. T., Roubos, J. A., van der Klei, I. J., van Peij, N. N., Veenhuis, M., von Dohren, H., Wagner, C., Wortman, J., Bovenberg, R. A., 2008. Genome sequencing and analysis of the filamentous fungus *Penicillium chrysogenum*. *Nat Biotechnol*. 26, 1161-8.
- van Zyl, C., Prior, B. A., Kilian, S. G., Kock, J. L., 1989. D-xylose utilization by *Saccharomyces cerevisiae*. *J Gen Microbiol*. 135, 2791-8.
- Vanhalewyn, M., Dumortier, F., Debast, G., Colombo, S., Ma, P., Winderickx, J., van Dijck, P., Thevelein, J. M., 1999. A mutation in *Saccharomyces cerevisiae* adenylate cyclase, Cyr1K1876M, specifically affects glucose- and acidification-induced cAMP signalling and not the basal cAMP level. *Mol Microbiol*. 33, 363-76.
- Vara-Ciruelos, D., Russell, F. M., Hardie, D. G., 2019. The strange case of AMPK and cancer: Dr Jekyll or Mr Hyde? *Open Biol*. 9, 190099.
- Vega, M., Riera, A., Fernandez-Cid, A., Herrero, P., Moreno, F., 2016. Hexokinase 2 is an intracellular glucose sensor of yeast cells that maintains the structure and activity of Mig1 protein repressor complex. *The Journal of biological chemistry*. 291, 7267-85.
- Verhoeven, M. D., Lee, M., Kamoen, L., van den Broek, M., Janssen, D. B., Daran, J. G., van Maris, A. J., Pronk, J. T., 2017. Mutations in PMR1 stimulate xylose isomerase activity and anaerobic growth on xylose of engineered *Saccharomyces cerevisiae* by influencing manganese homeostasis. *Sci Rep*. 7, 46155.
- Versele, M., de Winde, J. H., Thevelein, J. M., 1999. A novel regulator of G protein signalling in yeast, Rgs2, downregulates glucose-activation of the cAMP pathway through direct inhibition of Gpa2. *EMBO J*. 18, 5577-91.
- Vincent, O., Townley, R., Kuchin, S., Carlson, M., 2001. Subcellular localization of the Snf1 kinase is regulated by specific beta subunits and a novel glucose signaling mechanism. *Genes Dev*. 15, 1104-14.
- Wagner, M., Shen, L., Albersmeier, A., van der Kolk, N., Kim, S., Cha, J., Brasen, C., Kalinowski, J., Siebers, B., Albers, S. V., 2018. *Sulfolobus acidocaldarius* transports pentoses via a carbohydrate uptake transporter 2 (cut2)-type ABC transporter and metabolizes them through the aldolase-independent Weimberg pathway. *Appl Environ Microbiol*. 84.
- Walfridsson, M., Bao, X., Anderlund, M., Lilius, G., Bülow, L., Hahn-Hägerdal, B., 1996. Ethanolic fermentation of xylose with *Saccharomyces cerevisiae* harboring the *Thermus thermophilus xylA* gene, which expresses an active xylose (glucose) isomerase. *Appl Environ Microbiol*. 62, 4648-51.

- Wallace-Salinas, V., Brink, D. P., Ahren, D., Gorwa-Grauslund, M. F., 2015. Cell periphery-related proteins as major genomic targets behind the adaptive evolution of an industrial *Saccharomyces cerevisiae* strain to combined heat and hydrolysate stress. *BMC Genomics*. 16, 514.
- Warburg, O., Wind, F., Negelein, E., 1927. The metabolism of tumors in the body. *J Gen Physiol*. 8, 519-30.
- Wasserstrom, L., Portugal-Nunes, D., Almqvist, H., Sandström, A. G., Lidén, G., Gorwa-Grauslund, M. F., 2018. Exploring D-xylose oxidation in *Saccharomyces cerevisiae* through the Weimberg pathway. *AMB Express*. 8, 33.
- Wasylenko, T. M., Stephanopoulos, G., 2015. Metabolomic and (13)C-metabolic flux analysis of a xylose-consuming *Saccharomyces cerevisiae* strain expressing xylose isomerase. *Biotechnol Bioeng*. 112, 470-83.
- Watanabe, S., Fukumori, F., Nishiwaki, H., Sakurai, Y., Tajima, K., Watanabe, Y., 2019. Novel non-phosphorylative pathway of pentose metabolism from bacteria. *Scientific reports*. 9, 155.
- Watanabe, S., Kodaki, T., Makino, K., 2005. Complete reversal of coenzyme specificity of xylitol dehydrogenase and increase of thermostability by the introduction of structural zinc. *J Biol Chem*. 280, 10340-9.
- Watanabe, S., Shimada, N., Tajima, K., Kodaki, T., Makino, K., 2006. Identification and characterization of L-arabonate dehydratase, L-2-keto-3-deoxyarabonate dehydratase, and L-arabinolactonase involved in an alternative pathway of L-arabinose metabolism - Novel evolutionary insight into sugar metabolism. *Journal of Biological Chemistry*. 281, 33521-33536.
- Weierstall, T., Hollenberg, C. P., Boles, E., 1999. Cloning and characterization of three genes (*SUT1-3*) encoding glucose transporters of the yeast *Pichia stipitis*. *Mol Microbiol*. 31, 871-83.
- Weimberg, R., 1961. Pentose oxidation by *Pseudomonas fragi*. *Journal of Biological Chemistry*. 236, 629-635.
- Westholm, J. O., Nordberg, N., Muren, E., Ameer, A., Komorowski, J., Ronne, H., 2008. Combinatorial control of gene expression by the three yeast repressors Mig1, Mig2 and Mig3. *BMC Genomics*. 9, 601.
- Willey, J. M., Sherwood, L., Woolverton, C. J., 2017. *Prescott's Microbiology*. McGraw-Hill, New York, NY.
- Wilson, R. B., Tatchell, K., 1988. SRA5 encodes the low-Km cyclic AMP phosphodiesterase of *Saccharomyces cerevisiae*. *Mol Cell Biol*. 8, 505-10.
- Winder, W. W., Hardie, D. G., 1999. AMP-activated protein kinase, a metabolic master switch: possible roles in type 2 diabetes. *Am J Physiol*. 277, E1-10.
- Wohlbach, D. J., Kuo, A., Sato, T. K., Potts, K. M., Salamov, A. A., Labutti, K. M., Sun, H., Clum, A., Pangilinan, J. L., Lindquist, E. A., Lucas, S., Lapidus, A., Jin, M., Gunawan, C., Balan, V., Dale, B. E., Jeffries, T. W., Zinkel, R., Barry, K. W., Grigoriev, I. V., Gasch, A. P., 2011.

- Comparative genomics of xylose-fermenting fungi for enhanced biofuel production. *Proc Natl Acad Sci U S A.* 108, 13212-7.
- Xue, Y., Batlle, M., Hirsch, J. P., 1998. GPR1 encodes a putative G protein-coupled receptor that associates with the Gpa2p G-alpha subunit and functions in a Ras-independent pathway. *EMBO J.* 17, 1996-2007.
- Yamanaka, K., 1969. Inhibition of D-xylose isomerase by pentitols and D-lyxose. *Arch Biochem Biophys.* 131, 502-6.
- Yang, X., Jiang, R., Carlson, M., 1994. A family of proteins containing a conserved domain that mediates interaction with the yeast SNF1 protein kinase complex. *EMBO J.* 13, 5878-86.
- Yang, Z., Bisson, L. F., 1996. The SKS1 protein kinase is a multicopy suppressor of the *snf3* mutation of *Saccharomyces cerevisiae*. *Yeast.* 12, 1407-19.
- Yin, Z., Wilson, S., Hauser, N. C., Tournu, H., Hoheisel, J. D., Brown, A. J., 2003. Glucose triggers different global responses in yeast, depending on the strength of the signal, and transiently stabilizes ribosomal protein mRNAs. *Mol Microbiol.* 48, 713-24.
- Yukawa, T., Bamba, T., Guirimand, G., Matsuda, M., Hasunuma, T., Kondo, A., 2020. Optimization of 1,2,4-butanetriol production from xylose in *Saccharomyces cerevisiae* by metabolic engineering of NADH/NADPH balance. *Biotechnol Bioeng.*
- Zheng, L., Wei, S., Wu, M., Zhu, X., Bao, X., Hou, J., Liu, W., Shen, Y., 2020. Improving xylose fermentation in *Saccharomyces cerevisiae* by expressing nuclear-localized hexokinase 2. *Microorganisms.* 8.
- Zhou, Y. J., Buijs, N. A., Zhu, Z., Qin, J., Siewers, V., Nielsen, J., 2016. Production of fatty acid-derived oleochemicals and biofuels by synthetic yeast cell factories. *Nat Commun.* 7, 11709.
- Özcan, S., Dover, J., Johnston, M., 1998. Glucose sensing and signaling by two glucose receptors in the yeast *Saccharomyces cerevisiae*. *EMBO J.* 17, 2566-73.
- Özcan, S., Dover, J., Rosenwald, A. G., Wolfl, S., Johnston, M., 1996. Two glucose transporters in *Saccharomyces cerevisiae* are glucose sensors that generate a signal for induction of gene expression. *Proc Natl Acad Sci U S A.* 93, 12428-32.
- Özcan, S., Johnston, M., 1995. Three different regulatory mechanisms enable yeast hexose transporter (*HXT*) genes to be induced by different levels of glucose. *Mol Cell Biol.* 15, 1564-72.
- Özcan, S., Johnston, M., 1996. Two different repressors collaborate to restrict expression of the yeast glucose transporter genes *HXT2* and *HXT4* to low levels of glucose. *Mol Cell Biol.* 16, 5536-45.
- Özcan, S., Valli, L. G., Flick, J. S., Carlson, M., Johnston, M., 1997. Expression of the *SUC2* gene of *Saccharomyces cerevisiae* is induced by low levels of glucose. *Yeast.* 13, 127-37.

Paper I





Article

Characterization of the Weimberg Pathway in *Caulobacter crescentus*

Henrik Almqvist ^{1,*} , Sara Jonsdottir Glaser ^{1,†} , Celina Tufvegren ² , Lisa Wasserstrom ² and Gunnar Lidén ¹

¹ Department of Chemical Engineering, Lund University, P.O. Box 124, SE-221 00 Lund, Sweden; sara.jonsdottir_glaser@biotek.lu.se (S.J.G.); gunnar.liden@chemeng.lth.se (G.L.)

² Applied Microbiology, Department of Chemistry, Lund University, P.O. Box 124, SE-221 00 Lund, Sweden; celina.tufvegren@tmb.lth.se (C.T.); lisa.wasserstrom@tmb.lth.se (L.W.)

* Correspondence: henrik.almqvist@chemeng.lth.se; Tel.: +46-46-2228278

† Current address: Division of Biotechnology, Department of Chemistry, Lund University, P.O. Box 124, SE-221 00 Lund, Sweden.

Received: 7 May 2018; Accepted: 9 June 2018; Published: 12 June 2018



Abstract: *Caulobacter crescentus* is a gram-negative bacterium that can utilize xylose as a substrate using the Weimberg pathway, which converts xylose to α -ketoglutarate in five steps without carbon loss. This is an interesting pathway for heterologous expression in other organisms in order to enable xylose utilization in biorefinery processes. *C. crescentus* was grown on xylose, arabinose and glucose, and maximum specific growth rates determined for the three substrates were 0.11 h^{-1} , 0.05 h^{-1} , and 0.15 h^{-1} respectively. Growth was found to be significantly inhibited at sugar concentration of 20 g L^{-1} , shown primarily by an increased lag phase. Enzyme activity assays showed that the Weimberg pathway was active in cells grown, not only on xylose but also on arabinose. No activity was found for growth on glucose. Furthermore, substantial amounts of α -ketoglutarate—up to a yield of 0.4 g g^{-1} —was excreted during growth on xylose, but no other extracellular intermediates in the Weimberg pathway were detected during growth on xylose. Apparently, *C. crescentus* is not well adapted for efficient growth on high xylose levels, and responds by an extended lag phase and secretion of α -ketoglutarate.

Keywords: *Caulobacter crescentus*; Weimberg pathway; xylose; arabinose; physiological characterization; enzyme activity

1. Introduction

Caulobacter crescentus is an aquatic gram-negative bacterium, first described by [1] as *Caulobacter vibrioides*. The organism has been of interest for two main reasons; (a) its unusual cell cycle, and (b) its xylose degradation pathway. The cell cycle of *C. crescentus* involves two very different morphological forms, a motile swarmer cell and a non-motile stalked cell, making it a powerful model organism for studies of prokaryotic cell cycling [2–4]. The genetics of *C. crescentus* has been studied and the genome was fully sequenced by Nierman and co-workers [5]. The regulation and expression of the genes involved in replication has been reviewed by Curtis and Brun [3].

The aquatic natural environment of *C. crescentus* is nutrient poor. The ability of *C. crescentus* to utilize a wide range of substrates such as glucose, xylose, glucuronic acid, lactose, gluco-oligosaccharides and long-chain fatty acids is therefore important for its survival [6–10]. With respect to xylose metabolism, it is known that *C. crescentus* holds the Weimberg pathway [11]. The Weimberg pathway, first described in *Pseudomonas fragi* [12], is a rare pathway for xylose metabolism, found in only a handful of organisms [11]. The pathway consists of five enzymes that convert xylose to α -ketoglutarate (Figure 1).

First, xylose is reduced resulting in xylonolactone by an NAD^+ -dependent xylose dehydrogenase (XylB) and the xylonolactone is subsequently hydrolyzed to xylonate by xylonolactone lactonase (XylC) by the opening of the lactone ring. Subsequently, xylonate is dehydrated by xylonate dehydratase (XylD) into 2-keto-3-deoxy-xylonate which in turn is dehydrated by 2-keto-3-deoxy-xylonate dehydratase (XylX) to α -ketoglutarate semialdehyde. Finally, α -ketoglutarate semialdehyde is reduced to α -ketoglutarate by an NAD^+ -dependent α -ketoglutarate semialdehyde dehydrogenase (XylA). Through the Weimberg pathway xylose can be converted to α -ketoglutarate without loss of carbon, combined with a gain of 2 equivalents of NADH.

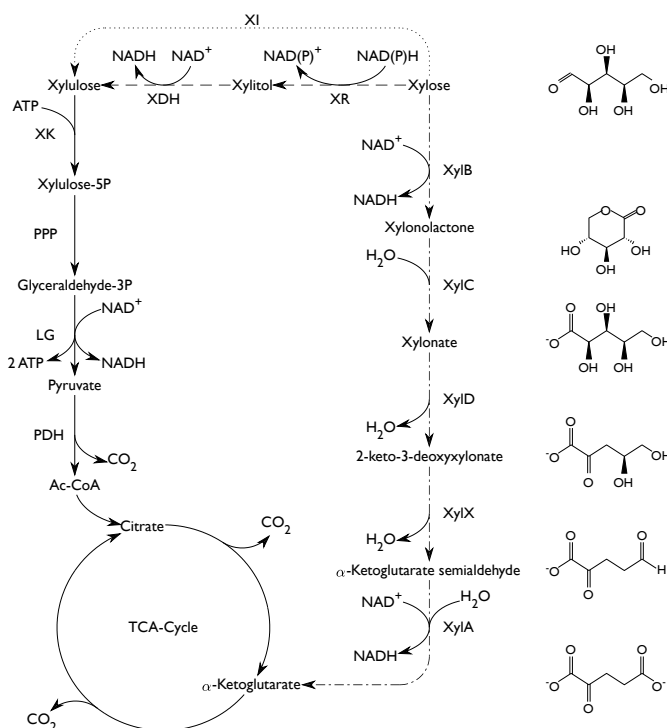


Figure 1. Schematic overview of the central carbon metabolism (solid lines) and the three xylose degradation pathways, the oxido-reductive pathway (dashed lines), the isomerase pathway (dotted lines) and the Weimberg pathway (dash-dot lines). Weimberg pathway enzymes are labeled with the gene encoding for each enzyme. Abbreviations: XR—Xylose Reductase, XDH—Xylitol Dehydrogenase, XI—Xylose Isomerase, PPP—Pentose Phosphate Pathway, LG—Lower Glycolysis, PDH—Pyruvate Dehydrogenase. Adapted from [13,14].

Xylose, a pentose sugar, is an important building block in hemicellulose, especially in hardwood and herbaceous plants where it can constitute up to 20% of the dry matter [15]. Efficient xylose utilization is thus an important goal in lignocellulose-based biorefineries. Natural xylose utilization ability is missing in several industrial host organisms, such as the yeast *Saccharomyces cerevisiae*, or the bacterium *Corynebacterium glutamicum* and heterologous pathways have to be introduced to enable xylose utilization [13,14]. Most frequently, either the oxido-reductive (xylose reductase and xylitol dehydrogenase - XR/XDH) pathway or the isomerase (XI) pathway have been used for this purpose (Figure 1). Both pathways convert xylose into xylulose, which is further metabolized in the pentose phosphate pathway (PPP), followed by conversion in the lower glycolysis to yield pyruvate.

Pyruvate is an important node, from which many products can be formed, e.g., ethanol, acetate and lactate. Since there is a net gain in ATP in the lower glycolysis these products can be formed anaerobically, but most of them result in a loss of carbon as CO₂. In aerobic processes, the carbon can instead be directed to the tricarboxylic acid cycle (TCA-cycle) to produce di- or tricarboxylic acids.

Recently, the Weimberg pathway has received significant interest from the scientific community as an alternative to the oxido-reductive and isomerase pathways, due to the fact that glycolysis is by-passed and no carbon is lost from decarboxylation. The end-product of the Weimberg pathway is α -ketoglutarate, an intermediate in the TCA-cycle, which makes the pathway an interesting option for production of carboxylic acids. The Weimberg pathway originating from *C. crescentus* has been established in *Pseudomonas putida* S12 [16] and in *Corynebacterium glutamicum* [13] enabling growth on xylose as the sole carbon source. In the study by Radek and co-workers, this was done as a step towards production of α -ketoglutarate or derivatives of α -ketoglutarate (e.g., L-glutamate) without carbon loss via the normal route through glycolysis. There have also been studies where only parts of the Weimberg pathway have been introduced, in order to produce the intermediate compound xylonate using both *Escherichia coli* [17,18] and *S. cerevisiae* [19].

The Weimberg pathway clearly represents a fundamentally different entry port of xylose in comparison to the more commonly used XR/XDH or XI pathways. However, despite the considerable interest in the heterologous expression of the Weimberg pathway, there are surprisingly few studies on the physiology of the natural host organism itself. Transcriptional profiling of *C. crescentus* grown on glucose and xylose has been reported [6] as well as protein synthesis during growth on glucose and gluco-oligosaccharides [9], but a physiological characterization of *C. crescentus* grown on xylose, glucose and arabinose is in fact lacking.

In the present study, the growth of *C. crescentus* on three different carbon source, xylose, glucose and arabinose, was assessed. Product formation and specific growth rates were determined in shake flask and bioreactor cultivations. Furthermore, the activity of the dehydrogenase enzyme, encoded by *xylB* was determined in crude cell extracts. Also, the activity of the Weimberg pathway downstream of xylonate, measured as the combined activity of the three enzymes encoded by *xylD*, *xylX* and *xylA*, was determined. These results give information on the working Weimberg pathway in a native host, and may guide metabolic engineering work for efficient heterologous expression of the Weimberg pathway from *C. crescentus* in other hosts.

2. Results

2.1. Growth in Shake Flasks

Growth characteristics of *C. crescentus* were investigated for three substrates—glucose, xylose, and arabinose each at three concentrations 5, 10, and 20 g L⁻¹ (Figure 2). The highest optical density (OD₆₂₀) was achieved on glucose followed by xylose, whereas growth on arabinose resulted in the lowest OD of the tested substrates. Using glucose as substrate, specific growth rates at 5 and 10 g L⁻¹ were similar (0.14 h⁻¹ and 0.15 h⁻¹, respectively) and as expected a higher final OD was obtained for 10 g L⁻¹. The sudden drop in OD at the end of the 5 g L⁻¹ glucose experiment was most likely due to biofilm formation and not a sudden decrease in biomass, since aggregated cells could be seen on the sides of the flask at the gas-liquid interface. At 20 g L⁻¹ the lag phase was considerably longer and the specific growth rate was lower, 0.12 h⁻¹. The culture had not reached the stationary phase when the experiment was terminated after 200 h. Slightly lower specific growth rates were found using xylose as a substrate, 0.10 h⁻¹ at 5 g L⁻¹ and 0.11 h⁻¹ at 10 g L⁻¹. At 20 g L⁻¹ the specific growth rate was markedly affected and reached only 0.05 h⁻¹. In addition, the final OD was lower at all substrate concentrations, especially at 20 g L⁻¹. Arabinose was in all aspects a poorer substrate than glucose and xylose, resulting in longer lag phase, lower growth rate, and lower final OD.

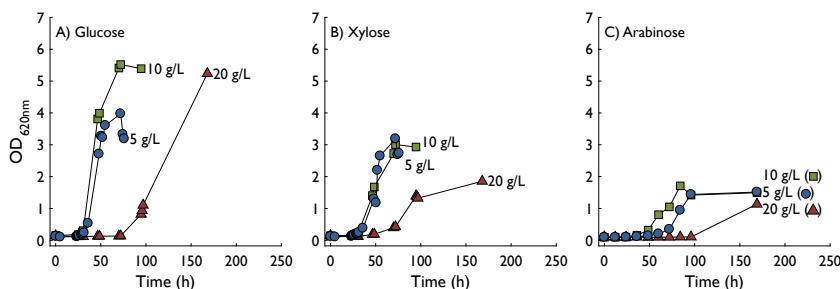


Figure 2. Optical density (620 nm) of cultures of *C. crescentus* in defined M2 medium supplemented with glucose (A), xylose (B) or arabinose (C) as substrate. Growth was monitored in three levels of substrate, 5 g L⁻¹ (circles), 10 g L⁻¹ (squares) or 20 g L⁻¹ (triangles). Data shown in this figure represents experiments performed in biological duplicates.

2.2. Enzyme Activity

Enzyme activities were assayed in crude cell extract from shake flask cultures. The activity of XylB was assessed, as well as the combined activity of XylD, XylX, and XylA, denoted as XylDXA. XylB activity was assessed by addition of xylose as a substrate and monitoring the formation of NADH. Since the assays were performed with crude cell extract, all enzymes in the Weimberg pathway are present in the reaction mixture. This means that the effect of product inhibition is reduced since the following enzymes in the pathway continuously convert the product of XylB to the final product. It also means that there might be some contribution to NADH formation by the final enzyme, XylA. Since neither XylD nor XylX activity results in any product measurable with spectroscopy, XylA activity was used to monitor the conversion of xylonate to the final product, assuming that no accumulation of intermediate metabolites occurred. As can be seen in Figure 3, all the assayed Weimberg pathway enzymes are synthesised in the presence of both xylose (Xyl) and arabinose (Ara), but not in the presence of glucose (Glu). In addition, the results show XylB activity using both xylose and arabinose as substrate, independent of which substrate the cells were grown on. The negative value for XylDXA activity in cells grown on glucose does not imply reverse activity but was rather an effect of background activity in the sample.

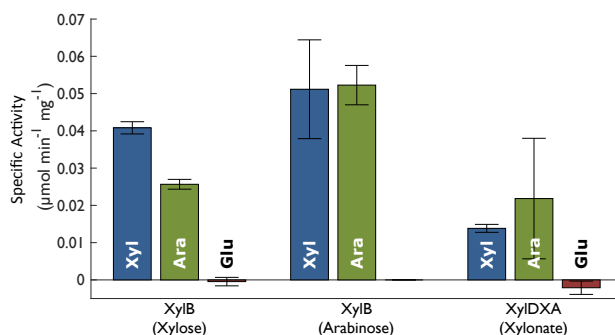


Figure 3. Enzyme activity in crude cell extract from *C. crescentus* grown on xylose (Xyl), arabinose (Ara) or glucose (Glu). Xylose dehydrogenase (XylB) was assayed with both xylose and arabinose as substrate and the compound activity of three enzymes (XylDXA), xylonate dehydratase (XylD), 2-keto-3-deoxyxylonate dehydratase (XylX) and α -ketoglutarate semialdehyde dehydrogenase (XylA). Substrates are indicated within round brackets. Error bars represent standard deviation.

2.3. Characterization in Bioreactors

Growth and product formation was studied in bioreactor experiments using either 10 g L⁻¹ glucose or xylose as substrate (Figure 4A,B). Growth was analyzed by measurement of optical density and cell dry weight. In addition, the fermentation broth was analyzed for metabolites using liquid chromatography. In the experiment with glucose as a substrate, biomass was the only product found in the medium. In contrast, α -ketoglutarate was found in the fermentation broth of the experiment with xylose. In the bioreactor experiment with glucose as a substrate the specific growth rate was 0.13–0.15 h⁻¹, which was similar to what was found in shake flask experiments at the same substrate concentration. In contrast to the shake flask, there was no lag-phase in the bioreactor. However, glucose was not depleted during the duration of the bioreactor experiment, as was the case in shake flasks, and consequently the final OD was markedly lower. The specific growth rate in the xylose bioreactor was 0.05–0.08 h⁻¹ which was lower than that in the corresponding shake flask experiment. Similarly to the glucose bioreactor, growth stopped before substrate was depleted. However, consumption of xylose did not cease and substantial amounts of α -ketoglutarate were formed at a specific production rate of 0.02–0.03 g gDW⁻¹ h⁻¹. The final α -ketoglutarate yield was 0.32–0.43 g g⁻¹. Bioreactor experiments were also carried out with 5 g L⁻¹ xylose (Figure 4C,D). After the initial lag-phase of about 36 h, xylose consumption and growth started. During the exponential growth phase, the specific growth rate varied from 0.04 to 0.13 h⁻¹ and the specific xylose consumption rate varied between 0.14 and 0.34 g gDW⁻¹ h⁻¹. In all cases, formation of α -ketoglutarate started after growth had begun and continued after cessation of growth, resulting in a yield of 0.25–0.43 g g⁻¹. In one case, where xylose was completely consumed, re-consumption of α -ketoglutarate occurred, although without growth during the consumption phase.

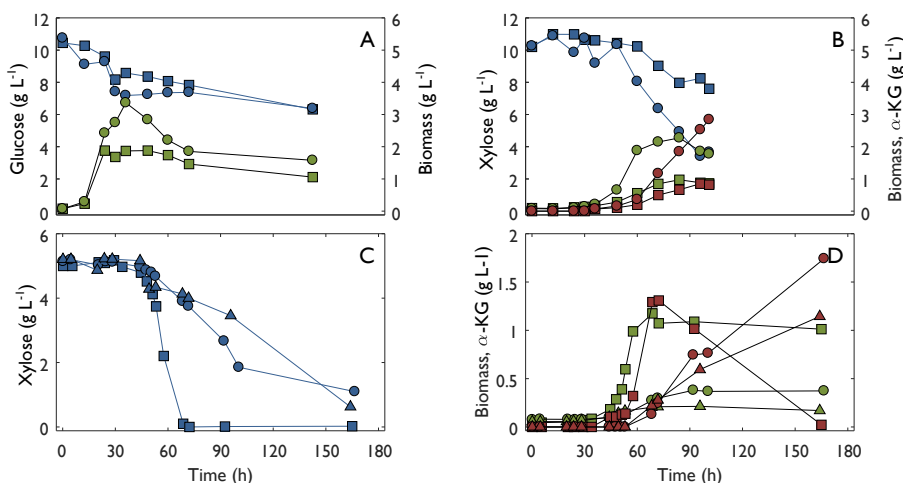


Figure 4. Metabolite profile from bioreactor experiments with *C. crescentus* in three conditions. The substrate was 10 g L⁻¹ of glucose (A), 10 g L⁻¹ of xylose (B) or 5 g L⁻¹ of xylose (C,D). Substrate is marked with blue symbols, biomass with green symbols and α -ketoglutarate with red symbols. Circles, squares and triangle are used to distinguish between different replicates of the experiment.

3. Discussion

The results from shake flask experiments suggested that glucose is a better substrate than xylose in terms of specific growth rate and final biomass concentration. However, growth on xylose was only slightly slower, indicating that the Weimberg pathway is almost as efficient as the Entner-Doudoroff pathway, which is used by *C. crescentus* [11], in terms of providing energy and biosynthetic precursors

for growth. The expression of the Weimberg pathway was found to be regulated, since the Weimberg pathway genes were expressed when grown on xylose but not on glucose. These findings agree with previous reports by Stephens and co-workers [11]. In the same work, these authors state that the Weimberg pathway may be involved in arabinose metabolism, even though the affinity for arabinose of XylB is much lower than xylose. However, they state that there may also be other ways for utilization of arabinose in *C. crescentus*. In the present study, it was found that both xylose and arabinose indeed trigger expression of the Weimberg pathway when provided in the growth medium. Additionally, XylB activity in crude cell extract was found using both xylose and arabinose, regardless of which of the two substrates was used to cultivate the cells. These findings together give strong support to the hypothesis that both xylose and arabinose are metabolized via the Weimberg pathway by the same enzymes. Although it cannot be ruled out that the NADH formation in presence of arabinose arose from other enzymes than XylB, the fact that this activity is induced by both xylose and arabinose makes it likely that it is one and the same enzyme, i.e., XylB.

A common feature for all substrates was the considerably longer lag phase in experiments with 20 g L^{-1} of substrate. The mechanism behind the inhibited growth is probably not substrate inhibition, but rather low osmotolerance since experiments at elevated salt concentrations (6 g L^{-1}) resulted in complete inhibition of growth. This fits well with the fact that the natural habitat of the organism is fresh water, which is an environment characterized by low concentration of solutes. It has been found that the sensitivity to osmotic stress of *C. crescentus* is due to an inability to accumulate intracellular solutes in response to the osmotic stress [20].

An interesting finding of this study was that *C. crescentus* grew better in shake flasks than bioreactors on both 10 g L^{-1} glucose and 10 g L^{-1} xylose. The maximum growth rate did not differ much between shake flasks and bioreactors for glucose, but for xylose the specific growth rate was clearly lower. For both substrates, the final OD was also significantly lower in the bioreactors. There was a substantial variability in the growth experiments. A possible explanation for this could be that *C. crescentus* may be sensitive to aeration. The aeration in shake flasks is much lower than in bioreactors, and in the initial bioreactor experiments preceding those described in this paper higher aeration was used, resulting in very slow or even complete absence of growth on both glucose and xylose. Therefore, a control strategy where aeration of the bioreactor was controlled by the dissolved oxygen tension had to be implemented. Furthermore, the xylose concentration was lowered to 5 g L^{-1} to enable complete substrate depletion. In one out of three cases, the growth rate even exceeded the rates found in shake flasks. However, also in these experiments a high variability was found, indicating that the environment in a bioreactor is unfavorable for growth of *C. crescentus* even at minimal sparging and low stirrer rates.

In the bioreactor experiments with xylose, significant amounts of α -ketoglutarate was found in the fermentation broth, and the formation of α -ketoglutarate coincides with cessation of growth. This implies that, as long as the cells are growing, the rate of α -ketoglutarate consumption by the TCA-cycle and amino acid synthesis matches the production of α -ketoglutarate in the Weimberg pathway. However, as growth ceases, the production of α -ketoglutarate in the Weimberg pathway is higher than the consumption, resulting in extracellular accumulation of α -ketoglutarate. The yield of α -ketoglutarate on xylose was high, reaching up to 0.43 g g^{-1} after growth had ceased. This is evidence that overflow metabolism on xylose occurs in *C. crescentus* as the α -ketoglutarate otherwise would have been respired to produce ATP for maintenance.

The medium from bioreactor experiments was analysed for extracellular metabolites using both HPLC and UHPLC methods and no measurable amounts of any metabolite apart from xylose and α -ketoglutarate were found. A mass balance on xylose was calculated with the sum of biomass, CO_2 and α -ketoglutarate, which amounted to 104 %, supporting the conclusion that no other major formation of metabolites occurred.

The maximum specific growth rate of *C. crescentus* on xylose was 0.13 h^{-1} which can be compared to that of engineered strains where the Weimberg pathway from *C. crescentus* has been

expressed in other organisms. For example, *C. glutamicum* expressing the full Weimberg pathway from *C. crescentus* was reported to have a maximum specific growth rate of 0.07 h^{-1} on xylose as a sole carbon and energy source [13], which is in the same range as *C. crescentus* itself. In another example, the full Weimberg pathway from *C. crescentus* was expressed in *P. putida* [16] resulting in a maximum specific growth rate of 0.21 h^{-1} when using xylose as a sole carbon and energy source. In that study, the activity of the Weimberg pathway enzymes were assayed. The activity of XylB was found to be $0.829\text{ }\mu\text{mol min}^{-1}\text{ mg}^{-1}$ which is more than twenty times higher than what we report for *C. crescentus* in this study ($0.0408\text{ }\mu\text{mol min}^{-1}\text{ mg}^{-1}$). The activity of XylDXA was found to be $0.0259\text{ }\mu\text{mol min}^{-1}\text{ mg}^{-1}$ which correlates well with the XylDXA activity obtained in our study ($0.0138\text{ }\mu\text{mol min}^{-1}\text{ mg}^{-1}$). This unbalance of activity in the engineered *P. putida* compared to the natural levels in *C. crescentus* may be one explanation to why the engineered organism overproduces xylonate. Compared to the engineered hosts, no intermediate metabolites, such as xylonate, were found in the fermentation broth from experiments with *C. crescentus*. This indicates that the activities of the enzymes in the pathway are finely balanced to achieve complete conversion of xylose to α -ketoglutarate.

In conclusion, this study clearly shows that the Weimberg pathway is expressed and functioning in *C. crescentus* growing on xylose and most likely also on arabinose. The growth rate on xylose was close to the growth rate on glucose. Non-growing cells produced α -ketoglutarate at high yields without formation of other metabolites. The slow growth of *C. crescentus*, its sensitivity to high concentrations of substrates and incompatibility with bioreactor cultivation, makes it unsuitable as a production organism for biorefinery purposes, justifying the efforts in the field of metabolic engineering attempting to introduce the Weimberg pathway in more suitable production organisms. The results of this study may prove valuable when introducing the Weimberg pathway in such organisms.

4. Materials and Methods

4.1. Microorganism

Caulobacter crescentus CB2 (DSM-4727) was purchased from DSMZ (Braunschweig, Germany) and kept frozen at $-80\text{ }^{\circ}\text{C}$ in glycerol stock.

4.2. Medium Composition

Two types of medium were used, a rich medium based on peptone and yeast extract (PYE) and a defined M2 medium [21]. PYE consisted of 2 g L^{-1} peptone, 1 g L^{-1} yeast extract, 0.8 mM MgSO_4 , and 0.5 mM CaCl_2 . The medium was sterilized at $121\text{ }^{\circ}\text{C}$ for 20 min in an autoclave. The defined M2 medium consisted of $1.74\text{ g L}^{-1}\text{ Na}_2\text{HPO}_4$, $1.06\text{ g L}^{-1}\text{ KH}_2\text{PO}_4$, $0.5\text{ g L}^{-1}\text{ NH}_4\text{Cl}$, 0.5 mM MgCl_2 , 0.5 mM CaCl_2 , $10\text{ }\mu\text{M FeSO}_4$ and $8\text{ }\mu\text{M}$ ethylenediaminetetraacetic acid (EDTA). A $10\times$ concentrated stock solution of Na_2HPO_4 , KH_2PO_4 and NH_4Cl was prepared and sterilized separately. The other minerals were prepared and sterilized separately, as three $100\times$ concentrated solutions, one containing MgCl_2 , the second containing CaCl_2 , and the third containing FeSO_4 and EDTA. Glucose, xylose and arabinose were prepared and sterilized separately as 200 g L^{-1} stock solutions. Prior to each experiment the components were mixed in the appropriate amounts and sterile, deionized water was used to dilute the solutions to reach the final concentration. All solutions were sterilized by autoclavation ($121\text{ }^{\circ}\text{C}$, 20 min) except the FeSO_4 solution which was filter sterilized using $0.2\text{ }\mu\text{m}$ syringe filters.

4.3. Shake-Flask Cultivation

Frozen stocks were revived in PYE medium in 250 mL E-flasks with 50 mL working volume. Growth tests were performed in M2 medium with 5, 10, or 20 g L^{-1} of glucose, xylose, or arabinose, a total of nine experiment conditions. Also here, 250 mL flasks with 50 mL working volume were used. Growth test experiments were inoculated from flasks with PYE medium.

The inoculation volume corresponded to an initial OD of 0.1, usually around 10% of the volume. All experiments were performed in duplicates at 33 °C and 200 rpm in an orbital shaker incubator (Kuhner, Basel, Switzerland).

4.4. Bioreactor Cultivation

Bioreactor experiments were performed in 2.5 L bioreactors (B. Braun International, Melsungen, Germany) with 1L working volume. The medium consisted of M2 medium supplemented with either glucose 10 g L⁻¹, xylose 10 g L⁻¹ or xylose 5 g L⁻¹. Temperature was set at 33 °C and the reactor was agitated with two Rushton turbines at 150 rpm. In experiments with 10 g L⁻¹ substrate aeration was set to 0.1 vvm (volume of air per volume of liquid and minute). In experiments with 5 g L⁻¹ xylose, aeration was controlled using dissolved oxygen tension (DOT) signal as input, maintaining a minimum DOT of 50%. Stirrer speed was manually increased if aeration rate exceeded 0.5 vvm, but not more than 350 rpm. A 3 M solution NaOH was used to control pH which was set at 6.5. Bioreactors were inoculated with cells that had been grown in M2 medium to reach late exponential phase and then centrifuged (3000× g, for 15 min) to remove the spent medium. The amount of cells used to inoculate the bioreactor corresponded to an initial OD of 0.1.

4.5. Biomass Measurements

Cell dry weight (CDW) was measured by centrifugation (2 min at 12,000× g) of 3 × 2 mL of medium from late exponential phase, to obtain a cell pellet. The supernatant was discarded and the cell pellet resuspended in 0.9% saline. After a second centrifugation, the cell pellet was resuspended in deionized water and transferred to a pre-dried and pre-weighed glass tube which was incubated at 105 °C for 16–24 h. After cooling down to room temperature in a desiccator the tubes were weighed to determine the cell dry weight. Optical density was measured at 620 nm using a spectrophotometer. One unit of optical density corresponded to 0.504 g L⁻¹ CDW. Maximum growth rate was estimated using Equation (1) on the data points forming the steepest slope of the growth curve.

$$\mu = \frac{\ln(\frac{x_2}{x_1})}{t_2 - t_1} \quad (1)$$

4.6. Analyses of Sugars and Organic Acids

Extracellular metabolites were analyzed on an HPLC system (Waters, Milford, MA, USA) after filtration of supernatant samples (0.2 µm cellulose acetate filters). Sugars were analyzed on a Bio-Rad Aminex HPX-87P column (Hercules, CA, USA) using ultra-pure water as mobile phase at a flow rate of 0.6 mL min⁻¹. Column temperature was 85 °C and an refractive index detector (RI) was used for detection. Organic acids were analyzed on a Bio-Rad Aminex HPX-87H column using 10 mM H₂SO₄ as mobile phase at flow rate of 0.6 mL min⁻¹. Acids were detected using an UV-detector at 210 nm. Samples were also analyzed for xylonate on a UHPLC system (Waters, Milford, MA, USA) equipped with an amide column and evaporative light scattering detector (ELSD, Waters, Milford, MA, USA) according to the method described by Almqvist and co-workers [22].

4.7. Enzymatic Assays

Cells were harvested at late exponential phase of growth in PYE supplemented with either xylose, arabinose or glucose. The cell samples were centrifuged at 3000× g, 8 °C for 15 min (Hermle Z513K, Wehingen, Germany). The supernatant was removed from the cell pellet and Yeast Protein Extraction Reagent (Y-PER; Thermo Fisher Scientific, Pierce Biotechnology, Waltham, MA, USA) was added at a proportion of 4 µL per mg cell pellet. The cells were resuspended in the reagent and incubated at 30 rpm, 25 °C for 20 min using a tilt board (Swelab Mixer 440, Boule, Spånga, Sweden). After incubation, the cell extract was centrifuged at 14,000× g, 25 °C for 10 min to remove cell debris. The supernatant containing the extracted protein was subsequently used in the enzyme

assays. A fraction of supernatant was transferred to a new Eppendorf tube and kept at -20°C for protein determination. Protein determination was done using the Bradford method [23] using bovine serum albumin (BSA) as standard. The enzymes encoded by XylB and XylA have NAD^{+} as a cofactor and hence the enzyme activity is directly proportional to reduction of NAD^{+} to NADH. The activity of XylB was measured using either xylose or arabinose as substrate. The activity of the dehydratases encoded by XylD and XylX were not directly measured but estimated from the sequential conversion of xylonate by the enzymes encoded by XylD, XylX and XylA, denoted XylDXA in the assays. The composition of the three reaction mixtures used for the assays is shown in Table 1 [16,24]. The activity of XylA was not assayed as α -ketoglutaric semialdehyde, the natural substrate of enzyme XylA was not commercially available. All components except the substrates were mixed together with the cell extract in the wells of the microtiter plate. Background activity in the sample was monitored and when stable the reaction was then initiated by addition of the substrate. NADH formation was continuously monitored at 340 nm during 10 min at 30°C in a thermostated microtiter plate reader (Ascent Multiscan, Thermo Fisher Scientific, Waltham, MA, USA). The enzyme activity was estimated by linear fitting of the absorbance measurements where the steepest linear slope, at least 1 min long was used.

Table 1. Stock solution composition for the enzyme assays.

	XylB	XylB	XylDXA
Tris-HCl, pH 8.0 (mM)	100.0	100.0	100.0
MgCl_2 (mM)	2.0	2.0	10.0
NAD^{+} (mM)	2.0	2.0	2.0
Xylose (mM)	83.3	-	-
Arabinose (mM)	-	83.3	-
Xylonate (mM)	-	-	80.0

Author Contributions: H.A., L.W. and G.L. conceived and designed the study. H.A., S.J.G., C.T. and L.W. performed the experiments and analysed the data. H.A. wrote the manuscript.

Funding: This work was part of the project XyloCut and financed within the ERA-Net for Applied Systems Biology.

Acknowledgments: The partners of the XyloCut project are acknowledged for their valuable input to this work.

Conflicts of Interest: The authors declare no conflict of interest.

Abbreviations

The following abbreviations are used in this manuscript:

CDW	Cell Dry Weight
DOT	Dissolved Oxygen Tension
HPLC	High Performance Liquid Chromatography
LG	Lower Glycolysis
$\text{NADH}/\text{NAD}^{+}$	Nicotinamide Adenine Dinucleotide (Reduced/Oxidized)
OD	Optical Density
PDH	Pyruvate dehydrogenase
PPP	Pentose Phosphate Pathway
TCA-Cycle	Tricarboxylic Acid Cycle
UHPLC	Ultra High Performance Liquid Chromatography
XDH	Xylulose Dehydrogenase
XI	Xylose Isomerase
XR	Xylose Reductase

References

- Henrici, A.T.; Johnson, D.E. Studies of Freshwater Bacteria: II. Stalked Bacteria, a New Order of Schizomycetes. *J. Bacteriol.* **1935**, *30*, 61–93. [[PubMed](#)]
- Skerker, J.M.; Laub, M.T. Cell-cycle progression and the generation of asymmetry in *Caulobacter crescentus*. *Nat. Rev. Microbiol.* **2004**, *2*, 325–337. [[CrossRef](#)] [[PubMed](#)]
- Curtis, P.D.; Brun, Y.V. Getting in the loop: Regulation of development in *Caulobacter crescentus*. *Microbiol. Mol. Biol. Rev. MMBR* **2010**, *74*, 13–41. [[CrossRef](#)] [[PubMed](#)]
- Tsokos, C.G.; Laub, M.T. Polarity and cell fate asymmetry in *Caulobacter crescentus*. *Curr. Opin. Microbiol.* **2012**, *15*, 744–750. [[CrossRef](#)] [[PubMed](#)]
- Nierman, W.C.; Feldblyum, T.V.; Laub, M.T.; Paulsen, I.T.; Nelson, K.E.; Eisen, J.; Heidelberg, J.F.; Alley, M.R.K.; Ohta, N.; Maddock, J.R.; et al. Complete genome sequence of *Caulobacter crescentus*. *Proc. Natl. Acad. Sci. USA* **2001**, *98*, 4136–4141. [[CrossRef](#)] [[PubMed](#)]
- Hottes, A.K.; Meewan, M.; Yang, D.; Arana, N.; Romero, P.; McAdams, H.H.; Stephens, C. Transcriptional profiling of *Caulobacter crescentus* during growth on complex and minimal media. *J. Bacteriol.* **2004**, *186*, 1448–1461. [[CrossRef](#)] [[PubMed](#)]
- Arellano, B.H.; Ortiz, J.D.; Manzano, J.; Chen, J.C. Identification of a dehydrogenase required for lactose metabolism in *caulobacter crescentus*. *Appl. Environ. Microbiol.* **2010**, *76*, 3004–3014. [[CrossRef](#)] [[PubMed](#)]
- Zalatan, F.; Black, P. Characterization of long-chain fatty acid uptake in *Caulobacter crescentus*. *Arch. Microbiol.* **2011**, *193*, 479–487. [[CrossRef](#)] [[PubMed](#)]
- Presley, G.N.; Payea, M.J.; Hurst, L.R.; Egan, A.E.; Martin, B.S.; Periyannan, G.R. Extracellular gluco-oligosaccharide degradation by *Caulobacter crescentus*. *Microbiology* **2014**, *160*, 635–645. [[CrossRef](#)] [[PubMed](#)]
- Wichelecki, D.J.; Graff, D.C.; Al-Obaidi, N.; Almo, S.C.; Gerlt, J.A. Identification of the in Vivo Function of the High-Efficiency D-Mannosate Dehydratase in *Caulobacter crescentus* NA1000 from the Enolase Superfamily. *Biochemistry* **2014**, *53*, 4087–4089. [[CrossRef](#)] [[PubMed](#)]
- Stephens, C.; Christen, B.; Fuchs, T.; Sundaram, V.; Watanabe, K.; Jenal, U. Genetic analysis of a novel pathway for D-xylose metabolism in *Caulobacter crescentus*. *J. Bacteriol.* **2007**, *189*, 2181–2185. [[CrossRef](#)] [[PubMed](#)]
- Weimberg, R. Pentose oxidation by *Pseudomonas fragi*. *J. Biol. Chem.* **1961**, *236*, 629–635. [[PubMed](#)]
- Radek, A.; Krumbach, K.; Gätgens, J.; Wendisch, V.F.; Wiechert, W.; Bott, M.; Noack, S.; Marienhagen, J. Engineering of *Corynebacterium glutamicum* for minimized carbon loss during utilization of D-xylose containing substrates. *J. Biotechnol.* **2014**, *192*, 156–160. [[CrossRef](#)] [[PubMed](#)]
- Karhumaa, K.; Garcia Sanchez, R.; Hahn-Hägerdal, B.; Gorwa-Grauslund, M.F. Comparison of the xylose reductase-xylytol dehydrogenase and the xylose isomerase pathways for xylose fermentation by recombinant *Saccharomyces cerevisiae*. *Microb. Cell Fact.* **2007**, *6*, 5, doi:10.1186/1475-2859-6-5. [[CrossRef](#)] [[PubMed](#)]
- Álvarez, C.; Reyes-Sosa, F.M.; Díez, B. Enzymatic hydrolysis of biomass from wood. *Microb. Biotechnol.* **2016**, *9*, 149–156. [[CrossRef](#)] [[PubMed](#)]
- Meijnen, J.P.; De Winde, J.H.; Ruijsenaars, H.J. Establishment of oxidative D-xylose metabolism in *Pseudomonas putida* S12. *Appl. Environ. Microbiol.* **2009**, *75*, 2784–2791. [[CrossRef](#)] [[PubMed](#)]
- Liu, H.; Valdehuesa, K.N.G.; Nisola, G.M.; Ramos, K.R.M.; Chung, W.J. High yield production of D-xylonic acid from D-xylose using engineered *Escherichia coli*. *Bioresour. Technol.* **2012**, *115*, 244–248. [[CrossRef](#)] [[PubMed](#)]
- Cao, Y.; Xian, M.; Zou, H.; Zhang, H. Metabolic Engineering of *Escherichia coli* for the Production of Xylonate. *PLoS ONE* **2013**, *8*, e67305, doi:10.1371/journal.pone.0067305. [[CrossRef](#)] [[PubMed](#)]
- Toivari, M.H.; Ruohonen, L.; Richard, P.; Penttilä, M.; Wiebe, M.G. *Saccharomyces cerevisiae* engineered to produce D-xylonate. *Appl. Microbiol. Biotechnol.* **2010**, *88*, 751–760. [[CrossRef](#)] [[PubMed](#)]
- Kohler, C.; Lourenço, R.F.; Bernhardt, J.; Albrecht, D.; Schüler, J.; Hecker, M.; Gomes, S.L. A comprehensive genomic, transcriptomic and proteomic analysis of a hyperosmotic stress sensitive α -proteobacterium. *BMC Microbiol.* **2015**, *15*, 71, doi:10.1186/s12866-015-0404-x. [[CrossRef](#)] [[PubMed](#)]
- Ely, B. Genetics of *Caulobacter crescentus*. *Methods Enzymol.* **1991**, *204*, 372–384. [[PubMed](#)]

22. Almqvist, H.; Sandahl, M.; Lidén, G. A rapid method for analysis of fermentatively produced D-xylonate using ultra-high performance liquid chromatography and evaporative light scattering detection. *Biosci. Biotechnol. Biochem.* **2017**, *81*, 1078–1080. [[CrossRef](#)] [[PubMed](#)]
23. Bradford, M. A rapid and sensitive method for the quantitation of microgram quantities of protein utilizing the principle of protein-dye binding. *Anal. Biochem.* **1976**, *72*, 248–254. [[CrossRef](#)]
24. Johnsen, U.; Dambeck, M.; Zaiss, H.; Fuhrer, T.; Soppe, J.; Sauer, U.; Schönheit, P. D-xylose degradation pathway in the halophilic archaeon *Haloferax volcanii*. *J. Biol. Chem.* **2009**, *284*, 27290–27303. [[CrossRef](#)] [[PubMed](#)]



© 2018 by the authors. Licensee MDPI, Basel, Switzerland. This article is an open access article distributed under the terms and conditions of the Creative Commons Attribution (CC BY) license (<http://creativecommons.org/licenses/by/4.0/>).

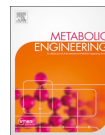
Paper II





Contents lists available at ScienceDirect

Metabolic Engineering

journal homepage: www.elsevier.com/locate/meteng

Identification of modifications procuring growth on xylose in recombinant *Saccharomyces cerevisiae* strains carrying the Weimberg pathway

Celina Borgström^{a,1}, Lisa Wasserström^{a,1,2}, Henrik Almqvist^{b,1}, Kristina Broberg^{b,3}, Bianca Klein^c, Stephan Noack^{c,d}, Gunnar Lidén^b, Marie F. Gorwa-Grauslund^{b,*}

^a Division of Applied Microbiology, Department of Chemistry, Lund University, PO Box 124, 221 00, Lund, Sweden

^b Department of Chemical Engineering, Lund University, PO Box 124, 221 00, Lund, Sweden

^c Institute of Bio- and Geosciences, IBG-1: Biotechnology, Forschungszentrum Jülich GmbH, Jülich, D-52425, Germany

^d Bioeconomy Science Center (BioSC), Forschungszentrum Jülich GmbH, Jülich, D-52425, Germany

ARTICLE INFO

Keywords:

Xylose
Weimberg pathway
 α -ketoglutarate semialdehyde dehydrogenase
Saccharomyces cerevisiae
 α -ketoglutarate

ABSTRACT

The most prevalent xylose-assimilating pathways in recombinant *Saccharomyces cerevisiae*, i.e. the xylose isomerase (XI) and the xylose reductase/xylitol dehydrogenase (XR/XDH) pathways, channel the carbon flux through the pentose phosphate pathway and further into glycolysis. In contrast, the oxidative and non-phosphorylative bacterial Weimberg pathway channels the xylose carbon through five steps into the metabolic node α -ketoglutarate (α KG) that can be utilized for growth or diverted into production of various metabolites.

In the present study, steps preventing the establishment of a functional Weimberg pathway in *S. cerevisiae* were identified. Using an original design where a *S. cerevisiae* strain was expressing the essential four genes of the *Caulobacter crescentus* pathway (*xylB*, *xylD*, *xylX*, *xylA*) together with a deletion of *FRA2* gene to upregulate the iron-sulfur metabolism, it was shown that the *C. crescentus* α KG semialdehyde dehydrogenase, *XylA* was not functional in *S. cerevisiae*. When replaced by the recently described analog from *Corynebacterium glutamicum*, *KsaD*, significantly higher *in vitro* activity was observed but the strain did not grow on xylose. Adaptive laboratory evolution (ALE) on a xylose/glucose medium on this strain led to a loss of *XylB*, the first step of the Weimberg pathway, suggesting that ALE favored minimizing the inhibiting xylonate accumulation by restricting the upper part of the pathway. Therefore three additional gene copies of the lower Weimberg pathway (*XylD*, *XylX* and *KsaD*) were introduced. The resulting *S. cerevisiae* strain (Δ *fra2*, *xylB*, 4x (*xylD*-*xylX*-*ksaD*)) was able to generate biomass from xylose and Weimberg pathway intermediates were detected. To our knowledge this is the first report of a functional complete Weimberg pathway expressed in fungi. When optimized this pathway has the potential to channel xylose towards value-added specialty chemicals such as dicarboxylic acids and diols.

1. Introduction

Large efforts are currently being made to replace non-renewable carbon sources with renewable alternatives in the production of fine and bulk chemicals, both to minimize environmental impacts and to secure a long-term supply of feedstocks. One promising renewable feedstock is lignocellulose that often contains high levels of the pentose sugar D-xylose (from now on referred to as xylose) in the hemicellulosic fraction, especially in hardwood and agricultural crops (Mutturi et al., 2014). However

xylose is not naturally used by the yeast *Saccharomyces cerevisiae*, a well-established cell factory due to the availability of advanced tools for genetic engineering and the tolerance to low pH, high osmolality and many of the inhibitors present in lignocellulosic hydrolysates (Sandström et al., 2014). Consequently, much research has been carried out to establish xylose assimilation pathways arising from natural hosts in *S. cerevisiae*.

In nature, assimilation of xylose occurs through isomerization, oxido-reduction or oxidative pathways (Fig. 1). The xylose isomerization pathway that starts with a one-step isomerization of xylose to

Abbreviations: ALE, adaptive laboratory evolution; FDR, false discovery rate; KGSADH, α -ketoglutarate semialdehyde dehydrogenase; PPP, pentose phosphate pathway; XDH, xylitol dehydrogenase; XI, xylose isomerase; XK, xylulose kinase; XR, xylose reductase; YNB, yeast nitrogen base; YPD, yeast extract-peptone-dextrose
* Corresponding author.

E-mail address: Marie-Francoise.Gorwa@tmb.lth.se (M.F. Gorwa-Grauslund).

¹ Equal contributions.

² Present address: Department of Clinical Microbiology, Division of Laboratory Medicine, Lund University Hospital, Lund, Sweden.

³ Present address: RISE AB, Ideon Science Park, Beta5, Scheelevägen 17, 223 70 Lund, Sweden.

<https://doi.org/10.1016/j.ymben.2019.05.010>

Received 4 April 2019; Received in revised form 14 May 2019; Accepted 27 May 2019

Available online 28 May 2019

1096-7176/© 2019 The Authors. Published by Elsevier Inc. on behalf of International Metabolic Engineering Society. This is an open access article under the CC BY license (<http://creativecommons.org/licenses/by/4.0/>).

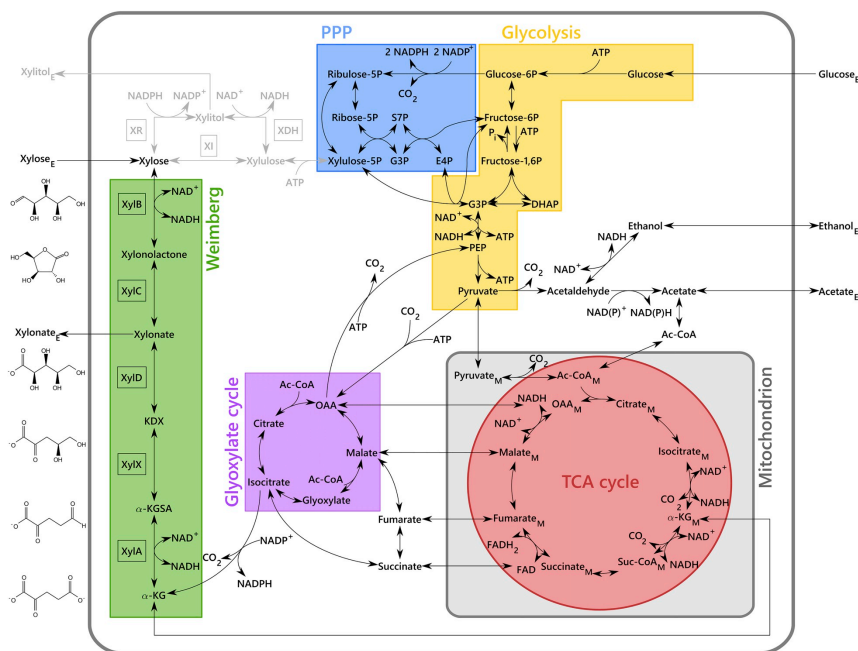


Fig. 1. Metabolic map of the central carbon metabolism of *S. cerevisiae* and the Weinberg pathway (green). The five reaction steps of the Weinberg pathway are catalyzed by xylose dehydrogenase (XylB), xylonolactonase (XylC), xylonate dehydratase (XylD), 3-keto-2-deoxy-xylonate dehydratase (XylX) and α -ketoglutarate semialdehyde dehydrogenase (KGSADH/XylA) and the end product of the pathway is cytosolic α -ketoglutarate that can enter the central carbon metabolism. For comparison, the main current xylose assimilation pathways in recombinant yeast are shown in light grey. Abbreviations: PPP - Pentose phosphate pathway, TCA cycle - Tricarboxylic acid cycle, G3P - Glyceraldehyde 3-phosphate, S7P - Sedoheptulose 7-phosphate, E4P - Erythrose 4-phosphate, DHAP - Dihydroxyacetone phosphate, PEP - Phosphoenolpyruvate, OAA - Oxaloacetic acid, Suc-CoA - Succinyl-Coenzyme A, Ac-CoA - Acetyl-Coenzyme A, α -KG - α -ketoglutaric acid, KDX - 2-keto-3-deoxy-xylonate, α -KGSa - α -ketoglutarate semialdehyde, XR - Xylose reductase, XDH - Xylitol dehydrogenase, XI - Xylose isomerase. (For interpretation of the references to color in this figure legend, the reader is referred to the Web version of this article.)

xylulose by the enzyme xylose isomerase (XI) is the most commonly described pathway in bacteria. In non-conventional yeasts, the most prevalent appears to be the oxido-reductive pathway, in which the conversion of xylose to xylulose is achieved in two steps, first a reduction catalyzed by xylose reductase (XR) followed by an oxidation catalyzed by xylitol dehydrogenase (XDH) (Du Preez and Prior, 1985; Jeffries, 1983). Both routes form xylulose from xylose that is further converted by xylulose kinase (XK) to xylulose-5-P and metabolized through the pentose phosphate pathway (PPP) and glycolysis (Wang et al., 1980).

In the - much less studied - oxidative pathways, xylose is first converted to 2-keto-3-deoxyxylonate through dehydrogenation, lactone ring opening and subsequent dehydration. Thereafter the oxidative pathway branches off to produce either pyruvate and glycoaldehyde (route I; Dahms, 1974), α -ketoglutarate (route II or Weinberg pathway; Weinberg, 1961) or pyruvate and glycolate in the recently described route III (Watanabe et al., 2019).

In *S. cerevisiae*, most engineering attempts have been based on the XR/XDH or XI pathways, largely for production of ethanol or acetyl-CoA derived products (see reviews by e.g. Hahn-Hägerdal et al., 2007; Kim et al., 2013; Krivoruchko et al., 2015). However, the fact that *S. cerevisiae* is able to grow at low pH makes it an interesting host for the

production of acids such as carboxylic acids, as shown in several studies (Abbott et al., 2009; Borodina and Nielsen, 2014; Buijs et al., 2013; Paddon et al., 2013). Producing carboxylic acids from xylose using the XR/XDH or XI pathways may not be optimal since it results in carbon loss in both the cytosol and the mitochondria before forming five-carbon carboxylic acids. Therefore, the Weinberg pathway provides an interesting route for production of xylose-derived α -ketoglutarate without carbon loss.

So far the upper part of the Weinberg pathway from *Caulobacter crescentus* that converts xylose to xylonate via two enzymatic steps catalyzed by a xylose dehydrogenase (XylB, encoded by *xylB*) and a xylonolactonase (XylC, encoded by *xylC*) has been successfully established in *S. cerevisiae* (Toivari et al., 2012) and *Escherichia coli* (Liu et al., 2012), enabling efficient conversion of xylose to xylonate. Further introduction of the lower part of the Weinberg pathway has also enabled production of glutaric acid and mesaconate in *E. coli* (Bai et al., 2016; Wang et al., 2018). Constitutive growth on xylose has also been recently established in *E. coli* by using a computational approach to optimize the enzyme levels (Rossoni et al., 2018). In *Corynebacterium glutamicum* (Radek et al., 2014, 2017) and *Pseudomonas putida* (Meijnen et al., 2009) introduction of the Weinberg pathway has also enabled growth on xylose as the sole carbon source.

Recently, the whole Weimberg pathway from *C. crescentus* was introduced in *S. cerevisiae* with the aim to establish growth on xylose; however, xylose was almost quantitatively converted to xylonate and not metabolized further in the pathway, despite the evaluation of five different xylonate dehydratase (XylD) genes (Wasserstrom et al., 2018). Most XylD proteins require an iron-sulfur (Fe-S) cluster to be loaded onto specific cysteine residues in the apoprotein for catalytic activity (Andberg et al., 2016). Accordingly it was shown that *C. crescentus* XylD activity was improved in yeast by upregulation of the iron metabolism through deletion of the iron regulon repressor *FRA2*, which allowed production of ethylene glycol, glycolic acid and lactic acid via the Dahms pathway in *S. cerevisiae* (Salusjärvi et al., 2017). However, to our knowledge, a functional Weimberg pathway that enables growth on xylose has not yet been established in fungal species.

In the present work, we introduced several modifications into the previously developed *S. cerevisiae* strain TMB4530 expressing the Weimberg pathway genes from *C. crescentus* (Wasserstrom et al., 2018) with the aim to establish growth on xylose. A novel, putative, α -ketoglutarate semialdehyde dehydrogenase from *C. glutamicum* encoded by *ksaD* (Brüsseler et al., 2019), was used instead of *C. crescentus* *xylA*. In addition, the Fe-S metabolism was upregulated by deletion of the iron regulon repressor *FRA2*. The resulting strain was subjected to adaptive laboratory evolution (ALE) on a mixture of xylose and glucose to select for additional modifications that would enable growth on xylose. Finally, the effect of modifying the enzyme ratio was evaluated and relevant metabolic intermediates were identified.

2. Materials and methods

2.1. Strains, plasmids and media

The plasmids and yeast strains used in the present study are listed in Tables 1 and 2, respectively. Details of strain and plasmid construction can be found in Fig. 2 and Annex A. Cultivations were made either in Yeast Peptone Dextrose (YPD) medium containing 10 g L⁻¹ yeast extract, 20 g L⁻¹ peptone and 20 g L⁻¹ glucose or Yeast Nitrogen Base (YNB; 6.7 g L⁻¹ YNB, with ammonium sulfate, without amino acids; Becton-Dickinson, NJ, USA) supplemented with different carbon sources as detailed below. For solid media agar was added at 15 g L⁻¹.

2.2. In vitro enzymatic activity measurements

Overnight cultures of yeast strains were grown at 30 °C and 180 rpm in 5 mL YNB supplemented with 20 g L⁻¹ glucose in 50 mL conical tubes with an initial OD_{620nm} of 1.0. Cells were harvested at late exponential phase, washed twice in 1 mL sterile H₂O and total protein was extracted using Y-PER extraction solution (Pierce, Rockford, IL, USA)

according to manufacturer's instructions. Total protein concentration was determined as previously described (Bradford, 1976; Wasserstrom et al., 2018). The enzyme activity of xylose dehydrogenase (XylB) and α -ketoglutarate semialdehyde dehydrogenase (KGSADH) were assayed by following the rate of NAD⁺ and NADP⁺ reduction through optical density at 340 nm as previously described (Wasserstrom et al., 2018). The measurements were performed in duplicates at 30 °C on a Multiskan Ascent reader (Thermo Electro Corporation, Waltham, MA, USA) using 96-well plates and a final volume of 200 μ L. The background formation of NADH was monitored and subtracted, if present, before substrate was added to the reactions. For all enzymatic assays, the standard mixture contained 100 mM Tris-HCl pH 8.0, 2 mM MgCl₂ and 2 mM NAD⁺ or 2 mM NADP⁺. A concentration of 100 mM of xylose was used as substrate for xylose dehydrogenase XylB (Toivari et al., 2012). For the KGSADH activity, the natural substrate α -ketoglutarate semialdehyde was not commercially available and therefore 5 mM glutaraldehyde was used as previously described (Johnsen et al., 2009).

2.3. Proteomics

A single colony of each strain was grown overnight at 30 °C and 180 rpm in 5 mL of YNB supplemented with 20 g L⁻¹ glucose and 25 mM potassium phthalate buffer set to pH 5.5 in 50 mL conical tubes. These cultures were used to inoculate 35 mL of the same media in 250 mL Erlenmeyer flasks. All strains were grown in biological duplicates until late exponential phase (OD_{620nm} = 3–4), split into three samples (10 mL each) and harvested in a swing-out rotor centrifuge at 3200 \times g for 5 min at 4 °C. The cells were flash frozen in liquid nitrogen and stored at -80 °C until proteomics analysis.

Prior to proteomics analysis, cell samples corresponding to approximately 10 mL were processed as described recently (Unrean et al., 2018).

Tryptic digestion of intracellular proteins was performed according to the protocol of Voges and Noack (2012). Peptide mixtures were separated by reversed phase HPLC using an Ascentis column (Sigma Aldrich, Schnelldorf, Germany), employing 0.1% formic acid in water and 0.1% formic acid in acetonitrile as buffers at a flowrate of 200 μ L min⁻¹.

For IDA and SWATH acquisition on a TripleTOF6600 (AB Sciex, Darmstadt, Germany), peptides were eluted with a gradient program in 90 min. Autosampler temperature was 6 °C and injection volume was 10 μ L. During the elution under the above-specified parameters the variable width Q1 windows were monitored in a non-scheduled manner. SWATH window width was calculated using SWATH Variable Window Calculator V1.0 (AB Sciex, Darmstadt, Germany). During the information-dependent acquisition all ions with m/z⁻¹ greater than 300, charge states of 2–4 and above an intensity of 150 were selected

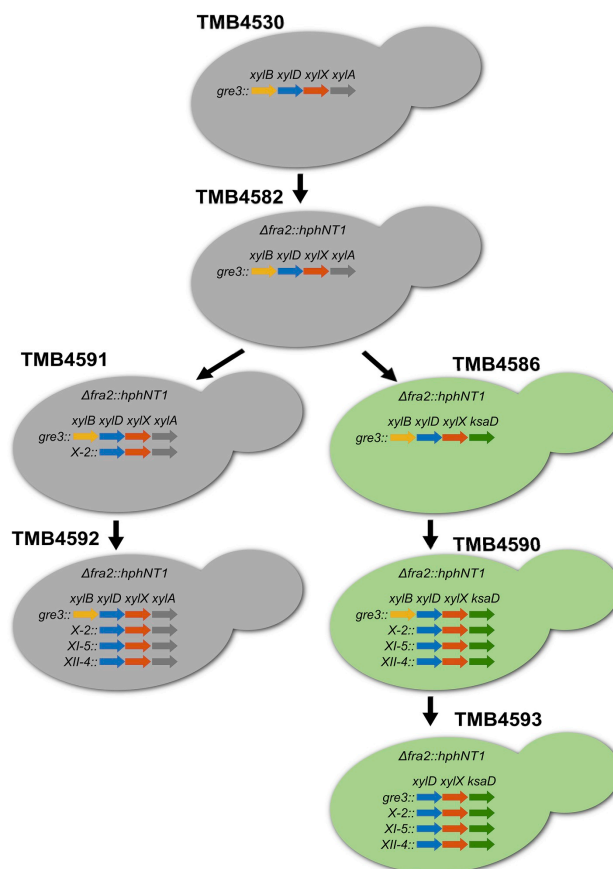
Table 1
List of plasmids used in the present study.

Plasmid name	Relevant genotype	Reference
pUG-amsSYM	(A.g.)TEF1p-amsS-(A.g.)TEF1	Solis-Escalante et al. (2013)
pUG-amsSYM2	Asc1-MCS; (A.g.)TEF1p-amsS-(A.g.)TEF1t; AsiSI	Wasserstrom et al. (2018)
pRS305H	Yfp1-LEU2_hphNT1	Taxis and Knop (2006)
Cas9-kanMX	TEF1p-Cas9-CYC1t_kanMX	Stovicek et al. (2015)
pAGS8	pUGamSYM2-xylD-xylX-xyIA	Wasserstrom et al. (2018)
pAGS8B	pUGamSYM2-xylB-xylD-xylX-xyIA	Wasserstrom et al. (2018)
gRNA.ADE2	SNR52p-gRNA.ADE2-SUP4t_natMX	Stovicek et al. (2015)
LWA45	pUGamSYM2-xylD-xylX-ksaD	This study
LWA46	pCFB3040-xylD-xylX-ksaD	This study
LWA48	p426-GDPp-ksaD-CYC1t	This study
LWA49	p426-GDPp-xyIA-CYC1t	This study
pUC57-ksaD	ksaD	This study
pCFB2899	X-2-MarkerFree	Jessop-Fabre et al. (2016)
pCFB3037	XI-5-MarkerFree	Jessop-Fabre et al. (2016)
pCFB3040	XII-4-MarkerFree	Jessop-Fabre et al. (2016)
pCFB3053	gRNA_X-2-XI-5-XII-4	Jessop-Fabre et al. (2016)

Table 2

List of strains used in the present study. For details on strain construction see Annex A.

Strain name	Relevant genotype	Encoded enzymes introduced into yeast	Reference
CEN.PK 113-5D	<i>MATa ura3-52 HIS3, LEU2 TRP1 MAL2-8c SUC2</i>	–	Entian and Kötter (2007)
CEN.PK 113-7D	<i>MATa URA3 HIS3 LEU2 TRP1 MAL2-8c SUC2</i>	–	Entian and Kötter (2007)
TMB4530	CEN.PK 113-7D, $\Delta gre3::AGS8B$	XylB, XylD, XylX, XylA	Wasserstrom et al. (2018)
TMB4582	TMB4530, <i>fra2::hphNT1</i>	XylB, XylD, XylX, XylA	This study
TMB4586	TMB4582, <i>xylA::ksaD</i>	XylB, XylD, XylX, KsaD	This study
TMB4590	TMB4586, X-2:: <i>xylD/xylX/ksaD</i> , XI-5:: <i>xylD/xylX/ksaD</i> , XII-4::LWA46	XylB, 4x(XylD, XylX, KsaD)	This study
TMB4591	TMB4582, X-2::pAGS8	XylB, 2x(XylD, XylX, XylA)	This study
TMB4592	TMB4591, XI-5::pAGS8 XII-4::pAGS8	XylB, 4x(XylD, XylX, XylA)	This study
TMB4593	TMB4590, $\Delta xylB::amdSYM$	4x(XylD, XylX, KsaD)	This study
TMB4594	CEN.PK113-5D, LWA48	KsaD	This study
TMB4595	CEN.PK113-5D, LWA49	XylA	This study

**Fig. 2.** Scheme of strain construction strategy. Construction details are found in Annex A.

for fragmentation. Acquired MS/MS spectra were matched to a *S. cerevisiae* Pasta Database (www.uniprot.org) using the Paragon algorithm with default parameters and default probabilities for modifications. A library of confidently identified peptides was generated for each sample using ProteinPilot (4.5, AB Sciex, Darmstadt, Germany). All peptides were assembled in a meta-library of *S. cerevisiae* covering 497 proteins.

For SWATH processing, the ProteinPilot library was imported into the MS/MS^{ALL} with SWATHTM Acquisition MicroApp within PeakView (2.1, AB Sciex, Darmstadt, Germany). For 12 fragments each of the ten most intense peptides (according to the MS1 precursor ion intensity from the IDA acquisition) the XIC were extracted from the SWATH spectra. Each ion trace was integrated and scored as implemented in the SWATHTM Acquisition MicroApp. A false discovery rate (FDR) was calculated as implemented in the SWATH MicroAPP. From all extracted 120 mass traces per protein only those with an FDR less than the threshold of 0.1% were exported and subjected to further analysis.

2.4. Dot plating

Pre-cultures were prepared as above but in YNB containing 2 g L⁻¹ glucose and 10 g L⁻¹ xylose. The overnight cultures were diluted with sterile 0.9% NaCl to an OD_{620nm} of 1.0, which corresponds to approximately 1 × 10⁶ CFU mL⁻¹. A five-fold serial dilution series was performed for each strain in a microtiter plate under sterile conditions. 5 µL of each dilution was carefully dot plated on YNB-agar plates supplemented with xylose (50 g L⁻¹) and incubated at 30 °C for 10 days.

2.5. Seed cultures prior to cultivation experiments

Experiments in shake flasks and bioreactors were preceded by a seed culture where cells from either plates or stocks frozen in glycerol were propagated in a shaker incubator operated at 30 °C and 170 rpm in 50 mL or 250 mL Erlenmeyer flasks containing 10 mL or 100 mL YPD supplemented with 25 mM potassium phthalate buffer set to pH 5.5. Cells from the seed cultures were separated from the growth medium by centrifugation at 5000 × g during 5 min, resuspended in water, and transferred to the shake flasks or bioreactors.

2.6. Aerobic cultivations in shake flasks

Shake-flask cultivations were performed in a shaker incubator operated at 30 °C and 170 rpm in baffled 250 mL Erlenmeyer flasks containing 50 mL defined medium with the following composition: glucose 5 g L⁻¹, xylose 10 g L⁻¹, ammonium sulfate 5 g L⁻¹, YNB (yeast nitrogen base without amino acids and ammonium sulfate) 1.7 g L⁻¹ and 25 mM potassium phthalate buffer set to pH 5.5. Cells from the seed culture were inoculated to an initial OD_{620nm} of 0.1.

2.7. Aerobic cultivations in bioreactors

Experiments were carried out in 2.5 L bioreactors (Biostat C, B. Braun International, Melsungen, Germany and Biostat A+, Sartorius, Göttingen, Germany) equipped with dual Ruston impellers, a pH electrode and a dissolved oxygen (pO₂) electrode. The bioreactors were operated at 30 °C with a stirrer speed of 500 rpm and sparged with air at a rate of 0.5 L min⁻¹ and pO₂ was monitored continuously. Automatic addition of potassium hydroxide (5 M) and sulfuric acid (1 M) was used to maintain pH at 5.50 ± 0.05. Continuous analysis of the CO₂ concentration in the off-gas was performed during all experiments using gas analysers connected to the bioreactors (Biostat C equipped with BlueOne Perm, BlueSens, Herten, Germany, Biostat A+ equipped with ElectroLab FerMac 368, Tewkesbury, UK). The experiments were performed in two stages: an initial growth phase on glucose and a second phase starting at 24 h, where glucose and xylose were added as a pulse. The initial medium composition, 1.0 L working

volume, was glucose 10 g L⁻¹, ammonium sulfate 5 g L⁻¹, YNB (yeast nitrogen base without amino acids and ammonium sulfate) 1.7 g L⁻¹. The reactors were sterilized with water and glucose at 121 °C for 20 min, after which separately autoclaved ammonium sulfate and filter sterilized YNB were added aseptically. Sterile water was used to make up the volume to 1.00 L, compensating for liquid lost as steam during sterilization. Cells from seed culture were used to inoculate the bioreactors at an initial OD_{620nm} of 0.4. An autoclaved mixture of 10 g glucose and 10 g xylose dissolved in 50 mL of water was added as a pulse at 24 h.

2.8. Adaptive laboratory evolution

A single colony of TMB4586 grown on YPD solid medium was inoculated into 5 mL of YP (10 g L⁻¹ yeast extract, 20 g L⁻¹ peptone) supplemented with 50 mM potassium phthalate buffer set to pH 5.5 and 2 g L⁻¹ glucose in a conical 50 mL tube, and incubated at 30 °C overnight. The culture was then used to inoculate a 250 mL shake flask with 25 mL YP containing 50 mM potassium hydrogen phthalate (pH 5.5), 2 g L⁻¹ glucose and 10 g L⁻¹ xylose to an initial OD_{620nm} of 0.1. The shake flask was incubated at 30 °C in a rotary shaker set to 170 rpm. After 48 h, samples were taken for determination of the biomass concentration as well as for extracellular metabolite composition; glycerol stocks of the culture were stored at -80 °C. The culture was then used to inoculate a new flask as described above. Re-inoculations were carried out every 48 h for a total of 25 times.

2.9. Biomass concentration

Biomass concentration was measured using spectrophotometry at 620 nm. Samples were diluted with water when exceeding 0.4 absorbance units. Optical density was correlated to cell dry weight determined at selected time points (endpoint for shake flasks and at 24 h, 48 h and endpoint for bioreactors). Cell dry weight was determined by centrifugation at 17 500 × g for 2 min of a sample with known volume (1.5–2.0 mL). The cell pellet was washed once with water, centrifuged and resuspended in water before being transferred to a pre-dried and weighed glass test tube. The cell pellet was dried at 105 °C in an oven for 12–18 h and then weighed.

2.10. Metabolite analysis

Samples for extracellular metabolite analysis were centrifuged at 17 500 × g for 2 min and the supernatant was filtered with 0.2 µm cellulose acetate syringe filters and stored at -20 °C before analysis. Ethanol, acetate and xylitol were analyzed using HPLC (Alliance 2695, Waters, Milford, MA, USA) equipped with an RI-detector (Shimadzu RID-6A). Separation was done on an Aminex HPX-87H column (300 × 7.8 mm, 9 µm, BIO-RAD, Hercules, CA, USA) at 60 °C using 5 mM H₂SO₄ in water (ELGA Purelab Flex, Veolia Water, Paris, France) as mobile phase at a flow rate of 0.6 mL min⁻¹. Glucose, xylose and xylonate were analyzed using UHPLC with ELS-detector (Acquity H-Class, Waters, Milford, MA, USA). A gradient method based on the Waters UPLC BEH Amide column (2.1 × 100 mm, 1.7 µm), especially developed for analysis of xylonate in the presence of xylose and glucose was used (Almqvist et al., 2017). Weimberg intermediates were analyzed using HPLC-MS (1260 Infinity II HPLC and 6545 QTOF, Agilent, Santa Clara, CA, USA). The chromatographic method was identical to the method used in UHPLC-ELS, except that the gradient re-equilibration time was extended with 2 min to compensate for the larger system volume of the HPLC-MS system compared to the UHPLC-ELS. The QTOF was operated in MS mode using negative electrospray ionization under the following conditions: drying gas temperature 200 °C, drying gas flow 8 L min⁻¹, sheath gas temperature 350 °C, sheath gas flow 12 L min⁻¹, nebulizer pressure 25 psig, capillary voltage 2000 V, nozzle

voltage 0 V, fragmentor voltage 125 V, skimmer voltage 45 V, octopole RF voltage 750 Vpp. Data was collected in the range 100–350 m/z^{-1} at a rate of 5 spectra s^{-1} . All standards were obtained from Sigma Aldrich (St. Louis, MO, USA) except α -ketoglutarate semialdehyde which was a kind gift from Jülich Research Centre.

3. Results and discussion

3.1. Proteomics reveal unexpected limitations of *C. crescentus* Weimberg pathway when introduced in *S. cerevisiae*

Previous introduction of the Weimberg pathway from *C. crescentus* into *S. cerevisiae* did not sustain growth on xylose; instead xylose was converted into the pathway intermediate xylonate, which accumulated in the broth (Wasserstrom et al., 2018). Based on these findings and other studies on the Dahms pathway (Salusjärvi et al., 2017), functional expression of the xylonate dehydratase enzyme (XylD) was foreseen as the main bottleneck of the pathway. To validate this hypothesis, untargeted proteomics was applied to the previously developed strain TMB4530 expressing *xylB*, *xylD*, *xylX* and *xylA* from *C. crescentus* and to the reference strain CEN.PK 113-7D not containing any of these genes. The results summarized in Fig. 3 and Supplementary Table B1 indicated significant differences in peptide numbers and abundances between TMB4530 and the reference strain, in particular for three of the four Weimberg pathway enzymes. For XylB, XylD and XylX 26, 12 and 74 peptides were identified with at least 95% confidence in either sample, summing up to 20-, 3- and 86-fold abundance increases in the TMB4530 sample compared to the control strain (Table B1). On the other hand, only two peptides associated with XylA were identified, ruling out safe identification of this protein in any of the samples analyzed. The absence or very low concentration of XylA was unexpected since *xylA* transcripts were previously identified in the TMB4530 strain (Wasserstrom et al., 2018), and there were no foreseen issues associated with establishing an α -ketoglutarate semialdehyde dehydrogenase activity from a bacterial XylA protein in yeast. In contrast, the XylD previously hypothesized as a major bottleneck of the Weimberg route was identified in TMB4530 on both mRNA and protein levels. Still xylonate dehydratase activity has not yet been proven in this strain background due to a lack of reliable enzymatic assay (Wasserstrom et al., 2018).

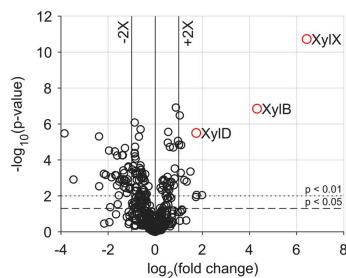


Fig. 3. Volcano plot for strain *S. cerevisiae* TMB4530 showing proteins with significantly altered abundances in comparison to the reference strain. While the heterologously expressed enzymes XylB, XylD and XylX of the Weimberg pathway showed the largest up-regulation across all intracellular proteins, no peptide was quantifiable for the last pathway enzyme XylA. In case of the reference strain, no peptides for any of the four enzymes were found and depicted fold changes were calculated from baseline signals.

3.2. XylA analog from *C. glutamicum* is actively expressed in *S. cerevisiae*

In light of the proteomics analysis, alternatives to the *C. crescentus* α -ketoglutarate semialdehyde dehydrogenase protein were searched for. It was recently shown that *C. glutamicum* could metabolize xylose via the Weimberg pathway after heterologous expression of only *xylD* or *xylX*, indicating the presence of endogenous enzymes for the other steps (Brüsseler et al., 2019). Indeed *C. glutamicum* α -ketoglutarate semialdehyde dehydrogenase KsaD (encoded by *ksaD*) was identified and shown to convert α -ketoglutarate semialdehyde to α -ketoglutarate *in vivo* and *in vitro* (Brüsseler et al., 2019). An amino acid alignment of KsaD with *C. crescentus* XylA revealed significant differences throughout the sequence with an identity of only 25%, but secondary structure predictions showed high similarity between the two proteins on a structural level (Brüsseler et al., 2019).

To assay the functionality of *C. glutamicum* KsaD in *S. cerevisiae*, the *ksaD* gene was expressed on a multicopy plasmid (generating strain TMB4594) and the enzymatic activity was assayed *in vitro*. For comparison, the *C. crescentus* *xylA* gene was expressed under similar conditions, generating strain TMB4595. The assay results indicated a 33-fold higher dehydrogenase activity for KsaD compared to XylA, using glutaraldehyde as substrate (Fig. 4). The modest activity of XylA in the multicopy expression system was consistent with the proteomics analysis where a single-integration *xylA* gene did not lead to identifiable XylA proteins.

C. crescentus *xylA* was therefore exchanged for *C. glutamicum* *ksaD* in the previously generated Weimberg strain TMB4530 (*xylB*, *xylD*, *xylX*, *xylA*) (Wasserstrom et al., 2018). In addition and to favor enhanced xylonate dehydratase (XylD) activity in yeast, the Fe-S metabolism was upregulated by deletion of the iron regulon repressor *FRA2*, as previously reported (Salusjärvi et al., 2017). The resulting strain, TMB4586 (Δ *fra2*, *xylB*, *xylD*, *xylX*, *ksaD*), was first evaluated for α -ketoglutarate semialdehyde dehydrogenase activity (KGSADH; Fig. 4). Due to the single integration of *ksaD*, a lower activity was measured than when using the multicopy strain TMB4594; still the activity was 20-fold higher than the Δ *fra2* strain TMB4582 containing the Weimberg pathway with the original *xylA* (Fig. 4).

Despite replacing *xylA* with *ksaD* and upregulating the Fe-S metabolism through *FRA2* deletion, TMB4586 (Δ *fra2*, *xylB*, *xylD*, *xylX*, *ksaD*) was still not able to grow on xylose and almost 100% of the xylose was converted to xylonate (data not shown). This indicated that the metabolic flux in the lower part of the pathway from xylonate to α -

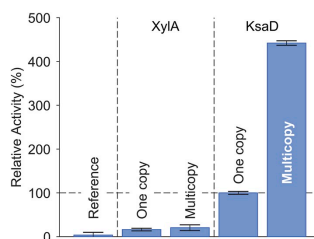


Fig. 4. KGSADH (α -ketoglutarate semialdehyde dehydrogenase) activity using glutaraldehyde as a substitute substrate. The assay was done for the reference strain (CEN.PK 113-7D), single integration of *xylA* (TMB4582), multicopy plasmid of *xylA* (TMB4595), single integration of *ksaD* (TMB4586) and multicopy plasmid of *ksaD* (TMB4594). Relative activities are shown with strain TMB4586 representing 100%. The absolute enzyme activity for TMB4586 was $0.13 \mu\text{mol min}^{-1} \text{mg}^{-1}$. Standard deviations were calculated from two biological and two technical replicates.

ketoglutarate still needed to be improved. Therefore, adaptive laboratory evolution (ALE) was performed on the strain to select for evolved cells able to grow on xylose.

3.3. Adaptive laboratory evolution of TMB4586 selects for pathway loss as result of xylonate accumulation

ALE of strain TMB4586 (Δ fra2, xylB, xylD, xylX, ksaD) was performed using serial batches and a mixture of glucose (2 g L^{-1}) and xylose (10 g L^{-1}). A low level of glucose was used to provide the growth needed for genetic mutations to occur, while xylose was supplied at a higher concentration to allow for mutants with increased growth on xylose to gain a competitive advantage and to become enriched over the course of the ALE experiment. The culture was grown for 48 h and then a small inoculum was transferred into a new shake flask with fresh medium. At each serial transfer event, cell dry weight, xylose consumption and xylonate production were measured (Fig. 5A).

For the first four cultures, the measured values remained relatively stable, but after the fifth culture, the residual xylose concentration decreased from 8 to 5 g L^{-1} , which was accompanied by a stoichiometric increase of xylonate from 4 to 7 g L^{-1} with only a minor improvement in biomass, from 2.4 to 2.9 g L^{-1} . These levels remained relatively stable for the following 14 cultures, with only a further 1 g L^{-1} decrease in residual xylose and a corresponding increase in xylonate. After culture 19, the ability of the cell community to assimilate xylose into xylonate started to decline, again without showing a

benefit towards biomass production. This trend continued until culture 25, where the ALE was terminated.

To further study the causes of the evolutionary effects seen during the ALE, culture 13 (ALE13) was chosen as a representative of the stable phase. Single clones from ALE13 were tested for growth on xylose as well as KGSADH (XylA/KsaD) enzyme activity and XylB enzyme activity from glucose-grown cells. Amongst 9 isolated clones, 3 grew on 50 g L^{-1} xylose plates (as did ALE13 itself) whereas the parental TMB4586 strain and the 6 other clones did not grow (Fig. 5B). There was an unexpected inverse correlation between growth and XylB activity, i.e. the clones that grew on xylose displayed a diminished XylB activity whereas the clones incapable of growth on xylose displayed intact XylB activities (Fig. 5B–C). The inability of these clones to grow on solid medium with xylose as the sole carbon source may be explained by the formation of the toxic Weimberg pathway intermediate xylonate. However, lack of xylonate formation alone was not sufficient to obtain growth on xylose, since xylose needs an entry point into metabolism. There are a number of endogenous reductases in *S. cerevisiae* that can act on xylose (Träff et al., 2002) and it has been shown that xylose uptake (although low) can be obtained when upregulating native oxidoreductases (Toivari et al., 2004). The well-known laboratory strain CEN.PK 113-7D, which has a substantial XR activity was indeed capable of slow aerobic growth on solid xylose medium (Fig. 5). For this reason, the main reductase gene, *GRE3*, had been deleted in all the Weimberg pathway strains used in the study. As the subpopulation that grew on xylose seemed to have strongly downregulated or completely lost the first enzyme of the Weimberg pathway, it seems plausible that the observed growth results from upregulation of other native aldose reductases triggered by the high selection pressure in the ALE; however, this could not be proven in the present case, since xylose reductase (XR) or xylitol dehydrogenase (XDH) activity could not be measured directly from the clones growing on xylose plate because the clones were unable to grow in liquid xylose medium. Enzymatic assays performed from glucose-grown clones showed, as expected, no activity (data not shown). The KGSADH activity stemming from the *ksaD* gene was retained in all the ALE13 clones and the XR/XDH enzyme assays above also ruled out that xylose was a substrate for KsaD.

To conclude, it seems that the toxicity of the xylonate affected the evolution more than the availability of extra carbon that could have been assimilated through a complete Weimberg pathway. Therefore rather than upregulating the lower Weimberg pathway the ALE community adapted to the selection pressure by downregulating the upper part of the pathway.

3.4. An increased ratio of lower to upper Weimberg pathway enzymes enables biomass assimilation in shake flasks

The unexpected effect of the ALE experiment underlined again the adverse effects of xylonate accumulation on *S. cerevisiae*. A way to address this problem would be to decrease the XylB activity to a level that matches the conversion rate of the downstream enzymes XylD, XylX and KsaD; however this would lead to an overall low carbon flux through the pathway. Instead, an increased activity of the lower Weimberg pathway enzymes was aimed for by introducing three additional copies of *xylD*, *xylX* and *ksaD* genes into strain TMB4586 (Δ fra2, xylB, xylD, xylX, ksaD). The resulting strain TMB4590 (Δ fra2, xylB, 4x(*xylD*, *xylX*, *ksaD*)) showed a fivefold higher *in vitro* activity of KGSADH compared to the single copy strain (TMB4586), both with NADH and NADPH as cofactors, whereas XylB activity was similar in all the Weimberg strains (Fig. 6).

Strain characterization in shake flask experiments in minimal medium containing glucose (5 g L^{-1}) and xylose (10 g L^{-1}) showed that the quadruple copy TMB4590 (Δ fra2, xylB, 4x(*xylD*, *xylX*, *ksaD*)) reached a $32 \pm 6\%$ higher cell dry weight compared to the CEN.PK reference strain, while the biomass concentration was not significantly

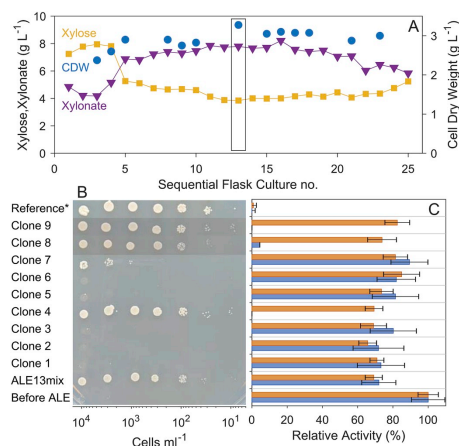


Fig. 5. Adaptive laboratory evolution of parental strain TMB4586 (Δ fra2, xylB, xylD, xylX, ksaD). A. End point (48 h) measurements of achieved cell dry weights (Circles), xylonate produced (Triangles) and residual xylose (Squares) of each sequential shake flask. During the entire experiment no residual glucose was found. Culture 13 is highlighted as a community chosen for further investigation (ALE13). B. Dot plating showing growth of reference CEN.PK 113-7D, ALE13 isolates, ALE13 total community and TMB4586 (Before ALE) on 50 g L^{-1} xylose on YNB-agar. C. KGSADH (orange) and XylB (blue) activities of corresponding clones/communities. For KGSADH the substitute substrate glutaraldehyde was used. Relative activities are shown with strain TMB4586 (Before ALE) representing 100% in each assay. The absolute enzyme activities before ALE were $0.16 \mu\text{mol min}^{-1} \text{ mg}^{-1}$ for KGSADH and $0.24 \mu\text{mol min}^{-1} \text{ mg}^{-1}$ for XylB. Standard deviations were calculated from two biological and two technical replicates. (For interpretation of the references to color in this figure legend, the reader is referred to the Web version of this article.)

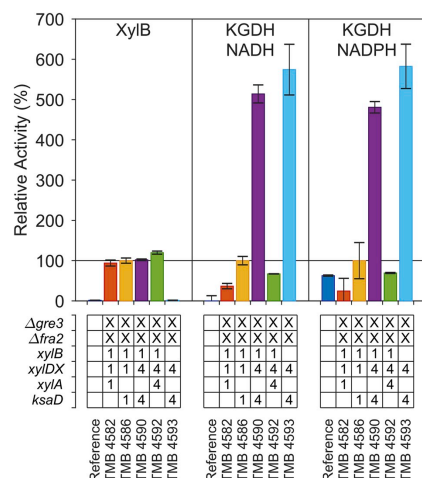


Fig. 6. Activities of xylose dehydrogenase (XylB) with xylose as substrate and NAD^+ as cofactor, and α -ketoglutarate semialdehyde dehydrogenase (KGSADH), using glutaraldehyde as a substitute substrate, with either NAD^+ or $NADP^+$ as cofactors. Relevant genotypes for the strains are reference: CEN.PK 113-7D; TMB4582: $\Delta fra2$, $xylB$ - $xylD$ - $xylX$ - $xylA$; TMB4586: $\Delta fra2$, $xylB$ - $xylD$ - $xylX$ - $ksaD$; TMB4590: $\Delta fra2$, $xylB$ - $4x(xylD$ - $xylX$ - $ksaD$); TMB4593: $\Delta fra2$, $xylB$ - $4x(xylD$ - $xylX$ - $xylA$); TMB4593: $\Delta fra2$, $4x(xylD$ - $xylX$ - $ksaD$). Relative activities are shown with strain TMB4586 representing 100% in each assay. The absolute enzyme activities for TMB4586 were $0.18 \mu\text{mol min}^{-1} \text{mg}^{-1}$ for XylB, $0.015 \mu\text{mol min}^{-1} \text{mg}^{-1}$ for KGSADH using NADH as cofactor, and $0.017 \mu\text{mol min}^{-1} \text{mg}^{-1}$ for KGSADH using NADPH as cofactor. Standard deviations were calculated from two biological and two technical replicates.

different between the single copy TMB4586 ($\Delta fra2$, $xylB$, $xylD$, $xylX$, $ksaD$) and the reference strain ($15 \pm 16\%$ increase) (Fig. 7). There were no major changes in consumed xylose and produced xylonate between the strains with one (TMB4586) and 4 (TMB4590) copies of $xylD$, $xylX$ and $ksaD$, but the xylonate yield of TMB4586 ($0.98 \text{ c-mol/c-mol xylose}$) was slightly higher than of TMB4590 ($0.91 \text{ c-mol/c-mol xylose}$). This indicated that the additional copies of $xylD$, $xylX$ and $ksaD$ enabled a higher carbon flux towards biomass synthesis in TMB4590, since an additional $0.07 \text{ C-mol/C-mol xylose}$ was made available for biomass incorporation. This agreed with the increased cell dry weight yield observed compared to the single copy strain TMB4586.

To verify that the biomass from xylose was formed via the Weimberg pathway in TMB4590 ($\Delta fra2$, $xylB$, $4x(xylD$, $xylX$, $ksaD$)) and not by upregulation of native XR and XDH enzymes, $xylB$ was deleted in TMB4590. The resulting strain TMB4593 ($\Delta fra2$, $4x(xylD$, $xylX$, $ksaD$)) that lacked XylB activity (Fig. 6) was not able to take up any xylose and grew equally well as the reference strain (Fig. 7). This confirmed that the lower Weimberg pathway, including KsaD, depended on the upper part of the Weimberg pathway for biomass synthesis in TMB4593 because other potential xylose oxido-reduction routes were not active. This also agrees with the fact that xylitol formation was not detected in any of the Weimberg strains in this experiment.

Strain TMB4582 expressing the original Weimberg pathway with *C. crescentus xylA* grew poorly in glucose and xylose media and reached a cell dry weight that was less than half of that of the reference strain. The reduced growth was also observed in rich glucose-only media in seed cultures (data not shown). The growth defect was even more pronounced when three additional copies of $xylD$, $xylX$ and $xylA$ were

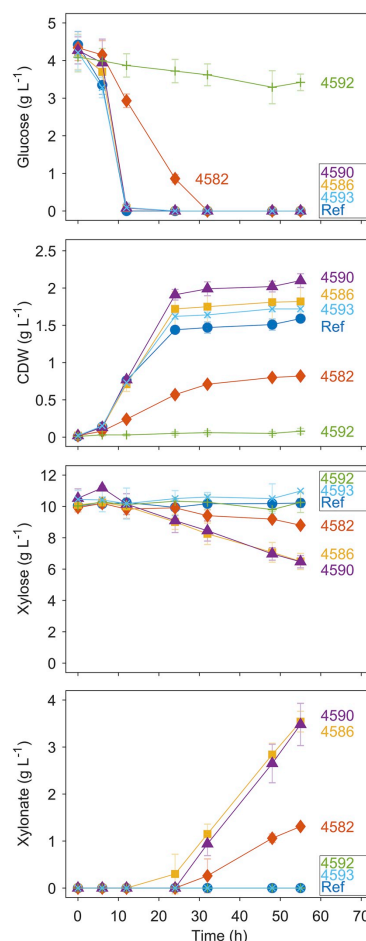


Fig. 7. Concentration profiles of glucose, xylose, cell dry weight and xylonate in shake flask cultivations in YNB medium. Six strains of *S. cerevisiae* are compared: Reference strain CEN.PK 113-7D (Circles), TMB4582 ($\Delta fra2$, $xylB$ - $xylD$ - $xylX$ - $xylA$; Diamonds), TMB4586 ($\Delta fra2$, $xylB$ - $xylD$ - $xylX$ - $ksaD$; Squares), TMB4590 ($\Delta fra2$, $xylB$ - $4x(xylD$ - $xylX$ - $ksaD$); Triangles), TMB4592 ($\Delta fra2$, $xylB$ - $4x(xylD$ - $xylX$ - $xylA$); +) and TMB4593 ($\Delta fra2$, $4x(xylD$ - $xylX$ - $ksaD$); X). Error bars indicate minimum/maximum value of duplicate experiments.

introduced, with the resulting strain TMB4592 ($\Delta fra2$, $xylB$, $4x(xylD$, $xylX$, $xylA$)) growing very poorly and even failing to consume all the glucose in the seed culture (data not shown) and in the glucose-xylose experiment (Fig. 7). The fact that both $xylA$ strains showed inhibited growth in rich media supplemented with only glucose, suggests that the issue is not solely toxic intermediates in the Weimberg pathway, but at least to some extent genotoxic effects of the gene product itself. Previous reverse transcriptase PCR experiments established that $xylA$ was

transcribed in *S. cerevisiae* (Wasserstrom et al., 2018); yet in the present study, proteomics analysis indicated that this *xyIA* transcript was not translated into a correctly folded, identifiable, protein. These results together with the clear growth defect of the *xyIA* strains even in glucose media suggests that the protein has a negative fitness effect on the cell.

3.5. TMB4590 can grow on xylose in bioreactor cultivations

Although the shake flask experiments indicated that TMB4590 ($\Delta fra2$, *xyIB*, $4x(xyID$, *xyIX*, *ksaD*)) could grow on xylose, the low biomass concentration resulted in low xylose volumetric consumption rate, which limited any difference in biomass during growth on xylose. In addition, the pH could not be maintained by the buffer system as the acidic intermediate xylonate was excreted in high concentrations, leading to a final extracellular pH of around 4. Finally, the oxygen transfer capacity in shake flask cultures was low, which may have led to oxygen deficiency preventing efficient growth through the oxidative Weinberg pathway. Therefore bioreactor experiments were carried out with strains TMB4590 ($\Delta fra2$, *xyIB*, $4x(xyID$, *xyIX*, *ksaD*)) and TMB4586 ($\Delta fra2$, *xyIB*, $1x(xyID$, *xyIX*, *ksaD*)). The experiments were set up using minimal medium in two steps: i) an initial batch phase (phase I) on glucose that lasted until depletion of all the glucose and the formed ethanol and acetate (24 h) followed by; ii) a pulse addition of glucose and xylose to allow bioconversion at high cell density (Fig. 8). In this second step two growth phases were observed: in phase II, glucose was metabolized to ethanol, acetate and biomass whereas xylose was used as the sole carbon source in phase III (Fig. 8).

For TMB4590 ($\Delta fra2$, *xyIB*, $4x(xyID$, *xyIX*, *ksaD*)), about 4 g L^{-1} of biomass was produced from 10 g L^{-1} glucose during phase I (Fig. 8A). The biomass doubled to about 8 g L^{-1} in phase II and there was a clear biomass increase of about 2 g L^{-1} in phase III during which the only available carbon source was xylose. The biomass formation during this phase was accompanied by xylose consumption and CO_2 evolution, which ceased at the time of xylose depletion and end of growth (Fig. 8C). The product yields in c-mol product/c-mol substrate (glucose + xylose) calculated from the start to the endpoint were 0.41 for biomass, 0.47 for CO_2 , 0.14 for xylonate, and 0.01 for xylitol. The total mass balance closed within 3% with these yields.

In contrast to the experiment with TMB4590 (4 copies of *xyID*, *xyIX* and *ksaD*), strain TMB4586 (1 copy of *xyID*, *xyIX* and *ksaD*) did not grow during phase III. Instead xylose was converted into xylonate at a yield of 0.87 c-mol/c-mol (Fig. 8D). For comparison, the corresponding xylonate yield for TMB4590 during phase III was 0.43 c-mol/c-mol xylose and the main other products were biomass (0.26 c-mol/c-mol) and CO_2 (0.35 c-mol/c-mol). This meant that more than half of the carbon was metabolized through the entire Weinberg pathway and the xylose conversion rate through the Weinberg pathway was high enough to enable growth.

3.6. Weinberg intermediate analysis indicates *XyID* as remaining rate limiting step

Further understanding of the limiting steps in the implemented Weinberg pathway was attempted by measuring whether pathway intermediates other than xylonate could be detected using the more sensitive LC-MS method. Samples were taken from the endpoint of the shake flask experiments with all the strains and from all time-points of the bioreactor experiment with TMB4590 (Fig. 9).

Xylonolactone, the product of *XyIB* activity, was found in shake flask cultures of all strains except the CEN.PK reference and the *xyIB*-inactivated strain TMB4593 ($\Delta fra2$, $4x(xyID$, *xyIX*, *ksaD*)), which confirmed that no other sources of *XyIB* activity were present in the strain background. In bioreactor experiments the xylonolactone concentration rose quickly after addition of xylose and thereafter remained on a stable level as the substrate was consumed. Altogether this confirmed earlier results (Salusjärvi et al., 2017; Wasserstrom et al., 2018) pointing out

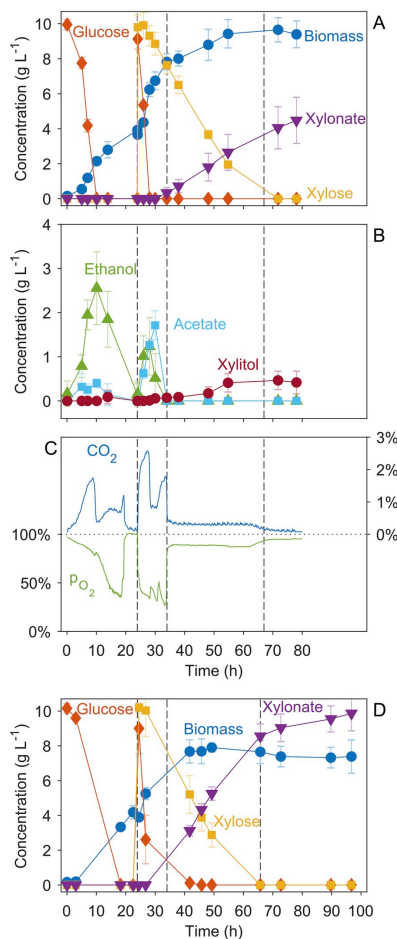


Fig. 8. Bioreactor experiment with *S. cerevisiae* TMB4590 ($\Delta fra2$, *xyIB*- $4x(xyID$, *xyIX*, *ksaD*)) in panels A–C and TMB4586 ($\Delta fra2$, *xyIB*-*xyID*-*xyIX*-*ksaD*) in panel D. The experiment used a fed-batch setup, and dashed lines separate the cultivation into phases: I) on only glucose; II) on glucose and xylose; III) on only xylose and IV) stationary phase. A & D. Concentration profile of glucose (Diamonds), xylose (Squares), cell dry weight (Circles) and xylonate (Triangles) for TMB4590 and TMB4586 respectively. B. Concentration profiles of ethanol (Triangles), acetate (Squares) and xylitol (Circles) for TMB4590. C. Concentration profiles of the off-gas CO_2 (top, blue) and dissolved oxygen ($p\text{O}_2$) in the cultivation medium (bottom, green) for TMB4590. Error bars indicate standard deviation of three experiments for TMB4590 and two experiments for TMB4586. (For interpretation of the references to color in this figure legend, the reader is referred to the Web version of this article.)

XyID as an enzyme for which sufficient activity is difficult to achieve in *S. cerevisiae*.

On the one hand, 2-keto-3-deoxyxylonate, the product of *XyID*

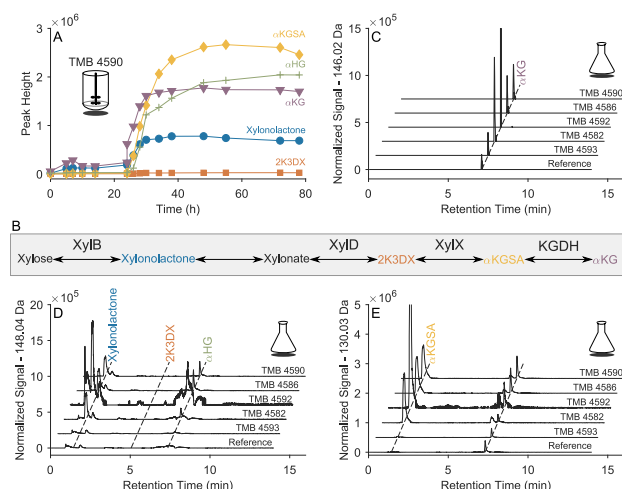


Fig. 9. LC-MS analysis of extracellular Weimberg pathway metabolites. A. Peak height of Weimberg metabolites over the bioreactor experiment with TMB4590 (Δ *fra2*, *xyIB*, *4x(xyID)*, *xyIX*, *ksaD*). B. Scheme of Weimberg intermediates with corresponding color code. C-E. Weimberg metabolites at the end points (56 h) of shake flask experiments for the following strains: GEN.PK113-7D (reference), TMB4593 (Δ *fra2*, *4x(xyID)*, *xyIX*, *ksaD*), TMB4582 (Δ *fra2*, *xyIB*, *1x(xyID)*, *xyIX*, *ksaD*), TMB4592 (Δ *fra2*, *xyIB*, *4x(xyID)*, *xyIX*, *ksaD*), TMB4586 (Δ *fra2*, *xyIB*, *1x(xyID)*, *xyIX*, *ksaD*), TMB4590 (Δ *fra2*, *xyIB*, *4x(xyID)*, *xyIX*, *ksaD*). Chromatographic profiles are given for different masses at 146.02 Da (C), 148.04 Da (D) and 130.03 Da (E). Mass abundance is normalized to cell concentration in shake flasks. (For interpretation of the references to color in this figure legend, the reader is referred to the Web version of this article.)

activity, was not found in any of the samples. On the other hand, α -ketoglutarate semialdehyde, the product of the fourth enzyme *XylX* (Fig. 1), was detected in all samples (except the reference strain and TMB4593). This indicated that *XylD* activity was probably not a rate-controlling step at the present stage. Also α -ketoglutarate semialdehyde levels were lower in the strains carrying *ksaD*, confirming the better efficiency of the *C. glutamicum* enzyme in the last step.

α -ketoglutarate was found in all shake flask cultures, which was expected since it is part of the TCA-cycle and can be transported in and out of the mitochondria via specific antiporters (Castegna et al., 2010; Palmieri et al., 2006). In the bioreactor experiments with TMB4590 (Δ *fra2*, *xyIB*, *4x(xyID)*, *xyIX*, *ksaD*) the excreted α -ketoglutarate was low during the glucose phase and quickly increased after the xylose pulse, supporting the hypothesis that the Weimberg pathway led to some α -ketoglutarate accumulation. Also another compound with the same monoisotopic molecular weight (184.04 Da) as xylonolactone and 2-keto-3-deoxyxylonate was detected during the xylose phase. It was identified as α -hydroxyglutarate, a compound that *S. cerevisiae* can form from α -ketoglutarate by cytosolic α -ketoglutarate reductases (Becker-Kettern et al., 2016). This further reinforced that cytosolic α -ketoglutarate was formed from xylose.

4. Conclusion

In the present study, xylose assimilation to α -ketoglutarate via the Weimberg pathway was demonstrated for the first time in a fungal species. An active pathway was obtained by introducing several modifications in the previously constructed strain TMB4530 carrying one copy of *C. crescentius xyIB/xyID/xyIX/xyIA* genes (Wasserstrom et al., 2018). First, the non-functional *XylA* enzyme was replaced by a more efficient analog from *C. glutamicum*, *KsaD*; secondly, Fe-S metabolism was upregulated by deleting the native *FRA2* gene, with the aim to increase *XylD* activity and finally, multiple gene copies of the lower part of the pathway enzymes (*XylD*, *XylX* and *KsaD*) were introduced. In the resulting strain, TMB4590, up to 57% of the carbon was metabolized into biomass and carbon dioxide. This opens the road for the production of carboxylic acids and diols from xylose, via α -ketoglutarate and the Weimberg route in fungal species.

Financial support

This work was supported by the European Union Commission (FP7 bioREFINE2G, project no. 613771) and by the Swedish Research Council (VR, Grant. No. 2015–06817) as part of the project “XyloCut – Shortcut to the carbon efficient microbial production of chemical building blocks from lignocellulose-derived D-xylose”, which is embedded in the ERASysAPP framework.

Declaration of interest

None.

Acknowledgements

We would like to thank Jan Marienhagen for providing us with the *KsaD* gene and protein sequences at an early stage. We would also like to thank the members of the XyloCut consortium for fruitful discussion and Herje Schagerlör for sharing his valuable insights in mass spectroscopy.

Annex A and B. Supplementary material and data

Supplementary material and data to this article can be found online at <https://doi.org/10.1016/j.jmben.2019.05.010>.

References

- Abbott, D.A., Zelle, R.M., Pronk, J.T., Van Maris, A.J.A., 2009. Metabolic engineering of *Saccharomyces cerevisiae* for production of carboxylic acids: current status and challenges. *FEMS Yeast Res.* 9, 1123–1136.
- Almqvist, H., Sandahl, M., Lidén, G., 2017. A rapid method for analysis of fermentatively produced D-xylonate using ultra-high performance liquid chromatography and evaporative light scattering detection. *Biosci. Biotech. Biochem.* 81, 1078–1080.
- Andberg, M., Aro-Kärkkäinen, N., Carlson, P., Oja, M., Bozonnet, S., Toivari, M., Hakulinen, N., O'Donoghue, M., Penttinen, M., Koivula, A., 2016. Characterization and mutagenesis of two novel iron-sulphur cluster pentonate dehydratases. *Appl. Microbiol. Biotechnol.* 100, 7549–7563.
- Bai, W.Q., Tai, Y.S., Wang, J.Y., Wang, J.L., Jambunathan, P., Fox, K.J., Zhang, K.C., 2016. Engineering nonphosphorylative metabolism to synthesize mesaconate from lignocellulosic sugars in *Escherichia coli*. *Metab. Eng.* 38, 285–292.
- Becker-Kettern, J., Paczia, N., Conrotte, J.F., Kay, D.P., Guignard, C., Jung, P.P., Linster, J., 2016. Engineering of *Escherichia coli* for the production of D-xylonolactone and D-xylonolactone derivatives. *Metab. Eng.* 38, 293–302.

- C.L., 2016. *Saccharomyces cerevisiae* forms D-2-hydroxyglutarate and couples its degradation to D-lactate formation via a cytosolic transhydrogenase. *J. Biol. Chem.* 291, 6036–6058.
- Borodina, I., Nielsen, J., 2014. Advances in metabolic engineering of yeast *Saccharomyces cerevisiae* for production of chemicals. *Biotechnol. J.* 9, 609–620.
- Bradford, M.M., 1976. A rapid and sensitive method for the quantitation of microgram quantities of protein utilizing the principle of protein-dye binding. *Anal. Biochem.* 72, 248–254.
- Brüsseler, C., Späth, A., Sokolowsky, S., Marienhagen, J., 2019. Alone at last - Heterologous expression of a single gene is sufficient for establishing the five-step Weinberg pathway in *Corynebacterium glutamicum*. *Metab. Eng. Commun.* 9, e00090.
- Buijs, N.A., Siewers, V., Nielsen, J., 2013. Advanced biofuel production by the yeast *Saccharomyces cerevisiae*. *Curr. Opin. Chem. Biol.* 17, 480–488.
- Castegna, A., Scarcia, P., Agrimi, G., Palmieri, L., Rottensteiner, H., Spera, L., Germinario, L., Palmieri, F., 2010. Identification and functional characterization of a novel mitochondrial carrier for citrate and oxoglutarate in *Saccharomyces cerevisiae*. *J. Biol. Chem.* 285, 17359–17370.
- Dahms, A.S., 1974. 3-Deoxy-D-pentulosonic acid aldolase and its role in a new pathway of D-xylose degradation. *Biochem. Biophys. Res. Commun.* 60, 1433–1439.
- Du Preez, J.C., Prior, B.A., 1985. A quantitative screening of some xylose-fermenting yeast isolates. *Biotechnol. Lett.* 7, 241–246.
- Entian, K.-D., Kötter, P., 2007. Yeast genetic strain and plasmid collections. In: In: Stanfield, L., Stark, M.J.R. (Eds.), *Methods in Microbiology*, vol. 36. Academic Press, pp. 629–666.
- Hahn-Hägerdal, B., Karhumaa, K., Fonseca, C., Spencer-Martins, I., Gorwa-Grauslund, M.F., 2007. Towards industrial pentose-fermenting yeast strains. *Appl. Microbiol. Biotechnol.* 74, 937–953.
- Jeffries, T.W., 1983. Utilization of Xylose by Bacteria, Yeasts, and fungi., Pentoses and Lignin. Springer, pp. 1–32.
- Jessop-Fabre, M.M., Jakóciunas, T., Stovicek, V., Dai, Z., Jensen, M.K., Keasling, J.D., Borodina, I., 2016. EasyClone-MarkerFree: a vector toolkit for marker-less integration of genes into *Saccharomyces cerevisiae* via CRISPR-Cas9. *Biotechnol. J.* 11, 1110–1117.
- Johnsen, U., Dambbeck, M., Zais, H., Fuhrer, T., Soppa, J., Sauer, U., Schonheit, P., 2009. D-Xylose degradation pathway in the halophilic archaeon *Haloflexax volcanii*. *J. Biol. Chem.* 284, 27290–27303.
- Kim, S.R., Park, Y.C., Jin, Y.S., Seo, J.H., 2013. Strain engineering of *Saccharomyces cerevisiae* for enhanced xylose metabolism. *Biotechnol. Adv.* 31, 851–861.
- Krivoruchko, A., Zhang, Y., Siewers, V., Chen, Y., Nielsen, J., 2015. Microbial acetyl-CoA metabolism and metabolic engineering. *Metab. Eng.* 28, 28–42.
- Liu, H., Valdehuesa, K.N.G., Nisola, G.M., Ramos, K.R.M., Chung, W.J., 2012. High yield production of D-xylonic acid from D-xylose using engineered *Escherichia coli*. *Bioresour. Technol.* 115, 244–248.
- Meijnen, J.P., de Winde, J.H., Ruijsendaal, H.J., 2009. Establishment of oxidative D-xylose metabolism in *Pseudomonas putida* S12. *Appl. Environ. Microbiol.* 75, 2784–2791.
- Mutturi, R., Palmqvist, B., Lidén, G., 2014. In: Waldron, K. (Ed.), *Advances in Biorefineries*. Woodhead Publishing, pp. 259–302.
- Paddon, C.J., Westfall, P.J., Pitera, D.J., Benjamin, K., Fisher, K., McPhee, D., Leavell, M.D., Tai, A., Main, A., Eng, D., Polichuk, D.R., Teoh, K.H., Reed, D.W., Treynor, T., Lenihan, J., Fleck, M., Bajad, S., Dang, G., Dengrove, D., Diola, D., Dorin, G., Ellens, K.W., Fickes, S., Galazzo, J., Gaucher, S.P., Geistlinger, T., Henry, R., Hepp, M., Horning, T., Iqbal, T., Jiang, H., Kizer, L., Lieu, B., Melis, D., Moss, N., Regentin, R., Secret, S., Tsuruta, H., Vazquez, R., Westbladt, L.F., Xu, L., Yu, M., Zhang, Y., Zhao, L., Lievens, J., Covello, P.S., Keasling, J.D., Reiling, K.K., Renninger, N.S., Newman, J.D., 2013. High-level semi-synthetic production of the potent antimalarial artemisinin. *Nature* 496, 528–532.
- Palmieri, F., Agrimi, G., Blanco, E., Castegna, A., Noia, M.A., Iacobazzi, V., Lasorsa, F.M., Marobio, C.M.T., Palmieri, L., Scarcia, P., 2006. Identification of mitochondrial carriers in *Saccharomyces cerevisiae* by transport assay of reconstituted recombinant proteins. *Biochim. Biophys. Acta Bioenerg.* 1757, 1249–1262.
- Radek, A., Krumbach, K., Gägens, J., Wendisch, V.F., Wiechert, W., Bott, M., Noack, S., Marienhagen, J., 2014. Engineering of *Corynebacterium glutamicum* for minimized carbon loss during utilization of D-xylose containing substrates. *J. Biotechnol.* 192, 156–160.
- Radek, A., Tenhaef, N., Muller, M.F., Brüsseler, C., Wiechert, W., Marienhagen, J., Polen, T., Noack, S., 2017. Miniaturized and automated adaptive laboratory evolution: evolving *Corynebacterium glutamicum* towards an improved D-xylose utilization. *Bioresour. Technol.* 245, 1377–1385.
- Rossoni, L., Carr, R., Baxter, S., Cortis, R., Thorpe, T., Eastham, G., Stephens, G., 2018. Engineering *Escherichia coli* to grow constitutively on D-xylose using the carbon-efficient Weinberg pathway. *Microbiology* 164, 287–298.
- Salusjärvi, L., Toivari, M., Vehkomäki, M.L., Koivistoinen, O., Mojitza, D., Niemela, K., Penttilä, M., Ruohonen, L., 2017. Production of ethylene glycol or glycolic acid from D-xylose in *Saccharomyces cerevisiae*. *Appl. Microbiol. Biotechnol.* 101, 8151–8163.
- Sandström, A.G., Almqvist, H., Portugal-Nunes, D., Neves, D., Lidén, G., Gorwa-Grauslund, M.F., 2014. *Saccharomyces cerevisiae*: a potential host for carboxylic acid production from lignocellulosic feedstock? *Appl. Microbiol. Biotechnol.* 98, 7299–7318.
- Solis-Escalante, D., Kuijpers, N.G., Nadine, B., Bolat, I., Bosman, L., Pronk, J.T., Daran, J.-M., Pascale, D.-L., 2013. amdSYM, a new dominant recyclable marker cassette for *Saccharomyces cerevisiae*. *FEMS Yeast Res.* 13, 126–139.
- Stovicek, V., Borodina, I., Forster, J., 2015. CRISPR-Cas system enables fast and simple genome editing of industrial *Saccharomyces cerevisiae* strains. *Metab. Eng. Commun.* 2, 13–22.
- Taxis, C., Knop, M., 2006. System of centromeric, episomal, and integrative vectors based on drug resistance markers for *Saccharomyces cerevisiae*. *Biotechniques* 40, 73–78.
- Toivari, M., Salusjärvi, L., Ruohonen, L., Penttilä, M., 2004. Endogenous xylose pathway in *Saccharomyces cerevisiae*. *Appl. Environ. Microbiol.* 70, 3681–3686.
- Toivari, M., Nygård, Y., Kumpulainen, E.-P., Vehkomäki, M.-L., Benčina, M., Valkonen, M., Masheimo, H., Andberg, M., Koivula, A., Ruohonen, L., 2012. Metabolic engineering of *Saccharomyces cerevisiae* for bioconversion of D-xylose to D-xylonate. *Metab. Eng.* 14, 427–436.
- Träff, K.L., Jonsson, L.J., Hahn-Hägerdal, B., 2002. Putative xylose and arabinose reductases in *Saccharomyces cerevisiae*. *Yeast* 19, 1233–1241.
- Unrean, P., Gatgens, J., Klein, B., Noack, S., Champreda, V., 2018. Elucidating cellular mechanisms of *Saccharomyces cerevisiae* tolerant to combined lignocellulosic-derived inhibitors using high-throughput phenotyping and multiomics analyses. *FEMS Yeast Res.* 18, foy106.
- Voges, R., Noack, S., 2012. Quantification of proteome dynamics in *Corynebacterium glutamicum* by (15)N-labeling and selected reaction monitoring. *J. Proteom.* 75, 2660–2669.
- Wang, P.Y., Johnson, B.F., Schneider, H., 1980. Fermentation of D-xylose by yeasts using glucose isomerase in the medium to convert D-xylose to D-xylulose. *Biotechnol. Lett.* 2, 273–278.
- Wang, J., Shen, X.L., Lin, Y.H., Chen, Z.Y., Yang, Y.P., Yuan, Q.P., Yan, Y.J., 2018. Investigation of the synergetic effect of xylose metabolic pathways on the production of glutaric acid. *ACS Synth. Biol.* 7, 24–29.
- Wasserstrom, L., Portugal-Nunes, D., Almqvist, H., Sandström, A.G., Lidén, G., Gorwa-Grauslund, M.F., 2018. Exploring D-xylose oxidation in *Saccharomyces cerevisiae* through the Weinberg pathway. *Amb. Express* 8, 33.
- Watanabe, S., Fukumori, F., Nishiwaki, H., Sakurai, Y., Tajima, K., Watanabe, Y., 2019. Novel non-phosphorylative pathway of pentose metabolism from bacteria. *Sci. Rep.* 9, 155.
- Weinberg, R., 1961. Pentose oxidation by *Pseudomonas fragi*. *J. Biol. Chem.* 236, 629–635.

Supporting Information[†] for:

Identification of modifications procuring growth on xylose in recombinant *Saccharomyces cerevisiae* strains carrying the Weimberg pathway

Celina Borgström^{a,1}, Lisa Wasserstrom^{a,1,2}, Henrik Almqvist^{b,1}, Kristina Broberg^{b,3}, Bianca Klein^c, Stephan Noack^{c,d}, Gunnar Lidén^b & Marie F Gorwa-Grauslund^{a,*}

^a Division of Applied Microbiology, Department of Chemistry, Lund University, PO Box 124, 221 00 Lund, Sweden

^b Department of Chemical Engineering, Lund University, PO Box 124, 221 00, Lund, Sweden

^c Institute of Bio- and Geosciences, IBG-1: Biotechnology, Forschungszentrum Jülich GmbH, Jülich, D-52425, Germany

^d Bioeconomy Science Center (BioSC), Forschungszentrum Jülich GmbH, Jülich, D-52425, Germany

*Corresponding author

E- mail: Marie-Francoise.Gorwa@tmb.lth.se

¹ Equal contributions

² Present address: Department of clinical Microbiology, Division of Laboratory Medicine, Lund University Hospital, Lund, Sweden

³ Present address: RISE AB, Ideon Science Park, Beta5, Scheelevägen 17, 223 70 Lund, Sweden

[†] Reformatted for increased readability by Celina Borgström Tufvegren

Supplementary Material - Borgström et al.

Annex A: Molecular biology methods and yeast strain construction

A.1 General molecular biology methods

For *S. cerevisiae*, competent yeast cells were prepared and transformed according to the high efficiency LiAc protocol (Gietz and Schiestl, 2007) but DMSO (10 % v/v) was added before heat shock at 42 °C for 20 min (Hill et al., 1991). *Escherichia coli* strain NEB5- α (New England Biolabs, Ipswich, MA, USA) was used for sub-cloning of plasmid DNA; cells were grown at 37 °C in Luria–Bertani (LB) broth containing 5 g L⁻¹ yeast extract, 10 g L⁻¹ peptone, 5 g L⁻¹ NaCl, pH 7.5. *E. coli* competent cells were prepared using the RbCl method (Green and Rogers, 2013) and transformants were selected on LB agar plates (15 g L⁻¹ agar) supplemented with 50 mg L⁻¹ ampicillin for 16 h at 37 °C.

Genomic *S. cerevisiae* DNA used for PCR amplification was extracted by boiling in 0.02 M NaOH for 10 minutes. All primers (Table A1) were purchased from Eurofins MWG Operon (Ebersberg, Germany). The FastDigest restriction enzymes, T4 ligase and DNA polymerase were obtained from Thermo Fisher Scientific (Waltham, MA, USA). All chemicals and sugars were purchased from Sigma Aldrich (St. Louis, MO, USA). Sanger sequencing of the constructed plasmid was done by Eurofins MWG Operon (Ebersberg, Germany). For diagnostic PCR reactions, DreamTaq DNA polymerase was used while cloning PCRs used Phusion Hot Start II Polymerase. GeneJET kits (Thermo Fisher Scientific) were used for extraction of plasmids, PCR products and agarose gels.

A.2 Plasmid and targeting fragment construction

Corynebacterium glutamicum gene *ksaD* was codon-optimized for *S. cerevisiae* and ordered using GeneArt (Thermo Fisher Scientific, Waltham, MA, USA). The gene sequence was retrieved from (Brüsseler et al., 2019).

pUGamdSYM2-*xylD*-*xylX*-*ksaD* (LWA45) was constructed by cleaving out *xylA* from the previously constructed plasmid AGS8 (Wasserstrom et al., 2018) using *PmeI*. The *ksaD* ORF was amplified from pUC-*ksaD* using primers 344/345 that contained 15 bp homology flanks to *PmeI* digested pAGS8. After verification of the fragments by agarose gel electrophoresis (AGE) the correct band was extracted. The vector and *ksaD* were combined using the In-Fusion HD Enzyme Mix (Takara Bio USA Inc., Mountain View, CA, USA) and transformed into *E. coli* NEB5- α .

p426-*GPD2p*-*ksaD*-*CYC1t* (LWA48) was constructed by cleaving out *ksaD* from pUC-*ksaD* using *Bam*HI and *Xho*I and ligating the fragment into the p426-*GPD2p* vector (Mumberg et al., 1995).

p426-*GPD2p*-*xylA*-*CYC1t* (LWA49) was constructed by PCR amplification of the *xylA* ORF from AGS8HB (Wasserstrom et al., 2018) and ligation into the *Bam*HI/*Xho*I restriction sites of the p426-*GPD2p* vector (Mumberg et al., 1995).

The *ksaD*-amdSYM PCR cassette for replacement of *xylA* in strain TMB4582 was constructed using overlap extension PCR. Three fragments, the *TPH* promoter, the *ksaD* ORF/*CYC1* terminator and the amdSYM marker were PCR amplified using primers 314/315, 316/329 and 328/330, respectively. The template for *TPH*p was genomic CEN.PK 113-7D DNA, for *ksaD*-

CYC1t plasmid LWA48 and for amdSYM plasmid pUGamdSYM. The three fragments contained 40 bp overlap to each other and could therefore be assembled using overlap extension PCR (OE-PCR).

To insert 3 more copies of the fragment containing *xylD*, *xylX* and *ksaD* into strain TMB4586, the CRISPR-Cas9 system was used together with a triple gRNA (pCfB3053) that enables simultaneous marker-less integration in the three intergenic regions named X-2, XI-5 and XII-4 (Jessop-Fabre et al., 2016). For the XII-4 region, the *xylD/xylX/ksaD* fragment was cleaved out from plasmid LWA45 using *EheI/AscI* and it was ligated into the vector pCfB3040 linearized with *PmiI/AscI*. The resulting vector containing *xylD*, *xylX* and *ksaD* with XII-4 homology regions upstream and downstream to the gene cassette was named LWA46. A similar strategy was tested for the other two regions (X-2 and XI-5) but was not successful; therefore a PCR based approach was used instead. 5' and 3' targeting fragments for the X-2 and XI-5 integration sites were amplified from pCfB2899 and pCfB3037, respectively, with specific primers that contained tails with homology to the *xylD-xylX-ksaD* gene cassette released from LWA45 by *EheI/AscI* cleaving. The X-2 fragments were amplified from pCfB2899 using primer pairs 346/347 (5') and 348/245 (3'), while amplification of the XI-5 region was done with primer pairs 349/350 (5') and 351/243 (3'). Primers 347 and 350 had 50 bp homology to the 5' end of LWA45 while primers 348 and 351 had 50 bp homology to the 3' end.

For integration of *xylD*, *xylX* and *xylA* from pAGS8 into TMB4582, the same targeting fragments were used as for integration of LWA45 (*xylD-xylX-ksaD*) into TMB4582 since the flanking regions are the same. About 200-600 bp of the 5' upstream region and 3' downstream region of X-2 and XI-5 was amplified from pCfB2899 and pCfB3037 as described above. In addition, targeting fragments for the XII-4 region were amplified from pCfB3040 using primer pairs 352/353 (5') and 354/355 (3'). The PCR products were verified using AGE and the 5' and 3' fragments for each integration site (X-2, XI-5, XII-4) were pooled together before ethanol precipitation using Novagen pellet paint (Thermo Fisher Scientific, Waltham, MA, USA).

For deletion of *xylB* in TMB4590 a PCR based gene targeting cassette was constructed using pUG-amdSYM as template and primers 356/357 (50 bp homology to *xylB* each).

FRA2 was deleted in strain TMB4530 using PCR based gene targeting and the hygromycin marker encoded by *hphNT1*. The *FRA2 hphNT1* deletion cassette was amplified from pRS305H (Taxis and Knop, 2006) using primers 325/326 that contained 50 bp homology flanks to the upstream and downstream region of the *FRA2* ORF.

A.3 Yeast strain engineering

All yeast strains were constructed in the CEN.PK 113-5D and CEN.PK 113-7D backgrounds as well as in the derived strain TMB4530 containing the Weimberg pathway from *C. crescentus* (Wasserstrom et al., 2018). A schematic picture of all constructed strains and their connection is given in Figure 2.

Transformants generated using the CRISPR-Cas9 system (Stovicek et al., 2015) were selected on YPD medium supplemented with 200 mg L⁻¹ geneticin and 100 mg L⁻¹ nourseothricin (Jena Bioscience, Germany) to allow selection of the Cas9-kanMX and gRNA-natMX plasmids. For transformants carrying the hygromycin resistance gene *hphNT1*, selection was performed using

YPD supplemented with 200 mg L⁻¹ hygromycin B. When *amdSYM* was used as a selection marker, transformants were plated on synthetic medium containing 600 mg L⁻¹ acetamide as the sole nitrogen source (SM-Ac), following the protocol described by Solis-Escalante et al. (2013). To select for cells that had recycled the *amdSYM* marker, cells were plated on SM containing 2.3 g L⁻¹ fluoroacetamide (SM-FAc).

A.3.1 Construction of strain TMB4582

To delete the wild type *FRA2* gene, the *fra2::hphNT1* deletion cassette was transformed into TMB4530 and correct integration was verified using diagnostic PCR with primer pairs 332/7 (5' integration), 333/336 (3' integration) and 334/335 (internal *FRA2* primers). The verified strain was saved as TMB4582.

A.3.2 Construction of strain TMB4586

To replace *xylA* with *ksaD* in strain TMB4582 a PCR based method was used with *amdSYM* as a selection marker, as described above. The final cassette contained *TPIIp-ksaD-CYC1t-amdSYM* with homology upstream and downstream to *xylA* in TMB4582. Transformants were selected on SM-Ac and correct integration was validated using primers 311/312 that amplify *ksaD* and primers 5 and 87 that anneal to *amdSYM* in the gene cassette and the *GRE3* locus present downstream of the integration site, respectively. Removal of *xylA* was verified with primers 222/223. Verified clones were sequenced and several point mutations were detected, however none leading to an amino acid replacement. The *amdSYM* marker was recycled as previously described (Solis-Escalante et al., 2013). *amdSYM* marker removal was confirmed with primers 311 and 87 and the strain was saved as TMB4586.

A.3.3 Construction of strain TMB4590

Three more copies of *xylD*, *xylX* and *ksaD* present in LWA45 were integrated into the three intergenic regions X-2, XI-5 and XII-4 in TMB4586 using CRISPR-Cas9 (Jessop-Fabre et al., 2016) and *in vivo* recombination. For integration in the X-2 and XI-5 loci, targeting fragments was prepared by PCR as described above, while integration in XII-4 was done by using the XII-4-*xylD-xylX-ksaD*-XII-4 cassette present on plasmid LWA46. Subsequently, TMB4586 expressing pCas9-kanMX was transformed with multiple fragments and plasmids including the gRNA plasmid pCfB3053, the X-2 and XI-5 targeting fragments, the gene cassette XII-4-*xylD-xylX-ksaD*-XII-4 cleaved out from LWA46 and the *xylD*, *xylX* and *ksaD* gene cassette released from LWA45. Correct integration of *xylD*, *xylX* and *ksaD* into X-2, XI-5 and XII-4 was verified with primer pairs 311/249, 311/250 and 311/251, respectively. The verified strain was saved as TMB4590.

A.3.4 Construction of strain TMB4592

As a control strain, three more copies of *xylD*, *xylX* and *xylA* present on pAGS8 were integrated into the three intergenic regions X-2, XI-5 and XII-4 in TMB4582 using CRISPR-Cas9 as described above. First, an intermediate strain, TMB4591, was constructed by integration of *xylD*, *xylX*, *xylA* into the X-2 locus. TMB4582 was transformed with targeting fragments for X-2, plasmid pAGS8 cleaved with *EheI*/*AscI* and the gRNA plasmid pCfB3020. The strain was verified using primers 222/249. Into this strain two more copies of *xylD*, *xylX*, *xylA* were

integrated into loci XI-5 and XII-4. TMB4591 expressing Cas9-kanMX was transformed with the targeting fragments for XI-5 and XII-4, the *xyiD-xyiX-xyiA* gene cassette released from pAGS8 and the gRNA plasmid pCfB3053. Correct integration of *xyiD*, *xyiX* and *xyiA* into XI-5 and XII-4 was verified with primer pairs 222/250 and 222/251, respectively. The verified strain was saved as TMB4592.

A.3.5 Construction of strain TMB4593

To construct another control strain, *xyiB* was deleted in strain TMB4590 resulting in strain TMB4593 containing four copies of *xyiD*, *xyiX* and *ksaD*. TMB4593 was generated by transforming the *xyiB* PCR fragment described above into TMB4590 and selecting for transformants on SM-Ac. Deletion of *xyiB* was verified by diagnostic PCR using primers 65/6 (5' integration), 5/38 (3' integration) and 224/225 (internal *xyiB* primers).

A.3.6 Construction of strain TMB4594 and TMB4595

Two strains were made that contained episomal plasmids overexpressing *ksaD* and *xyiA* by transforming CEN.PK 113-5D (*ura3⁻*) with the plasmids LWA48 (p426-*ksaD*) and LWA49 (p426-*xyiA*). Transformants were selected in YNB media supplemented with 20 g L⁻¹ glucose. Verified strains were saved as TMB4594 (*ksaD*) and TMB4595 (*xyiA*).

References

- Brüsseler, C., Späth, A., Sokolowsky, S., Marienhagen, J., 2019. Alone at last! - Heterologous expression of a single gene is sufficient for establishing the five-step Weimberg pathway in *Corynebacterium glutamicum*. *Metabolic Engineering Communications*. 9, e00090.
- Gietz, R. D., Schiestl, R. H., 2007. High-efficiency yeast transformation using the LiAc/SS carrier DNA/PEG method. *Nature protocols*. 2, 31-34.
- Green, R., Rogers, E. J., 2013. Transformation of chemically competent *E. coli*. *Methods Enzymol*. 529, 329-36.
- Hill, J., Donald, K. A., Griffiths, D. E., Donald, G., 1991. DMSO-enhanced whole cell yeast transformation. *Nucleic Acids Research*. 19, 5791-5792.
- Jessop-Fabre, M. M., Jakočiūnas, T., Stovicek, V., Dai, Z., Jensen, M. K., Keasling, J. D., Borodina, I., 2016. EasyClone-MarkerFree: A vector toolkit for marker-less integration of genes into *Saccharomyces cerevisiae* via CRISPR-Cas9. *Biotechnology Journal*. 11, 1110-1117.
- Mumberg, D., Muller, R., Funk, M., 1995. Yeast vectors for the controlled expression of heterologous proteins in different genetic backgrounds. *Gene*. 156, 119-22.
- Solis-Escalante, D., Kuijpers, N. G., Nadine, B., Bolat, I., Bosman, L., Pronk, J. T., Daran, J.-M., Pascale, D.-L., 2013. amdSYM, a new dominant recyclable marker cassette for *Saccharomyces cerevisiae*. *FEMS Yeast Research*. 13, 126-139.
- Stovicek, V., Borodina, I., Forster, J., 2015. CRISPR-Cas system enables fast and simple genome editing of industrial *Saccharomyces cerevisiae* strains. *Metabolic Engineering Communications*. 2, 13-22.

- Taxis, C., Knop, M., 2006. System of centromeric, episomal, and integrative vectors based on drug resistance markers for *Saccharomyces cerevisiae*. *Biotechniques*. 40, 73-78.
- Wasserstrom, L., Portugal-Nunes, D., Almqvist, H., Sandström, A. G., Lidén, G., Gorwa-Grauslund, M. F., 2018. Exploring D-xylose oxidation in *Saccharomyces cerevisiae* through the Weimberg pathway. *AMB Express*. 8, 33.

Table A1. List of primers used in the present study. Uppercase letters indicate the primer annealing region while lowercase contains extra features such as enzyme cleavage sites or homology regions. Bold lowercase letters indicate a direct repeat region in the primer.

Name	Amplification target	Sequence (5' to 3')
5_ amdSYM down	amdSYM	CCAGATGCGAAGTTAAGTGC
7_ kanMXTEFp up	TEFp	GCACGTCAAGACTGTCAAGG
87_3'GRE3_r_AGS7	GRE3	GCTTTGCTCTCTTGGTGTCT
103_gRNA SNR52p_r	gRNA	GATCATTTATCTTTCACTGC
222_RT_XYLA_f	<i>xylA</i>	TACATTGACATTGCCGCATC
223_RT_XYLA_r	<i>xylA</i>	ATGATAGTCAACTCCCCGACG
243_XI-5down_r	XI-5	GAGAAAACAACAACCACCTGG
245_X2down_rev	X-2	AGACGTAAAGTCAGGCAAGG
249_X-2 ver	X-2	ACGCCACCAAGACAATATCC
250_XI-5 ver	XI-5	CACAGTGTACCAACGATTCC
251_XII-4 ver	XII-4	GTGAAATCTCTTTGCGGTAG
310_gRNA-xylA	gRNA	gacattgccgcatcagaggggttttagagctagaaatagcaag
311_cg0535_RT-PCR_f	cg0535	CAGATCAATTGCACCAAGTC
312_cg0535_RT-PCR_r	cg0535	TCACCTATCGATTTCTCTTGG
314_TPI1p_f	TPI1p	cccgacagggaaggcctatagcaccacaatactgacagta ctaaataattTATATCTAGGAACCCATCAG
315_TPI1p_r	TPI1p	ccgtgcaaggcagtagcagtaaatcatTTTTAGTTTA TGTATGTGTT
316_cg0535_TPI1pflank	cg0535	aacacatacataaactaaaaATGATTACTGCTAC TGCCTT
320_OE-PCR_f	TPI1p	CCCGACAGGGAAGGCCTATAGC
325_FRA2del5'Hyg_FW	pRS305H	tccgactgtgtattggaataagttttcggtgttatatatacat atatGATCTGTTTAGCTTGCCTCG
326_FRA2del3'Hyg_RV	pRS305H	ttcaatgccgtctccttcgaaacttaataaaaaaacaatcat cctttTCAAGAACGAATTCGAGCTC
328_ amdSYMCYC1tflank kDR_fw	amdSYM	gctcgaaggcttaatttgcaatgttgatatacttttctgc ctgtggtgcatccacg TGAAGCTTCGTACGC TGCAG
329_CYC1tflankamdSY M_r	CYC1t	gaaaaagtatatccaacattGCAAATTAAAGCCT TCGAGC
330_ amdSYMrGREfl	amdSYM	acacatacacgcatcggaatgagggaaattgttcatacgt cgttgagGCATAGGCCACTAGTGGATCT G

Table A1. (cont'd)

Name	Amplification target	Sequence (5' to 3')
331_OE-PCR_r		ACACATATACAGCATCGGAATG
332_G1_FRA2	FRA2	AAACCCCTAACCAACCAGTC
333_G4_FRA2	FRA2	GCTGTTGATGATAGTACTGC
334_I1_FRA2	FRA2	AGGTGAAAGAATTGAAAAGG
335_I2_FRA2	FRA2	TCATACCACAATCTTAGACC
336_HygDOWN	hphNT1	ATGGCTGTGTAGAAGTACTCG
344_cg0535_AGS8	cg0535	acatattcaaagttaaacATGATTACTGCTACT GCCTTGAC
345_cg0535_AGS8	cg0535	tttgaattaacgttaaacTCACCTATCGATTTCT CTTGGAACA
346_X2up_f	X-2	CTATGAGGAGACTGTTAGTTGG
347_X2up_flank to AGS8cg_r	X-2	acaaatcttaaagtcatacattgcacgactacacgtgacccg ggggcgcgACGTGACCACTTCGAGAG
348_X2down_flank to AGS8cg_f	X-2	gtttaattttatttcattctggaactcttcgagttctttgtggga ggcCATAATCGGCCTCACAGAG
349_XI5up_f	XI-5	AAGTCGTTGATAGCATTTCGG
350_XI5up_flank to AGS8cg_r	XI-5	acaaatcttaaagtcatacattgcacgactacacgtgacccg ggggcgcgTGGTGCACGGAGTTTATGG
351_XI5down_flank to AGS8cg_f	XI-5	gtttaattttatttcattctggaactcttcgagttctttgtggga ggcCATTCTTTCAATTTTGCACCTC
352_XII-4-up_f	XII-4	AAGATTGGCCATTTTGTGAG
353_XII-4-up_flank to AGS8_r	XII-4	acaaatcttaaagtcatacattgcacgactacacgtgacccg ggggcgcgCTATTTTATACGCTCGAACG
354_XII-4-down_flank to AGS8_f	XII-4	gtttaattttatttcattctggaactcttcgagttctttgtggga ggcTGTACAATTCCCCATTAGAG
355_XII-4-down_r	XII-4	CTTAACAAATCCCTAAACTGG
356_xylBamdSYM_f	amdSYM	gtttaattacaaaatgtcatcagccatttatccctcgtaaagg gtaaaTGAAGCTTCGTACGCTGCAG
357_xylBamdSYM_r	amdSYM	tcaatctcttatctccagcctgcataatccagtactcatggc cagtacGCATAGGCCACTAGTGATCTG

Annex B: Supplementary data

B1. Proteomics data

Table B1. Differentially expressed proteins of *S. cerevisiae* TMB4530 in comparison to the control yeast strain CEN.PK 113-7D. Proteins with statistically significant changes (p-value < 0.01, Log2(Fold-Change) > 0.5 for upregulated proteins and Log2(Fold-Change) < -0.5 for down-regulated proteins) are shown.

Identified protein	Corresponding gene	Yeast systematic gene name	Fold change	p-value
XylX_Caulobacter_crescentus	<i>xylX</i>	---	85.910	1.87E-11
D-xyllose 1-dehydrogenase OS=Caulobacter crescentus (strain NA1000 / CB15N) GN=xylB PE=1 SV=1	<i>xylB</i>	---	19.918	1.40E-07
Heat shock protein SSA1	<i>SSA1</i>	YAL005C	3.963	9.04E-03
Homoserine kinase	<i>THR1</i>	YHR025W	3.370	8.81E-03
Xylonate dehydratase xylD OS=Caulobacter crescentus (strain NA1000 / CB15N) GN=xylD PE=3 SV=1	<i>xylD</i>	---	3.334	3.15E-06
NADPH-dependent methylglyoxal reductase GRE2	<i>GRE2</i>	YOL151W	3.311	1.15E-02
Protein SCP160	<i>SCP160</i>	YJL080C	2.816	4.40E-04
Histone H2A.1	<i>HTA1</i>	YDR225W	2.520	1.60E-03
Polyamine N-acetyltransferase 1	<i>PAA1</i>	YDR071C	2.486	2.31E-01
Ribose-5-phosphate isomerase	<i>RKI1</i>	YOR095C	2.349	1.31E-03
60S ribosomal protein L27-A	<i>RPL27A</i>	YHR010W	2.212	6.34E-02
Nicotinamidase	<i>PNC1</i>	YGL037C	2.192	5.74E-02
60S ribosomal protein L25	<i>RPL25</i>	YOL127W	2.144	1.48E-05
Nuclear localization sequence-binding protein	<i>NSR1</i>	YGR159C	2.116	5.20E-04
Isocitrate dehydrogenase [NAD] subunit 2, mitochondrial	<i>IDH2</i>	YOR136W	2.100	7.71E-02
GrpE protein homolog, mitochondrial	<i>MGE1</i>	YOR232W	2.065	2.43E-01
10 kDa heat shock protein, mitochondrial	<i>HSP10</i>	YOR020C	2.055	3.33E-07
40S ribosomal protein S28-A	<i>RPS28A</i>	YOR167C	2.012	1.41E-05
Single-stranded DNA-binding protein RIM1, mitochondrial	<i>RIM1</i>	YCR028C-A	0.478	3.66E-03
Aromatic/aminoadipate aminotransferase 1	<i>ARO8</i>	YGL202W	0.475	3.36E-03
Uncharacterized protein YBR085C-A	---	YBR085C-A	0.468	1.26E-01
3,4-dihydroxy-2-butanone 4-phosphate synthase	<i>RIB3</i>	YDR487C	0.467	4.10E-03
Putative nitroreductase HBN1	<i>HBN1</i>	YCL026C-B	0.465	2.75E-01
T-complex protein 1 subunit eta	<i>CCT7</i>	YJL111W	0.458	3.64E-01
Phenylalanine--tRNA ligase beta subunit	<i>FRS1</i>	YLR060W	0.458	7.73E-02
Acyl-CoA-binding protein	<i>ACB1</i>	YGR037C	0.455	2.30E-04
5-methyltetrahydropteroyltriL-glutamate--homocysteine methyltransferase	<i>MET6</i>	YER091C	0.453	2.60E-04
Asparagine synthetase [glutamine-hydrolyzing] 1	<i>ASN1</i>	YPR145W	0.440	1.18E-03
Protein ARG5,6, mitochondrial	<i>ARG5,6</i>	YER069W	0.434	6.90E-03
Ubiquitin-like protein SMT3	<i>SMT3</i>	YDR510W	0.433	1.49E-01
L-2-aminoadipate reductase	<i>LYS2</i>	YBR115C	0.419	1.39E-03
Glucan 1,3-beta-glucosidase I/II	<i>EXG1</i>	YLR300W	0.418	3.63E-03
Heat shock protein 26	<i>HSP26</i>	YBR072W	0.411	2.16E-05

Table B1. (cont'd)

Identified protein	Corresponding gene	Yeast systematic gene name	Fold change	p-value
Pyrroline-5-carboxylate reductase	<i>PRO3</i>	YER023W	0.406	1.97E-03
60S ribosomal protein L17-A	<i>RPL17A</i>	YKL180W	0.404	1.37E-03
Diphosphomevalonate decarboxylase	<i>MVD1</i>	YNR043W	0.400	1.20E-03
Glutamine--fructose-6-phosphate aminotransferase [isomerizing]	<i>GFA1</i>	YKL104C	0.400	5.30E-04
Dethiobiotin synthetase	<i>BIO4</i>	YNR057C	0.396	3.05E-03
Protein MMF1, mitochondrial	<i>MMF1</i>	YIL051C	0.390	3.80E-04
Glycine--tRNA ligase 1, mitochondrial	<i>GRS1</i>	YBR121C	0.386	5.45E-05
D-3-phosphoglycerate dehydrogenase 2	<i>SER33</i>	YIL074C	0.379	5.48E-05
60S ribosomal protein L24-B	<i>RPL24B</i>	YGR148C	0.379	1.20E-03
Cofilin	<i>COF1</i>	YLL050C	0.358	1.21E-03
Uncharacterized protein MRP8	<i>MRP8</i>	YKL142W	0.348	1.59E-03
General transcriptional corepressor TUP1	<i>TUP1</i>	YCR084C	0.343	9.33E-03
DNA-directed RNA polymerases I and III subunit RPAC2	<i>RPC19</i>	YNL113W	0.332	2.90E-02
Glucan 1,3-beta-glucosidase	<i>BGL1</i>	YLR300W	0.326	5.65E-05
RNA polymerase II degradation factor 1	<i>DEF1</i>	YKL054C	0.325	2.61E-03
Phosphoglycerate kinase	<i>PGK1</i>	YCR012W	0.319	7.20E-04
UTP--glucose-1-phosphate uridylyltransferase	<i>UGP1</i>	YKL035W	0.316	1.06E-01
Transketolase 1	<i>TKL1</i>	YPR074C	0.308	7.00E-04
Peroxiredoxin TSA1	<i>TSA1</i>	YML028W	0.305	3.33E-05
Adenosylhomocysteinase	<i>SAH1</i>	YER043C	0.276	9.20E-04
FK506-binding protein 1	<i>FPR1</i>	YNL135C	0.266	4.22E-02
Ribonucleoside-diphosphate reductase small chain 2	<i>RNR4</i>	YGR180C	0.260	2.89E-01
Ubiquitin-60S ribosomal protein L40	<i>RPL40A</i>	YIL148W	0.257	2.99E-05
26S proteasome regulatory subunit RPN1	<i>RPN1</i>	YHR027C	0.234	6.80E-04
Regulation of enolase protein 1	<i>REE1</i>	YJL217W	0.223	3.45E-01
Heat shock protein SSB2	<i>SSB2</i>	YNL209W	0.221	5.90E-04
Protein HOR7	<i>HOR7</i>	YMR251W-A	0.192	2.91E-03
Dihydroxyacetone kinase 1	<i>DAK1</i>	YML070W	0.191	4.91E-06
Lysine--tRNA ligase, cytoplasmic	<i>KRS1</i>	YDR037W	0.090	1.22E-03
Inositol-3-phosphate synthase	<i>INO1</i>	YJL153C	0.069	3.32E-06

Paper III



RESEARCH

Open Access



Real-time monitoring of the sugar sensing in *Saccharomyces cerevisiae* indicates endogenous mechanisms for xylose signaling

Daniel P. Brink^{*†}, Celina Borgström[†], Felipe G. Tueros and Marie F. Gorwa-Grauslund

Abstract

Background: The sugar sensing and carbon catabolite repression in Baker's yeast *Saccharomyces cerevisiae* is governed by three major signaling pathways that connect carbon source recognition with transcriptional regulation. Here we present a screening method based on a non-invasive in vivo reporter system for real-time, single-cell screening of the sugar signaling state in *S. cerevisiae* in response to changing carbon conditions, with a main focus on the response to glucose and xylose.

Results: The artificial reporter system was constructed by coupling a green fluorescent protein gene (*yEGFP3*) downstream of endogenous yeast promoters from the *Snf3p/Rgt2p*, *SNF1/Mig1p* and *cAMP/PKA* signaling pathways: *HXT1p/2p/4p*; *SUC2p*, *CAT8p*; *TPS1p/2p* and *TEF4p* respectively. A panel of eight biosensors strains was generated by single copy chromosomal integration of the different constructs in a W303-derived strain. The signaling biosensors were validated for their functionality with flow cytometry by comparing the fluorescence intensity (FI) response in the presence of high or nearly depleted glucose to the known induction/repression conditions of the eight different promoters. The FI signal correlated with the known patterns of the selected promoters while maintaining a non-invasive property on the cellular phenotype, as was demonstrated in terms of growth, metabolites and enzyme activity.

Conclusions: Once verified, the sensors were used to evaluate the signaling response to varying conditions of extracellular glucose, glycerol and xylose by screening in 96-well microtiter plates. We show that these yeast strains, which do not harbor any recombinant pathways for xylose utilization, are lacking a signaling response for extracellular xylose. However, for the *HXT2p/4p* sensors, a shift in the flow cytometry population dynamics indicated that internalized xylose does affect the signaling. These results suggest that the previously observed effects of this pentose on the *S. cerevisiae* physiology and gene regulation can be attributed to xylose and not only to a lack of glucose.

Keywords: *Saccharomyces cerevisiae*, Biosensor, Sugar sensing, Signaling, Xylose, GFP, cAMP/PKA, *Snf3p/Rgt2p*, *SNF1/Mig1p*, Flow cytometry

Background

Baker's yeast *Saccharomyces cerevisiae* can grow naturally in a variety of niches, ranging from plants and ripening fruit to soil and insect guts, that are diverse in nutrient type and content [1, 2]. The cellular uptake and metabolism of carbon sources in this yeast are regulated by a complex network of sensing and signaling cascades

which allow the cells to recognize and respond to variations in the environmental carbon availability and to reprogram the phosphorylation and metabolite patterns and transcription levels accordingly [3–6]. Despite its broad variability in sensing and utilizing different carbon sources, wild type *S. cerevisiae* cannot efficiently utilize pentoses such as xylose and arabinose, and although endogenous genes for xylose utilization are present in the genome, they are inadequately expressed to support growth [7]. In addition, this yeast exhibits strong carbon catabolite repression on metabolism of alternative

*Correspondence: daniel.brink@tmb.lth.se

[†]Daniel P. Brink and Celina Borgström contributed equally to this work
Applied Microbiology, Department of Chemistry, Lund University, P.O. Box 124, 22100 Lund, Sweden

carbon sources when cultivated on glucose, its favored carbon source [6]. *S. cerevisiae* has become a eukaryotic model organism for studies in this field, and the signaling responses to glucose and other alternative fermentable carbon sources such as sucrose, maltose and galactose in this yeast are well-known [3, 6]. The signaling response to xylose, however, is not.

By virtue of its robustness, manageability and high genetic manipulability, *S. cerevisiae* has become an imperative protagonist in industrial bioprocesses and is a promising host for production of value-added chemicals from lignocellulosic biomass [8, 9]. However, a major research challenge in establishing lignocellulosic biomass as a sustainable feedstock for this yeast is that the xylose stream cannot yet be fully valorized—which is a particular issue as xylose is the second most abundant sugar in lignocellulosic hydrolysates [8, 9]. Although *S. cerevisiae* has been successfully engineered for pentose utilization by introduction of exogenous pathways from other yeasts [10–12], growth rates and productivity are significantly lower on this sugar compared with glucose and thus not industrially competitive [9]. In fact, the recombinant strains, despite being successfully engineered to utilize xylose, do not seem to recognize this carbon source as a fermentable sugar, as has been implied in multiple studies [13–19]. Taken together, these advances suggest something is lacking in the sensing and signaling of xylose in *S. cerevisiae*, and that this is a plausible bottleneck that has to be overcome in order to improve productivity of e.g. ethanol from xylose.

Sugar sensing in *S. cerevisiae* is governed by three cross-talking signaling pathways (Fig. 1): the Snf3p/Rgt2p pathway senses extracellular hexoses and induces transcription of an array of hexose transporters (*HXT1-17*) [3, 20, 21]; the SNF1/Mig1p pathway (here represented by *SUC2* and *CAT8*) is a conveyor of catabolite repression by internalized glucose [6], and regulates induction of alternative carbon sources (including e.g. ethanol, glycerol and galactose) during glucose depletion by a not entirely elucidated interaction with Hexokinase isoenzyme 2 (Hxk2p; see Fig. 1) [22–24]; finally, the cAMP/PKA pathway responds to both internalized and external glucose through the Ras1p/2p paralogs or the Gpr1p/Gpa2p complex, respectively, and in accordance to this regulates the environmental stress response, cell cycle progression and homeostasis (here assessed by the *TPS1/2* genes) [5, 25]. Together, these pathways have evolved to support growth on versatile niches [2, 3]; consequently, *S. cerevisiae* gene expression is highly regulated by carbon-source dependent promoters (for a review see [26]).

In this study, we utilized a Green Fluorescent Protein (GFP) to design a panel of biosensors that allow for real-time single-cell evaluation of the sugar signaling state in

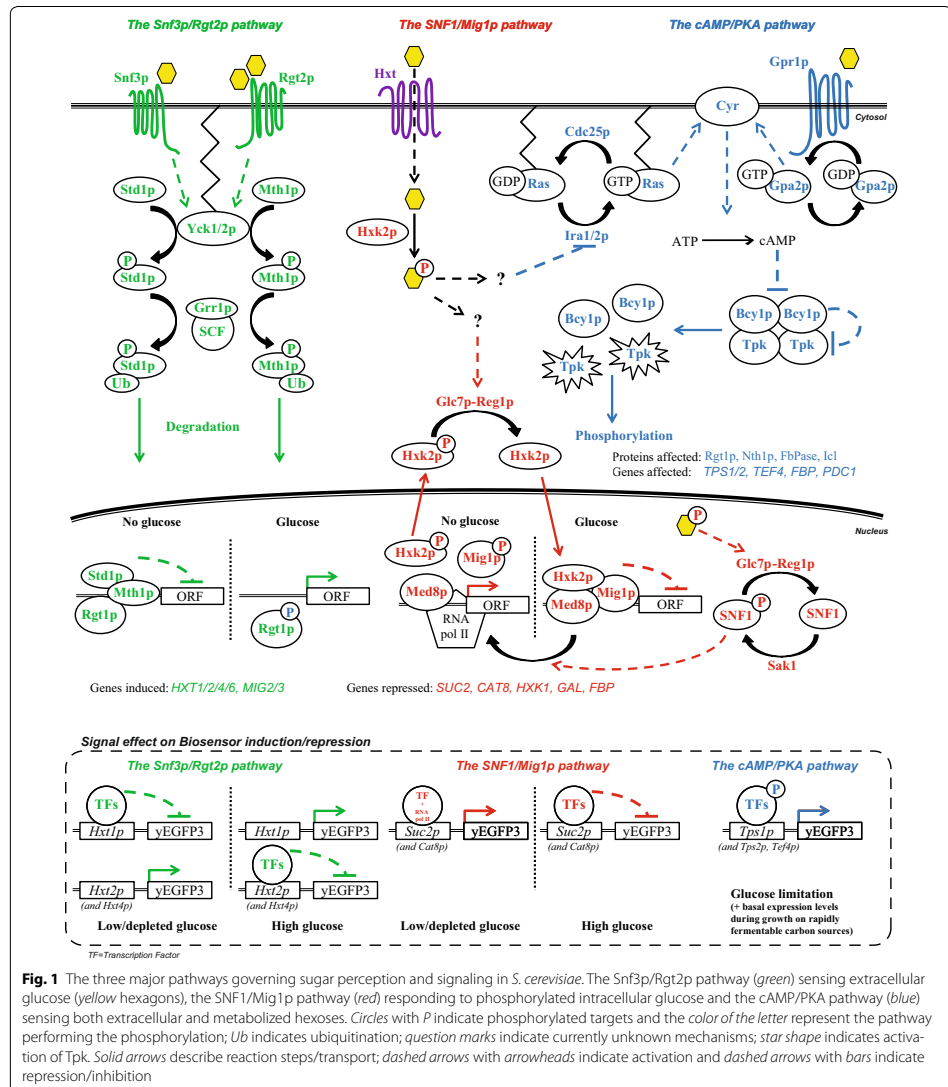
S. cerevisiae using flow cytometry, which in turn comes with the possibility of detecting and analyzing population heterogeneities. Here, the promoter regions from eight genes (*HXT1p/2p/4p*; *SUC2p*, *CAT8p*; *TPS1p/2p*, *TEF4p*) under control by the Snf3/Rgt2, Snf1/Glc7 and RAS-cAMP-PKA pathways respectively were coupled to the established yeast reporter gene *yEGFP3* (yeast enhanced green fluorescent protein) [27] and were introduced in *S. cerevisiae*. Due to the non-invasive and heritable features of the small and inert GFP molecule [28], fluorescent protein biosensors have become a highly applied tool within the field of yeast biology [29–35]. The glucose repressed *JEN1* promoter (under control of the SNF1 complex) has previously been used as a biosensor to detect different concentrations of glucose based on GFP-intensity [36]; however, this study did not focus on any *S. cerevisiae* sensing of other sugars than glucose.

Despite recent attempts at resolving the Gordian knot of xylose sensing in *S. cerevisiae* by heterologous expression of bacterial xylose-responsive transcription regulators (XylRs) [37, 38], as well as engineering of carbon catabolite repression, by e.g. deletion of *MIG1/2*, in recombinant xylose utilizing strains [39], little is still known about how or even if xylose is sensed by this yeast. To our knowledge, the current study is the first time a fluorescent biosensor has been implemented to monitor the hexose-pentose signaling state of this yeast. Determining the position(s) in the cascade where the signal differentiates for xylose and glucose will allow us to find novel engineering targets for improving xylose uptake and utilization in *S. cerevisiae*.

Methods

Strains

The *S. cerevisiae* strains that were used in this study are listed in Table 1. The W303-1A strain [ATCC® 208352], from which the engineered strains were derived, was purchased from ATCC (Manassas, VA, US). Competent *Escherichia coli* NEB5α (New England BioLabs, Ipswich, MA, US) was used for subcloning. *E. coli* DH5α containing the M3499 plasmid (Addgene plasmid #51674) was purchased from Addgene (Cambridge, MA, US). All strains were stored in 25% (v/v) glycerol at –80 °C. The yeast strains were maintained on Yeast Nitrogen Base (YNB)-glucose agar plates (6.7 g/L YNB w.o. amino acids, 20 g/L glucose, 20 g/L agar-agar) supplemented with amino acids (tryptophan 75 mg/L, histidine 125 mg/L, leucine 500 mg/L and uracil 150 mg/L [40] and adenine 100 mg/L [41]) depending on the strain requirements. Solid media cultivations were considered fresh for two weeks before new plates were streaked from the –80 °C stock.



Molecular biology methods

Standard molecular biology methods were used for all cloning procedures [42]. Restriction enzymes, Phusion DNA polymerase and T4 ligase were obtained from Thermo Scientific (Waltham, MA, US), with the

exception of the *ZraI* restriction enzyme that was purchased from New England Biolabs (Ipswich, MA, US). PCR primers were ordered from Eurofins MWG Operon (Ebersberg, Germany); all primers that were used in this study can be found in Additional file 1: Table S1. Plasmid

Table 1 Yeast strains and plasmids used in the present study

Strain	Genotype	Reference
W303-1A	<i>MAΔ trp1-1 leu2-3,112 his3-11 ade2-1 ura3-1 can1-100</i>	[54]; ATCC® 208352
TMB3700	<i>W303-1A TRP1 HIS3, ura3::M3499 (ADE2)</i>	This study
TMB3711	<i>TMB3700; can1::Ylp211; SPB1/PBN1::Ylp128</i>	This study
TMB3712	<i>TMB3700, can1::YlpGFP-Hxt1p; SPB1/PBN1::Ylp128</i>	This study
TMB3713	<i>TMB3700, can1::YlpGFP-Hxt2p; SPB1/PBN1::Ylp128</i>	This study
TMB3714	<i>TMB3700, can1::YlpGFP-Hxt4p; SPB1/PBN1::Ylp128</i>	This study
TMB3715	<i>TMB3700, can1::YlpGFP-Suc2p; SPB1/PBN1::Ylp128</i>	This study
TMB3716	<i>TMB3700, can1::YlpGFP-Cat8p; SPB1/PBN1::Ylp128</i>	This study
TMB3717	<i>TMB3700, can1::YlpGFP-Tps1p; SPB1/PBN1::Ylp128</i>	This study
TMB3718	<i>TMB3700, can1::YlpGFP-Tps2p; SPB1/PBN1::Ylp128</i>	This study
TMB3719	<i>TMB3700, can1::YlpGFP-Tef4p; SPB1/PBN1::Ylp128</i>	This study
CEN.PK 113-7D	<i>MAΔ, MAL2-8^S, SUC2</i>	[76]; EUROSCARF collection
Plasmid	Relevant genotype	Reference
Ylpac128	<i>Amp^R; LEU2</i>	[50]
Ylpac211	<i>Amp^R; URA3</i>	[50]
YEplK01	<i>YEplacHXT; URA3; GPD2p-yEGFP3-PGK1t</i>	[33]
YlpGFP	<i>Ylpac211::yEGFP3-PGK1t</i>	This study
YlpGFP-HXT1p	<i>YlpGFP:HXT1p-yEGFP3-PGK1t</i>	This study
YlpGFP-HXT2p	<i>YlpGFP:HXT2p-yEGFP3-PGK1t</i>	This study
YlpGFP-HXT4p	<i>YlpGFP:HXT4p-yEGFP3-PGK1t</i>	This study
YlpGFP-SUC2p	<i>YlpGFP:SUC2p-yEGFP3-PGK1t</i>	This study
YlpGFP-CAT8p	<i>YlpGFP:CAT8p-yEGFP3-PGK1t</i>	This study
YlpGFP-TPS1p	<i>YlpGFP:TPS1p-yEGFP3-PGK1t</i>	This study
YlpGFP-TPS2p	<i>YlpGFP:TPS2p-yEGFP3-PGK1t</i>	This study
YlpGFP-TEF4p	<i>YlpGFP:TEF4p-yEGFP3-PGK1t</i>	This study
M3499	<i>Amp^R; ura3::ADE2</i>	[52]

purification was done using the GeneJet plasmid Mini-Prep kit (Thermo Scientific, Waltham, MA, US) and PCR products were purified using the GeneJET PCR purification kit from the same manufacturer. DNA extractions from agarose gels were made using the QIAquick gel extraction kit (Qiagen, Hilden, Germany). All genetic constructs were verified by sequencing (Eurofins MWG Operon, Ebersberg, Germany). The genomic DNA sequences from the CEN.PK and W303 strains that were used for the design of the cloning were retrieved from the *Saccharomyces* Genome Database (SGD; <http://www.yeastgenome.org>) [43]. Extraction of genomic yeast DNA was performed using the LiOAC-SDS method [44].

Competent *E. coli* NEB5 α cells were prepared and transformed according to the method of Inoue and colleagues [45]; *E. coli* transformants were selected on Luria-Bertani medium (10 g/L tryptone, 5 g/L yeast extract and 10 g/L NaCl, agar 15 g/L) supplemented with 100 μ g/mL ampicillin. *S. cerevisiae* cells were transformed according to the lithium acetate method [46] with addition of DMSO (10% v/v) prior to heat shock [47], and were streaked on selective medium.

Construction of expression cassettes, targeting fragments and plasmids

The *yEGFP3-PGK1t* expression cassette containing the yeast enhanced GFP (*yEGFP3*) [27] and the *PGK1* terminator was PCR amplified from the YEplK01 plasmid [33] using the *yEGFP-F1-KpnI* and *yEGFP-R1-SacI* primers. The promoter regions (ca 1 kb upstream of each ORF) from eight genes involved in the *S. cerevisiae* sugar signaling (*HXT1*, *HXT2*, *HXT4*, *SUC2*, *CAT8*, *TPS1*, *TPS2* and *TEF4*) were PCR amplified from genomic CEN.PK 113-7D DNA. The CEN.PK strain was originally intended to be used throughout the project, but following the construction of the biosensors plasmids it was found that this strain family has deficiencies in the cAMP/PKA pathway [48, 49], and the W303 strain was instead chosen for the sensor evaluation. Flanking *Sall* and *BamHI* restriction sites were introduced in each expression cassette respectively. Expression cassettes for the recovery of the tryptophan and histidine auxotrophies in W303-1A were also PCR amplified from CEN.PK 113-7D genomic DNA.

The YlpGFP plasmid was constructed by ligating the *yEGFP3-PGK1t* cassette into the integrative yeast shuttle

vector YIplac211 [50] using the flanking *KpnI* and *SacI* restriction enzyme sites that were introduced when the cassette was PCR amplified from YEpJK01. The eight promoter-GFP reporter plasmids (YIpGFP-HXT1p, YIpGFP-HXT2p, YIpGFP-HXT4p, YIpGFP-SUC2p, YIpGFP-CAT8p, YIpGFP-TEF4p, YIpGFP-TPS1p and YIpGFP-TPS2p) were generated by ligation of each promoter cassette into YIpGFP through the *Sall* and *BamHI* sites respectively and the plasmids were transformed into *E. coli*. A schematic illustration of the plasmid map is found in Additional file 1: Figure S2, and all plasmids that were used in this study are listed in Table 1.

Targeting fragments for nested double homologous integration of the YIpGFP plasmids into the yeast genome were constructed by PCR amplification (previously described in e.g. [51]). A schematic illustration of the integration strategy is found in Additional file 1: Figure S1. The two targeting fragments for integration of the biosensor plasmids were generated by amplifying 300 bp regions in the 5'- and 3'-ends of the *CAN1* ORF from W303-1A genomic DNA with addition of 50 bp tails with homology to the flanks of the linear sequence of YIplac211 (after digestion with the blunt cutting *ZraI*). The tail regions of the fragments were achieved by using 74 bp "tail" primers with 24 bp primers annealing to the chromosomal DNA. Likewise, 475 bp targeting fragments for integration of YIplac128 in the *SPB1/PBN1* intergenic locus were generated using primers modified from Flagfeldt et al. [51].

Yeast reporter strain construction

All yeast strains used in this study (Table 1) were constructed from the parental strain W303-1A. The strains were made prototrophic by sequential transformation with the *TRP1* and *HIS3* expression cassettes and the M3499 plasmid (*ura3::ADE2*) [52], followed by one of the eight GFP-reporter plasmids containing the *URA3* marker (YIpGFP-HXT1p, YIpGFP-HXT2p, YIpGFP-HXT4p, YIpGFP-SUC2p, YIpGFP-CAT8p, YIpGFP-TEF4p, YIpGFP-TPS1p, YIpGFP-TPS2p) respectively. Finally, the leucine auxotrophy was cured in all GFP-strains by integration of an empty YIplac128 (*LEU2*⁺) plasmid in the *SPB1/PBN1* intergenic locus [51].

Since the uracil auxotrophy in W303-1A is caused by a single point mutation in the *Ura3-1* allele and is known to revert [53, 54], the *URA3* locus in the reporter strains was deleted to avoid the possibility of reversion to the wild type locus during the sequential transformations. This was made with the M3499 *ura3::ADE2* Disruptor Converter plasmid (Addgene plasmid #51674; a gift from David Stillman); digestion and red-white screening was performed according to the authors' instructions [52].

The eight GFP-reporter plasmids and the empty YIplac128 plasmid (*LEU2*⁺) were linearized with *ZraI* and were integrated in the yeast genome by double homologous recombination with the targeting fragments described above. The correct integration of all plasmids was verified with PCR amplification of genomic DNA from transformant colonies.

Cultivation conditions

Single colonies from the reporter strains were taken from YNB-glucose-plates and were cultivated in two steps prior to the experiments. The first step (pre-pre-cultivation) was performed in 50 mL conical tubes with 5 mL YNB-glucose20 medium (6.7 g/L YNB w.o. amino acids, 20 g/L glucose supplemented with potassium hydrogen phthalate buffer 50 mM pH 5.5) in order to gain sufficient biomass (10 h cultivation time). The second step consisted of a pre-cultivation with repressing conditions; depending on the induction/repression conditions of each GFP-reporter strain (Table 2) the liquid YNB-medium was complemented with either excess glucose (40 g/L; cultivated for 12 h in order not to deplete the glucose and induce the promoters) or ethanol (3% v/v; cultivated for 32 h to reach a sufficient biomass) in order to repress GFP-expression. For the *TEF4* biosensor (TMB3719) pre-culture, glucose 20 g/L and 24 h cultivation was used to achieve better repression. For the batch culture experiments, the pre-cultures were grown in 250 mL baffled shake flasks (25 mL YNB-glucose40 or YNB-EtOH3 medium) with an initial optical density (OD_{620nm}) of 0.05. The pre-cultures for the microtiter plate experiments were performed in a similar manner, with the difference that 50 mL conical tubes (5 mL YNB-glucose40 or YNB-EtOH3 medium; initial OD_{620nm} = 0.05) were used. All yeast incubations were performed at 30 °C and 180 rpm unless otherwise specified.

The pre-cultures were harvested by centrifugation at 3000 rpm for 5 min (5810R centrifuge, Eppendorf, Hamburg, Germany) and the cell pellets were washed twice in 5 mL YNB-KHPthalate without glucose, were resuspended in 1 mL YNB-KHPthalate medium without glucose and were used to inoculate 1000 mL baffled shake flasks with a total end-volume of 100 mL and an initial OD_{620nm} of 0.5. From here on, aerobic batch cultivations were carried out in liquid YNB-KHPthalate medium complemented with either high (20 g/L) or low (1 g/L) glucose concentrations (according to previous studies; Table 2). Aerobic conditions were chosen not to impact the GFP signal as the protein is known to require oxygen to mature [27]; furthermore, since this yeast is Crabtree positive [55], respiro-fermentative growth will occur

Table 2 Summary of the documented induction/repression conditions for the *S. cerevisiae* promoters chosen for the GFP-reporter constructs

Promoter	Name/function	Signaling pathway	Induced/derepressed by	Repressed by	References
HXT1	Low-affinity hexose transporter	Snf3p/Rgt2p	High glucose (4% w/v) ^a	Low glucose (0.1% w/v)	[20]
HXT2	High-affinity hexose transporter	Snf3p/Rgt2p	Low glucose (0.1% w/v)	High glucose (4% w/v)	[20]
HXT4	High-affinity hexose transporter	Snf3p/Rgt2p	Low glucose (0.1% w/v)	High glucose (4% w/v); more glucose-repressed than HXT2	[20, 77]
SUC2	Invertase	SNF1/Mig1p	Low glucose (0.1% w/v)	High glucose (2% w/v) and depleted glucose (0% w/v)	[78]
CAT8	Alternative carbon source response-activator	SNF1/Mig1p	Low glucose (0.2% w/v)	High glucose (4% w/v)	[79]
TPS1	Trehalose-6-phosphate synthase (56 kD subunit)	cAMP/PKA	Glucose limitation, stress conditions (e.g. heat, nutrient starvation, oxidative stress)	High glucose; however, a basal expression level has been observed when growing on rapidly fermentable sugars	[80, 81]
TPS2	Trehalose-6-phosphate synthase (102.8 kD subunit)	cAMP/PKA			
TEF4	Translation elongation factor	cAMP/PKA	–	Stress conditions	[82, 83]

^a Glucose 4% (w/v) corresponds to 40 g/l

during these conditions. Two biological replicates were performed for each strain and condition.

Microtiter plate based experiments were carried out in a similar fashion to the shake flask experiments. The pre-cultures were harvested in a benchtop centrifuge in 2 mL conical tubes at 2300 RCF for 2 min (5415R centrifuge, Eppendorf, Hamburg, Germany) and washed twice in 1.5 mL YNB-KHPthalate medium without glucose. The cells were inoculated in pre-sterilized 96 U-well microtiter plates (Microtest Plate 96 well R, Sarstedt, Nümbrecht, Germany) with a 250 µL total volume per well and initial $OD_{620nm} = 0.5$. The microtiter plates were incubated at room temperature (24–25 °C) in microtiter plate shaker (IKA MS3 Basic, Staufen, Germany) at 800 rpm both during and in-between flow cytometry analysis since the flow cytometer could not be incubated. The single-cell fluorescence was evaluated in eight different conditions in YNB-KHPthalate medium with the following supplements: no glucose; glucose 1, 20 and 5 g/L; glycerol 3% (v/v); xylose 50 g/L; xylose 50 g/L with glucose 5 g/L; xylose 50 g/L with glycerol 3% (v/v). The autosampler was paused after half of the wells had been injected, and the remaining wells were mixed thoroughly by pipetting the liquid in each well up and down in order to counteract cell sedimentation. The strains were analysed in two biological replicates with two technical replicates per strain, condition and plate.

Analyses and sampling procedures

Growth and metabolite profiles

Growth of the cell cultures were monitored by optical density (OD) at 620 nm using an Ultrospec 2100 Pro

spectrophotometer (Amersham Biosciences, Uppsala, Sweden). Extracellular glucose, glycerol, acetate and ethanol were quantified with a Waters HPLC system (Mildford, MA, USA). The separation was performed with an HPX-87H ion exchange column (Bio-Rad, Hercules, CA, USA). The mobile phase consisted of 5 mM H₂SO₄ at a flow rate of 0.6 mL/min and a column temperature of 60 °C. A refractive index detector (RID-6a, Shimadzu, Kyoto, Japan) was used for detection. Growth and metabolite analyses were performed in technical duplicates for every sample.

Flow cytometry

The yeast GFP-reporter strains were evaluated for fluorescence intensity (FI) with a BD Accuri C6 flow cytometer equipped with a BD CSampler autosampler (Becton–Dickinson, NJ, US). A laser with an excitation wavelength of 488 nm was used and fluorescence emission levels were measured with a 533/30 bandpass filter. Quality control was performed prior to each experiment with Spherotech 8-peak and 6-peak validation beads (Becton–Dickinson, NJ, US). A flow rate of 14 µL/min and a core size of 10 µm were used when analysing cells. The threshold was set to 8000 at the forward scatter-height (FSC-H) channel and 100,000 events were collected per sample. Every cell sample was followed by an auto-sampler wash cycle and a 2 min injection of deionised water in order to minimize sample carryover between injections. For the microtiter plate cultivations, 10,000 events were collected per sample and the mean of the technical replicates was used in the data analysis of each biological replicate; this could be done since the

technical replicates were highly consistent within each pair (in terms of standard deviation). The raw data has been deposited at FlowRepository (<https://flowrepository.org/>) [56] with accession numbers FR-FCM-ZZRA, FR-FCM-ZZRB, FR-FCM-ZZRC, FR-FCM-ZZRD and FR-FCM-ZZRE.

Flow cytometry raw data was exported from the Accuri software as fcs-files and was processed and analyzed with the Knijnenburg morphology correction model [57] in Matlab (Release R2015a, The MathWorks, Inc., Natick, MA, US) using the FCS data reader function (version 28 May 2014; L. Balkay, University of Debrecen, Hungary; downloaded from <http://www.mathworks.com/matlabcentral>). FlowJo (v10; Treestar, Inc., San Carlos, CA) was used to produce overlay histograms for certain visualisation purposes. A custom, in-house Matlab script was developed to allow high-throughput, automated signal-to-cell size normalization and visualization of the population average based on the geometrical mean of the FL1-H channel (GFP) histograms. The script identifies .fcs raw data for each time point and calls the Knijnenburg model to normalize the fluorescence intensity (FI) to cell size and outputs plots of the normalized FI over time for each strain. Non-Gaussian histograms were predominantly observed in the raw FI data from the glucose 1 g/L cultures; it was however found that this was caused by size heterogeneities in the cultures, as the morphology-normalized data proved to compensate for skewed distributions in the in-data. A complementary custom in-house Python script was developed to facilitate renaming of file names and sorting in the required folder hierarchy in order for the custom Matlab script to function properly. See also Additional file 1 for a more detailed description of the custom scripts. The custom scripts and operation instructions have been deposited on Github (<https://github.com/tmbyeast/Flow-cytometry-tools>), and this is also where possible future updates will be stored. Users will have to download the Knijnenburg model separately according to the authors' instructions [57].

A mean, time-independent FI baseline [corresponding to the autofluorescence of the negative control TMB3711 at the FL1-H channel and excitation wavelength (488 nm)] was calculated as the average FI of the biological replicates for the glucose 20 and 1 g/L cultures (four replicates in total). The baseline was only used to indicate the approximate autofluorescence of the utilized strains in order to facilitate comparisons with the FI induction/repression patterns of the biosensor strains (TMB3712-3719).

Matlab (Release R2015a, The MathWorks, Inc., Natick, MA, US) was also used to perform one-way ANOVA tests (*anova1*) coupled with a multiple comparison test (*multcompare*).

RT-qPCR assay

Culture samples for mRNA analysis were quenched in cold methanol (-80°C ; 1.4 mL methanol per 1 mL cell culture [58]) and centrifuged at 1800 RCF and 0°C for 5 min. The supernatants were decanted and the cell pellets were stored in -80°C . RNA was extracted using the RNeasy Mini Kit (Qiagen, Hilden, Germany) using mechanical lysis: the quenched cell samples were resuspended in RLT buffer previously mixed with 2-mercaptoethanol, and were lysed by bead beating in a Precellys 24 (6500 rpm, 3 cycles \times 60 with 30 s pauses in-between cycles; Bertin Technologies, France) with a Cryolys temperature controller (Bertin Technologies, France) cooled with liquid nitrogen. Residual DNA was removed from the extract with rDNase I (Ambion, Life Technologies, Carlsbad, CA, US). Conventional PCR was used to verify that no residual DNA was left in the RNA extract. The RNA content was quantified using a BioDrop (BioDrop Ltd, Cambridge, UK). The superscript IV Reverse Transcriptase kit and Oligo(DT)₂₀ primers (Invitrogen, Life Technologies, Carlsbad, CA, US) were used to synthesise cDNA from extracted RNA (using 0.5 mg/mL of RNA extract per sample). RT-qPCR was performed using the Ex Taq DNA polymerase kit (Takara Bio, Kusatsu, Shiga, Japan), EvaGreen dye (Biotium, Hayward, CA, US), bovine serum albumin (20 mg/mL; Thermo Scientific, Waltham, MA, US) and a LightCycler 2.0 (Roche Life Science, Basel, Switzerland). Quantification cycle (C_q)-values and melting curve analyses were determined using the LightCycler software 4.1 (Roche Life Science, Basel, Switzerland). *ACT1*, *UBC6* and *TAF10* were evaluated as reference gene candidates [59]. Due to its stability during the evaluated conditions, *ACT1* was chosen as the reference gene (using primers *ACT1_F/ACT1_R*; *yEGFP3* and *SUC2* were used as target genes (primers *yEGFP3_F1790_RT/yEGFP3_R1918_RT* and *SUC2_F263_RT/SUC2_R397_RT* respectively). The following RT-qPCR program was used to analyze all three genes: denaturation 95°C 2 min; 45 cycles of 95°C 10 s, 55°C 10 s, 72°C 30 s; melting curve analysis: 50°C 1 min hold time, ramp to 95°C with 0.05°C/s ; cooling: 40°C , 30 s. Standard curves for calculation of RT-qPCR efficiency and assessment of gene relative expressions were performed according to the Pfaffl method [60]. Each sample was analyzed in biological and technical triplicates.

Invertase enzyme assay

Enzymatic activity of invertase (EC: 3.2.1.26; encoded by *SUC2*) was assessed in yeast cell extracts according to previous protocols [61, 62] with the exception that the carcinogenic *o*-dianisidine was substituted with 4-aminophenazone/phenol [63]. A detailed description of the adapted protocol and calculation of the specific invertase

activity can be found in Additional file 1. Assays were performed in biological triplicates.

Sampling procedures

The 100 mL batch shake flask cultures were sampled for OD (500 μ L) and FI (200 μ L) measurements every hour, for metabolite concentrations (2 mL) every second h for the first 8 h and at 24 h, and for mRNA (4 mL) at 0, 15, 30, 45 and 60 min. Enzyme assay samples were collected every 30 min for the first 3 h from cultures grown in 1 g/L glucose. The sample volumes were designed to minimize the influence of sampling on the culture, by having at least 50% of the starting volume left in the flask after the final sample point. The microtiter plates were sampled by the Accuri autosampler at 0, 3 and 6 h. Each run lasted ~90 min (a technical limitation of the flow cytometer).

Results

Design and construction of the yeast biosensor strains

A panel of eight *S. cerevisiae* sugar-responsive biosensor strains were constructed by coupling select promoters from the three main sugar sensing pathways in this yeast (Snf3p/Rgt2p, SNF1/Mig1p and cAMP/PKA; Fig. 1) with a green fluorescent protein (GFP) gene followed by genomic integration (one biosensor/strain). The biosensor expression cassettes were produced by cloning of endogenous *S. cerevisiae* promoters circa 1 kb upstream from the *HXT1/2/4*, *SUC2*, *CAT8*, *TPS1/2* and *TEF4* genes in front of the *yEGFP3* cassette [27] in the YIpac211 vector [50] (cf. Additional file 1: Figure S2). The promoter length was roughly based on the known binding motifs of these regions (Additional file 1: Table S2). The promoters were chosen for their known interactions with said pathways (Table 2) [3, 6], and/or based upon changes in their transcriptomics profiles in deletion mutant strains, compared to the wild type [64].

In vivo recombination and double homologous integration of nested DNA fragments [51] was used to integrate the biosensor cassettes in single-copy in the TMB3700 strain, that in turn was derived from *S. cerevisiae* W303-1A (Table 1). In addition to the eight biosensor strains, a ninth strain was integrated with an empty YIp211 plasmid (i.e. lacking *yEGFP3* and promoter) and was used as a negative control in order to measure the cellular auto-fluorescence at the GFP emission wavelength.

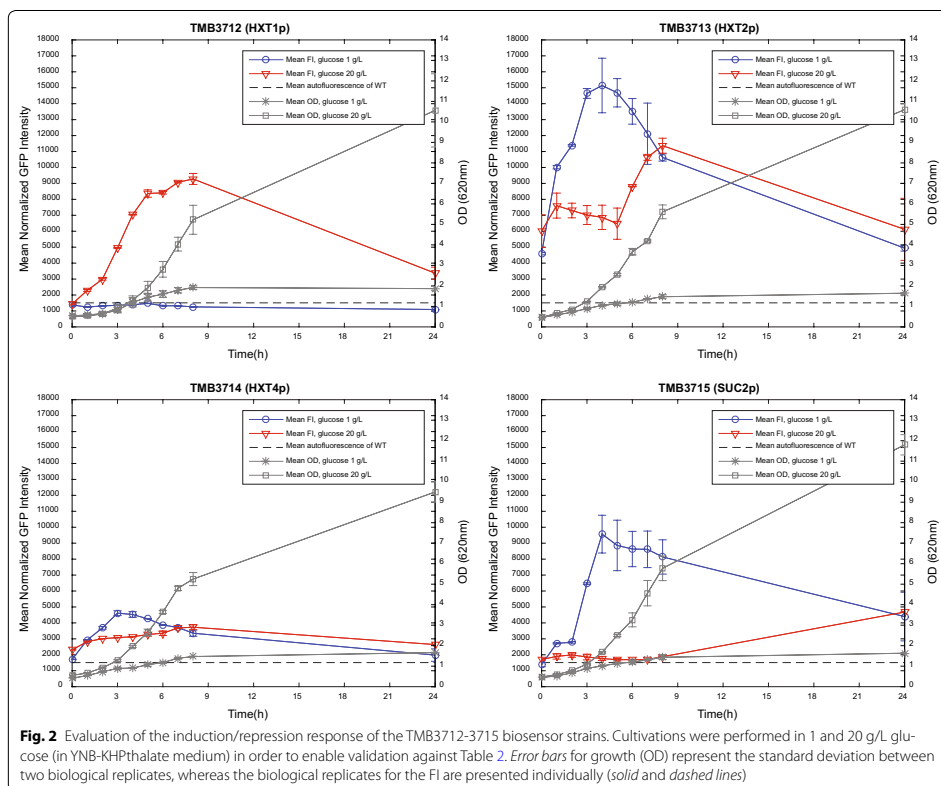
Validation of the induction/repression patterns of the sugar signaling biosensors

In order to allow for assessment of the *S. cerevisiae* signaling response to xylose, the response of the eight biosensors were first validated on high (20 g/L) and low (1 g/L) glucose by comparing the fluorescence intensity (FI)

with the already well documented induction/repression patterns of the eight promoters (Table 2). Flow cytometry was used to measure the FI at a single-cell level; this methodology was chosen for the biosensor protocols since it allows for identification of possible population heterogeneities (subpopulations) and can later on be used with cell sorting experiments (i.e. by FACS: fluorescence-activated cell sorting); the non-pooled, single-cell approach of this methodology will therefore be able to generate data that complements traditional pooled-sample strategies like transcriptomics and RT-qPCR. KHPthalate buffer was added to the culture media to minimize pH stress on the cell, as stress conditions are known to induce/repress *TPS1p/2p* and *TEF4p* (Table 2).

The negative control strain TMB3711 (no GFP-cassette) was used to identify the cellular auto-fluorescence at the GFP emission wavelength over time (Additional file 1: Figure S4) and was used to establish a mean, time-independent FI baseline for the biosensor strains (Figs. 2, 3). Also evident from Additional file 1: Figure S4, is that the (size normalized) auto-fluorescence does not change neither during true growth (glucose 20 g/L) nor during carbon starvation (glucose 1 g/L). To account for the fact that larger cells display a higher fluorescence than smaller ones, all FI signals were normalized to cell size using the Knijnenburg morphology correction model for Matlab [57], resulting in improved Gaussian distributions in the FI histograms. An example of the look of the FI histograms before and after normalization is available in Additional file 1: Figure S3.

By comparing the FI curves from the different conditions in Figs. 2, 3 with the known physiological outcomes for the corresponding strain and condition (listed in Table 2) it was found that the fluorescent response of the TMB3712-3718 biosensor constructs correlated with the reported induction/repression conditions from literature. This shows that GFP constructs such as these are indeed conceivable systems for monitoring the signaling state of the yeast cell. As was expected, the growth profiles (OD; Figs. 2, 3) and maximum specific growth rates (μ_{\max} ; Additional file 1: Table S3) were similar between the nine strains, which corroborates that the physiology of these strains was unaffected by the integration of the biosensor cassettes. Furthermore, the metabolite profiles of extracellular glucose, glycerol, acetate and ethanol were also tantamount across the panel of strains (Additional file 1: Figure S5), showing that the integration of the sensor constructs did not interfere with the central metabolism. It was found that approximately 7 g/L remained in the 20 g/L glucose cultures after 8 h, which would still be high enough not to alter the induction/repression pattern (Table 2). Full carbon depletion occurred between 8 h and 24 h (Additional file 1: Figure S5).



TMB3719, however, proved to be very challenging to repress during the pre-culture, as this promoter (*TEF4p*) is known to be repressed by stress conditions (Table 2). Attempts were made with high glucose (40 g/L for 12 h) and respiratory conditions (Ethanol 3% v/v; 48 and 72 h) before settling on glucose 20 g/L for 24 h. Although this proved to be a more stressful, and thus more repressing, condition than in the other attempts, the sensor was still highly induced at 0 h (Fig. 3).

To further validate that the observed GFP response indeed reflects the signaling patterns in these strains during high and low glucose conditions, and, more importantly, to ensure that the second promoter copy present in the genome after integration of the biosensor plasmids did not affect the endogenous expression, the transient mRNA levels were assessed with an RT-qPCR assay. Since the genetic construct, integration locus and plasmid copy number (double homologous integration)

was identical for all the biosensor strains, except for the promoter region preceding the *yEGFP3* cassette, mRNA profile validation was performed for one biosensor strain (TMB3715; *SUC2p*) and the negative control strain (TMB3711). *SUC2* was chosen since it encodes an enzyme (invertase) that can be easily assayed (which is not the case for many of the other biosensor genes, e.g. the hexose transporters); thus *SUC2* was used as a model to validate the biosensor construct versus the native gene on both the transcript and protein level—with respect to the integration locus of the cassette and the promoter copy number (one endogenous, one in the biosensor cassette). It was found that there was no significant difference in expression profile for the endogenous *SUC2* gene between the two strains and that the profile of the endogenous *SUC2* matched the one of the *SUC2p-yEGFP3* construct in TMB3715 (Fig. 4). This demonstrated that (1) the integration of the biosensor cassette did not alter

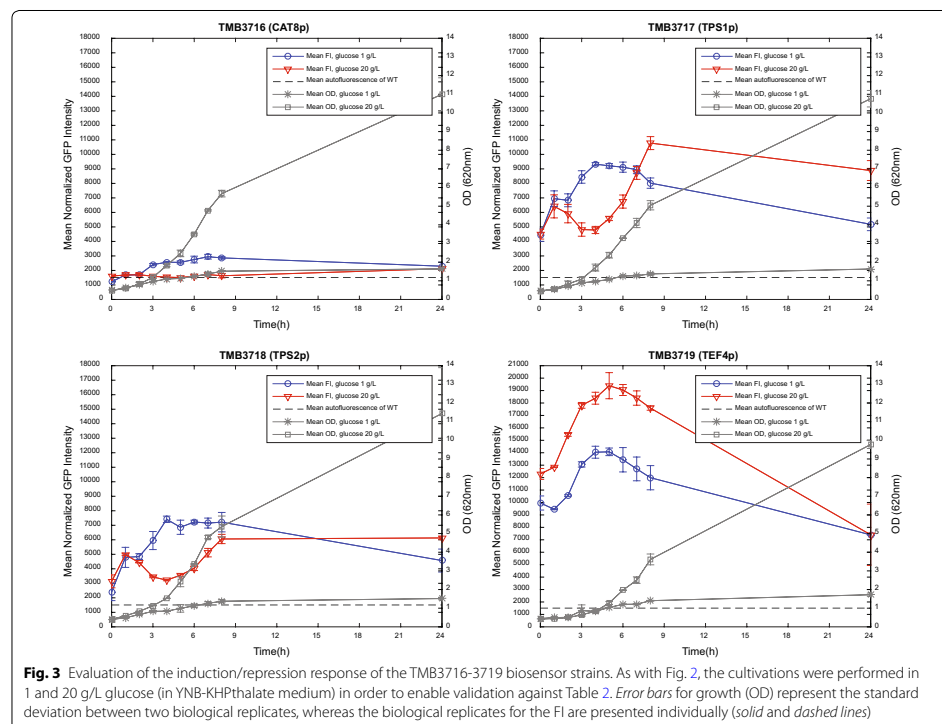


Fig. 3 Evaluation of the induction/repression response of the TMB3716-3719 biosensor strains. As with Fig. 2, the cultivations were performed in 1 and 20 g/L glucose (in YNB-KHPthalate medium) in order to enable validation against Table 2. Error bars for growth (OD) represent the standard deviation between two biological replicates, whereas the biological replicates for the FI are presented individually (solid and dashed lines)

the transcription phenotype despite there being two copies of the promoter in the genome (one endogenous, and one in the sensor construct; here: *SUC2p*), (2) that the observed (cumulative) increase in GFP signal (Fig. 2) was reciprocal to the transient GFP-transcript pulse (Fig. 4) and (3) that the chosen integration locus (*CAN1*) resulted in lower fold expression levels than the endogenous *SUC2* but that this did not obstruct the functionality of the sensor. It should be noted that though the behavior of *SUC2p* cannot be superimposed on that of the other promoters of this study, the correlation of Figs. 2, 3 with Table 2 have already given good indications to the functionality of all eight biosensors of this study.

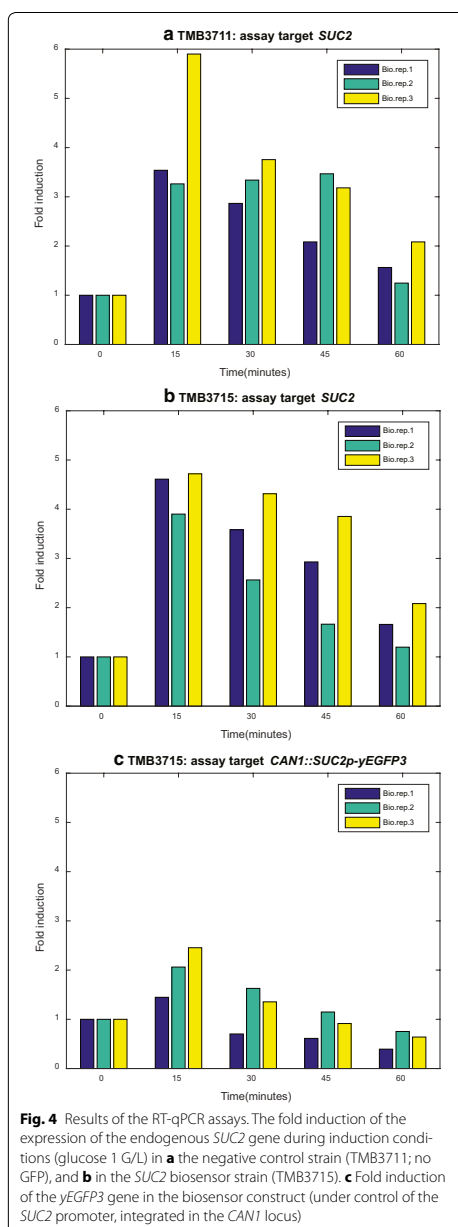
Finally, to fully ascertain that the biosensor constructs truly were non-invasive, the phenotype of the *SUC2p*-*yEGFP3* strain was also assessed on the protein level by benchmarking the enzymatic activity of invertase (the protein product of *SUC2*) in TMB3715 to that of the negative control TMB3711. The endpoint invertase activity in cell extracts did not differ significantly between the two strains when cultivated in 1 g/l (inducing conditions

for *SUC2*/invertase) (Additional file 1: Figure S6). Assay saturation (equivalent to 500 mM glucose without sucrose [62]) was reached in the samples from 2.5 to 3 h of cultivation, and therefore marked the end of the assay.

It should be noted that it is easy to follow the build-up of GFP in our biosensor system, but that the post-peak signal should preferably only be used for trends. This can be attributed to the facts that gene expression at that time will undergo a growth phase coupled shift [65] and that the fluorescent half-life of the yeast *yEGFP3* protein is circa 7.5 h [66]. Alternative GFP cassettes with significantly lower half-life (34 min) exist [66], but is out of the question for the current study due to the invasive properties of the ATP-dependent degradation process [67] of the alternative GFP construct.

Screening of the signaling response to xylose and other carbon sources

Once verified, the biosensor strains were used to screen for the signaling response on a panel of different carbon sources with a main focus on different combinations of



xylose. To accomplish this, a protocol for microtiter plate screening was developed based on the Accuri C6 flow cytometer autosampler. Data analysis was again performed with our custom in-house Matlab and Python scripts and Knijnenburg model [57] (cf. [Methods section](#)), producing a high-throughput in silico pipeline from data acquisition to post-data analysis. For each condition in this dataset, the fold change from the 0 h sample of the same condition was calculated in order to enable comparisons between conditions and to facilitate the overview of the microtiter plate data (Table 3; Additional file 1: Table S4).

Glucose 1 g/L and 20 g/L displayed the same trend in the microtiter plates as in the previous shake flask cultivations (calculated as the fold change from the 0 h baseline; Additional file 1: Figure S7). This demonstrates that the scale-down to microtiter plate cultures did not affect the biosensor signal, while conserving the reproducibility of the assay. It can however be noted that the microplate 0 h-measurement of the *TPS1p/2p* sensors rather seem to reflect the 1 h-point of the shake flask cultures; due to the behavior of the FI pattern in the 1–6 h interval for these two sensors (Fig. 3), a different fold change response direction was therefore found in the microtiter plate experiment compared to the shake flasks (Additional file 1: Figure S7).

Xylose has in previous studies commonly been supplied to engineered *S. cerevisiae* strains in high concentration (50 g/L) in order to improve the uptake rate, as only unspecific pentose transporters exists in this species [12, 68]. Consequently, 50 g/L xylose was used to screen the strains for any signaling response to this pentose sugar. Xylose did not elicit any significant response in any of the strains (Table 3) and the fold change at 3 and 6 h (compared to the signal at 0 h) was comparable to true carbon starvation as was assessed using YNB-KHPthalate medium without any added carbon source (Additional file 1: Table S4).

It has previously been observed that the xylose uptake can be improved by co-substrate cultures with low concentrations of glucose [69]. In order for the glucose to quickly be consumed, but not start out low enough to induce the biosensors strains known to be induced by 1 g/L glucose (Table 2), a xylose (50 g/L) and glucose (5 g/L) co-culture was evaluated, as well as glucose 5 g/L alone in order to be able to distinguish between pentose and hexose effect. It was found that for the biosensors based on hexose transporter promoters (TMB3712–3714), this co-substrate cultivation resulted in a slightly higher fold-change than glucose 5 g/L alone (Table 3). In fact, it was found that the xylose–glucose co-culture was significantly different from the glucose 5 g/L results for

Table 3 Results of the microtiter-plate screening of the biosensors strains on glucose, xylose and a co-culture thereof, given in terms of FI fold induction

Strain	Glucose 5 g/L ^a		Xylose 50 g/L + Gluc. 5 g/L		Xylose 50 g/L ^b	
	3 h	6 h	3 h	6 h	3 h	6 h
TMB3711 (No GFP)	1.00 ± 0.010	0.92 ± 0.056	1.04 ± 0.010*	1.02 ± 0.041 *	0.79 ± 0.017	0.78 ± 0.023
TMB3712 (<i>HXT1p</i>)	1.21 ± 0.016	1.23 ± 0.013	1.48 ± 0.011*	1.70 ± 0.011 *	0.83 ± 0.015	0.84 ± 0.010
TMB3713 (<i>HXT2p</i>)	1.10 ± 0.264	1.34 ± 0.11	1.37 ± 0.26	2.01 ± 0.55*	0.89 ± 0.039	0.89 ± 0.046
TMB3714 (<i>HXT4p</i>)	1.77 ± 0.058	2.47 ± 0.22	2.15 ± 0.31*	3.45 ± 0.62*	1.08 ± 0.25	1.31 ± 0.51
TMB3715 (<i>SUC2p</i>)	0.98 ± 0.15	3.51 ± 0.75	1.13 ± 0.10	5.15 ± 0.62*	0.95 ± 0.12	1.06 ± 0.21
TMB3716 (<i>CAT8p</i>)	0.98 ± 0.002	1.14 ± 0.039	1.08 ± 0.037*	1.13 ± 0.037	0.82 ± 0.003	0.84 ± 0.018
TMB3717 (<i>TPS1p</i>)	0.74 ± 0.051	1.23 ± 0.075	0.70 ± 0.048	0.77 ± 0.047*	0.92 ± 0.006	0.91 ± 0.029
TMB3718 (<i>TPS2p</i>)	0.85 ± 0.026	1.61 ± 0.084	0.95 ± 0.076*	1.05 ± 0.032*	0.85 ± 0.012	0.85 ± 0.026
TMB3719 (<i>TEF4p</i>)	1.35 ± 0.013	1.46 ± 0.010	1.28 ± 0.018*	1.42 ± 0.0032	0.87 ± 0.012	0.96 ± 0.010

The FI signal was normalized to the corresponding 0 h signal of the given condition and strain. A value of 1 corresponds to repression (i.e. no fold change since time 0 h). A one-way ANOVA with a multiple comparison test was performed to statistically compare the results from the different conditions

* Significantly different from the glucose 5 g/L fold change from the same hour (one-way ANOVA with a multiple comparison test; $p \leq 0.05$)

^a Glucose 5 g/L was significantly different from the xylose 50 g/L in all strains and times except for 3 h for TMB3713, TMB3715, TMB3718 and 6 h for TMB3713

^b Xylose 50 g/L was significantly different from the xylose-glucose co-culture in all strains and times except for TMB3715 at 3 h

13 out of the 18 measured time points in Table 3, showing that the higher fold change in the co-substrate cultures was not an effect of the glucose alone, but of the presence of both sugars (Table 3). The xylose that was used in the study had a reported Lot purity of 99.7%, and it is therefore unlikely that the response from the high-affinity transporters is caused by low levels of contaminating sugars. To confirm this, the xylose stock solution that was used throughout this study was analyzed by HPLC, and no other peaks than the expected xylose peak were found (Limit-of-detection: 0.8 g/L).

On the same note, co-substrate cultures of xylose (50 g/L) and glycerol (3% v/v) was used to assess the effect of xylose during respiratory growth. Since it has been hypothesized that xylose exhibits a “non-fermentable carbon source”—response in *S. cerevisiae* [13, 14, 17], evaluation of the sugar signaling during respiratory conditions was performed. However, neither glycerol alone nor in co-culture with xylose, resulted in any major induction fold change throughout the course of the screening (Additional file 1: Table S4).

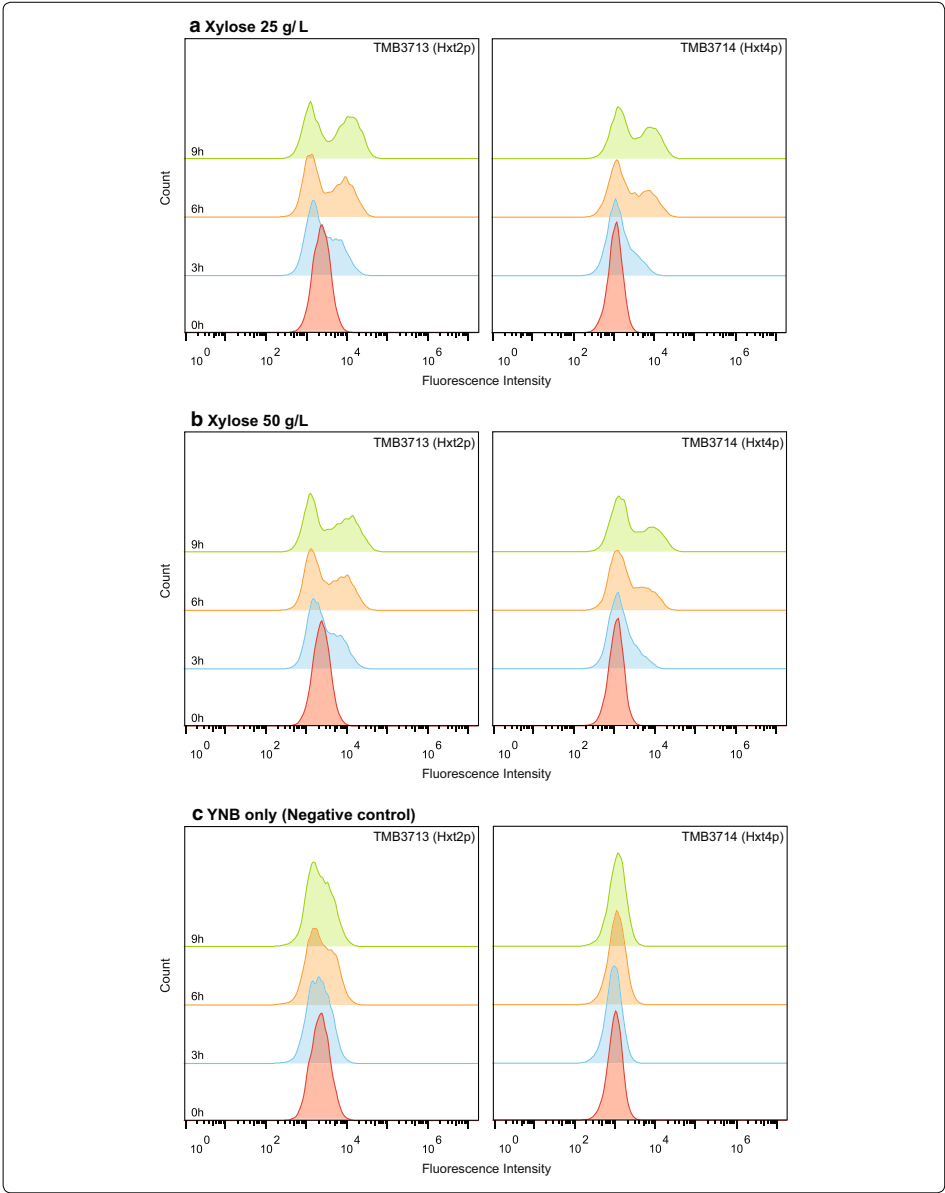
In order to determine if xylose could have any dose-dependent effect on the cellular signaling, all strains were also evaluated in microtiter plates with xylose

concentrations ranging from 25 up to 100 g/L. The analysis time was also extended from 6 h to 9 h to fully assure that any possible lag in the sensor signal would not interfere with the results. For most reporter genes the fluorescence intensity fold-changes again showed unremarkable patterns (Additional file 1: Table S5); the *HXT* sensors, however, consistently displayed higher fold change levels than the remaining biosensors. Furthermore, a study of the raw, non-normalized fluorescence data, revealed that while TMB3712 (*HXT1p*) only showed one, well-defined, fluorescence population (Additional file 1: Figure S8), strains TMB3713 and TMB3714 (*HXT2p* and *HXT4p*, respectively) showed two distinct fluorescence subpopulations (Fig. 5). These two subpopulations were neither visible at the start of the experiment, nor did they appear for cultivations in YNB-KHPthalate only.

In order to evaluate the potential induction characteristics of the two populations, the FI histograms were manually gated and geometric means were calculated for the lower and higher intensity populations, respectively. The intensity values were then compared to the mean intensity of the starting population at 0 h (Table 4). These estimations, along with Fig. 5, made it evident that the percentage of fluorescence events belonging

(See figure on next page.)

Fig. 5 Overlay histogram plots from the raw (non-normalized) data of TMB3713 (*HXT2p*) and TMB3714 (*HXT4p*). Graphs show the distribution of the Fluorescence Intensity per registered event in the sample at each of the four time points (0, 3, 6 and 9 h). The Gaussian distribution seen at time 0 h for all strains signified homogenous populations, whereas deviations from the normal distribution implied population heterogeneities. The strains were cultivated in xylose 25 and 50 g/L and YNB-KHPthalate medium without any carbon source. It evident from **a** and **b** that two subpopulations appear from 3 h and forward, and that this is not the case in the negative control (YNB only). The left subpopulations are equivalent to the cellular autofluorescence (cf. **c**), whereas the right subpopulations are clearly induced



the higher intensity population increased over time and that this percentage was slightly higher for TMB3713 (*HXT2p*) independent on sampling point (Table 4). After 3 h in xylose 25 g/L the higher intensity populations for TMB3713 and TMB3714 had reached fold-changes of 2.69 ± 0.10 and 4.40 ± 0.10 respectively (Table 4), which was comparable to the induction achieved by glucose 1 g/L during the same time period (3.62 ± 0.130 and 4.27 ± 0.50 , respectively; Additional file 1: Table S4).

Discussion

Extracellular xylose is not in itself sensed by *S. cerevisiae*

Over the years, transcriptomics, metabolomics and metabolic flux analysis studies have uncovered the unusual cellular response that xylose assimilation triggers in *S. cerevisiae*. Several significant differences between xylose and glucose on the regulation of the central carbon metabolism have been highlighted in the past, including: catabolite repression patterns [70], respiratory metabolism during oxygen limited cultivations with xylose as the sole carbon source (as opposed to the expected respiro-fermentative metabolism) [19]; expression of respiratory pathway genes on xylose during anaerobiosis [13, 71]; a decrease in the concentration of glycolysis- and pentose phosphate pathway-related precursor metabolites when shifting from glucose to xylose [17]; and an accumulation of aromatic amino acids in yeast cultivated on xylose, that was comparable to the response of starving cells [18, 72]. Taken together, these results have hinted towards a major issue in the xylose sensing and recognition of *S. cerevisiae*, and we believe that this issue is likely to be a cause of the current bottleneck(s) hindering efficient yeast valorization of lignocellulosic material.

The current study has indicated that endogenous mechanisms for xylose signaling do exist in *S. cerevisiae* and that this signal does not seem to originate from sensing of extracellular xylose. Most of our biosensors remained unresponsive to xylose, regardless of it being presented to the cell as a sole carbon source or together with other, fermentable or non-fermentable, carbon sources. These findings would indicate that, for the majority of its carbon sensing pathways, *wild type* non-xylose utilizing *S. cerevisiae* cannot sense extracellular xylose, but would rather sense the lack of fermentable carbon sources (previously suggested in e.g. [16]). However, as will be discussed below, we hypothesize that this is not necessarily the fact for *internalized* xylose.

Flow cytometry illuminates otherwise unseen population heterogeneities on xylose

A key feature of the chosen methodology is that it allows for the assessment of sugar sensing population heterogeneities through the means of flow cytometry. Since all

strains (and therefore all cells in each measured population) have been engineered to have one single copy of the biosensor, any occurrence of subpopulations can be considered to be of true physiological relevance. When a consistently higher mean FI was discovered for the *HXT1/2/4* biosensors in the xylose titer dataset (Additional file 1: Table S5), we traced the effect down to the population distribution level; this allowed us to identify subpopulations expressing significantly higher amounts of GFP in non-growing TMB3713 (*HXT2p*) and TMB3714 (*HXT4p*) incubated with 25–100 g/L xylose (Fig. 5; Table 4 highlights the results of the 25 and 50 g/L cultivations). This heterogeneous population distribution on the FI channel would have gone undetected with conventional fluorimetry or transcriptomics, where only population averages are considered (i.e. methods that will detect changes in average signal, but cannot identify subpopulations). In both the TMB3713 and TMB3714 strains, the higher of the two FI populations showed FI fold-changes (Fig. 5; Table 4) comparable to the induction patterns found for 1 g/L glucose (Additional file 1: Table S4), the condition considered to yield the highest induction for these gene targets. Despite the slightly higher mean FI of TMB3712 (*HXT1p*; Additional file 1: Table S5), this strain did not display any subpopulations during these conditions (Additional file 1: Figure S8).

The presence of these fluorescent subpopulations allowed us to surmise a few of the characteristics of this apparent xylose sensing effect. We hypothesize that this sensing requires xylose to be transported into the cell. Out of the two sensors controlling *HXT1/2/4* induction, *Snf3p* and *Rgt2p*, the former has been reported to be glucose repressed while the latter is expressed at low levels regardless of glucose or xylose concentrations [14, 20, 73], indicating that during incubation with xylose all cells would have the same probability of sensing the extracellular xylose at any specific time point. Were the xylose sensing only contingent on recognition at the cell membrane, all cells would be equally susceptible to induction and the fluorescence profiles would remain single-population, but this is not the case in the current results for TMB3713–3714. Another factor weighing into this conclusion is that none of the *Snf3p/Rgt2p* pathway regulated genes showed any split FI-histogram populations under glucose conditions (data not shown). We therefore hypothesize that at least one component of the natural *Snf3p/Rgt2p* signaling pathway is missing for xylose, and this missing piece is likely to be the system for extracellular recognition.

During the pre-cultivations, the biosensor strains were grown in conditions that were repressing towards their particular gene target. In the case of TMB3713 (*HXT2p*) and TMB3714 (*HXT4p*), a high glucose content (40 g/L

Table 4 Population heterogeneities for the hexose transporter-based biosensors during xylose cultivations

Strain	Population	FI fold changes (25 g/L xylose)			FI fold changes (50 g/L xylose)		
		3 h	6 h	9 h	3 h	6 h	9 h
TMB3712 (<i>HXT1p</i>)	Single	1.24 ± 0.17	1.10 ± 0.10	1.00 ± 0.32	1.26 ± 0.36	1.23 ± 0.26	1.13 ± 0.31
	% of total population	100	100	100	100	100	100
TMB3713 (<i>HXT2p</i>)	High FI	2.69 ± 0.10	3.90 ± 0.28	5.16 ± 0.060	3.23 ± 0.21	3.70 ± 0.020	4.52 ± 0.082
	% of total population	36 ± 0.1	43 ± 6.1	51 ± 2.1	32 ± 4.1	42 ± 0.5	49 ± 2.1
	Low FI	0.66 ± 0.004	0.58 ± 0.031	0.58 ± 0.004	0.71 ± 0.018	0.60 ± 0.017	0.58 ± 0.030
TMB3714 (<i>HXT4p</i>)	% of total	64 ± 0.1	57 ± 6.1	49 ± 2.1	68 ± 4.1	58 ± 0.5	51 ± 2.1
	High FI	4.40 ± 0.10	6.39 ± 0.15	7.76 ± 0.10	5.29 ± 1.22	6.01 ± 0.26	8.14 ± 0.024
	% of total population	19 ± 3.3	37 ± 3.2	42 ± 2.7	13 ± 8.3	29 ± 1.8	35 ± 0.2
	Low FI	1.02 ± 0.004	1.04 ± 0.007	1.21 ± 0.012	1.11 ± 0.11	1.07 ± 0.047	1.15 ± 0.068
	% of total population	8.1 ± 3.3	63 ± 3.2	58 ± 2.7	87 ± 8.3	71 ± 1.8	65 ± 0.2

Peak fold changes and population distributions (percent of total cell population) during cultivation in 25 and 50 g/L xylose in non-normalized data (for the normalized data from this experiment, cf. Additional file 1: Table S5). TMB3712 (*HXT1p*) displayed an increase in FI after already 3 h, but the analyzed samples were consistently distributed in a single peak population. TMB3713 (*HXT2p*) and TMB3714 (*HXT4p*) were highly heterogeneous on the FL-1 (GFP) channel with two distinct peaks (one with low and one with high FI). The histograms of TMB3713–3714 are also displayed in Fig. 5. The experiments were performed in biological and technical duplicates

for 12 h) was used as the repressing condition. While this condition will repress the high-affinity hexose transporters, low-affinity transporters such as *HXT1* will be in an induced stage at the end of the pre-culture/start of the xylose incubation. Although these low-affinity transporters have been reported to have an affinity for xylose so low that they cannot support growth of otherwise xylose-utilizing yeast strains [74], it is known that they do have some transport capacity for this pentose [75]. It is therefore possible that the Hxt1p membrane transport protein, or any of the other glucose induced transporter proteins, are present on the cell membrane when the yeast cells are transferred from the glucose 40 g/L pre-culture to the xylose-containing media. From here—and this is the core of the present hypothesis—a stochastic event decides whether or not the cell will take up the xylose (via the expressed hexose transporters). For the subpopulation in which this event occurred, the internalized xylose molecules were then able to induce/derepress the *HXT2/4* genes, as was demonstrated by the population distributions observed in Fig. 5.

Partial derepression of high-affinity hexose transporter genes for *S. cerevisiae* was also found in a transcriptomics study by Salusjarvi et al. [14], comparing expression profiles while metabolizing xylose or in different states of catabolite repression. Although the authors also suggest a potential xylose effect on the Snf3/Rgt2 pathway, their study cannot differentiate between sensing of extracellular or intracellular xylose, especially since xylose was confirmed to be taken up and metabolized. In contrast, our study focused on the inherent effect of xylose—and not its metabolites—on native yeast, as well as elucidating the population heterogeneities obscured by transcriptomic approaches.

Conclusions

Through this study, we have generated and validated a panel of in vivo biosensors that allows for rapid assessment of the sugar signaling state of the *S. cerevisiae* cell. Furthermore, this study has, to our knowledge, demonstrated that extracellular xylose itself does not trigger a regulatory response, as the current results imply that the previously reported respiratory response on xylose is due to the lack of glucose and is not an effect of the presence of extracellular xylose. Furthermore, the results of the current study indicate for the first time a cellular mechanism for recognition of internalized xylose in *S. cerevisiae*; however, future work dedicated to this hypothesis is required in order to fully ascertain this. Accordingly, this creates a strong impetus for metabolic engineering of the sugar signaling pathways as the next logical step in order to improve xylose utilization and valorization in this yeast.

Additional file

Additional file 1. Additional materials and methods, figures and tables.

Abbreviations

FI: fluorescence intensity; GFP: green fluorescent protein; ORF: open reading frame; YNB: yeast nitrogen base.

Authors' contributions

DB participated in the design of the study, constructed the strains and drafted the initial manuscript. DB and FT designed and performed the flow cytometry analyses and enzymatic assay. CB participated in the design of the study, and together with DB performed the molecular biology experiments, wrote the custom scripts and finalized the manuscript. FT designed and performed the microtiter plate screening setup and the RT-qPCR gene-expression analysis. MGG conceived the study and revised the manuscript. All authors read and approved the final manuscript.

Acknowledgements

We want to thank Magnus Carlquist for fruitful discussions on experimental design for flow cytometry and enzymatic assays, Johannes Hedman for valuable input on RT-qPCR assay design and Peter Rådström for critical reading of the manuscript.

Competing interests

The authors declare that they have no competing interests.

Availability of data and materials

The datasets supporting the conclusions of this article are available in the FlowRepository repository (<https://flowrepository.org/>) with accession numbers FR-FCM-ZZRA, FR-FCM-ZZRB, FR-FCM-ZZRC, FR-FCM-ZZRD and FR-FCM-ZZRE. The custom Matlab and Python scripts are available in Supporting Information S2 and at the authors' Github repository (<https://github.com/tmbyeast/Flow-cytometry-tools>).

Funding

This work was financially supported by the Swedish National Energy Agency (Energimyndigheten, Project No. P35350-1). The funders had no role in the design of the study, collection, analysis, and interpretation of data or writing of the manuscript.

Received: 29 May 2016 Accepted: 14 October 2016

Published online: 24 October 2016

References

- Goddard MR, Greig D. *Saccharomyces cerevisiae*: a nomadic yeast with no niche. *FEMS Yeast Res*. 2015;15(3):009.
- Dashko S, Zhou N, Compagno C, Piskur J. Why, when, and how did yeast evolve alcoholic fermentation? *FEMS Yeast Res*. 2014;14:826–32.
- Santangelo GM. Glucose signaling in *Saccharomyces cerevisiae*. *Microbiol Mol Biol Rev*. 2006;70:253–82.
- Conrad M, Schothorst J, Kankipati HN, Van Zeebroeck G, Rubio-Teixeira M, Thevelein JM. Nutrient sensing and signaling in the yeast *Saccharomyces cerevisiae*. *FEMS Microbiol Rev*. 2014;38:254–99.
- Zaman S, Lippman SI, Schnepel L, Slonim N, Broach JR. Glucose regulates transcription in yeast through a network of signaling pathways. *Mol Syst Biol*. 2009;5(1):245.
- Gancedo JM. Yeast carbon catabolite repression. *Microbiol Mol Biol Rev*. 1998;62:334–61.
- Toivari MH, Salusjarvi L, Ruohonen L, Penttilä M. Endogenous xylose pathway in *Saccharomyces cerevisiae*. *Appl Environ Microbiol*. 2004;70:3681–6.
- Laluce C, Schenberg ACG, Gallardo JCM, Coradello LFC, Pombeiro-Sponchiado SR. Advances and developments in strategies to improve strains of *Saccharomyces cerevisiae* and processes to obtain the lignocellulosic ethanol-A review. *Appl Biochem Biotechnol*. 2012;166:1908–26.
- Hahn-Hägerdal B, Karhumaa K, Fonseca C, Spencer-Martins I, Gorwa-Grauslund MF. Towards industrial pentose-fermenting yeast strains. *Appl Microbiol Biotechnol*. 2007;74:937–53.
- Kötter P, Ciriacy M. Xylose fermentation by *Saccharomyces cerevisiae*. *Appl Microbiol Biotechnol*. 1993;38:776–83.
- Brat D, Boles E, Wiedemann B. Functional expression of a bacterial xylose isomerase in *Saccharomyces cerevisiae*. *Appl Environ Microbiol*. 2009;75:2304–11.
- Karhumaa K, Wiedemann B, Hahn-Hägerdal B, Boles E, Gorwa-Grauslund MF. Co-utilization of L-arabinose and D-xylose by laboratory and industrial *Saccharomyces cerevisiae* strains. *Microb Cell Fact*. 2006;5(1):1.
- Jin YS, Laplaza JM, Jeffries TW. *Saccharomyces cerevisiae* engineered for xylose metabolism exhibits a respiratory response. *Appl Environ Microbiol*. 2004;70:6816–25.
- Salusjarvi L, Kankainen M, Soliymani R, Pitkanen JP, Penttilä M, Ruohonen L. Regulation of xylose metabolism in recombinant *Saccharomyces cerevisiae*. *Microb Cell Fact*. 2008;7(1):1.
- Souto-Maior AM, Runquist D, Hahn-Hägerdal B. Crabtree-negative characteristics of recombinant xylose-utilizing *Saccharomyces cerevisiae*. *J Biotechnol*. 2009;143:119–23.
- Matsushika A, Goshima T, Hoshino T. Transcription analysis of recombinant industrial and laboratory *Saccharomyces cerevisiae* strains reveals the molecular basis for fermentation of glucose and xylose. *Microb Cell Fact*. 2014;13(1):1.
- Bergdahl B, Heer D, Sauer U, Hahn-Hägerdal B, van Niel EW. Dynamic metabolomics differentiates between carbon and energy starvation in recombinant *Saccharomyces cerevisiae* fermenting xylose. *Biotechnol Biofuels*. 2012;5(1):1.
- Klimacek M, Krahulec S, Sauer U, Nidetzky B. Limitations in xylose-fermenting *Saccharomyces cerevisiae*, made evident through comprehensive metabolite profiling and thermodynamic analysis. *Appl Environ Microbiol*. 2010;76:7566–74.
- Feng X, Zhao H. Investigating glucose and xylose metabolism in *Saccharomyces cerevisiae* and *Scheffersomyces stipitis* via C-13 metabolic flux analysis. *AIChE J*. 2013;59:3195–202.
- Özcan S, Johnston M. Three different regulatory mechanisms enable yeast hexose transporter (hxt) genes to be induced by different levels of glucose. *Mol Cell Biol*. 1995;15:1564–72.
- Dietvorst J, Karhumaa K, Kielland-Brandt MC, Brandt A. Amino acid residues involved in ligand preference of the Snf3 transporter-like sensor in *Saccharomyces cerevisiae*. *Yeast*. 2010;27:131–8.
- Moreno F, Ahuatz D, Riera A, Palomino CA, Herrero P. Glucose sensing through the Hxk2-dependent signalling pathway. *Biochem Soc Trans*. 2005;33:265–8.
- Kraakman LS, Winderickx J, Thevelein JM, de Winder JH. Structure-function analysis of yeast hexokinase: structural requirements for triggering cAMP signalling and catabolite repression. *Biochem J*. 1999;343:159–68.
- García-Salcedo R, Lubitz T, Beltran G, Elbing K, Tian Y, Frey S, Wolkenhauer O, Krantz M, Klipp E, Hohmann S. Glucose de-repression by yeast AMP-activated protein kinase SNF1 is controlled via at least two independent steps. *FEBS J*. 2014;281:1901–17.
- Thevelein JM, Cauwenberg L, Colombo S, de Winder JH, Donatoni M, Dumortier F, Kraakman L, Lemaire K, Ma P, Nauwelaers D, et al. Nutrient-induced signal transduction through the protein kinase A pathway and its role in the control of metabolism, stress resistance, and growth in yeast. *Enzyme Microb Technol*. 2000;26:819–25.
- Weinhandl K, Winkler M, Glieder A, Camattari A. Carbon source dependent promoters in yeasts. *Microb Cell Fact*. 2014;13(1):1.
- Cormack BP, Bertram G, Egerton M, Gow NR, Falkow S, Brown AJP. Yeast-enhanced green fluorescent protein (yEGFP): a reporter of gene expression in *Candida albicans*. *Microbiology*. 1997;143:303–11.
- Chalfie M. GFP: lighting up life. *Proc Natl Acad Sci USA*. 2009;106:10073–80.
- Peng B, Williams TC, Henry M, Nielsen LK, Vickers CE. Controlling heterologous gene expression in yeast cell factories on different carbon substrates and across the diauxic shift: a comparison of yeast promoter activities. *Microb Cell Fact*. 2015;14:91.
- Thierfelder S, Ostermann K, Göbel A, Rödel G. Vectors for glucose-dependent protein expression in *Saccharomyces cerevisiae*. *Appl Biochem Biotechnol*. 2011;163:954–64.
- Ishii J, Izawa K, Matsumura S, Wakamura K, Tanino T, Tanaka T, Ogino C, Fukuda H, Kondo A. A simple and immediate method for simultaneously evaluating expression level and plasmid maintenance in yeast. *J Biochem*. 2009;145:701–8.
- Carlquist M, Fernandes RL, Helmark S, Heins AL, Lundin L, Sørensen SJ, Gernaey KV, Lantz AE. Physiological heterogeneities in microbial populations and implications for physical stress tolerance. *Microb Cell Fact*. 2012;11:1.
- Knudsen JD, Carlquist M, Gorwa-Grauslund M. NADH-dependent biosensor in *Saccharomyces cerevisiae*: principle and validation at the single cell level. *AMB Express*. 2014;4:81.
- Kacmar J, Zamamiri A, Carlson R, Abu-Absi NR, Srien F. Single-cell variability in growing *Saccharomyces cerevisiae* cell populations measured with automated flow cytometry. *J Biotechnol*. 2004;109:239–54.
- Attfield PV, Choi HY, Veal DA, Bell PJL. Heterogeneity of stress gene expression and stress resistance among individual cells of *Saccharomyces cerevisiae*. *Mol Microbiol*. 2001;40:1000–8.
- Chambers P, Issaka A, Palecek SP. *Saccharomyces cerevisiae* JEN1 promoter activity is inversely related to concentration of repressing sugar. *Appl Environ Microbiol*. 2004;70:8–17.

37. Wang M, Li S, Zhao H. Design and engineering of intracellular-metabolite-sensing/regulation gene circuits in *Saccharomyces cerevisiae*. *Biotechnol Bioeng*. 2016;113(1):206–15.
38. Teo WS, Chang MW. Bacterial XylRs and synthetic promoters function as genetically encoded xylose biosensors in *Saccharomyces cerevisiae*. *Biotechnol J*. 2015;10:315–22.
39. Roca C, Haack MB, Olsson L. Engineering of carbon catabolite repression in recombinant xylose fermenting *Saccharomyces cerevisiae*. *Appl Microbiol Biotechnol*. 2004;63:578–83.
40. Pronk JT. Auxotrophic yeast strains in fundamental and applied research. *Appl Environ Microbiol*. 2002;68:2095–100.
41. Kokina A, Kibildis J, Liepins J. Adenine auxotrophy – be aware: some effects of adenine auxotrophy in *Saccharomyces cerevisiae* strain W303-1A. *FEMS Yeast Res*. 2014;14:697–707.
42. Sambrook J, Russell DW. *Molecular cloning: a laboratory manual*. 3rd ed. Cold Spring Harbor: Cold Spring Harbor Laboratory Press; 2001.
43. Cherry JM, Hong EL, Amundsen C, Balakrishnan R, Binkley G, Chan ET, Christie KR, Costanzo MC, Dwight SS, Engel SR, et al. *Saccharomyces* genome database: the genomics resource of budding yeast. *Nucleic Acids Res*. 2012;40:D700–5.
44. Lööke M, Kristjuhan K, Kristjuhan A. Extraction of genomic DNA from yeasts for PCR-based applications. *Biotechniques*. 2011;50(5):325.
45. Inoue H, Nojima H, Okayama H. High-efficiency transformation of *Escherichia coli* with plasmids. *Gene*. 1990;96:23–8.
46. Gietz RD, Schiestl RH. High-efficiency yeast transformation using the LiAc/SS carrier DNA/PEG method. *Nat Protoc*. 2007;2:31–4.
47. Hill J, Donald KAIG, Griffiths DE. DMSO-enhanced whole cell yeast transformation. *Nucleic Acids Res*. 1991;19:5791–2.
48. Vanhalewyn M, Dumortier F, Debat G, Colombo S, Ma PS, Winderickx J, Van Dijk P, Thevelein JM. A mutation in *Saccharomyces cerevisiae* adenylate cyclase, *Cyr 1* (K1876 M), specifically affects glucose- and acidification-induced cAMP signalling and not the basal cAMP level. *Mol Microbiol*. 1999;33:363–76.
49. Nijkamp JF, van den Broek M, Datema E, de Kok S, Bosman L, Luttk M, Daran-Lapujade P, Vongsangnak W, Nielsen J, Heijne HM, et al. De novo sequencing, assembly and analysis of the genome of the laboratory strain *Saccharomyces cerevisiae*, a model for modern industrial biotechnology. *Microb Cell Fact*. 2012;11(1):1.
50. Gietz RD, Sugino A. New yeast-*Escherichia coli* shuttle vectors constructed with in vitro mutagenized yeast genes lacking six-base pair restriction sites. *Gene*. 1988;74:527–34.
51. Flagfeldt DB, Siewers V, Huang L, Nielsen J. Characterization of chromosomal integration sites for heterologous gene expression in *Saccharomyces cerevisiae*. *Yeast*. 2009;26:545–51.
52. Voth WP, Jiang YW, Stillman DJ. New 'marker swap' plasmids for converting selectable markers on budding yeast gene disruptions and plasmids. *Yeast*. 2003;20:985–93.
53. Brachmann CB, Davies A, Cost GJ, Caputo E, Li JC, Hieter P, Boeke JD. Designer deletion strains derived from *Saccharomyces cerevisiae* S288C: a useful set of strains and plasmids for PCR-mediated gene disruption and other applications. *Yeast*. 1998;14:115–32.
54. Thomas BJ, Rothstein R. Elevated recombination rates in transcriptionally active DNA. *Cell*. 1989;56:619–30.
55. Pronk JT, Steensma HY, vanDijken JP. Pyruvate metabolism in *Saccharomyces cerevisiae*. *Yeast*. 1996;12:1607–33.
56. Spidlen J, Breuer K, Brinkman R. Preparing a minimum information about a flow cytometry experiment (MIFlowCyt) compliant manuscript using the international society for advancement of cytometry (ISAC) FCS file repository (FlowRepository.org). *Curr Protocol Cytomet*. 2012;10(18):11–26.
57. Knijnenburg TA, Roda O, Wann YK, Nolan GP, Aitchison JD, Shmulevich I. A regression model approach to enable cell morphology correction in high-throughput flow cytometry. *Mol Syst Biol*. 2011;7(1):531.
58. Ismail KSK, Sakamoto T, Hasunuma T, Kondo A. Time-based comparative transcriptomics in engineered xylose-utilizing *Saccharomyces cerevisiae* identifies temperature-responsive genes during ethanol production. *J Ind Microbiol Biotechnol*. 2013;40:1039–50.
59. Teste MA, Duquenne M, Francois JM, Parrou JL. Validation of reference genes for quantitative expression analysis by real-time RT-PCR in *Saccharomyces cerevisiae*. *BMC Mol Biol*. 2009;10(1):1.
60. Pfaffl MW. A new mathematical model for relative quantification in real-time RT-PCR. *Nucleic Acids Res*. 2001;29(9):45.
61. Weiß P, Huppert S, Kolling R. ESCRT-III protein Snf7 mediates high-level expression of the *SUC2* gene via the Rim101 pathway. *Eukaryot Cell*. 2008;7:1888–94.
62. Harkness TAA, Amason TG. A simplified method for measuring secreted invertase activity in *Saccharomyces cerevisiae*. *Biochem Pharmacol*. 2014;3:151.
63. Bauminger BB. Micro method for manual analysis of true glucose in plasma without deproteinization. *J Clin Pathol*. 1974;27:1015–7.
64. Apweiler E, Sameith K, Margaritis T, Brabers N, van de Pasch L, Bakker LV, van Leenen D, Holstege FCP, Kemmeren P. Yeast glucose pathways converge on the transcriptional regulation of trehalose biosynthesis. *BMC Genom*. 2012;13(1):1.
65. Wu J, Zhang NS, Hayes A, Panoutsopoulou K, Oliver SG. Global analysis of nutrient control of gene expression in *Saccharomyces cerevisiae* during growth and starvation. *Proc Natl Acad Sci USA*. 2004;101:3148–53.
66. Mateus C, Avery SV. Destabilized green fluorescent protein for monitoring dynamic changes in yeast gene expression with flow cytometry. *Yeast*. 2000;16:1313–23.
67. Glickman MH, Rubin DM, Fried VA, Finley D. The regulatory particle of the *Saccharomyces cerevisiae* proteasome. *Mol Cell Biol*. 1998;18:3149–62.
68. Bergdahl B, Sandström AG, Borgström C, Boonyawan T, van Niel EWJ, Gorwa-Grauslund MF. Engineering yeast hexokinase 2 for improved tolerance toward xylose-induced inactivation. *PLoS ONE*. 2013;8(9):75055.
69. Lee WJ, Kim MD, Ryu YW, Bisson LF, Seo JH. Kinetic studies on glucose and xylose transport in *Saccharomyces cerevisiae*. *Appl Microbiol Biotechnol*. 2002;60:186–91.
70. Belinchón MM, Gancedo JM. Xylose and some non-sugar carbon sources cause catabolite repression in *Saccharomyces cerevisiae*. *Arch Microbiol*. 2003;180:293–7.
71. Runquist D, Hahn-Hägerdal B, Bettiga M. Increased expression of the oxidative pentose phosphate pathway and gluconeogenesis in anaerobically growing xylose-utilizing *Saccharomyces cerevisiae*. *Microb Cell Fact*. 2009;8:1.
72. Matsushika A, Nagashima A, Goshima T, Hoshino T. Fermentation of xylose causes inefficient metabolic state due to carbon/energy starvation and reduced glycolytic flux in recombinant industrial *Saccharomyces cerevisiae*. *PLoS ONE*. 2013;8(7):69005.
73. Özcan S, Dover J, Rosenwald AG, Wolf S, Johnston M. Two glucose transporters in *Saccharomyces cerevisiae* are glucose sensors that generate a signal for induction of gene expression. *Proc Natl Acad Sci USA*. 1996;93:12428–32.
74. Hamacher T, Becker J, Gardonyi M, Hahn-Hägerdal B, Boles E. Characterization of the xylose-transporting properties of yeast hexose transporters and their influence on xylose utilization. *Microbiology*. 2002;148:2783–8.
75. Sedlak M, Ho NW. Characterization of the effectiveness of hexose transporters for transporting xylose during glucose and xylose co-fermentation by a recombinant *Saccharomyces* yeast. *Yeast*. 2004;21:671–84.
76. Entian KD, Köttler P. Yeast genetic strain and plasmid collections. *Yeast Gene Anal*. 2007;36:629–66.
77. Özcan S, Johnston M. Two different repressors collaborate to restrict expression of the yeast glucose transporter genes *HXT2* and *HXT4* to low levels of glucose. *Mol Cell Biol*. 1996;16:5536–45.
78. Özcan S, Vallier LG, Flick JS, Carlson M, Johnston M. Expression of the *SUC2* gene of *Saccharomyces cerevisiae* is induced by low levels of glucose. *Yeast*. 1997;13:127–37.
79. Hedges D, Proft M, Entian KD. CAT8, a new zinc cluster-encoding gene necessary for derepression of gluconeogenic enzymes in the yeast *Saccharomyces cerevisiae*. *Mol Cell Biol*. 1995;15:1915–22.
80. Parrou JL, Enjalbert B, Plourde L, Bauche A, Gonzalez B, Francois J. Dynamic responses of reserve carbohydrate metabolism under carbon and nitrogen limitations in *Saccharomyces cerevisiae*. *Yeast*. 1999;15:191–203.
81. Winderickx J, de Winde JH, Crauwels M, Hino A, Hohmann S, Van Dijk P, Thevelein JM. Regulation of genes encoding subunits of the trehalose synthase complex in *Saccharomyces cerevisiae*: novel variations of STRE-mediated transcription control? *Mol Gen Genet*. 1996;252:470–82.
82. Olarewaju O, Ortiz PA, Chowdhury WQ, Chatterjee I, Kinzy TG. The Translation Elongation Factor eEF1B Plays a Role in the Oxidative Stress Response Pathway. *RNA Biol*. 2004;1:89–94.
83. Groust I, Ivanov P, Malcova I, Pomphach P, Frydlova I, Slaba R, Senohrabkova L, Novakova L, Hasek J. Heat shock-induced accumulation of translation elongation and termination factors precedes assembly of stress granules in *S. cerevisiae*. *PLoS ONE*. 2013;8(3):57083.

Supporting Information[†] for:

Real-time monitoring of the sugar sensing in *Saccharomyces cerevisiae* indicates endogenous mechanisms for xylose signaling

Daniel P Brink[¶], Celina Borgström[¶], Felipe G Tueros and Marie F Gorwa-Grauslund*

Applied Microbiology, Department of Chemistry, Lund University, Lund, Sweden

*Corresponding author

E- mail: Marie-Francoise.Gorwa@tmb.lth.se

[¶]These authors contributed equally to this work

[†] Reformatted for increased readability by Celina Borgström Tufvegren

Supplementary Materials and Methods

High-throughput cell size normalization script for flow cytometry

Flow cytometry, not unlike genome sequencing and RNA-seq, generates *Big Data* due to its single cell analysis over multiple channels. This calls for novel *in silico* tools for facilitating post-data processing, especially in experimental designs where the number of runs, replicates and conditions start to increase. We have designed Matlab (Release R2015a, The MathWorks, Inc., Natick, MA, US) and Python (v3, The Python Software Foundation, US) scripts that within minutes processes raw .fcs-files (here outputted by the BD Accuri flow cytometer; Becton-Dickinson, NJ, US), normalizes the fluorescence intensity (FI) on channel FL1-H to cell size by calling the Knijnenburg morphology normalization model [1], and plots the geometrical mean of each normalized histogram versus time as either scatter or bar plots. Thus we have generated a high-throughput pipeline from data acquisition to post-processing that significantly decreases the hands-on analysis time. Since there is no set limitation in the number of strains, replicates and conditions that can be assessed with these custom scripts, they are applicable both to batch and microtiter plate cultivation data.

The main script that needs to be called in order to run the pipeline is the *FI_size_normalization_loader.m* (Matlab). Users will have to download the Knijnenburg model separately according to the author's instructions [1] and store *FI_size_normalization_loader.m* in the root of the Knijnenburg model folder. Our custom Matlab script recognises .fcs-files stored in the following folder hierarchy: *<strain>/<biological replicate>/<conditions>*. Filenames must include the sample time (in hours) and the folder names are used to keep track of the files during the processing. In order to facilitate the control of filenames and folder hierarchy, a custom Python script (v3, The Python Software Foundation, US) was also written.

The *batch_name_change_accuri_fc_data.py* script was specifically designed for use with .fcs-files output by the Accuri software. A specific feature of this software is that it adds the acquisition position of the sample to each sample with exported as .fcs: e.g. A01 TMB3711 1g.L 0h. The Python script uses the position in the acquisition matrix (rows A-H, columns 01-12) to rename and sort the files in the required hierarchy. The user inputs the desired names in the *accuri_data_matrix.txt* template and when run the script outputs data that can directly be used as in-data for *FI_size_normalization_loader.m* script in Matlab. Although it is however possible to rename the .fcs files manually (as long as the file names end with Xh.fcs, where X is the sample time), we recommend users to use the *batch_name_change_accuri_fc_data.py-FI_size_normalization_loader.m* pipeline for convenience.

The *FI_size_normalization_loader.m* comes with a number of options to customize the output of the processed data. The user will have to choose if they want scatter plots (*styler='time'*) or bar plots (*styler='bar'*). Optional settings are: plot each replicate individually (*err='0'*; default) or as means with standard deviation errorbars (*err='1'*); and to show the results of the normalized histograms (*norm_plot='1'*) or not

(`norm_plot='0'; default`). For more information on the scripts, please see the readme-file in the script archive.

At the moment, the script can only normalize and plot data from one channel of the flow cytometer as this was the desired feature for the current study. Users are welcome to modify the scripts to fit with their own projects as long as the current study is cited. An archive containing all custom scripts developed for the current study is available in Supplementary File S2 and has also been deposited on Github (<https://github.com/tmbyeast/Flow-cytometry-tools>). Possible future updates to the custom scripts will be stored on the Github page.

Adapted invertase assay

The invertase assay used in the current study was adapted from three previous protocols in order to generate a protocol for assessment of cell extracts that did not rely on the commonly used, but highly carcinogenic, o-dianisidine chromophore, but instead on the non-carcinogenic 4-aminoantipyrine/phenol reaction [2-4]. The assay is based on three coupled enzymatic reactions: invertase in cell extracts converts added sucrose into fructose and glucose, followed by oxidation of the latter by glucose oxidase, producing D-glucono-1,5-lactone and hydrogen peroxide. In the third step hydrogen peroxide is used by horseradish peroxidase to produce a colored chromophore from an added substrate [3].

Cells were grown in 100 mL shake flask cultures with 1 g/L glucose as inducing condition (preceded by pre-pre- and pre-cultures as described in the *Cultivation conditions* section in the main publication). Samples of 5 mL were harvested by centrifugation (1800 RCF, 5 min at room temperature), washed once in 5 mL sterile water prior to supernatant removal with an FTA-1 aspirator (Biosan, Riga, Latvia). Cell pellets were stored in -80°C and all samples were kept on ice during subsequent cell lysis and sample pre-processing.

For the enzyme assay, the frozen cell pellets were thawed on ice and resuspended in 600 µL 0.1 M NaC₂ H₃ O₂ (Na-Ac). Lysis of cells was done by glass bead beating in a Precellys 24 (Bertin Technologies, France; 5000 rpm, 3 cycles, 45s/cycle, 30 s pause between cycles) cooled by a Cryolus temperature controller (Bertin Technologies, France) with dry-ice. 400 µL of the supernatant was transferred to a fresh 1.5 mL tube and centrifuged at 500 RCF and 0°C for 5 minutes [4]. The supernatant was then transferred to 150 µL of 0.1 M Na-Ac, generating the final product of the sample pre-processing. 5 µL of this solution was used for the invertase assay by adding it to 100 µL fresh 0.1 M Na-Ac [4].

The first assay step (using the invertase in the cell extracts) was started by adding 25 µL freshly prepared 0.5 M sucrose to the assay tubes and incubating in a 37°C water bath for 20 minutes [3]. Four controls were prepared for each assay: I) cells without sucrose, II) sucrose without cells, III) 250 mM glucose and IV) 500 mM glucose [3]. The invertase reaction was stopped by addition of 150 µL 0.2 M K₂HPO₄ and boiling for 3 minutes in a heat block [3].

To start the second and third assay steps (glucose oxidase and peroxidase), 0.5 mL 4-aminoantipyrine-based coloring reagent solution (0.1 M K_2HPO_4 , pH 7; 2.5 mg/mL glucose oxidase ($>15,000$ U/g; Sigma-Aldrich, St. Louis, MO, USA); 0.5 mg/mL Type II horseradish peroxidase (200 U/mg; Sigma-Aldrich, St. Louis, MO, USA) [4]; 1.48 mM 4-aminoantipyrine; 21.25 mM phenol [2]; wrapped in foil and stored at 4°C) was added to the tubes that were then incubated in a 37°C water bath for an additional 20 minutes. Finally, absorbance was measured at 540nm in technical duplicates using a Ultrospec 2100 Pro spectrophotometer (Amersham Biosciences, Uppsala, Sweden).

Total protein content in the cell extracts samples were quantified using the Coomassie (Bradford) Protein Assay Kit (Thermo Scientific; Waltham, MA, US) with 5 μL of each cell extract sample. The assay outcome was determined with a Multiscan Ascent microtiter plate reader (Thermo Scientific; Waltham, MA, US) at 595nm.

The end-point invertase concentration for every sample was calculated using Lambert-Beer's law and the molar absorptivity $13,900 \text{ M}^{-1}\text{cm}^{-1}$ for the resulting product of the 4-aminoantipyrine/phenol assay (4-N-(1,4-benzoquinoneimine)-antipyrine) [5]. The specific invertase activity was then determined by dividing the invertase concentration with the corresponding total protein content and invertase reaction time (20 min), yielding the unit $\mu\text{mol } \mu\text{g}^{-1} \text{ min}^{-1}$.

Supplementary Figures

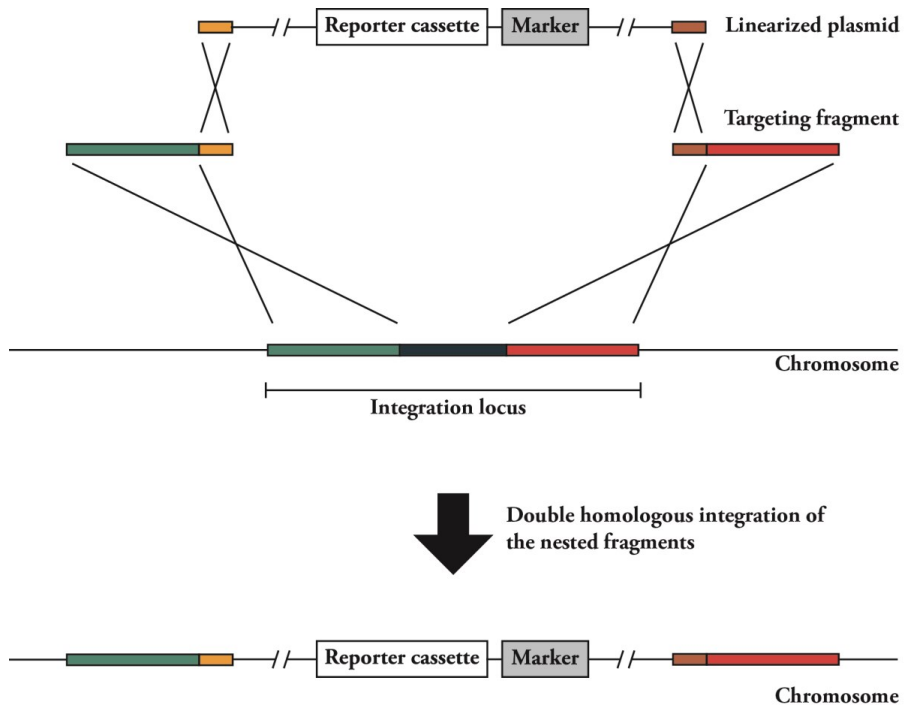


Fig S1. Schematic representation of the utilized strategy for double homologous, single-copy integration of the GFP-reporter plasmids in the *S. cerevisiae* genome. Correct integration of the linearized plasmid was aided by targeting fragments with homology to both the plasmid and the integration locus. Colors represent homologous regions.

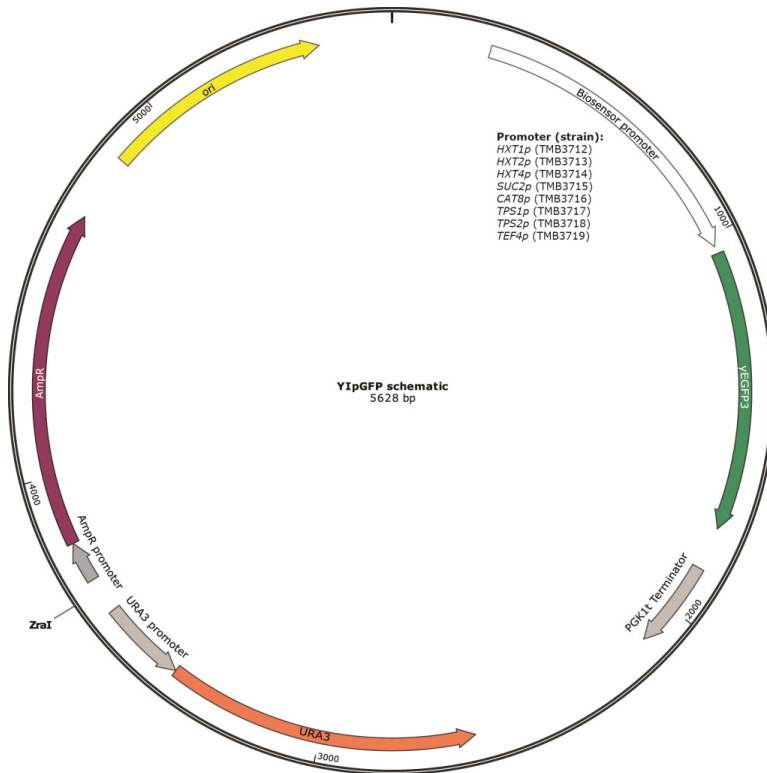
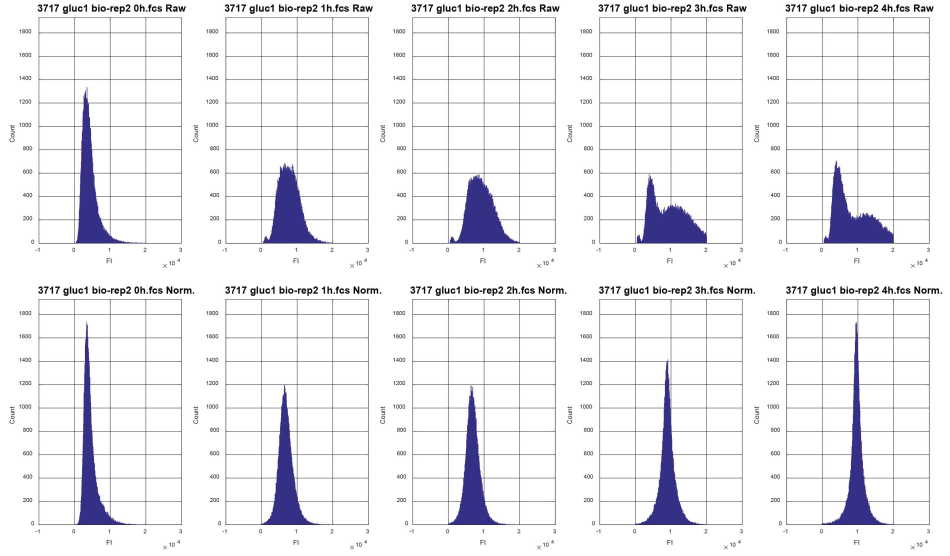


Fig S2. Schematic illustration of the biosensor plasmids. The biosensor promoter cassette was varied between the eight biosensor plasmids (see note next to cassette). *ZraI* restriction enzyme was used linearize the plasmid prior to yeast integration.

A



B

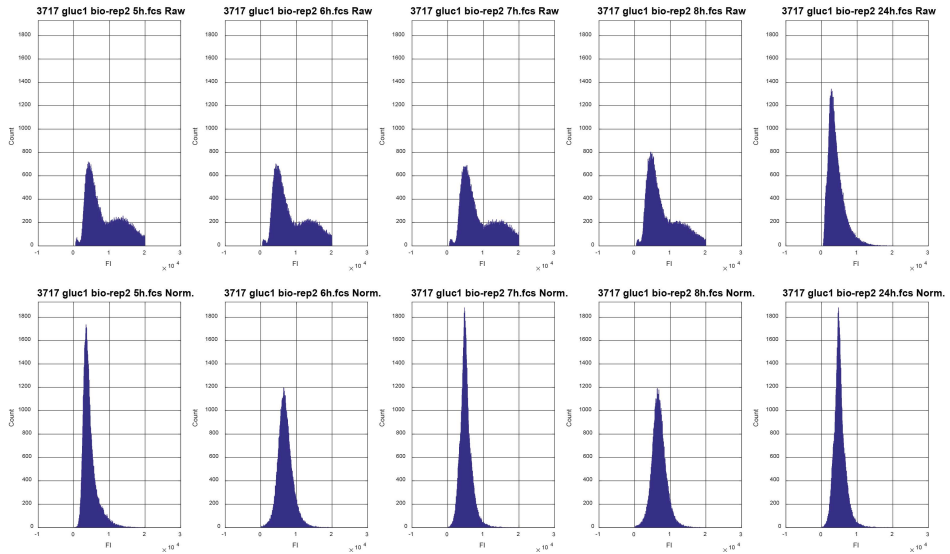


Fig S3. Example of the look of the FI histograms before and after normalization. The second biological replicate of strain TMB3717 cultivated with glucose 1g/L is here used as an example. The X-axes of the histograms represent the FI signal for GFP and the Y-axes the counts. A: results for 0-4h. B: results for 5-24h. Bottom rows of A and B show the normalized data from the corresponding raw data in the row above.

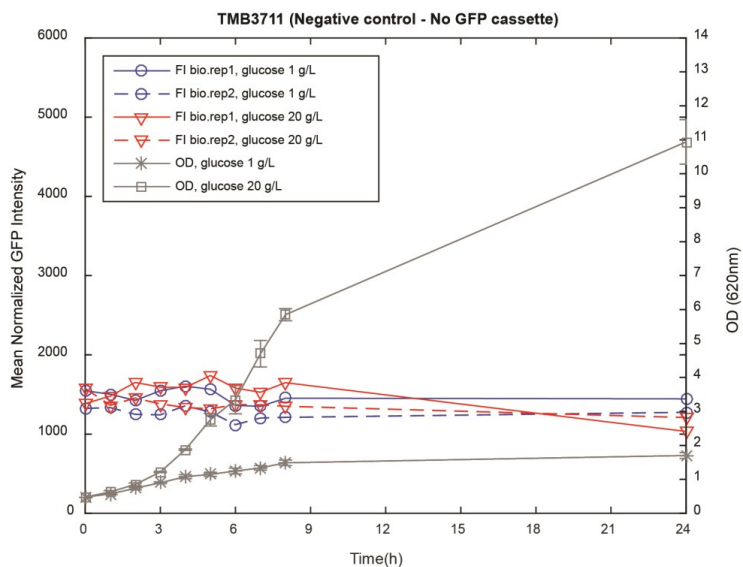
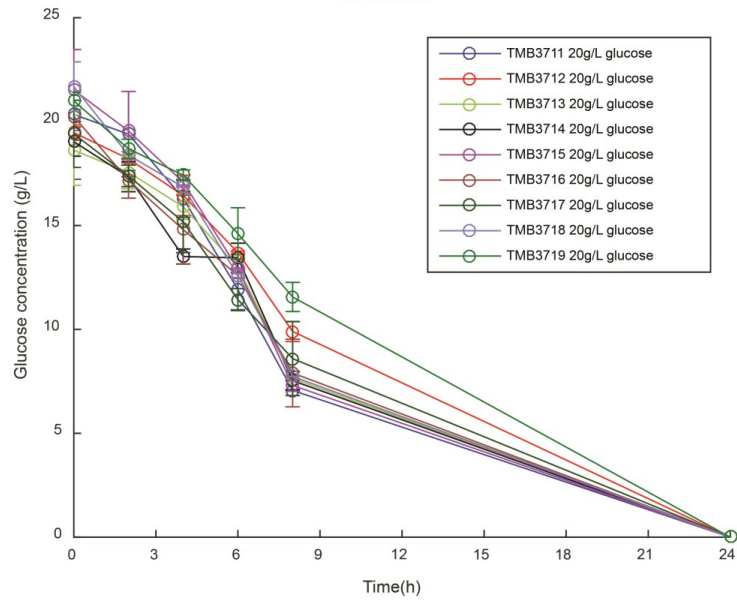
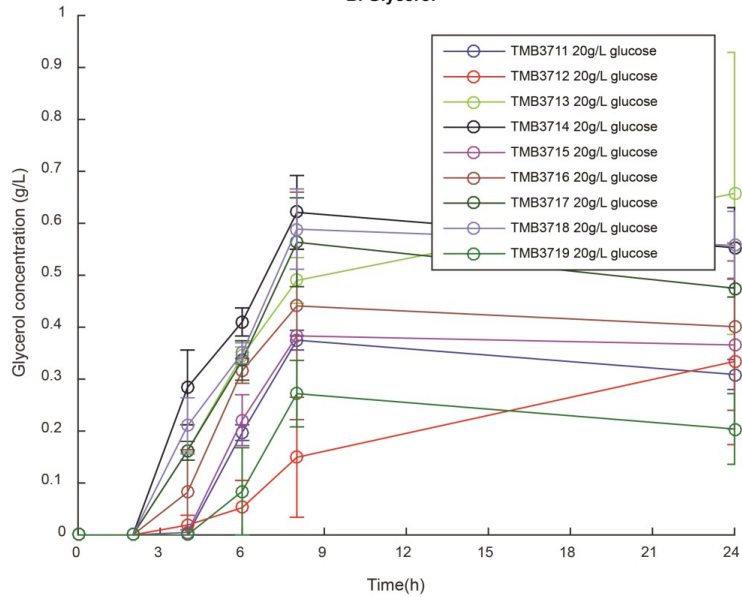


Fig S4. Evaluation of strain TMB3711 (negative control strain without the *yEGFP3* cassette) in terms of growth (OD) and fluorescence intensity (FI). Cultivations were performed in 1 g/L and 20 g/L glucose (YNB-KHPthalate medium) in two biological replicates. Due to the lack of the *GFP* gene in this strain, the above FI represents the autofluorescence of the TMB371X biosensor strains at the current excitation wavelength (488 nm).

A. Glucose



B. Glycerol



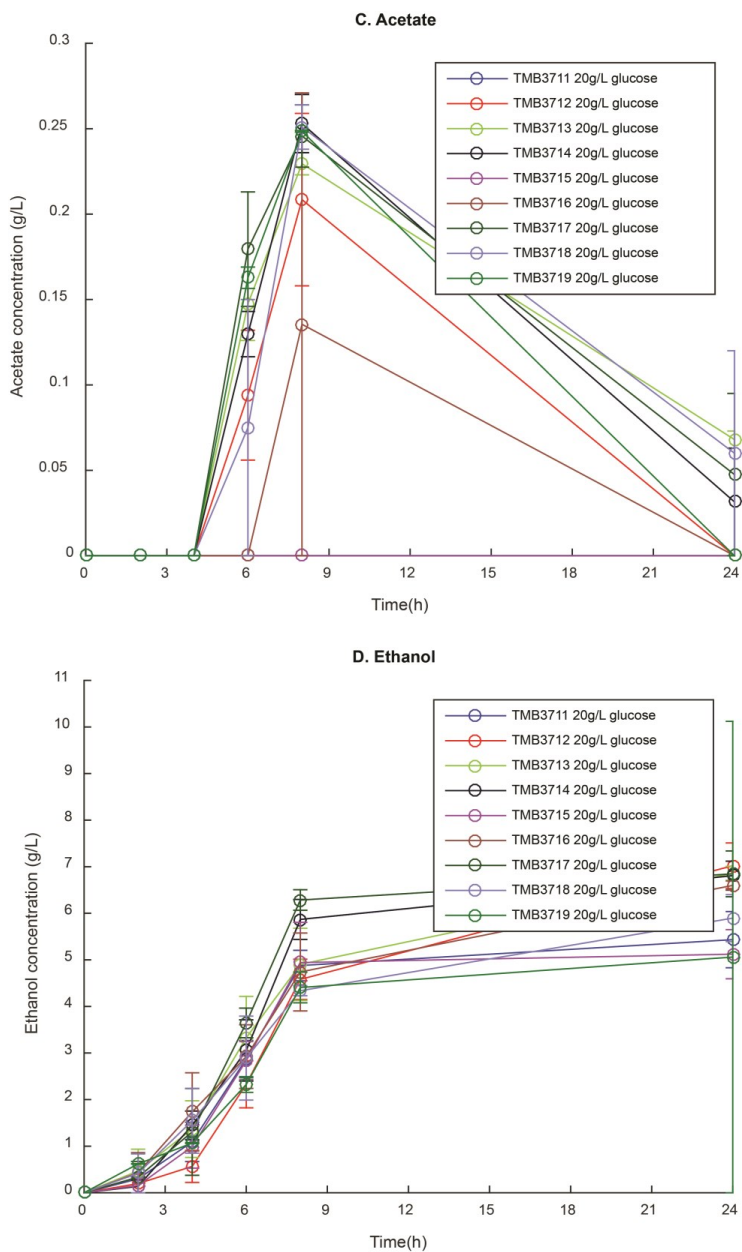


Fig S5. Metabolite profiles of the 24h 100 mL batch cultivations of the biosensor strains, as determined by HPLC. Acetate peaks were observed in all strains but could not always be quantified as some peaks were below the limit of detection of the standard curve (<0.05 g/L). The analysis was performed in two biological and two technical replicates.

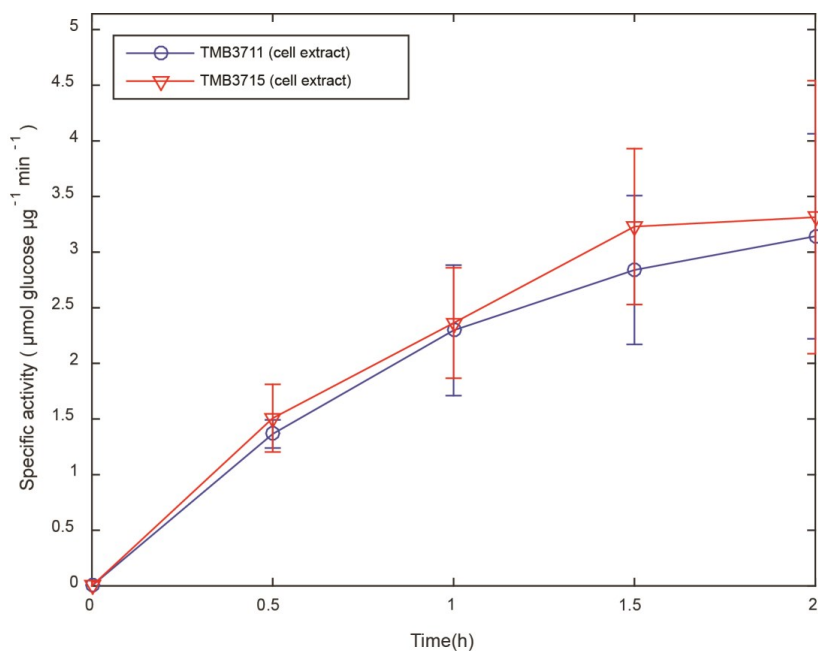
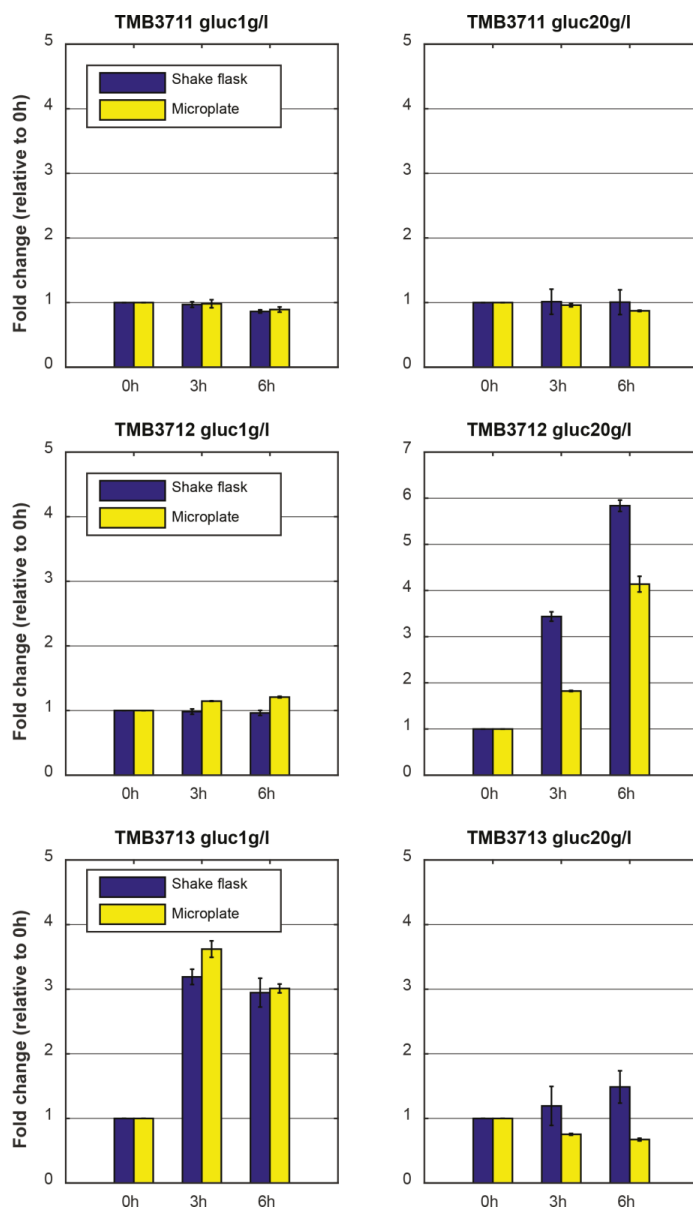
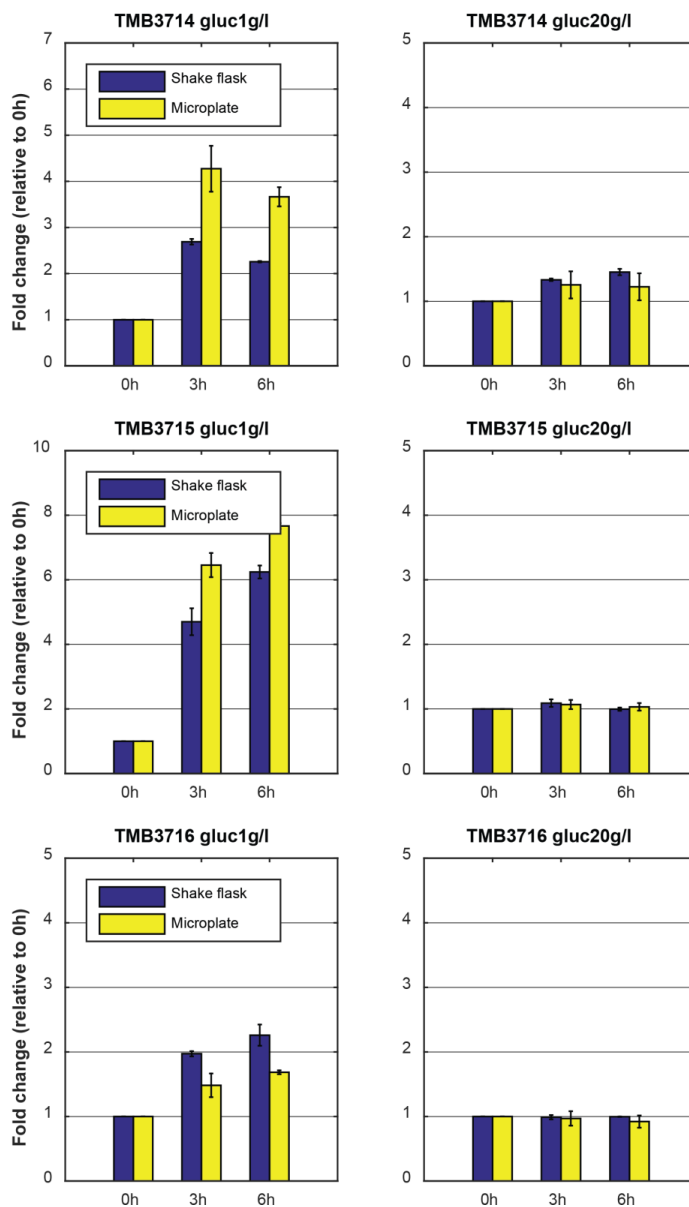


Figure S6. Invertase assay results. Specific invertase activity in cell extracts from TMB3711 (negative control) and TMB3715 (*SUC2p-yEGFP3* biosensor strain). The assay was performed in biological triplicates and the vertical bars indicate the standard deviation between the replicates.

A.



B.



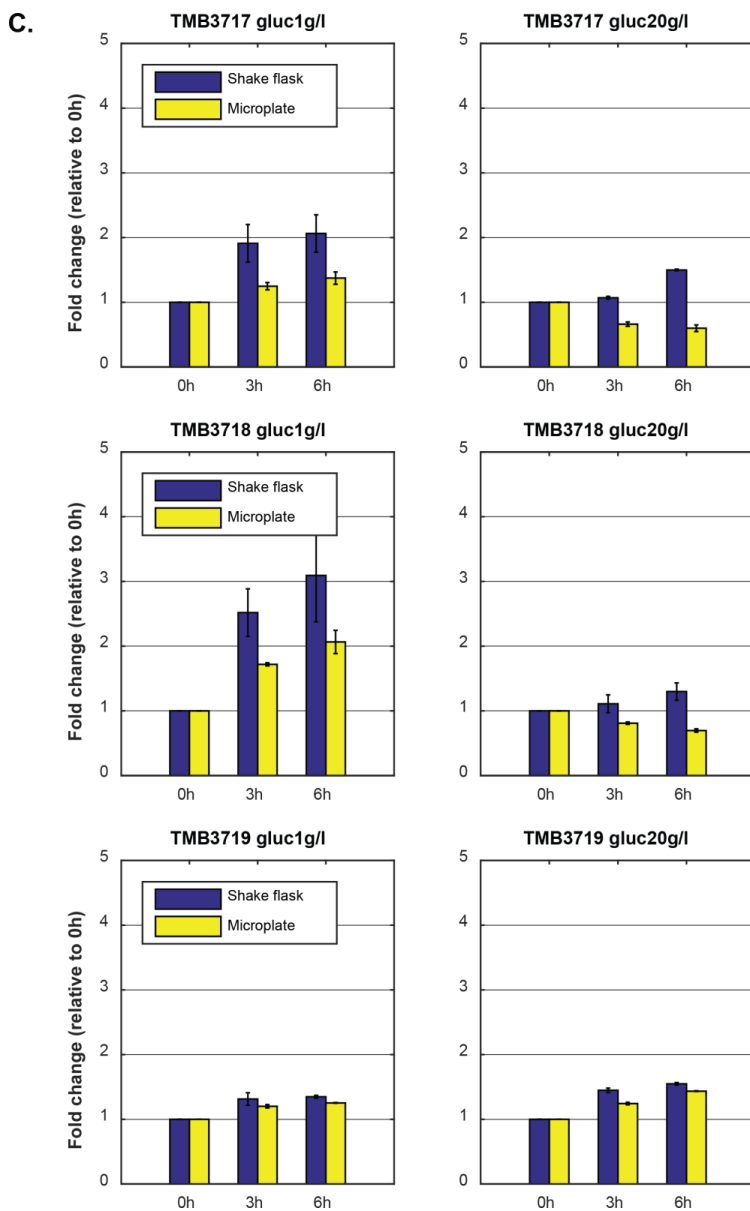


Figure S7. Comparison the FI results from the shake flask cultivations and the corresponding microplate cultivations, in terms of fold change relative to 0h. Data from Figure 2 & 3 in the main paper was converted to fold change (blue bars) for the glucose 1 g/l and 20 g/l conditions for each biosensor strain (A-C). This is presented alongside the data from Table D (yellow bars) for the 0h, 3h and 6h time points (as no other times were measured in the microtiter plate experiment).

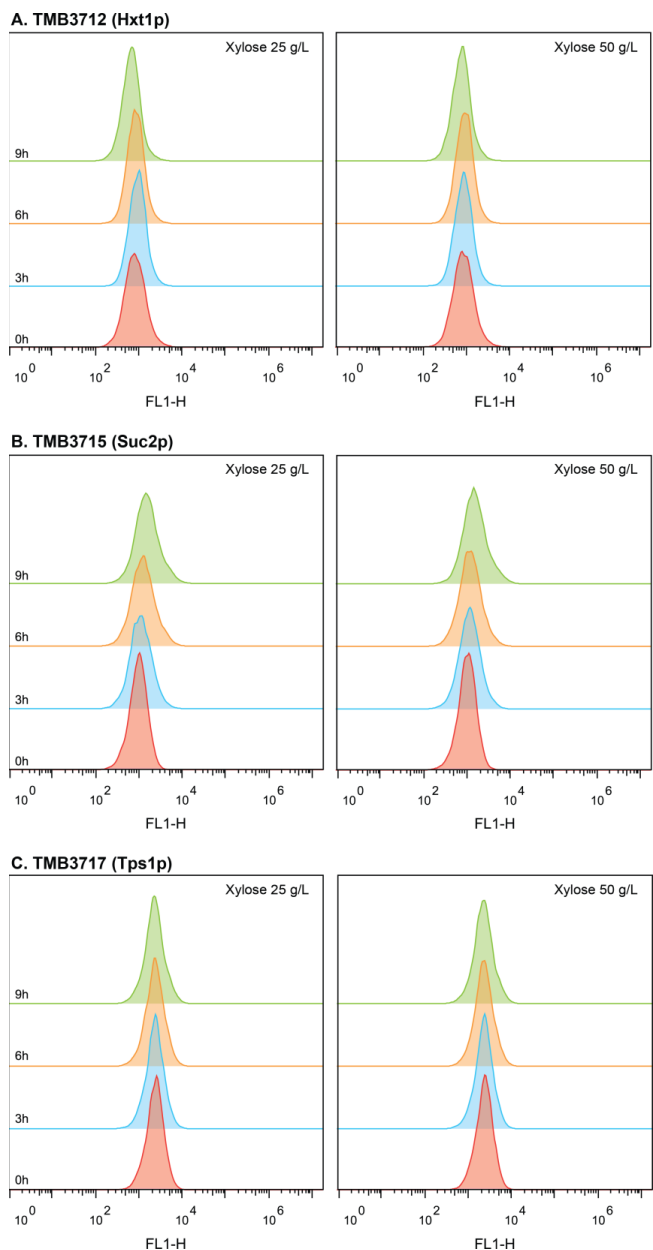


Fig S8. Selected histograms from the data of Supplementary Table D. The subfigures show the FI signal distribution over 9h during two different xylose conditions (25 and 50 g/L). The histograms are representative of the distributions of strains TMB3712 and TMB3715-3719 and contrast the histograms of strains TMB3713-14 (Fig 6 in the main article) by not being affected by the presence of xylose.

Supplementary Tables

Table S1. Primers used in the present study. Underscored regions indicate introduced restriction enzyme sites. Lower case letters indicate tailing regions used for making targeting fragments.

Name	Description	Sequence	Reference
TRP1_f	Cloning of <i>TRP1</i> , forward primer	CTGTTATTAATTTTCAC	[6]
TRP1_r	Cloning of <i>TRP1</i> , reverse primer	TCTTAGCATTTTTG	[6]
HIS3_flank_f	Cloning of <i>HIS3</i> , forward primer	TATCGTTTGAACACGG	[6]
HIS3_flank_r	Cloning of <i>HIS3</i> , reverse primer	AGTTCAGCCATAATATG	[6]
ADE2_F2	Verification of M3499 chromosomal integration	ATGGATTCTAGAACAG TTGGTATATTAG	[7]
URA3_CHR5_F627	“	GGGAAGACAAGCAACG AAAC	This study
yEGFP_F1_KpnI	Cloning of yEGFP3-PGK1t cassette with <i>KpnI</i> restriction site, forward primer	TGCGGT <u>ACCA</u> AAAAATG TCTAAAGCTGAAG	This study
yEGFP_R1_SacI	Cloning of yEGFP3-PGK1t cassette with <i>SacI</i> restriction site, forward primer	TGAGCTCTGAACATAGA AATATCGAATG	This study
HXT1p_f	Cloning of <i>HXT1</i> promotor, forward primer with <i>SaII</i> site	TACGTCGACTAGCAGGG CGAGATTGGTGC	This study
HXT1p_r	Cloning of <i>HXT1</i> promotor, reverse primer with <i>BamHI</i> site	ATGGGATCCTGATTTTAC GTATATCAACTAGTTGAC GATTATG	This study
HXT2p_f	Cloning of <i>HXT2</i> promotor, forward primer with <i>SaII</i> site	ATCGTCGACCTATTTTAC TTAAACGAAGATAGGGTT TCGTAATC	This study
HXT2p_r	Cloning of <i>HXT2</i> promotor, reverse primer with <i>BamHI</i> site	ATGGGATCCTATGTTGCT TTATAAGTCTTTTTGTAAT	This study
HXT4p_f	Cloning of <i>HXT4</i> promotor, forward primer with <i>SaII</i> site	AACGTCGACCAACGATGT TGCCAAATAGTCGTACCTG	This study
HXT4p_r	Cloning of <i>HXT4</i> promotor, reverse primer with <i>BamHI</i> site	ATGGGATCCGGCAGATTTT ATTGTAAAAGTGTTCAAA ACCAAAC	This study
SUC2p_f	Cloning of <i>SUC2</i> promotor, forward primer with <i>SaII</i> site	ATCGTCGACTTCCCAATG AACAAAGGACAGG	This study
SUC2p_r	Cloning of <i>SUC2</i> promotor, reverse primer with <i>BamHI</i> site	TTAGGATCCCATATACGT TAGTGAAAAGAAAAGCTT TTTGTTTTGC	This study

Table S1. (cont'd)

Name	Description	Sequence	Reference
CAT8p_f	Cloning of <i>CAT8</i> promotor, forward primer with <i>SaII</i> site	AACGTCGACTAATATACG GCTCTAGCGTCACC	This study
CAT8p_r	Cloning of <i>CAT8</i> promotor, reverse primer with <i>BamHI</i> site	TGGGGATCCCTTGTGTCTTC TCTTTTACTCAACTTGTA ATTCTC	This study
TEF4p_f	Cloning of <i>TEF4</i> promotor, forward primer with <i>SaII</i> site	TGCGTCGACCTTAATATCC TCTCCTCTTCTTCATC	This study
TEF4p_r	Cloning of <i>TEF4</i> promotor, reverse primer with <i>BamHI</i> site	ATCGGATCCCTTGAATCTA TCGAGGGCCAAAATC	This study
TPS1p_f	Cloning of <i>TPS1</i> promotor, forward primer with <i>SaII</i> site	TGAGTCGACGAATTTTACG ATAGAGCCAGAGAC	This study
TPS1p_r	Cloning of <i>TPS1</i> promotor, reverse primer with <i>BamHI</i> site	ATCGGATCCAGTTCTATGT CTTAATAAGTCTGTATGTG	This study
TPS2p_f	Cloning of <i>TPS2</i> promotor, forward primer with <i>SaII</i> site	TGCGTCGACTAAACCAAG GAGTGCCCTCAGCGAAAC CACTG	This study
TPS2p_r	Cloning of <i>TPS2</i> promotor, reverse primer with <i>BamHI</i> site	ACGGGATCCCTTCGGCACAG AAATAGTGACAGGCAGTGT TATTTTGG	This study
CAN1_Targ1_F	Cloning of targeting fragment for introduction of the GFP plasmids in <i>CAN1</i>	GCTCTTTCCCGACGAGAGT AAATG	This study
CAN1_Targ1_Rtail	“	Ataacaatagggtccgcgcacattcc ccgaaaagtgccacctgacAAGAGGA TGTAACAGGG ATGAATG	This study
CAN1_Targ2_Ftail	“	Atacgcctattttatagggttaatgtcatgataa taatggtttcttagacAACAAGTTGGC TCCTAAATTCCTG	This study
CAN1_Targ2_R	“	CATAAATGTGGCCGCATAAT AAGC	This study
CAN1_CHR5_F201	Verification of chromosomal integration of reporter plasmids	CCGAATCAGGGAATCCCCTT	[8]
AmpR_R130	“	AATGATACCGCGAGACCCAC TTGTA CTGGCGGATAATGC	This study
URA3_R550	“	CTTAG	This study
CAN1_CHR5_R129	“	GCAAGATTGTTGTGGTGAAT CATCG	This study; mod. from [8]
YIpGFP-prom_R2	“	TTAAGGTCAATTTACCGTAA GTAGCATC	This study
SPB1_Targ1_F	Cloning of targeting fragment for introduction of the YIpac128 plasmid in the <i>SPB1/PBN1</i> intergenic region	TTTGCCAGATTGGTTTTTAG AAG	This study

Table S1. (cont'd)

Name	Description	Sequence	Reference
SPB1_ Targ1_Rtail	“	Atttagaaaaataaacaataaggggttcgcg cacatttccccgaaaagtgccacctgacAAG GGAATGGAAAAATAATGCTC	This study; modified from [9]
PBN1_ Targ2_Ftail	“	Tggcctcgtgatacgccctattttataggtaatg tcatgataataatggtttcttagacATCATC AAAAAACTTATAGGAAACC	This study; mod. from [9]
PBN1_ Targ2_R	“	CGAGATAAGGCATGGGGTTC	[9]
SPB1_ verif_F	Verification of chromosomal integration of the YIplac128 plasmid	AGGAAGAATGGACCGGTTTT	[9]
PBN1_ verif_R	“	GGAGGATGGACGATGGTAAA	[9]
LEU2_R	“	TTAAGCAAGGATTTTCTTAA CTTCTTCG	This study
ACT1_F	RT-qPCR reference gene	TGGATTCCGGTGATGGTGTT	[10]
ACT1_R	“	TCAAAATGGCGTGAGGTAG AGA	[10]
yEGFP3_ F1790_RT	RT-qPCR assay of the <i>yEGFP3</i> gene	TGGTGATGGTCCAGTCTTGTT	This study
yEGFP3_ R1918_RT	“	TGGGTAATACCAGCAGCAGT	This study
SUC2_ F263_RT	RT-qPCR assay of the <i>SUC2</i> gene	AACCCATTGCTATCGCTCCC	This study
SUC2_ R397_RT	“	AAGTCCAAATCGCAACGCAT	This study

Table S2. Characterization of some known regulatory elements of the *S. cerevisiae* promoters that were chosen for the sugar signaling study. The table was partially adapted from Weinhandl *et al.* [11]. Abbreviations - STRE: Stress response element; UAS: Upstream activating sequence; RGE: Rapid Growth Element.

Promoter	Binding protein and promoter regulatory motifs		Reference
<i>HXT1p</i>	Rgt1p:	-957 to -951; -921 to -915; -772 to -766; -736 to -730; -481 to -475; -451 to -445; -399 to -393; -227 to -221	[12, 13]
	Mig1p:	-60 to 49	
<i>HXT2p</i>	Rgt1p:	-577 to -571; -430 to -424	[12]
		-393 to -387	
	Mig1p:	-427 to -415; -504 to -493	
	UAS:	-291 to -218	
<i>HXT4p</i>	Rgt1p:	-645 to -639; -424 to -418	[12, 14]
		-295 to -289	
	Mig1p:	-566 to -554; -498 to -486	
<i>SUC2p</i>	Mig1p/2p:	-499 to -480; -442 to -425	[15]
	Sko1p:	-627 to -617	
	UAS:	-650 to -418	
	TATA-box:	-133	
<i>CAT8p</i>	Mig1p:	-204 to -223	[16]
<i>TPS1p</i>	STRE:	-467; -354; -300; -273; -244; -233	[17]
<i>TPS2p</i>	STRE:	-517; -484; -435; -415; -303	[17]
<i>TEF4p</i>	Rgt1p:	-737 to -730	[12, 18]
	RGE:	-403 to -398	
	Tbflp:	-187	

Table S3. Average maximum specific growth rate (μ_{\max}) of the biosensor strains during cultivation on glucose 20 g/L, including standard deviations. The cultivations were performed in biological duplicates. The corresponding growth curves can be found in Figures 3 and 4 in the main publication.

Strain	μ_{\max} (h^{-1})
TMB3711 (No GFP)	0.34 ± 0.03
TMB3712 (<i>HXT1p</i>)	0.37 ± 0.01
TMB3713 (<i>HXT2p</i>)	0.36 ± 0.02
TMB3714 (<i>HXT4p</i>)	0.33 ± 0.01
TMB3715 (<i>SUC2p</i>)	0.35 ± 0.02
TMB3716 (<i>CAT8p</i>)	0.35 ± 0.03
TMB3717 (<i>TPS1p</i>)	0.32 ± 0.03
TMB3718 (<i>TPS2p</i>)	0.35 ± 0.01
TMB3719 (<i>TEF4p</i>)	0.37 ± 0.07

Table S4. Results of the microtiter plate screening of the biosensors strains in terms of FI fold induction.
The FI signal was normalized to the corresponding 0h signal of the given condition and strain. A value of 1 corresponds to repression (i.e. no fold change since time 0h). Values in bold indicate a fold change of >2.

Strain	YNB only (no carbon source)		Glucose 1 g/L		Glucose 20 g/L		Glucose 5 g/L	
	3h	6h	3h	6h	3h	6h	3h	6h
TMB3711	0.92 ±	0.91	0.98	0.89	0.96	0.87	1.00	0.92
(No GFP)	0.023	±0.024	±0.062	±0.040	±0.026	±0.010	±0.010	±0.056
TMB3712	0.84	0.83	1.15	1.21	1.82	4.14	1.21	1.23
(HXT1p)	±0.010	±0.031	±0.010	±0.012	±0.01	±0.17	±0.016	±0.013
TMB3713	1.13	1.28	3.62	3.01	0.75	0.67	1.10	1.34
(HXT2p)	±0.034	±0.091	±0.130	±0.068	±0.013	±0.021	±0.264	±0.11
TMB3714	1.04	1.15	4.27	3.67	1.25	1.22	1.77	2.47
(HXT4p)	±0.088	±0.18	±0.50	±0.21	±0.21	±0.21	±0.058	±0.22
TMB3715	1.10	1.44	6.45	7.66	1.07	1.03	0.98	3.51
(SUC2p)	±0.22	±0.56	±0.37	±0.089	±0.071	±0.059	±0.15	±0.75
TMB3716	1.01	1.27	1.48	1.69	0.97	0.92	0.98	1.14
(CAT8p)	±0.010	±0.041	±0.18	±0.030	±0.11	±0.094	±0.002	±0.039
TMB3717	1.04	1.08	1.25	1.37 ±	0.66	0.60	0.74	1.23
(TPS1p)	±0.001	±0.018	±0.056	0.095	±0.033	±0.051	±0.051	±0.075
TMB3718	1.00	1.11	1.72	2.06	0.81	0.70	0.85	1.61
(TPS2p)	±0.017	±0.022	±0.023	±0.18	±0.018	±0.024	±0.026	±0.084
TMB3719	0.95	1.01	1.20	1.25	1.24	1.44	1.35	1.46
(TEF4p)	±0.025	±0.043	±0.025	±0.010	±0.018	±0.010	±0.013	±0.010
Strain	Glycerol 3% (v/v)		Xylose 50 g/L		Xylose 50 g/L + Gluc. 5 g/L		Xyl. 50 g/L + Glyc. 3% (v/v)	
	3h	6h	3h	6h	3h	6h	3h	6h
TMB3711	0.82	0.79	0.79	0.78	1.04	1.02	0.76	0.72
(No GFP)	±0.024	±0.017	±0.017	±0.023	±0.010	±0.041	±0.014	±0.013
TMB3712	0.75	0.79	0.83	0.84	1.48	1.70	1.22	1.14
(HXT1p)	±0.013	±0.051	±0.015	±0.010	±0.011	±0.011	±0.097	±0.064
TMB3713	1.09	1.28	0.89	0.89	1.37	2.01	0.89	0.91
(HXT2p)	±0.037	±0.064	±0.039	±0.046	±0.26	±0.55	±0.012	±0.009
TMB3714	0.98	1.06	1.08	1.31	2.15	3.45	0.96	1.09
(HXT4p)	±0.087	±0.16	±0.25	±0.51	±0.31	±0.62	±0.14	±0.33
TMB3715	0.98	1.20	0.95	1.06	1.13	5.15	0.91	1.02
(SUC2p)	±0.20	±0.40	±0.12	±0.21	±0.10	±0.62	±0.17	±0.27
TMB3716	0.89	1.09	0.82	0.84	1.08	1.13	0.80	0.78
(CAT8p)	±0.027	±0.049	±0.003	±0.018	±0.037	±0.037	±0.004	±0.009
TMB3717	0.92	0.91	0.92 ±	0.91	0.70	0.77	0.91	0.91
(TPS1p)	±0.006	±0.029	0.006	±0.029	±0.048	±0.047	±0.007	±0.026
TMB3718	0.93	1.03	0.85	0.85	0.95	1.05	0.84	0.82
(TPS2p)	±0.020	±0.029	±0.012	±0.026	±0.076	±0.032	±0.012	±0.025
TMB3719	0.97	1.07	0.87	0.96	1.28	1.42±	0.87	0.95
(TEF4p)	±0.015	±0.040	±0.012	±0.010	±0.018	0.0032	±0.010	±0.0027

Table S5. Effect of different concentrations of xylose on the biosensor strains. The effect of xylose was investigated in terms of FI fold induction (normalized to 0h for the given condition and strain), as well as prolonged cultivation time (9h; cf. Table 3 in the main article). A value of 1 corresponds to repression (i.e. no fold change since time 0h).

Strain	YNB only (no carbon source)			Xylose 25 g/L			Xylose 50 g/L			Xylose 75 g/L			Xylose 100 g/L		
	3h	6h	9h	3h	6h	9h	3h	6h	9h	3h	6h	9h	3h	6h	9h
TMB3711 (No GFP)	0.92 ±0.01	1.00 ±0.03	1.07 ±0.10	0.91 ±0.04	0.96 ±0.01	1.00 ±0.01	0.90 ±0.01	0.92 ±0.02	0.94 ±0.03	0.89 ±0.01	0.90 ±0.04	0.91 ±0.06	0.88 ±0.01	0.88 ±0.05	0.89 ±0.07
TMB3712 (HXT1p)	1.03 ±0.02	0.84 ±0.01	0.79 ±0.01	1.32 ±0.26	1.20 ±0.22	1.19 ±0.50	1.21 ±0.26	1.12 ±0.20	1.00 ±0.24	1.22 ±0.12	1.02 ±0.06	0.97 ±0.07	1.25 ±0.07	1.12 ±0.01	1.09 ±0.02
TMB3713 (HXT2p)	1.00 ±0.02	1.03 ±0.07	0.97 ±0.05	1.20 ±0.046	1.76 ±0.01	2.35 ±0.06	1.21 ±0.02	1.72 ±0.04	2.25 ±0.03	1.17 ±0.02	1.63 ±0.01	1.91 ±0.027	1.09 ±0.04	1.31 ±0.01	1.51 ±0.03
TMB3714 (HXT4p)	0.99 ±0.01	1.04 ±0.03	1.02 ±0.03	1.36 ±0.10	2.34 ±0.05	2.94 ±0.22	1.33 ±0.11	1.88 ±0.17	2.78 ±0.02	1.27 ±0.07	1.56 ±0.03	1.97 ±0.11	1.15 ±0.04	1.25 ±0.02	1.36 ±0.01
TMB3715 (SUC2p)	1.04 ±0.06	1.12 ±0.01	1.21 ±0.09	1.06 ±0.11	1.18 ±0.14	1.22 ±0.09	1.06 ±0.12	1.12 ±0.12	1.17 ±0.10	1.03 ±0.09	1.06 ±0.06	1.10 ±0.03	1.01 ±0.07	1.03 ±0.05	1.04 ±0.02
TMB3716 (CAT8p)	1.12 ±0.14	1.22 ±0.10	1.31 ±0.03	1.07 ±0.10	1.19 ±0.17	1.26 ±0.19	1.04 ±0.070	1.09 ±0.09	1.16 ±0.13	1.01 ±0.03	1.04 ±0.03	1.04 ±0.03	0.98 ±0.01	1.00 ±0.01	0.99 ±0.013
TMB3717 (TPS1p)	0.97 ±0.08	0.92 ±0.001	0.90 ±0.02	0.97 ±0.05	0.99 ±0.08	0.95 ±0.06	0.97 ±0.04	0.97 ±0.042	0.94 ±0.05	0.98 ±0.04	0.94 ±0.02	0.88 ±0.006	0.98 ±0.04	0.94 ±0.01	0.84 ±0.007
TMB3718 (TPS2p)	1.07 ±0.08	1.08 ±0.002	1.08 ±0.07	1.04 ±0.05	1.06 ±0.007	1.08 ±0.012	1.03 ±0.05	1.00 ±0.02	1.02 ±0.02	1.01 ±0.03	0.97 ±0.06	0.93 ±0.05	1.00 ±0.03	0.96 ±0.05	0.92 ±0.07
TMB3719 (TEF4p)	0.93 ±0.004	0.74 ±0.01	0.60 ±0.01	1.04 ±0.04	0.96 ±0.008	0.85 ±0.032	0.95 ±0.02	1.00 ±0.02	0.88 ±0.02	0.90 ±0.03	0.93 ±0.07	0.92 ±0.02	0.86 ±0.012	0.86± 0.03	0.90 ±0.07

References

1. Knijnenburg TA, Roda O, Wan YK, Nolan GP, Aitchison JD, Shmulevich I. A regression model approach to enable cell morphology correction in high-throughput flow cytometry. *Mol Syst Biol.* 2011;7(531). doi: 10.1038/msb.2011.64. PubMed PMID: 21952134.
2. Bauminger BB. Micro Method for Manual Analysis of True Glucose in Plasma without Deproteinization. *J Clin Pathol.* 1974;27(12):1015-7. doi: 10.1136/jcp.27.12.1015. PubMed PMID: 4452743.
3. Harkness TAA, Arnason TG. A Simplified Method for Measuring Secreted Invertase Activity in *Saccharomyces cerevisiae*. *Biochemistry & Pharmacology: Open Access.* 2014;3(6):151. doi: 10.4172/2167-0501.1000151.
4. Weiß P, Huppert S, Kolling R. ESCRT-III Protein Snf7 Mediates High-Level Expression of the SUC2 Gene via the Rim101 Pathway. *Eukaryot Cell.* 2008;7(11):1888-94. doi: 10.1128/Ec.00194-08. PubMed PMID: 18806212.
5. Kayyali US, Moore TB, Randall JC, Richardson RJ. Neurotoxic Esterase (Nte) Assay - Optimized Conditions Based on Detergent-Induced Shifts in the Phenol/4-Aminoantipyrine Chromophore Spectrum. *J Anal Toxicol.* 1991;15(2):86-9. PubMed PMID: 2051750.
6. Knudsen JD, Carlquist M, Gorwa-Grauslund M. NADH-dependent biosensor in *Saccharomyces cerevisiae*: principle and validation at the single cell level. *AMB Express.* 2014;4(1):81. doi: 10.1186/s13568-014-0081-4. PubMed PMID: 25401080.
7. Tokuhiko K, Muramatsu M, Ohto C, Kawaguchi T, Obata S, Muramoto N, Hirai M, Takahashi H, Kondo A, Sakuradani E, Shimizu S. Overproduction of Geranylgeraniol by Metabolically Engineered *Saccharomyces cerevisiae*. *Appl Environ Microb.* 2009;75(17):5536-43. doi: 10.1128/Aem.00277-09. PubMed PMID: 19592534.
8. Solis-Escalante D, van den Broek M, Kuijpers N, Pronk J, Boles E, Daran J, Daran-Lapujade P. The genome sequence of the popular hexose-transport-deficient *Saccharomyces cerevisiae* strain EBY. VW4000 reveals LoxP/Cre-induced translocations and gene loss. *FEMS Yeast Res.* 2015;15(2). doi: 10.1093/femsyr/fou004. PubMed PMID: 25673752.
9. Flagfeldt DB, Siewers V, Huang L, Nielsen J. Characterization of chromosomal integration sites for heterologous gene expression in *Saccharomyces cerevisiae*. *Yeast.* 2009;26(10):545-51. doi: 10.1002/Yea.1705. PubMed PMID: 19681174.
10. Ismail KSK, Sakamoto T, Hatanaka H, Hasunuma T, Kondo A. Gene expression cross-profiling in genetically modified industrial *Saccharomyces cerevisiae* strains during high-temperature ethanol production from xylose. *J Biotechnol.* 2013;163(1):50-60. doi: 10.1016/j.jbiotec.2012.10.017. PubMed PMID: 23131464.

11. Weinhandl K, Winkler M, Glieder A, Camattari A. Carbon source dependent promoters in yeasts. *Microb Cell Fact.* 2014;13(5). doi: 10.1186/1475-2859-13-5. PubMed PMID: 24401081.
12. Kim JH. DNA-binding properties of the yeast Rgt1 repressor. *Biochimie.* 2009;91(2):300-3. doi: 10.1016/j.biochi.2008.09.002. PubMed PMID: 18950675.
13. Sinha S, Tompa M. Discovery of novel transcription factor binding sites by statistical overrepresentation. *Nucleic Acids Res.* 2002;30(24):5549-60. doi: 10.1093/Nar/Gkf669. PubMed PMID: 12490723.
14. Özcan S, Johnston M. Two different repressors collaborate to restrict expression of the yeast glucose transporter genes HXT2 and HXT4 to low levels of glucose. *Mol Cell Biol.* 1996;16(10):5536-45. doi: 10.1128/MCB.16.10.5536. PubMed PMID: 8816466.
15. Bu Y, Schmidt MC. Identification of cis-acting elements in the SUC2 promoter of *Saccharomyces cerevisiae* required for activation of transcription. *Nucleic Acids Res.* 1998;26(4):1002-9. doi: DOI 10.1093/nar/26.4.1002. PubMed PMID: 9461460.
16. Randez-Gil F, Bojunga N, Proft M, Entian KD. Glucose derepression of gluconeogenic enzymes in *Saccharomyces cerevisiae* correlates with phosphorylation of the gene activator Cat8p. *Mol Cell Biol.* 1997;17(5):2502-10. doi: 10.1128/MCB.17.5.2502. PubMed PMID: 9111319.
17. Moskvina E, Schuller C, Maurer CTC, Mager WH, Ruis H. A search in the genome of *Saccharomyces cerevisiae* for genes regulated via stress response elements. *Yeast.* 1998;14(11):1041-50. doi: 10.1002/(Sici)1097-0061(199808)14:11<1041::Aid-Yea296>3.0.Co;2-4. PubMed PMID: 9730283.
18. Bosio MC, Negri R, Dieci G. Promoter architectures in the yeast ribosomal expression program. *Transcription.* 2011;2(2):71-7. doi: 10.4161/trns.2.2.14486. PubMed PMID: 21468232.

Paper IV



RESEARCH ARTICLE

Assessing the effect of D-xylose on the sugar signaling pathways of *Saccharomyces cerevisiae* in strains engineered for xylose transport and assimilation

Karen O Osiro, Daniel P Brink[†], Celina Borgström, Lisa Wasserstrom, Magnus Carlquist and Marie F Gorwa-Grauslund*

Applied Microbiology, Department of Chemistry, Lund University, Kemikentrum, Naturvetarvägen 14, Lund 223 62, Sweden

*Corresponding author: Applied Microbiology, Department of Chemistry, Lund University, Kemikentrum, Naturvetarvägen 14, Lund 223 62, Sweden.

Tel: +46 46 222 0619; E-mail: Marie-Francoise.Gorwa@tmb.lth.se

One sentence summary: In this study, in vivo single-cell biosensors were used to assess the sensing of glucose and xylose sugars by *Saccharomyces cerevisiae*, in order to understand its low xylose utilization rate.

Editor: Pascale Daran-Lapujade

[†]Daniel P Brink, <http://orcid.org/0000-0003-4041-0250>

ABSTRACT

One of the challenges of establishing an industrially competitive process to ferment lignocellulose to value-added products using *Saccharomyces cerevisiae* is to get efficient mixed sugar fermentations. Despite successful metabolic engineering strategies, the xylose assimilation rates of recombinant *S. cerevisiae* remain significantly lower than for the preferred carbon source, glucose. Previously, we established a panel of in vivo biosensor strains (TMB371X) where different promoters (HXT1/2/4p; SUC2p, CAT8p; TPS1p/2p, TEF4p) from the main sugar signaling pathways were coupled with the yEGFP3 gene, and observed that wild-type *S. cerevisiae* cannot sense extracellular xylose. Here, we expand upon these strains by adding a mutated galactose transporter (GAL2-N376F) with improved xylose affinity (TMB372X), and both the transporter and an oxidoreductase xylose pathway (TMB375X). On xylose, the TMB372X strains displayed population heterogeneities, which disappeared when carbon starvation was relieved by the addition of the xylose assimilation pathway (TMB375X). Furthermore, the signal in the TMB375X strains on high xylose (50 g/L) was very similar to the signal recorded on low glucose (≤ 5 g/L). This suggests that intracellular xylose triggers a similar signal to carbon limitation in cells that are actively metabolizing xylose, in turn causing the low assimilation rates.

Keywords: *Saccharomyces cerevisiae*; sugar sensing/signaling; xylose; XR/XDH; GFP biosensor; cAMP/PKA; Snf3p/Rgt2p; SNF1/Mig1p; flow cytometry

ABBREVIATIONS

FI: fluorescence intensity
GFP: green fluorescent protein
OD: optical density
OE-PCR: overlap extension PCR
ORF: open reading frame

PCR: polymerase chain reaction
PPP: pentose phosphate pathway
XDH: xylitol dehydrogenase
XK: xylulokinase
XR: xylose reductase
YPD: yeast peptone dextrose

Received: 8 November 2017; Accepted: 27 December 2017

© FEMS 2018. This is an Open Access article distributed under the terms of the Creative Commons Attribution Non-Commercial License (<http://creativecommons.org/licenses/by-nc/4.0/>), which permits non-commercial re-use, distribution, and reproduction in any medium, provided the original work is properly cited. For commercial re-use, please contact journals.permissions@oup.com

BACKGROUND

The lignocellulose-based biorefinery has been foreseen as a candidate process to supply the future global demand for sustainable energy sources that can replace the non-renewable sources used today, and has shown good potential to decrease the environmental impact compared to the conventional processes (Uihlein and Schebek 2009). Up to one-third of the composition of lignocellulose is constituted of D-xylose, the second most abundant sugar in nature (Limayem and Ricke 2012), meaning that in order to fully take advantage of the carbon content of this renewable feedstock, future biorefineries will require microbes that can efficiently convert not only hexose (C₆), but also pentose (C₅) sugars such as xylose, preferably simultaneously. Although some microorganisms are naturally able to ferment and produce valuable chemical compounds from xylose, they are seldom suitable for industrial applications due to their poor performance under high osmotic stress, low pH, strict anaerobic environments and/or in the presence of the wide range of inhibitory compounds released during lignocellulose pretreatment (Skoog and Hahn-Hägerdal 1988; Hahn-Hägerdal et al. 2007a; Rudolf et al. 2008; Kwak and Jin 2017). Instead, the industrially robust, natural ethanol-producing organism *Saccharomyces cerevisiae* (Baker's yeast) has for a long time been considered a promising host for metabolic engineering to enable pentose conversion (Jeffries and Jin 2004; van Maris et al. 2007).

Over the years, different strategies have been developed in order to introduce and improve xylose metabolism in *S. cerevisiae*. As the endogenous genes for xylose catabolism already present in this yeast are insufficiently expressed (Toivari et al. 2004; Attfield and Bell 2006), exogenous genes from natural xylose assimilating microbes have been used to enable pentose catabolism in *S. cerevisiae* (Kötter et al. 1990; Kötter and Ciriacy 1993; Brat, Boles and Wiedemann 2009). The oxidoreductase pathway that was used in the present study consists of a xylose reductase (XR) and a xylitol dehydrogenase (XDH) that converts xylose to xylulose via xylitol; xylose can then enter the non-oxidative pentose phosphate pathway (PPP) via the endogenous xylulokinase (XK) and be further shunted to the central carbon metabolism (Kötter and Ciriacy 1993). Xylose utilization can be further improved by also overexpressing the endogenous TAL1 and TKL1 genes in order to increase the metabolic flux through the PPP (Hahn-Hägerdal et al. 2007b).

Despite these modifications, growth and productivity are still significantly lower on xylose than on glucose (Hahn-Hägerdal et al. 2007a). Redox imbalance is an issue with the oxidoreductase pathway, as the commonly used *Scheffersomyces stipitis* XR has a higher preference for NADPH over NADH while the XDH is strictly NAD⁺-dependent, resulting in an insufficient recycling of NADPH and NAD⁺ (Bruinenberg et al. 1983; Kötter and Ciriacy 1993). However, the recently identified XR of *Spathaspora passalidarum* (encoded by XYL1.2) that prefers NADH over NADPH can be used to significantly decrease the redox issues of the XR/XDH pathway in *S. cerevisiae* (Cadete et al. 2016).

Cofermmentation of hexose and pentose sugar also prove challenging as glucose is preferentially consumed over xylose (Zaldivar et al. 2002; Moysés et al. 2016), because of the lack of specific xylose transporters (Kim et al. 2012). Although xylose can be taken up by some of the native hexose transporters, during mixed sugar cultivations, these transporters have a naturally higher affinity for glucose (Kotyk 1967; Hamacher et al. 2002). Nevertheless, a couple of recent studies have demonstrated improved xylose uptake by engineering hexose and galactose

transporters for improved xylose specificity (Farwick et al. 2014; Nijland et al. 2014, 2016; Apel et al. 2016).

At the present stage, xylose can be fermented to ethanol by recombinant *S. cerevisiae*, but at such low rates that it has been hypothesized that xylose still is not recognized as a fermentable sugar (Jin, Laplaza and Jeffries 2004; Salusjarvi et al. 2006; Runquist, Hahn-Hägerdal and Bettiga 2009; Klimacek et al. 2010; Bergdahl et al. 2012; Feng and Zhao 2013). This indicates possible issues with the intra- and/or extracellular sensing of xylose in *S. cerevisiae*. A handful of studies have shown the influence of xylose on glucose signaling (Fernandez et al. 1986; Jin, Laplaza and Jeffries 2004; Salusjarvi et al. 2006; Salusjarvi et al. 2008; Alff-Tuomala et al. 2016; Zeng et al. 2016), but the mechanism by which *S. cerevisiae* could potentially sense xylose is still mainly unknown. Therefore, increased comprehension of the xylose effect on the main glucose signaling pathways may lead to new strategies for enhancing xylose utilization.

There are three main signaling pathways that control glucose sensing in *S. cerevisiae* (Fig. 1): the Snf3p/Rgt2p pathway, the Snf1/Mig1p pathway and the cAMP/protein kinase A (PKA) pathway (Santangelo 2006). We recently reported on the construction of a panel of fluorescent biosensors strains that allows for real-time single-cell monitoring of these three signaling pathways during different carbon conditions. The promoter regions of eight different genes (HXT1/2/4p; SUC2p, CAT8p; TPS1/2p, TEF4p)—each controlled by one of the three signaling pathways—were coupled to the yEGFP3 (yeast enhanced green fluorescent protein) reporter gene and integrated in the chromosome in single copy (Brink et al. 2016). The HXT1/2/4p biosensors represent the Snf3p/Rgt2p pathway, which regulates the expression of hexose transporters by sensing extracellular glucose (Boles and Hollenberg 1997; Özcan, Dover and Johnston 1998; Santangelo 2006). The SUC2p and CAT8p biosensors are reporters for the Snf1/Mig1p pathway that is responsible for carbon catabolite repression and is regulated mainly by intracellular glucose. This pathway can induce genes for alternative carbon source utilization during glucose depletion (Özcan et al. 1997; Santangelo 2006). The TPS1/2 promoters represent the cAMP/PKA pathway, which responds to both internal and external glucose and governs, among others, the gluconeogenesis and environmental stress response (Rolland, Winderickx and Thevelein 2002; Santangelo 2006). The PKA is activated in the presence of glucose, which leads to a phosphorylation of several metabolic enzymes, transcription factors and, consequently, gene regulation (Kraakman et al. 1999; Kim, Polish and Johnston 2003; Mosley et al. 2003; Santangelo 2006). It has also been demonstrated that SUC2 and HXT1 are in part regulated by the cAMP/PKA pathway, meaning that these signaling pathways are cross-talking (Kaniak et al. 2004; Kim and Johnston 2006; Gancedo, Flores and Gancedo 2015).

Previously, we applied the biosensor strains to investigate whether the signal on glucose differentiated from that on xylose in any of the three signaling routes in non-xylose metabolizing *S. cerevisiae*. It was found that the biosensors remained unresponsive to extracellular xylose, and that certain population heterogeneities indicated that xylose that had been internalized (e.g. through promiscuous hexose transporters) was being sensed by some parts of the glucose signaling pathway (Brink et al. 2016). The current study pursues the investigation of the sugar signaling response of *S. cerevisiae*, this time for strains where a transporter with increased affinity for xylose is overexpressed (Farwick et al. 2014), or for strains that can fully metabolize xylose, by addition of the same transporter gene, the XR/XDH

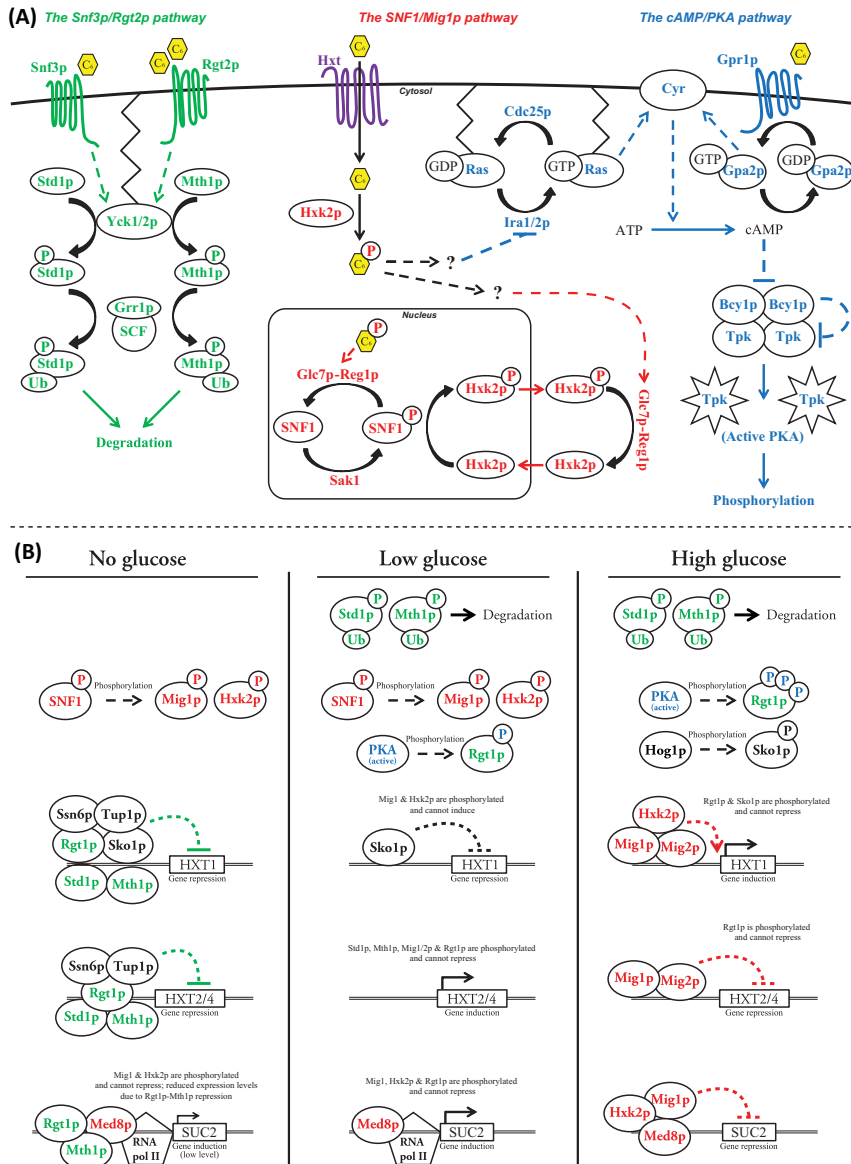


Figure 1. (A) The three main glucose signalling pathways in *S. cerevisiae*. The *Snf3p/Rgt2p* pathway (green) controls expression of hexose transporters and responds to extracellular glucose (yellow hexagons with C_6); the *SNF1/Mig1p* pathway (red) controls expression of genes related to utilization of alternative carbon sources and senses intracellular phosphorylated (P) glucose; the *cAMP/PKA* pathway (blue) controls homeostasis and stress response and senses both extra- and intracellular glucose. Solid arrows represent reactions/transport and dashed arrows represent induction (arrowhead) or repression (hammerhead). This figure was adapted from a previous study (Brink et al. 2016). **(B)** Known induction/repression effects on the *HXT1*, *HXT2/4* and *SUC2* genes during absence of glucose, low-glucose (typically < 1 g/L) and high-glucose conditions (typically > 10 g/L). Note that *Mig1p/2p* are known to act redundantly on their targets, meaning that both enzymes are normally not needed for target gene induction.

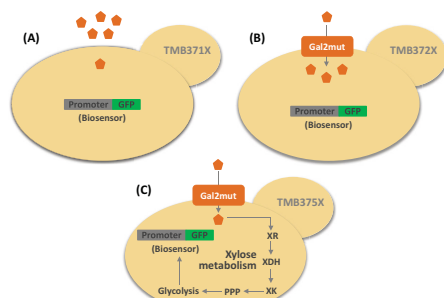


Figure 2. Schematic representation of the different biosensors strains. The biosensors were previously analyzed in TMB371X strains lacking xylose transport (i.e. no Gal2mut transporter) and assimilation (Brink et al. 2016) (A). In this study, the biosensors were further evaluated with the overexpression of a xylose transporter (Gal2mut) in TMB372X strains (B). In the third case, a pathway for xylose utilization was added to the strains with Gal2mut transporter, resulting in the TMB375X strains (C).

xylose pathway gene and overexpressed TAL1 and TKL1 genes in the PPP (Fig. 2).

MATERIALS AND METHODS

Strains

The yeast strains used in the study are based on previously constructed biosensors strains (Brink et al. 2016), and are described in Table 1. Strains TMB3701–TMB3709 are collectively referred as TMB370X strains and this nomenclature is also used for the different series of derived strains (e.g. TMB371X, TMB372X and TMB375X; Table 1). Depending on the experimental requirements, the strains were grown on either yeast peptone dextrose (YPD; yeast extract 10 g/L, peptone 20 g/L, glucose 20 g/L) or yeast nitrogen base (YNB; 6.7 g/L YNB without amino acids; Becton-Dickinson, NJ, USA) supplemented with different carbon sources (detailed below). *Escherichia coli* NEB5- α (New England BioLabs, Ipswich, MA, USA) was used for routine plasmid subcloning and was cultivated in Lysogeny broth (LB) medium (10 g/L tryptone, 5 g/L yeast extract, 5 g/L NaCl, pH 7.0). Solid plates were obtained by adding 15 g/L agar-agar to the above media. All strains were stored at -80°C in 25% (v/v) glycerol; CRISPR-Cas9 transformants were stored in the presence of their respective antibiotics (detailed below).

Molecular biology methods

All cloning procedures were performed according to standard molecular biology methods (Sambrook and Russell 2001). Genomic yeast DNA was extracted according to the LiOAc-SDS method (Löke, Kristjuhan and Kristjuhan 2011) and polymerase chain reaction (PCR) products were purified with GeneJET PCR purification kit (Thermo Fisher Scientific, Waltham, MA, USA). All primers (Table S5, Supporting Information) were obtained from Eurofins MWG Operon (Ebersberg, Germany). Restriction enzymes, T4 ligase and Phusion DNA polymerase were purchased from Thermo Fisher Scientific, except for *ZraI* that was purchased from New England Biolabs. Plasmid purification was performed with GeneJET plasmid MiniPrep kit (Thermo Fisher Scientific).

The lithium acetate transformation protocol (Gietz and Schiestl 2007), modified with the addition of DMSO (10% v/v) prior to heat shock (Hill, Donald and Griffiths 1991), was used for all the *S. cerevisiae* transformations. Competent *E. coli* cells were prepared and transformed according to the method of Inoue, Nojima and Okayama (1990). Selection of *E. coli* transformants was performed on LB medium supplemented with 50 $\mu\text{g}/\text{mL}$ of ampicillin.

Plasmids and transformation fragments

The plasmids that were used in the study are listed in Table 2. The TDH3p-GAL2.N376F-CYC1t cassette containing the mutated GAL2 transporter (GAL2.N376F) was constructed from the pRS62N.GAL2.N376F plasmid (Farwick et al. 2014) that was a gift from Prof. E. Boles. Since the antibiotic marker and truncated HXT7p promoter in pRS62N.GAL2.N376F was not desired in the current study, the GAL2.N376F cassette was cloned into a new vector. This was made in two steps: first, the cassette was amplified from the original plasmid using the GAL2-F1.SmaI and GAL2.R1.XhoI primers and was ligated between the TDH3 promoter and the CYC1 terminator in the p426-GPD Mumberg vector (Mumberg, Muller and Funk 1995), thus generating the p426-GPD-GAL2.N376F plasmid; second, the TDH3p-GAL2.N376F-CYC1t cassette was amplified from p426-GPD-GAL2.N376F plasmid using the TDH3p-F2.SacI and CYC1t-R2-SphI primers. The final plasmid (YIplac128-GAL2.N376F) was constructed by ligating the TDH3p-GAL2.N376F-CYC1t cassette to YIplac128 (LEU2) using the SacI and SphI restriction sites.

Construction of the XR-XDH-XK integrative plasmids

Saccharomyces cerevisiae promoters TEF1p and PG11p, terminators GPM1t and PYK1t, as well as the XKS1 ORF (open reading frame)-encoding XK (Ho, Chen and Brainard 1998), were PCR amplified individually from genomic DNA isolated from *S. cerevisiae* CEN.PK 113-7D with primers generating a 40 bp homology between promoter, gene and terminator. *Scheffersomyces stipitis* gene SsXDH encoding XDH (Kötter et al. 1990) was amplified from the plasmid YIpRC5 (Cadete et al. 2016). Following agarose gel electrophoresis, the amplified PCR products were gel-purified. Each individual gene expression cassette (TEF1p-SsXDH-GPM1t and PG11p-XKS1-PYK1t) was assembled by overlap extension PCR (OE-PCR) using primer pairs 65/70 (XDH cassette) and 71/76 (XKS1 cassette) with each part added in equimolar amounts. In order to enable In-fusion HD cloning (In-Fusion® HD Cloning Kit User Manual, Clontech Laboratories, CA, USA), 15 bp homology regions between the two cassettes and the plasmid YIpRC5 was included in the primers. Following electrophoresis, the OE-PCR products were gel-purified. Two microgram of plasmid YIpRC5, already carrying the SpXYL1.2 gene cassette for XR from *Sp. paspalidarum*, was cleaved with FastDigest PstI and SacI and separated by gel electrophoresis followed by gel purification (GeneJET Gel Extraction Kit; Thermo Fisher Scientific). Gene cassettes and PstI/SacI digested YIpRC5 containing the remaining XR-encoding gene were added in equimolar amount to 5 \times In-fusion HD enzyme premix following the In-fusion HD cloning kit user manual (Raman and Martin 2014). The obtained plasmid was verified using restriction enzymes SacI and PstI and agarose gel electrophoresis. The plasmid was Sanger sequenced (Eurofins MWG Operon) using primers 78–83 and named pLWA20.

The xylose pathway from pLWA20 was recloned into pCfB2899, pCf3037 and pCf3040 to allow integration of three copies of the cassette using a CRISPR-Cas9 system into the intergenic regions X-2, XI-5 and XII-4, respectively (Jessop-Fabre

Table 1. Yeast strains constructed and/or utilized in this study.

Strain	Relevant genotype	Reference
W303-1A TMB3700	MATa trp1-1 leu2-3112 his3-11 ade2-1 ura3-1 can1-100 W303-1A; TRP1 HIS3, ura3::M3499 (ADE2)	Thomas and Rothstein (1989); ATCC® 208352 Brink et al. (2016)
TMB370X series		
TMB3701	TMB3700; can1::Ylp211	Brink et al. (unpublished)
TMB3702	TMB3700; can1::YlpGFP-Hxt1p	
TMB3703	TMB3700; can1::YlpGFP-Hxt2p	
TMB3704	TMB3700, can1::YlpGFP-Hxt4p	
TMB3705	TMB3700; can1::YlpGFP-Suc2p	
TMB3707	TMB3700; can1::YlpGFP-Tps1p	
TMB3708	TMB3700; can1::YlpGFP-Tps2p	
TMB3709	TMB3700; can1::YlpGFP-Tef4p	
TMB371X series		
TMB3711	TMB3701; can1::Ylp211; SPB1/PBN1::Ylp128	Brink et al. (2016)
TMB3712	TMB3702; can1::YlpGFP-Hxt1p; SPB1/PBN1::Ylp128	
TMB3713	TMB3703; can1::YlpGFP-Hxt2p; SPB1/PBN1::Ylp128	
TMB3714	TMB3704; can1::YlpGFP-Hxt4p; SPB1/PBN1::Ylp128	
TMB3715	TMB3705; can1::YlpGFP-Suc2p; SPB1/PBN1::Ylp128	
TMB3717	TMB3707; can1::YlpGFP-Tps1p; SPB1/PBN1::Ylp128	
TMB3718	TMB3708; can1::YlpGFP-Tps2p; SPB1/PBN1::Ylp128	
TMB3719	TMB3709; can1::YlpGFP-Tef4p; SPB1/PBN1::Ylp128	
TMB372X series		
TMB3721	TMB3701; SPB1/PBN1::Ylp128GAL2mut	This study
TMB3722	TMB3702; SPB1/PBN1::Ylp128GAL2mut	
TMB3723	TMB3703; SPB1/PBN1::Ylp128GAL2mut	
TMB3724	TMB3704; SPB1/PBN1::Ylp128GAL2mut	
TMB3725	TMB3705; SPB1/PBN1::Ylp128GAL2mut	
TMB3727	TMB3707; SPB1/PBN1::Ylp128GAL2mut	
TMB3728	TMB3708; SPB1/PBN1::Ylp128GAL2mut	
TMB3729	TMB3709; SPB1/PBN1::Ylp128GAL2mut	
TMB375X series		
TMB3751	TMB3721; Vac17/MRC1::TKL-TAL ^a ; Chr X-2/XI-5/XII-4::XR-XDH-XK ^b	This study
TMB3752	TMB3722; Vac17/MRC1::TKL-TAL; Chr X-2/XI-5/XII-4::XR-XDH-XK	
TMB3753	TMB3723; Vac17/MRC1::TKL-TAL; Chr X-2/XI-5/XII-4::XR-XDH-XK	
TMB3754	TMB3724; Vac17/MRC1::TKL-TAL; Chr X-2/XI-5/XII-4::XR-XDH-XK	
TMB3755	TMB3725; Vac17/MRC1::TKL-TAL; Chr X-2/XI-5/XII-4::XR-XDH-XK	
TMB3757	TMB3727; Vac17/MRC1::TKL-TAL; Chr X-2/XI-5/XII-4::XR-XDH-XK	
TMB3758	TMB3728; Vac17/MRC1::TKL-TAL; Chr X-2/XI-5/XII-4::XR-XDH-XK	
TMB3759	TMB3729; Vac17/MRC1::TKL-TAL; Chr X-2/XI-5/XII-4::XR-XDH-XK	

^aTKL-TAL = pFBA1-TKL1-tPDC1, pTPI1-TAL1-tCPS1.^bXR-XDH-XK = pTDH3-SpXYL1.2-tADH1, pTEF1-SaXDH-tGPM1, pPGI1-XKS1-tPYK1.

et al. (2016), resulting in plasmids pLWA31, pLWA32 and pLWA33. To construct pLWA32 and pLWA33, the XR/XDH/XKS1 ORFs were amplified from pLWA20 using primers 247/248 that contained sites for *AscI* and *SbfI*, while the pCfB2899/pCfB3040 backbone was amplified using primers 239 and 240 followed by cleaving with *AscI* and *SbfI*. The template vector was removed by *DpnI* cleaving. All fragments were gel-purified after cleaving and subsequently ligated. The resulting plasmids were verified by PCR using primers 245/246 for pLWA32 (pCfB2899-pLWA20) and 244/246 for pLWA33 (pCfB3040-pLWA20) and by restriction digest with *FastDigest SmaI*. The resulting plasmids were sequenced using primers 79–83. To clone the xylose pathway cassette into pCfB3037 XDH, XKS1 and XR were cleaved out from pLWA20 using *AscI/PmlI* and the 6642 bp fragment was purified from the gel. The plasmid backbone of pCfB3037 (including the 5' and 3' genomic target sequences XI-5) was amplified using primers 239 and 240 and cleaved with *MscI/AscI*. The template vector was removed by *DpnI* cleaving. All fragments were gel-purified after cleaving and subsequently ligated. The obtained plasmid,

pLWA31, was verified by restriction digest using *SmaI* and by sequencing using primers that anneal in the plasmid backbone and the TDH3p region (Seq_forward, Seq_reverse and TDH3p-F2-SacI).

Construction of the TKL-TAL integrative plasmid (pLWA19)

Saccharomyces cerevisiae promoters FBA1p and TPI1p, terminators PDC1t and CPS1t and the TKL1 and TAL1 ORFs were PCR amplified individually from *S. cerevisiae* CEN.PK 113-7D genomic DNA generating 40 bp homology between promoter, gene and terminator. Following agarose gel electrophoresis, the amplified PCR products were gel-purified (Thermo Fisher Scientific). Each individual gene expression cassette (FBA1p-TKL1-PDC1t and TPI1p-TAL1-CPS1t) was assembled by OE-PCR using primer pairs 45/50 (TKL1) and 51/56 (TAL1) with each part added in equimolar amounts. To enable In-fusion HD cloning, as described above for pLWA20, 15 bp homology regions between the two cassettes and the plasmid pUG-amdSYM (Solis-Escalante et al. 2013) were included in the primers. Following agarose gel electrophoresis,

Table 2. Plasmids used in this study.

Plasmid	Relevant genotype	Reference
Ylplac128	<i>AmpR</i> ; <i>LEU2</i>	Gietz and Sugino (1988)
p426-GPD	<i>URA3</i> ; <i>TDH3p-CYC1t</i>	Mumberg, Muller and Funk (1995)
YlpRCS	<i>URA3</i> ; <i>TDH3p-XYL1-ADH1t</i> ; <i>PGK1p-XYL2-PGK1t</i> ; <i>SpXYL1.2</i> (from <i>Sp. passalidarum</i> UFMG-CM-Y469)	Cadete et al. (2016)
pUG-amdSYM	<i>AmpR</i> ; <i>AnTEF2p-amdSYM-AnTEF2t</i> (from <i>Aspergillus nidulans</i>)	Solis-Escalante et al. (2013)
pRS62N_GAL2.N376F	<i>HXT7p- GAL2.N376F-CYC1t</i>	Farwick et al. (2014)
Ylplac128-GAL2.N376F	<i>Ylplac128: TDH3p- GAL2.N376F-CYC1t</i>	This study
pCfB2312	<i>TEFp-Cas9-CYC1t</i> ; <i>kanMX</i>	Stovicek, Borodina and Forster (2015)
pCfB2899	<i>X-2-MarkerFree backbone</i>	Jessop-Fabre et al. (2016)
pCfB3037	<i>XI-5- MarkerFree backbone</i>	Jessop-Fabre et al. (2016)
pCfB3040	<i>XII-4- MarkerFree backbone</i>	Jessop-Fabre et al. (2016)
pCfB3053	<i>CRISPR-cas9 gRNA targeting the X-2 (NCA3/NSF1), XI-5 (FRE2/COS9) and XII-4 (NIT3/YLR352W) regions; natMX</i>	Jessop-Fabre et al. (2016)
pLWA19	<i>pFBA1-TKL1-tPDC1</i> , <i>pTPI1-TAL1-tCPS1</i> ; <i>amdSYM</i>	This study
pLWA20	<i>Ylp-TDH3p-XYL-ADH1t-TEF1p-XDH-GPM1t-PG1p-XKS1-PYK1t;URA3</i>	This study
pLWA26	<i>gRNA-VAC17/MRC1</i> ; <i>natMX</i>	This study
pLWA31	<i>pCfB3037</i> ; <i>pTDH3-SpXYL1.2-tADH1</i> , <i>pTEF1-SsXDH-tGPM1</i> , <i>pPGI1-XKS1-tPYK1</i>	This study
pLWA32	<i>pCfB2899</i> ; <i>pTDH3-SpXYL1.2-tADH1</i> , <i>pTEF1-SsXDH-tGPM1</i> , <i>pPGI1-XKS1-tPYK1</i>	This study
pLWA33	<i>pCfB3040</i> ; <i>pTDH3-SpXYL1.2-tADH1</i> , <i>pTEF1-SsXDH-tGPM1</i> , <i>pPGI1-XKS1-tPYK1</i>	This study

the OE-PCR products were gel-purified. Two microgram of plasmid pUG-amdSYM2 was cleaved with *SpeI* and *SacII* and gel-purified. Gene cassettes and *SpeI/SacII* digested pUG-amdSYM2 were added in equimolar amount to 5× In-fusion HD enzyme premix following the In-fusion HD cloning kit user manual (Raman and Martin 2014). The plasmid was verified by sequencing using primers 5, 51, 57–60 and was named pLWA19.

pLWA19 was designed to be cleaved with *SfaAI* and *NotI* and integrated by nested double homologous integration aided by 5' and 3' homologous targeting fragments. Fragments for integration of the resulting TKL-TAL(*SfaAI/NotI*) cassette in the *VAC17/MRC1* intergenic locus were amplified from W303 genomic DNA using the following primers: 88.f and 107.r for the 5' *VAC17/MRC1* fragment and 108.f and *MRC1.TF.r* for the 3' *VAC17/MRC1* fragment.

Strain generation

TMB372X series

The TMB372X strains containing the different biosensors together with the mutated *Gal2p* transporter were constructed from the TMB370X (*Leu⁻*) strains by integration of the *Ylplac128-GAL2.N376F (Leu⁺)* plasmid at the *SPB1/PBN1* intergenic locus. This locus was previously used to cure the leucine auxotrophy with an empty *Ylplac128* plasmid (*LEU2*) in the TMB371X strains (Brink et al. 2016), meaning that all yeast strains in this study have a comparable genetic makeup in this region. Targeting fragments for double homologous integration of the *Ylplac128-GAL2.N376F* plasmid (linearized with *ZraI*) were PCR amplified using the *SPB1*. *Targ1.F/SPB1*. *Targ1.Rtail* and *PBN1*. *Targ2.Ftail/PBN1*. *Targ2.R* primer pairs, and were used for single-copy integration into the yeast genome as previously described (Brink et al. 2016).

TMB375X series

The TMB372X strains were used to construct the TMB375X strains by sequential integration of a cassette for overexpres-

sion of *TKL1* and *TAL1* genes, followed by three copies of the cassette containing the xylose pathway genes (*SpXYL1.2*, *SsXDH* and *XKS1*). These integrations were performed using a *S. cerevisiae* CRISPR-Cas9 system (Stovicek, Borodina and Forster 2015). First, the different TMB372X strains were transformed with the pCfB2312 plasmid containing the *Cas9* gene (Stovicek, Borodina and Forster 2015) and selected for on YPD with 200 µg/mL geneticin. Following this, the *TKL-TAL(SfaAI/NotI)* fragment was inserted in the *VAC17/MRC1* intergenic region. One microgram gRNA plasmid (pLWA26), 2 µg linear DNA fragments of *TKL-TAL(SfaAI/NotI)* and 0.5 µg of each 5'/3' targeting fragments were used and strains were selected for with 200 µg/mL geneticin and 100 µg/mL clonNAT. Cultivations in YPD with 200 µg/mL geneticin only (i.e. without clonNAT) were performed to cure the cells of the pLWA26 gRNA plasmid prior to the next transformation. Second, the xylose pathway genes were integrated in three different intergenic loci: *X-2* (chrX; *NCA3/NSF1*), *XI-5* (chrXI; *FRE2/COS9*) and *XII-4* (chrXII; *NIT3/YLR352W*) (Jessop-Fabre et al. 2016). One microgram gRNA plasmid (pCfB3053; Jessop-Fabre et al. 2016) and 1 µg of each *SmaI* linearized plasmid (pLWA31, pLWA32 and pLWA33) were used, and transformants were selected on YPD with 200 µg/mL geneticin and 100 µg/mL clonNAT. Correct integration of pLWA31 (*XI-5*), pLWA32 (*X-2*) and pLWA33 (*XII-4*) was verified using primer pairs 246/250, 246/249 and 246/251, respectively.

Sampling and analysis

Enzymatic assays

Single yeast colonies from the TMB375X strains (maintained on YPD agar plates with 200 µg/mL geneticin) were used to inoculate 5 mL of YPD medium in 50 mL conical centrifuge tubes. Cells were grown overnight at 30 °C and 180 rpm, and were harvested at 3000 rpm for 5 min. The whole-cell protein was extracted by treating the cell pellet with Y-PER (Yeast Protein Extraction Reagent; Pierce, Rockford, IL, USA) according to the manufacturer's instructions. The Micro-BCA kit (Pierce) and Bovine

Table 3. Biosensor induction and repression condition and cultivation time used in the study, based on and modified from our previously established protocol (Brink et al. 2016).

Strain	Promoter	Function	Signaling pathway	Repression condition	Induction condition
TMB37X1	Empty plasmid	Negative control	–	–	–
TMB37X2	HXT1p	Low-affinity hexose transporter	Snf3p/Rgt2p	Glucose 5 g/L (14 h)	Glucose 40 g/L (6 h)
TMB37X3	HXT2p	High-affinity hexose transporter	Snf3p/Rgt2p	Glucose 40 g/L (14 h)	Glucose 1 g/L (6 h)
TMB37X4	HXT4p	High-affinity hexose transporter	Snf3p/Rgt2p	Glucose 40 g/L (14 h)	Glucose 1 g/L (6 h)
TMB37X5	SUC2p	Invertase	SNF1/Mig1p	Glucose 40 g/L (14 h)	Glucose 1g/L (6 h)
TMB37X7	TPS1p	Trehalose-6-phosphate synthase	cAMP/PKA	Glucose 40 g/L (14 h)	Glucose 1 g/L (6 h)
TMB37X8	TPS2p	Trehalose-6-phosphate phosphatase	cAMP/PKA	Glucose 40 g/L (14 h)	Glucose 1 g/L (6 h)
TMB37X9	TEF4p	Translation elongation factor	cAMP/PKA	EtOH 3% (v/v) (26 h)	Glucose 40 g/L (6 h)

Albumin standard (Thermo Fisher Scientific) were used to determine the total protein concentration.

XR and XDH microtiter plate assays were adapted from previous protocols (Smiley and Bolen 1982; Rizzi et al. 1989). XR activity was determined by following NADH oxidation at 340 nm on a Multiskan Ascent (Thermo Electro Corporation, Finland) with constant read mode (one measurement every 3 s, 60 measurements points in total). The reaction consisted of 100 mM triethanolamine pH 7.0, 0.2 mM NADH, 350 mM xylose as a substrate and 5 μ L sample (protein extract from the TMB375X strains) for a total reaction volume of 250 μ L, and was initiated by the addition of the substrate. XDH activity was assayed with the same setup, but NAD⁺ reduction was now followed. The assay (250 μ L total volume) consisted of 100 mM glycine pH 9.0, 50 mM MgCl₂, 0.3 mM NAD⁺, 150 mM xylitol as a substrate and 5 μ L sample. The specific activity was defined as the amount of enzyme required to catalyze the formation/disappearance of 1 μ mol of NADH (ϵ NADH = 6220 L/mol cm) per min and mg protein (Horecker and Kornberg 1948; Burnett 1972). The enzymatic assays were done in biological duplicates and technical triplicates.

Growth curve

Single colonies from the TMB375X strains were inoculated in 5 mL of YPD medium in a 50 mL tube for overnight cultivation at 30°C, 180 rpm. The cells were then inoculated in a pre-sterilized Microtest Plate 96 Well R (Sarstedt, Nümbrecht, Germany) with YNB medium supplemented with either 20 g/L glucose or 20 g/L xylose. A starting optical density at 620nm (OD₆₂₀) of 0.5 and a total volume of 240 μ L were used. The plate was shaken at 1000 rpm in a 30°C incubator. Measurements were taken every hour for 8 h in total. YNB medium without cells and supplemented with the carbon source used for each specific growth curve was used as a negative control. Growth was recorded in biological duplicates and technical triplicates.

Flow cytometry analysis

A BD Accuri C6 flow cytometer equipped with a BD CSampler autosampler (Becton–Dickinson) was used to analyze the single-cell fluorescence intensity (FI) of the TMB372X and TMB375X GFP-reporter strains on different carbon sources. Cells were inoculated in YNB medium buffered with 50 mM potassium hydrogen phthalate at pH 5.5 (from here on denoted as YNB-KHPthalate medium) complemented with one of the following: xylose 50 g/L, xylose 5 g/L, xylose 50 g/L with glucose 5 g/L, glucose 5 g/L. A 488 nm excitation wavelength and 533/30 bandpass filter (from here on referred as the FL1-H channel) were used. The setup and handling of the Accuri flow cytometer was performed as previously reported (Brink et al. 2016). Data analysis was performed

with the FlowJo software (v10; Treestar, Inc., San Carlos, CA). Although TMB37X1 did not contain any biosensor, repression and induction were performed in glucose 40 g/L and glucose 1 g/L, respectively, in order to assess the autofluorescence under different conditions.

Two pre-cultivations were performed prior to the flow cytometry assay in order to gain sufficient biomass and biosensor repression at time 0 h of the experiment. The repression was performed to establish a FI baseline with an as low as possible intensity at the start of the experiment. The first pre-cultivations were prepared by inoculating a single colony in 5 mL of YNB-KHPthalate complemented with glucose 20 g/L (50 mL conical tubes) and incubation for 14 h at 30°C and 180 rpm. Following this, the strains were submitted to a second pre-cultivation in repressing conditions according to the known regulatory conditions of each biosensor promoter (Table 3). For the second pre-cultivation, cells were inoculated in 5 mL (in 50 mL conical tubes) at and initial OD₆₂₀ of 0.05 and were grown for 14 h. The strains were analyzed with the previously developed microtiter plate protocol (Brink et al. 2016), with some improvements regarding the repression and induction conditions for some of the biosensor strains (Table 3). The TEF4p biosensor proved challenging to repress, and the cells were therefore cultivated from an initial OD₆₂₀ of 0.1 for 26 h on YNB-KHPthalate supplemented with ethanol 3% (v/v) as a repressing condition; for the inducing condition, YNB-KHPthalate with glucose 20 g/L was used. For the repressing condition of the HXT1p biosensor, cultivations for 14 h in YNB-KHPthalate with glucose 5 g/L were used. For each strain and condition, biological triplicates and technical duplicates were performed.

Population heterogeneities on the GFP channel (FL1-H) were identified numerically and classified into low and high FI populations using two-component Gaussian Mixture modeling. The analysis was performed with Matlab (Release R2015a, The MathWorks, Inc., Natick, MA, USA) and is further outlined in the Supporting Information.

RESULTS

Strain construction and validation

We previously reported on the construction and validation of a non-invasive fluorescent *in vivo* reporter system for real-time monitoring of the three major glucose signaling pathways in *S. cerevisiae* (Brink et al. 2016). The present study complements the previous work by expanding the biosensor panel with 16 new strains divided in two strain series: TMB372X and TMB375X (Table 1). The TMB372X strain contains the different GFP-coupled biosensors from the previous study (HXT1/2/4p, SUC2p,

TPS1p/2p, TEF4p) together with a mutated galactose transporter (GAL2-N376F). This transporter has been reported to have increased affinity for D-xylose while having lost the ability to transport hexoses (Farwick et al. 2014). The TMB372X strains were constructed from the TMB370X (*Leu*⁻) series by integration of the GAL2-mutated gene at the SPB1/PBN1 intergenic locus with LEU2 as the selection marker. The TMB375X strains were then constructed from the TMB372X strains by overexpressing two of the non-oxidative PPP genes (TAL1 and TKL1) and integrating three gene copies of an oxidoreductase xylose pathway (XR-XDH-XK; cf. Table 1 and the section Materials and Methods for details). All integrations were verified using yeast colony PCR.

In order to ascertain the in-series comparability of the strains of the TMB375X series, the XR and XDH enzymatic activities were assayed, and it was confirmed that the activities of the respective enzymes were all in the same range across all strains (Fig. S3, Supporting Information). Likewise, growth experiments in glucose 20 g/L or xylose 20 g/L were also performed, and all strains demonstrated a similar growth pattern and rate (Table S6, Supporting Information; Fig. S2, Supporting Information).

Screening of the biosensors response to glucose and xylose

The strains from this and the previous studies were designed to analyze the effect of xylose on biosensors for three different scenarios for the uptake and metabolism of xylose (Fig. 2): extracellular xylose only, intracellular non-metabolized xylose and intracellular metabolized xylose. The wild type, non-xylose utilizing TMB371X strains (Fig. 2A) were used to assess the effect of xylose on the sugar signaling when most of xylose was extracellular (Brink et al. 2016). The previous study on these strains indicated that *S. cerevisiae* did not sense extracellular xylose, but that there was a response towards intracellular xylose, possibly transported inside the cell by hexose transporters capable to also transport xylose to some degree (Brink et al. 2016). In the current study, the TMB372X strains were used to analyze the biosensor response when xylose could efficiently be transported inside the cell via an engineered transporter, although it was not further metabolized (Fig. 2B). The final case (intracellular metabolized xylose) was assessed with the TMB375X strains, containing the transporter as well as a recombinant pathway for xylose assimilation (Fig. 2C).

The induction and repression conditions used in this study were performed as previously described (Brink et al. 2016) with slight modifications to improve the repression profile of the HXT1p and TEF4p biosensor strains (Table 3). The results of the flow cytometry screening of the biosensor strains on different concentrations of glucose and xylose are presented in Fig. 3 (TMB372X strains) and Fig. 4 (TMB375X strains). The corresponding data analysis—including peak means, coefficient of variation and subpopulation identification—for all strains and replicates is found in the Supporting Information and Tables S1–S4. The fold change results of the TMB375X (transporter + assimilation) strains are also summarized in heat map form in Fig. 5 (see also Fig. S4, Supporting Information, for an extended heat map with all strains of TMB371X–5X). It was found that the assessed biosensors were repressed and induced on glucose as expected (Table 3; Figs 3 and 4). However, not all strains could be completely repressed (dotted vertical red line in Figs 3 and 4), meaning that they had higher fluorescence than the cellular auto-FI of the control strains without GFP (black vertical line in Figs 3 and 4). This was previously observed for the strains TMB371X (Brink

et al. 2016), and was therefore not an attribute of the added genetic constructs in strains TMB372X (transporter) and TMB375X (transporter + assimilation). This discrepancy between repression and autofluorescence signal was mainly observed for the HXT2p, TPS1/2p and TEF4p biosensors (Fig. 3; Fig. 4C, F, G and H).

A shift in intensity and/or population heterogeneity was observed for the TMB3721 strain, the negative control strain without GFP that was used to determine the cellular autofluorescence. When inoculated in low glucose concentration (1 and 5 g/L) and/or in xylose (that the strain cannot metabolize), a decreased fluorescence was emitted compared to the control conditions for induction and repression (Fig. 3A, histograms I and R). TMB3751, the negative control that was able to grow on xylose, instead displayed an FI for xylose conditions comparable the repressing condition (Fig. 4A). The variations in autofluorescence observed for the TMB3721 strain can likely be explained by a decrease/variation in cell size due to carbon limitation due to low glucose concentration and the lack of xylose metabolism.

The biosensors for the Snf3p/Rgt2p signaling pathway gave a partial response in the presence of xylose. Both strains with the sensor for the HXT1p low-affinity hexose transporter (TMB3722 and TMB3752) showed a slightly higher fluorescence for the mixture of xylose 50 g/L and glucose 5 g/L, but no change in signal was detected for glucose 5 g/L, xylose 5 g/L or xylose 50 g/L (Figs 3B and 4B). HXT2p and HXT4p, the high-affinity hexose transporters, behaved similar to each other, with population heterogeneities detected in the presence of xylose for the xylose transporter strains TMB3723 and TMB3724 (Fig. 3C and D; Table S1, Supporting Information). However, when the xylose pathway was added (TMB3753 and TMB3754), a distinctive change in signaling pattern was observed with the disappearance of the subpopulations (Fig. 4C and D; Table S2, Supporting Information); this was also manifested in the TMB375X heat map (Fig. 5), where the two strains showed an induction signal on xylose similar to the inducing control condition (glucose 1 g/L). Cultivating the biosensors on YNB medium without any carbon source did not impact the signal response in any of the strains (Table S7, Supporting Information), meaning that the observed response on xylose can be attributed to xylose itself and not to a lack of (recognizable) carbon.

The promoter of the invertase-encoding gene *SUC2* was chosen as a representative biosensor for the SNF1/Mig1p signaling pathway; the previously assayed *Cat8p* as a potential sensor for this pathway (Brink et al. 2016) was not considered this time since it behaved like *SUC2p* but with lower overall FI, therefore giving less resolution. The *SUC2p* biosensor was slightly affected by the presence of low xylose concentration (5 g/L) when strain TMB3725 (transporter) was analyzed (Fig. 3E). In TMB3755 (transporter + assimilation), metabolized xylose clearly induced this biosensor both in a high or low concentration but with different FI intensity (Fig. 5), whereas it was less induced by the mixture of xylose 50 g/L and glucose 5 g/L, and by glucose 5 g/L (Figs 4E and 5).

The biosensors for the cAMP/PKA signaling pathway were not induced by intracellular non-metabolized xylose (TMB3727–28). In fact, the left subpopulation of the TPS1/2p strains was more repressed during xylose conditions than during the repression condition (Fig. 3F and G; Table S1, Supporting Information). Nevertheless, when the strains carrying the TPS1/2p biosensors were engineered to metabolize xylose (TMB3757–58), the population heterogeneities disappeared, and xylose triggered a small induction (Fig. 4F and G; Table S2, Supporting Information). In the case of TEF4p, only the strain that was able to metabolize xylose (TMB3759) was induced by high xylose (xylose 50 g/L)

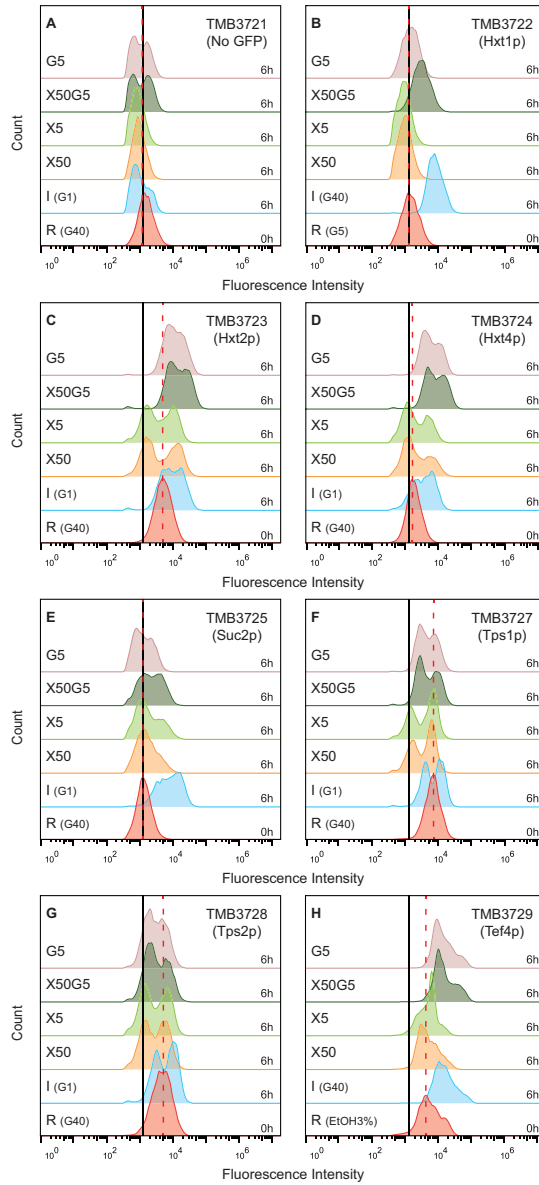


Figure 3. Histograms from flow cytometry analysis in microtiter plates of TMB372X strains in different conditions after 6 h. R: repression condition (see Table 3); I: induction condition (see Table 3); X50: xylose 50 g/L; X5: xylose 5 g/L; X50G5: xylose 50 g/L with glucose 5 g/L; G5: glucose 5 g/L. Black line is the reference for the auto-FI based on the negative control (TMB3721). The red dotted line marks the repression condition intensity for each biosensor. The histograms displayed in the figure are single replicates and are representative of their corresponding biological and technical replicates.

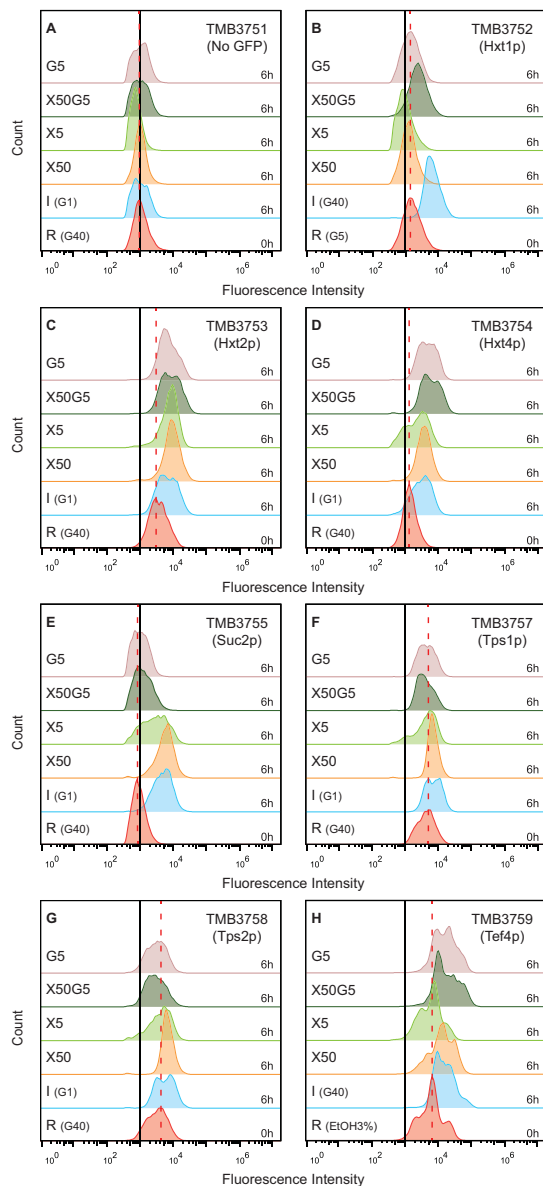


Figure 4. Histograms from flow cytometry analysis in microtiter plates of TMB375X strains in different conditions after 6 h: R: repression condition (see Table 3); I: induction condition (see Table 3); X50: xylose 50 g/L; X5: xylose 5 g/L; X50G5: xylose 50 g/L with glucose 5 g/L; G5: glucose 5 g/L. Black line is the reference for auto-FI based on the negative control (TMB3751). The red dotted line marks the repression condition intensity for each biosensor. The histograms displayed in the figure are single replicates and are representative of their corresponding biological and technical replicates.

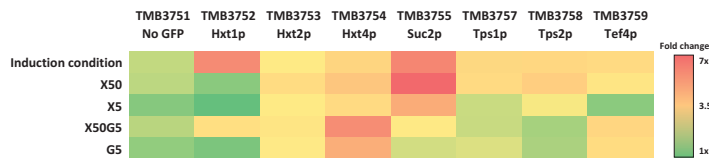


Figure 5. Heat map of the GFP FI of the TMB375X (transporter + assimilation) strains with the FI fold change from 0 to 6 h. The different conditions were as follows: induction condition (see Table 3), xylose 50 g/L (X50), xylose 5 g/L (X5), xylose 50 g/L with glucose 5 g/L (X50G5) and glucose 5 g/L (G5). The heat map values were taken from the average of the geometric mean FI of all the biological triplicates (including the technical duplicates).

(Fig. 4). As was also reported in the previous study (Brink et al. 2016), the TEF4p biosensor is very challenging to repress, which is evident when compared with other biosensors, and especially with the control TMB3751 lacking GFP (Fig. 4).

The main difference observed between the two strain series, TMB372X (transporter) and TMB375X (transporter + assimilation), was that the subpopulations that appeared in the TMB372X strains in some of the conditions, often disappeared after the xylose assimilation capacity was added (TMB375X strains; Table S2, Supporting Information). Most of the TMB375X biosensors were induced by sole xylose, except for HXT1p which did not demonstrate any influence from xylose 5 g/L or 50 g/L; in fact, no major change could be seen between the histograms of TMB3722 (Fig. 3B) and TMB3752 (Fig. 4B). For the strains that could metabolize xylose (TMB375X) and are known to be induced by glucose 1 g/L (HXT2p, HXT4p, SUC2p, TPS1p and TPS2p; Table 3), it was noticed that the chosen induction condition resulted in a similar response as with xylose 50 g/L, causing GFP expression for these biosensors under both conditions (Fig. 5).

DISCUSSION

Although metabolic engineering has conveyed and improved xylose assimilation in *S. cerevisiae*, xylose utilization rates are still low in comparison to the native glucose assimilation rates (Matsushika et al. 2009). As a number of studies have suggested that xylose is not recognized as a fermentable sugar by recombinant *S. cerevisiae* strains (Jin, Laplaza and Jeffries 2004; Salusjarvi et al. 2006; Salusjarvi et al. 2008; Zeng et al. 2016), we created a system of in vivo biosensors to investigate how xylose influences the sugar signaling pathways in Baker's yeast (Brink et al. 2016) and analyze them in conjunction with engineered xylose transport and assimilation. The major outcomes are discussed below.

Population heterogeneity on xylose is alleviated in the transporter strains after the xylose pathway is introduced

The in vivo biosensor system was designed with single-copy integration for single-cell measurements, meaning that any population heterogeneity/subpopulation in the GFP data are of physiological relevance, and not artifacts of the biosensor design (Brink et al. 2016). In the first generation of biosensors (TMB371X; no transporter nor xylose pathway), we have previously observed an effect of internalized xylose on HXT2/4p sensors. Subpopulations were only observed for the HXT2/4p biosensors during xylose conditions (25 and 50 g/L), and not for any other strains or conditions (Brink et al. 2016).

In the present study, it was found that the addition of the mutated GAL2 transporter gene (TMB372X) resulted in popu-

lation heterogeneities in more strains than just the HXT2/4p biosensors on xylose 5 g/L and on xylose 50 g/L (Fig. 3). It was then observed that these heterogeneities were alleviated after the xylose pathway was added (TMB375X), as the biosensors induced by low glucose (1 g/L) were completely induced in high xylose (50 g/L) when the strains became able to metabolize xylose (Fig. 4). The overall disappearance of the subpopulations in the TMB375X strains able to grow on xylose indicate that it could be either the intracellular xylose and/or the background expression of the yeast's endogenous xylose metabolism (Toivari et al. 2004) that are behind these heterogeneities.

Xylose resulted in a similar signal to that of limited glucose conditions in strains able to metabolize xylose

Assessment of the xylose sensing in the *S. cerevisiae* strains engineered to transport and grow on xylose (TMB375X) revealed a link between the signal during xylose conditions and the signal at glucose 1 g/L (Fig. 4). As the population heterogeneities disappeared in favor of a more homogenous population distribution in TMB375X (Table S2, Supporting Information), it became evident that, for sensors induced by low glucose, the signal on both xylose 50 and 5 g/L was highly similar to the signal of low glucose (Fig. 4). This is intriguing since it indicates that when *S. cerevisiae* senses intracellular and metabolized xylose, it triggers a low glucose response that might actually hinder efficient xylose utilization.

HXT1p was the only biosensor which did not show population heterogeneity in any of the three constructions (Fig. 2): the wild-type strains (TMB371X), the Gal2p mutant strains (TMB372X) or the strains in which xylose can be both taken up and metabolized (TMB375X), see Figs 3B and 4B. HXT1p is also the only biosensor in this panel that is repressed by low glucose (Table 3), and this effect was also achieved by high xylose (Fig. 4B). It is known that the expression of HXT1 is well-regulated by different proteins of the sugar sensing pathways—Snf3p/Rgt2p (Rgt1p), SNF1/Mig1p (Hxk2p), cAMP/PKA (PKA and Rgt1p)—and the osmotolerance pathway Hog1/MAPK (Sko1p) (Tomás-Cobos et al. 2004; Palomino, Herrero and Moreno 2005; Kim and Johnston 2006). Therefore, we cannot currently elucidate if the xylose repression on Hxt1p is a result of (i) the internalized and metabolized xylose; (ii) the lack of extracellular glucose signal; or both. Although the HXT1p biosensor did not show an induction either for extracellular, intracellular and metabolized xylose or for glucose 5 g/L, the induction effect observed on the mix of glucose 5 g/L and xylose 50 g/L (Figs 3B and 4B) might be caused by the high molarity from xylose 50 g/L combined along with effects of the cell sensing glucose. The Hog1/MAPK pathway is activated during conditions of high osmotic stress (e.g. high concentrations of sugars or salts), and regulates among other targets Sko1p which is a repressor of HXT1 (Fig. 1B). Upon

activation of Hog1/MAPK, Sko1p is phosphorylated and released from the *HXT1* promoter, allowing the expression of the gene (Tomás-Cobos et al. 2004).

HXT2/4p are known to be repressed during glucose absence (by e.g. Rgt1p), and also at high-glucose concentrations (by e.g. Mig1p), resulting in an *HXT2/4* expression window when glucose is present only in low concentrations (Özcan and Johnston 1996); interestingly, this window also seems to span xylose conditions (Fig. 4C and D). Mig1p simultaneously affects *SUC2*: at low glucose concentrations SNF1 is activated and phosphorylates Mig1p (Fig. 1B) leading to a derepression of the high-affinity hexose transporters *HXT2/4* and *SUC2* (Westholm et al. 2008). Indeed, it was observed that xylose triggers the SNF1/Mig1p signaling pathway (Fig. 4E) in the same manner that it triggers the low glucose concentration-sensing *HXT2/4p*. The behavior of the *SUC2p* biosensor (TMB3755) also matches that of a transcriptomics study on *S. cerevisiae* engineered for xylose utilization, which showed a peak expression of *SUC2* occurring during xylose conditions, leading the authors to hypothesize that xylose does not activate the glucose repression pathways in the same way as glucose does (Salusjärvi et al. 2008).

TPS1/2 are known to be induced by stress conditions (including glucose limitation) (Winderickx et al. 1996), but interestingly, the wild-type biosensors (neither xylose transport nor assimilation) remained repressed with xylose 50 g/L after 6 h (TMB3717-18; Brink et al. 2016). The current study, however, showed that in xylose condition the low FI subpopulations of these biosensors with just the transporter (TMB3727-28) were more repressed than the repression condition (glucose 40 g/L; Fig. 3F–G). On the other hand, the corresponding biosensor strains with transporter and xylose pathway (TMB3757-58; Fig. 4F–G) were induced in presence of xylose. This indicates that internalized and metabolized xylose has an effect on *TPS1/2* similar to that of low/limited glucose, while the lack of induction of these biosensors in the Gal2p mutant strains (TMB3727-28) is comparable to the signal of when they were submitted to YNB with no carbon source (Table S7, Supporting Information).

From a signaling pathway point of view (Fig. 1), we could observe the following effects of xylose on TMB375X: the Snf3p/Rgt2p pathway was partially induced on xylose, that is the Snf3p-regulated gene (*HXT2p/4p*) was induced, whereas the Rgt2p side (*HXT1p*) was repressed; the SNF1/Mig1p pathway was induced (*SUC2p*); finally, the cAMP/PKA was repressed (inversely proportional to *TPS1/2p*, which were activated). Interestingly, by taking this holistic view on the biosensor results, we observed that the pathway induction pattern fits with the known induction pattern of protein kinase A (PKA), a protein that to some extent is known to regulate all three of these pathways. PKA is activated by cAMP which in turn is activated by sensing of extra- and/or intracellular glucose (Santangelo 2006; Peeters and Thevelein 2014). Active PKA leads to activation of *HXT1p* (Kim and Johnston 2006; Jouandot, Roy and Kim 2011), repression of *SUC2p* (Gancedo, Flores and Gancedo 2015) and repression of *TPS1/2p* (Boy-Marcotte et al. 1998; Roosen et al. 2005). The results of the current study suggest that since *HXT1p* was repressed and *SUC2p* and *TPS1/2p* were induced on xylose (Fig. 4), it follows that xylose cannot fully activate PKA. In that case, the PKA behavior may be one of the key signaling differences between glucose and xylose; this is graphically summarized in Fig. 6. PKA is also inactivated during stress conditions, which subsequently triggers activation of the environmental stress response through e.g. *Msn2p/4p* (Smith, Ward and Garrett 1998; Thevelein and De Winde 1999), meaning that the xylose utilizing strains may have an active stress response running simultaneously to the carbon

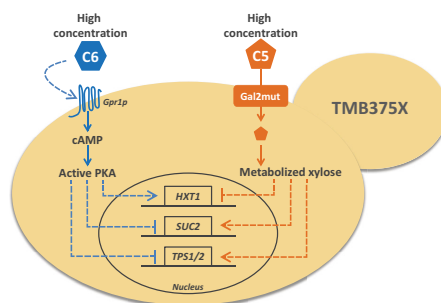


Figure 6. The effect of glucose-activated PKA on the signaling system compared to the observed effect of high-xylose concentrations in the TMB375X (transporter + assimilation) strains. For *HXT1*, *SUC2* and *TPS1/2*, the signal response of high xylose is the direct opposite of that high glucose. From this, it is hypothesized that high concentrations of xylose is sensed as low concentration glucose by *S. cerevisiae* (see the Discussion section for details). Solid arrows: reactions/transport; dashed arrows: induction (arrowhead) or repression (hammerhead). Note that PKA is not necessarily the only regulator of these genes (cf. Fig. 1).

metabolism which in turn would lead to a state of suboptimal growth.

Furthermore, it is known that Hexokinase 2 (Hxk2p) has an important regulatory function in sugar signaling and glucose carbon catabolite repression, and is, e.g., required both to fully induce *HXT1* during high-glucose conditions (through Rgt1p), and to de-repress *SUC2* during low-glucose conditions (through Mig1p) (Özcan and Johnston 1995; Moreno and Herrero 2002), cf. Fig. 1B. *In vitro* studies have shown that Hxk2p is inactivated by D-xylose through an autophosphorylation at the active site (Fernandez et al. 1986; Heidrich et al. 1997); moreover, HXK2 is repressed by Rgt1p in the absence of glucose (Palomino, Herrero and Moreno 2005), meaning that the low glucose–high xylose effect that we observed have two different mechanistic explanations with similar outcome when we consider Hxk2p as a key signaling regulator. The lack of signal in the *HXT1p* biosensors (TMB3722 and 3752) during conditions with xylose as sole carbon source (Figs 3 and 4) would then be explained by the fact that this transporter is repressed by low glucose levels (Fig. 1B; Table 3) and that one of its inducers, Hxk2p, is inactivated by (intracellular) xylose. Furthermore, deletion studies have shown that genes of low-affinity hexose transporters (e.g. *HXT1*) were downregulated in $\Delta h x k 2$ strains, whereas high-affinity transporters (e.g. *HXT2/4*) were upregulated (Özcan and Johnston 1995; Petit et al. 2000). The observed signal for the *HXT2/4p* high-affinity transporters on xylose in all the three strain series (TMB3713-14, Brink et al. 2016; TMB3723-24, Fig. 3; TMB3753-54, Fig. 4), could, at least partly, also be explained in relation to Hxk2p: intracellular xylose inactivates hexokinase, which then de-represses the high-affinity transporters. However, the case seems to be slightly different for *SUC2p*—a gene that is also regulated by Hxk2p (Moreno and Herrero 2002)—which was not fully induced on xylose until strain TMB3755 (transporter + assimilation; Fig. 4E vs. Fig. 3E). Studies have shown that Hxk2p only controls the long-term repression of *SUC2* on glucose (de Winde et al. 1996; Sanz, Nieto and Prieto 1996), which, together with the fact that the *HXT* and *SUC2* genes are controlled by different signaling pathways (Snf3p/Rgt2p and SNF1/Mig1p respectively), could explain the different results of these biosensors.

It should also be noted that the observed overall decrease in population heterogeneity in TMB375X (transporter + assimilation) compared to TMB372X (transporter) might also suggest that the sugar signaling pathways are affected by intermediate metabolites formed from xylose during its catabolism, since the main difference between these strain series is the addition of the XR/XDH/XKS and TAL1/TKL1 cassettes (Table 1). The recombinant xylose pathways shunt carbon to the glycolysis via the PPP, which means that the observed biosensor induction on xylose in the TMB375X strains (transporter + assimilation; Fig. 4) can have resulted from signaling feedback from the lower glycolysis and central carbon metabolism.

CONCLUSIONS

We have identified two major problems in how xylose is sensed by *S. cerevisiae*: (i) xylose is not sensed extracellularly (TMB371X; Brink et al. 2016) and (ii) xylose-utilizing strains produce a similar signal for high xylose as for low glucose. The consequences of xylose not being sensed in the extracellular space leads to a cascade of signaling reactions that involves all three sugar signaling pathways: for instance, if xylose is not sensed outside the cell it does not induce the extracellular receptors of the Snf3p/Rgt2 and cAMP/PKA pathways, which in turn does not trigger a complete expression of hexose transporters (mainly the low-affinity hexose transporters such as HXT1 remain unexpressed) and inactivates PKA. Furthermore, a high-xylose signal (which we postulate to be similar to a low-glucose signal) leads to an activation of the SNF1/Mig1p pathway by inactivating Hxk2p, allowing for the expression of alternative-carbon utilization genes (e.g. SUC2), while low-affinity hexose transporters again are repressed. This study also shows that the sensing of intracellular xylose changes when strains are engineered to transport, and to assimilate xylose, and implies that further studies aimed to improve xylose utilization in this yeast need to be performed in strains engineered to grow on xylose instead of wild-type strains.

SUPPLEMENTARY DATA

Supplementary data are available at [FEMSLE](https://www.frontiersin.org) online.

ACKNOWLEDGEMENTS

The authors would like to acknowledge Felipe G. Tueros for his assistance in generating some of the strains used in the study. The pRS62N-GAL2-N376F plasmid was kindly provided by Eckhard Boles (Goethe University, Frankfurt, Germany). We would also like to thank Irina Borodina, Vratislav Stovicek and Jochen Förster (Technical University of Denmark, Copenhagen, Denmark) for providing plasmids for the CRISPR-Cas9 system used in this study.

AUTHOR CONTRIBUTIONS

KOO, MC and MGG designed the study. KOO performed the strain construction, enzymatic assays, flow cytometry analysis, data analysis and drafted the initial manuscript. DB participated in the molecular biology work, strain construction, data analysis (e.g. the Gaussian Mixture modeling) and manuscript revision. CB participated in the data analysis and manuscript revision. LW designed and constructed the XK/XDH and TAL/TKL cassettes (pLWA plasmids). KOO and DB finalized the manuscript.

MGG conceived the study and revised the manuscript. All authors read and approved the final manuscript.

FUNDING

This work was supported by The Swedish Research Council (Vetenskapsrådet) [grant number 2016-05297.VR] and The Brazilian National Council for Scientific and Technological Development (National Council for Scientific and Technological Development - CNPq) [“Science Without Borders (Ciência sem Fronteiras - CsF)” scholarship awarded to KOO].

Conflict of interest. None declared.

REFERENCES

- Alff-Tuomala S, Salusjärvi L, Barth D et al. Xylose-induced dynamic effects on metabolism and gene expression in engineered *Saccharomyces cerevisiae* in anaerobic glucose-xylose cultures. *Appl Microbiol Biot* 2016;100:969–85.
- Apel AR, Ouellet M, Szmidt-Middleton H et al. Evolved hexose transporter enhances xylose uptake and glucose/xylose co-utilization in *Saccharomyces cerevisiae*. *Sci Rep* 2016;6:19512.
- Attfield PV, Bell PJ. Use of population genetics to derive nonrecombinant *Saccharomyces cerevisiae* strains that grow using xylose as a sole carbon source. *FEMS Yeast Res* 2006;6:862–8.
- Bergdahl B, Heer D, Sauer U et al. Dynamic metabolomics differentiates between carbon and energy starvation in recombinant *Saccharomyces cerevisiae* fermenting xylose. *Biotechnol Biofuels* 2012;5:34.
- Boles E, Hollenberg CP. The molecular genetics of hexose transport in yeasts. *FEMS Microbiol Rev* 1997;21:85–111.
- Boy-Marcotte E, Perrot M, Bussereau F et al. Msn2p and Msn4p control a large number of genes induced at the diauxic transition which are repressed by cyclic AMP in *Saccharomyces cerevisiae*. *J Bacteriol* 1998;180:1044–52.
- Brat D, Boles E, Wiedemann B. Functional Expression of a Bacterial Xylose Isomerase in *Saccharomyces cerevisiae*. *Appl Environ Microb* 2009;75:2304–11.
- Brink DP, Borgström C, Tueros FG et al. Real-time monitoring of the sugar sensing in *Saccharomyces cerevisiae* indicates endogenous mechanisms for xylose signaling. *Microb Cell Fact* 2016;15:183.
- Bruinenberg PM, de Bot PH, van Dijken JP et al. The role of redox balances in the anaerobic fermentation of xylose by yeasts. *Eur J Appl Microbiol* 1983;18:287–92.
- Burnett RW. Accurate measurement of molar absorptivities. *J Res Nat Bur Stand A* 1972;76:483.
- Cadete RM, de las Heras AM, Sandström AG et al. Exploring xylose metabolism in *Spathaspora* species: XYL1. 2 from *Spathaspora passalidarum* as the key for efficient anaerobic xylose fermentation in metabolic engineered *Saccharomyces cerevisiae*. *Biotechnol Biofuels* 2016;9:167.
- de Winde JH, Crauwels M, Hohmann S et al. Differential requirement of the yeast sugar kinases for sugar sensing in establishing the catabolite-repressed state. *FEBS J* 1996;241:633–43.
- Farwick A, Bruder S, Schadeweg V et al. Engineering of yeast hexose transporters to transport D-xylose without inhibition by D-glucose. *P Natl Acad Sci USA* 2014;111:5159–64.
- Feng X, Zhao H. Investigating glucose and xylose metabolism in *Saccharomyces cerevisiae* and *Scheffersomyces stipitis* via C-13 metabolic flux analysis. *AIChE J* 2013;59:3195–202.

- Fernandez R, Herrero P, Fernandez M et al. Mechanism of inactivation of hexokinase PII of *Saccharomyces cerevisiae* by D-xylose. *Microbiology* 1986;132:3467–72.
- Gancedo JM, Flores C-L, Gancedo C. The repressor Rgt1 and the cAMP-dependent protein kinases control the expression of the SUC2 gene in *Saccharomyces cerevisiae*. *Biochim Biophys Acta* 2015;1850:1362–7.
- Gietz RD, Schiestl RH. High-efficiency yeast transformation using the LiAc/SS carrier DNA/PEG method. *Nat Protoc* 2007;2:31–4.
- Gietz RD, Sugino A. New yeast-*Escherichia coli* shuttle vectors constructed with in vitro mutagenized yeast genes lacking six-base pair restriction sites. *Gene* 1988;74:527–34.
- Hahn-Hägerdal B, Karhumaa K, Fonseca C et al. Towards industrial pentose-fermenting yeast strains. *Appl Microbiol Biot* 2007a;74:937–53.
- Hahn-Hägerdal B, Karhumaa K, Jeppsson M et al. Metabolic engineering for pentose utilization in *Saccharomyces cerevisiae*. *Adv Biochem Eng Biot* 2007b;108:147–77.
- Hamacher T, Becker J, Gardonyi M et al. Characterization of the xylose-transporting properties of yeast hexose transporters and their influence on xylose utilization. *Microbiology* 2002;148:2783–8.
- Heidrich K, Otto A, Behlke J et al. Autophosphorylation–inactivation of hexokinase 2 in *Saccharomyces cerevisiae*. *Biochemistry* 1997;36:1960–4.
- Hill J, Donald KA, Griffiths DE et al. DMSO-enhanced whole cell yeast transformation. *Nucleic Acids Res* 1991;19:5791.
- Ho NW, Chen Z, Brainard AP. Genetically engineered *Saccharomyces* yeast capable of effective cofermentation of glucose and xylose. *Appl Environ Microb* 1998;64:1852–9.
- Horecker BL, Kornberg A. The extinction coefficients of the reduced band of pyridine nucleotides. *J Biol Chem* 1948;175:385–90.
- Inoue H, Nijima H, Okayama H. High-Efficiency Transformation of *Escherichia coli* with Plasmids. *Gene* 1990;96:23–8.
- Jeffries T, Jin Y-S. Metabolic engineering for improved fermentation of pentoses by yeasts. *Appl Microbiol Biot* 2004;63:495–509.
- Jessop-Fabre MM, Jakóciunas T, Stovicek V et al. EasyClone-MarkerFree: a vector toolkit for marker-less integration of genes into *Saccharomyces cerevisiae* via CRISPR-Cas9. *Biotechnol J* 2016;11:1110–7.
- Jin YS, Laplaza JM, Jeffries TW. *Saccharomyces cerevisiae* engineered for xylose metabolism exhibits a respiratory response. *Appl Environ Microb* 2004;70:6816–25.
- Jouandot D, Roy A, Kim JH. Functional dissection of the glucose signaling pathways that regulate the yeast glucose transporter gene (HXT) repressor Rgt1. *J Cell Biochem* 2011;112:3268–75.
- Kaniak A, Xue Z, Macool D et al. Regulatory network connecting two glucose signal transduction pathways in *Saccharomyces cerevisiae*. *Eukaryot Cell* 2004;3:221–31.
- Kim J-H, Johnston M. Two glucose-sensing pathways converge on Rgt1 to regulate expression of glucose transporter genes in *Saccharomyces cerevisiae*. *J Biol Chem* 2006;281:26144–9.
- Kim J-H, Polish J, Johnston M. Specificity and regulation of DNA binding by the yeast glucose transporter gene repressor Rgt1. *Mol Cell Biol* 2003;23:5208–16.
- Kim SR, Ha S-J, Wei N et al. Simultaneous co-fermentation of mixed sugars: a promising strategy for producing cellulosic ethanol. *Trends Biotechnol* 2012;30:274–82.
- Klimacek M, Krahulec S, Sauer U et al. Limitations in xylose-fermenting *Saccharomyces cerevisiae*, made evident through comprehensive metabolite profiling and thermodynamic analysis. *Appl Environ Microb* 2010;76:7566–74.
- Kötter P, Amore R, Hollenberg CP et al. Isolation and characterization of the *Pichia stipitis* xylitol dehydrogenase gene, XYL2, and construction of a xylose-utilizing *Saccharomyces cerevisiae* transformant. *Curr Genet* 1990;18:493–500.
- Kötter P, Ciriacy M. Xylose fermentation by *Saccharomyces cerevisiae*. *Appl Microbiol Biot* 1993;38:776–83.
- Kotyk A. Properties of the sugar carrier in baker's yeast. *Folia Microbiol* 1967;12:121–31.
- Kraakman LS, Winderickx J, Thevelein JM et al. Structure-function analysis of yeast hexokinase: structural requirements for triggering cAMP signalling and catabolite repression. *Biochem J* 1999;343:159–68.
- Kwak S, Jin Y-S. Production of fuels and chemicals from xylose by engineered *Saccharomyces cerevisiae*: a review and perspective. *Microb Cell Fact* 2017;16:82.
- Limayem A, Ricke SC. Lignocellulosic biomass for bioethanol production: current perspectives, potential issues and future prospects. *Prog Energy Combust* 2012;38:449–67.
- Lööke M, Kristjuhan K, Kristjuhan A. Extraction of genomic DNA from yeasts for PCR-based applications. *Biotechniques* 2011;50:325.
- Matsushika A, Inoue H, Kodaki T et al. Ethanol production from xylose in engineered *Saccharomyces cerevisiae* strains: current state and perspectives. *Appl Microbiol Biot* 2009;84:37–53.
- Moreno F, Herrero P. The hexokinase 2-dependent glucose signal transduction pathway of *Saccharomyces cerevisiae*. *FEMS Microbiol Rev* 2002;26:83–90.
- Mosley AL, Lakshmanan J, Aryal BK et al. Glucose-mediated phosphorylation converts the transcription factor Rgt1 from a repressor to an activator. *J Biol Chem* 2003;278:10322–7.
- Moyes DN, Reis VC, Almeida JR et al. Xylose fermentation by *Saccharomyces cerevisiae*: challenges and prospects. *Int J Mol Sci* 2016;17:207.
- Mumberg D, Müller R, Funk M. Yeast vectors for the controlled expression of heterologous proteins in different genetic backgrounds. *Gene* 1995;156:119–22.
- Nijland JG, Shin HY, de Jong RM et al. Engineering of an endogenous hexose transporter into a specific D-xylose transporter facilitates glucose-xylose co-consumption in *Saccharomyces cerevisiae*. *Biotechnol Biofuels* 2014;7:168.
- Nijland JG, Vos E, Shin HY et al. Improving pentose fermentation by preventing ubiquitination of hexose transporters in *Saccharomyces cerevisiae*. *Biotechnol Biofuels* 2016;9:158.
- Özcan S, Dover J, Johnston M. Glucose sensing and signaling by two glucose receptors in the yeast *Saccharomyces cerevisiae*. *EMBO J* 1998;17:2566–73.
- Özcan S, Johnston M. Three different regulatory mechanisms enable yeast hexose transporter (Hxt) genes to be induced by different levels of glucose. *Mol Cell Biol* 1995;15:1564–72.
- Özcan S, Johnston M. Two different repressors collaborate to restrict expression of the yeast glucose transporter genes HXT2 and HXT4 to low levels of glucose. *Mol Cell Biol* 1996;16:5536–45.
- Özcan S, Vallier LG, Flick JS et al. Expression of the SUC2 gene of *Saccharomyces cerevisiae* is induced by low levels of glucose. *Yeast* 1997;13:127–37.
- Palomino A, Herrero P, Moreno F. Rgt1, a glucose sensing transcription factor, is required for transcriptional repression of the HXK2 gene in *Saccharomyces cerevisiae*. *Biochem J* 2005;388:697–703.
- Peeters K, Thevelein JM. Glucose sensing and signal transduction in *Saccharomyces cerevisiae*. In: Piškur J,

- Compagno C (eds.) *Molecular Mechanisms in Yeast Carbon Metabolism*. Berlin, Heidelberg: Springer-Verlag, 2014, 21–56.
- Petit T, Diderich JA, Kruckeberg AL et al. Hexokinase regulates kinetics of glucose transport and expression of genes encoding hexose transporters in *Saccharomyces cerevisiae*. *J Bacteriol* 2000;182:6815–8.
- Raman M, Martin K. One solution for cloning and mutagenesis: In-Fusion® HD Cloning Plus. *Nat Methods* 2014;11:3–5.
- Rizzi M, Harwart K, Erlemann P et al. Purification and properties of the NAD⁺-xylitol-dehydrogenase from the yeast *Pichia stipitis*. *J Ferment Bioeng* 1989;67:20–4.
- Rolland F, Winderickx J, Thevelein JM. Glucose-sensing and signalling mechanisms in yeast. *FEMS Yeast Res* 2002;2:183–201.
- Rosen J, Engelen K, Marchal K et al. PKA and Sch9 control a molecular switch important for the proper adaptation to nutrient availability. *Mol Microbiol* 2005;55:862–80.
- Rudolf A, Baudel H, Zacchi G et al. Simultaneous saccharification and fermentation of steam-pretreated bagasse using *Saccharomyces cerevisiae* TMB3400 and *Pichia stipitis* CBS6054. *Biotechnol Bioeng* 2008;99:783–90.
- Runquist D, Hahn-Hägerdal B, Bettiga M. Increased expression of the oxidative pentose phosphate pathway and gluconeogenesis in anaerobically growing xylose-utilizing *Saccharomyces cerevisiae*. *Microb Cell Fact* 2009;8:1.
- Salusjärvi L, Kankainen M, Soliymani R et al. Regulation of xylose metabolism in recombinant *Saccharomyces cerevisiae*. *Microb Cell Fact* 2008;7:18.
- Salusjärvi L, Pitkanen JP, Aristidou A et al. Transcription analysis of recombinant *Saccharomyces cerevisiae* reveals novel responses to xylose. *Appl Biochem Biotech* 2006;128:237–61.
- Sambrook J, Russell DW. *Molecular Cloning: A Laboratory Manual*, 3rd Edn. Cold Spring Harbor, New York: Cold Spring Harbor Laboratory Press, 2001.
- Santangelo GM. Glucose signaling in *Saccharomyces cerevisiae*. *Microbiol Mol Biol R* 2006;70:253–82.
- Sanz P, Nieto A, Prieto JA. Glucose repression may involve processes with different sugar kinase requirements. *J Bacteriol* 1996;178:4721–3.
- Skog K, Hahn-Hägerdal B. Xylose fermentation. *Enzyme Microb Tech* 1988;10:66–80.
- Smiley KL, Bolen PL. Demonstration of D-xylose reductase and D-xylitol dehydrogenase in *Pachysolen tannophilus*. *Biotechnol Lett* 1982;4:607–10.
- Smith A, Ward MP, Garrett S. Yeast PKA represses Msn2p/Msn4p-dependent gene expression to regulate growth, stress response and glycogen accumulation. *EMBO J* 1998;17:3556–64.
- Solis-Escalante D, Kuijpers NG, Nadine B et al. amdSYM, a new dominant recyclable marker cassette for *Saccharomyces cerevisiae*. *FEMS Yeast Res* 2013;13:126–39.
- Stovicek V, Borodina I, Forster J. CRISPR-Cas system enables fast and simple genome editing of industrial *Saccharomyces cerevisiae* strains. *Metab Eng Commun* 2015;2:13–22.
- Thevelein JM, De Winde JH. Novel sensing mechanisms and targets for the cAMP-protein kinase A pathway in the yeast *Saccharomyces cerevisiae*. *Mol Microbiol* 1999;33:904–18.
- Thomas BJ, Rothstein R. Elevated recombination rates in transcriptionally active DNA. *Cell* 1989;56:619–30.
- Toivari MH, Salusjärvi L, Ruohonen L et al. Endogenous xylose pathway in *Saccharomyces cerevisiae*. *Appl Environ Microb* 2004;70:3681–6.
- Tomás-Cobos L, Casadomé L, Mas G et al. Expression of the HXT1 low affinity glucose transporter requires the coordinated activities of the HOG and glucose signalling pathways. *J Biol Chem* 2004;279:22010–9.
- Uihlein A, Schebek L. Environmental impacts of a lignocellulose feedstock biorefinery system: an assessment. *Biomass Bioenerg* 2009;33:793–802.
- van Maris A, Winkler A, Kuypers M et al. Development of efficient xylose fermentation in *Saccharomyces cerevisiae*: xylose isomerase as a key component. *Adv Biochem Eng Biot* 2007;108:179–204.
- Westholm JO, Nordberg N, Murén E et al. Combinatorial control of gene expression by the three yeast repressors Mig1, Mig2 and Mig3. *BMC Genomics* 2008;9:601.
- Winderickx J, de Winde JH, Crauwels M et al. Regulation of genes encoding subunits of the trehalose synthase complex in *Saccharomyces cerevisiae*: Novel variations of STRE-mediated transcription control? *Mol Gen Genet* 1996;252:470–82.
- Zaldivar J, Borges A, Johansson B et al. Fermentation performance and intracellular metabolite patterns in laboratory and industrial xylose-fermenting *Saccharomyces cerevisiae*. *Appl Microbiol Biot* 2002;59:436–42.
- Zeng W-Y, Tang Y-Q, Gou M et al. Transcriptomes of a xylose-utilizing industrial flocculating *Saccharomyces cerevisiae* strain cultured in media containing different sugar sources. *AMB Express* 2016;6:51.

Supporting Information[†] for:

Assessing the effect of D-xylose on the sugar signaling pathways of *Saccharomyces cerevisiae* in strains engineered for xylose transport and assimilation

Karen O Osiro, Daniel P Brink, Celina Borgström, Lisa Wasserstrom, Magnus Carlquist,
Marie F Gorwa-Grauslund*

Applied Microbiology. Department of Chemistry. Lund University. Lund. Sweden

*Corresponding author

E- mail: Marie-Francoise.Gorwa@tmb.lth.se

[†] Reformatted for increased readability by Celina Borgström Tufvegren

Supplementary Material and Methods

Identification of subpopulations using Gaussian Mixture modelling

Throughout the screening of the strains constructed in this study, it was found that some of the conditions resulted in population heterogeneities on the main channel of interest, i.e. the GFP channel (FL1-H). In order to be able to account for the reproducibility of the heterogeneities over the biological and technical replicates that were performed for each strain and condition, the histograms of the FL1-H dataset were analyzed for normal distributions, and all non-Gaussian distributions were subjected to Gaussian Mixture modeling in order to identify the beginning and end of each subpopulation.

For the dataset of the present study it was assumed that all non-Gaussian histograms were composed of two normally distributed components, i.e. two underlying subpopulations. Once the intersection point between the two subpopulations was identified, the population was classified into a low and high Fluorescence Intensity (FI) clusters. Examples of the outcome of this workflow are shown in Figure S1. The clusters were used to calculate the percent of the total population (n=10 000 events) that fell into each FI cluster (Table S1-S2), as well as the Coefficient of Variance (CV; Table S1-2) and mean FI of each cluster (Table S3; Table S4). Notably, the analysis showed that mainly the TMB372X strains (transporter) displayed population heterogeneities, with only a few occurring in the TMB375X (transporter + assimilation) data, see Table S1-S4. A custom Matlab (Release R2015a, The MathWorks, Inc., Natick, MA, US) script was written using scripts shared by other developers online. The modelling was performed using the *gaussian_mixture_model.m* script (v1.1; written by Matthew Roughan; downloaded from <http://www.mathworks.com/matlabcentral>) and curve intersections were identified using the *Fast and Robust Curve Intersections* script (v2.0; written by Douglas Schwarz; downloaded from <http://www.mathworks.com/matlabcentral>).

Supplementary Figures

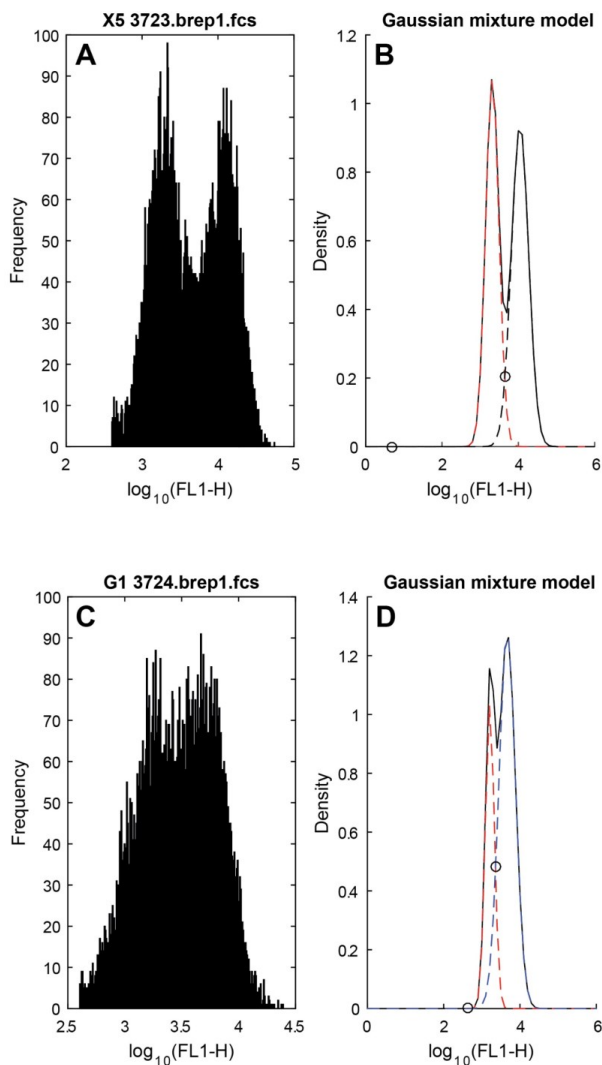


Figure S1. Example of the Gaussian Mixture modelling workflow. A&C: Histograms of the FL1-H channel data from a typical heterogeneous signal (A: TMB3723 on xylose 5 g/L after 6h; C: TMB3724 on glucose 1 g/L after 6h). B & D: Density histograms showing the Gaussian mixture modelling of the data from A and C respectively, that was used to identify the FL1-H value that marked the separation of the two subpopulations. Mixture plot legend: red dotted line= 1st component/normal distribution, blue dotted line= 2nd component/normal distribution, black solid line= compound model (1st component + 2nd component), circles = intersections between the 1st and 2nd component. Only intersections that occurred within the area under the compound model were considered.

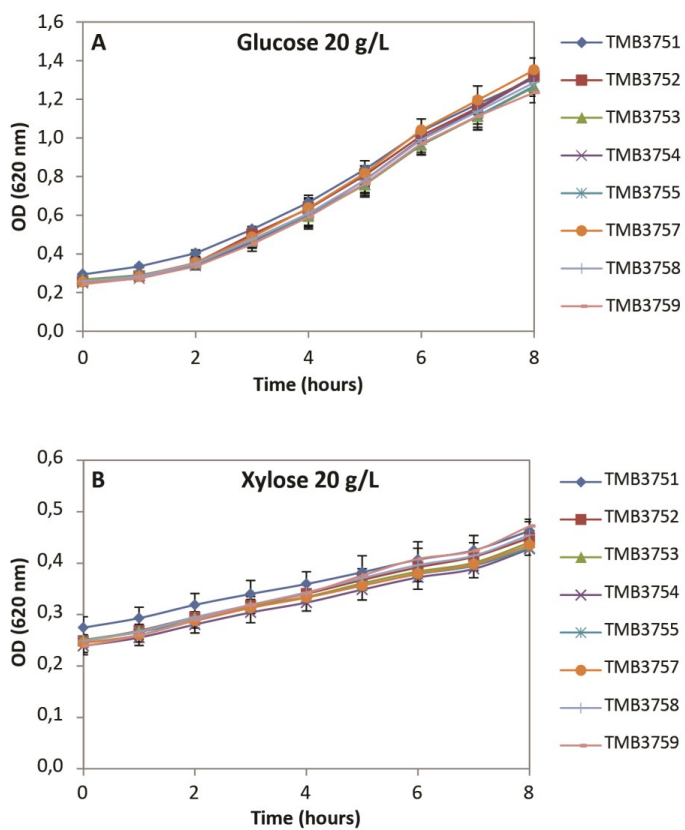


Figure S2. Growth of strains TMB375X (carrying genes for xylose transport and assimilation). Cultivations were performed in YNB medium containing A: glucose 20 g/L; B: xylose 20 g/L.

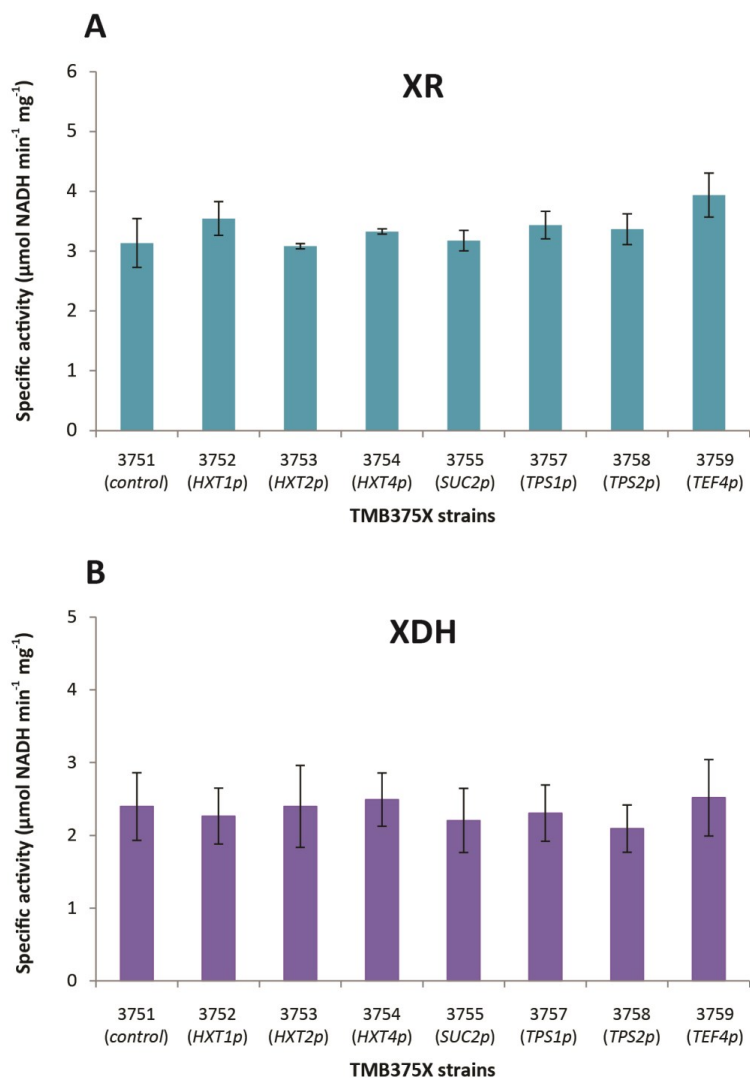


Figure S3. Enzymatic activities of A) xylose reductase (XR) and B) xylitol dehydrogenase (XDH) in the TMB375X strains. The error bars represent the standard deviations of the biological replicates.

Supplementary Tables

Table S1. Distribution and Coefficient of Variation (CV) of the TMB372X subpopulations on the FL1-H channel. The non-normal distributed histograms were subjected to Gaussian Mixture modelling in order to identify the underlying subpopulations. The experiment was performed in three biological replicates with two technical replicates each. FI=fluorescence intensity; N/A=no subpopulations (i.e. the histogram followed normal distribution); I=induction condition; R=repression condition. 100% corresponds to 10 000 flow cytometry events.

Strain	Condition	Time	Percent Lower subpop (FL1-H)	Percent Upper subpop (FL1-H)	CV Lower subpop (FL1-H)	CV Upper subpop (FL1-H)
3721	G5	6h	N/A			
	X50G5	6h	N/A			
	X5	6h	N/A			
	X50	6h	N/A			
	I(G1)	6h	N/A			
	R(G40)	0h	N/A			
3722	G5	6h	N/A			
	X50G5	6h	N/A			
	X5	6h	N/A			
	X50	6h	N/A			
	I(G40)	6h	N/A			
	R(G5)	0h	N/A			
3723	G5	6h	76% \pm 7	24% \pm 7	0.43 \pm 0.03	0.33 \pm 0.02
	X50G5	6h	66% \pm 3	34% \pm 3	0.42 \pm 0.02	0.34 \pm 0.02
	X5	6h	43% \pm 3	57% \pm 3	0.35 \pm 0.03	0.51 \pm 0.02
	X50	6h	46% \pm 2	54% \pm 2	0.35 \pm 0.02	0.60 \pm 0.03
	I(G1)	6h	52% \pm 5	48% \pm 5	0.41 \pm 0.01	0.41 \pm 0.02
	R(G40)	0h	N/A			
3724	G5	6h	77% \pm 10	23% \pm 10	0.40 \pm 0.03	0.29 \pm 0.03
	X50G5	6h	62% \pm 5	38% \pm 5	0.39 \pm 0.01	0.34 \pm 0.01
	X5	6h	42% \pm 2	58% \pm 2	0.23 \pm 0.03	0.48 \pm 0.03
	X50	6h	46% \pm 3	54% \pm 3	0.22 \pm 0.01	0.63 \pm 0.02
	I(G1)	6h	34% \pm 3	66% \pm 3	0.24 \pm 0.03	0.47 \pm 0.02
	R(G40)	0h	N/A			
3725	G5	6h	N/A			
	X50G5	6h	N/A			
	X5	6h	40% \pm 4	60% \pm 4	0.19 \pm 0.01	0.60 \pm 0.02
	X50	6h	56% \pm 6	44% \pm 6	0.20 \pm 0.02	0.56 \pm 0.02
	I(G1)	6h	51% \pm 1	49% \pm 1	0.43 \pm 0.01	0.43 \pm 0.02
	R(G40)	0h	N/A			

Table S1. (cont'd)

Strain	Condition	Time	Percent Lower subpop (FL1-H)	Percent Upper subpop (FL1-H)	CV Lower subpop (FL1-H)	CV Upper subpop (FL1-H)
3727	G5	6h	N/A			
	X50G5	6h	57% \pm 5	43% \pm 5	0.32 \pm 0.01	0.38 \pm 0.01
	X5	6h	35% \pm 3	65% \pm 3	0.30 \pm 0.02	0.39 \pm 0.02
	X50	6h	38% \pm 1	62% \pm 1	0.28 \pm 0.01	0.38 \pm 0.01
	I(G1)	6h	51% \pm 4	49% \pm 4	0.34 \pm 0.01	0.32 \pm 0.01
	R(G40)	0h	N/A			
3728	G5	6h	47% \pm 8	53% \pm 8	0.25 \pm 0.02	0.52 \pm 0.02
	X50G5	6h	N/A			
	X5	6h	37% \pm 3	63% \pm 3	0.25 \pm 0.01	0.49 \pm 0.01
	X50	6h	37% \pm 1	63% \pm 1	0.23 \pm 0.01	0.49 \pm 0.02
	I(G1)	6h	49% \pm 2	51% \pm 2	0.36 \pm 0.01	0.36 \pm 0.01
	R(G40)	0h	N/A			
3729	G5	6h	76% \pm 9	24% \pm 9	0.42 \pm 0.07	0.42 \pm 0.09
	X50G5	6h	79% \pm 1	21% \pm 1	0.47 \pm 0.01	0.36 \pm 0.02
	X5	6h	N/A			
	X50	6h	49% \pm 8	51% \pm 8	0.28 \pm 0.02	0.57 \pm 0.01
	I(G40)	6h	88% \pm 1	12% \pm 1	0.55 \pm 0.01	0.29 \pm 0.01
	R(EtOH3%)	0h	58% \pm 5	42% \pm 5	48% \pm 2	38% \pm 2

Table S2. Distribution and Coefficient of Variation (CV) of the TMB375X subpopulations on the FL1-H channel. The non-normal distributed histograms were subjected to Gaussian Mixture modelling in order to identify the underlying subpopulations. The experiment was performed in three biological replicates with two technical replicates each. FI=fluorescence intensity; N/A=no subpopulations (i.e. the histogram followed normal distribution); I=induction condition; R=repression condition. 100% corresponds to 10 000 flow cytometry events.

Strain	Condition	Time	Percent Lower subpop (FL1-H)	Percent Upper subpop (FL1-H)	CV Lower subpop (FL1-H)	CV Upper subpop (FL1-H)
3751	G5	6h		N/A		
	X50G5	6h		N/A		
	X5	6h		N/A		
	X50	6h		N/A		
	I(G1)	6h		N/A		
	R(G40)	0h		N/A		
3752	G5	6h		N/A		
	X50G5	6h		N/A		
	X5	6h		N/A		
	X50	6h		N/A		
	I(G40)	6h		N/A		
	R(G5)	0h		N/A		
3753	G5	6h		N/A		
	X50G5	6h		N/A		
	X5	6h		N/A		
	X50	6h		N/A		
	I(G1)	6h		N/A		
	R(G40)	0h		N/A		
3754	G5	6h		N/A		
	X50G5	6h		N/A		
	X5	6h		N/A		
	X50	6h		N/A		
	I(G1)	6h		N/A		
	R(G40)	0h		N/A		
3755	G5	6h		N/A		
	X50G5	6h		N/A		
	X5	6h	18% \pm 5	82% \pm 5	0.16 \pm 0.02	0.61 \pm 0.04
	X50	6h		N/A		
	I(G1)	6h		N/A		
	R(G40)	0h		N/A		
3757	G5	6h		N/A		
	X50G5	6h		N/A		
	X5	6h	10% \pm 1%	90% \pm 1	0.18 \pm 0.01	0.49 \pm 0.02
	X50	6h		N/A		
	I(G1)	6h	48% \pm 5	52% \pm 5	0.28 \pm 0.01	0.36 \pm 0.02
	R(G40)	0h		N/A		

Table S2. (cont'd)

Strain	Condition	Time	Percent Lower subpop (FL1-H)	Percent Upper subpop (FL1-H)	CV Lower subpop (FL1-H)	CV Upper subpop (FL1-H)
3758	G5	6h	N/A			
	X50G5	6h	N/A			
	X5	6h	25% ±18	75% ±18	0.23 ±0.11	0.48 ±0.08
	X50	6h	N/A			
	G1	6h	N/A			
	R(G40)	0h	N/A			
3759	G5	6h	79% ±9	21% ±9	0.52 ±0.09	0.34 ±0.11
	X50G5	6h	78% ±2	22% ±2	0.52 ±0.03	0.36 ±0.02
	X5	6h	N/A			
	X50	6h	N/A			
	I(G40)	6h	64% ±47	36% ±47	0.52 ±0.21	0.39 ±0.30
	R(EtOH3%)	0h	80% ±11	20% ±11	0.59 ±0.05	0.27 ±0.04

Table S3. Reproducibility of the TMB372X samples on the FL1-H channel as determined by the geometrical mean of the histograms. The non-normal distributed histograms were subjected to Gaussian Mixture modelling in order to identify the underlying subpopulations. For Coefficient of Variation (CV) for the identified subpopulations. see Table S1. The experiment was performed in three biological replicates with two technical replicates each. FI=fluorescence intensity; N/A=no subpopulations (i.e. the histogram followed normal distribution); I=induction condition; R=repression condition. Each flow cytometry sample was recorded with 10 000 events.

Strain	Condition	Time	Mean FI lower population (FL1-H)	Mean FI upper population (FL1-H)	Mean FI total population (FL1-H)	CV total population (FL1-H)
3721	G5	6h	N/A		957 ±70	0.39 ±0.03
	X50G5	6h	N/A		1146 ±57	0.41 ±0.02
	X5	6h	N/A		862 ±18	0.33 ±0.02
	X50	6h	N/A		961 ±10	0.35 ±0.01
	I(G1)	6h	N/A		1070 ±23	0.38 ±0.04
	R(G40)	0h	N/A		1452 ±40	0.47 ±0.01
3722	G5	6h	N/A		1323 ±90	0.47 ±0.01
	X50G5	6h	N/A		2903 ±216	0.62 ±0.02
	X5	6h	N/A		972 ±89	0.43 ±0.04
	X50	6h	N/A		1032 ±47	0.41 ±0.02
	I(G40)	6h	N/A		8031 ±234	0.56 ±0.01
	R(G5)	0h	N/A		1457 ±57	0.54 ±0.02
3723	G5	6h	8075 ±411	26872 ±2796	10601 ±221	0.73 ±0.03
	X50G5	6h	9335 ±328	31710 ±540	13409 ±318	0.73 ±0.03
	X5	6h	1899 ±121	9824 ±960	4248 ±244	0.86 ±0.04
	X50	6h	1945 ±95	11704 ±840	4493 ±197	1.01 ±0.03
	I(G1)	6h	5330 ±576	19206 ±1668	9523 ±396	0.74 ±0.01
	R(G40)	0h	N/A		5203 ±139	0.63 ±0.02
3724	G5	6h	4354 ±238	13765 ±1474	5563 ±375	0.67 ±0.02
	X50G5	6h	5315 ±153	17477 ±675	7967 ±223	0.70 ±0.02
	X5	6h	1451 ±62	5513 ±620	2362 ±196	0.77 ±0.03
	X50	6h	1459 ±39	5414 ±374	2315 ±164	0.92 ±0.03
	I(G1)	6h	1693 ±136	5264 ±541	3173 ±303	0.67 ±0.01
	R(G40)	0h	N/A		1897 ±57	0.50 ±0.02
3725	G5	6h	N/A		1359 ±169	0.58 ±0.08
	X50G5	6h	N/A	2357 ±313	0.72 ±0.03	
	X5	6h	1372 ±38	4449 ±252	1954 ±75	0.83 ±0.04
	X50	6h	1418 ±47	3638 ±267	1604 ±108	0.77 ±0.04
	I(G1)	6h	3869 ±232	14769 ±758	7132 ±402	0.76 ±0.02
	R(G40)	0h	N/A		1351 ±19	0.52 ±0.10
3727	G5	6h	N/A		4710 ±156	0.70 ±0.03
	X50G5	6h	2847 ±85	9373 ±370	4575 ±161	0.72 ±0.02
	X5	6h	1741 ±106	6999 ±175	3775 ±149	0.66 ±0.02
	X50	6h	1782 ±79	6193 ±251	3503 ±113	0.64 ±0.02
	I(G1)	6h	4121 ±150	13405 ±558	7135 ±320	0.64 ±0.02
	R(G40)	0h	N/A		6854 ±248	0.54 ±0.01

Table S3. (cont'd)

Strain	Condition	Time	Mean FI lower population (FL1-H)	Mean FI upper population (FL1-H)	Mean FI total population (FL1-H)	CV total population (FL1-H)
3728	G5	6h	1773 ±119	5240 ±460	2944 ±90	0.76 ±0.04
	X50G5	6h	<i>N/A</i>		3216 ±78	0.78 ±0.03
	X5	6h	1564 ±25	6132 ±176	3069 ±148	0.74 ±0.02
	X50	6h	1532 ±36	5227 ±230	2838 ±56	0.72 ±0.01
	G1	6h	3135 ±172	11153 ±663	5803 ±407	0.68 ±0.01
	R(G40)	0h	<i>N/A</i>		4661 ±86	0.65 ±0.02
3729	G5	6h	9885 ±911	37984 ±7424	13210 ±747	0.87 ±0.02
	X50G5	6h	11636 ±295	48585 ±1890	14739 ±305	0.88 ±0.02
	X5	6h	<i>N/A</i>		5018 ±988	0.76 ±0.04
	X50	6h	2849 ±261	8827 ±1195	4813 ±568	0.82 ±0.03
	I(G40)	6h	13271 ±255	60705 ±2277	14246 ±392	0.87 ±0.01
	R(EtOH3%)	0h	4702 ±277	19464 ±1559	8265 ±547	0.80 ±0.02

Table S4. Reproducibility of the TMB375X samples on the FL1-H channel as determined by the geometrical mean of the histograms. The non-normal distributed histograms were subjected to Gaussian Mixture modelling in order to identify the underlying subpopulations. The experiment was performed in three biological replicates with two technical replicates each. FI=fluorescence intensity; N/A=no subpopulations (i.e. the histogram followed normal distribution); I=induction condition; R=repression condition. Each flow cytometry sample was recorded with 10 000 events.

Strain	Condition	Time	Mean FI lower population (FL1-H)	Mean FI upper population (FL1-H)	Mean FI total population (FL1-H)	CV total population (FL1-H)
3751	G5	6h	N/A		991 ±69	0.40 ±0.08
	X50G5	6h	N/A		1154 ±70	0.43 ±0.04
	X5	6h	N/A		935 ±181	0.39 ±0.09
	X50	6h	N/A		1166 ±140	0.42 ±0.10
	I(G1)	6h	N/A		1191 ±179	0.44 ±0.11
	R(G40)	0h	N/A		802 ±627	0.48 ±0.02
3752	G5	6h	N/A		1243 ±94	0.51 ±0.04
	X50G5	6h	N/A		2610 ±165	0.62 ±0.01
	X5	6h	N/A		1099 ±96	0.55 ±0.04
	X50	6h	N/A		1338 ±54	0.55 ±0.03
	I(G40)	6h	N/A		6796 ±297	0.58 ±0.01
	R(G5)	0h	N/A		1123 ±876	0.64 ±0.03
3753	G5	6h	N/A		7103 ±133	0.73 ±0.02
	X50G5	6h	N/A		7690 ±95	0.72 ±0.02
	X5	6h	N/A		6953 ±602	0.53 ±0.01
	X50	6h	N/A		9299 ±436	0.61 ±0.02
	I(G1)	6h	N/A		6942 ±406	0.75 ±0.03
	R(G40)	0h	N/A		3766 ±180	0.66 ±0.02
3754	G5	6h	N/A		4326 ±747	0.64 ±0.03
	X50G5	6h	N/A		5702 ±780	0.68 ±0.02
	X5	6h	N/A		2496 ±366	0.58 ±0.03
	X50	6h	N/A		3357 ±569	0.54 ±0.05
	I(G1)	6h	N/A		2673 ±403	0.62 ±0.04
	R(G40)	0h	N/A		964 ±748	0.53 ±0.05
3755	G5	6h	N/A		1044 ±61	0.49 ±0.08
	X50G5	6h	N/A		1275 ±38	0.63 ±0.06
	X5	6h	1344 ±81	4730 ±570	3008 ±504	0.71 ±0.06
	X50	6h	N/A		4952 ±531	0.60 ±0.02
	I(G1)	6h	N/A		4150 ±413	0.68 ±0.01
	R(G40)	0h	N/A		665 ±518	0.45 ±0.04
3757	G5	6h	N/A		4503 ±82	0.63 ±0.04
	X50G5	6h	N/A		4195 ±259	0.63 ±0.01
	X5	6h	1372 ±18	5515 ±229	4211 ±120	0.56 ±0.02
	X50	6h	N/A		7145 ±308	0.41 ±0.01
	I(G1)	6h	4573 ±281	11830 ±744	7392 ±279	0.58 ±0.02
	R(G40)	0h	N/A		2771 ±2148	0.65 ±0.03

Table S4. (cont'd)

Strain	Condition	Time	Mean FI lower population (FL1-H)	Mean FI upper population (FL1-H)	Mean FI total population (FL1-H)	CV total population (FL1-H)
3758	G5	6h	<i>N/A</i>		2909 ±203	0.70 ±0.04
	X50G5	6h	<i>N/A</i>		2854 ±148	0.73 ±0.04
	X5	6h	1873 ±652	5809 ±1127	3796 ±232	0.61 ±0.03
	X50	6h	<i>N/A</i>		6648 ±151	0.44 ±0.01
	I(G1)	6h	<i>N/A</i>		5742 ±178	0.65 ±0.02
	R(G40)	0h	<i>N/A</i>		2134 ±1654	0.71 ±0.03
3759	G5	6h	10895 ±2507	47089 ±12444	14114 ±1574	0.88 ±0.06
	X50G5	6h	12117 ±1187	52084 ±4957	15477 ±1271	0.89 ±0.03
	X5	6h	<i>N/A</i>		6752 ±1456	0.78 ±0.05
	X50	6h	<i>N/A</i>		11930 ±1023	0.76 ±0.04
	I(G40)	6h	10242 ±6722	58644 ±31798	14573 ±309	0.85 ±0.03
	R(EtOH3%)	0h	7037 ±1294	28707 ±6572	5662 ±4450	0.77 ±0.03

Table S5. Primers used in the present study

Primer	Description	Sequence 5' – 3'	Reference
5_3'amdSYM down	Used to construct pLWA19	ccagatgcgaagttaagtgc	This study
45_FBA1p_f	“	tatcagatccactagtaggtcatgcattagcgcgccAC AATACTGACAGTACTAAATAATTG C	This study
47_TKL_f	“	gtaatacatattcaaacgccggcgaaaATGACTCA ATTCAGTGACATTG	This study
48_TKL_r	“	TaattagagattaaatcgccacgtgTTAGAAAGC TTTTTCAAAGG	This study
49_PDC1t_f	“	aaaaaagctttctaacacgtgGCGATTTAATCT CTAATTATTAGTTAAAG	This study
50_PDC1t_r	“	atataCCTAGGGGCAGTTTTGAATTGA GTAACC	This study
51_TPI1p_f	“	tgcccctaggTATATCTAGGAACCCATC AG	This study
52_TPI1p_r	“	gagctggttcagacattttgtcgacTTTTAGTTTA TGTATGTGTTTTTG	This study
53_TAL1_f	“	atacataaactaaaagtcgacaaaATGTCTGAAC CAGCTCAAAAG	This study
54_TAL1_r	“	ctattcaatcattgcgccccgggTTAAGCGGTA ACTTCTCTTTTC	This study
55_CPS1t_f	“	agaaagtaccgcttaacccgggGCGCAATGAT TGAATAGTCAAA	This study
56_CPS1t_r	“	gagaccggcagatccGCGGGATTGACAC TTGATTGACACTTC	This study
57_PPPseq1_f	“	TGGTTACGGTTCCTTGCATG	This study
58_PPPseq2_r	“	TCTTGTGGAACAACAAAGG	This study
59_PPPseq3_r	“	GGGTGTCCAGGTGTAACATC	This study
60_PPPseq4_r	“	ATTAATGCAGGTAACTGG	This study
61_FBA1p_r	Verification of <i>TKL-TAL</i> integration in <i>VAC17/MRC1</i> ; used to construct pLWA19	tgaattgagtcattttcgccggcgTTTGAATATG TATTACTTGGTTATGG	This study
65_TEF1_f	Used to construct pLWA20	tcgttcttccacactgcagATAGCTTCAAAAT GTTCTACTCC	This study
66_TEF1_r	“	ttagcagtcattttcgggccgcTTTGTAATTAAA ACTTAGATTAGATTGC	This study
67_XDH_f	“	ctaagttttaattacaagcgccgcgaaaATGACTG CTAACCCCTTCCTTG	This study
68_XDH_r	“	tcatttctcagacctcgagtaCTCAGGGCCGTC AATGAG	This study
69_GPM1t_f	“	ctcattgacggccctgagtaactcgagGTCTGAAG AATGAATGATTG	This study
70_GPM1t_r	“	ttgttactagtTATTCGAAGTCCCCATTCA G	This study
71_PGI1p_f	“	aataactagtAACAAAAATCACGATCTG GGTGGGT	This study
72_PGI1p_r	“	actgaacacaacattatgctagcTTTTAGGCTGG TATCTTGATTC	This study
73_XKS1_f	“	aagataccagcctaaaagctagcataATGTTGTG TTCAGTAATTACAG	This study
74_XKS1_r	“	tcaatcatgattcttttccgggTTAGATGAGAG TCTTTCCAG	This study

Table S5. (cont'd)			
Primer	Description	Sequence 5' – 3'	Reference
75_ PYK1t_f	“	aaagactctcatctaaccgggAAAAAGAATC ATGATTGA	This study
76_ PYK1t_r	“	cggccagtgaattcgagctcatgcacacgtgGCATT TATGTACCCATGTA	This study
78_XXX_seq1_r	“	ACGTGGTCTGGCAACTTGAC	This study
79_XXX_seq2_f	Used to construct pLWA20/31/32/33	ACGAATACAAGAGCGGTCAC	This study
80_XXX_seq3_r	Used to construct pLWA20/31/32/33	GTCCTGGTTAATGGCGAGAC	This study
81_XXX_seq4_f	Used to construct pLWA20/31/32/33	TCAGAGACAGACAAGAGAGG	This study
82_XXX_seq5_r	Used to construct pLWA20/31/32/33	CTTGAATTATAGCGATCCC	This study
83_XXX_seq6_r	Used to construct pLWA20/31/32/33	AGGGTTTTCCCAGTCACGAC	This study
88_5'Vac17new_f	Amplification of 5' <i>VAC17</i> end fragment for homology recombination, verification of <i>TKL-TAL</i> integration in <i>VAC17/MRC1</i> ; used to construct pLWA19	ACGATCAGATACACATACGG	This study
92_3'GRE3_f	Used to construct pLWA20	gtttccaagaactaacttggagggtatatacgggtacat aatgccacGCACTAAATGCCAACATCA G	This study
93_3'GRE3_r	“	GCTTTGCTCTCTTGGTGTCT	This study
98_5'GRE3_f	Used to construct pLWA20	CTACTTCTAGGGGGCCTATC	This study
99_5'GRE3_r	“	CTGGATGCCAGCTTAAAAAG	This study
107_ VAC17_r	Amplification of 5' <i>VAC17</i> end fragment for homology recombination; used to construct pLWA19	gtatagcatacattatacgaagtattattaagggttctcgag agctcgcgCAAAAAAAGCTGAAGATAT TCTG	This study
108_MRC1_f	Amplification of 3' <i>MRC1</i> end fragment for homology recombination; used to construct pLWA19	cataaccttatgtatcacacacacagatttaggtgacacta tagaacgcCTAGACTCGGGTGCCATCT	This study
MRC1_TF_r	Amplification of 3' <i>MRC1</i> end fragment for homology recombination; used to construct pLWA19	CAAAAGCTTCTATCACATATATGG G	This study
239_Easyclone_f	Used to construct pLWA31/32/33	aggaCACGTGgccgtgtttacaacgtcg	This study
240_Easyclone_r	“	aggaggcgcgccTAGCATGAGGTCGCTC ATCG	This study
Seq_forward	Used to construct pLWA31	AGGCTCAGTCGAAAGACTGG	This study
Seq_reverse	“	CGACTCACTATAGAAGTTCC	This study
244_XII-4 down_r	Used to construct pLWA33	ATTGCCCCAACCTTATAAGC	This study

Table S5. (cont'd)

Primer	Description	Sequence 5' – 3'	Reference
Seq_reverse	“	CGACTCACTATAGAAGTTCC	This study
244_XII-4 down_r	Used to construct pLWA33	ATTGCCCCAACCTTATAAGC	This study
245_X-2 down_r	Used to construct pLWA32	AGACGTAAAGTCAGGCAAGG	This study
246_XKS1_down_f	Verification of <i>XR-XDH-XK</i> integration in the X-2, XI-5 and XII-4 loci; Used to construct pLWA32/33	GAAACACCAAACTCATGTGC	This study
247_PYK1t_rev	Used to construct pLWA31/32/33	agattacctgcaggAGGGTTTTCCAGTCA CGAC	This study
248_TDH3p_fw	“	agattagcgcgcccCACAGGAAACAGCTA TGACC	This study
249_X-2 ver	Verification of <i>XR-XDH-XK</i> integration in the X-2 locus; Used to construct pLWA31/32/33	ACGCCACCAAGACAATATCC	This study
250_XI-5 ver	Verification of <i>XR-XDH-XK</i> integration in the XI-5 locus; Used to construct pLWA31/32/33	CACAGTGTACCAACGATTCCG	This study
251_XII-4 ver	Verification of <i>XR-XDH-XK</i> integration in the XII-4 locus; Used to construct pLWA31/32/33	GTGAAATCTCTTTGCGGTAG	This study
LW11	Amplification of <i>ALD6</i> (positive control for PCR)	GAAC TTCACCACCTTAGAGC	This study
LW12	“	TAGCACCTTGGAAGTTAGCC	This study
GAL2-F1_SmaI	Cloning of the <i>GAL2_N376F</i> cassette	ACCCGGGAAAAATGGCAGTTGAGGA GAAC	This study
GAL2_R1_XhoI	“	TGCTCGAGTTATTCTAGCATGGCCT TGTACCAC	This study
TDH3p-F2-SacI	Cloning of the <i>TDH3p-GAL2-N376F-CYC1t</i> cassette	TAAGAGCTCAGTTTATCATTATCAA TACTCGCCATTTC	This study
CYC1t-R2-SphI	“	GACCAGCATGCCAAATTAAAGCCT TCGAGCGTC	This study
SPB1_Targ1_F	Cloning of targeting fragments for introduction of the <i>Ylplac128-GAL2_N376F</i> plasmid in the <i>SPB1/PBN1</i> intergenic region	TTTGCCAGATTGGTTTTTAGAAG	Brink, et al. (2016)
SPB1_Targ1_Rtail	“	atttagaaaaataacaaatagggttcgcgcacattcc ccgaaaagtgccacctgacAAGGGAATGGAA AAATAATGCTC	Brink, et al. (2016)
PBN1_Targ2_Ftail	“	tggcctcgtgatacgctattttataggtaatgtcatgata ataatggtttcttagacATCATCAAAAAACTT ATAGGAAACC	Brink, et al. (2016)
PBN1_Targ2_Ftail	“	CGAGATAAGGCATGGGGTTC	Brink, et al. (2016)

Table S6. Maximum specific growth rates (μ_{\max}) of strains TMB375X (transport + assimilation). The cultivations were performed in YNB medium containing glucose 20 g/L and xylose 20 g/L and two biological replicates.

Strain	Glucose 20 g/L μ_{\max} (h ⁻¹)	Xylose 20 g/L μ_{\max} (h ⁻¹)
TMB3751 (No GFP)	0.235 ± 0.008	0.064 ± 0.002
TMB3752 (HXT1p)	0.258 ± 0.003	0.074 ± 0.001
TMB3753 (HXT2p)	0.253 ± 0.005	0.070 ± 0.005
TMB3754 (HXT4p)	0.268 ± 0.004	0.074 ± 0.001
TMB3755 (SUC2p)	0.254 ± 0.003	0.070 ± 0.005
TMB3757 (TPS1p)	0.267 ± 0.001	0.074 ± 0.002
TMB3758 (TPS2p)	0.258 ± 0.049	0.078 ± 0.001
TMB3759 (TEF4p)	0.265 ± 0.001	0.088 ± 0.002

Table S7. Signal response on the FL1-H channel during cultivations in YNB medium without any carbon source. Peak mean fluorescence intensity (FI) at 0h and 6h, and the FI fold change from 0h to 6h. The experiment was performed in two biological replicates.

Condition	Strain	Mean FI 0h	Mean FI 6h	FI Fold change
YNB without carbon source	TMB3751	1079 ±10.5	890 ±6.5	0.825 ±0.020
	TMB3752	1353 ±4.5	1051 ±11.5	0.777 ±0.016
	TMB3753	2155 ±7.5	2027 ±10	0.941 ±0.002
	TMB3754	1441 ±19	1309 ±36	0.908 ±0.018
	TMB3755	817 ±3.5	885 ±14.5	1.083 ±0.032
	TMB3757	2496 ±18.5	2204 ±15	0.883 ±0.001
	TMB3758	2119 ±9	1972 ±1.5	0.93 ±0.005
	TMB3759	2130 ±42	2367 ±52.5	1.111 ±0.004

References

Brink DP, Borgström C, Tueros FG, Gorwa-Grauslund MF. Real-time monitoring of the sugar sensing in *Saccharomyces cerevisiae* indicates endogenous mechanisms for xylose signaling. *Microb Cell Fact* 2016;**15**: 183.

Paper V



Using phosphoglucose isomerase-deficient *Saccharomyces cerevisiae* to further understand the role of glycolytic intermediates in strains engineered for D-xylose utilization

Celina Borgström¹, Oksana Rogova², Karen O. Osiro¹, Ester Lundberg¹,
Peter Spégel² & Marie F. Gorwa-Grauslund¹

¹ Division of Applied Microbiology, Department of Chemistry, Lund University, Lund, Sweden.

² Centre for Analysis and Synthesis, Department of Chemistry, Lund University, Lund, Sweden

Abstract

Despite massive engineering efforts worldwide, recombinant *Saccharomyces cerevisiae* are still less efficient at converting the non-natural D-xylose sugar to ethanol, compared to the preferred sugar D-glucose. Using biosensors reporting for the three main sugar sensing routes, we have recently demonstrated that the sensing response on D-xylose is similar to the response observed on low concentrations of D-glucose. In order to understand to which extent glycolytic intermediates are involved in the sensing response, the *PGII* gene, encoding phosphoglucose isomerase that catalyzes the conversion of glucose-6-phosphate to fructose 6-phosphate, was deleted. When evaluating the signaling response with biosensors for the main sugar sensing routes, *PGII* deletion was shown to alter the signaling response and decrease similarities in the response to high D-xylose and low D-glucose sensing response. This indicated that the metabolic node around Pgi1p is of importance for further engineering of the yeast sugar sensing for improved D-xylose utilization.

Introduction

With the increasing demand for renewable and environmentally friendly products, biorefineries, where a microorganism uses biomass from waste streams to produce fuels and specialty chemicals, such as bioethanol and polyhydroxyalkanoates (PHAs), is attracting increasing attention (Venkata Mohan et al., 2016). Baker's yeast *Saccharomyces cerevisiae* is a popular choice for the bioconversion process since this GRAS eukaryote has high tolerance towards inhibitors found in e.g. hydrolysates of agricultural and forestry waste streams (Almeida et al., 2007; Hahn-Hägerdal et al., 2007). However, since it cannot utilize the pentose sugar D-xylose that constitutes up to 30 % of wood materials, *S. cerevisiae* has been genetically engineered by introducing the xylose isomerase (XI) or the xylose reductase/xylitol dehydrogenase (XR/XDH) pathways. Together with overexpression of genes encoding xylulokinase (XK) and enzymes from the non-oxidative pentose phosphate pathway (PPP), this enables a substantial flux of D-xylose-derived substrates to enter glycolysis at the level of fructose-6-phosphate (F6P) and glyceraldehyde-3-phosphate (G3P) (Fig. 1). Ethanol production from D-xylose has now reached the maximum theoretical yield, but the rate of D-xylose consumption is still significantly lower than that of D-glucose (Jin and Jeffries, 2004; Chu and Lee, 2007). Also, co-consumption of D-xylose and D-glucose is not yet possible. Competition for transport into the cell may partly explain the sequential utilization of the sugars (Subtil and Boles, 2012); however, strains expressing engineered transporters with increased affinity for D-xylose are still not able to

achieve sufficient co-consumption (Nijland et al., 2014; Reider Apel et al., 2016).

D-xylose is not a natural carbon source for *S. cerevisiae* and all genes of the engineered pathways are highly expressed in the presence of D-glucose (Karhumaa et al., 2009); therefore it is not expected to be regulated by catabolite repression that controls the preference of *S. cerevisiae* to consume D-glucose over other carbon sources. Catabolite repression in *S. cerevisiae* is tightly regulated by the level of D-glucose and by the presence or absence of other naturally used carbon sources (Gancedo, 1998). Still it is unclear whether and how the non-natural carbon source D-xylose is sensed by *S. cerevisiae*.

Using a biosensor system responsive to variations in the D-glucose signaling routes (Brink et al., 2016), it was recently shown that extracellular and assimilated D-xylose is sensed in recombinant yeast carrying the XR/XDH pathway, something that does not occur in wild-type *S. cerevisiae* (Osiro et al., 2018). However, the observed response to D-xylose resembled the one observed on low concentrations of D-glucose. This gave rise to the hypothesis that during the incorporation of carbon from D-xylose into glycolysis, one or more metabolic intermediates with sugar signaling functionalities was/were formed.

Glucose-6-phosphate (G6P), trehalose-6-phosphate (T6P), and fructose-1,6-bisphosphate (F1,6bP) have been proposed as the major sugar signaling intermediates for D-glucose catabolism (Gancedo, 1998; Peeters et al., 2017; Aguilera, 1987; Vicente et al., 2018). On D-xylose, *S. cerevisiae* can produce

ethanol via F1,6bP but also glycogen via G6P (Portugal-Nunes et al., 2017), indicating that both G6P and F1,6bP intermediates are available (Fig. 1). G6P production from D-xylose requires phosphoglucose isomerase activity (Pgi1p) encoded by the *PGI1* gene (*YBR196c*), to interconvert G6P and F6P.

In the present study, *PGI1* gene was deleted in recombinant xylose-utilizing strains so that the levels of glycolytic

intermediates could be manipulated, depending on the type and levels of carbon sources added to the medium. Alterations in D-xylose and D-glucose metabolism and changes in sugar signaling were examined with the previously developed biosensor system and with profiling of intracellular sugar phosphates, with the objective to identify possible connections between sensing and the measured intermediates.

Materials and Methods

Strains and media

The plasmids and yeast strains used in the present study are presented in Tables 1 and 2, respectively. Primers used for amplification and confirmation of DNA fragment integration are found in Supplementary Table S1. *S. cerevisiae* strains were grown at 30 °C on solid or liquid YP (10 g L⁻¹ yeast extract; 20 g L⁻¹ peptone) or YNB (6.7 g L⁻¹ yeast nitrogen base without amino acids; 50 mM potassium hydrogen phthalate buffer, pH 5.5) with or without 15 g L⁻¹ agar and supplemented with suitable sugars. YP supplemented with 20 g L⁻¹ D-fructose and 1 g L⁻¹ D-glucose (YPFG) was routinely used for the *PGI1* deletants. Geneticin (G418; 200 mg L⁻¹) was supplemented to the medium to maintain the episomal plasmid pCfB2312 and aureobasidin A (AbA; 0.3 mg L⁻¹) was supplemented to the medium for selection

of uptake of the pUG62AUR-F12.Pgi1 plasmid.

Escherichia coli strain NEB5 α (New England Biolabs, Ipswich, MA, USA) was used for preparation and amplification of plasmids and was grown in liquid or solid Lysogeny Broth (LB) medium (10 g L⁻¹ tryptone, 5 g L⁻¹ yeast extract, 5 g L⁻¹ NaCl; with or without 15 g L⁻¹ agar) supplemented with 100 mg L⁻¹ ampicillin, at 37 °C.

Genetic methods

S. cerevisiae DNA sequences were amplified with PCR using either Phusion High-Fidelity DNA polymerase or DreamTaq polymerase, from Thermo Fisher Scientific (Waltham, MA, USA). Primers (Suppl. Table S1) were designed based on DNA sequences for W303 strains obtained from *Saccharomyces cerevisiae* Genome Database (SGD; <http://www.yeastgenome.org>) and were

Table 1. Plasmids used in the present study. US: region upstream of *PGI1*; DS: region downstream of *PGI1*.

Plasmid	Relevant genotype	Reference
pCfB2312	<i>TEF1p-Cas9-CYC1t; kanMX</i>	Stovicek et al. (2015)
pUG62AUR	LoxP – AbA ^R - LoxP;	Bergdahl et al. (2013)
pUG62AUR-F12.Pgi1	<i>PGI1</i> (US)-pUG62AUR- <i>PGI1</i> (DS)	This study

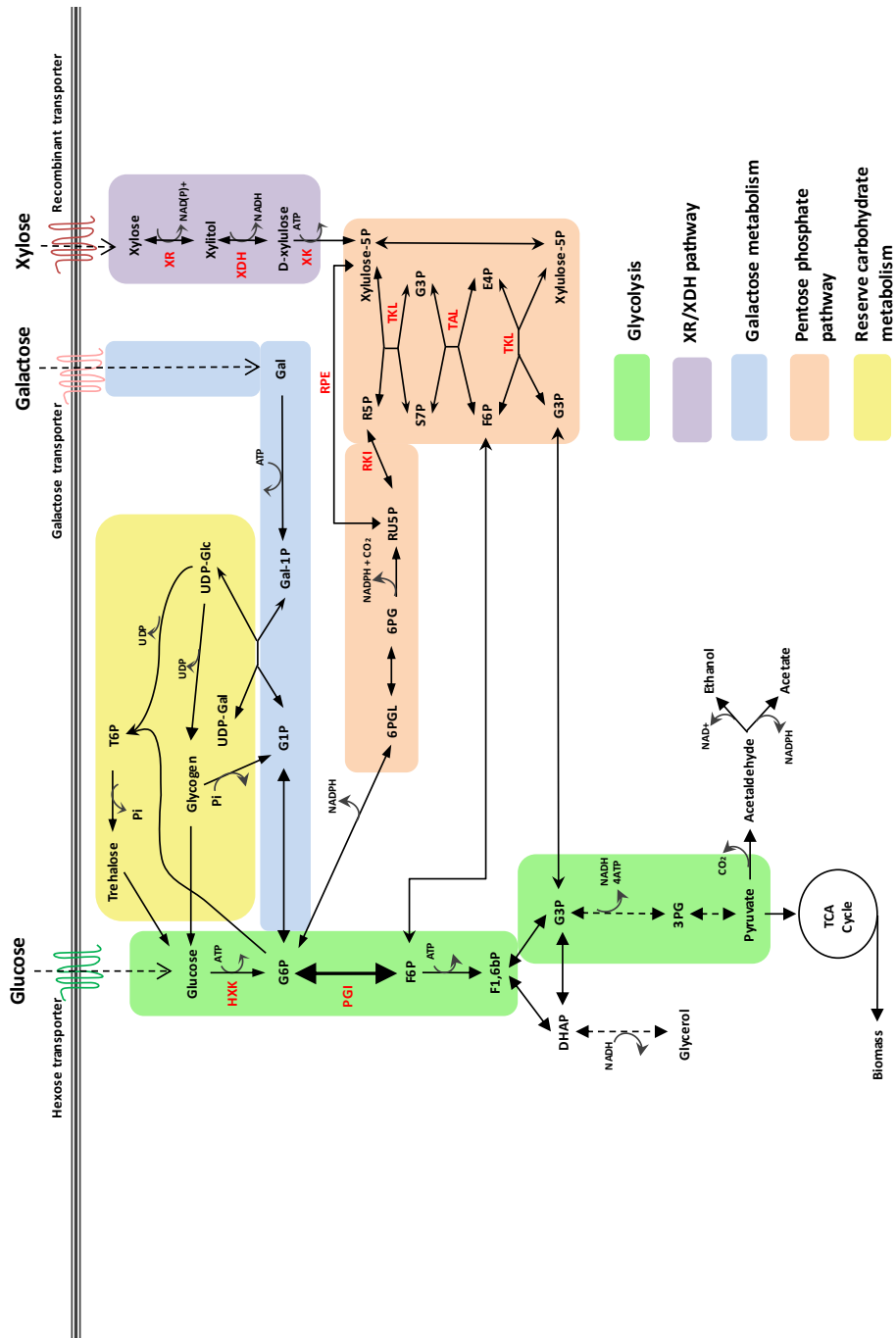


Figure 1. Metabolic map of *S. cerevisiae*, including D-xylose assimilation through the xylose reductase/xylitol dehydrogenase pathway, as established in strains TMB3752, TMB3755 and TMB3757. Abbreviations: Glc: D-glucose; Gal: D-galactose; G6P: glucose-6-phosphate; F6P: fructose-6-phosphate; F1,6bP: fructose-1,6-bisphosphate; DHAP: dihydroxyacetone phosphate; G3P: glyceraldehyde-3-phosphate; 3PG: 3-phosphoglycerate; TCA cycle: tricarboxylic acid cycle; G1P: glucose-1-phosphate; Gal-1-P: galactose-1-phosphate; UDP: uridine diphosphate; T6P: trehalose-6-phosphate; 6PGL: 6-phosphogluconolactone; 6PG: 6-phosphogluconate; RU5P: ribulose-5-phosphate; R5P: ribose-5-phosphate; S7P: sedoheptulose-7-phosphate; E4P: erythrose-4-phosphate; NADH: nicotinamide adenine dinucleotide; NADPH: nicotinamide adenine dinucleotide phosphate; ATP: adenosine triphosphate; HKX: hexokinase; PGI: phosphoglucose isomerase; XR: xylose reductase; XDH: xylitol dehydrogenase; XK: xylulokinase; RPE: ribulose-5-phosphate 3-epimerase; RKI: ribose-5-phosphate keto-isomerase; TKL: transketolase; TAL: transaldolase.

ordered from Eurofins Genomics (Ebersberg, Germany). PCR products were purified with GeneJET PCR Purification Kit and plasmids were purified with GeneJET Plasmid Miniprep Kit (Thermo Fisher Scientific). DNA concentrations were measured with BioDrop Duo spectrophotometer at 280 nm (BioDrop, Cambridge, UK). Genomic yeast DNA was extracted by physical means with the “smash and grab” method

using glass beads as previously described (Hoffman and Winston, 1987). Restriction enzymes and T4 DNA ligase (5 U μL^{-1}) were purchased from Thermo Fisher Scientific. Digestions and DNA amplifications were verified with gel electrophoresis using 0.8 % (w/v) agarose. DNA extractions from agarose gels were made with GeneJET Gel Extraction Kit (Thermo Fisher Scientific).

Table 2. *S. cerevisiae* strains used in the present study.

Strain	Biosensor promoter	Relevant genotype	Reference
TMB3752	<i>HXT1p</i>	TMB3700 (<i>SPB1/PBN1::Gal2mut</i> ; <i>VAC17/MRC1::TKL-TAL</i> ; <i>Chr X-2/XI-5/XII-4::XR-XDH-XK</i>) <i>can1::HXT1p-GFP</i> ; pCfB2312	Osiro et al. (2018)
TMB3755	<i>SUC2p</i>	TMB3700 (<i>SPB1/PBN1::Gal2mut</i> ; <i>VAC17/MRC1::TKL-TAL</i> ; <i>Chr X-2/XI-5/XII-4::XR-XDH-XK</i>) <i>can1::SUC2p-GFP</i> ; pCfB2312	Osiro et al. (2018)
TMB3757	<i>TPS1p</i>	TMB3700 (<i>SPB1/PBN1::Gal2mut</i> ; <i>VAC17/MRC1::TKL-TAL</i> ; <i>Chr X-2/XI-5/XII-4::XR-XDH-XK</i>) <i>can1::TPS1p-GFP</i> ; pCfB2312	Osiro et al. (2018)
TMB3902	<i>HXT1p</i>	TMB3752; <i>PGI1::AbA^R</i>	This study
TMB3905	<i>SUC2p</i>	TMB3755; <i>PGI1::AbA^R</i>	This study
TMB3907	<i>TPS1p</i>	TMB3757; <i>PGI1::AbA^R</i>	This study

Competent *E. coli* cells were prepared and transformed with the method described by Inoue and colleagues (1990). Competent *S. cerevisiae* cells were prepared and transformed with the lithium acetate method described by Gietz and Schiestl (2007), with an addition of 10 % (v/v)

DMSO prior to the heat shock (Hill et al., 1991). Transformations and gene integration sites were verified using diagnostic colony PCR.

Vector construction

Two sequences corresponding to 500 bp upstream and 500 bp downstream of *PGII* were amplified from genomic yeast DNA isolated from strain TMB3752, using primers 1-4 (Suppl. Table S1). The two fragments were ligated at the *NheI* site introduced by the forward primer of flank 1 and the reverse primer of flank 2, producing fragment F12 that was subsequently PCR amplified and inserted into the backbone vector pUG62AUR using restriction enzymes *AvrII/SaII*, producing the pUG62AUR-F12-PGI1 plasmid.

Construction of *PGII* deletants

PGII deletants were constructed by replacing the endogenous *PGII* gene with the linearized plasmid containing the AbA resistance marker gene (AbA^R) through homologous recombination by transforming *NheI* linearized pUG62AUR-F12-*PGII* into strains TMB3752, TMB3755 and TMB3757. After transformation, the strains were incubated in liquid YPFG medium for two hours before selective plating. Transformants were selected on YPFG agar plates containing AbA and G418. Colonies were re-streaked on solid media with YPFG and YP supplemented with 20 g L⁻¹ D-glucose (YPD). Colonies that were able to grow on YPFG but not on YPD were selected and used in colony PCR to verify the *PGII* deletion using primers 5 and 6 (Suppl. Table S1).

Enzymatic assays

Single colonies were grown in 5 mL YPFG medium in 50 mL conical tubes overnight. Cells were then washed, resuspended and incubated in YPD for two hours before harvesting and protein extraction using Y-PER (Thermo Fisher Scientific, Waltham, MA, USA)

according to the supplier's instructions. Total protein concentrations were determined using the Coomassie (Bradford) Protein Assay Kit (Thermo Fisher Scientific) microplate procedure according to the supplier's instructions, using bovine serum albumin as standard. Phosphoglucose isomerase activity was determined in technical and biological duplicates, using the method of Maitra and Lobo (1971).

Shake flasks cultures

Single colonies were inoculated into 5 mL YPFG in 50 mL conical tubes and incubated in 30°C and 180 rpm overnight. Pre-cultures were then used to inoculate 25 mL YPFG in 250 mL baffled shake flasks to an OD_{620nm} of approximately 0.1. Cultures were carried out in biological duplicates, 30 °C and 180 rpm. Optical density at 620 nm was followed using the Ultrospec 2100 pro spectrophotometer (Amersham Biosciences, Chicago, IL, USA).

Microtiter plate cultures

Pre-cultures were prepared by inoculation of single colonies into 5 mL YPFG medium in 50 mL conical tubes and incubation in 30 °C and 180 rpm overnight, after which they were used to inoculate 96-well microtiter plates to an OD_{620nm} of approximately 0.1 in YNB medium supplemented with various carbon sources. OD_{620nm} was measured with an automated spectrophotometer (Multiskan Ascent, Thermo Electron Corporation, Waltham, MA, USA) every 10 minutes for 64 hours. Growth was evaluated in biological duplicates. To confirm that an increase in absorbance was a result of growth and not the microtiter plate drying out or an artefact of the instrumentation, all wells were manually checked for cell pellets at the end of the cultivations. Negative controls,

consisting of YNB supplemented with 20 g L⁻¹ D-fructose and 1 g L⁻¹ D-glucose (YNB-FG) inoculated with sterile water only were also to verify that no growth was obtained. Maximal growth rates (μ_{\max}) were calculated as the highest linear slope found when the natural logarithms of the optical densities were plotted against time whereas lag phase duration was determined as the time point where maximal growth rate was initiated.

Measurements of intracellular metabolites

Culture conditions

Single colonies were inoculated into 25 mL of YPFG in 250 mL shake flasks and incubated at 30 °C at 180 rpm until late exponential phase. Cells were then inoculated into 50 mL of YNB supplemented with 20 g L⁻¹ of either D-glucose or D-xylose in 500 mL shake flasks at an initial OD_{620nm} of 0.5. Cultures were incubated at 30 °C and 180 rpm for 30 min before sampling for metabolites.

Sample preparation

Quenching of metabolism and sampling for sugar metabolite profiling were performed as described by (Bergdahl et al., 2012). Briefly, 10 mL cell culture was added to 40 mL -40 °C methanol (60 % in water). Samples were incubated for 5 min at -40 °C before centrifugation at -9 °C and 3220*g for 5 min. The supernatant was discarded and the cell pellet stored at -80 °C.

Intracellular metabolites were extracted using either the boiling ethanol method (Gonzalez et al., 1997) or mechanical disruption in methanol (Pluskal et al., 2010). Buffered ethanol (75 % in water, 70 mM HEPES, pH 7.4) at 80 °C were used to resuspend the cell pellet and the suspension was boiled for 3 min. cell

debris was precipitated by incubation on ice for 2 h followed by centrifugation at 21,130*g at 4 °C for 10 min.

For mechanical disruption, cells were resuspended in 80 % methanol (in water) and bead beaten with the Precellys 24 homogenizer (Bertin Instruments, Montigny-le-Bretonneux, France) using the Precellys lysing kit with the following program: 3 cycles of 30 s of agitation at 6,500 rpm with 30 s rest in between. The Cryolys cooling unit (Bertin Instruments, Montigny-le-Bretonneux, France) was used with liquid nitrogen to cool the samples during bead beating. Cell debris and beads were removed by centrifugation at 21,130*g and 4 °C for 5 min.

Prior to metabolite extraction, all samples were centrifuged (4 °C, 14000 rpm, 10 min). From each sample 150 μ L was placed into 1.5 mL Eppendorf tubes and 50 μ L of chloroform added to yield a chloroform/alcohol ratio of 3/7. Subsequently, samples were vortexed for 5 s and left in the cold (-20 °C) for 2 h. Then, 10 μ L of 20 μ g mL⁻¹ 2-deoxyglucose 6-phosphate (internal standard, IS) was added and samples extracted twice with ice-cold water (2 x 200 μ L). The aqueous layers were pooled and evaporated to dryness in modular concentrator miVac (Genevac Ltd., Ipswich, United Kingdom).

The derivatization consisted of two steps. First, 20 μ L of methoxy-amination reagent (MOX; Thermo Fisher Scientific) was added to the dried samples, and the sample was mixed by vortexing and left at room temperature overnight. Then, 6 μ L of 1-methylimidazol and 12 μ L of propionic acid anhydride were added and the sample was again mixed by vortexing. Finally, the derivatization reaction was allowed to continue for 30 min at 37 °C, after which the samples were evaporated

to dryness under a flow of nitrogen gas (Pierce Reacti-Vap III; Thermo Fisher Scientific, Minneapolis, MN). Prior to LC/MS analysis, 100 μ L of water containing 0.1% HCOOH was added to the samples.

LC/MS analysis

Sugar phosphates were analyzed on an Agilent 1290 Infinity UHPLC system coupled with an Agilent 6495 QqQ-MS (Agilent Technologies, Santa Clara, CA) operated in dynamic multiple-reaction-monitoring (MRM) mode, as previously described in detail (Rende et al., 2019). Briefly, chromatographic separation was performed on a Waters Acquity HSS-T3 1.8 μ m, 2.1 \times 50 mm column (Waters Corporation, Milford, MA). Mobile phase A was composed of water and mobile phase B of MeOH, both containing 2 % of HCOOH. The gradient was: 5 % B for 1 min, then linear gradients from 5 to 30 % B from 1 to 3 min, then 30 to 40 % B from 3 to 6 min, hold at 40 % B from 6 to 10 min, then 40 to 70 % B from 10 to 12.5 min, hold at 70 % B from 12.5 to 15 min, and then 70 to 99 % B from 15 to 17 min hold at 99 % B for 0.5 min, then the column was re-equilibrated to 5 % B in 0.5 min and to 0.1 % B in 2 min. The flow rate was 0.5 mL min⁻¹, the column temperature 40 °C, and the injection volume 1 μ L. The mass spectrometer was operated in negative electrospray ionization (ESI) mode with a gas temperature of 150 °C, a gas flow of 16.1 L min⁻¹, a nebulizer pressure of 20 psi, a sheath gas temperature of 350 °C and flow-rate of 11 L min⁻¹, a capillary voltage of 3000 V, a nozzle voltage of 1000 V, an iFunnel high pressure RF of 80 V, an iFunnel low pressure RF of 40 V, a fragmentor voltage of 380 V, and a cell acceleration voltage of 5 V. MRM transitions are given in Suppl. Table S3.

Data processing and statistical analysis

Data were processed using MassHunter Qualitative Analysis and Quantitative Analysis software (Agilent Technologies, Santa Clara, CA). Pentose phosphates were partially co-eluting and therefore integrated as a sum, except for one of the ribose-5-phosphate tautomers which was clearly resolved from the others. The second, most intense, of the two tautomers for glucose 6-phosphate was integrated. UDP-glucose and UDP-galactose co-eluted and are reported as a single signal. Statistical analysis was performed in R (version 3.6.0.). Method relative standard deviation (RSD) was determined from eight independently extracted and derivatized samples analyzed in triplicate over 16 h and instrument RSD from analysis of a single sample, which was analyzed after every 8 samples over 16 h, 5 times in total. Peak areas were normalized to the area of the IS and log2-transformed to conform to normality. Principal component analysis (PCA) was conducted using prcomp (*factoextra*). Fold changes and significance levels for volcano plots were derived from linear models (lm, *car*) and anova (Anova, *car*), and graphs were produced using ggplot (*ggplot2*).

Fluorescence measurements

Fluorescence intensity (FI) was analysed at the single-cell level using a BD Accuri C6 flow cytometer connected to a BD CSampler autosampler (Becton-Dickinson, NJ, US) with detection at 488 nm and 533/30 bandpass filter (FL1-H channel).

For fluorescence intensities associated with metabolite measurements, samples were taken from shake flasks at time point 0 h and 6 h.

For measurements in microtiter plates, pre-cultivation was performed from a single colony inoculation into a 50 mL conical tube containing 5 mL of YPFG medium and that was incubated overnight at 30 °C and 180 rpm. The pre-culture was used to inoculate a microtiter plate or shake flask containing YNB supplemented with various carbon sources

with an initial OD_{620nm} of 0.5 and incubation was performed at 30 °C, 800 rpm, for 6 h.

Per sample, 10 000 events were collected with a threshold of 800 for the FL1-H channel. FlowJo v10 software (Treestar, Inc., San Carlos, CA, USA) was used to analyse the data from biological replicates.

Results and Discussion

Construction and validation of the *PGII* deletants

In order to manipulate the intracellular level of glycolytic intermediates, and G6P in particular, *PGII* gene was deleted in recombinant xylose-fermenting strains carrying either the *HXT1p-GFP* biosensor (TMB3752), the *SUC2p-GFP* biosensor (TMB3755) or the *TPS1p-GFP* (TMB3757) biosensor, reporting for the Snf3p/Rgt2p, the SNF1/Mig1p and the cAMP/PKA sugar signaling pathways, respectively. *PGII* was deleted through homologous recombination using flanks of 500 base pairs upstream and downstream of the *PGII* open reading frame (ORF). The structural gene was replaced with *AbA^R*, a gene variant of the native *AUR1* (YKL004W), conferring resistance to aureobasidin A, and transformants were selected on a medium containing the antibiotic. *PGII* deletion was confirmed by diagnostic PCR (Suppl. 1) and enzymatic activity measurements (Fig. 2). The specific activity of the background strains was approximately 0.04-0.09 $\mu\text{mol min}^{-1} \text{mg}^{-1}$ whereas the specific activity of the *PGII*-deleted strains was below 0.003 $\mu\text{mol min}^{-1} \text{mg}^{-1}$ (Fig. 2). This indicated that the deletion of *PGII* was successful, but it also confirmed that there was no other enzyme

catalyzing the interconversion between G6P and F6P.

S. cerevisiae strains with inactive Pgilp have been reported to lose their ability to grow on single monomeric sugars such as D-glucose and D-fructose (Ciriacy and Breitenbach, 1979; Aguilera and Zimmermann, 1986). Abolishment of growth on D-glucose has been attributed to the inability to channel carbon into the lower glycolysis for energy and precursor production, because the flux through the PPP was considered too low (Aguilera and Zimmermann, 1986; Aguilera, 1987). Using D-fructose as sole carbon source would theoretically result in production of ATP, through substrate-level and oxidative phosphorylation, as well as of many biomass precursors via lower glycolysis and the tricarboxylic acid (TCA). However, G6P that is needed, among others, in the formation of cell wall phospholipids, glycoproteins and glucans (Willey et al., 2017), can only be generated by gluconeogenesis because of the irreversible decarboxylation of 6-phosphogluconate in the PPP (Fig. 1). This explains why *PGII* deletants did not grow on D-fructose as a sole carbon source but did grow on D-fructose supplemented with a small amount (1 g L⁻¹) of D-glucose (Aguilera, 1986).

In the present study, growth abolishment of *PGII* deletants on D-glucose was confirmed on solid media using YP supplemented with 20 g L⁻¹ D-glucose (YPD) (Suppl. 1). In parallel, *PGII* deletants were shown to grow on 20 g L⁻¹

D-fructose supplemented with 1 g L⁻¹ D-glucose medium (YPFG) as in previous studies using other strain backgrounds (Aguilera, 1986) (Suppl. 1). YPFG medium was further used for strain maintenance and all pre-cultures.

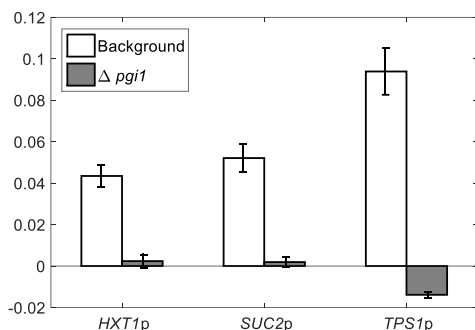


Figure 2. *PGI1* deletion confirmation in the biosensor strains. Pgi1p specific activity in the background strains (white) and the *PGI1* deletants (grey). For the enzyme assay cultures were incubated with 20 g L⁻¹ glucose for 2h before harvesting, to ensure full expression of any available gene.

Growth of *PGII* deletants in shake flasks

Aerobic shake flask cultures were performed on two of the constructed biosensors and their respective deletant strains in YPFG medium. The *PGII* deletants exhibited a clear growth delay compared to the background strains (Fig. 3): whereas the background strains

displayed a lag phase of three to five hours before entering exponential growth, the *PGII* deletants had corresponding lag phases that lasted for around 18h. Also, the deletants showed 50% reduced maximum specific growth rates as compared to the background strains (0.22-0.25 vs. 0.44-0.45 h⁻¹, respectively).

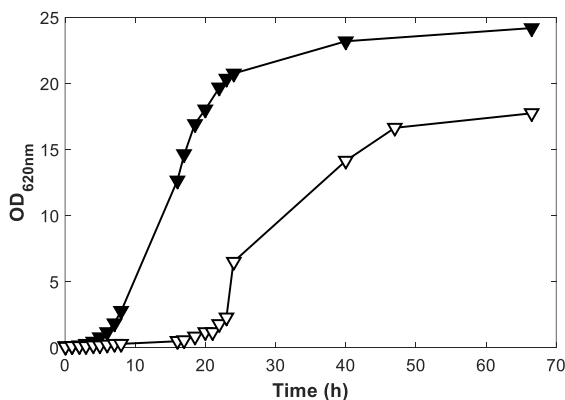


Figure 3. Representative growth curves (OD_{620nm}) of *PGII*-deficient strain (open symbols) and background strain (closed symbols) in shake flasks with YP medium with 20 g L⁻¹ D-fructose and 1 g L⁻¹ D-glucose. Curves are shown for the *HXT1p-GFP* biosensor strains, and similar patterns were exhibited for the *SUC2p-GFP* and *TPS1p-GFP* biosensor strains as well.

There was no discernible difference in growth pattern between strains carrying the *HXT1p-GFP* biosensor and those carrying the *SUC2p-GFP* or *TPS1p-GFP* biosensor, neither in the background nor in the *pgi1Δ* phenotype. This confirmed that the chosen biosensor system was non-invasive.

Microtiter plate screening indicates extended lag phase for *PGII* deletion on several carbon sources

In order to screen the growth response of the *PGII* deletants to a larger number of carbon source combinations, including D-xylose, micro-scale cultivations were carried out in 96-well microplates. The tested carbon sources were 20 g L⁻¹ D-fructose, 20 g L⁻¹ D-fructose with 1 g L⁻¹ D-glucose, 20 g L⁻¹ D-galactose, 50 g L⁻¹ D-xylose, and 50 g L⁻¹ D-xylose with 1 g L⁻¹ D-glucose (Fig. 4).

Although this set-up has limitations (for example incomplete aeration, evaporation, non-linear behavior for

OD_{620nm} values above 1), repeatable data concerning lag phases and the first stages of growth were obtained.

The longer lag phase exhibited by the *PGII* deletants on YPFG in aerobic shake flasks was also observed in the microscale cultures on YNB-FG, although with larger variations (Fig. 4A). In the background strains, exponential growth on single fermentable sugars (D-fructose, D-glucose and D-galactose) started almost immediately, as expected (Fig. 4B-D; Tables 3-4). The lag phases were slightly longer on D-galactose (13 h) than on D-glucose and D-fructose where exponential growth was recorded after 8.3 h. The highest maximum specific growth rate (μ_{\max} of 0.52 h⁻¹) was recorded on D-glucose while a lower μ_{\max} of 0.28 h⁻¹ was achieved on D-fructose and on D-galactose. Growth was also recorded on D-xylose for the background strains, (engineered with the XR/XDH pathway), albeit with a substantial lag phase (22.7 h) and a linear growth pattern (Fig. 4E).

Table 3. Lag phase duration (hours), as determined by the start of maximal growth rate, for the tested biosensors. Unless otherwise stated, averages and standard deviations stem from four replicates, two from each of the *HXT1p* and *SUC2p* biosensors.

	Frc20 + Glc1	Frc20	Glc20	Gal20	Xyl20	Xyl20 + Glc1
Back-ground	4.3 ±2.9	8.3 ±0.8	8.3 ±1.1	13.0 ±1.4	22.7 ±1.1	21.9 ±0.5
<i>pgi1Δ</i>	14.1 ±4.9	37.7 ±4.3	31.3 ±1.9 *	39.7 ±3.5 **	n.d.	> 60 h **

Frc20: 20 g L⁻¹ D-fructose, Glc1: 1 g L⁻¹ D-glucose, Glc20: 20 g L⁻¹ D-glucose, Gal20: 20 g L⁻¹ D-galactose, Xyl20: 20 g L⁻¹ D-xylose, n.d.: Not determined.

* measured on the 3 out of 4 replicates that grew

** measured on the 2 out of 4 replicates that grew

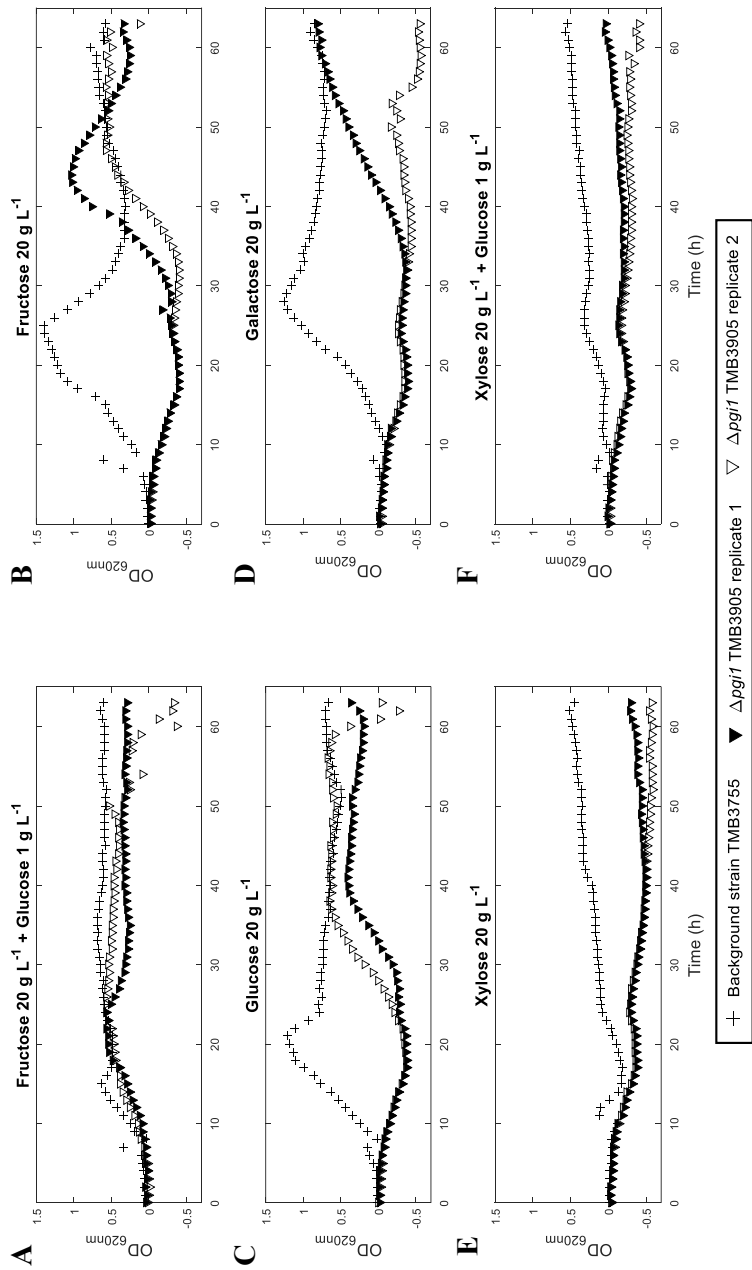


Figure 4. Growth curves from microscale cultivations. Carbon sources: 20 g L⁻¹ D-fructose with 1 g L⁻¹ D-glucose (A), 20 g L⁻¹ D-fructose (B), 20 g L⁻¹ D-glucose (C), 20 g L⁻¹ D-galactose (D), 50 g L⁻¹ D-xylose (E), 50 g L⁻¹ D-xylose with 1 g L⁻¹ D-glucose (F). Two replicates for the deletion strain (TMB3905, open and closed triangles) and one replicate for the background strain (TMB3755, plusses) are shown for the *SUC2p* biosensor. In each case, growth was also confirmed by cell pellet formation in the corresponding well.

Table 4. Maximal growth rate (h^{-1}) achieved for microscale cultivations, for the tested biosensors. Unless otherwise stated, averages and standard deviations stem from four replicates, two from each of the *HXT1p* and *SUC2p* biosensors.

	Frc20 + Glc1	Frc20	Glc20	Gal20	Xyl20	Xyl20 +Glc1
Back-ground	0.30 ± 0.09	0.29 ± 0.05	0.52 ± 0.13	0.28 ± 0.06	0.65 ± 0.46	0.32 ± 0.13
<i>pgi1</i>Δ	0.39 ± 0.09	0.66 ± 0.31	1.48 ± 0.78 *	0.69 ± 0.08 **	n.d.	n.d.

Frc20: 20 g L⁻¹ D-fructose, Glc1: 1 g L⁻¹ D-glucose, Glc20: 20 g L⁻¹ D-glucose, Gal20: 20 g L⁻¹ D-galactose, Xyl20: 20 g L⁻¹ D-xylose, n.d.: Not determined.

* measured on the 3 out of 4 replicates that grew

** measured on the 2 out of 4 replicates that grew

Surprisingly and in contrast to previous reports, the *PGII* deletants were able to grow on the single sugars D-glucose, D-galactose and D-fructose, albeit with significantly prolonged lag phases. Additionally, an increased heterogeneity between biological replicates, both in terms of lag phase duration and maximal growth rates was observed (Fig. 4B-E; Tables 3-4). Also, not all biological replicates would initiate growth, which is a trait that was not observed with the background strains. A possible explanation for this growth lies in the genetic makeup of the background strains: the strains have been engineered to ferment D-xylose, by introduction of heterologous XR and XDH genes, overexpression of a more xylose-selective mutated Gal2p transporter (Farwick et al., 2014), and by overexpression of the PPP genes *TKL1* and *TAL1* (Karhumaa et al., 2005). The latter modifications are of importance since PPP is thought to be the limiting factor for growth on D-glucose in wild-type strains deleted for *PGII* (Aguilera, 1986).

In fact, a doubling of the activities of 6-phosphogluconate de-hydrogenase (GND), ribulose-5-phosphate 3-epimerase (RPE) and transaldolase (TAL) (Fig. 1) has been shown to be one of the

mechanisms used in suppressor mutants of *pgi1* Δ strains (Dickinson et al., 1995). Also, *pgi1* Δ mutants of the yeast *Kluyveromyces lactis* were able to grow on D-glucose only, but lost this ability upon additional disruptions in the PPP (Goffrini et al., 1991).

However, upregulation of PPP genes cannot explain growth on D-fructose in the xylose-engineered strains of the present study, since G6P cannot be generated under these conditions. In a previous study it was shown that during early exponential growth on YPFG media, *pgi1* Δ mutants accumulated G6P, UDP-glucose and the storage carbon glycogen (Corominas et al., 1992). Since the pre-cultures of the present study all consist of YPFG, it is possible that the cells being inoculated into D-fructose medium had sufficient storage of glycogen to be broken down into D-glucose and provide enough G6P precursors to support growth on D-fructose. The growth phase of the pre-culture may be crucial as glycogen was shown to decrease fourfold between early and late exponential phase (Corominas et al., 1992), which might be an explanation, together with the benefit of the upregulated PPP, to why other studies also employing YPFG as pre-

culture did not observe growth on D-fructose for their *pgi1Δ*-strains.

D-Galactose enters the yeast central metabolism at the level of G6P through isomerization, phosphorylation, UDP-transfer and phosphate transfer (Fig. 1). This assimilation requires UDP-glucose which, as mentioned above, has been shown to accumulate in *pgi1Δ* mutants pre-grown on YPFG. In conjunction with higher PPP, this may also explain the growth observed on sole D-galactose in the *PGII* deletants.

In the cultivations containing D-xylose as a single carbon source, no growth was recorded for the *PGII* deletants (Fig. 4E), whereas the addition of D-glucose at 1 g L⁻¹ enabled some growth in about half of the replicates, but with a lag phase over 60 h (Fig. 4F). D-Xylose is expected to enter glycolysis at the F6P and G3P nodes (Fig. 1), implying *PGII* deletants could theoretically grow on D-xylose through the same mechanisms as on D-fructose. However, lower carbon flux on D-xylose and limited glycogen production might exceed the maintenance needs and prevent growth.

Metabolomics

To further study the phenotype of the *PGII* deletants assimilating various carbon sources, the abundance of intracellular sugar phosphates was determined in the background and deletion strains TMB3757 and TMB3907, respectively, carrying the TPS1p-GFP biosensor. Cells were incubated with

either D-glucose or D-xylose for 30 min prior to quenching and extraction of intracellular metabolites. Two different extraction methods— boiling ethanol and mechanical disruption in methanol – were employed to reduce potential biases in the data.

Intracellular extracts were then analyzed using LC/MS/MS (Rende et al., 2019). The repeatability of the instrumental analysis was on average 13.5 % for the detected sugar phosphates whereas the repeatability for the entire method, including extraction and derivatization was 21.0 % (Suppl. Table S1).

First, a PCA was performed to generate an overview of the metabolic alterations associated with the *PGII* deletion and the sugar source. This analysis revealed systematic changes in intracellular sugar phosphate patterns in the two strains on the two sugar sources. The first principal component (Dim1), explaining 35.2 % of the variation in the data, clearly distinguished between the culture conditions (D-glucose vs. D-xylose) in the deletion strain (Fig. 5A). The second component (Dim2; 25.3 %), separated the background and the deletion strain while the third component (Dim3; 20.5 %) distinguished between D-glucose and D-xylose for the background strain (Fig. 5B). Overall, 81.0 % of the variation in the data was mapped in the first three components of the PCA, showing that both strain and culture condition yielded systematic alterations in the levels of sugar phosphates.

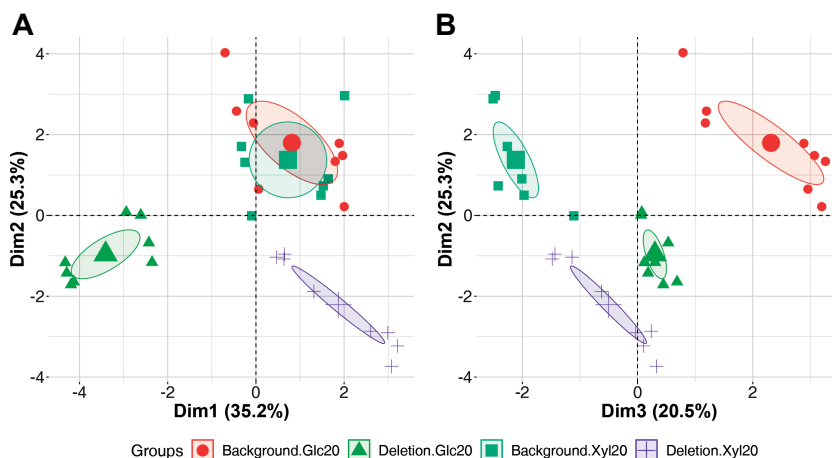


Figure 5. Loading plot of principal component analysis of intracellular metabolite data. A: First (Dim1) and second (Dim2) principal components, explaining 60.5 % of variance; B: Third (Dim3) and second (Dim2) principal components, explaining 45.8 % of variance. Data points are categorized by strain and condition: Background strain on D-glucose (orange dots), deletion strain on D-glucose (green triangles), background strain on D-xylose (blue squares) and deletion strain on D-xylose (purple plusses).

Next, intracellular metabolites were investigated in a univariate fashion. The *pgi1Δ* strain displayed the expected hyper-accumulation of G6P, as well as of intermediates formed from G6P through glycogen and trehalose synthesis (trehalose 6-P; T6P, UDP-glucose /galactose; UDP-G, glucose 1-P; G1P, galactose 1-P; Gal1P) or via the PPP (seduheptulose 7-P; S7P and erythrose 4-P; E4P), compared to the background strain under the same condition (Fig. 6A). In contrast, the deletion strain was depleted for metabolites downstream of the phosphoglucose isomerase reaction in glycolysis, which could be expected as a direct consequence of the *PGI1* deletion: fructose 1,6-biphosphate, F1,6bP; dihydroxyacetone phosphate, DHAP; glyceraldehyde 3-phosphate, G3P and fructose 6-phosphate, F6P (Fig. 6A). Depletion was also observed for 6-phosphogluconate (6PG), an intermediate of the oxidative PPP whose regeneration is dependent on gluconeogenesis to G6P,

which does not happen in the deletion strain.

In the background (TMB3757) and deletion (TMB3907) strains, D-xylose is converted via the XR/XDH pathway, followed by the non-oxidative PPP and carbon enters lower glycolysis at the F6P and G3P nodes (Fig. 1). As *Pgi1p* is not directly part of the D-xylose assimilation pathway, the deletion of *PGI* was not expected to substantially alter the intracellular metabolite concentrations between the two strains within only 30 min of incubation with this sugar. However, the LC/MS data showed significant accumulation of nearly all assayed metabolites in the deletion strain (Fig. 6B). The most pronounced accumulation was observed for the metabolites within lower glycolysis (F1,6bP; G3P; 3-phosphoglycerate, 3PG; DHAP and F6P) as well as Gal1P, but also PPP intermediates (S7P; pentose 5-P; E4P and ribose 5-P, R5P) and metabolites

involved in glycogen and trehalose synthesis (G1P and G6P). Accumulation of PPP and lower glycolytic intermediates implied a limitation in the D-xylose assimilation pathway in the deletion strain, in conjunction with its impaired growth compared to the background strain. The increased concentrations within glycogen and trehalose

metabolism, on the other hand, can be explained by accumulation from D-glucose during the preculture, as reported previously (Corominas et al., 1992) and also observed in the deletion strain on D-glucose (Fig. 6A). None of the assayed metabolites were found in excess in the background strain on D-xylose.

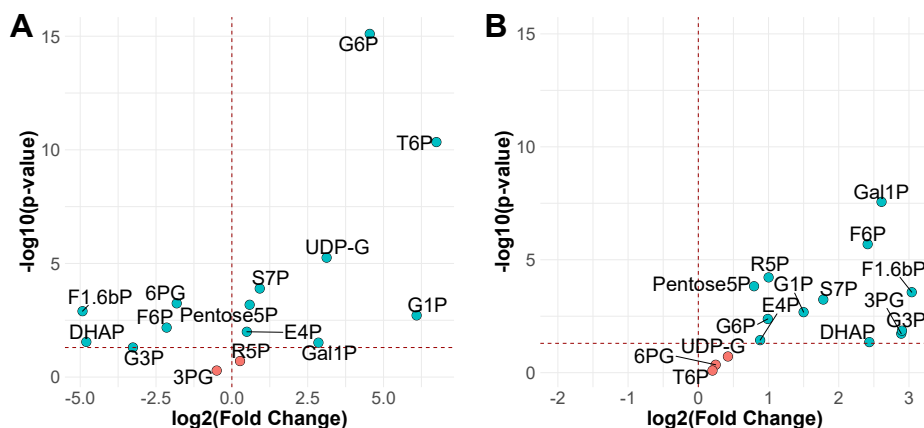


Figure 6. Volcano plots showing $-\log_{10}$ p-values (Y-axis) and \log_2 fold-change (X-axis) for the differences in metabolite abundance between background and *PGII* deletion strains. Positive values on the x-axis (\log_2 fold-change) implies higher abundance in the deletion strain; negative values indicate higher abundance in the background strain. A: Incubated on D-glucose; B: Incubated on D-xylose (B). Significant ($p < 0.05$) alterations are colored blue and insignificantly ($p > 0.05$) altered metabolites red.

Correlation between sugar phosphate abundance and sugar signaling response

The biosensor response of the background and the *PGII* deletion strains was recorded during incubation on D-glucose or D-xylose and fluorescence intensities (FIs) were plotted against the changes in intracellular levels of sugar phosphate obtained above in order to identify putative correlations (Fig. 7). For some metabolites, the *pgi1Δ* strain consuming D-glucose produced intracellular abundances around 30-70 times higher than any other strain and condition combination. These hyper-accumulated

metabolites included G6P, G1P and T6P, and were sometimes omitted in graphs to increase clarity. Uncropped graphs can be found in the Supplementary material (Fig. S2). As expected, the biosensor profile of G6P was found to be very similar to that of external D-glucose (Brink et al., 2016) (Fig. 7A), with increasing expression of *HXT1* and spikes of *SUC2* and *TPS1* expression that rapidly declined with the increase of G6P abundance (Fig. 7B-C). Similar profiles were also found for G1P, T6P, UDP-G and 6PG (Suppl. Fig. S1). This indicates a significant importance of the G6P node for the sugar signaling response, regardless of whether D-glucose or D-xylose is used.

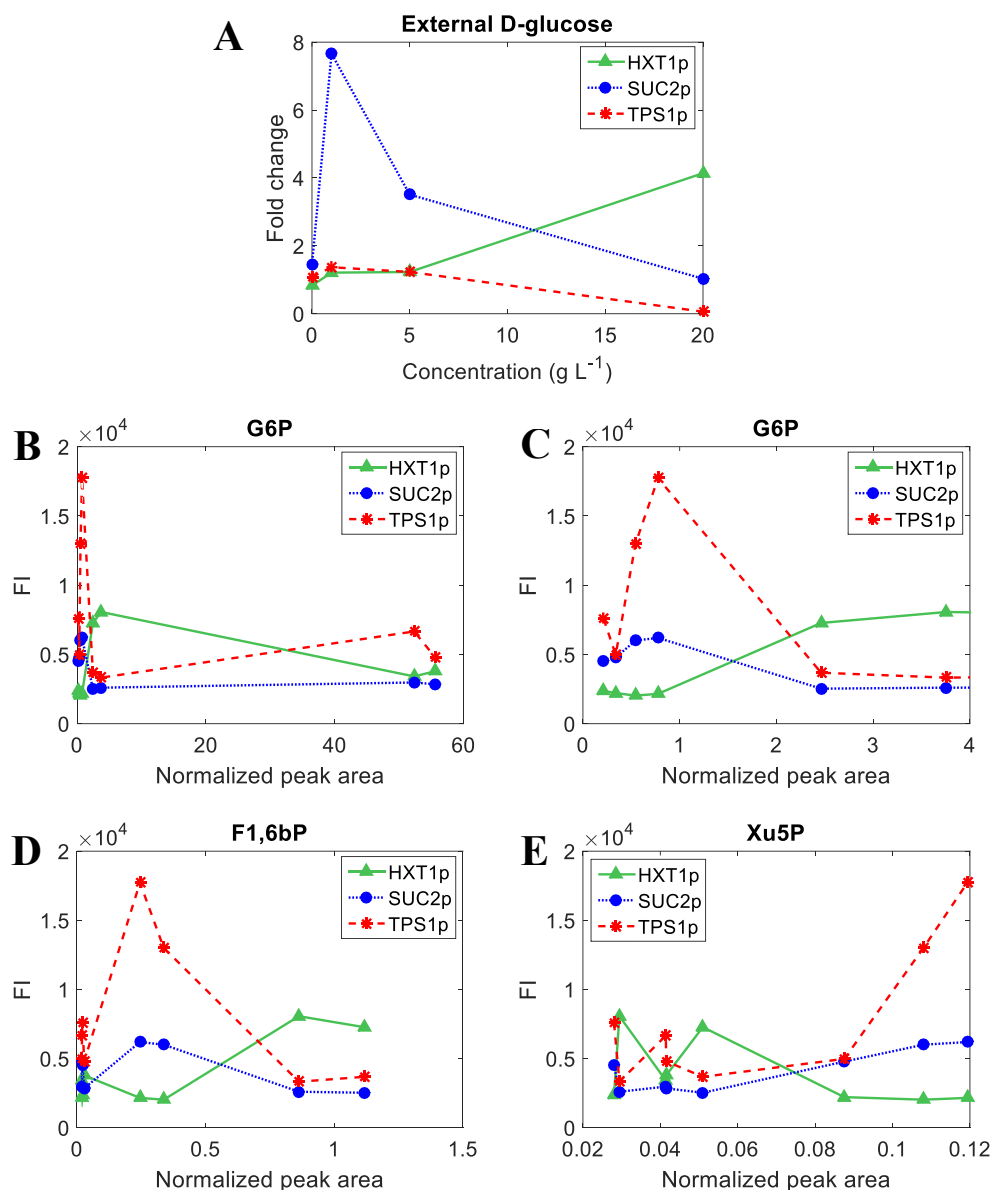


Figure 7. Fluorescence intensity (FI) as a function of the corresponding metabolite abundances, obtained from the background and deletion strains grown on D-glucose or D-xylose. The biosensor for *HXT1p* (triangles, green solid line) reports on the Rgt2p/Snf3p pathway, *SUC2p* (circles, blue dotted lines) the SNF1/Mig1p pathway and *TPS1p* (crosses, red dashed lines) the cAMP/PKA pathway. A: Extracellular D-glucose (adapted from Brink et al., 2016); B: Intracellular glucose-6-phosphate; C: Intracellular glucose-6-phosphate zoomed in at abundances lower than 4; D: Intracellular fructose-1,6-bisphosphate; and E: Intracellular xylulose-5-phosphate.

F1,6bP has previously been implicated in the regulation of the cAMP/PKA signaling pathway (Peeters et al., 2017), which affects the expression of genes such as *TPS1*. However, here the abundance of F1,6bP could also be correlated to the signaling response of *HXT1* (Rgt2p/Snf3p pathway) and *SUC2* (SNF1/Mig1p pathway) (Fig. 7D).

Other intracellular metabolites displayed a complex pattern of biosensor expression at low abundances but they clearly showed a signaling state similar to the response to a low D-glucose concentration: high expression of *SUC2p* and *TPS1p* coupled with repression of *HXT1p*; these metabolites included intermediates of the non-oxidative PPP: xylulose 5-P (Xu5P; Fig. 7D), E4P, S7P and F6P, as well as Gal1P (Suppl. Fig. S1). As D-xylose assimilation requires flux through the PPP, elevated concentrations of its intermediates could, at least partially, explain the low D-glucose signal recorded during growth on D-xylose.

Effect of *PGII* deletion on sugar sensing

The yeast sugar signaling response was further explored by recording the biosensor response in background and *pgi1Δ* strains on several sugars. For this, two biosensors were selected: *HXT1p*, whose expression increases with extracellular D-glucose concentration, and *SUC2p*, where the expression peaks at low D-glucose levels and decreases at higher D-glucose concentrations (Fig. 7A). Although the intracellular metabolite abundances are not known for all the tested sugars, some general conclusions could be made.

The background and deletion strains were incubated in the sugar concentrations previously evaluated for growth (20 g L⁻¹)

except for D-xylose, where 50 g L⁻¹ was used to be comparable to earlier sensing studies (Osiro et al., 2019; Brink et al., 2016; Osiro et al., 2018). Since D-xylose has previously been observed to elicit signals resembling those on low levels of D-glucose (Osiro et al., 2018), D-glucose and D-galactose concentrations of 1 g L⁻¹ were also included in the study. Cells were incubated for 6 h, as in earlier studies, which prevented growth in any of the strain or conditions (cf. Table 3).

Average FIs are shown as a heat map in Table 5 and in Suppl. Fig. S2. Subpopulations were observed in some histograms, however only in the background strains and only when cells were incubated on D-glucose and on high D-fructose media (Suppl. Fig. S2). Therefore, they were not considered for the overall interpretation.

The *HXT1p* biosensor

In the background strain, the *HXT1p* sensor did not respond to carbon starvation, whereas a slight upregulation was observed at low levels of D-glucose, high levels of D-galactose and D-xylose, and combinations thereof. The only conditions to clearly induce *HXT1p* were high levels of D-glucose or D-fructose. This is consistent with the Rgt2p and Snf3p sensors only responding to repressive sugars and their extracellular level (Dietvorst et al., 2010). On D-xylose, D-galactose or a combination thereof only a slight decrease in FI was observed in the *PGII* deletion strain, with a fold change around 0.9. However, on D-glucose and D-fructose, the change was more dramatic. On 1 g L⁻¹ of D-glucose, with or without addition of D-xylose, the expression of *HXT1p* doubled in the deletion strain, possibly due to

accumulation of G6P. At higher glucose levels (20 g L⁻¹), however, or on D-fructose, FI levels were half of those observed in the deletion strain. In the D-glucose condition, the abundances of G6P, G1P and T6P were around 30-70 times higher in the *PGII* deletant than in the background strain. These abundances

might be beyond what the cell would deem physiologically possible, which could result in a shutdown of the metabolism, with low/no induction. Analogous reasoning could be used to explain the D-fructose case, with expected but unconfirmed accumulation of, for instance, F6P, F1,6bP, G3P and DHAP.

Table 5. Heat map of *HXT1p* and *SUC2p* fluorescence responses after 6h incubation in different media for the background (BG) strains and for the *PGI1* deletants. Fluorescence at time 0 (similar for all media) is also displayed. Fold changes are the ratio between average FI of the *PGI1* deletant and that of the corresponding background strain, for each incubation condition.

	BG <i>HXT1p</i>	<i>pgi1Δ</i> <i>HXT1p</i>	fold change	BG <i>SUC2p</i>	<i>pgi1Δ</i> <i>SUC2p</i>	fold change
0h D-fructose 20 g L ⁻¹ + D-glucose 1 g L ⁻¹	1701	2264	1.33	2516	3390	1.35
D-xylose 50 g L ⁻¹	2289	2091	0.91	4657	6100	1.31
D-glucose 1 g L ⁻¹	1922	3648	1.90	6447	6003	0.93
D-xylose 50 g L ⁻¹ + D-glucose 1 g L ⁻¹	2697	5479	2.03	8157	6685	0.82
D-galactose 1 g L ⁻¹	1859	1600	0.86	3750	4973	1.33
D-xylose 50 g L ⁻¹ + D-galactose 1 g L ⁻¹	2208	1975	0.89	4875	6955	1.43
D-glucose 20 g L ⁻¹	7669	3599	0.47	2564	2910	1.13
D-galactose 20 g L ⁻¹	2121	1718	0.81	4813	5781	1.20
D-fructose 20 g L ⁻¹	3174	1773	0.56	2578	3808	1.48
No carbon source	1008	1169	1.16	2178	4116	1.89

BG: Background strain

The *SUC2p* biosensor

In a *pgi1Δ* strain, reduced sensitivity to D-glucose repression was previously observed upon pulses of D-glucose, D-fructose or D-galactose (Sierkstra et al., 1993). These trends were also seen in the present study, as high levels of D-glucose,

D-fructose, D-galactose and D-xylose all caused higher *SUC2* expression in the deletion strain than in the background strain (Table 5). This pointed towards the *Pgi1p* reaction being of importance to D-glucose repression in yeast. *SUC2* is known to be induced by low

concentrations of D-glucose (Özcan et al., 1997). The induction was confirmed in the background strain, but it was not increased by the *PGII* deletion, indicating that the level of G6P may not be the primary mechanism for *SUC2* induction. In the deletant, the induction was increased on D-xylose or D-galactose, which could hint towards other key metabolites than G6P. Finally, *SUC2* induction was even reduced in a medium combining D-glucose and D-xylose, which may indicate opposite effects from different metabolic intermediates on sugar sensing.

Conclusions

The present study aimed to clarify the role of intracellular metabolite levels on sugar sensing in *S. cerevisiae* using metabolomics and biosensor strains carrying or not a deletion of the *PGII* gene.

Several metabolites gave a similar biosensor induction pattern as the one observed for external D-glucose (G6P, G1P, T6P, UDP-G and 6PG), for instance maximum expression at relatively low concentrations followed by repression at higher concentrations for *SUC2* and *TPS1* biosensors, and steady increase for *HXT1* biosensor. On the other side of the spectrum, high abundances of Xu5P, E4P, S7P, F6P, and Gal1P displayed a signaling state similar to that found on low D-glucose concentrations.

On D-glucose, *PGII* deletion led to the accumulation of intermediates upstream of the Pgilp reaction and depletion of sugar phosphates downstream of the reaction. On D-xylose, however, the deletion strain was found to accumulate almost all the identified sugar phosphates, probably due to an inefficient catabolism.

The signaling response on a variety of carbon sources confirmed the importance of glycolytic intermediates on sugar sensing.

Financial support

This work was supported by The Swedish Research Council (Vetenskapsrådet) under grant number 2016-05297_VR, the Swedish Energy Agency (grant number 2018-004378), and The Brazilian National Council for Scientific and Technological Development (Conselho Nacional de Desenvolvimento Científico e Tecnológico - CNPq) [scholarship awarded for KOO].

Acknowledgements

The authors would like to thank Dominika Miroszewska for her contribution to the first design of the *PGII* deletion, Dr. Magnus Carlquist for helpful discussion on the flow cytometry experiments and The authors are also grateful to Sofia Essén for the support in LC/MS analysis.

References

- Aguilera, A., 1986. Deletion of the phosphoglucose isomerase structural gene makes growth and sporulation glucose dependent in *Saccharomyces cerevisiae*. *Molecular and General Genetics* 204, 310-316.
- Aguilera, A., 1987. Mutations suppressing the effects of a deletion of the phosphoglucose isomerase gene *PGII* in *Saccharomyces cerevisiae*. *Current Genetics*. 11, 429-434.
- Aguilera, A., Zimmermann, F. K., 1986. Isolation and molecular analysis of the phosphoglucose isomerase structural gene of *Saccharomyces cerevisiae*. *Molecular and General Genetics*. 202, 83-89.
- Almeida, J. R. M., Modig, T., Petersson, A., Hahn-Hägerdal, B., Lidén, G., Gorwa-Grauslund, M. F., 2007. Increased tolerance and conversion of inhibitors in lignocellulosic hydrolysates by *Saccharomyces cerevisiae*. *J Chem Technol Biot*. 82, 340-349.
- Bergdahl, B., Heer, D., Sauer, U., Hahn-Hägerdal, B., van Niel, E. W., 2012. Dynamic metabolomics differentiates between carbon and energy starvation in recombinant *Saccharomyces cerevisiae* fermenting xylose. *Biotechnol Biofuels*. 5, 34.
- Bergdahl, B., Sandström, A. G., Borgström, C., Boonyawan, T., van Niel, E. W., Gorwa-Grauslund, M. F., 2013. Engineering yeast hexokinase 2 for improved tolerance toward xylose-induced inactivation. *PloS one*. 8.
- Brink, D. P., Borgström, C., Tueros, F. G., Gorwa-Grauslund, M. F., 2016. Real-time monitoring of the sugar sensing in *Saccharomyces cerevisiae* indicates endogenous mechanisms for xylose signaling. *Microbial Cell Factories*. 15, 183.
- Chu, B. C. H., Lee, H., 2007. Genetic improvement of *Saccharomyces cerevisiae* for xylose fermentation. *Biotechnology advances*. 25, 425-441.
- Ciriacy, M., Breitenbach, I., 1979. Physiological effects of seven different blocks in glycolysis in *Saccharomyces cerevisiae*. *Journal of Bacteriology*. 139, 152-160.
- Corominas, J., Clotet, J., Fernández-Bañares, I., Boles, E., Zimmerman, F. K., Guinovart, J. J., Ariño, J., 1992. Glycogen metabolism in a *Saccharomyces cerevisiae* phosphoglucose isomerase (*pgi1*) disruption mutant. *FEBS Letters*. 310, 182-186.
- Dickinson, J. R., Sobanski, M. A., Hewlins, M. J., 1995. In *Saccharomyces cerevisiae* deletion of phosphoglucose isomerase can be suppressed by increased activities of enzymes of the hexose monophosphate pathway. *Microbiology*. 141, 385-391.
- Dietvorst, J., Karhumaa, K., Kielland-Brandt, M. C., Brandt, A., 2010. Amino acid residues involved in ligand preference of the Snf3 transporter-like sensor in *Saccharomyces cerevisiae*. *Yeast*. 27, 131-8.
- Farwick, A., Bruder, S., Schadeweg, V., Oreb, M., Boles, E., 2014. Engineering of yeast hexose transporters to transport D-xylose without inhibition by D-glucose. *Proceedings of the National Academy of Sciences*. 111, 5159-5164.

- Gancedo, J. M., 1998. Yeast carbon catabolite repression. *Microbiology and Molecular Biology Reviews*. 62, 334-361.
- Gietz, R. D., Schiestl, R. H., 2007. High-efficiency yeast transformation using the LiAc/SS carrier DNA/PEG method. *Nature Protocols*. 2, 31-34.
- Goffrini, P., Wésolowski-Louvel, M., Ferrero, I., 1991. A phosphoglucose isomerase gene is involved in the Rag phenotype of the yeast *Kluyveromyces lactis*. *Molecular and General Genetics*. 228, 401-409.
- Gonzalez, B., Francois, J., Renaud, M., 1997. A rapid and reliable method for metabolite extraction in yeast using boiling buffered ethanol. *Yeast*. 13, 1347-55.
- Hahn-Hägerdal, B., Karhumaa, K., Fonseca, C., Spencer-Martins, I., Gorwa-Grauslund, M. F., 2007. Towards industrial pentose-fermenting yeast strains. *Applied Microbiology & Biotechnology*. 74, 937-53.
- Hill, J., Donald, K. A., Griffiths, D. E., Donald, G., 1991. DMSO-enhanced whole cell yeast transformation. *Nucleic Acids Research*. 19, 5791-5792.
- Hoffman, C. S., Winston, F., 1987. A ten-minute DNA preparation from yeast efficiently releases autonomous plasmids for transformation of *Escherichia coli*. *Gene*. 57, 267-272.
- Jin, Y.-S., Jeffries, T. W., 2004. Stoichiometric network constraints on xylose metabolism by recombinant *Saccharomyces cerevisiae*. *Metabolic Engineering*. 6, 229-238.
- Karhumaa, K., Hahn-Hägerdal, B., Gorwa-Grauslund, M. F., 2005. Investigation of limiting metabolic steps in the utilization of xylose by recombinant *Saccharomyces cerevisiae* using metabolic engineering. *Yeast* 22, 359-368.
- Karhumaa, K., Pahlman, A. K., Hahn-Hägerdal, B., Levander, F., Gorwa-Grauslund, M. F., 2009. Proteome analysis of the xylose-fermenting mutant yeast strain TMB 3400. *Yeast*. 26, 371-82.
- Maitra, P. K., Lobo, Z., 1971. A kinetic study of glycolytic enzyme synthesis in yeast. *Journal of Biological Chemistry*. 248, 475-488.
- Nijland, J. G., Shin, H. Y., de Jong, R. M., de Waal, P. P., Klaassen, P., Driessen, A. J., 2014. Engineering of an endogenous hexose transporter into a specific D-xylose transporter facilitates glucose-xylose co-consumption in *Saccharomyces cerevisiae*. *Biotechnol Biofuels*. 7, 168.
- Osiro, K. O., Borgström, C., Brink, D. P., Fjölnisdóttir, B. L., Gorwa-Grauslund, M. F., 2019. Exploring the xylose paradox in *Saccharomyces cerevisiae* through *in vivo* sugar signalomics of targeted deletants. *Microbial Cell Factories* (Submitted).
- Osiro, K. O., Brink, D. P., Borgström, C., Wasserstrom, L., Carlquist, M., Gorwa-Grauslund, M. F., 2018. Assessing the effect of D-xylose on the sugar signaling pathways of *Saccharomyces cerevisiae* in strains engineered for xylose transport and assimilation. *FEMS Yeast Research*. 18.
- Peeters, K., van Leemputte, F., Fischer, B., Bonini, B. M., Quezada, H., Tsytlonok, M., Haesen, D., Vanthienen, W., Bernardes, N., Gonzalez-Blas, C. B., Janssens, V., Tompa, P., Versees, W., Thevelein, J. M., 2017. Fructose-1,6-bisphosphate couples glycolytic flux to activation of Ras. *Nat Commun*. 8, 922.

- Pluskal, T., Nakamura, T., Villar-Briones, A., Yanagida, M., 2010. Metabolic profiling of the fission yeast *S. pombe*: quantification of compounds under different temperatures and genetic perturbation. *Mol Biosyst.* 6, 182-98.
- Portugal-Nunes, D. J., Pawar, S. S., Lidén, G., Gorwa-Grauslund, M. F., 2017. Effect of nitrogen availability on the poly-3-D-hydroxybutyrate accumulation by engineered *Saccharomyces cerevisiae*. *AMB Express*.
- Reider Apel, A., Ouellet, M., Szmidt-Middleton, H., Keasling, J. D., Mukhopadhyay, A., 2016. Evolved hexose transporter enhances xylose uptake and glucose/xylose co-utilization in *Saccharomyces cerevisiae*. *Nature Scientific Reports*. 6, 19512.
- Rende, U., Niittyta, T., Moritz, T., 2019. Two-step derivatization for determination of sugar phosphates in plants by combined reversed phase chromatography/tandem mass spectrometry. *Plant Methods*. 15, 127.
- Sierkstra, L. N., Silljé, H. H. W., Verbakel, J. M. A., Verrips, C. T., 1993. The glucose-6-phosphate-isomerase reaction is essential for normal glucose repression in *Saccharomyces cerevisiae*. *European Journal of Biochemistry*. 214, 121-127.
- Stovicek, V., Borodina, I., Forster, J., 2015. CRISPR–Cas system enables fast and simple genome editing of industrial *Saccharomyces cerevisiae* strains. *Metabolic Engineering Communications*. 2, 13-22.
- Subtil, T., Boles, E., 2012. Competition between pentoses and glucose during uptake and catabolism in recombinant *Saccharomyces cerevisiae*. *Biotechnol Biofuels*. 5, 14.
- Venkata Mohan, S., Nikhil, G. N., Chiranjeevi, P., Nagendranatha Reddy, C., Rohit, M. V., Kumar, A. N., Sarkar, O., 2016. Waste biorefinery models towards sustainable circular bioeconomy: Critical review and future perspectives. *Bioresource technology*. 215, 2-12.
- Vicente, R. L., Spina, L., Gómez, J. P. L., Dejean, S., Parrou, J.-L., Francois, J. M., 2018. Trehalose-6-phosphate promotes fermentation and glucose repression in *Saccharomyces cerevisiae*. *Microbial Cell*. 5, 444-459.
- Özcan, S., Vallier, L. G., Flick, J. S., Carlson, M., Johnston, M., 1997. Expression of the *SUC2* gene of *Saccharomyces cerevisiae* is induced by low levels of glucose. *Yeast*. 13, 127-137.

Supporting Information for:

Using phosphoglucose isomerase-deficient *Saccharomyces cerevisiae* to further understand the role of glycolytic intermediates in strains engineered for D-xylose utilization

Celina Borgström¹, Oksana Rogova², Karen O. Osiro¹, Ester Lundberg¹, Peter Spégel², Marie F. Gorwa-Grauslund¹

¹ Division of Applied Microbiology, Department of Chemistry, Lund University, Lund, Sweden.

² Centre for Analysis and Synthesis, Department of Chemistry, Lund University, Lund, Sweden

List of primers

The complete list of primers used in the present study is shown in Table S1 below.

Table S1. Primers used in the study. Inserted restriction sites are presented in bold.

Primer number	Primer name	Inserted restriction site	Sequence (5'-3')	Purpose
1	F1_FP	<i>NheI</i>	AAG CTAGC ATCGACCAGCA T TAGTAGGGG	Amplification of flanking region upstream of <i>PGI1</i> promoter
2	F1_RP	<i>AvrII</i>	TAC CTAGG ATCACGTACTTC TCACCGTCAAG	
3	F2_FP	<i>SalI</i>	TA GTCGAC ATGAAAGATACT CGCACTGGAAG	Amplification of flanking region DS of <i>PGI1</i> terminator
4	F2_RP	<i>NheI</i>	AAG CTAGC ATGTAGAGCCG TGTTTTGTTC	
5	F1_US_FP	-	GAAATGTATGTTGCTGGCA C	Verification of <i>PGI1</i> deletion
6	F2_DS_RP	-	CAAGTTCCAGGCTAAAGAA G	

Table S2. Multiple-reaction-monitoring (MRM) transitions and retention times of LC-MS analysis of sugar phosphates. Relative standard deviations (RSD) were obtained as described in Materials and Methods.

Compound	RT (min)	Quantifier	CE	Qualifier	CE	Method RSD (%)	Instrumental RSD (%)
3-phosphoglyceric acid	0.7	241→79	50	241→151	5	18.03	14.72
Glyceraldehyde 3-P	3.2	254→79	50	254→180	5	42.48	31.34
Dihydroxyacetone phosphate	2.9	254→79	50	254→180	5	17.41	10.57
Fructose-1,6-PP	4.2	536→79	50	536→159	21	26.96	11.01
Erythrose-4-P	5.3	340→79	50	340→266	5	25.13	56.6
Xylulose-5-P	7.4	426→79	49	426→37	9	9.7 (Sugars 5-P)	3.57 (Sugars 5-P)
Ribulose-5-P	7.7	426→79	49	426→37	9	11.97 (Ribose-5-P)	4.99 (Ribose-5-P)
Ribose-5-P	8.7	426→79	49	426→37	9		
2-Deoxyglucose 6-P (IS)	7.9	440→79	41	-	-	16.95	13.77
Galactose-1-P	9.1	483→79	37	483→427	13	14.15	8.46
Glucose-1-P	9.9	483→79	37	483→427	13	25.71	1.28
Fructose-6-P	11.6	512→79	37	512→153	13	27.10	11.91
Glucose-6-P	11.7	512→79	37	512→153	13	10.11	3.94
Seduheptulose-7-P	12.6	598→79	49	598→542	17	14.73	2.63
UDP-glucose/ UDP- galactose	12.5	901→497	41	901→545	37	15.25	8.29
Trehalose-6-P	13.3	813→79	50	813→757	25	55.73	33.11
6-Phosphogluconate	6.9	499→79	37	-	-	15.28	3.02

RT: Retention time, CE: Collision energy, RSD: Relative standard deviation.

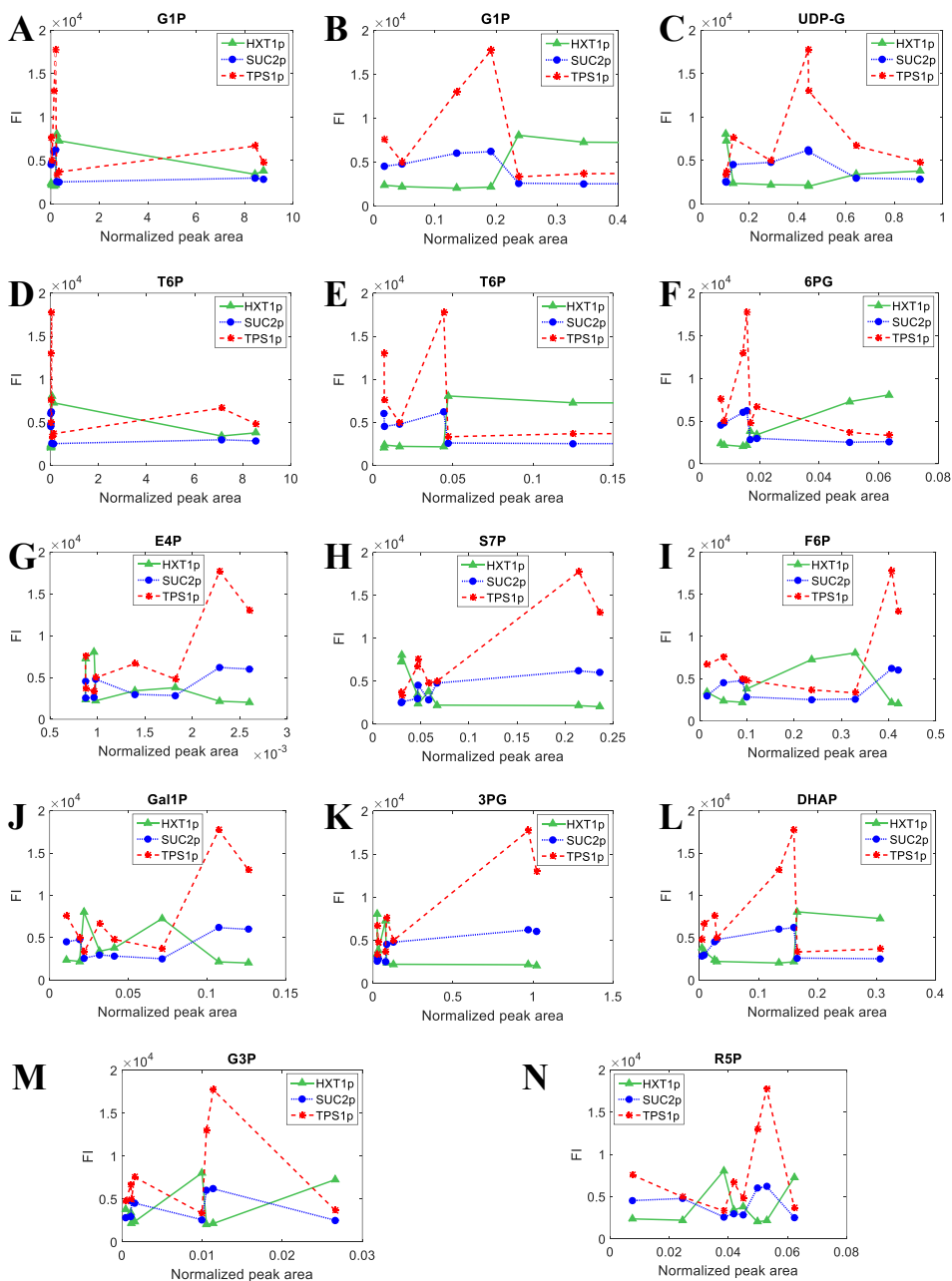


Figure S1. Fluorescence intensity (FI) as a function of the corresponding intracellular metabolite abundances, obtained from the background and deletion strains grown on D-glucose or D-xylose. The biosensor for *HXT1p* (triangles, green solid line) reports on the Rgt2p/Snf3p pathway, *SUC2p* (circles, blue dot-lines) the SNF1/Mig1p pathway and *TPS1p* (crosses, red dashed lines) the cAMP/PKA pathway. A: Glucose-1-phosphate; B: Glucose-1-phosphate zoomed in at abundances lower than 0.4; C: Uridine diphosphate (UDP)-glucose and UDP-galactose; D: Trehalose-6-phosphate; E: Trehalose-6-phosphate, zoomed in at abundances lower than 0.15; F: 6-phosphogluconate; G: Erythrose-4-phosphate; H: Sedoheptulose-7-phosphate; I: Fructose-6-phosphate; J: Galactose-1-phosphate; K: 3-phosphoglycerate; L: Dihydroxyacetone phosphate; M: Glyceraldehyde-3-phosphate; N: Ribose-5-phosphate.

Histograms from *HXT1p* and *SUC2p* biosensors

The fluorescence histograms for the *HXT1p*- and *SUC2p*- biosensors with and without *PGII* deletion are disclosed in Fig. S2. In the background strain (Fig. S2A & S2C) subpopulations with two fluorescence peaks are observed when cells are incubated with both high and low levels of D-glucose, or with high levels of D-fructose. Subpopulations produced by the biosensor strains incubated on D-glucose have been observed previously (Brink et al., 2016; Osiro et al., 2018); in this case the heterogeneities are not severe enough to call for separate consideration, so they are treated as one population. These doubled peaks were also not present in the *pgi1Δ*-strains of the respective reporters on the same media (Fig. S2B and S2D), and the deleted strains displayed more homogenous fluorescence populations than the background strains.

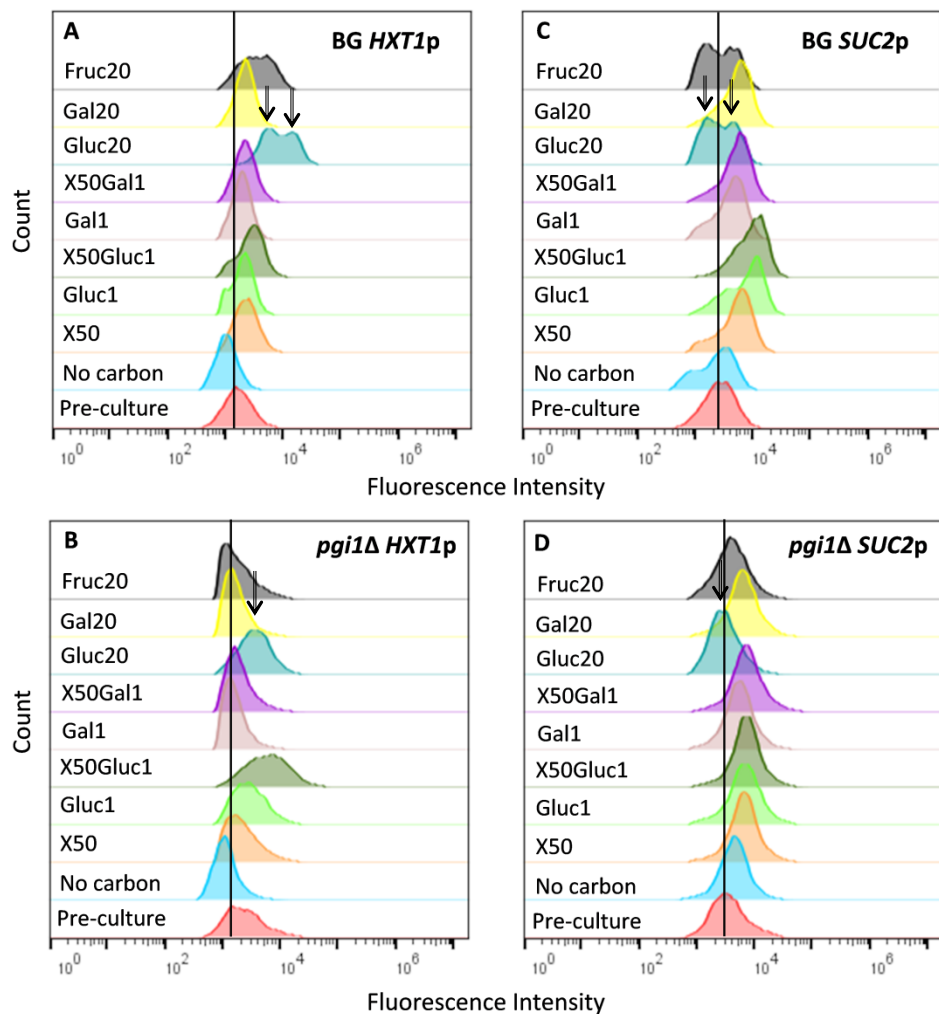


Figure S2. Histogram of biosensors *HXT1p* (A, B) and *SUC2p* (C, D) without (A, C) and with (B, D) *PGI1* gene deletion. The four strains were analysed at 0h (=pre-culture conditions), and after 6h for the following conditions: no carbon; 50 g L⁻¹ D-xylose (X50); 1 g L⁻¹ D-glucose (Gluc1); 50 g L⁻¹ D-xylose and 1 g L⁻¹ D-glucose (X50Gluc1); 1 g L⁻¹ D-galactose (Gal1); 50 g L⁻¹ D-xylose and 1 g L⁻¹ D-galactose (X50Gal1); 20 g L⁻¹ D-glucose (Gluc20); 20 g L⁻¹ D-galactose (Gal20); and 20 g L⁻¹ D-fructose (Fruc20). Arrows indicate one example of a condition (20 g L⁻¹ D-glucose) where the background strains (A,C) displayed subpopulations in fluorescence intensity, but for both *PGI1*-deleted strains (B, D) single populations were observed.

References

- Brink, D. P., Borgström, C., Tueros, F. G., Gorwa-Grauslund, M. F., 2016. Real-time monitoring of the sugar sensing in *Saccharomyces cerevisiae* indicates endogenous mechanisms for xylose signaling. *Microbial Cell Factories*. 15, 183.
- Osiro, K. O., Brink, D. P., Borgström, C., Wasserstrom, L., Carlquist, M., Gorwa-Grauslund, M. F., 2018. Assessing the effect of D-xylose on the sugar signaling pathways of *Saccharomyces cerevisiae* in strains engineered for xylose transport and assimilation. *FEMS Yeast Research*. 18.

Paper VI



Engineering Yeast Hexokinase 2 for Improved Tolerance Toward Xylose-Induced Inactivation

Basti Bergdahl*, Anders G. Sandström, Celina Borgström, Tarinee Boonyawan[‡], Ed W. J. van Niel, Marie F. Gorwa-Grauslund

Division of Applied Microbiology, Department of Chemistry, Lund University, Lund, Sweden

Abstract

Hexokinase 2 (Hxk2p) from *Saccharomyces cerevisiae* is a bi-functional enzyme being both a catalyst and an important regulator in the glucose repression signal. In the presence of xylose Hxk2p is irreversibly inactivated through an autophosphorylation mechanism, affecting all functions. Consequently, the regulation of genes involved in sugar transport and fermentative metabolism is impaired. The aim of the study was to obtain new Hxk2p-variants, immune to the autophosphorylation, which potentially can restore the repressive capability closer to its nominal level. In this study we constructed the first condensed, rationally designed combinatorial library targeting the active-site in Hxk2p. We combined protein engineering and genetic engineering for efficient screening and identified a variant with Phe159 changed to tyrosine. This variant had 64% higher catalytic activity in the presence of xylose compared to the wild-type and is expected to be a key component for increasing the productivity of recombinant xylose-fermenting strains for bioethanol production from lignocellulosic feedstocks.

Citation: Bergdahl B, Sandström AG, Borgström C, Boonyawan T, van Niel EWJ, et al. (2013) Engineering Yeast Hexokinase 2 for Improved Tolerance Toward Xylose-Induced Inactivation. PLoS ONE 8(9): e75055. doi:10.1371/journal.pone.0075055

Editor: Paul Hoskisson, University of Strathclyde, United States of America

Received: June 29, 2013; **Accepted:** August 5, 2013; **Published:** September 6, 2013

Copyright: © 2013 Bergdahl et al. This is an open-access article distributed under the terms of the Creative Commons Attribution License, which permits unrestricted use, distribution, and reproduction in any medium, provided the original author and source are credited.

Funding: This work was financially supported by the Swedish National Energy Agency (www.energimyndigheten.se, Project No. P35350-1). The funders had no role in study design, data collection and analysis, decision to publish, or preparation of the manuscript.

Competing Interests: The authors have declared that no competing interests exist.

* E-mail: basti.bergdahl@tmb.lth.se

‡ Current address: Centre of Medical Excellence, Chiang Mai University, Chiang Mai, Thailand

Introduction

The yeast *Saccharomyces cerevisiae* has three structural genes encoding enzymes that catalyse the phosphorylation of glucose to glucose 6-phosphate: *HXK1*, *HXK2* and *GLK1* [1]. *HXK1* and *HXK2* encode hexokinases which, in addition to glucose, also can phosphorylate fructose and mannose. These two proteins share a protein identity of 77%. *GLK1* encodes a glucokinase which has an identity of 38% with the two hexokinases and lacks the ability to phosphorylate fructose [1]. During growth on fermentable carbon sources hexokinase 2 (Hxk2p) provides the main sugar-phosphorylating capability [2]. When the conditions change to non-fermentable carbon sources the *HXK2* gene becomes repressed and the *HXK1* and *GLK1* genes are rapidly de-repressed [3].

Hexokinase 2 has a bi-functional role in yeast metabolism; in addition to its catalytic function it also has an important regulatory function in the glucose catabolite repression mechanism [4,5], being an essential Snf1p-antagonist and co-repressor with Mig1p. The Snf1p pathway controls the expression of genes required for growth on less preferred fermentable carbon sources (e.g. galactose, sucrose and maltose) and non-fermentable carbon sources like glycerol and ethanol [6]. Snf1p is activated upon glucose depletion through phosphorylation by three kinases: Sak1p, Elm1p and Tos3p [7]. Addition of glucose effectively inactivates Snf1p by stimulating the activity of the Glc7p/Reg1p phosphatase complex, located in the cytosol [8]. Hxk2p is essential in this deactivation mechanism by enabling Glc7p/Reg1p to dephosphorylate Snf1p [8]. Hence, in a *hxx2Δ* mutant, Snf1p

never becomes dephosphorylated and target genes are constitutively expressed, even at high concentrations of glucose [9,10]. In the presence of glucose Hxk2p is transported into the nucleus by the karyopherin α/β carrier complex Kap60p/Kap95p [11,12]. Inside the nucleus, Hxk2p interacts with Mig1p and forms a DNA-binding repressor complex [13,14]. Mig1p is the transcription factor responsible for the repression of genes needed for utilization of alternative fermentable carbon sources [6]. The Hxk2p/Mig1p complex binds to the Mig1p-recognition sites upstream of target genes and in the case of *SUC2* repression, Hxk2p also interacts with Med8p which supposedly hinders the activation of RNA polymerase [4,5,15]. In de-repressing conditions active Snf1p is transported into the nucleus and phosphorylates Mig1p leading to its transport out from the nucleus [16]. Active Snf1p can also phosphorylate Hxk2p at residue Ser15 (numbered according to the translated mRNA sequence) which prevents Hxk2p from entering the nucleus [11]. In the absence of Hxk2p, Mig1p is constitutively phosphorylated in the nucleus and transported out with loss of repressive capacity as a result [13]. Transcriptional analysis of a *hxx2Δ*-strain showed significant upregulation of genes with binding sites for Mig1p and/or Cat8p (e.g. *FBP1*, *MDH2*, *MDH3*, *MLS1*, *ICL1*, *IDP2* and *PCK1*) [17,18]. This confirms the significant role of Hxk2p in the Snf1p circuit of the glucose signalling mechanism. In addition, Hxk2p also participates in the control of genes encoding sugar transporters [17,18,19]. The presence of Hxk2p is required to fully induce *HXT1* at high glucose concentrations and *HXT2* and *HXT4* at low concentrations [19]. Hxk2p is also needed to repress the expression of *HXT2*

and *HXT4* at high glucose concentration [19]. Finally, a specific role for Hxk2p in modulating mitochondrial cytochrome content and respiratory activity has been suggested [20]. This is supported by a diminished Crabtree effect in *hxk2Δ* mutants, resulting in a nearly complete respiratory metabolism at high glucose concentration [18]. In light of these findings, the Hxk2p protein can be regarded as a global glycolytic regulator that is essential for mediating the complete glucose repression signal.

Early studies on glucose catabolite repression revealed that xylose can induce a decrease in the glucose phosphorylating activity [2]. *In vitro* experiments confirmed that Hxk2p becomes irreversibly inactivated by xylose through an autophosphorylation mechanism in the presence of ATP [21]. The target residue for the autophosphorylation was later identified as Ser158 situated in the active site [22]. The exchange of this amino acid indeed abolished the autophosphorylation but also severely reduced catalytic activity [22]. The induced inactivation by xylose also caused an increase in invertase activity (encoded by *SUC2*), demonstrating that both the catalytic and regulatory functions of Hxk2p are affected by the modification [2]. Normally the catalytic and regulatory functions operate independently through different parts of the protein [14], indicating that the phosphorylation of Ser158 has a profound influence on Hxk2p functionality. Alteration of Ser158 significantly reduces the ability of Hxk2p to stimulate the Ras/cAMP signal [23,24], a signal that induces a fast and comprehensive modulation of the transcriptional organization with the aim to enhance cellular metabolism and growth [25].

In the production of bioethanol from lignocellulosic biomass, an efficient conversion of xylose is of great importance to increase the economic feasibility of the process [26]. *S. cerevisiae* lacks the ability to ferment xylose and requires extensive genetic engineering to obtain such a trait [27]. However, xylose is not recognised as a fermentable carbon source by this yeast, as shown in several transcription analyses [28,29,30] and profiling of intracellular metabolite concentrations [31,32]. Due to the distinguished role of Hxk2p in glucose repression signalling we hypothesised that the inactivation by xylose leads to a reduced capability to regulate expression of genes involved in sugar transport and fermentative metabolism. The aim of the current study was to identify new variants of Hxk2p, immune to autophosphorylation by xylose, which were expected to increase the sugar consumption rate during fermentation of a glucose/xylose mixture by restoring the repressive capability closer to its nominal level, thus increasing ethanol productivity. The over-expression of one such variant did indeed result in a faster xylose uptake rate and a faster initial growth rate on xylose but other regulatory factors, normally induced by glucose, are still needed to significantly increase the ethanol productivity from xylose.

Materials and Methods

Strains and culture conditions

Plasmids and yeast strains used are listed in Table 1. Frozen yeast strains were recovered on solid YPD or YPGal plates (10 g L⁻¹ yeast extract, 20 g L⁻¹ peptone, 20 g L⁻¹ glucose or galactose, 15 g L⁻¹ agar) for two days at 30°C. Yeast cultures were grown in liquid YPD or YPGal medium for 12–16 h at 30°C and 180 rpm in an orbital shaker. Competent yeast cells were prepared and transformed according to the high efficiency protocol [33]. Transformants were selected on solid Yeast Nitrogen Base (YNB) medium (6.7 g L⁻¹ YNB without amino acids, 15 g L⁻¹ agar) with 20 g L⁻¹ glucose or galactose as carbon source. When required, uracil and leucine were supplemented at 50 mg L⁻¹ and 220 mg L⁻¹, respectively, and the antibiotics gentiicin and aureobasidin

were supplemented at 200 mg L⁻¹ and 0.15 mg L⁻¹, respectively. In shake flask cultivations, YNB medium contained 50 mM potassium hydrogen phthalate buffer at pH 5.5. Anaerobic continuous cultivations were made in a defined mineral medium [34] using 5 g L⁻¹ glucose and 50 g L⁻¹ xylose or 15 g L⁻¹ glucose with or without 30 g L⁻¹ xylose in the feed reservoir. All media used for anaerobic cultivations were supplemented with Tween 80 (400 mg L⁻¹) and ergosterol (10 mg L⁻¹).

E. coli strain NEB5α (New England Biolabs, USA) was used for sub-cloning of plasmid DNA. Heat shock competent cells were prepared according to the Inoue method [35] and transformed according to the supplier's instructions. Transformants were selected from solid LB plates (5 g L⁻¹ yeast extract, 10 g L⁻¹ tryptone, 10 g L⁻¹ NaCl, 15 g L⁻¹ agar, pH 7.0), supplemented with 100 mg L⁻¹ of ampicillin, after incubation for 16 h at 37°C. Cultures of transformed cells were grown in liquid LB medium with ampicillin, for 14–16 h at 37°C and 180 rpm.

Structural analysis of Hxk2p

A homology model of *S. cerevisiae* Hxk2p was generated based on the closed conformation of the *S. cerevisiae* Hxk1p scaffold with a glucose moiety in the active site (PDB: 3B8A_X). The models were generated using SWISS-MODEL [36] by submitting the Hxk2p (GenBank: E1W10681.1) and the later obtained Hxk2p-Y amino acid sequences for automatic homology modelling. Structural analysis of the model was done manually using PyMOL (<http://www.pymol.org>). Further information regarding the structural analysis is described in the Results section.

Construction of an *E. coli* library of Hxk2p-variants

The native *HXK2* gene was amplified from genomic DNA of *S. cerevisiae* CEN.PK2-1C. This fragment also contained a 700 bp upstream promoter-sequence and a 300 bp downstream terminator-sequence. The cloned *HXK2* locus was verified by sequencing and the resulting plasmid was named YlpBB5 (Table 1). The cloned *HXK2* locus was used as template for introducing specific mutations using six degenerate primer pairs (Table S3). The primers were designed such that the 3'-end of each region overlapped with the 5'-end of the following region, enabling the use of overlap-extension PCR (OE-PCR) [37] to link all regions together in a combinatorial manner, generating a heterogeneous mix of the complete locus (see Fig. S1). The plasmid library was generated according to the MEGAWHOP protocol [38] in which the heterogeneous DNA mix were used as megaprimers and the YlpBB5 plasmid as template. The newly synthesised plasmids were subsequently cloned in commercial heat shock competent *E. coli* NEB5α and the presence of all mutations introduced were confirmed by sequencing (Fig. S2). Detailed information on the procedures can be found in the Supporting information.

Construction of the yeast screening strain TMB3463

The genes *HXK2*, *HXK1* and *GLK1* were deleted sequentially from strain TMB3042 (Table 1). The regions used for homologous recombination were amplified from genomic DNA and flanked the intended ORF to ensure complete gene replacement. Three deletion cassettes with different selection markers were created by OE-PCR (Table 1, Table S4). Correct integration of the cassettes was verified by PCR (Fig. S3B) and the new strains were named TMB3460 (*hxk2-Δ*), TMB3461 (*hxk2-Δ hxk1-Δ1*) and TMB3462 (*hxk2-Δ hxk1-Δ1 glk1-Δ*) (Table 1). The deletions were also verified using primers specific for each gene (Table S5). However, this analysis revealed that the *HXK1* gene was still present in the genome even though the deletion cassette was in the correct locus and the strain was expected to be haploid (Fig. S3C). To delete the

Table 1. Strains and plasmids used in this study.

Name	Relevant genotype ^a	Reference
Plasmids		
p424	<i>TRP1</i>	[54]
p426	<i>URA3</i>	[54]
pUG6	<i>LoxP-KanMX-LoxP</i>	[55]
pUG6AUR	<i>LoxP-AUR1-LoxP</i>	[56]
pUG62AUR-HXK1USDS	<i>HXK1</i> (−294—−21 bp), <i>HXK1</i> (+1780—+1999 bp), <i>LoxP-AUR1-LoxP</i>	This study
Ylplac128	<i>LEU2</i>	[57]
Ylplac211	<i>URA3</i>	[57]
YlpDR1	Ylplac128: <i>TDH3p-GXF1-CYC1t</i>	[58]
YlpDR7	Ylplac211: <i>TDH3p-XYL1(N272D)-ADH1t</i> ; <i>PGK1p-XYL2-PGK1t</i>	[46]
YlpBB5	Ylplac128: <i>HXK2p-HXK2-HXK2t</i>	This study
YlpBB8	Ylplac128: <i>TDH3p-HXK2-CYC1t</i>	This study
YlpBB8Y	Ylplac128: <i>TDH3p-HXK2(F159Y)-CYC1t</i>	This study
Deletion cassettes		
<i>HXK2</i>	<i>HXK2</i> (−500—−1 bp)- <i>TRP1-HXK2</i> (+1461—+1960 bp)	This study
<i>HXK1</i>	<i>HXK1</i> (−1000—−451 bp)- <i>URA3-HXK1</i> (+2040—+2353 bp)	This study
<i>GLK1</i>	<i>GLK1</i> (−673—−121 bp)- <i>LoxP-KanMX-LoxP-GLK1</i> (+1858—+2359 bp)	This study
Yeast strains		
TMB3042	CEN.PK2-1C; <i>gre3-Δ</i> ; <i>his3::PGK1p-XKS1-PGK1t</i> , <i>HIS3</i> ; <i>tal1::PGK1p-TAL1-PGK1t</i> ; <i>tkl1::PGK1p-TKL1-PGK1t</i> ; <i>rki1::PGK1p-RKI1-PGK1t</i> ; <i>rpe1::PGK1p-RPE1-PGK1t</i> ; <i>trp1</i> , <i>ura3</i> , <i>leu2</i>	[45]
TMB3460	TMB3042; <i>hxx2-Δ::TRP1</i> ; <i>ura3</i> , <i>leu2</i>	This study
TMB3461	TMB3460; <i>hxx1-Δ1::URA3</i> ; <i>leu2</i>	This study
TMB3462	TMB3461; <i>glk1-Δ::LoxP-KanMX-LoxP</i> ; <i>leu2</i>	This study
TMB3463	TMB3462; <i>hxx1-Δ2::pUG62AUR-HXK1USDS</i> ; <i>leu2</i>	This study
TMB3466	TMB3463; <i>leu2::YlpBB8</i>	This study
TMB3467	TMB3463; <i>leu2::YlpBB8Y</i>	This study
TMB3490	TMB3460; <i>ura3::YlpDR7</i> ; <i>leu2</i>	This study
TMB3492	TMB3490; <i>leu2::YlpBB8</i>	This study
TMB3493	TMB3490; <i>leu2::YlpBB8Y</i>	This study

^aSequence numbering for some constructs are numbered in relation to the first base in the ATG starting codon of the ORF in question.
doi:10.1371/journal.pone.0075055.t001

second copy of *HXK1* a new deletion vector was constructed based on the pUG6AUR plasmid (Table 1). Additional restriction sites were introduced in the pUG6AUR plasmid by ligating a linker (Fig. S4) into the *SalI*/*NdeI*-digested plasmid, generating plasmid pUG62AUR (Fig. S5). The linker contained recognition sequences for *KpnI*, *SmaI*, *SphI* and *AvrII*. Homologous regions flanking the *HXK1* gene were amplified by PCR from genomic DNA (Table S6), generating an upstream sequence of 273 bp (−294—−21 bp) and a downstream sequence of 219 bp (+1780—+1999 bp). The upstream and downstream fragments were digested with *SphI*/*AvrII* and *SphI*/*KpnI*, respectively, and ligated into pUG62AUR generating the deletion vector pUG62AUR-HXK1USDS (Fig. S6). Correct integration of the vector was verified by PCR (Table S7) and enzyme activity measurements confirmed the absence of any glucose phosphorylating activity (Fig. S7). The final screening strain was named TMB3463 (Table 1). Detailed information on these procedures can be found in the Supporting information.

Large-scale transformation of TMB3463

A single colony of TMB3463 was inoculated in 5 mL YPGal in a 50 mL conical tube and cultivated for 20 h. This pre-culture was used to inoculate 50 mL YPGal in a 500 mL baffled shake flask at

OD = 0.1. After 10.5 h of cultivation the cells were in mid-exponential phase and used to inoculate four shake flasks of 1 L containing 100 mL YPGal each at OD = 0.02. After 14.5 h of growth the cultures reached an OD = 1 and were harvested, washed and transformed according the Large-scale PEG/LiAc protocol [39]. The transformation was performed for 90 min at 42°C in an orbital shaker at 65 rpm, using 300 μg of the plasmid library linearized with *Afl*III. After washing the cells, different volumes were spread on solid YNB medium with galactose. The remaining transformants were inoculated in 1.5 L of defined mineral medium [34] with 20 g L^{−1} galactose as carbon source. The propagation was performed in a 2.5 L Braun bioreactor with a stirring rate of 800 rpm and a sparging rate of 1 L air min^{−1}. The pH was automatically maintained at 5.5 by addition of 3 M KOH. Silicon antifoam RD emulsion (Dow Corning, USA) was added at a concentration of 0.5 mL L^{−1}. After four days colonies were counted on the plates and the total size of the yeast library was estimated to 1.4 × 10⁶ ± 3% cfus, which is 6 times larger than the size required for 100% coverage [40].

Selection of a new Hxk2p-variant

Screening of the yeast Hxk2p-library for variants with increased resistance to autophosphorylation by xylose was performed in anaerobic glucose-limited continuous cultivation. After propagating the yeast library aerobically on galactose the culture volume was reduced to 1 L, sparging was changed to N₂-gas at a flow rate of 0.2 L min⁻¹ and the stirring rate was set to 200 rpm. The feed reservoir, containing 5 g L⁻¹ glucose and 50 g L⁻¹ xylose, was supplied at a rate giving a dilution rate of 0.072 h⁻¹. After 96 h the dilution rate was increased to 0.40 h⁻¹ initiating a washout of all cells. During the washout, samples for OD and HPLC analysis were collected every hour. After 12 h a final sample was collected and diluted to yield single colonies on solid YNB medium with glucose. The plates were incubated for two days and ten random colonies were selected for sequencing of the *HXK2* gene. The ten *HXK2* ORFs were amplified from genomic DNA by PCR using primers HXK2_seq_f (5'-GAA AAG ATT GTA GGA ATA TAA TTC TC-3') and HXK2_seq_r (5'-CAC ATA ATT AAA AAA AGG GCA CCT TC-3'). Each reaction mixture (50 µL) contained 1X Buffer, 1.5 mM MgCl₂, 0.2 mM of each dNTP, 0.5 mM of forward and reverse primer and 1 U High Fidelity Phusion Hotstart II Polymerase (Thermo Scientific, USA). The amplification program was as follows: 30 s denaturation at 98°C, 30 cycles of 10 s denaturation at 98°C, 15 s annealing at 58.3°C, 45 s extension at 72°C and 1 cycle of 10 min final extension at 72°C. The PCR-products were purified using GeneJet PCR Purification Kit (Thermo Scientific, USA) and sent for sequencing.

Construction of strains TMB3466, 3467, 3492 and 3493

The native *HXK2* gene was amplified by PCR from plasmid YlpBB5 using primers HXK2-F1-SpeI (5'-CTA GAA CTA GTA AAT GGT TCA TTT AGG TCC AAA AAA ACC ACA AG-3') and HXK2-R1-SalI (5'-GAG GTC GAC TTA GAC ACC GAT GAT ACC AAC GG-3'). The amplification program was as follows: 30 s denaturation at 98°C, 30 cycles of 10 s denaturation at 98°C, 30 s annealing at 65°C (−0.5°C decrease per cycle), 1 min extension at 72°C and 1 cycle of 10 min final extension at 72°C. The gene encoding the selected variant Hxk2p(F159Y) was amplified from genomic DNA of one of the selected clones using the same program. The two *HXK2* genes were digested with *SpeI* and *SalI* and inserted between the *TDH3*-promoter and *CYC1*-terminator in the vector YlpDR1, yielding the two plasmids YlpBB8 and YlpBB8Y (Table 1). The cloned genes were verified by DNA-sequencing.

Strains with a single hexokinase gene were constructed by transforming TMB3463 with YlpBB8 or YlpBB8Y, both linearized with *ClaI*. The new strains were named TMB3466 and TMB3467, respectively (Table 1). Xylose-fermenting strains were constructed by transforming TMB3460 with YlpDR7, linearized with *EcoRV*, generating strain TMB3490. This strain was further transformed with YlpBB8 or YlpBB8Y generating the strains TMB3492 and TMB3493, respectively (Table 1).

Carbon limited continuous cultivations

The sensitivity of the native Hxk2p and Hxk2p-Y toward xylose was evaluated in anaerobic glucose-limited continuous cultivations. Strains TMB3466 and TMB3467 (Table 1) were pre-grown in YNB medium with glucose until late exponential phase and inoculated into 3 L stirred-tank bioreactors (Applikon, Schiedam, The Netherlands) equipped with ADI 1025 Bio-Console and ADI 1010 Bio-Controller (Applikon, Schiedam, The Netherlands). Cultivations were performed with a working volume of 1 L of defined mineral medium [34] at 30°C. The medium was continuously stirred at 200 rpm and sparged with N₂-gas at a

rate of 0.2 L min⁻¹. The pH was automatically maintained at 5.5 by addition of 3 M KOH. The condenser was connected to a Heto CBN 8–30 cooling bath (Jouan Nordic A/S, Allerød, Denmark) and cooled to 4°C. The off-gas was analysed on-line for O₂, CO₂ and ethanol using an INNOVA 1313 Fermentation Monitor (LumaSense Technologies A/S, Denmark). Silicon antifoam RD emulsion (Dow Corning, USA) was added at a concentration of 0.2 mL L⁻¹. An initial steady-state was established at *D* = 0.21 h⁻¹ using a feed reservoir with 15 g L⁻¹ glucose. The cells were then exposed to a gradual increase in xylose concentration by changing to a feed reservoir with 15 g L⁻¹ glucose and 30 g L⁻¹ xylose. Samples were collected after 5 and 7.5 volume changes with each feed composition, as well as at different time points during the accumulation of xylose. Cell samples (5 mL) were collected on ice and centrifuged for 5 min at 4000 rpm and 4°C. Cell pellets for enzyme activity measurements were stored at −80°C until needed. Fermentation experiments were performed in biological duplicates.

Anaerobic batch fermentations

Cells were pre-grown in YNB medium with glucose until late exponential phase and inoculated into the bioreactor at a concentration of 0.03 g CDW L⁻¹. Fermentation experiments were performed in 3 L stirred-tank bioreactors (Applikon, Schiedam, The Netherlands) as described above except that 1 L of 2× YNB with 20 g L⁻¹ glucose and 50 g L⁻¹ xylose was used as cultivation medium. Fermentation experiments were performed in biological duplicates.

Enzyme activity assays

Cell-free extracts were prepared by thawing frozen cell pellets on ice and wash once with water. After a centrifugation step of 5 min at 4000 rpm and 4°C, the cells were treated with 250 µL Y-PER (Thermo Scientific, USA) per 100 mg of wet cell pellet according to the suppliers instructions. Protein concentrations were determined with the Coomassie Protein Assay Reagent (Thermo Scientific, USA) using BSA (Thermo Scientific, USA) as standard. Glucose phosphorylating activity was determined in a 1 mL reaction mixture containing: 20 mM HEPES (pH 7.6), 5 mM glucose, 5 mM MgCl₂, 1 mM NADP, 1 mM ATP and 1.16 U of glucose 6-phosphate dehydrogenase. The formation of NADPH was measured at 340 nm in a cuvette with light path length of 1 cm using a Ultrospec 2100 Pro spectrophotometer (Amersham Biosciences Corp., USA) controlled by computer software SWIFT Reaction Kinetics v. 2.05 (Biochrom Ltd., Cambridge, UK). The absorbance was converted to concentration units using the molar extinction coefficient of NADPH ($\epsilon_{340\text{ nm}} = 6220\text{ L mol}^{-1}\text{ cm}^{-1}$). The slope was determined within an interval of at least 1 min, using at least three different dilutions of the cell extract. Only the slopes within the range 0.05–0.2 A min⁻¹ were considered acceptable. One unit is defined as the conversion of 1 µmole of glucose per min.

Biomass determination and analysis of metabolites

Optical density was measured at 620 nm using an Ultrospec 2100 Pro spectrophotometer (Amersham Biosciences Corp., USA). Cell dry weight was measured in triplicate by filtering a known volume of the culture through a pre-weighed nitrocellulose filter with 0.45 µm pore size. The filters were washed with three volumes of water, dried in a microwave oven for eight minutes at 350 W and weighed after equilibrating to room temperature in a desiccator.

Concentrations of glucose, xylose, xylitol, glycerol, acetate and ethanol were analysed by HPLC (Waters, USA). Metabolites were

separated using an Aminex HPX-87H ion exchange column (Bio-Rad, USA) at 45°C with 5 mM H₂SO₄ as mobile phase at a flow rate of 0.6 mL min⁻¹. All compounds were detected with a RID-10A refractive index detector (Shimadzu, Japan).

Calculation of metabolic rates

Maximum specific consumption rates of glucose and production rates of glycerol, acetate and ethanol were calculated from Equation 1.

$$r_j^{\max} = Y_{j/x} \cdot \mu_{\max} \quad (1)$$

The biomass yield coefficients ($Y_{j/x}$) were calculated as the slope in a linear regression of cumulative consumption or production of metabolite j vs. the biomass concentration. Yield coefficients were calculated from at least eight data points. Maximum specific growth rates on glucose were calculated as the slope in a linear regression of ln(CDW) vs. time from four data points. Due to the non-exponential growth on xylose, Equation 1 cannot be used for calculating specific rates. The maximum specific consumption rates of xylose and production rates of xylitol, glycerol, acetate and ethanol during xylose consumption were instead calculated as the slope in linear regression of metabolite concentration divided by biomass concentration vs. time. These rates were calculated using at least four data points from the phase when xylose was the only carbon source. The significance of a difference between two mean values was calculated using a two-tailed t-test assuming equal variance of the two samples. Comparison of mean values from steady state cultures had a degree of freedom of six ($n_1 = n_2 = 4$) whereas all other comparisons had two degrees of freedom ($n_1 = n_2 = 2$).

Results

Amino acid residues potentially influencing the xylose-induced inactivation

The aim of the study was to identify a new variant of Hxk2p which i) is immune to autophosphorylation by xylose, ii) maintains its regulatory capability, and iii) has high catalytic activity in the presence of xylose. Ser158 in the active site is known to be the target for autophosphorylation [22] and modulation of this residue disrupts the catalytic function as well as the regulatory capability [23]. To fulfil the above mentioned criteria we used a focused protein engineering strategy, targeting the active site of Hxk2p.

A homology model of Hxk2p was generated with a glucose moiety in the active site, based on the closed conformation of the *S. cerevisiae* Hxk1p scaffold. The generated model allowed the study of the amino acid residues directly involved in substrate binding. Several amino acids in different regions surrounding the active site were assessed for their mutability. This assessment was based on both the structural features of the amino acids and on their orientation towards the glucose moiety. The initial set of residues included those within a 6 Å radius volume centred on the C-6 of the β-D-glucopyranose structure. The residues with a side-chain orientation pointing away from the active site were, however, removed from the set. The final set of potentially mutable positions contained 13 amino acid residues (Table 2). The chosen degeneracy introduced mutations in each position creating a codon for either one or three alternative amino acids, or the native amino acid (Table 2). With this approach a condensed library was generated. Although limited in diversity, such a focused library design strategy was previously shown to efficiently select for

favourable epistatic effects on another enzyme [41]. Often only discreet changes are needed to induce a required adjustment of substrate preference. Thus, the alternative residue(s) were chosen to have chemical properties similar to the wild-type residue, while chain length and size of the residue were varied. Some substitutions, such as Gly271Cys, were assumed to promote residue-residue interactions and cause slight backbone conformation changes. The isoleucine in position 231 was assumed to be a key residue for distinguishing between the binding of D-glucopyranose and D-xylopyranose [42] as it is pointing directly at the C-6 of glucose. Hence, four different residues (including the wild-type residue) were possible at this position. The theoretical combinatorial protein library was calculated to contain 16,384 variants. In practice, a total size of ca. 57,000 cfus was obtained after transforming *E. coli* with the plasmid library, which corresponded to a 97% coverage of the theoretical variants [40].

Identification of a new Hxk2p variant with a single amino acid substitution

Strain TMB3463, which is unable to grow on glucose due to the absence of hexokinase activity, was constructed to couple the screening to the survival of the host on this carbon source. Hence, when transformed with the library only strains carrying catalytically functional enzyme variants could grow on glucose. To select for a variant immune to inactivation by xylose the population had to be exposed to this sugar and it had to be taken up by the cells. Unfortunately, glucose and xylose are taken up by the same transporters [43] and due to the much higher affinity for glucose the concentration of this sugar has to be as low as possible to maintain a high xylose-mediated selection pressure. For this reason glucose-limited continuous cultivation was chosen for the screening. Due to the role of Hxk2p in fermentative metabolism, anaerobic conditions were chosen for the screening to generate an additional selection pressure for a variant with maintained regulatory function.

After transforming strain TMB3463 with the plasmid library the transformants were propagated in aerobic batch cultivation with galactose as carbon source in order to include variants that might

Table 2. Mutations included in the condensed Hxk2p library.

#	Selected residue	Alternative residue(s)	Codon degeneracy ^a
1	Ser158	Thr	ASC
2	Phe159	Tyr	TWC
3	Arg173	Lys	ARA
4	Lys176	Arg	ARA
5	Asp211	Glu	GAK
6	Thr212	Ser	ASC
7	Ile231	Asp/Phe/Tyr	WWC
8	Gly233	Ser	RGC
9	Thr234	Ser	ASC
10	Gly235	Ala	GSA
11	Glu269	Asp	GAK
12	Gly271	Cys	KGC
13	Glu302	Asp	GAK

The table lists the amino acid residues chosen for mutagenesis, the alternative residues in each position and the codon degeneracy used.

^aCodon degeneracy: S = C or G; W = A or T; R = A or G; K = G or T.

doi:10.1371/journal.pone.0075055.t002

have poor glucose phosphorylating capability. When all galactose was consumed the conditions were changed to anaerobiosis and the chemostat was initiated by supplying the feed, containing 5 g L^{-1} glucose and 50 g L^{-1} xylose, at a rate of 1.16 mL min^{-1} giving a dilution rate of 0.072 h^{-1} . At this rate it took ca. 56 h to reach a concentration of 49 g L^{-1} of xylose inside the reactor. During this period all variants, which were either unable to phosphorylate glucose or significantly inactivated by xylose, were expected to wash out from the culture. After 96 h of cultivation the dilution rate was increased to 0.40 h^{-1} and being higher than the maximum growth rate under anaerobic conditions, it initiated a washout of all cells. When the optical density was sufficiently low, the largest fraction of the remaining cells was expected to constitute the variants with the highest growth rate.

Immediately upon increasing the flow rate the population was able to grow at a rate of 0.17 h^{-1} (Fig. 1). After 4 h the concentration of glucose had increased above 3 g L^{-1} which was enough to reduce the transport of xylose into the cells and as a consequence the growth rate increased to 0.29 h^{-1} (Fig. 1). It took 12 h to reduce the OD from 1.2 to 0.2 at which point the culture was diluted and plated on solid medium to yield single colonies. Ten random colonies were selected for sequencing of the *Hxk2* gene. Four of these sequences gave inconclusive results due to the detection of more than one nucleotide in some positions and were thus discarded. The remaining six sequences were of good quality and the majority (4 out of 6) had mutations corresponding to a single amino acid substitution: Phe159Tyr. This variant was designated Hxk2p-Y.

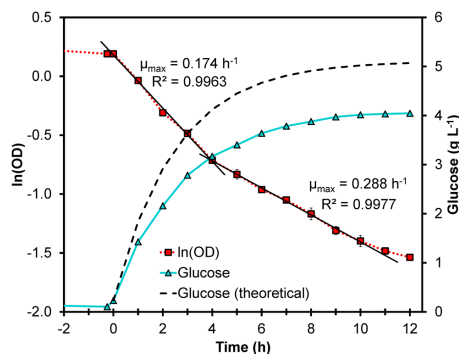


Figure 1. Selection of Hxk2p variants. The selection of Hxk2p variants was performed in anaerobic glucose limited chemostat cultivation with feed containing 5 g L^{-1} glucose and 50 g L^{-1} xylose. After 96 h of continuous cultivation of TMB3463 transformed with the *Hxk2*-library at $D=0.072 \text{ h}^{-1}$, the dilution rate was increased to $D=0.40 \text{ h}^{-1}$ (indicated as $t=0 \text{ h}$). During the washout the specific growth rate was calculated from the equation $d \ln(OD) dt^{-1} = \mu_{max} - D$. The natural logarithm of OD is shown as red squares (■). The washout profile displays two growth phases and the switching point occurs when the residual glucose concentration (▲) exceeds 3 g L^{-1} . After 10 h the glucose concentration stabilized at 4 g L^{-1} which reduced the selection pressure by inhibiting the uptake of xylose and thus slowed down the washout of cells. The measured accumulation of glucose was less than the theoretical (dashed line), calculated according to $S = S_{in} + (S_0 - S_{in}) \cdot e^{(1-D)t}$, showing that the consumption was not negligible. doi:10.1371/journal.pone.0075055.g001

The Phe159Tyr substitution confers increased resistance to xylose-induced inactivation

To evaluate the effect of the Phe159Tyr substitution on the catalytic activity, two new yeast strains were constructed: TMB3466 (Hxk2p-wt) and TMB3467 (Hxk2p-Y). Both strains lacked all genes encoding hexo- and glucokinases and the expression of the reintroduced gene was controlled by the constitutive *TDH3*-promoter to avoid glucose-controlled gene expression. Both strains were cultivated in anaerobic, glucose-limited chemostat at $D=0.22 \pm 0.01 \text{ h}^{-1}$, first with only glucose in the feed. When steady state had been established the feed was changed to also contain 30 g L^{-1} xylose which led to an accumulation of xylose inside the reactor. At steady state on glucose the two strains exhibited nearly the same specific glucose phosphorylating activity (Fig. 2); hence, the Phe159Tyr substitution had no detrimental effect on the catalytic function. At the second steady state, in the presence of ca. 30 g L^{-1} xylose, the wild-type enzyme lost 59% of the activity whereas the Hxk2p-Y variant only lost 40% (Fig. 2). During the accumulation of xylose there were no statistically significant differences between the two enzymes, although the activity profiles suggested that the wild-type enzyme lost the activity more rapidly than the Hxk2p-Y variant. Still, the 64% higher activity of the variant in the presence of xylose was statistically significant ($P=0.007$) showing that this single mutation indeed conferred higher resistance to xylose-induced inactivation without decreasing the normal catalytic capability.

Physiological responses of yeast strains harbouring the Hxk2p-Y variant

In the continuous cultivations of strains TMB3466 (Hxk2p-wt) and TMB3467 (Hxk2p-Y) with only glucose, there were significant

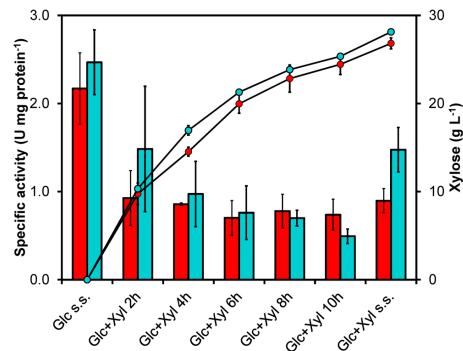


Figure 2. Specific glucose phosphorylating activity during xylose-induced inactivation of Hxk2p-wt and Hxk2p-Y. Specific glucose phosphorylating activity (bars) in strains TMB3466 (Hxk2p-wt) (red colour) and TMB3467 (Hxk2p-Y) (turquoise colour) in anaerobic glucose-limited chemostat cultivations. At steady state (s.s.) on glucose (Glc) the two strains exhibited similar activity but during the accumulation of xylose (Xyl; ●) the wild-type enzyme became inhibited faster than the variant. At steady state in the presence of xylose the variant had 64% higher specific activity compared with the wild-type. Specific activities were determined from duplicate biological experiments. At steady state conditions two different samples were collected with at least 2.5 volume changes in between. doi:10.1371/journal.pone.0075055.g002

differences in the yields of glycerol and biomass (Table 3). Strain TMB3467 had 23% ($P=0.04$) and 2.6% ($P=0.015$) higher yields of glycerol and biomass, respectively, compared to TMB3466. Yet, in this condition there was no significant difference in the glucose uptake rate (Table 3). In the presence of xylose, the glucose consumption rate in TMB3466 was reduced by 15% ($P=5\cdot10^{-5}$) while the consumption rate in TMB3467 was only reduced by 5% ($P=0.052$). Hence, the Hxk2p-Y variant enabled a 15% higher ($P=4\cdot10^{-4}$) specific glucose uptake rate in the presence of xylose compared with Hxk2p-wt. Despite the reduced consumption rate of glucose, TMB3466 did not change its physiology significantly with regard to production rates or product yields when exposed to xylose (Table 3). TMB3467, on the other hand, reduced the yield of biomass by 5.8% ($P=6\cdot10^{-5}$) but increased the ethanol production rate by 6.5% ($P=0.048$) (Table 3). Hence, TMB3467 had a 8.9% faster ($P=0.10$) ethanol production rate compared with the control strain in the presence of xylose (Table 3). Furthermore, the specific uptake rate of xylose by TMB3467 was 34% lower ($P=0.03$) compared to TMB3466 (Table 3). This might be due to improved repression of genes encoding unspecific aldose reductases that can convert xylose to xylitol [44]. In line with this observation, TMB3467 also had a 34% lower ($P=0.044$) xylitol yield compared to TMB3466 (Table 3), matching the difference in xylose uptake rate very well.

To investigate whether the increased resistance toward xylose-induced inactivation affected batch fermentation of a glucose/

xylose mixture, two new strains were constructed: TMB3492 (Hxk2p-wt) and TMB3493 (Hxk2p-Y). These strains assimilate xylose via the oxido-reductive pathway, consisting of a xylose reductase (XR) and a xylitol dehydrogenase (XDH) from *Scheffersomyces stipitis* and contain modifications known to improve xylose fermentation, such as increased activity of the enzymes in the non-oxidative pentose phosphate pathway and xylulokinase [45] as well as an engineered XR-variant with improved NADH preference [46]. The fermentation of 20 g L⁻¹ glucose and 50 g L⁻¹ xylose was evaluated in anaerobic batch cultivations (Fig. 3). However, there were no statistically significant differences between the two strains with regard to product yields per consumed xylose (Table S1) or per total amount of sugar consumed (Table S2). Strain TMB3493 had, however, a 64% faster ($P=0.095$) maximum specific consumption rate of xylose compared to the control strain (Table S1). During the period of fastest xylose consumption, TMB3493 also had a maximum growth rate more

Table 3. Specific consumption rates, production rates and yields in anaerobic glucose-limited chemostat cultures of TMB3466 (Hxk2p-wt) and TMB3467 (Hxk2p-Y).

	Glucose steady state		Glucose + xylose steady state	
	TMB3466	TMB3467	TMB3466	TMB3467
Specific rates (mmol g CDW⁻¹ h⁻¹)				
Glucose	-12.9±0.08	-13.2±0.5	-10.9±0.4	-12.5±0.3
Xylose	-	-	-2.75±0.59	-1.82±0.27
Glycerol	2.19±0.03	2.76±0.29	2.34±0.41	2.53±0.04
Acetate	0.15±0.02	0.23±0.09	0.21±0.08	0.20±0.02
Ethanol	20.6±2.43	21.7±1.0	21.3±1.9	23.2±0.6
Xylitol	-	-	0.32±0.09	0.22±0.05
CO ₂ ^a	21.6±2.44 ^b	22.9±0.9	22.4±1.8	24.3±0.6
Yields (g g sugar⁻¹)				
Glycerol	0.087±0.001	0.107±0.015	0.092±0.022	0.092±0.004
Acetate	0.004±0.001	0.006±0.002	0.006±0.002	0.005±0.000
Ethanol	0.391±0.045	0.402±0.003	0.395±0.010	0.404±0.018
Xylitol	-	-	0.020±0.005	0.013±0.002
Biomass	0.092±0.001	0.094±0.001	0.090±0.007	0.089±0.001
CO ₂	0.410±0.044	0.422±0.002	0.414±0.007	0.423±0.017
Carbon balance	99.1±8.7 ^b	103.7±1.5	102.2±1.1	103.1±3.5
Redox balance (%)	98.6±8.6 ^b	103.4±1.6	101.9±1.3	102.8±3.5

Values are given as mean ± standard deviation of four measurements from two biological experiments.

^aThe production rate of CO₂ was calculated from the production rates of ethanol, acetate and biomass according to the following relationships: 1 mol mol ethanol⁻¹, 1 mol mol acetate⁻¹ and 0.1 mol C-mol biomass⁻¹.

^bThe high standard deviation of these values was due to a single deviating measurement of ethanol in one experiment.

doi:10.1371/journal.pone.0075055.t003

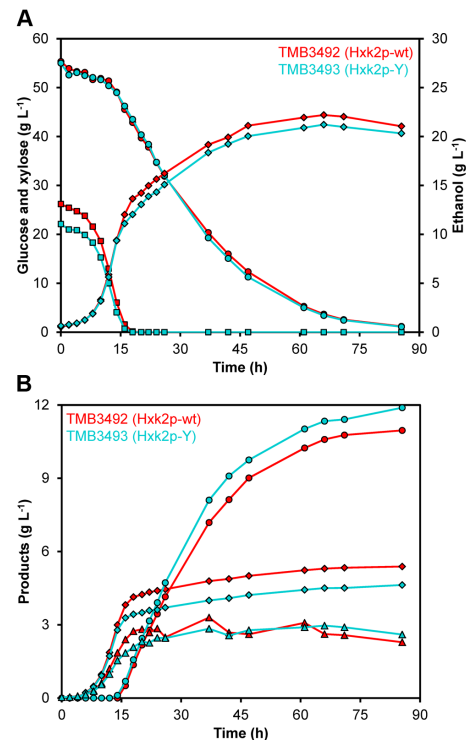


Figure 3. Anaerobic batch fermentation profiles of a glucose/xylose mixture. Fermentation experiments were performed using 2 × YNB medium containing 20 g L⁻¹ glucose and 50 g L⁻¹ xylose. Figures show representative values from one experiment out of two biological duplicates using TMB3492 (Hxk2p-wt) (red) and TMB3493 (Hxk2p-Y) (turquoise). **A)** Fermentation profiles of glucose (■) and xylose (●) consumption and production of ethanol (◆). **B)** Fermentation profiles of xylitol (●), glycerol (◆) and biomass (▲) formation. doi:10.1371/journal.pone.0075055.g003

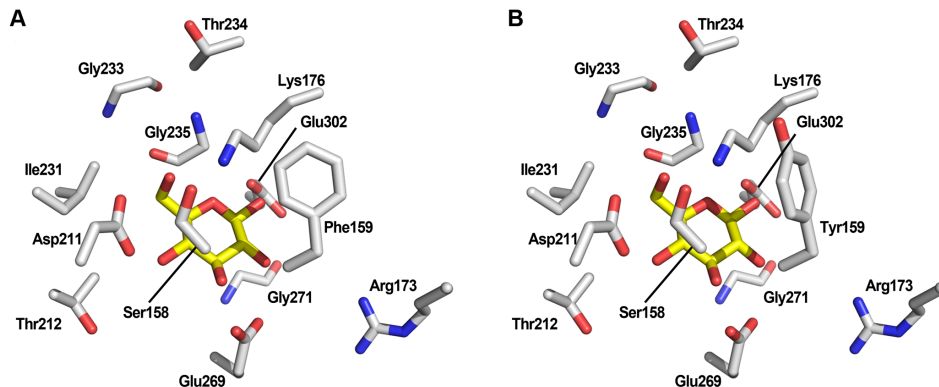


Figure 4. Homology models of the Hxk2p active site. The key residues in the active site of Hxk2p that selected for mutagenesis are displayed with corresponding label (see also Table 2). The position and orientation of the Phe159 and Tyr159 residues are shown in **A**) and **B**), respectively. Both figures show the orientation of the β -D-glucopyranose structure (yellow colour) in the active site.
doi:10.1371/journal.pone.0075055.g004

than double that of the control strain (0.027 h^{-1} and 0.013 h^{-1} , respectively) (Table S1). Although this difference was statistically significant at $P=0.037$, the limited extension of this growth rate resulted in nearly identical overall productivities of the two strains (Table S2).

Discussion

Previous studies on Hxk2p active-site have focused on the key catalytic residues involved in phosphate transfer, Ser158 or Asp211, by site-directed mutagenesis [22,23]. In this study we describe the first condensed, rationally designed combinatorial library [41,47] targeting the active-site in Hxk2p and the subsequent screening for mutations in the *HXX2* gene beneficial for resisting xylose-induced inactivation. This resulted in the identification of a protein variant, with the single amino acid substitution Phe159Tyr, which provides an increased glucose-phosphorylating activity in the presence of xylose.

The Phe159Tyr substitution does not impact negatively on the normal catalytic activity (Fig. 2), which is consistent with a widespread occurrence of tyrosine in position 159 among several hexokinases. For example, the Tyr159 residue is found in *S. cerevisiae* Hxk1p (PDB: 3B8A_X) and also in Hxk1p from the xylose-utilizing *Sc. stipitis* (NCBI RefSeq: XP_001386689). The occurrence of Tyr159 in the only hexokinase enzyme present in the xylose-utilizing *Sc. stipitis* supports our finding that it is beneficial for resisting xylose-induced inactivation. The Tyr159 residue is pointing towards the ATP-binding pocket and the additional hydroxyl group on the aromatic ring can generate a more polar environment at the edge of the glucose-binding pocket (Fig. 4). It is conceivable that the increased polarity generates an electron-rich draw on the phosphate group in ATP during the transition state, resulting in a lowered risk of autophosphorylation of the spatially close Ser158. Further studies are, however, needed to quantitate to what extent this novel substitution impacts i) the potential for autophosphorylation, ii) the kinetics of the enzyme and iii) the regulatory function.

The screening method used for identifying the Hxk2p-Y variant was designed to be rapid but still allowing the cells to grow at

maximum growth rate under the given conditions. A short cultivation time reduces the extent of unknown adaptive modifications [48] and biofilm formation, which could lead to an inefficient selection for fast-growing strains as cells attached to surfaces and cells suspended in the broth would compete for the available nutrients [49]. There is, however, a significant drawback with the adopted method, i.e. the loss of selection pressure. The decrease in cell concentration during the washout reduced the capacity to consume glucose. Hence, the residual glucose inevitably accumulated over time, preventing xylose from entering the cells and act on the Hxk2p enzyme. To avoid this problem, screening should be performed in a turbidostat [49,50] which can operate close to the maximum growth rate of the population while maintaining a low residual glucose concentration and high selection pressure.

The significant differences observed between strains TMB3466 and TMB3467 in xylose conversion at steady state (Table 3) suggest that Hxk2p has a role in the regulation of the endogenous xylose pathway in *S. cerevisiae*. There are four genes in *S. cerevisiae* encoding xylose reductases: *YJR096W*, *GCT1*, *GRE3* and *YPR1* [44]. Since the *GRE3* gene is disrupted in the parental strain TMB3042 used in this study, the observed conversion of xylose to xylitol is most likely catalysed by the *GCT1* or *YPR1* gene products. The BioGRID database (<http://thebiogrid.org>) lists one study in which a negative genetic interaction between *HXX2* and *GCT1* has been identified [51]. Hxk2p is known to regulate the expression of genes required for utilization of alternative carbon sources such as sucrose and galactose through the physical interactions with Med8p (*SUC2*) [15] and Rpt5p (*GAL1-10*) [52]. If xylose is also considered an alternative carbon source by *S. cerevisiae* it is plausible that the genes required for its utilization are also regulated by Hxk2p. However, further information is needed to confirm this hypothesis.

The new Hxk2p-Y variant can be applied in strains producing ethanol from lignocellulosic feedstocks. The hydrolysates produced from some of those materials are often rich in xylose [53]. Our hypothesis was that expressing a variant with improved repressive capability would increase the ethanol productivity by increasing the sugar consumption rate. This hypothesis is based on

experimental results showing that Hxk2p acts as an activator of *HXT1*-expression and as a repressor of *HXT2* and *HXT4-7* [18,19]. Hxt1p is a sugar transporter with low affinity and high transport capacity of both glucose and xylose; Hxt4p-7p, on the other hand, are high-affinity, low-capacity transporters [43]. When xylose is the sole carbon source mainly the low capacity transporters are present, even at high concentrations [28,29,30]. This makes the transport process inefficient since the available transporters easily become saturated with xylose. A fully functional Hxk2p in the presence of xylose might be enough to shift the expression of genes toward high-capacity transporters, leading to an increased uptake rate at high concentrations. The results presented here from anaerobic batch fermentations of glucose and xylose did indeed show a faster xylose uptake rate by the strain with the Hxk2p-Y variant (Table S1) which is in good agreement with the hypothesis. The increased uptake rate did, however, not lead to an increased production of ethanol but rather seemed to enable a faster initial growth rate on xylose. Unfortunately the extent of this growth period was very short indicating that the improved transport capacity must be combined with other regulatory factors induced by glucose. The identification of these factors requires further investigations. Still, the result obtained in this study is a first, but significant, step towards establishing a xylose repression signal in *S. cerevisiae*. Such a signal is most likely a prerequisite for an efficient conversion of xylose to bioethanol using recombinant *S. cerevisiae*.

Supporting Information

Figure S1 Construction of the mutated HXK2 megaprimer. The figure outlines the OE-PCR-based strategy used to construct the mutated *HXK2* megaprimer. The reader is referred to the Supporting information for detailed information. (TIFF)

Figure S2 Sequencing of the HXK2-library. The nucleotide sequences of the mutated regions are shown to the left. The top sequence is the native sequence and the bottom sequence contains the introduced degeneracy. Codons that were modified are underlined and the native and alternative amino acid residues are indicated with bold and white-on-black letters, respectively. The right panel shows the corresponding region from the electropherogram (note that Region 6 is shown as the reverse complement). Arrows indicate the point of the degeneracy and the dual signals show that the mutations are indeed introduced in the megaprimer. (TIFF)

Figure S3 Verification results of integration and gene deletion. A) Primers used with template from CEN.PK2-1C (positive control) and TMB3462. B) Amplification results of the set-up shown in A). C) Amplification of each gene using specific primers listed in Table S5. The reaction with template from TMB3462 contained primers for all genes. (TIFF)

Figure S4 Illustration of the 39 bases long linker used to create a multiple cloning site into the pUG6AUR plasmid. (TIFF)

References

1. Lobo Z, Maitra PK (1977) Physiological role of glucose-phosphorylating enzymes in *Saccharomyces cerevisiae*. Arch Biochem Biophys 182: 639–645.
2. Fernandez R, Herrero P, Gascon S, Moreno F (1984) Xylose-induced decrease in hexokinase PII activity confers resistance to carbon catabolite repression of invertase synthesis in *Saccharomyces carlsbergensis*. Arch Microbiol 139: 139–142.

Figure S5 The pUG62AUR plasmid with a multiple cloning site consisting of the *AvrII*, *SphI*, *SmaI* and *KpnI* restriction sites. (TIFF)

Figure S6 The pUG62AUR-HXK1USDS plasmid containing homologous regions flanking the *HXK1* gene. (TIFF)

Figure S7 The glucose phosphorylating activity in strains TMB3462 (3A) and TMB3463 (4A) relative to the wild-type CEN.PK2-1C strain. (TIFF)

Table S1 Maximum specific consumption rates, production rates and yields in anaerobic batch fermentation of 20 g L⁻¹ glucose and 50 g L⁻¹ xylose by TMB3492 (Hxk2p-wt) and TMB3493 (Hxk2p-Y). Values are given as mean \pm standard deviation of two independent experiments. (DOC)

Table S2 Overall yields and production rates in anaerobic batch fermentation of 20 g L⁻¹ glucose and 50 g L⁻¹ xylose by TMB3492 (Hxk2p-wt) and TMB3493 (Hxk2p-Y). Values are given as mean \pm standard deviation of two independent experiments. (DOC)

Table S3 Primers used to construct the mutated *HXK2* megaprimer. (DOC)

Table S4 Primers used to construct deletion cassettes. (DOC)

Table S5 Primers used to confirm correct integration and gene deletion. (DOC)

Table S6 Primers used to amplify additional fragments upstream and downstream the *HXK1* gene. Restriction sites are indicated in bold. (DOC)

Table S7 Primers used to confirm correct integration of pUG62AUR-HXK1USDS and *HXK1*-gene deletion. (DOC)

Methods S1 Engineering yeast hexokinase 2 for improved tolerance toward xylose-induced inactivation. (PDF)

Acknowledgments

We wish to acknowledge Mirna Sallaku for her help with the structural analysis of Hxk2p.

Author Contributions

Conceived and designed the experiments: BB AGS. Performed the experiments: BB AGS CB TB. Analyzed the data: BB AGS EWJvN MFGG. Wrote the paper: BB AGS.

5. Gancedo C, Flores CL (2008) Moonlighting proteins in yeasts. *Microbiol Mol Biol Rev* 72: 197–210.
6. Schuller HJ (2003) Transcriptional control of nonfermentative metabolism in the yeast *Saccharomyces cerevisiae*. *Curr Genet* 43: 139–160.
7. Sutherland CM, Hawley SA, McCartney RR, Leech A, Stark MJR, et al. (2003) Elm1p is one of three upstream kinases for the *Saccharomyces cerevisiae* SNF1 complex. *Curr Biol* 13: 1299–1305.
8. Sanz P, Alms GR, Haystead TAJ, Carlson M (2000) Regulatory interactions between the Reg1-Glc7 protein phosphatase and the Snf1 protein kinase. *Mol Cell Biol* 20: 1321–1328.
9. Treitel MA, Kuchin S, Carlson M (1998) Snf1 protein kinase regulates phosphorylation of the Mig1 repressor in *Saccharomyces cerevisiae*. *Mol Cell Biol* 18: 6273–6280.
10. Ludin K, Jiang R, Carlson M (1998) Glucose-regulated interaction of a regulatory subunit of protein phosphatase 1 with the Snf1 protein kinase in *Saccharomyces cerevisiae*. *Proc Natl Acad Sci USA* 95: 6245–6250.
11. Fernandez-Garcia P, Pelaez R, Herrero P, Moreno F (2012) Phosphorylation of yeast hexokinase 2 regulates its nucleocytoplasmic shuttling. *J Biol Chem* 287: 42151–42164.
12. Pelaez R, Fernandez-Garcia P, Herrero P, Moreno F (2012) Nuclear import of the yeast hexokinase 2 protein requires alpha/beta-Importin-dependent pathway. *J Biol Chem* 287: 3518–3529.
13. Ahuatzí D, Riera A, Pelaez R, Herrero P, Moreno F (2007) Hxk2 regulates the phosphorylation state of Mig1 and therefore its nucleocytoplasmic distribution. *J Biol Chem* 282: 4485–4493.
14. Pelaez R, Herrero P, Moreno F (2010) Functional domains of yeast hexokinase 2. *Biochem J* 432: 181–190.
15. de la Cera T, Herrero P, Moreno-Herrero F, Chaves RS, Moreno F (2002) Mediator factor Med8p interacts with the hexokinase 2: Implication in the glucose signalling pathway of *Saccharomyces cerevisiae*. *J Mol Biol* 319: 703–714.
16. DeVit MJ, Johnston M (1999) The nuclear exportin Msn5 is required for nuclear export of the Mig1 glucose repressor of *Saccharomyces cerevisiae*. *Curr Biol* 9: 1231–1241.
17. Schuurmans JM, Rossell SL, van Tuijl A, Bakker BM, Hellingwerf KJ, et al. (2008) Effect of *hsk2* deletion and *HAP1* overexpression on fermentative capacity in *Saccharomyces cerevisiae*. *FEMS Yeast Res* 8: 195–203.
18. Schuurmans JM, Boersma A, Lascaris R, Hellingwerf KJ, Teixeira de Mattos MJ (2008) Physiological and transcriptional characterization of *Saccharomyces cerevisiae* strains with modified expression of catabolic regulators. *FEMS Yeast Res* 8: 26–34.
19. Özcan S, Johnston M (1995) Three different regulatory mechanisms enable yeast hexose transporter (*HXT*) genes to be induced by different levels of glucose. *Mol Cell Biol* 15: 1564–1572.
20. Noubhani A, Bonoust O, Bonini BM, Thevelein JM, Devin A, et al. (2009) The trehalose pathway regulates mitochondrial respiratory chain content through hexokinase 2 and cAMP in *Saccharomyces cerevisiae*. *J Biol Chem* 284: 27229–27234.
21. Fernandez R, Herrero P, Fernandez MT, Moreno F (1986) Mechanism of inactivation of hexokinase PII of *Saccharomyces cerevisiae* by D-xylose. *J Gen Microbiol* 132: 3467–3472.
22. Heidrich K, Otto A, Behlke J, Rush J, Wenzel KW, et al. (1997) Autophosphorylation-inactivation site of hexokinase 2 in *Saccharomyces cerevisiae*. *Biochemistry* 36: 1960–1964.
23. Kraakman LS, Windericks J, Thevelein JM, De Winde JH (1999) Structure-function analysis of yeast hexokinase: structural requirements for triggering cAMP signalling and catabolic repression. *Biochem J* 343: 159–168.
24. Rolland F, de Winde JH, Lemaire K, Boles E, Thevelein JM, et al. (2000) Glucose-induced cAMP signalling in yeast requires both a G-protein coupled receptor system for extracellular glucose detection and a separable hexose kinase-dependent sensing process. *Mol Microbiol* 38: 348–358.
25. Zaman S, Lippman SI, Schnepel L, Slonim N, Broach JR (2009) Glucose regulates transcription in yeast through a network of signaling pathways. *Mol Syst Biol* 5.
26. Sasser P, Galhe M, Zacchi G (2008) Techno-economic evaluation of bioethanol production from three different lignocellulosic materials. *Biomass Bioenergy* 32: 422–430.
27. Hahn-Hagerdal B, Karhumaa K, Fonseca C, Spencer-Martins I, Gorwa-Grauslund MF (2007) Towards industrial pentose-fermenting yeast strains. *Appl Microbiol Biotechnol* 74: 937–953.
28. Runquist D, Hahn-Hagerdal B, Bettiga M (2009) Increased expression of the oxidative pentose phosphate pathway and microencapsulation in anaerobically growing xylose-utilizing *Saccharomyces cerevisiae*. *Microb Cell Fact* 8.
29. Salusjärvi I, Pitkanen JP, Aristidou A, Ruohonen L, Penttilä M (2006) Transcription analysis of recombinant *Saccharomyces cerevisiae* reveals novel responses to xylose. *Appl Biochem Biotechnol* 128: 237–261.
30. Jin YS, Laplaza JM, Jeffries TW (2004) *Saccharomyces cerevisiae* engineered for xylose metabolism exhibits a respiratory response. *Appl Environ Microbiol* 70: 6816–6825.
31. Klimacek M, Krahulec S, Sauer U, Nidetzky B (2010) Limitations in xylose-fermenting *Saccharomyces cerevisiae*, made evident through comprehensive metabolite profiling and thermodynamic analysis. *Appl Environ Microbiol* 76: 7566–7574.
32. Bergdahl B, Heer D, Sauer U, Hahn-Hagerdal B, van Niel EW (2012) Dynamic metabolomics differentiates between carbon and energy starvation in recombinant *Saccharomyces cerevisiae* fermenting xylose. *Biotechnol Biofuels* 5: 34.
33. Gietz RD, Schiestl RH (2007) High-efficiency yeast transformation using the LiAc/SS carrier DNA/PEG method. *Nat Protoc* 2: 31–34.
34. Verdun C, Postma E, Scheffers WA, Van Dijken JP (1992) Effect of benzoic acid on metabolic fluxes in yeasts: a continuous-culture study on the regulation of respiration and alcoholic fermentation. *Yeast* 8: 501–517.
35. Sambrook J, Fritsch EF, Maniatis T (1989) Molecular cloning: A laboratory manual. Cold Spring Harbor: Cold Spring Harbor Laboratory Press.
36. Arnold K, Bordoli L, Kopp J, Schwede T (2006) The SWISS-MODEL workspace: a web-based environment for protein structure homology modelling. *Bioinformatics* 22: 195–201.
37. Horton RM, Hunt HD, Ho SN, Pullen JK, Pease LR (1989) Engineering hybrid genes without the use of restriction enzymes: gene splicing by overlap extension. *Gene* 77: 61–68.
38. Miyazaki K (2003) Creating random mutagenesis libraries by megaprimer PCR of whole plasmid (MEGAWHOP). *Methods Mol Biol* 231: 23–28.
39. Gietz RD, Schiestl RH (2007) Large-scale high-efficiency yeast transformation using the LiAc/SS carrier DNA/PEG method. *Nat Protoc* 2: 38–41.
40. Firth AE, Patrick WM (2005) Statistics of protein library construction. *Bioinformatics* 21: 3314–3315.
41. Sandström AG, Wikmark Y, Engström K, Nyhlen J, Backvall JE (2012) Combinatorial reshaping of the *Candida antarctica* lipase A substrate pocket for enantioselectivity using an extremely condensed library. *Proc Natl Acad Sci USA* 109: 78–83.
42. Hoog C, Widmalm G (2001) Free energy simulations of D-xylose in water and methyl D-xylopyranoside in methanol. *J Phys Chem B* 105: 6375–6379.
43. Saloheimo A, Rauta J, Stasyk OV, Sibiryi AA, Penttilä M, et al. (2007) Xylose transport studies with xylose-utilizing *Saccharomyces cerevisiae* strains expressing heterologous and homologous permeases. *Appl Microbiol Biotechnol* 74: 1041–1052.
44. Träff KL, Jönsson LJ, Hahn-Hagerdal B (2002) Putative xylose and arabinose reductases in *Saccharomyces cerevisiae*. *Yeast* 19: 1233–1241.
45. Karhumaa K, Hahn-Hagerdal B, Gorwa-Grauslund MF (2005) Investigation of limiting metabolic steps in the utilization of xylose by recombinant *Saccharomyces cerevisiae* using metabolic engineering. *Yeast* 22: 359–368.
46. Runquist D, Hahn-Hagerdal B, Bettiga M (2010) Increased ethanol productivity in xylose-utilizing *Saccharomyces cerevisiae* via a randomly mutagenized xylose reductase. *Appl Environ Microbiol* 76: 7796–7802.
47. Reetz MT, Wu S (2008) Greatly reduced amino acid alphabets in directed evolution: making the right choice for saturation mutagenesis at homologous enzyme positions. *Chem Commun*: 5499–5501.
48. Sauer U (2001) Evolutionary engineering of industrially important microbial phenotypes. *Adv Biochem Eng Biotechnol* 73: 129–169.
49. Gostomski P, Muhlemann M, Lin YH, Mormino R, Bungay H (1994) Auxostats for continuous-culture research. *J Biotechnol* 37: 167–177.
50. Bryson V (1952) Microbial Selection Part 2. The turbidostat selector - A device for automatic isolation of bacterial variants. *Science* 116: 48–51.
51. Costanzo M, Baryshnikova A, Bellay J, Kim Y, Spear ED, et al. (2010) The genetic landscape of a cell. *Science* 327: 425–431.
52. Guerrero C, Milenković T, Pržulj N, Kaiser P, Huang I (2008) Characterization of the proteasome interaction network using a QTAG-based tag-team strategy and protein interaction network analysis. *Proc Natl Acad Sci USA* 105: 13333–13338.
53. Gírio FM, Fonseca C, Carvalheiro F, Duarte LC, Marques S, et al. (2010) Hemicelluloses for fuel ethanol: A review. *Bioresour Technol* 101: 4775–4800.
54. Mumberg D, Müller R, Funk M (1995) Yeast vectors for the controlled expression of heterologous proteins in different genetic backgrounds. *Gene* 156: 119–122.
55. Guldener U, Heck S, Fielder T, Beinhauer J, Hegemann JH (1996) A new efficient gene disruption cassette for repeated use in budding yeast. *Nucleic Acids Res* 24: 2519–2524.
56. Johansson B (2001) Metabolic Engineering of the Pentose Phosphate Pathway of Xylose Fermenting *Saccharomyces cerevisiae* [Doctoral Thesis]. Lund: Lund University.
57. Gietz RD, Sugino A (1988) New yeast-*Escherichia coli* shuttle vectors constructed with in vitro mutagenized yeast genes lacking six-base pair restriction sites. *Gene* 74: 527–534.
58. Runquist D, Fonseca C, Rådström P, Spencer-Martins I, Hahn-Hagerdal B (2009) Expression of the Gx1 transporter from *Candida intermedia* improves fermentation performance in recombinant xylose-utilizing *Saccharomyces cerevisiae*. *Appl Microbiol Biotechnol* 82: 123–130.

Supporting Information[†] for:

Engineering yeast hexokinase 2 for improved tolerance toward xylose-induced inactivation

Basti Bergdahl^{1,*}, Anders G. Sandström¹, Celina Borgström¹, Tarinee Boonyawan^{1,†}, Ed W.J. van Niel¹ and Marie F. Gorwa-Grauslund¹

¹ Division of Applied Microbiology, Department of Chemistry, Lund University, P.O. Box 124, SE-22100 Lund, Sweden

[†] Current address: Centre of Medical Excellence, Faculty of Medicine, Chiang Mai University, 110 Intavaroros, Amphur Muang, Chiang Mai 50200, Thailand.

* To whom correspondence should be addressed. E-mail: basti.bergdahl@tmb.lth.se (B.B.)

[†] Reformatted for increased readability by Celina Borgström Tufvegren

Contents

Supplementary Methods	2
Construction of the <i>E. coli</i> library of Hxk2p-variants	2
Cloning of the <i>HXK2</i> locus.....	2
Generating the plasmid library using the MEGAWHOP procedure.....	4
Construction of strains TMB3460, TMB3461 and TMB3462	6
Construction of TMB3460 (<i>hxx2-Δ</i>)	6
Construction of TMB3461 (<i>hxx2-Δ hxx1-Δ1</i>).....	6
Construction of TMB3462 (<i>hxx2-Δ hxx1-Δ1 glk1-Δ</i>)	7
Construction of the screening strain TMB3463	8
Generation of plasmid pUG62AUR	8
Construction of TMB3463 (<i>hxx2-Δ hxx1-Δ1 glk1-Δ hxx1-Δ2</i>).....	9
Supplementary Tables S1 to S7.....	12

Supplementary Methods

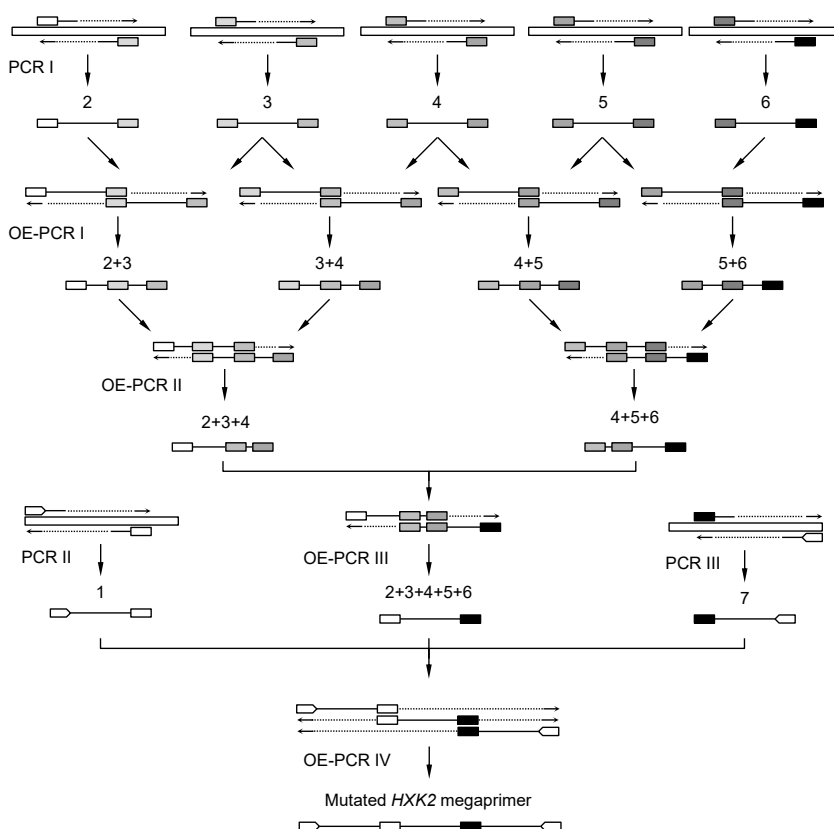
Construction of the *E. coli* library of Hxk2p-variants

Cloning of the *HXK2* locus

The locus was amplified using primers HXK2_loc_f (5'-GCT TGC ATG CAC GCC ATA GAA GAG CAA TTT CCG TCC-3') and HXK2_loc_r (5'-CCG GGG ATC CGA GAG GGT TAA AAT TGG CGT GCA ATT TTA TGA AG-3'). The high fidelity Phusion Hotstart II polymerase (Thermo Scientific, USA) was used with the following PCR program: 30 s initial denaturation at 98°C, 30 cycles of 10 s denaturation at 98°C, 30 s annealing at 65°C and 1 min elongation at 72°C, and a final 10 min elongation step at 72°C. The resulting DNA fragment was digested with *Bam*HI and *Sph*I (FastDigest, Thermo Scientific, USA) at 37°C for 30 min and ligated into YIplac128, linearized with the same restriction enzymes. The ligation system was subsequently used to transform *E. coli* NEB5α.

Construction of the mutated *HXK2* megaprimer

The strategy used to construct the mutated *HXK2* megaprimer is outlined in Figure S1 and the primers are listed in Table S3.



Supplementary Figure S1. Construction of the mutated *HXK2* megaprimer

Unless stated otherwise the PCR reactions contained 1× HF Buffer, 0.2 mM of each dNTP, 0.01 U μL^{-1} Phusion Hotstart DNA Polymerase II and 0.5 μM each of forward and reverse primers. The reaction volume was 50 μL . OE-PCR reactions contained 30 fmol of each fragment. DNA fragments amplified by PCR were purified using GeneJet PCR Purification Kit (Thermo Scientific, USA) unless stated otherwise.

PCR I: Mutated fragments were amplified from YIpBB5 using the following PCR program: 30 s denaturation at 98°C, 30 cycles of 10 s denaturation at 98°C, 5 s annealing and extension at 72°C and 1 cycle of 10 min extension at 72°C. Primers were used according to the following scheme:

Fragment 2: Group_1_f and Group_2_r

Fragment 3: Group_2_f and Group_3_r

Fragment 4: Group_3_f and Group_4_r

Fragment 5: Group_4_f and Group_5_r

Fragment 6: Group_5_f and Group_6_r

PCR II: The non-mutated fragments were amplified from YIpBB5 using the following PCR program: 30 s denaturation at 98°C, 20 cycles of 10 s denaturation at 98°C, 15 s annealing at 72°C (-0.5°C cycle⁻¹), 30 s extension at 72°C, 16 cycles of 10 s denaturation at 98°C, 15 s annealing at 62.4°C, 30 s extension at 72°C and 1 cycle of 10 min extension at 72°C. Primers were used according to the following scheme:

Fragment 1: Yip128-F1 and Group_1_r

Fragment 7: Group_6_f and Yip128-R1

OE-PCR I: The two fragments were joined using 1× GC buffer in the reaction mix and the following PCR program: 30 s denaturation at 98°C, 16 cycles of 10 s denaturation at 98°C, 30 s annealing at 70°C (-0.5°C cycle⁻¹) and 30 s extension at 72°C. At this point the reaction was halted at 4°C until primers had been added after which the program was repeated. The program was finished with a final 10 min extension at 72°C. The primers were added to a final concentration of 0.52 μM according to the following scheme:

Fragment 2+3: Group_1_f and Group_3_r

Fragment 3+4: Group_2_f and Group_4_r

Fragment 4+5: Group_3_f and Group_5_r

Fragment 5+6: Group_4_f and Group_6_r

OE-PCR II: The two fragments were joined using the same procedure as in OE-PCR I. The primers were added to a final concentration of 0.52 μM according to the following scheme:

Fragment 2+3+4: Group_1_f and Group_4_r

Fragment 4+5+6: Group_3_f and Group_6_r

OE-PCR III: The two fragments were joined using the same procedure as in OE-PCR I. The primers Group_1_f Group_6_r and were added to a final concentration of 0.52 μM .

OE-PCR IV: The three fragments were joined using the following PCR program: 30 s denaturation at 98°C, 16 cycles of 10 s denaturation at 98°C, 30 s annealing at 70°C (-0.5°C cycle⁻¹), 30 s extension at 72°C and 1 cycle of 5 min extension at 72°C. At this point the reaction was halted at 4°C until primers had been added after which the program was repeated. The program was finished with a final 10 min extension at 72°C. The primers Yip128-F1 and Yip128-R1 were added to a final concentration of 0.52 µM.

The final megaprimer was purified from 0.8% agarose gel using the QIAquick Gel Extraction Kit (Qiagen, Germany).

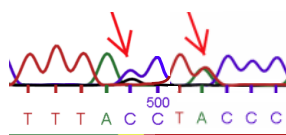
Generating the plasmid library using the MEGAWHOP procedure

The MEGAWHOP reaction mixture (50 µL) contained the following: 1× HF Buffer, 0.2 mM of each dNTP, 503 ng of HXK2 megaprimer, 50.1 ng of template plasmid YIpBB5 and 0.02 U µL⁻¹ Phusion Hotstart DNA Polymerase II. The whole plasmid amplification was performed using the following PCR program: 30 s denaturation at 98°C, 25 cycles of 10 s denaturation at 98°C, 15 s annealing at 58°C and 3 min extension at 72°C.

After completing the PCR reaction, 0.8 µL *DpnI* (20 U µL⁻¹) was added to 40 µL of the MEGAWHOP reaction mixture and incubated for 2 h at 37°C. AT the same time a negative control (40 µL) containing 1× HF Buffer and 1 ng µL⁻¹ YIpBB5 was treated equally. 2 µL and 5 µL of *DpnI*-treated MEGAWHOP reaction was used to transform commercial heat shock competent *E. coli* NEB5α (High Efficiency, New England Biolabs, USA) according to the supplier's instructions. Transformants were selected on solid LB-medium supplemented with 100 mg L⁻¹ ampicillin. Both transformations generated ca. 7700 cfu mL⁻¹. 5 µL of the negative control did not result in any transformants. Five additional transformation reactions of NEB5α were performed generating a total *E. coli* library of 57,370 ± 3261 cfu. These transformants were inoculated in 100 mL of LB-medium supplemented with 100 mg mL⁻¹ of ampicillin and grown for 16 h at 37°C. The resulting culture was aliquoted in 25% glycerol and stored at -80°C. Part of the culture was used to purify and sequence the plasmids. This confirmed that all mutations were present in the plasmid mix (Fig. S2).

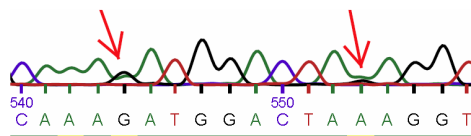
Region 1

F S F P
 469 TTTTCTTCCCA
 |||.:.|:||||
 469 TTTASCTWCCCA
 F **T** **Y** P



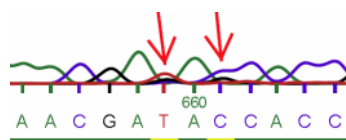
Region 2

Q R W T K G
 514 CAAAGATGGACTAAAGGT
 ||||:|||||||:||||
 514 CAAARATGGACTARAGGT
 Q **K** W T **R** G



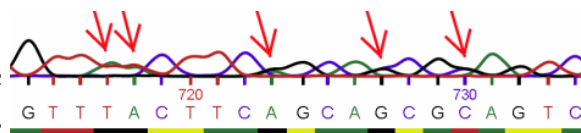
Region 3

N D T T
 628 AACGACACTACC
 |||||.|:..|||
 628 AACGAKASCACC
 N **D** **S** T



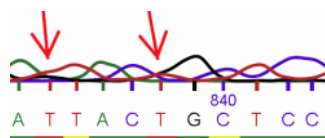
Region 4

V I F G T G V
 688 GTTATCTTCGGTACTGGTGTC
 |||:|||||.|.|.|.|.|||
 688 GTTWWCTTCRGCASCAGSAGTC
 V **N** F **S** **S** **A** V



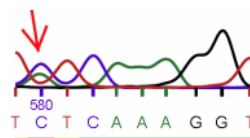
Region 5

E Y G S
 805 GAATACGGTTC
 ||.||||:|.|||
 805 GAKTACKGCTCC
D Y **C** S



Region 6

F E K
 901 TTTGAAAA
 |||||.|||
 901 TTTGAKAAA
 F **D** K



OBS. Reverse sequence.

Supplementary Figure S2. Sequencing of the HXK2-library

The nucleotide sequences of the mutated regions are shown to the left. The top sequence is the native sequence and the bottom sequence contains the introduced degeneracy. Codons that were modified are underlined and the native and alternative amino acid residues are indicated with bold and white-on-black letters, respectively. The right panel shows the corresponding region from the electropherogram (note that Region 6 is shown as the reverse complement). Arrows indicate the point of the degeneracy and the dual signals show that the mutations are indeed introduced in the megaprimer.

Construction of strains TMB3460, TMB3461 and TMB3462

Unless stated otherwise the PCR reactions contained 1× HF Buffer, 0.2 mM of each dNTP, 0.01 U μL^{-1} Phusion Hotstart DNA Polymerase II and 0.5 μM each of forward and reverse primers (Table S4). The reaction volume was 50 μL . OE-PCR reactions contained 200 fmol of each fragment. DNA fragments amplified by PCR were purified from 0.8% agarose gel using the QIAquick Gel Extraction Kit (Qiagen, Germany) unless stated otherwise.

Verification of correct integration and gene deletion was performed using the primers listed in Table S5 and the following reaction mix: 1× DreamTaq Buffer, 0.2 mM of each dNTP, 0.3 μM each of forward and reverse primers and 1 U μL^{-1} DreamTaq DNA Polymerase.

Construction of TMB3460 (*hxx2-Δ*)

The upstream and downstream fragments flanking the *HXX2* gene were amplified from genomic DNA from *S. cerevisiae* CEN.PK2-1C using the following PCR program: 30 s denaturation at 98°C, 30 cycles of 10 s denaturation at 98°C, 30 s annealing at 65°C (-0.5°C cycle⁻¹), 15 s extension at 72°C and 1 cycle of 10 min extension at 72°C.

The auxotrophic marker cassette *TRP1* was amplified from plasmid p424 using the following PCR program: 30 s denaturation at 98°C, 30 cycles of 10 s denaturation at 98°C, 30 s annealing at 65°C (-0.5°C cycle⁻¹), 1 min extension at 72°C and 1 cycle of 10 min extension at 72°C.

The deletion cassette *HXX2_US-TRP1-HXX2_DS* was created by OE-PCR using the following PCR program: 30 s denaturation at 98°C, 16 cycles of 10 s denaturation at 98°C, 30 s annealing at 68°C (-0.5°C cycle⁻¹) and 1 min extension at 72°C. At this point the reaction was halted at 4°C until primers *HXX2_US_f* and *HXX2_DS_r* had been added after which the program continued: 30 s denaturation at 98°C, 20 cycles of 10 s denaturation at 98°C, 30 s annealing at 63°C (-0.4°C cycle⁻¹) and 1 min extension at 72°C. The program was finished with a final 10 min extension at 72°C.

The amplified deletion cassette was purified and used to transform TMB3042. Transformants were selected on solid YNB medium with 2% glucose, 50 mg L⁻¹ uracil and 220 mg L⁻¹ leucine. Correct integration was verified by PCR amplification from chromosomal DNA of randomly selected colonies using primers *HXX2_823US_f* and *TRP1_71_r*. One positive clone was named TMB3460.

Construction of TMB3461 (*hxx2-Δ hxx1-Δ1*)

The upstream and downstream fragments flanking the *HXX1* gene were amplified from genomic DNA from *S. cerevisiae* CEN.PK2-1C. The auxotrophic marker cassette *URA3* was amplified from plasmid p426. All fragments were amplified using the following PCR program: 30 s denaturation at 98°C, 30 cycles of 10 s denaturation at 98°C, 30 s annealing at 65°C (-0.5°C cycle⁻¹), 1 min s extension at 72°C and 1 cycle of 10 min extension at 72°C.

The deletion cassette HXK1_US-*URA3*-HXK1_DS was created by OE-PCR using the following PCR program: 30 s denaturation at 98°C, 16 cycles of 10 s denaturation at 98°C, 30 s annealing at 68°C (-0.5°C cycle⁻¹) and 1 min extension at 72°C. At this point the reaction was halted at 4°C until primers HXK1_US_f and HXK1_DS_r had been added after which the program continued: 30 s denaturation at 98°C, 20 cycles of 10 s denaturation at 98°C, 30 s annealing at 67°C (-0.4°C cycle⁻¹) and 1 min extension at 72°C. The program was finished with a final 10 min extension at 72°C.

The amplified deletion cassette was purified and used to transform TMB3460. Transformants were selected on solid YNB medium with 2% galactose and 220 mg L⁻¹ leucine. Correct integration was verified by PCR amplification from chromosomal DNA of randomly selected colonies using primers HXK1_1510US_f and *URA3*_120_r. One positive clone was named TMB3461.

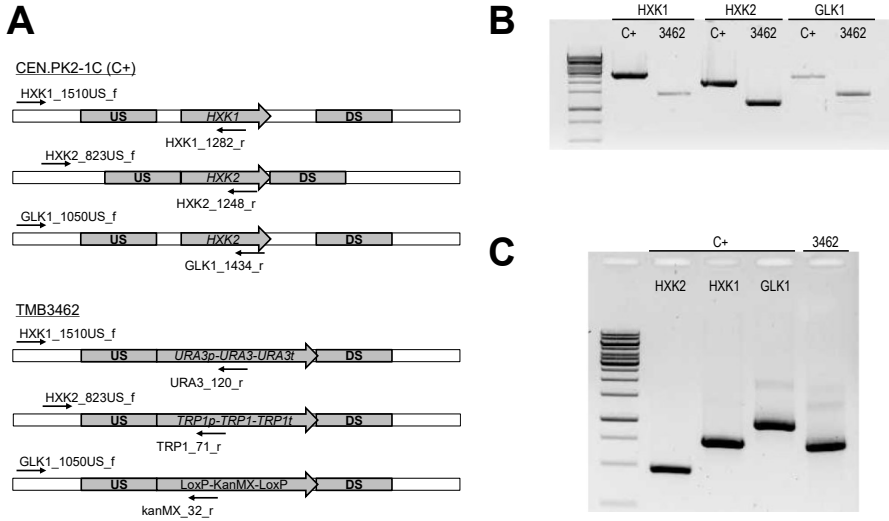
Construction of TMB3462 (*hxx2-Δ hxx1-Δ1 glk1-Δ*)

The upstream and downstream fragments flanking the *GLK1* gene were amplified from genomic DNA from *S. cerevisiae* CEN.PK2-1C. The antibiotic marker cassette *LoxP-KanMX-LoxP* was amplified from plasmid pUG6. All fragments were amplified using the following PCR program: 30 s denaturation at 98°C, 30 cycles of 10 s denaturation at 98°C, 30 s annealing at 67°C (-0.5°C cycle⁻¹), 1 min extension at 72°C and 1 cycle of 10 min extension at 72°C.

The deletion cassette GLK1_US-[*LoxP-KanMX-LoxP*]-GLK1_DS was created by OE-PCR using the following PCR program: 30 s denaturation at 98°C, 16 cycles of 10 s denaturation at 98°C, 30 s annealing at 68°C (-0.5°C cycle⁻¹) and 1 min extension at 72°C. At this point the reaction was halted at 4°C until primers GLK1_US_f and GLK1_DS_r had been added after which the program continued: 30 s denaturation at 98°C, 20 cycles of 10 s denaturation at 98°C, 30 s annealing at 68.5°C (-0.4°C cycle⁻¹) and 1 min extension at 72°C. The program was finished with a final 10 min extension at 72°C.

The amplified deletion cassette was purified and used to transform TMB3461. Transformants were selected on solid YNB medium with 2% galactose, 220 mg L⁻¹ leucine and 200 mg L⁻¹ geneticin. Correct integration was verified by PCR amplification from chromosomal DNA of randomly selected colonies using primers GLK1_1050US_f and *kanMX*_32_r. One positive clone was named TMB3462.

Investigation of the glucose phosphorylating activity in strain TMB3462 revealed a significant level of activity despite confirmation of all deletion cassettes. Amplification of each gene using specific primers (Table S5) revealed that *HXX1* was still present in the genome (Fig. S3).



Supplementary Figure S3. Verification results of integration and gene deletion.

A) Primers used with template from CEN.PK2-1C (positive control) and TMB3462. **B)** Amplification results of the set-up shown in **A)**. **C)** Amplification of each gene using specific primers listed in Table S5. The reaction with template from TMB3462 contained primers for all genes.

Construction of the screening strain TMB3463

Generation of plasmid pUG62AUR

To facilitate the use of pUG6AUR, a new multiple cloning site was created near the LoxP site upstream of the aureobasidin A resistance gene using linkers. These linkers consisted of two long oligonucleotides, 37 and 35 bases, respectively, and were complimentary except for the sticky ends. These were instead complementary to the restriction sites *SalI* and *NdeI* present in the pUG6AUR plasmid. All in all, the linkers included six different restriction sites: *SalI*, *KpnI*, *SmaI*, *SphI*, *AvrII* and *NdeI* (Fig. S4).

Linker oligomers:

5'-TCGACCTGAGGTACCCGGGCATGCATCCTAGGTGCA-3'
 3'-GGACTCCATGGGGCCGTACGTAGGATCCACGTAT-5'
 SalI *KpnI* *SmaI* *SphI* *AvrII* *NdeI*

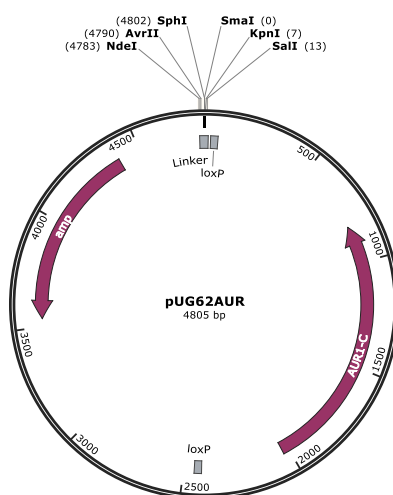
Restriction sites:

<i>SalI</i>	5'...G [^] ATCGAC...3'	<i>SmaI</i>	5'...CC [^] CGGG...3'	<i>AvrII</i>	5'...C [^] ATAGG...3'
	3'...CAGCTAG...5'		3'...GGG [^] ACCC...5'		3'...GGATC [^] AG...5'
<i>KpnI</i>	5'...GGGTAC...3'	<i>SphI</i>	5'...GCATG...3'	<i>NdeI</i>	5'...CA [^] TATG...3'
	3'...C [^] ATGGA...5'		3'...C [^] GTACG...5'		3'...GTA [^] TAC...5'

Supplementary Figure S4. Illustration of the 39 bases long linker used to create a multiple cloning site into the pUG6AUR plasmid.

The linker oligomers were annealed to each other by mixing 500 pmol of each oligonucleotide with 6 μmol NaCl in 1 \times DreamTaq Buffer (final volume 30 μL) and incubated at 100°C in a Thermocycler for 5 min. The temperature was then lowered slowly at 1°C min⁻¹ until a temperature of 4°C was reached. The salt was removed through alcohol precipitation. 1 mL 99.5 % ethanol was added to the 30 μL mix and incubated at -80°C for 10 min. The tube was centrifuged for 12 min at 4°C and the supernatant was discarded. The pellet was washed once with 500 μL of 70% ethanol after which the pellet was dried in room temperature for 10 min. The small pellet was finally dissolved in 25 μL TE buffer giving an estimated concentration of 20 μM (ca. 475 ng μL^{-1}).

The annealed linkers were ligated to pUG6AUR, previously digested with *SalI* and *NdeI*, in a 20 μL reaction containing the following: 1 \times Fast Digest Green Buffer, 50 ng μL^{-1} linker, 12.5 ng μL^{-1} linear pUG6AUR, 5% (w v⁻¹) PEG 4000, 0.5 mM ATP and 0.125 U μL^{-1} T4 DNA Ligase. The ligation mixture was incubated at room temperature for 60 min after which the ligase was inactivated at 70°C for 5 min. 2 μL of the ligation mix was removed and diluted to a final concentration of 2.5 ng plasmid μL^{-1} . 5 μL of the diluted ligation mix was used to transform heat shock competent *E. coli* NEB5 α . Transformants were selected on LB-medium with 100 mg L⁻¹ ampicillin. Successful ligation was determined by digesting the purified plasmids with *KpnI/SphI* or *KpnI/AvrII* which are specific for the presence of the linker. The resulting plasmid was named pUG62AUR (Fig. S5).



Supplementary Figure S5. The pUG62AUR plasmid with a multiple cloning site consisting of the *AvrII*, *SphI*, *SmaI* and *KpnI* restriction sites.

Construction of TMB3463 (*hxx2-Δ hxx1-Δ1 glk1-Δ hxx1-Δ2*)

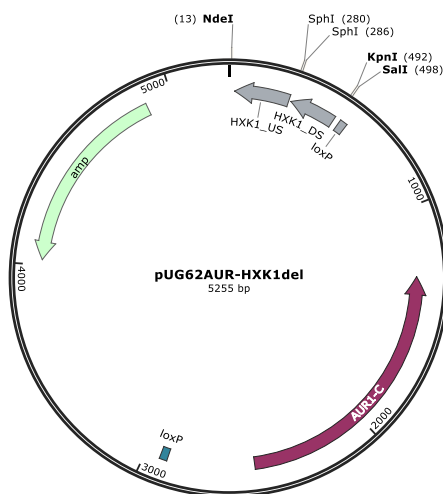
Unless stated otherwise the PCR reactions contained 1 \times GC Buffer, 0.2 mM of each dNTP, 0.01 U μL^{-1} Phusion Hotstart DNA Polymerase II and 0.5 μM each of forward and reverse primers (Table S6). The reaction volume was 50 μL . DNA fragments amplified by PCR were

purified from 0.8% agarose gel using the QIAquick Gel Extraction Kit (Qiagen, Germany) unless stated otherwise.

Verification of correct integration and gene deletion was performed using the primers listed in Table S7 and the following reaction mix: 1× DreamTaq Buffer, 0.2 mM of each dNTP, 0.3 μM each of forward and reverse primers and 1 U μL⁻¹ DreamTaq DNA Polymerase.

The additional upstream and downstream fragments flanking the *HXK1* gene were amplified from genomic DNA from *S. cerevisiae* CEN.PK2-1C using the following PCR program: 30 s denaturation at 98°C, 5 cycles of 10 s denaturation at 98°C, 15 s annealing at 60.9°C, 8 s extension at 72°C, 25 cycles of 10 s denaturation at 98°C, 20 s annealing and extension at 72°C and 1 cycle of 10 min extension at 72°C.

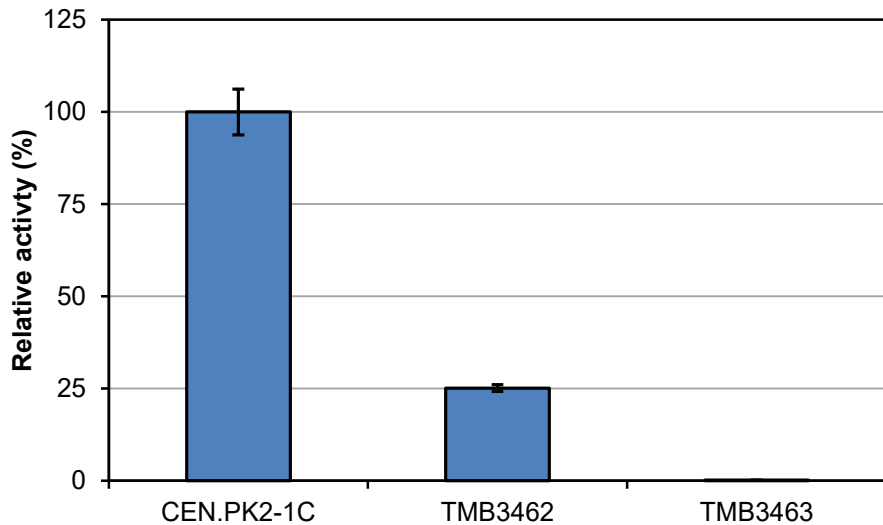
The purified upstream and downstream fragments were digested with *SphI*/*AvrII* and *KpnI*/*SphI*, respectively. The digested fragments were ligated into pUG62AUR, previously digested with *KpnI*/*AvrII*, using a 3:1 molar ratio of insert to vector and an incubation time of 2 h at room temperature. 5 μL of the ligation mix was used for transformation of heat shock competent *E. coli* NEB5α. Transformants were selected on LB-medium with 100 mg L⁻¹ ampicillin. Successful ligation was determined by colony PCR using primers HXK1_DS2_f and HXK1_US2_r and the resulting plasmid was named pUG62AUR-HXK1USDS (Fig. S6).



Supplementary Figure S6. The pUG62AUR-HXK1USDS plasmid containing homologous regions flanking the *HXK1* gene.

TMB3462 was transformed with pUG62AUR-HXK1USDS, linearized with *FspI*, according to High efficiency protocol. Before plating the transformants the cells were resuspended in 1 mL of YP with 2% galactose and incubated at 30°C for 2.25 h. Transformants were selected on solid YNB medium containing 2% galactose, 220 mg L⁻¹ leucine and 0.15 mg L⁻¹ aureobasidin A. Correct integration was verified by colony PCR on randomly selected

colonies using primers HXK1_US_f and AmpR-R130. Attempts to amplify the *HXK1* gene using primers HXK1_547_f and HXK1_1282_r did not result in any amplification, indicating the gene had been deleted. This was confirmed by a very low glucose phosphorylating activity in one positive clone which was named TMB3463 (Fig. S7).



Supplementary Figure S7. The glucose phosphorylating activity in strains TMB3462 (3Δ) and TMB3463 (4Δ) relative to the wild-type CEN.PK2-1C strain.

Supplementary Tables

Supplementary Table S1. Maximum specific consumption rates, production rates and yields in anaerobic batch fermentation of 20 g L⁻¹ glucose and 50 g L⁻¹ xylose by TMB3492 (Hxk2p-wt) and TMB3493 (Hxk2p-Y).

Values are given as mean \pm standard deviation of two independent experiments.

	Glucose phase		Xylose phase	
	TMB3492	TMB3493	TMB3492	TMB3493
μ_{\max} (h ⁻¹)	0.35 \pm 0.02	0.34 \pm 0.01	0.013 \pm 0.000	0.027 \pm 0.004
Specific rates (mmol g CDW⁻¹ h⁻¹)				
$r_{\max, \text{glc}}$	-20.6 \pm 3.2	-21.8 \pm 0.4	—	—
$r_{\max, \text{xyl}}$	—	—	-3.48 \pm 0.35	-5.72 \pm 0.99
$r_{\max, \text{xylt}}$	—	—	0.909 \pm 0.017	0.960 \pm 0.014
$r_{\max, \text{glyc}}$	6.31 \pm 0.49	6.61 \pm 0.42	0.085 \pm 0.041	0.052 \pm 0.037
$r_{\max, \text{ac}}$	1.04 \pm 0.02	1.22 \pm 0.09	0.040 \pm 0.021	0.028 \pm 0.005
$r_{\max, \text{etoh}}$	39.1 \pm 5.6	41.3 \pm 2.5	1.60 \pm 0.40	1.34 \pm 0.98
Yields (g g sugar⁻¹)				
$Y_{\text{xylt/s}}$	—	—	0.261 \pm 0.007	0.270 \pm 0.003
$Y_{\text{glyc/s}}$	0.129 \pm 0.005	0.127 \pm 0.007	0.028 \pm 0.001	0.027 \pm 0.000
$Y_{\text{ac/s}}$	0.015 \pm 0.002	0.015 \pm 0.000	0.009 \pm 0.003	0.008 \pm 0.002
$Y_{\text{etoh/s}}$	0.398 \pm 0.012	0.392 \pm 0.036	0.251 \pm 0.003	0.255 \pm 0.009
$Y_{\text{X/s}}$	0.078 \pm 0.005	0.070 \pm 0.002	0.056 \pm 0.013	0.055 \pm 0.008

Supplementary Table S2. Overall yields and production rates in anaerobic batch fermentation of 20 g L⁻¹ glucose and 50 g L⁻¹ xylose by TMB3492 (Hxk2p-wt) and TMB3493 (Hxk2p-Y).

Values are given as mean \pm standard deviation of two independent experiments.

	Overall yields (g g total sugar ⁻¹)			Overall production rates (g L ⁻¹ h ⁻¹)	
	TMB3492	TMB3493		TMB3492	TMB3493
$Y_{\text{xylt/s}}$	0.144 \pm 0.010	0.158 \pm 0.002	q_{xylt}	0.133 \pm 0.007	0.139 \pm 0.000
$Y_{\text{glyc/s}}$	0.061 \pm 0.008	0.059 \pm 0.002	q_{glyc}	0.057 \pm 0.008	0.052 \pm 0.003
$Y_{\text{ac/s}}$	0.011 \pm 0.002	0.012 \pm 0.001	q_{ac}	0.010 \pm 0.002	0.010 \pm 0.001
$Y_{\text{etoh/s}}$	0.258 \pm 0.004	0.262 \pm 0.004	q_{etoh}	0.240 \pm 0.000	0.231 \pm 0.001
$Y_{\text{X/s}}$	0.032 \pm 0.005	0.036 \pm 0.003	q_{X}	0.029 \pm 0.004	0.031 \pm 0.002

Supplementary Table S3. Primers used to construct the mutated *HXK2* megaprimer.

Name	Sequence (with wobble positions in bold letters)
Degenerate primers	
Group_1_f	5'-CATTGGGTTTCACCTTTASCT W CCCAGCTTCTCAAAAC-3'
Group_1_r	5'-GTTTTGAGAAGCTGGG W AGSTAAAGGTGAAACCCAATG-3'
Group_2_f	5'-GAAGGTATCTTGCAAA R ATGGACTA R AGGTTTTGATATTCC-3'
Group_2_r	5'-GGAATATCAAAACCT Y TAGTCCAT Y TTTGCAAGATACCTTC-3'
Group_3_f	5'-GTTGCTTTGATAAACG A KASCACCGGTACTTTGGTTG-3'
Group_3_r	5'-CAACCAAAGTACCGGTG S TMTCGTTTATCAAAGCAAC-3'
Group_4_f	5'-GAAACTAAGATGGGTGTT W WCTTC R GCASCGSAGTCAATGGTGCTTAC-3'
Group_4_r	5'-GTAAGCACCATTGACTSCG S TGCGYAAG W WAACACCCATCTTAGTTTC-3'
Group_5_f	5'-CAATGGCCATCAACTGTG A KTACKGCTCCTTCGATAATGAAC-3'
Group_5_r	5'-GTTCAATTATCGAAGGAGC M GTAMTCACAGTTGATGGCCATTG-3'
Group_6_f	5'-CAGGCCAACAAACCTTTG A KAAAAATGTCTTCTGGTTAC-3'
Group_6_r	5'-GTAACCAGAAGACATTTT M TCAAAGGTTTGTGGCCTG-3'
Additional primers	
YIp128-F1	5'-GGCCTTTTGCTGGCCTTTTG-3'
YIp128-R1	5'-AAGGGGGATGTGCTGCAAGG-3'

Supplementary Table S4. Primers used to construct deletion cassettes.

Name	Sequence
HXK2_US_f	5'-GGTACCTAGAAATGGCTATCATGC-3'
HXK2_US_r	5'-TATATATAGTAATGTCGTTTATTTAATTAGCGTACTTATTATGTGTGG-3'
HXK2_DS_f	5'-GATAGGGTTGAGTGTTGTTACTTAATTTGTAATAAAGTTGAACAACAAG-3'
HXK2_DS_r	5'-AGAAGAATCCACGCGTAAAAATCG-3'
TRP1_f	5'-TAAGTACGCTAATTAATAAACGACATTACTATATATATAATATAGGAAG-3'
TRP1_r	5'-CTTAATTTACAAATTAAGTAACAACACTCAACCCTATCTAGGTC-3'
HXK1_US_f	5'-TGGCGTGGGGTGGGGTGATT-3'
HXK1_US_r	5'-GTTAAGCCAGCCCCGACACCGGGCACGTGCGGGAGTTT-3'
HXK1_DS_f	5'-GTCTATCAGGGCGATGGCCGCGACCCAGATTGCAGAAGATCCC-3'
HXK1_DS_r	5'-AGGTGCCCTTGCTAGCAT-3'
URA3_f	5'-AAACTCCCGCACGTGTGCCCGGTGTCGGGGCTGGCTTAAC-3'
URA3_r	5'-GGGATCTTCTGCAATCTGGGTGCGGGGCCATCGCCCTGATAGAC-3'
GLK1_US_f	5'-AGAGGAGGCGAGCAGCAGGG-3'
GLK1_US_r	5'-GTCGACCTGCAGCGTACGAAAGTGCCCACCGTTTGAGCGT-3'
GLK1_DS_f	5'-ATCAGATCCACTAGTGGCCTATGCGACAGCCTCGCCCTCTCCGT-3'
GLK1_DS_r	5'-CGGGCAGTGCAAGTGAGGG-3'
loxPKanMX_f	5'-ACGCTCAAACGGTGGGCACTTTTCGTACGCTGCAGGTGCAC-3'
loxPKanMX_R	5'-ACGGAAGAGGGCGAGGCTGTCGCATAGGCCACTACCTCTCCGT-3'

Supplementary Table S5. Primers used to confirm correct integration and gene deletion.

Name	Sequence	Application
HXK2_823US_f	5'-ACCACACGCATGCCTTCATTCC-3'	Chromosomal integration
TRP1_71_r	5'-GCGGCCTCTGTGCTCTGCAA-3'	
HXK2_773_f	5'-TTCCACCATCTGTCCAATGGC-3'	Gene deletion
HXK2_1248_r	5'-TGCAGCAATGTGACCGGTCTTG-3'	
HXK1_1510US_f	5'-AGCGGTTTCGCTTCCAGCACC-3'	Chromosomal integration
URA3_120_r	5'-GGTGGTACGAACATCCAATGAAGCA-3'	
HXK1_547_f	5'-GTCGAAGGCCACGATGTCGTCC-3'	Gene deletion
HXK1_1282_r	5'-CCCTTAGCGGCGGCTTCCTT-3'	
GLK1_1050US_f	5'-ACGGCGACAGCCGTTGGCTT-3'	Chromosomal integration
kanMX_32_r	5'-CGCGGCCTCGAAACGTGAGT-3'	
GLK1_433_f	5'-CCGGACGAGTTGGCCAAGGG-3'	Gene deletion
GLK1_1434_r	5'-CCTCTACCCCTCGGCACCCA-3'	

Supplementary Table S6. Primers used to amplify additional fragments upstream and downstream the *HXK1* gene. Restriction sites are indicated in bold.

Name	Sequence	Restriction site
HXK1_US2_f	5'-TAGGCAT GC GCATTGGTACCTTAGGACCGTTGAG-3'	<i>Sph</i> I
HXK1_US2_r	5'-CGCCTAGGGATTGAGTTGTTGGGTGAGTTTG-3'	<i>Avr</i> II
HXK1_DS2_f	5'-ACTGGTACCTTGGTCTTCTTCATGCATCATTTCA-3'	<i>Kpn</i> I
HXK1_DS2_r	5'-TTGGCAT GC ATCAGCTATAAGAGACGAAATTGCT-3'	<i>Sph</i> I

Supplementary Table S7. Primers used to confirm correct integration of pUG62AUR-HXK1USDS and *HXK1*-gene deletion.

Name	Sequence	Application
HXK1_1510US_f	5'-AGCGGTTTCGCTTCCAGCACC-3'	Chromosomal integration
AmpR-R130	5'-AATGATACCGCGAGACCCAC-3'	
HXK1_547_f	5'-GTCGAAGGCCACGATGTCGTCC-3'	Gene deletion
HXK1_1282_r	5'-CCCTTAGCGGCGGCTTCCTT-3'	

Paper VII



RESEARCH

Open Access



Exploring the xylose paradox in *Saccharomyces cerevisiae* through in vivo sugar signalomics of targeted deletants

Karen O. Osiro, Celina Borgström, Daniel P. Brink, Birta Líf Fjölnisdóttir and Marie F. Gorwa-Grauslund*

Abstract

Background: There have been many successful strategies to implement xylose metabolism in *Saccharomyces cerevisiae*, but no effort has so far enabled xylose utilization at rates comparable to that of glucose (the preferred sugar of this yeast). Many studies have pointed towards the engineered yeast not sensing that xylose is a fermentable carbon source despite growing and fermenting on it, which is paradoxical. We have previously used fluorescent biosensor strains to in vivo monitor the sugar signalome in yeast engineered with xylose reductase and xylitol dehydrogenase (XR/XDH) and have established that *S. cerevisiae* senses high concentrations of xylose with the same signal as low concentration of glucose, which may explain the poor utilization.

Results: In the present study, we evaluated the effects of three deletions (*ira2Δ*, *isu1Δ* and *hog1Δ*) that have recently been shown to display epistatic effects on a xylose isomerase (XI) strain. Through aerobic and anaerobic characterization, we showed that the proposed effects in XI strains were for the most part also applicable in the XR/XDH background. The *ira2Δisu1Δ* double deletion led to strains with the highest specific xylose consumption- and ethanol production rates but also the lowest biomass titre. The signalling response revealed that *ira2Δisu1Δ* changed the low glucose-signal in the background strain to a simultaneous signalling of high and low glucose, suggesting that engineering of the signalome can improve xylose utilization.

Conclusions: The study was able to correlate the previously proposed beneficial effects of *ira2Δ*, *isu1Δ* and *hog1Δ* on *S. cerevisiae* xylose uptake, with a change in the sugar signalome. This is in line with our previous hypothesis that the key to resolve the xylose paradox lies in the sugar sensing and signalling networks. These results indicate that the future engineering targets for improved xylose utilization should probably be sought not in the metabolic networks, but in the signalling ones.

Keywords: *Saccharomyces cerevisiae*, Sugar sensing/signalling, Xylose, GFP biosensor, cAMP/PKA, Snf3p/Rgt2p, SNF1/Mig1p, $\Delta ira2$, $\Delta isu1$, $\Delta hog1$

Introduction

Microbial fermentation and bioconversion can be used for sustainable production of bulk and fine chemicals from renewable feedstocks. Of particular interest is fermentation of lignocellulose, a non-edible plant matter which is found in e.g. forestry and agricultural residues and municipal paper waste and that, unlike fermentation

of crops such as corn and sugarcane, does not compete for arable land [1]. An industrially feasible lignocellulose biorefinery will require a microbe that not only can withstand the harsh conditions in the lignocellulosic hydrolysate (e.g. low pH, osmotic stress and inhibitory compounds) but also is able to process all the sugars in the feedstock, i.e. both hexose (C_6) and pentose (C_5) sugars [2, 3]. One of the most commonly used microorganisms in this context is Baker's yeast *Saccharomyces cerevisiae*, which can be used to produce e.g. bioethanol from lignocellulosic hydrolysates since it naturally

*Correspondence: marie-francoise.gorwa@tmb.lth.se
Applied Microbiology, Department of Chemistry, Lund University, Lund, Sweden



© The Author(s) 2019. This article is distributed under the terms of the Creative Commons Attribution 4.0 International License (<http://creativecommons.org/licenses/by/4.0/>), which permits unrestricted use, distribution, and reproduction in any medium, provided you give appropriate credit to the original author(s) and the source, provide a link to the Creative Commons license, and indicate if changes were made. The Creative Commons Public Domain Dedication waiver (<http://creativecommons.org/publicdomain/zero/1.0/>) applies to the data made available in this article, unless otherwise stated.

ferments glucose at high efficiency and has a basal inherent robustness to several of the stressors in the hydrolysate [4, 5]. However, wild type *S. cerevisiae* cannot utilize pentose sugars [6], and there is therefore a large interest to metabolically engineer this yeast to rapidly catabolize C₅-sugars in general, and xylose—the second most abundant sugar in nature [7]—in particular.

There are currently two successfully implemented strategies for xylose utilization by *S. cerevisiae*: the oxido-reductive pathway [8, 9] and the isomerase pathway [10, 11]. The oxido-reductive strategy uses a xylose reductase (XR) and a xylitol dehydrogenase (XDH) to convert xylose to xylitol and xylitol to xylulose respectively [9]. The reactions are NAD(P)H-dependent, meaning that the cellular redox balance has to be considered when implementing this pathway. The isomerase strategy, on the other hand, relies on a xylose isomerase (XI) that converts xylose directly to xylulose without the requirement of any cofactors [10]. The XI is however easily inhibited by xylitol formation from endogenous reductases acting on the xylose, such as Gre3p [10]. Commonly, XR/XDH pathways are of fungal origin, whereas XI is bacterial [12], meaning that the former genes are more straightforward to express in *S. cerevisiae*. From xylulose, the endogenous xylulokinase (XK) will shunt the carbon into the non-oxidative part of the pentose phosphate pathway (PPP), where it will eventually reach the central carbon metabolism [9]. Xylose catabolism can be improved by modification of a number of endogenous genes in the PPP, such as overexpression of *XKS1* (encoding XK) [13, 14], *TAL1* and *TKL1* [15], and deletion of *GRE3* [16, 17] and *PHO13* [18, 19]. It can also be noted that the redox issue in the XR/XDH pathway can be improved by the expression of an XR with preference for NADH over NADPH [20], and that novel XIs that are less inhibited by xylitol have been discovered [21]. Deletion of the *GRE3* reductase is also beneficial for XIs, as *gre3Δ* results in less endogenous xylitol formation from xylose [22]. Xylose uptake is another issue in *S. cerevisiae*: there are no specialized xylose transporters and the uptake takes place through hexose transporters that have some affinity for xylose, but the simultaneous presence of glucose impairs

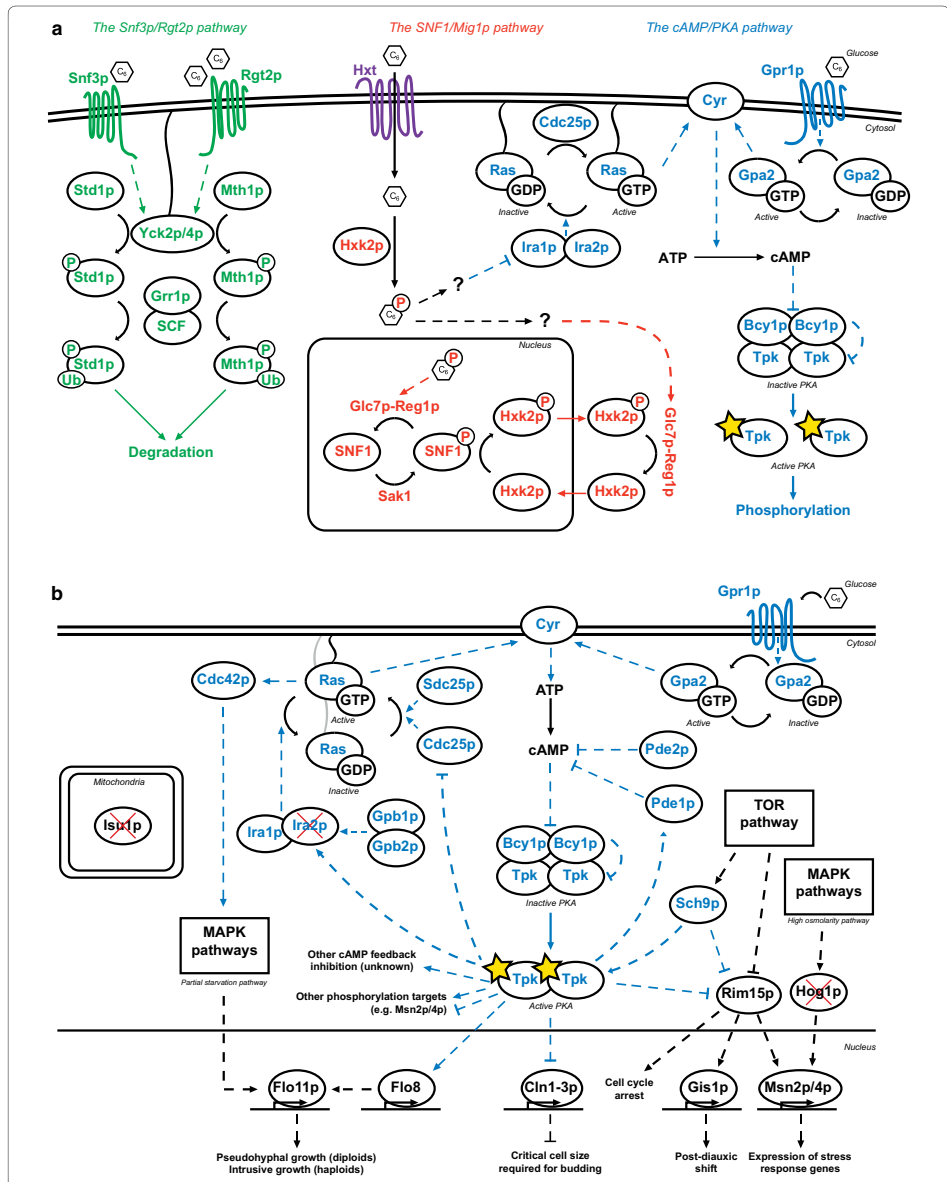
xylose uptake [23]. Therefore some hexose and galactose transporters have been engineered for improved xylose specificity [24–27].

However, despite many successful metabolic engineering strategies, xylose utilization by recombinant *S. cerevisiae* is still lagging behind the performance on glucose. For example there are now strains with yields of ethanol from xylose [20, 28] close to the maximum theoretical yield of 0.51 g/g substrate [29], but the specific productivities on xylose of these strains are about 3–8 times lower than what is normally seen on glucose (typically around 2 g ethanol/g cell dry weight⁻¹ h⁻¹ on glucose; [30]). Co-consumption of glucose and xylose is another issue, as xylose is typically only taken up after most of the glucose has been depleted [12, 31], which leads to inefficient fermentation times. Because of these phenotypes, it has been suggested that xylose triggers a non-fermentative response in the recombinant *S. cerevisiae* and evidenced by e.g. transcript and metabolite profiling and observed respiratory behaviour [32–37].

This xylose paradox—that xylose is fermented to ethanol despite the cellular signals suggesting otherwise—has led us to believe that the root of the poor productivity and co-consumption may be found in the sugar sensing and signalling pathways of *S. cerevisiae*. Previously, we constructed and validated a panel of in vivo fluorescent biosensors [38] that allows for single-cell real-time monitoring of the signals of the three main sugar sensing pathways in this yeast: the Snf3p/Rgt2p pathway, the SNF1/Mig1p pathway and the cAMP/protein kinase A (PKA) pathway (Fig. 1a). It was found that in *S. cerevisiae* strains that had not been engineered for xylose utilization, extracellular xylose did not trigger any signals, but a certain population heterogeneity on xylose indicated that there might be an endogenous sensing of intracellular xylose [38]. When the same biosensors were later applied to strains that had been engineered for xylose uptake with the XR/XDH pathway and a xylose transporter, high xylose concentrations triggered the same signal as low glucose concentrations did; this indicated that xylose resulted in the opposite signal to that of glucose and that it may

(See figure on next page.)

Fig. 1 Schematic representation of the signalling pathways and deletions investigated in the current study. **a** The three main sugar signalling pathways in *S. cerevisiae*, adapted from [39]. The Snf3p/Rgt2p pathway (green) handles expression of hexose transporters in response to extracellular glucose. The SNF1/Mig1p pathway (red) handles expression of genes related to alternative (non-glucose) carbon sources in response to intracellular phosphorylated glucose. The cAMP/PKA pathway (blue) handles e.g. cellular growth, homeostasis and stress response. **b** Detailed schematic map of the cAMP/PKA pathway with the genes that were deleted in the current study marked with a red cross. Note that two of the three genes (*IRA2*, *HOG1*) are closely related to the pathway, whereas the third one (*ISU1*) is located in the mitochondria and seemingly unrelated to the cAMP/PKA pathway. **b** was adapted from [46, 47, 56, 63, 81–85]. Solid arrows represent reactions/transport and dashed arrows represent induction (arrowhead) or repression (hammerhead)



trigger a starvation response rather than a fermentation response [39].

These previous findings led us to look in the literature for genetic modifications that may affect the sugar signalling pathways in favour of xylose, that we could assay further with our biosensor system. In a recent study by Sato and colleagues, adaptive evolution and reverse engineering was used to discover previously unknown epistatic interactions between different genes that, when deleted, improved xylose uptake and utilization: *HOG1*, *IRA2*, *ISU1* and *GRE3* [40]. Their results showed that combinations of these deletions led to improved growth, xylose consumption and specific ethanol productivity on strains engineered with the XI pathway during anaerobic conditions; they also observed that *isu1Δ* and *hog1Δ* enabled aerobic xylose respiration [40]. *IRA2* and *HOG1* are known to be connected to the sugar and stress signalling networks (cAMP/PKA pathway and MAP kinase (MAPK) cascades respectively) [41, 42] and are therefore along the lines of our hypothesis of the importance of the signalling networks for solving the xylose paradox (Fig. 1b). The *ISU1* gene, which encodes a mitochondrial Fe-S cluster scaffold protein [43, 44], had however not been previously connected to xylose metabolism, but was recently pinpointed by two independent studies [40, 45]. As for *GRE3*, it may primarily improve the XI pathway—by decreasing the xylitol concentration and thus XI inhibition [22].

In the current study, we investigated the effects of the deletions found by Sato et al. on the sugar signalling pathways by introducing them in our biosensor strains, with a focus on the epistatic interactions of *HOG1*, *IRA2*, and *ISU1*. In particular, we wanted to answer the following research questions: are the observed xylose fermentation improvements also achievable with XR/XDH? Did the improvement of xylose consumption come from a change in the sugar signalome (i.e. all the sugar signalling pathways in the cell)? We here report on the fermentation profiles and biosensor responses of the combinatorial deletions of these genes in three of our XR/XDH-equipped biosensor strain lines.

Results

Deletion of key genes in biosensor strains

Deletions of *ISU1*, *HOG1* and *IRA2* were recently shown to epistatically improve anaerobic xylose metabolism in XI-containing strains of *S. cerevisiae* and the effect was reproducible in two different *S. cerevisiae* strain backgrounds (BY4741 and CEN.PK113-5D) [40]. In the current study, xylose utilizing strains from our previously established XR/XDH biosensor panel (TMB375X; [39]) were used to evaluate the effect of *isu1Δ*, *hog1Δ*, and

ira2Δ on the three main sugar signalling pathways: strains TMB3752 (*HXT1p*-GFP) for the Snf3p/Rgt2p pathway, TMB3755 (*SUC2p*-GFP) for SNF1/Mig1p pathway and TMB3757 (*TPS1p*-GFP) for the cAMP/PKA pathway, Fig. 1a. The strain TMB3751 (same background but without biosensor) was used as a control strain. All biosensor strains were derived from *S. cerevisiae* W303-1A, which is a common host for signalling studies in *S. cerevisiae* [46–48]; CEN.PK strains, on the other hand, are less suitable for sugar sensing studies since they are known to have accumulated mutations in the cAMP/PKA network [49, 50], whereas this is not the case in W303 [51].

In total, 24 strains were constructed for the study (Table 1). The deletions were performed as single and combinatorial knock-outs. Single gene deletions (*isu1Δ*, *hog1Δ* and *ira2Δ*) were made in each of the three previously mentioned biosensor strain lines (TMB3752 (*HXT1p*-GFP), TMB3755 (*SUC2p*-GFP), and TMB3757 (*TPS1p*-GFP)) as well as the control strain (TMB3751; no biosensor). Strains TMB376X (*ira2Δ*) and TMB377X (*isu1Δ*) were used as the background to construct the double deletion (*ira2Δisu1Δ* and *isu1Δhog1Δ*) strains, respectively, and TMB379X strains (*ira2Δisu1Δ*) were used to generate the triple deletion strains (*ira2Δisu1Δhog1Δ*), see Table 1. All deletions were confirmed by yeast colony PCR (data not shown). The effect of the deletions were then analysed in terms of strain characterization and fermentation profiles, and the biosensor signals were measured by flow cytometry and used to assess how the deletions affected the *S. cerevisiae* sugar signalling network.

The reported improvements of *ira2Δ*, *hog1Δ* and *isu1Δ* with the XI pathway also occurred in strains with the XR/XDH pathway

Anaerobic conditions

In the original study of the deletants [40], rich medium (YPX; Yeast extract, Peptone and Xylose) was used for the evaluation. Whereas this is a good strategy to assess the fermentation process performance, it is not necessarily the most suited medium for physiological characterisation. In contrast, a defined medium ensures that the cell will synthesise all its required components *in vivo* instead of taking it up from a rich medium [52]. Therefore, we performed the anaerobic evaluation of the three combinatorial deletions (*ira2Δ*, *ira2Δisu1Δ*, *ira2Δisu1Δhog1Δ*) in both YPX and YNBX (Yeast Nitrogen Base Xylose; a defined medium) in order to be able to compare to the previous results with the XI strain while making an in-depth physiological characterisation. As a proof-of-concept and to keep the number of strains down to a manageable amount, the effects of the deletions were

Table 1 *S. cerevisiae* biosensor strains constructed and/or utilized in this study

Strains	Biosensor	Relevant genotype	References
TMB375X series (background strains)			
TMB3751	Control	can1::Ylp211; <i>SPB1/PBN1::Ylp128GAL2mut</i> ; <i>Vac17/MRC1::TKL-TAL</i> ; <i>Chr X-2/XI-5/XII-4::XR-XDH-XK</i>	[39]
TMB3752	<i>HXT1p</i>	can1::YlpGFP-Hxt1p; <i>SPB1/PBN1::Ylp128GAL2mut</i> ; <i>Vac17/MRC1::TKL-TAL</i> ; <i>Chr X-2/XI-5/XII-4::XR-XDH-XK</i>	
TMB3755	<i>SUC2p</i>	can1::YlpGFP-Suc2p; <i>SPB1/PBN1::Ylp128GAL2mut</i> ; <i>Vac17/MRC1::TKL-TAL</i> ; <i>Chr X-2/XI-5/XII-4::XR-XDH-XK</i>	
TMB3757	<i>TPS1p</i>	can1::YlpGFP-Tps1p; <i>SPB1/PBN1::Ylp128GAL2mut</i> ; <i>Vac17/MRC1::TKL-TAL</i> ; <i>Chr X-2/XI-5/XII-4::XR-XDH-XK</i>	
TMB361X series			
TMB3761	Control	TMB3751; <i>ira2Δ</i>	This study
TMB3762	<i>HXT1p</i>	TMB3752; <i>ira2Δ</i>	
TMB3765	<i>SUC2p</i>	TMB3755; <i>ira2Δ</i>	
TMB3767	<i>TPS1p</i>	TMB3757; <i>ira2Δ</i>	
TMB377X series			
TMB3771	Control	TMB3751; <i>isu1Δ</i>	This study
TMB3772	<i>HXT1p</i>	TMB3752; <i>isu1Δ</i>	
TMB3775	<i>SUC2p</i>	TMB3755; <i>isu1Δ</i>	
TMB3777	<i>TPS1p</i>	TMB3757; <i>isu1Δ</i>	
TMB378X series			
TMB3781	Control	TMB3751; <i>hog1Δ</i>	This study
TMB3782	<i>HXT1p</i>	TMB3752; <i>hog1Δ</i>	
TMB3785	<i>SUC2p</i>	TMB3755; <i>hog1Δ</i>	
TMB3787	<i>TPS1p</i>	TMB3757; <i>hog1Δ</i>	
TMB379X series			
TMB3791	Control	TMB3761 (<i>ira2Δ</i>); <i>isu1Δ</i>	This study
TMB3792	<i>HXT1p</i>	TMB3762 (<i>ira2Δ</i>); <i>isu1Δ</i>	
TMB3795	<i>SUC2p</i>	TMB3765 (<i>ira2Δ</i>); <i>isu1Δ</i>	
TMB3797	<i>TPS1p</i>	TMB3767 (<i>ira2Δ</i>); <i>isu1Δ</i>	
TMB385X series			
TMB3851	Control	TMB3771 (<i>isu1Δ</i>); <i>hog1Δ</i>	This study
TMB3852	<i>HXT1p</i>	TMB3772 (<i>isu1Δ</i>); <i>hog1Δ</i>	
TMB3855	<i>SUC2p</i>	TMB3775 (<i>isu1Δ</i>); <i>hog1Δ</i>	
TMB3857	<i>TPS1p</i>	TMB3777 (<i>isu1Δ</i>); <i>hog1Δ</i>	
TMB386X series			
TMB3861	Control	TMB3791 (<i>ira2Δisu1Δ</i>); <i>hog1Δ</i>	This study
TMB3862	<i>HXT1p</i>	TMB3792 (<i>ira2Δisu1Δ</i>); <i>hog1Δ</i>	
TMB3865	<i>SUC2p</i>	TMB3795 (<i>ira2Δisu1Δ</i>); <i>hog1Δ</i>	
TMB3867	<i>TPS1p</i>	TMB3797 (<i>ira2Δisu1Δ</i>); <i>hog1Δ</i>	

assessed in the *SUC2p*-GFP biosensor line (TMB37X5; Table 1).

In both media and under anaerobic conditions, increased specific rates of xylose consumption and ethanol production were obtained in the deletion strains compared to the control strain (Table 2). In parallel, the anaerobic biomass titre decreased with each sequential deletion compared to the control strain (Fig. 2d, h). As for ethanol titres, *ira2Δ* (TMB3765) had the highest maximum titre in YPX and YNBX (Fig. 2c, g), although there was no change in ethanol yield (Table 2). Deletion of *ISU1* in the *ira2Δ* background negatively impacted the xylose,

xylitol, ethanol and biomass titres, whereas the additional deletion of *HOG1* (*ira2Δisu1Δhog1Δ*) was partly able to recover the decrease in titre caused by *ira2Δisu1Δ* (Fig. 2). For comparison, Sato et al. observed a different trend for growth since they reported an increased growth rate with each sequential deletion; however, biomass and ethanol titres were not reported [40].

A stepwise increase in specific xylose consumption rate was previously observed with each additional deletion in the XI strain [40]. In the present study, the consumption rates of the deletion strains all increased compared to the control, but peaked in the *ira2Δisu1Δ* strain, and

Table 2 Anaerobic specific rates and yields in YPX and YNBX media

Strain	Specific xylose consumption rate g/(g CDW L h)	Specific xylitol formation rate g/(g CDW L h)	Specific ethanol formation rate g/(g CDW L h)	Yield ethanol per xylose g/g	Yield xylitol per xylose g/g
YPX (0–48 h)					
TMB3755 (background strain)	1.57 ± 0.09	0.17 ± 0.00	0.51 ± 0.09	0.32 ± 0.04	0.11 ± 0.01
TMB3765 (<i>ira2Δ</i>)	2.06 ± 0.05	0.24 ± 0.02	0.74 ± 0.04	0.36 ± 0.01	0.12 ± 0.01
TMB3795 (<i>ira2Δ isu1Δ</i>)	3.22 ± 0.56	0.36 ± 0.07	1.14 ± 0.22	0.35 ± 0.01	0.11 ± 0.00
TMB3865 (<i>ira2Δ isu1Δ hog1Δ</i>)	1.94 ± 0.09	0.23 ± 0.01	0.70 ± 0.02	0.36 ± 0.01	0.12 ± 0.00
YNBX (0–70 h)					
TMB3755 (background strain)	1.41 ± 0.14	0.16 ± 0.02	0.45 ± 0.01	0.32 ± 0.03	0.11 ± 0.00
TMB3765 (<i>ira2Δ</i>)	2.19 ± 0.09	0.24 ± 0.01	0.75 ± 0.07	0.34 ± 0.02	0.11 ± 0.00
TMB3795 (<i>ira2Δ isu1Δ</i>)	4.23 ± 0.93	0.24 ± 0.05	1.50 ± 0.18	0.36 ± 0.04	0.06 ± 0.00
TMB3865 (<i>ira2Δ isu1Δ hog1Δ</i>)	2.12 ± 0.01	0.29 ± 0.00	0.60 ± 0.05	0.28 ± 0.03	0.14 ± 0.00

The cultivations were performed in two biological replicates. Additional cultivation rates can be found in Additional file 1: Tables S1, S2

not in the triple deletion strain (Table 2; both in YPX and YNBX). In fact, the specific xylose consumption and ethanol formation rates in the *ira2Δisu1Δ* strain on YNBX were roughly three times higher than that of the background strain (Additional file 1: Table S2), as a consequence of the severe decrease in biomass formation (Fig. 2d, h), since the specific consumption rate is normalized to the biomass concentration. This implies that the double deletion strain shunted more carbon away from biomass formation and towards the product, as is seen in the specific ethanol productivity of this strain compared to the others (Table 2). In terms of yield of ethanol from xylose, there was no significant change in TMB3795 (*ira2Δisu1Δ*) compared to the control. From a process point-of-view, this strain actually had the worst combination of deletions, since it decreased the *volume* consumption and productivity (Additional file 1: Tables S1, S2).

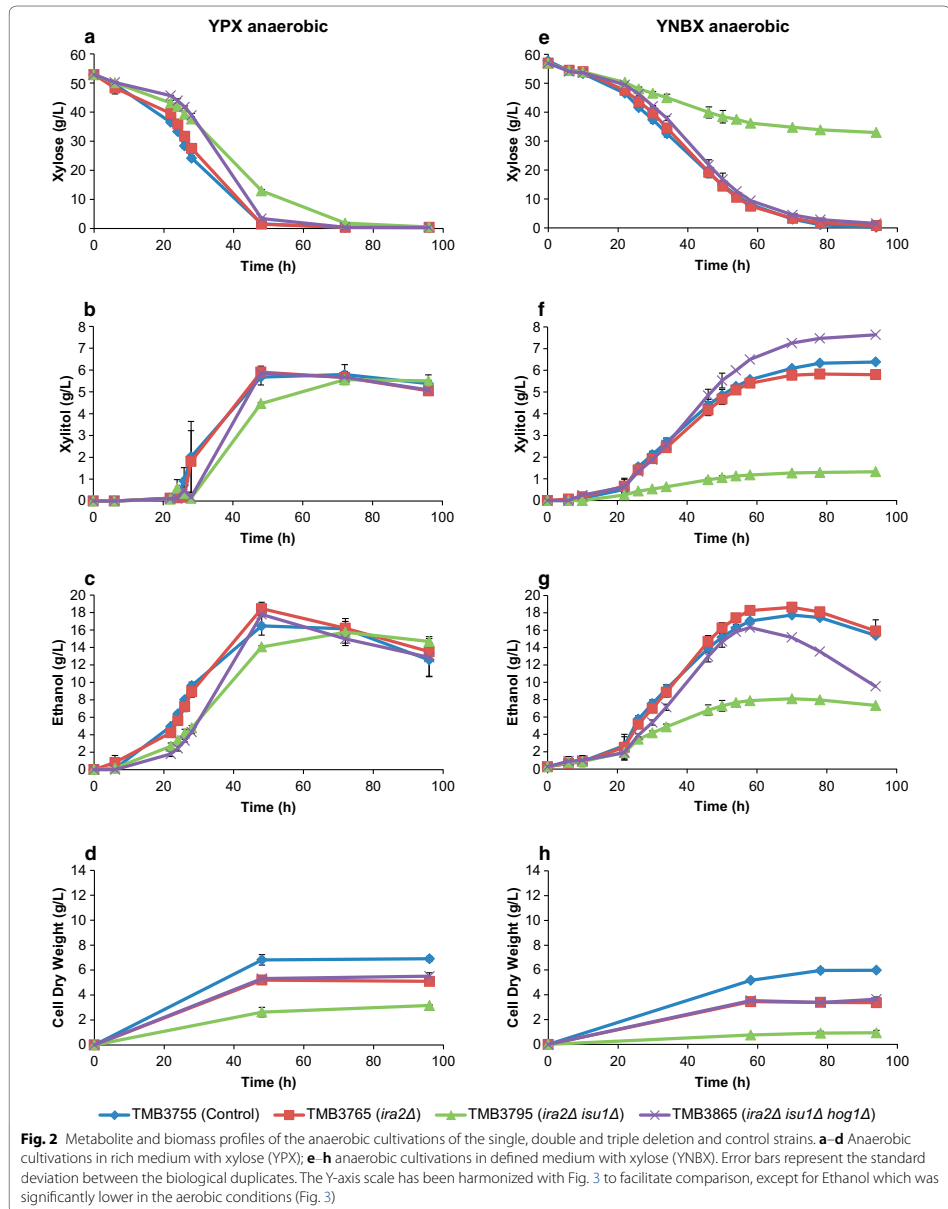
When cultivated on YNBX, the double deletion strain TMB3795 (*ira2Δisu1Δ*) showed a significantly lower fitness and overall performance compared to the other three strains (Fig. 2e–h). This strain clearly benefited from the rich nature of YPX (Fig. 2a–d), and struggled to cope with the minimal medium. It is also evident that fermentation on YNBX (Fig. 2e, f) took longer time than on YPX (Fig. 2a–d)—70 h vs. 48 h to peak Ethanol, for instance; Fig. 2—although the trends were similar. Due to the undefined nature of some of the rich medium components, it was decided to pursue the study with YNBX only.

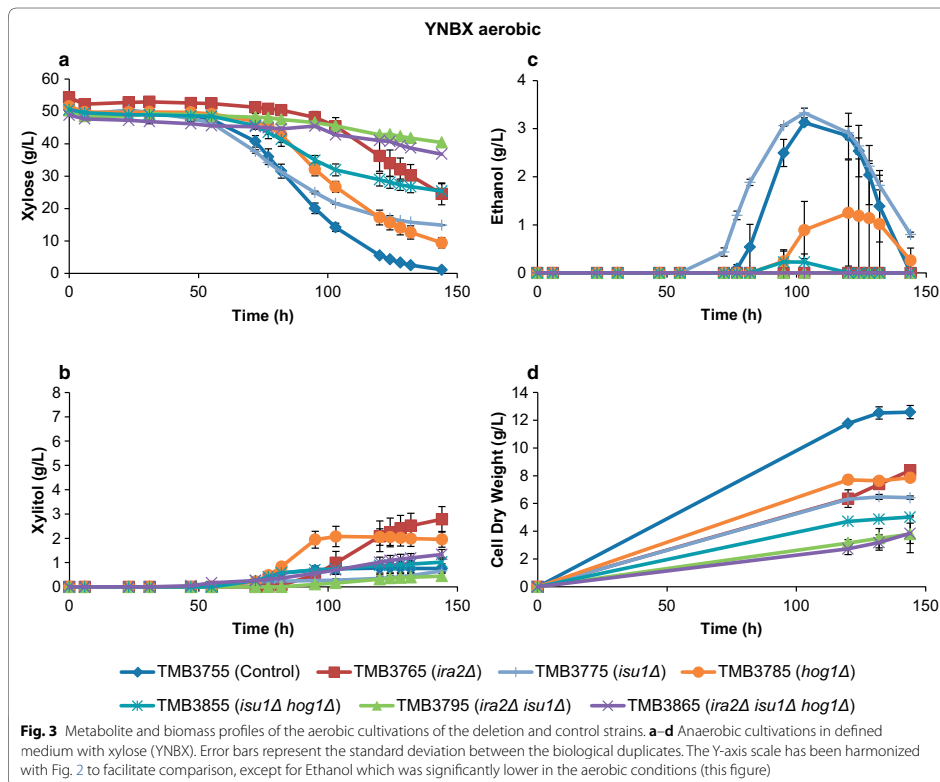
Aerobic conditions

It was previously suggested that during aerobic conditions, the *isu1Δ* single deletion relieved the starvation response on xylose and that *isu1Δhog1Δ* further

improved the specific xylose consumption rate [40]. To be able to investigate whether this also applied to the XR/XDH strains, three more strains were assayed in addition to the four that were used anaerobically: TMB3775 (*isu1Δ*), TMB3785 (*hog1Δ*), TMB3855 (*isu1Δhog1Δ*). The aerobic results on YNBX with the seven strains are shown in Fig. 3. As expected from respiratory growth, the aerobic cultivations in general led to higher biomass yields, but every deletion led to a decrease in final cell dry weight compared to the control strain. The lag time was significantly longer than during anaerobiosis, which has been observed before in XR/XDH strains engineered with a XR with preference for NADH [53].

isu1Δ was the best deletion in XR/XDH strains in terms of improved aerobic specific xylose consumption rate (Additional file 1: Table S3). However, any combination that included *isu1Δ* (*isu1Δhog1Δ*, *ira2Δisu1Δ*, *ira2Δisu1Δhog1Δ*) turned out to be worse than the single deletion in terms of specific rates of xylose and ethanol (Additional file 1: Table S3), thereby infirming any epistatic effect of *isu1Δhog1Δ* in the XR/XDH background. The results also demonstrated that the *ira2Δ* single deletion severely decreased the aerobic fitness in every regard: poor xylose consumption, increased xylitol accumulation and decreased production of ethanol and biomass (Fig. 3), which corroborates previous results [40]. It is also notable that, except for TMB3775 (*isu1Δ*) and TMB3785 (*hog1Δ*), no ethanol was detected in the aerobic cultures of the deletion strains (Fig. 3; Additional file 1: Table S3), which indicates that this is either a secondary effect of the decreased rate of xylose consumption (Fig. 3), or that these deletions makes the yeast Crabtree-negative during growth on xylose.





Signalome responses to *ira2Δ*, *hog1Δ* and *isu1Δ*

Following up on the proposed epistatic interactions between *ira2Δ*, *isu1Δ* and *hog1Δ* [40], the effect of these deletions on the three main sugar signalling pathways were investigated. The TMB3751 strain that lacks any GFP-coupled biosensor was used as a control in order to determine the background fluorescence intensity of the biosensor strains (autofluorescence) and how this was affected by potential changes in cell size and morphology caused by the mutations. When analysing TMB3751 and its derivatives either in the presence of xylose 50 g/L or without any carbon source (YNB only), an autofluorescence increase was observed for the strains with *HOG1* and *IRA2* single deletions, in *hog1Δ* and *ira2Δ* in combination with *isu1Δ*, as well as in the triple deletion case (Fig. 4a). It was also observed that the tendency to flocculate increased with each subsequent deletion, and that the average cell morphology also changed from

yeast-shaped to a circular shape (Additional file 1: Figure S5), which has previously been reported for e.g. loss-of-function mutants of *IRA2* [54]. Therefore, it was also of importance to normalize each signal to the autofluorescence of each background strain (TMB37X1; no biosensor) to account for effects linked to changes in morphology. The fluorescence results are illustrated in the form of a heat map with the fold change from the corresponding background strain (with the same deletion) to each strain and condition (Fig. 5); e.g. TMB3772 (*HXT1p*) was normalized to TMB3771 (no biosensor) and so on. We also acknowledged that the change in morphology/flocculation tendency made OD measurement unreliable, since it led to increases in apparent OD; instead, we used cell dry weight to quantify biomass, which circumvented the morphology issue. The signalling profiles were very similar in the aerobic, anaerobic conditions and microtiter plates experiments (Additional file 1: Figure S6), and

for the sake of throughput, the results of Figs. 4 and 5 are from the microtiter plates (micro-aerobic conditions) only.

***ira2Δisu1Δ* simultaneously leads to high and low glucose signals in different sugar signalling pathways**

As was shown in the characterisation section above, *ira2Δisu1Δ* resulted in the highest anaerobic specific xylose consumption rate. On the biosensor level, it was observed that *ira2Δisu1Δ* constitutively induced the *HXT1p* biosensor (usually activated by high glucose concentrations) in all the conditions, including low glucose (5 g/L), high xylose (50 g/L) and the repressing conditions (Fig. 5a and Additional file 1: Figure S2). The *high glucose*-signal from *ira2Δisu1Δ* displayed by the *HXT1p* biosensor (Snf3p/Rgt2p signalling pathway) was also confirmed with the *TPS1p* biosensor (cAMP/PKA pathway) that is normally inducible in low glucose and repressed in high glucose [38] (Additional file 1: Figure S4). *TPS1p*-GFP was repressed by *ira2Δ* and *ira2Δisu1Δ* not only in the repression condition, but also in conditions that induced the background strain (TMB3757), for instance, low glucose (G5) and high xylose (X50); Fig. 5c. Thus, *ira2Δisu1Δ* promoted a high glucose signal even in low glucose conditions or in conditions that previously gave a low glucose signal (i.e. xylose 50 g/L) [39].

Paradoxically, *SUC2p*, a biosensor that is induced by low glucose signals [38], was also highly induced by *ira2Δisu1Δ* on xylose. Therefore, on xylose, *ira2Δisu1Δ* both conferred a low glucose signal, (as shown by the *SUC2p* biosensor), and a high glucose signal (*HXT1p* induction and *TPS1p* repression), but in different signalling pathways (Snf1/Mig1p, Snf3p/Rgt2p vs. cAMP/PKA). In fact, the *ira2Δ* and *ira2Δisu1Δ* biosensors were induced on xylose in the *HXT1p* and *SUC2p* biosensor strains and downregulated in *TPS1p* when compared to their corresponding background strains (TMB375X), Fig. 5. Taken together, the biosensor analysis and the anaerobic fermentation data showed that all three signalling pathways (Snf3p/Rgt2p, Snf1/Mig1p and cAMP/PKA) were simultaneously activated by *ira2Δisu1Δ* in the high xylose condition (X50).

The single deletion of *IRA2* exhibited two distinct subpopulations for the *SUC2p* biosensor in xylose 50 g/L, with cell counts evenly distributed among them (left subpopulation: 43.8% of total cell count; right subpopulation: 56.2%; Fig. 4e-*ira2Δ*). Nonetheless, the additional deletion of *ISU1* strongly alleviated the left subpopulation compared to the single *ira2Δ*. A similar effect was observed among *isu1Δ* and *hog1Δ* and its combination.

hog1Δ* weakens the high glucose signal triggered by *ira2Δisu1Δ

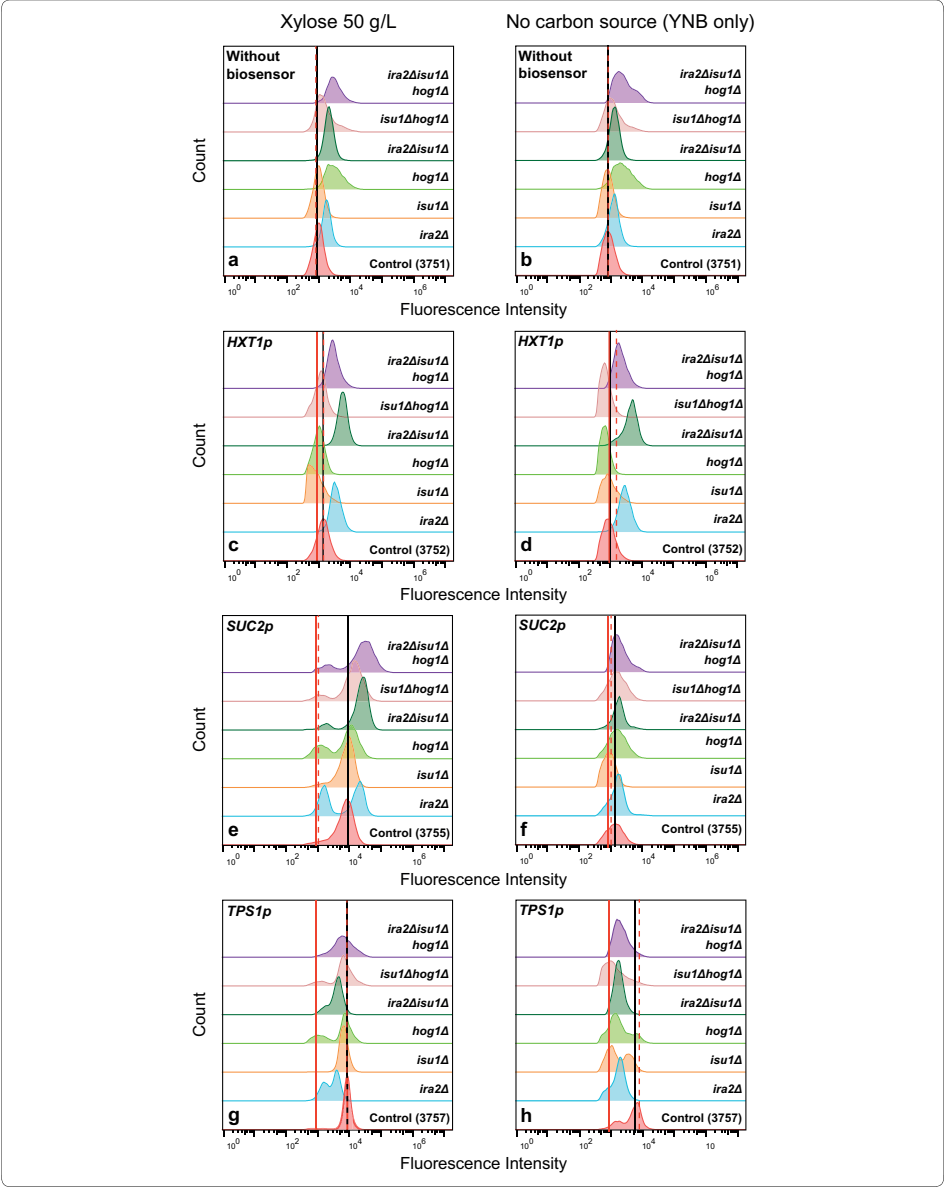
While *ira2Δisu1Δ* constitutively induced the *HXT1p* biosensor (Fig. 4c), the single deletion of *HOG1* resulted in a repression of *HXT1p*-GFP in almost all of the assayed conditions (Fig. 5a and Additional file 1: Figure S2). This repression also occurred in combination with *isu1Δ* (TMB3852: *isu1Δhog1Δ*) and to some extent with *ira2Δisu1Δ* (TMB3862: *ira2Δisu1Δhog1Δ*). In terms of fluorescence intensity (FI) signal, the triple deletion did not give the same high glucose signal as *ira2Δisu1Δ* (Fig. 4). At the same time, the addition of *hog1Δ* in TMB3792 (*ira2Δisu1Δ*) did not counteract the *SUC2p* low glucose-signal conferred by *ira2Δisu1Δ* since the major population of *SUC2p* biosensor on TMB3865 (*ira2Δisu1Δhog1Δ*) was still highly induced in all conditions, including xylose 50 g/L (Fig. 4e and Additional file 1: Figure S3). This high FI from the *SUC2p* biosensor implies that the triple deletion strain maintained the same low glucose-signal as the *ira2Δisu1Δ* strain (and the background strain TMB3755, cf. [39]), independently of carbon source. Finally, the impact of *hog1Δ* on *TPS1p* biosensor was mainly observed on the mixture of xylose 50 g/L and glucose 5 g/L, which seemed to keep this biosensor in an induced state (Fig. 5c; Additional file 1: Figure S4).

Discussion

In the current study, we showed that the epistatic interactions identified between *IRA2*, *ISU1* and *HOG1* gene deletions in a XI strain [40] were also valid for XR/XDH engineered *S. cerevisiae* strains. However, the biggest increase in specific xylose consumption and -ethanol

(See figure on next page.)

Fig. 4 Flow cytometry results on xylose 50 g/L (**a, c, e and g**) and no carbon source—YNB only (**b, d, f and h**) after 6 h. The histograms represent: strains without biosensor (**a and b**), *HXT1p* (**c and d**), *SUC2p* (**e and f**) and *TPS1p* (**g and h**), respectively. Each control strain (**a and b**: 3751, **c and d**: 3752, **e and f**: 3755 and **g and h**: 3757) is presented with all its deletion derivatives: single (*isu1Δ*, *hog1Δ*, and *ira2Δ*), double (*ira2Δisu1Δ* and *isu1Δhog1Δ*) and triple (*ira2Δisu1Δhog1Δ*) deletion. The black line indicates the autofluorescence of each control strain. The red dotted line shows the Fluorescence Intensity (FI) of the repression condition of each control strain (see Additional file 1: Figures S2–S4 (0 h)). The red solid line indicates the autofluorescence of control strain 3751 under the same condition (**a, b**). The cultivations were performed in oxygen limited microtiter plates, but the results are highly similar to those of the anaerobic and aerobic shake flasks (Additional file 1: Figure S6)





formation rates occurred in the *ira2Δisu1Δ* strains (and not in the *ira2Δisu1Δhog1Δ* strains as in [40]). Also the increase in specific rates was mostly connected to a corresponding decrease in final biomass, and not to an increase in volumetric rates. The present study also showed that there was a clear medium effect when using YPX (rich medium) that overshadowed some of the physiological effects of the deletions, and that defined medium (e.g. YNBX) should be preferred for this type of study. Furthermore, the clear impact of the deletions on the signalome confirmed our previous hypothesis that the efficiency of xylose uptake is connected to one or several of the sugar signalling routes [39].

Is there a connection between the increase in anaerobic specific xylose consumption rate and the simultaneous signalling of high and low glucose?

Previously, we have shown that high xylose concentrations gives the same response as low glucose concentrations in the three sugar signalling pathways in *S. cerevisiae* engineered with the XR/XDH pathway [39]. This low glucose-signal on xylose was hypothesised to be one of the reasons why xylose is not recognised as a fermentable carbon source by XR/XDH engineered *S. cerevisiae* [39]; presented schematically in Fig. 6a. In light of this hypothesis, the results with the *ira2Δisu1Δ* strains are noteworthy since the deletions do not only improve the specific xylose and ethanol rates, but also change the signalling to confer a high glucose-signal in

the Snf3p/Rgt2p and cAMP/PKA pathways (*HXT1p* and *TPS1p* biosensors, respectively), while maintaining the low glucose-signal in the SNF1/Mig1p pathway (*SUC2p* biosensor), see Fig. 6b. The improved specific rates in the *ira2Δisu1Δ* strains are directly related to the lower biomass production and the question that remains is whether the decreased biomass is a consequence of the changes in the signalome. This led us towards the cAMP/PKA pathway, which is known to regulate cell cycle progression, proliferation and homeostasis [55], and is a common denominator for the *ira2Δ* and *hog1Δ* deletions (Fig. 1b).

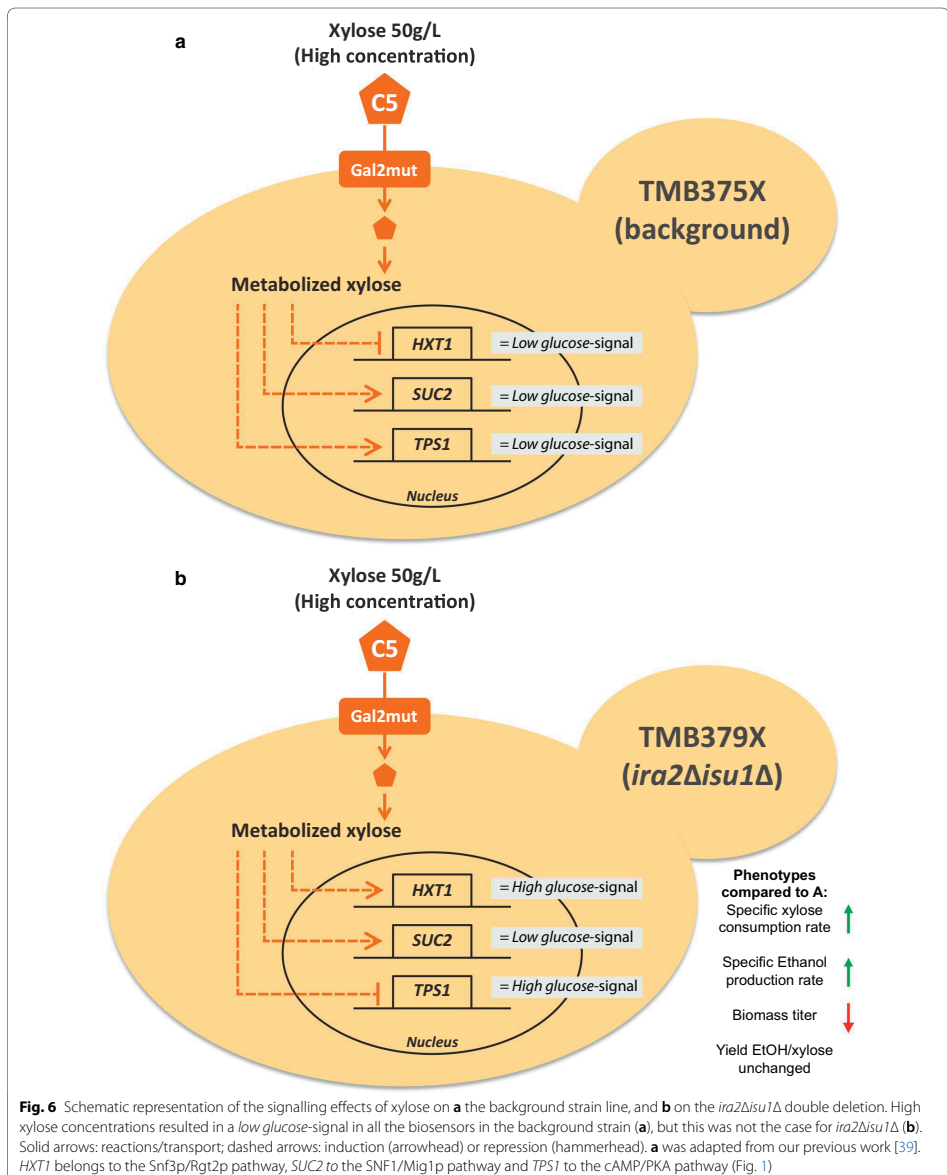
In very general terms, the level of active PKA in *S. cerevisiae* is glucose-regulated, and is high during growth on glucose and low during growth on alternative carbon sources [55]. cAMP and PKA levels are controlled intracellularly through the RAS-complex and extracellularly through glucose sensing by Gpr1p [46, 47]. Ira1/2p are regulators of RAS that induce the change of RAS from its active, cAMP-promoting form (RAS-GTP) to its inactive form (RAS-GDP) [41, 56]. *ira2Δ* has been reported to lead to constitutively activated RAS-GTP, which in turn leads to elevated levels of cAMP and PKA [46, 57], see Fig. 1b. Mechanistically, *ira2Δ* diminishes the self-regulatory feedback loop of PKA [46], which allows for continuous production of cAMP. This implies that *ira2Δ*-containing strains should have elevated cAMP/PKA levels compared to control strains, which fits with the overall high glucose-signal in the *TPS1p* biosensor strains (as indicated by *TPS1p* repression; Fig. 5c). PKA activation is dependent on cAMP, which is formed from ATP [58, 59]. In a study on the effect of benzoic acid on *S. cerevisiae*, it was found that addition of moderate levels of benzoic acid in the medium led to increased glycolytic and respiratory rates to compensate for the ATP consumed by pumping protons out of the cell, and to lower biomass [60]. In our case, the observed decrease in biomass production and increased sugar uptake rate in strains with *ira2Δ* in single and combinatorial deletion (Fig. 2h) could therefore be related to a constant ATP drainage from constitutive cAMP/PKA signals that should be very costly in terms of ATP.

Boosted PKA levels have been correlated with a number of phenotypes, some of which were also seen in the deletion strain of the current study. To name a few: PKA leads to lower levels of stress signals through its repression of the *MSN2/4* stress response genes [61], increased pseudohyphal growth [62] and increased critical cell size needed for budding [63] (Fig. 1b). The two latter in particular have also been reported for *ira2Δ* strains along with increased flocculation [54], and could explain the overall change in morphology observed in

the *ira2Δ*-containing strains (Additional file 1: Figure S5). It is possible that the changes in cell morphology and increased flocculation in the deletion strains are more pronounced in the W303 strain background that was used in the present study. W303 has, in comparison to the gold standard *S. cerevisiae* S288C genome, a number of non-synonymous mutations in flocculation genes that may make it more prone to flocculation [51]. PKA also contributes to the induction of low-affinity hexose transporters (i.e. *HXT1*) by phosphorylation of the Rgt1p protein, thus counteracting the repressive effect of Rgt1p on the low-affinity hexose transporter genes [39, 64]. This is not the only signal needed to induce *HXT1* [48, 65], but it is a supporting mechanism towards the high glucose-signal on xylose seen in the *ira2Δisu1Δ* strains (Figs. 4 and 6b).

While the above cAMP/PKA reasoning can explain the signal and phenotype of *ira2Δ*, it is clear that *isu1Δ* in conjunction with *ira2Δ* reinforces the high- and low glucose signal. *ISU1* encodes a mitochondrial Fe-S cluster protein and its deletion leads to accumulation of mitochondrial iron, which has been suggested to play a role in cellular iron homeostasis [66]. Deletion of *ISU1* is known to decrease the activity of respiratory enzymes that require Fe-S clusters, and thus results in poor respiratory growth [44], which is also evident from Fig. 3d. It has been reported that *isu1Δ* helped maintain low levels of reactive oxygen species (ROS) during ethanol stress (which was not the case of other Fe-S cluster deletants) [67] and that the elevated mitochondrial iron helped suppressing oxidative damage in *S. cerevisiae* cells lacking the *SOD1* superoxide dismutase [66]. This is likely to be a contributing factor to the enabled xylose respiration that was shown in *isu1Δ* strains when the oxidative phosphorylation was experimentally blocked [40].

The anaerobic effect of *isu1Δ*—or rather its effect together with *ira2Δ* (Fig. 2)—are more puzzling, as the mitochondrion is primarily involved in respiration. Also, proteomics analysis of the *isu1Δ* XI strains revealed a difference compared to the control strain during aerobic conditions, but not during anaerobic conditions [40]. The mitochondrial Isu proteins have however been suggested to also be necessary for maturation of cytosolic Fe-S clusters [68]. Since *isu1Δ* changes the iron homeostasis by accumulation of mitochondrial iron [66], it is likely that these cells have a constitutive iron stress. High iron levels inactivate a transcription factor (Aft1p) by migrating it from the mitochondria to the cytosol, meaning that it cannot induce its targets, which include *ISU1/2* and metal transporters [69], and would thus contribute to a decrease in Fe-S cluster formation. How this would lead to the observed decrease in biomass formation and increased specific ethanol production of the current



study is difficult to say, but it could be speculated that the cell would benefit from producing ethanol during the iron stress, so that it can grow on it when the stress is relieved. This would however require more experiments than the current study.

It is also noteworthy that *SUC2* is still induced in *ira2Δisu1Δ* strains, indicating that there is a *low glucose* signal to this pathway—this was in fact, observed in all of the deletion strains (Figs. 4 and 5). Whereas the *high glucose* signal to the other two signalling pathways suggest that the deletions do tune the cell towards understanding that xylose is fermentable (Fig. 6b), the *low glucose* signal to the SNF1/Mig1p pathway as indicated by the *SUC2p* induction, suggests that yeast could simultaneously sense xylose as a non-fermentable carbon source. Aerobically, the comparative proteomics results of Sato et al. suggested that the *isu1Δ* XI strains did not emit a starvation response on xylose which is normally seen in *S. cerevisiae*, and that the mechanisms for non-fermentable carbon sources were repressed [40]. However, our *SUC2p* biosensor strains suggest that there indeed was an induction signal for the alternative carbon pathways during aerobic conditions (Fig. 4e). *SUC2p* transcription has been found to be induced by PKA during low glucose levels, and repressed by PKA during absence of glucose [70], i.e. PKA can both induce and repress *SUC2p*. The likely elevated PKA levels in the *ira2Δisu1Δ* strains in the current study, coupled with proposed *low glucose*-signal from xylose in the XR/XDH background [39] could therefore explain why the *SUC2p* biosensors are induced in the *ira2Δisu1Δ* double deletants.

The biggest difference between the current study and that of Sato et al. is that the *ira2Δisu1Δhog1Δ* triple deletion was not the best strain in terms of specific xylose and ethanol rates but *ira2Δisu1Δ* was. The main signalling difference between these two deletions was that *HXT1p* was more induced in the *ira2Δisu1Δ* than in *ira2Δisu1Δhog1Δ* strain (Fig. 4), which could imply that it is of essence to have high expression of low affinity hexose transporters (e.g. *HXT1p*) in order to improve the specific xylose consumption. It should however be noted that the triple deletion did recover the decreases in concentration and volumetric rates of the double deletion (Fig. 4; Additional file 1: Table S2), meaning that the *ira2Δisu1Δhog1Δ* strains might still be of interest from a process point-of-view.

Are *ira2Δ* and *isu1Δ* desired genotypes for anaerobic xylose fermentation processes?

In the previous section we hypothesize that the simultaneous *high*- and *low glucose* signals were one of the reasons for the improved xylose phenotypes of the *ira2Δisu1Δ* strains. However, this comes with clear

physiological drawbacks: they consume less xylose, produce less ethanol and biomass (Fig. 4) and tend to flocculate (Additional file 1: Figure S5). The *ira2Δ* single deletion results in an improved strain in terms of specific rates because of the decrease in biomass production. Anaerobic cultivations lead to significantly lower biomass production than aerobic cultivations and *ira2Δ* decreases an already low biomass concentration to even lower levels. This explains why the anaerobic xylose, xylitol and ethanol titres are roughly the same between the control and *ira2Δ* strains while the specific rates increased. As *ira2Δ* leads to constitutive activation of PKA, the cell will have a repressed stress response system (e.g. *MSN2/4*) and thus feel less stress; however, this is a “false happiness”, since the strain cannot really activate its stress system. Lignocellulose hydrolysate is rich in inhibitory compounds such as furans and aromatics, and *ira2Δ* might therefore be a less suitable deletion for this type of fermentation process. The XR/XDH pathway does have an edge over XI here, as XR has 5-hydroxymethyl-furfural detoxifying effect [71]. Adding the *isu1Δ* deletion, that according to literature leads to hyperaccumulation of mitochondrial iron [66], will likely trigger an iron stress and Fe–S cluster insufficiencies, that possibly is masked by the repression of the stress response system by the high PKA levels. Dos Santos et al. who also discovered the effects of the *isu1Δ* the same year as Sato et al. hypothesized that *isu1Δ* might be beneficial to XI strains since XI is a metalloenzyme [45], which is also the case for yeast XDHs [72]. Therefore *ira2Δisu1Δ* is a double edged sword: aerobically it is the worst combination in terms of fitness and titres (Fig. 3), but anaerobically it is one of the best in terms of specific rates (Table 2).

The discussed deletions are undeniably a step in the right direction for improving xylose utilization and signalling in *S. cerevisiae*. But the physiological drawbacks warrant us to ask what a desired genotype for xylose fermentation would look like. It is likely that a balance is needed for signalling that may be difficult to achieve by null mutants alone. Turning specific genes on or off is likely to kill or damage the cell, and a more careful gene attenuation would probably be beneficial, e.g. by CRISPRi methods [73]. The biosensor system for monitoring the sugar signalling pathways will be a valuable tool towards this end, as it allows modifications to be assessed by both physiological characterization and signalling patterns.

Conclusions

We previously showed that xylose is not sensed extracellularly by *S. cerevisiae* [38] and that XR/XDH engineered strains gave a *low glucose*-signal when grown in high xylose concentrations, implying low PKA activity [39]. In the present study, the deletions of *IRA2* and *ISU1* were

used to look further into this hypothesis. We were able to show that the deletions did convey xylose fermentation improvements in XR/XDH strains, and that this phenotype was linked to changes in the sugar signalome. The simultaneous *high*- and *low* glucose signal achieved by *ira2Δisu1Δ* on xylose 50 g/L suggests that these deletions to some extent alleviate the *low* glucose-signal we saw in the parental XR/XDH biosensor strains [39], and that genetic modifications of this kind are likely a step towards making *S. cerevisiae* recognize xylose as a fermentable carbon source.

Materials and methods

Strains and media

The *S. cerevisiae* strains used in the present study are based on previously constructed strains that contain biosensors that couple the promoters from different genes regulated by the sugar signalling pathways to a green fluorescent protein (GFP) [38, 39]. In the current study, the TMB375X series of strains (Table 1; [39]) were used to further study the genetics of the signalome. Besides the different GFP biosensors, the TMB375X strains contain a single-copy of the mutated *GAL2* transporter from the pRS62N_GAL2_N376F plasmid [24], overexpression of two pentose phosphate pathway genes (*TAL1*, *TKL1*) and three copies of XR/XDH/XK xylose pathway [39]. All the strains used in the study are listed in Table 1.

The yeast strains were maintained on Yeast Peptone Dextrose (YPD; 10 g/L yeast extract, 20 g/L peptone, 20 g/L glucose). Physiological characterization was performed in Yeast Peptone (YP) and/or Yeast Nitrogen Base (YNB; 6.7 g/L Yeast Nitrogen Base without amino acids [Becton–Dickinson and Company, USA] buffered with 50 mM potassium hydrogen phthalate at pH 5.5) media supplemented with different concentrations of glucose and/or xylose as a carbon source (see details below). For sub-cloning of plasmids, *Escherichia coli* NEB5- α (New England BioLabs, Ipswich, MA, US) was used and was cultivated in Lysogeny Broth (LB) medium (10 g/L tryptone, 5 g/L yeast extract, 5 g/L NaCl, pH 7.0). Yeast mineral medium (3 g/L KH_2PO_4 , 0.5 g/L $\text{MgSO}_4 \cdot 7\text{H}_2\text{O}$, 6.6 g/L K_2SO_4 , 1 mL/L trace elements, 1 mL/L vitamin solution, pH 6.0 adjusted with KOH) [60] was used for the amdSYM transformations [74]. When using solid plates, 15 g/L of agar was added to the medium. All strains were stored in 25% (v/v) glycerol at -80°C and, when relevant, transformed cells were also stored with their corresponding antibiotics.

Molecular biology methods

Standard methods were used to perform cloning experiments [75]. The primers used in the study, acquired from Eurofins MWG Operon (Ebersberg, Germany), are listed

in Additional file 1: Table S4. Competent *E. coli* cells were prepared and transformed according to the methods of Inoue and colleagues [76]; transformants were selected for in LB medium supplemented with 50 $\mu\text{g/mL}$ of ampicillin. The Lithium Acetate transformation protocol [77] with the addition of DMSO (10% v/v) prior to heat shock [78] was used for the *S. cerevisiae* transformations. All yeast transformants were selected according to their specific selection marker and verified by colony PCR [79].

Deletion of *ISU1* and *HOG1* with CRISPR–Cas9

Construction of gRNA plasmids

The pCfB3496 (hphMX marker) [80] and LWA26 (natMX marker) [39] plasmids were used as templates to construct gRNA plasmids to target *ISU1* and *HOG1*. The plasmids were PCR amplified using Phusion High-Fidelity DNA Polymerase (Thermo Fisher Scientific, Waltham, MA, USA) and phosphorylated primers. The forward primers (105_ISU1_f and 105_HOG1_f) contained a 5' tail with the new 20 bp targeting sequence (Additional file 1: Table S4), and were used together with the 103_r reverse primer to generate the plasmids to target *ISU1* and *HOG1* respectively. The amplicons were purified with GeneJET PCR purification kit (Thermo Fisher Scientific) according to the manufacturer's protocol. The purified products were digested with *DpnI* followed by plasmid ligation with T4 DNA ligase (Thermo Fisher Scientific). The obtained plasmids were propagated in *E. coli*, extracted with the GeneJET Plasmid Miniprep Kit (Thermo Fisher Scientific) and verified by Sanger sequencing (Eurofins MWG Operon) using standard primer T3. The final plasmids were named gRNA_ISU1 and gRNA_HOG1 (Additional file 1: Table S5). Two different selection markers were chosen for these plasmids to avoid marker recycling after yeast transformation: gRNA_ISU1 had Hygromycin B (hphMX) and gRNA_HOG1 had ClonNAT (natMX).

Construction of donor DNA and deletion of *ISU1* and *HOG1*

A fragment of the bacterial AmpR ampicillin resistance gene (330 bp) was amplified to be used as a junk-donor DNA to delete *ISU1* and *HOG1* with CRISPR–Cas9. Primers with 50 bp tails with homology to the upstream and downstream regions of *ISU1* (primers Amp_ISU1_f and Amp_ISU1_r) and *HOG1* (primers Amp_HOG1_f and Amp_HOG1_r) were used to amplify the fragment. Agarose gel electrophoresis was performed to confirm the presence of the desired PCR products. The fragment was purified with the GeneJET PCR purification kit (Thermo Fisher Scientific).

All yeast strains used in this study already had the pCfB2312 plasmid containing a Cas9 gene [80]. The strains were transformed by the addition of 1 μg gRNA

plasmid and 0.5 µg of donor DNA, specific for each deletion. *ISU1* and *HOG1* transformants were selected on YPD plates with 200 µg/mL geneticin supplemented with either 200 µg/mL Hygromycin B or 100 µg/mL clonNAT, respectively.

Deletion of *IRA2* with *amdSYM*

IRA2 proved difficult to delete with the CRISPR–Cas9 system, which was possibly due to the large size of this gene (9240 bp). Instead, the *amdSYM* strategy [74] was used for this deletion. The *amdSYM* cassette was amplified from the pUG-*amdSYM* plasmid [74] with *IRA2_S1_**amdSYM_f* and *IRA2_S2_**amdSYM_r* primers containing 50 bp homology to the upstream and downstream region of *IRA2*. The fragment was purified with the GeneJet PCR purification kit (Thermo Fisher Scientific) and 1 µg purified product was used for the yeast transformations. The transformants were selected for growth on mineral medium [60] with 0.6 g/L acetamide; the same medium but with 2.3 g/L fluoroacetamide was used to recycle the *amdSYM* marker. Recycling of *amdSYM* marker was accomplished by inoculating a single colony in 10 mL of YPD in a 50 mL of conical centrifuge tubes at 30 °C, 180 rpm followed by plating on mineral medium [60] with 2.3 g/L fluoroacetamide. Colony PCR was used to verify the recycling.

Flow cytometry

Single-cell fluorescence intensity (FI) was measured with a BD Accuri C6 flow cytometer in connection with a BD CSampler autosampler (Becton–Dickinson, NJ, US). Detection was done at 488 nm and 533/30 bandpass filter (FL1-H channel). Pre-cultivations, induction/repression conditions and sample preparations were performed as previously described [38, 39]. Cells were inoculated in a microtiter plate starting with an $OD_{620nm} = 0.5$ and were incubated for 6 h, at 800 rpm and 30 °C. Different media were tested during the incubation: YNB-KHPthalate medium with glucose 1 g/L, 5 g/L and 40 g/L; xylose 50 g/L; xylose 50 g/L combined with glucose 5 g/L and with no carbon source (YNB only). The threshold was set to 800 at FL1-H channel and 10 000 events were collected per sample. Flow cytometry data from technical and biological replicates were analyzed with the FlowJo v10 software (Treestar, Inc., San Carlos, CA).

Aerobic and anaerobic cultivations

Prior to the aerobic and anaerobic fermentation, pre-cultivations were carried out as in the flow cytometry experiment [39]. The aerobic cultivations were performed with 100 mL of YNB-KHPthalate supplemented with 50 g/L of xylose (YNBX) in 1 L baffled shake flasks. For the

anaerobic cultivations, YNB-KHPthalate supplemented with 50 g/L of xylose (YNBX) and YP supplemented with 50 g/L of xylose (YPX) were used, respectively. 100 mL media were added to 1 L non-baffled shake flasks sealed with a curved neck attached to a rubber stopper. Nitrogen gas was sparged through an inlet port connected to a 0.22 µm sterile filter. Glycerol (2 mL) was added into the curved neck to maintain the anaerobic environment while allowing for gas release. A separate outlet was used for sampling.

All cultivations (anaerobic and aerobic) were performed at 30 °C and 180 rpm and in biological duplicates. Samples for optical density at 620 nm (OD_{620}), metabolites, and flow cytometry (at 0 h and 6 h) were taken and stored at 4 °C. The samples were not frozen since it has been observed that storage at –20 °C negatively affects the quantification of high xylose concentrations.

Biomass and metabolite analysis

Biomass was determined both as OD_{620} with an Ultrospec 2100 Pro spectrophotometer (Amersham Biosciences, Uppsala, Sweden) and as cell dry weight (CDW). CDW was performed by vacuum filtering 5 mL culture through pre-weighed Supor 450 Membrane Disc Filters (0.45 µm; Pall Corporation, NY, USA), followed by washing with distilled water and drying for 8 min at 350 W in a microwave. The dried filters were stored in a desiccator prior to weighing.

A Waters HPLC system (Milford, MA, USA) was used to quantify extracellular metabolites in the cultivations. The system was run with an Aminex HPX-87H ion exchange column (Bio-Rad, Hercules, CA, USA) at 60 °C, and a mobile phase of 5 mM H_2SO_4 flowing at 0.6 mL/min. Compounds were detected with a refractive index detector (Waters model 2414; Milford, MA, USA).

Additional file

Additional file 1. Additional Methods, Figures and Tables.

Abbreviations

CDW: cell dry weight; FI: fluorescence intensity; GFP: green fluorescent protein; OD: optical density; PCR: polymerase chain reaction; XDH: xylitol dehydrogenase; XI: xylose isomerase; XK: xylulokinase; XR: xylose reductase; YNB: Yeast Nitrogen Base; YNBX: Yeast Nitrogen Base Xylose; YPD: Yeast extract Peptone Dextrose; YPX: Yeast extract Peptone Xylose.

Acknowledgements

The authors are grateful to Gunnar Lidén and Henrik Almqvist (Department of Chemical Engineering, Lund University) for giving us time on their anaerobic shake flask system and assisting with its setup. We would like to thank Magnus Carlquist for his input on the flow cytometry methods. Plasmids for the *S. cerevisiae* CRISPR–Cas9 system that was used in this study were kindly provided by Irina Borodina, Vratislav Stovicek and Jochen Förster (Technical

University of Denmark, Copenhagen, Denmark). We would also like to thank Eckhard Boles (Goethe University, Frankfurt, Germany) for providing the pRS62N_GAL2_N376F plasmid that was integrated in the background strains used in the study.

Authors' contributions

KOO, CB and MFGG designed the experimental plan. KOO and BLF constructed the strains and performed the initial flow cytometry experiments (microtiter plates). KOO and CB performed the shake flask cultivations and the flow cytometry. DB performed the HPLC analysis. KOO, CB, DB and MFGG analysed the data. DB wrote the manuscript based on a draft from KOO, and KOO, CB and MFGG contributed with input on the writing. MFGG conceived the study and revised the manuscript. All authors read and approved the final manuscript.

Funding

This work was supported by The Swedish Research Council (Vetenskapsrådet) under grant number 2016-05297_VR, the Swedish Energy Agency (grant number 2018-004378), and The Brazilian National Council for Scientific and Technological Development (Conselho Nacional de Desenvolvimento Científico e Tecnológico) [scholarship awarded for KOO].

Availability of data and materials

Flow cytometry and fermentation data are available upon request.

Ethics approval and consent to participate

Not applicable.

Consent for publication

Not applicable.

Competing interests

The authors declare that they have no competing interests.

Received: 23 March 2019 Accepted: 17 May 2019

Published online: 23 May 2019

References

- Nanda S, Azargohar R, Dalai AK, Kozinski JA. An assessment on the sustainability of lignocellulosic biomass for biorefining. *Renew Sustain Energy Rev*. 2015;50:925–41.
- Hahn-Hägerdal B, Karhumaa K, Fonseca C, Spencer-Martins I, Gorwa-Grauslund MF. Towards industrial pentose-fermenting yeast strains. *Appl Microbiol Biotechnol*. 2007;74:937–53.
- Buschke N, Schäfer R, Becker J, Wittmann C. Metabolic engineering of industrial platform microorganisms for biorefinery applications—optimization of substrate spectrum and process robustness by rational and evolutive strategies. *Biores Technol*. 2013;135:544–54.
- Laluce C, Schenberg ACG, Gallardo JCM, Coradello LFC, Pombeiro-Sponchiado SR. Advances and developments in strategies to improve strains of *Saccharomyces cerevisiae* and processes to obtain the lignocellulosic ethanol—a review. *Appl Biochem Biotechnol*. 2012;166:1908–26.
- Almeida JR, Modig T, Petersson A, Hahn-Hägerdal B, Lidén G, Gorwa-Grauslund MF. Increased tolerance and conversion of inhibitors in lignocellulosic hydrolysates by *Saccharomyces cerevisiae*. *J Chem Technol Biotechnol Int Res Process Environ Clean Technol*. 2007;82:340–9.
- Jeffries T, Jin Y-S. Metabolic engineering for improved fermentation of pentoses by yeasts. *Appl Microbiol Biotechnol*. 2004;63:495–509.
- Limayem A, Ricke SC. Lignocellulosic biomass for bioethanol production: current perspectives, potential issues and future prospects. *Prog Energy Combust Sci*. 2012;38:449–67.
- Kötter P, Amore R, Hollenberg CP, Ciriacy M. Isolation and characterization of the *Pichia stipitis* xylitol dehydrogenase gene, *XYL2*, and construction of a xylose-utilizing *Saccharomyces cerevisiae* transformant. *Curr Genet*. 1990;18:493–500.
- Kötter P, Ciriacy M. Xylose Fermentation by *Saccharomyces cerevisiae*. *Appl Microbiol Biotechnol*. 1993;38:776–83.
- Brat D, Boles E, Wiedemann B. Functional expression of a bacterial xylose isomerase in *Saccharomyces cerevisiae*. *Appl Environ Microbiol*. 2009;75:2304–11.
- Kuyper M, Harhangi HR, Stave AK, Winkler AA, Jetten MS, de Laat WT, den Ridder JJ, Op den Camp HJ, van Dijken JP, Pronk JT. High-level functional expression of a fungal xylose isomerase: the key to efficient ethanol fermentation of xylose by *Saccharomyces cerevisiae*? *FEMS Yeast Res*. 2003;4:69–78.
- Moysés DN, Reis VCB, Almeida JRMD, Moraes LMPD, Torres FAG. Xylose fermentation by *Saccharomyces cerevisiae*: challenges and prospects. *Int J Mol Sci*. 2016;17:207.
- Eliasson A, Christensson C, Wahlborn CF, Hahn-Hägerdal B. Anaerobic xylose fermentation by recombinant *Saccharomyces cerevisiae* carrying *XYL1*, *XYL2*, and *XKS1* in mineral medium chemostat cultures. *Appl Environ Microbiol*. 2000;66:3381–6.
- Jin Y-S, Ni H, Laplaza JM, Jeffries TW. Optimal growth and ethanol production from xylose by recombinant *Saccharomyces cerevisiae* require moderate D-xylulokinase activity. *Appl Environ Microbiol*. 2003;69:495–503.
- Walfridsson M, Hallborn J, Penttilä M, Keränen S, Hahn-Hägerdal B. Xylose-metabolizing *Saccharomyces cerevisiae* strains overexpressing the *TKL1* and *TAL1* genes encoding the pentose phosphate pathway enzymes transketolase and transaldolase. *Appl Environ Microbiol*. 1995;61:4184–90.
- Träff Bjerre K, Jeppsson M, Hahn-Hägerdal B, Gorwa-Grauslund MF. Endogenous NADPH-dependent aldose reductase activity influences product formation during xylose consumption in recombinant *Saccharomyces cerevisiae*. *Yeast*. 2004;21:141–50.
- Kuyper M, Hartog MM, Toirkens MJ, Almering MJ, Winkler AA, van Dijken JP, Pronk JT. Metabolic engineering of a xylose-isomerase-expressing *Saccharomyces cerevisiae* strain for rapid anaerobic xylose fermentation. *FEMS Yeast Res*. 2005;5:399–409.
- Van Vleet JH, Jeffries TW, Olsson L. Deleting the para-nitrophenyl phosphatase (*pNPase*), *PHO13*, in recombinant *Saccharomyces cerevisiae* improves growth and ethanol production on D-xylose. *Metab Eng*. 2008;10:360–9.
- Ni H, Laplaza JM, Jeffries TW. Transposon mutagenesis to improve the growth of recombinant *Saccharomyces cerevisiae* on D-xylose. *Appl Environ Microbiol*. 2007;73:2061–6.
- Cadete RM, Heras AM, Sandström AG, Ferreira C, Gírio F, Gorwa-Grauslund MF, Rosa CA, Fonseca C. Exploring xylose metabolism in *Spathaspora* species: *XYL1*. 2 from *Spathaspora passalidarum* as the key for efficient anaerobic xylose fermentation in metabolic engineered *Saccharomyces cerevisiae*. *Biotechnol Biofuels*. 2016;9:167.
- Ha S-J, Kim SR, Choi J-H, Park MS, Jin Y-S. Xylitol does not inhibit xylose fermentation by engineered *Saccharomyces cerevisiae* expressing *xylA* as severely as it inhibits xylose isomerase reaction in vitro. *Appl Microbiol Biotechnol*. 2011;92:77–84.
- Träff K, Cordero RO, Van Zyl W, Hahn-Hägerdal B. Deletion of the *GRE3* aldose reductase gene and its influence on xylose metabolism in recombinant strains of *Saccharomyces cerevisiae* expressing *thxylA* and *XKS1* genes. *Appl Environ Microbiol*. 2001;67:5668–74.
- Subtil T, Boles E. Competition between pentoses and glucose during uptake and catabolism in recombinant *Saccharomyces cerevisiae*. *Biotechnol Biofuels*. 2012;5:14.
- Farwick A, Bruder S, Schadeweg V, Oreb M, Boles E. Engineering of yeast hexose transporters to transport D-xylose without inhibition by D-glucose. *Proc Natl Acad Sci USA*. 2014;111:5159–64.
- Nijland JG, Shin HY, de Jong RM, De Waal PP, Klaassen P, Driessen AJ. Engineering of an endogenous hexose transporter into a specific D-xylose transporter facilitates glucose-xylose co-consumption in *Saccharomyces cerevisiae*. *Biotechnol Biofuels*. 2014;7:168.
- Reider Apel A, Ouellet M, Szmidt-Middleton H, Keasling JD, Mukhopadhyay A. Evolved hexose transporter enhances xylose uptake and glucose/xylose co-utilization in *Saccharomyces cerevisiae*. *Scientific Rep*. 2016;6:19512.
- Shin HY, Nijland JG, Waal PP, Jong RM, Klaassen P, Driessen AJ. An engineered cryptic *Hxt11* sugar transporter facilitates glucose-xylose co-consumption in *Saccharomyces cerevisiae*. *Biotechnol Biofuels*. 2015;8:176.
- Zhou H, Cheng J-S, Wang BL, Fink GR, Stephanopoulos G. Xylose isomerase overexpression along with engineering of the pentose phosphate pathway and evolutionary engineering enable rapid xylose utilization

- and ethanol production by *Saccharomyces cerevisiae*. *Metab Eng*. 2012;14:611–22.
29. McMillan J. Xylose fermentation to ethanol. A review. Golden: National Renewable Energy Lab; 1993.
 30. Taherzadeh MJ, Niklasson C, Lidén G. Acetic acid—friend or foe in anaerobic batch conversion of glucose to ethanol by *Saccharomyces cerevisiae*? *Chem Eng Sci*. 1997;52:2653–9.
 31. Zaldivar J, Borges A, Johansson B, Smits H, Villas-Bôas S, Nielsen J, Olsson L. Fermentation performance and intracellular metabolite patterns in laboratory and industrial xylose-fermenting *Saccharomyces cerevisiae*. *Appl Microbiol Biotechnol*. 2002;59:436–42.
 32. Jin Y-S, Laplaza JM, Jeffries TW. *Saccharomyces cerevisiae* engineered for xylose metabolism exhibits a respiratory response. *Appl Environ Microbiol*. 2004;70:6816–25.
 33. Salusjärvi L, Pitkänen J-P, Aristidou A, Ruohonen L, Penttilä M. Transcription analysis of recombinant *Saccharomyces cerevisiae* reveals novel responses to xylose. *Appl Biochem Biotechnol*. 2006;128:237–73.
 34. Runquist D, Hahn-Hägerdal B, Bettiga M. Increased expression of the oxidative pentose phosphate pathway and gluconeogenesis in anaerobically growing xylose-utilizing *Saccharomyces cerevisiae*. *Microb Cell Fact*. 2009;8:1.
 35. Klimacek M, Krahulec S, Sauer U, Nidetzky B. Limitations in xylose-fermenting *Saccharomyces cerevisiae*, made evident through comprehensive metabolite profiling and thermodynamic analysis. *Appl Environ Microbiol*. 2010;76:7566–74.
 36. Bergdahl B, Heer D, Sauer U, Hahn-Hägerdal B, van Niel EWJ. Dynamic metabolomics differentiates between carbon and energy starvation in recombinant *Saccharomyces cerevisiae* fermenting xylose. *Biotechnol Biofuels*. 2012;5:34.
 37. Feng X, Zhao H. Investigating glucose and xylose metabolism in *Saccharomyces cerevisiae* and *Scheffersomyces stipitis* via C-13 metabolic flux analysis. *AIChE J*. 2013;59:3195–202.
 38. Brink DP, Borgström C, Tueros FG, Gorwa-Grauslund MF. Real-time monitoring of the sugar sensing in *Saccharomyces cerevisiae* indicates endogenous mechanisms for xylose signaling. *Microb Cell Fact*. 2016;15:183.
 39. Osiro KO, Brink DP, Borgström C, Wasserstrom L, Carlquist M, Gorwa-Grauslund MF. Assessing the effect of d-xylose on the sugar signaling pathways of *Saccharomyces cerevisiae* in strains engineered for xylose transport and assimilation. *FEMS Yeast Res*. 2018. <https://doi.org/10.1093/femsyr/fox096>.
 40. Sato TK, Tremaine M, Parreiras LS, Hebert AS, Myers KS, Higbee AJ, Sardi M, McDwain SJ, Ong JM, Breuer RJ. Directed evolution reveals unexpected epistatic interactions that alter metabolic regulation and enable anaerobic xylose use by *Saccharomyces cerevisiae*. *PLoS Genet*. 2016;12:e1006372.
 41. Tanaka K, Nakafuku M, Tamanoi F, Kaziro Y, Matsumoto K, Toh-e A. IRA2, a second gene of *Saccharomyces cerevisiae* that encodes a protein with a domain homologous to mammalian ras GTPase-activating protein. *Mol Cell Biol*. 1990;10:4303–13.
 42. Reiser V, Ruis H, Ammerer G. Kinase activity-dependent nuclear export opposes stress-induced nuclear accumulation and retention of Hog1 mitogen-activated protein kinase in the budding yeast *Saccharomyces cerevisiae*. *Mol Biol Cell*. 1999;10:1147–61.
 43. Mühlenhoff U, Gerber J, Richhardt N, Lill R. Components involved in assembly and dislocation of iron–sulfur clusters on the scaffold protein Isu1p. *EMBO J*. 2003;22:4815–25.
 44. Schilke B, Voisine C, Beinert H, Craig E. Evidence for a conserved system for iron metabolism in the mitochondria of *Saccharomyces cerevisiae*. *Proc Natl Acad Sci*. 1999;96:10206–11.
 45. Dos Santos LV, Carazzolle MF, Nagamatsu ST, Sampaio NMV, Almeida LD, Pirolla RAS, Borelli G, Corrêa TLR, Argueso JL, Pereira GAG. Unraveling the genetic basis of xylose consumption in engineered *Saccharomyces cerevisiae* strains. *Scientific Rep*. 2016;6:38676.
 46. Colombo S, Ronchetti D, Thevelein JM, Winderickx J, Martegani E. Activation state of the Ras2 protein and glucose-induced signaling in *Saccharomyces cerevisiae*. *J Biol Chem*. 2004;279:46715–22.
 47. Kraakman L, Lemaire K, Ma P, Teunissen AW, Donaton MC, Van Dijk P, Winderickx J, De Winde JH, Thevelein JM. A *Saccharomyces cerevisiae* G-protein coupled receptor, Gpr1, is specifically required for glucose activation of the cAMP pathway during the transition to growth on glucose. *Mol Microbiol*. 1999;32:1002–12.
 48. Belinchón MM, Gancedo JM. Different signalling pathways mediate glucose induction of SUC2, HXT1 and pyruvate decarboxylase in yeast. *FEMS Yeast Res*. 2006;7:40–7.
 49. Nijkamp JF, van den Broek M, Datema E, de Kok S, Bosman L, Luttik MA, Daran-Lapujade P, Vongsangnak W, Nielsen J, Heijne WHM, et al. De novo sequencing, assembly and analysis of the genome of the laboratory strain *Saccharomyces cerevisiae* CEN.PK113-7D, a model for modern industrial biotechnology. *Microb Cell Fact*. 2012;11:36.
 50. Vanhalewyn M, Dumortier F, Debast G, Colombo S, Ma PS, Winderickx J, Van Dijk P, Thevelein JM. A mutation in *Saccharomyces cerevisiae* adenylyl cyclase, Cyr 1 (K1876 M), specifically affects glucose- and acidification-induced cAMP signalling and not the basal cAMP level. *Mol Microbiol*. 1999;33:363–76.
 51. Matheson K, Parsons L, Gammie A. Whole-genome sequence and variant analysis of W303, a widely-used strain of *Saccharomyces cerevisiae*. *G3 Genes Genomes Genet*. 2017;7:2219–26.
 52. Hahn-Hägerdal B, Karhumaa K, Larsson CU, Gorwa-Grauslund M, Görgens J, Van Zyl WH. Role of cultivation media in the development of yeast strains for large scale industrial use. *Microb Cell Fact*. 2005;4:31.
 53. de las Heras AM, Portugal-Nunes DJ, Rizza N, Sandström AG, Gorwa-Grauslund MF. Anaerobic poly 3-D-hydroxybutyrate production from xylose in recombinant *Saccharomyces cerevisiae* using a NADH-dependent acetoacetyl-CoA reductase. *Microb Cell Fact*. 2016;15:197.
 54. Halme A, Bumgarner S, Styles C, Fink GR. Genetic and epigenetic regulation of the FLO gene family generates cell-surface variation in yeast. *Cell*. 2004;116:405–15.
 55. Rolland F, Winderickx J, Thevelein JM. Glucose-sensing and signalling mechanisms in yeast. *FEMS Yeast Res*. 2002;2:183–201.
 56. Santangelo GM. Glucose signaling in *Saccharomyces cerevisiae*. *Microbiol Mol Biol Rev*. 2006;70:253–82.
 57. Park J-I, Grant CM, Dawes IW. The high-affinity cAMP phosphodiesterase of *Saccharomyces cerevisiae* is the major determinant of cAMP levels in stationary phase: involvement of different branches of the Ras-cyclic AMP pathway in stress responses. *Biochem Biophys Res Commun*. 2005;327:311–9.
 58. Cook WH, Lipkin D, Markham R. The formation of a cyclic dianhydride-dienyl acid (I) by the alkaline degradation of adenosine-5'-triphosphoric acid (II). *J Am Chem Soc*. 1957;79:3607–8.
 59. Uno I, Nyuoya H, Ishikawa T. Effects of 2-deoxy-D-glucose and quinidine on the fruiting body formation in *Coprinus macrorhizus*. *J Gen Appl Microbiol*. 1981;27:219–28.
 60. Verdruyn C, Postma E, Scheffers WA, Van Dijken JP. Effect of benzoic acid on metabolic fluxes in yeasts: a continuous-culture study on the regulation of respiration and alcoholic fermentation. *Yeast*. 1992;8:501–17.
 61. Smith A, Ward MP, Garrett S. Yeast PKA represses Msn2p/Msn4p-dependent gene expression to regulate growth, stress response and glycogen accumulation. *EMBO J*. 1998;17:3556–64.
 62. Robertson LS, Causton HC, Young RA, Fink GR. The yeast A kinases differentially regulate iron uptake and respiratory function. *Proc Natl Acad Sci*. 2000;97:5984–8.
 63. Tokiwa G, Tyers M, Volpe T, Futcher B. Inhibition of G1 cyclin activity by the Ras/cAMP pathway in yeast. *Nature*. 1994;371:342.
 64. Kim J-H, Johnston M. Two glucose-sensing pathways converge on Rgt1 to regulate expression of glucose transporter genes in *Saccharomyces cerevisiae*. *J Biol Chem*. 2006;281:26144–9.
 65. Tomás-Cobos L, Casadomé L, Mas G, Sanz P, Posas F. Expression of the HXT1 low affinity glucose transporter requires the coordinated activities of the HOG and glucose signalling pathways. *J Biol Chem*. 2004;279:22010–9.
 66. Garland SA, Hoff K, Vickery LE, Culotta VC. *Saccharomyces cerevisiae* ISU1 and ISU2: members of a well-conserved gene family for iron-sulfur cluster assembly. *J Mol Biol*. 1999;294:897–907.
 67. Perez-Gallardo RV, Briones L, Díaz-Pérez AL, Gutiérrez S, Rodríguez-Zavala JS, Campos-García J. Reactive oxygen species production induced by ethanol in *Saccharomyces cerevisiae* increases because of a dysfunctional mitochondrial iron–sulfur cluster assembly system. *FEMS Yeast Res*. 2013;13:804–19.
 68. Gerber J, Neumann K, Prohl C, Mühlenhoff U, Lill R. The yeast scaffold proteins Isu1p and Isu2p are required inside mitochondria for maturation of cytosolic Fe/S proteins. *Mol Cell Biol*. 2004;24:4848–57.

69. Yamaguchi-Iwai Y, Ueta R, Fukunaka A, Sasaki R. Subcellular localization of Aft1 transcription factor responds to iron status in *Saccharomyces cerevisiae*. *J Biol Chem*. 2002;277:18914–8.
70. Gancedo JM, Flores CL, Gancedo C. The repressor Rgt1 and the cAMP-dependent protein kinases control the expression of the SUC2 gene in *Saccharomyces cerevisiae*. *Biochimica et Biophysica Acta (BBA)-General Subjects*. 2015;1850:1362–7.
71. Almeida JR, Modig T, Röder A, Lidén G, Gorwa-Grauslund M-F. *Pichia stipitis* xylose reductase helps detoxifying lignocellulosic hydrolysate by reducing 5-hydroxymethyl-furfural (HMF). *Biotechnol Biofuels*. 2008;1:12.
72. Lunzer R, Mamnun Y, Haltrich D, Kulbe KD, Nidetzky B. Structural and functional properties of a yeast xylitol dehydrogenase, a Zn²⁺ + -containing metalloenzyme similar to medium-chain sorbitol dehydrogenases. *Biochem J*. 1998;336:91–9.
73. Gilbert LA, Larson MH, Morsut L, Liu Z, Brar GA, Torres SE, Stern-Ginossar N, Brandman O, Whitehead EH, Doudna JA. CRISPR-mediated modular RNA-guided regulation of transcription in eukaryotes. *Cell*. 2013;154:442–51.
74. Solis-Escalante D, Kuijpers NG, Nadine B, Bolat I, Bosman L, Pronk JT, Daran J-M, Daran-Lapujade P. *amdSYM*, a new dominant recyclable marker cassette for *Saccharomyces cerevisiae*. *FEMS Yeast Res*. 2013;13:126–39.
75. Sambrook J, Russell DW. *Molecular cloning: a laboratory manual*. 3rd ed. New York: Cold Spring Harbor Laboratory Press; 2001.
76. Inoue H, Nojima H, Okayama H. High-efficiency transformation of *Escherichia coli* with plasmids. *Gene*. 1990;96:23–8.
77. Gietz RD, Schiestl RH. High-efficiency yeast transformation using the LiAc/SS carrier DNA/PEG method. *Nat Protoc*. 2007;2:31–4.
78. Hill J, Donald KA, Griffiths DE. DMSO-enhanced whole cell yeast transformation. *Nucleic Acids Res*. 1991;19:5791.
79. Bergkessel M, Guthrie C. Colony PCR. In: *Methods in enzymology*, vol. 529. Amsterdam: Elsevier; 2013. p. 299–309.
80. Stovicek V, Borodina I, Forster J. CRISPR–Cas system enables fast and simple genome editing of industrial *Saccharomyces cerevisiae* strains. *Metab Eng Commun*. 2015;2:13–22.
81. Vandamme J, Castermans D, Thevelein JM. Molecular mechanisms of feedback inhibition of protein kinase A on intracellular cAMP accumulation. *Cell Signal*. 2012;24:1610–8.
82. Tamaki H. Glucose-stimulated cAMP-protein kinase A pathway in yeast *Saccharomyces cerevisiae*. *J Biosci Bioeng*. 2007;104:245–50.
83. Urban J, Soulard A, Huber A, Lippman S, Mukhopadhyay D, Deloche O, Wanke V, Anrather D, Ammerer G, Riezman H. Sch9 is a major target of TORC1 in *Saccharomyces cerevisiae*. *Mol Cell*. 2007;26:663–74.
84. Bisschops MM, Zwartjens P, Keuter SG, Pronk JT, Daran-Lapujade P. To divide or not to divide: a key role of Rim15 in calorie-restricted yeast cultures. *Biochimica et Biophysica Acta (BBA) Mol Cell Res*. 2014;1843:1020–30.
85. Chen RE, Thorner J. Function and regulation in MAPK signaling pathways: lessons learned from the yeast *Saccharomyces cerevisiae*. *Biochimica et Biophysica Acta-Mol Cell Res*. 2007;1773:1311–40.

Publisher's Note

Springer Nature remains neutral with regard to jurisdictional claims in published maps and institutional affiliations.

Ready to submit your research? Choose BMC and benefit from:

- fast, convenient online submission
- thorough peer review by experienced researchers in your field
- rapid publication on acceptance
- support for research data, including large and complex data types
- gold Open Access which fosters wider collaboration and increased citations
- maximum visibility for your research: over 100M website views per year

At BMC, research is always in progress.

Learn more biomedcentral.com/submissions



Supporting Information[†] for:

Exploring the xylose paradox in *Saccharomyces cerevisiae* through *in vivo* sugar signalomics of targeted deletants

Karen O Osiro, Celina Borgström, Daniel P Brink, Birta Líf Fjölnisdóttir and
Marie F Gorwa-Grauslund*

Applied Microbiology, Department of Chemistry, Lund University, Lund, Sweden

*Corresponding author

E- mail: marie-francoise.gorwa@tmb.lth.se

[†] Reformatted for increased readability by Celina Borgström Tufvegren

Additional Methods

Uncompensated and compensated carbon balances

The carbon balances for the anaerobic and aerobic shake flask cultivations were calculated based on the measured concentrations of xylose, xylitol, glycerol, acetate and ethanol in C-mols/L (Table S1-3), see Eq. 1. C_n in the equation is the number of C-mols of compounds n , and one C-mol biomass of *S. cerevisiae* was approximated with $\text{CH}_{1.62}\text{O}_{0.47}\text{N}_{0.21}$ [1]. A degree-of-reduction (DR) balance was made in parallel to solve the equation system (Eq. 2), with each coefficient being the degree-of-reduction of the compound.

$$C_{xylose} = C_{xylitol} + C_{glycerol} + C_{acetate} + C_{EtOH} + C_{biomass} \quad (\text{Eq. 1})$$

$$4 \cdot C_{xylose} = 4.4 \cdot C_{xylitol} + 4.67 \cdot C_{glycerol} + 4 \cdot C_{acetate} + 6 \cdot C_{EtOH} + 4.11 \cdot C_{biomass} \quad (\text{Eq. 2})$$

Since the anaerobic DR balances only closed around 90% (Table S1-3), a compensated balance was made where it was assumed that there were two missing compounds: Ethanol and CO_2 and that their addition would close the DR balance to 100%. The missing degree-of-reduction (ΔDR) and missing carbon balance (ΔC) in the measured data was thus as assumed to consist of:

$$\Delta\text{DR} = \text{DR}_{in} - \text{DR}_{out} = 6 \cdot C_{EtOH} + 0 \cdot C_{\text{CO}_2} \quad (\text{Eq. 3})$$

$$\Delta\text{C} = C_{in} - C_{out} = C_{EtOH} + C_{\text{CO}_2} \quad (\text{Eq. 4})$$

where 6 and 0 are the degree-of-reduction coefficients of Ethanol and CO_2 respectively. The compensated balances (Table S1-S3) did improve the Carbon balance closure, but they still only close at 70-75%. This implies that the HPLC quantification did not capture all the carbon, and that there was carbon that probably was lost due to the N_2 -sparging.

Additional Figures

Control strain (without biosensor)

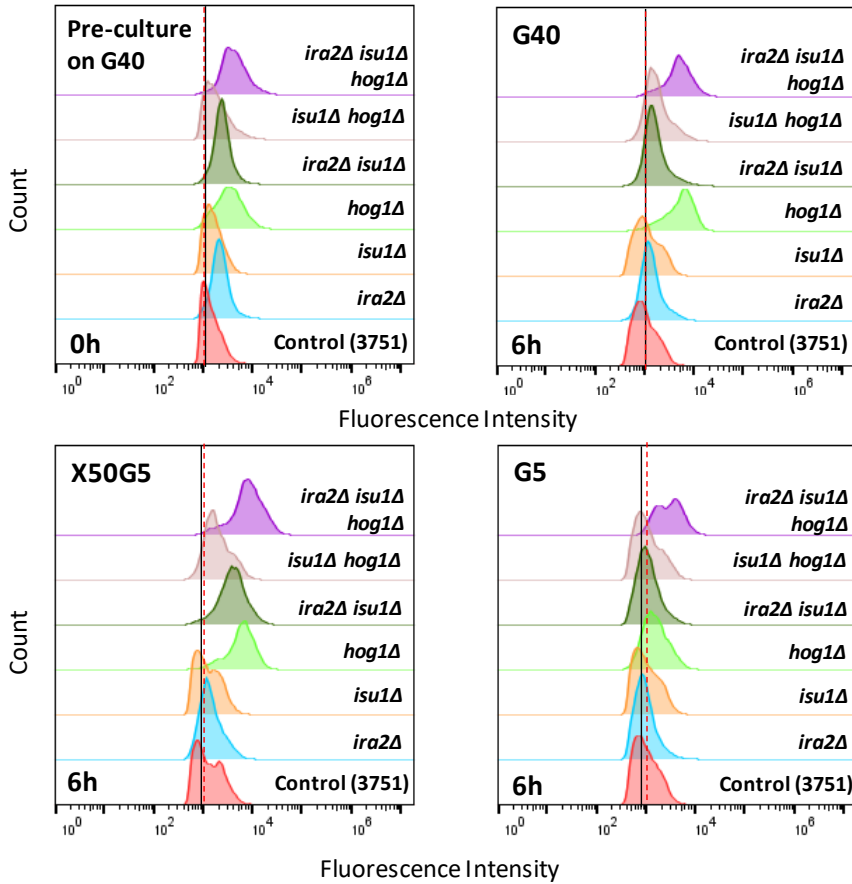


Figure S1. Histogram of the control strain (without biosensor) and all its derivatives (TMB 3XX1) at different carbon sources: pre-culture on G40 (0h), glucose 40 g/L (G40), mixture of xylose 50 g/L and glucose 5 g/L (X50G5) and glucose 5 g/L (G5). Black line indicates the autofluorescence of each control strain. Red dotted line shows the Fluorescence Intensity (FI) of the repression condition of control strain. The experiments were performed in microtiter plates.

HXT1p biosensor

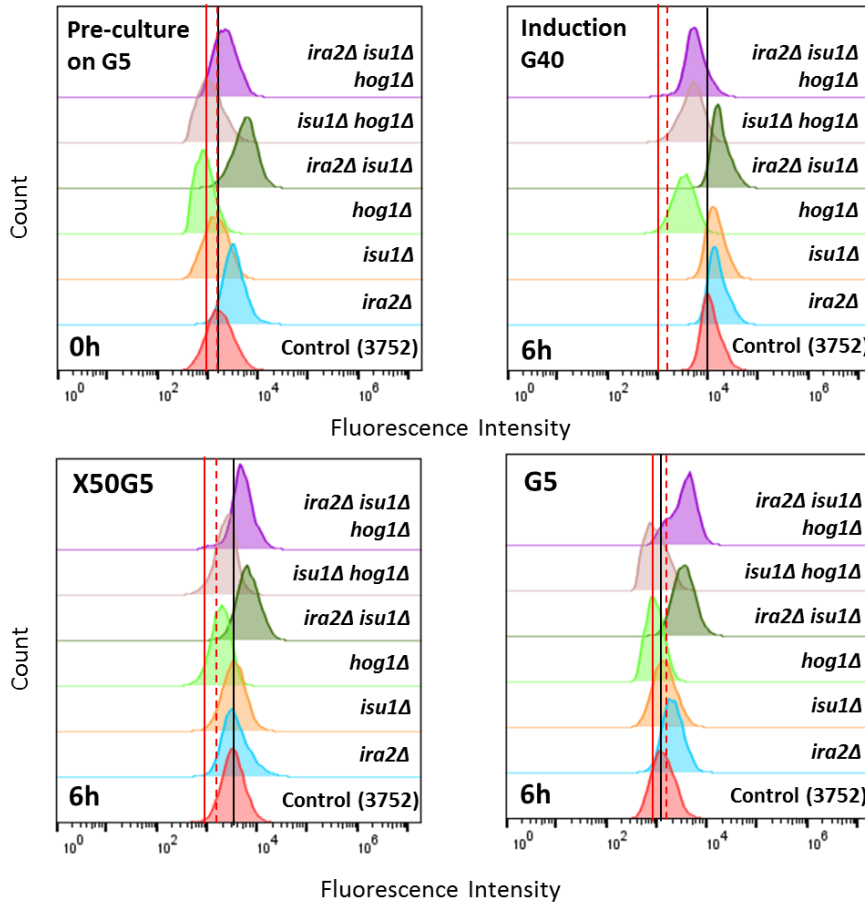


Figure S2. Histogram of the *HXT1p* biosensor and all its derivatives (TMB 3XX2) at different carbon sources: pre-culture on G40 (0h), glucose 40 g/L (G40), mixture of xylose 50 g/L and glucose 5 g/L (X50G5) and glucose 5 g/L (G5). Black line indicates the autofluorescence of each control strain. Red dotted line shows the Fluorescence Intensity (FI) of the repression condition of control strain. Red solid line indicates the autofluorescence of control strain 3751 under same condition as presented on each graph. The experiments were performed in microtiter plates.

SUC2p biosensor

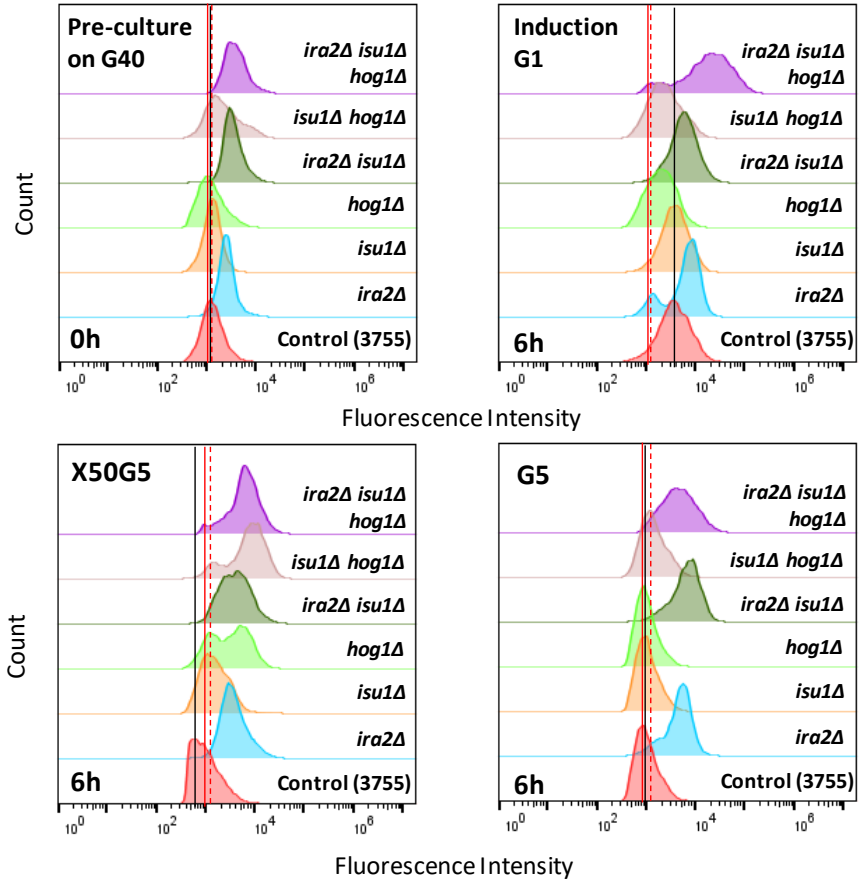


Figure S3. Histogram of the SUC2p biosensor and all its derivatives (TMB 3XX5) at different carbon sources: pre-culture on G40 (0h), glucose 40 g/L (G40), mixture of xylose 50 g/L and glucose 5 g/L (X50G5) and glucose 5 g/L (G5). Black line indicates the autofluorescence of each control strain. Red dotted line shows the Fluorescence Intensity (FI) of the repression condition of control strain. Red solid line indicates the autofluorescence of control strain 3751 under same condition as presented on each graph. The experiments were performed in microtiter plates.

TPS1p biosensor

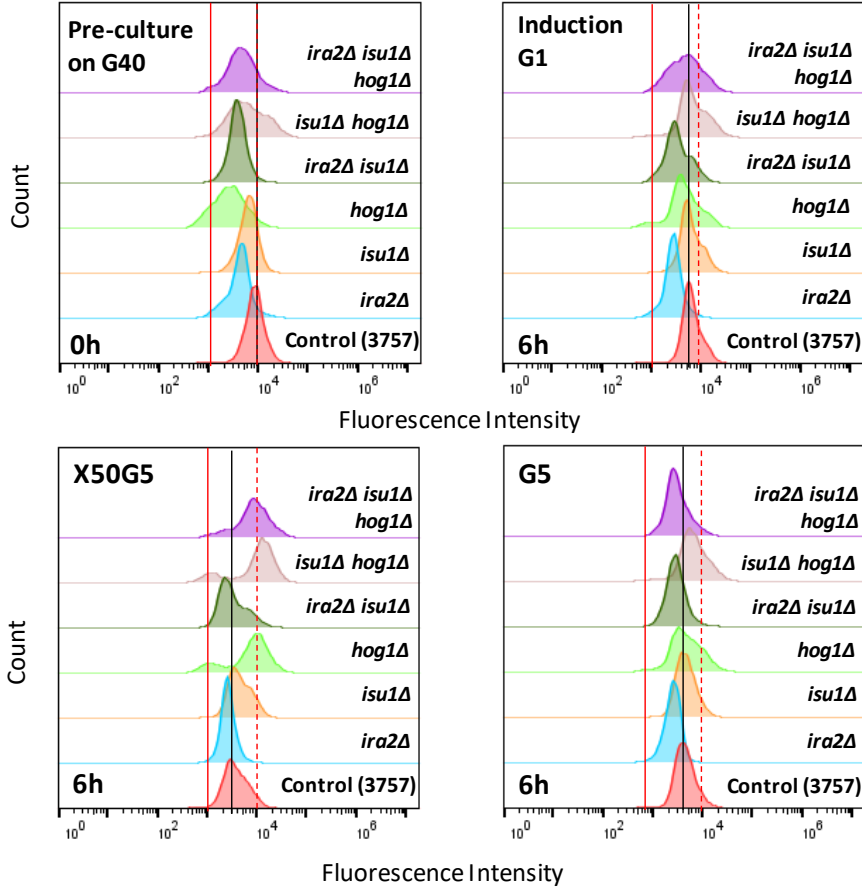


Figure S4. Histogram of the TPS1p biosensor and all its derivatives (TMB 3XX7) at different carbon sources: pre-culture on G40 (0h), glucose 40 g/L (G40), mixture of xylose 50 g/L and glucose 5 g/L (X50G5) and glucose 5 g/L (G5). Black line indicates the autofluorescence of each control strain. Red dotted line shows the Fluorescence Intensity (FI) of the repression condition of control strain. Red solid line indicates the autofluorescence of control strain 3751 under same condition as presented on each graph. The experiments were performed in microtiter plates.

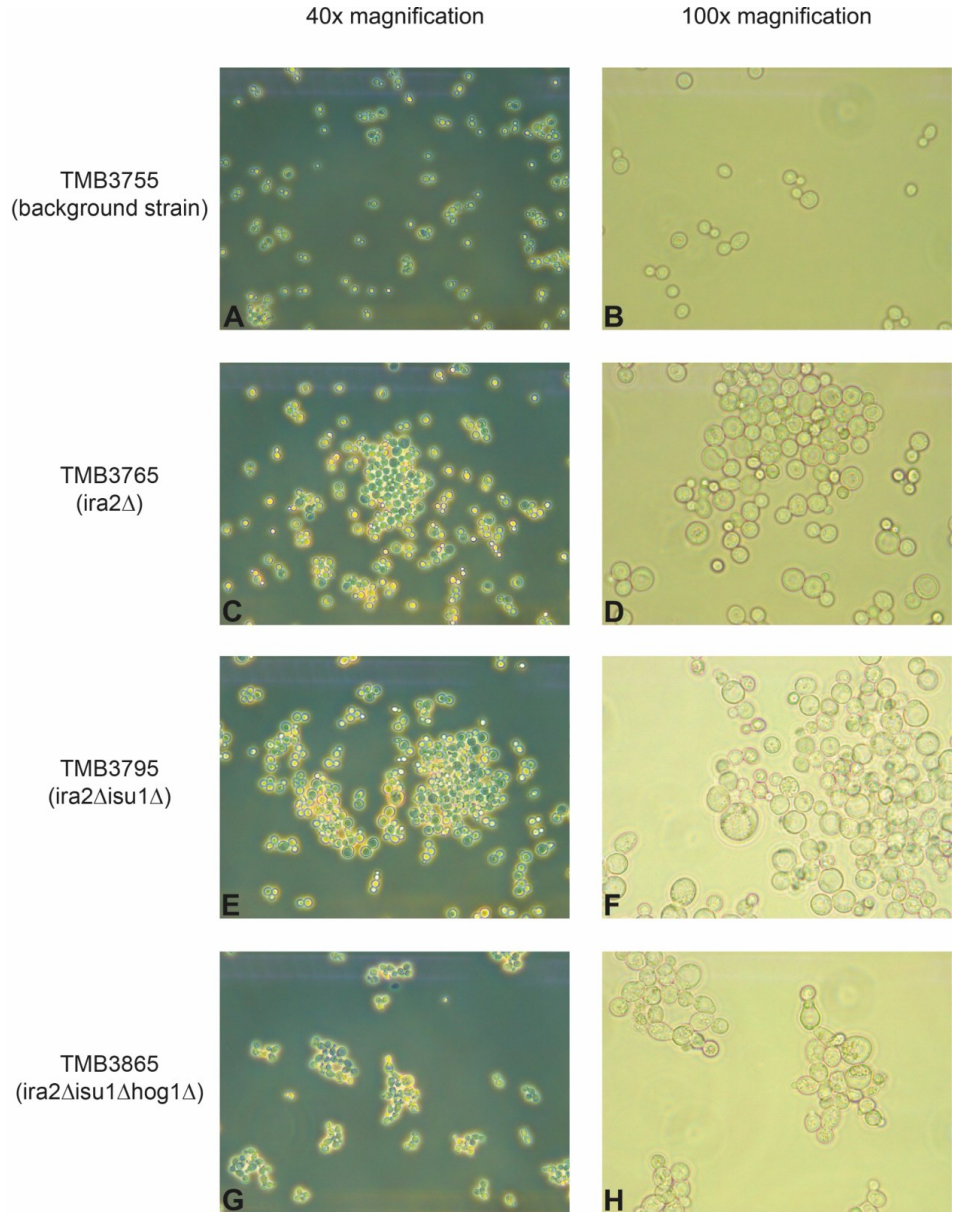


Figure S5. Microscopy photos of the overnight cultures in glucose 40 g/L of the background strain for the *SUC2p* biosensor (TMB3755) and the subsequent deletions of *ira2Δ*, *isu1Δ*, *hog1Δ*. Note the changes in flocculation tendency and cell morphology with each deletion. Left hand side: 40x magnification; right hand side: 100x magnification. Photos were taken with a Leica ICC50W microscope camera (Leica Microsystems, Germany).

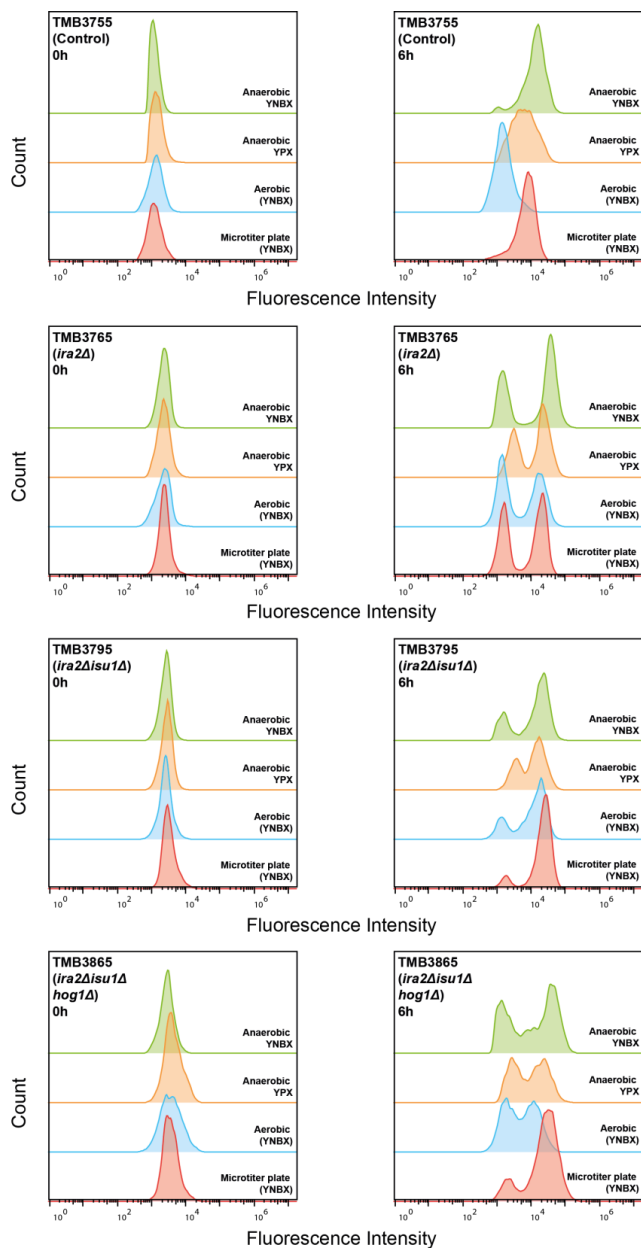


Figure S6. Comparison of the signal of the *SUC2p* biosensors across the anaerobic and aerobic shake flask experiments, and the microtiter plate experiment. Representative histograms were used for each condition. Note that the signal intensity (X-axis) is comparable across the different oxygenations and vessel volumes, except in the aerobic experiment for the background strain.

Additional Tables

Table S1. Rates, yields and carbon balance data from the **anaerobic** shake flasks with **YPX** (0-48h), performed in two biological replicates.

	TMB3755 (background strain)	TMB3765 (Δira2)	TMB3795 (Δira2 Δsul)	TMB3865 (Δira2 Δsul Δhog1)
Volumetric Xylose consumption rate (g · L ⁻¹ · h ⁻¹)	10.684 ± 0.318	10.701 ± 0.253	8.323 ± 0.317	10.305 ± 0.310
Volumetric Xylitol formation rate (g · L ⁻¹ · h ⁻¹)	1.182 ± 0.107	1.230 ± 0.081	0.930 ± 0.015	1.218 ± 0.012
Volumetric Glycerol formation rate (g · L ⁻¹ · h ⁻¹)	0.141 ± 0.079	0.027 ± 0.038	0.181 ± 0.026	0.022 ± 0.031
Volumetric Acetate formation rate (g · L ⁻¹ · h ⁻¹)	0.149 ± 0.028	0.157 ± 0.020	0.134 ± 0.028	0.143 ± 0.034
Volumetric Ethanol formation rate (g · L ⁻¹ · h ⁻¹)	3.430 ± 0.312	3.841 ± 0.214	2.928 ± 0.045	3.706 ± 0.038
Specific Xylose consumption rate (g · g CDW ⁻¹ · L ⁻¹ · h ⁻¹)	1.571 ± 0.090	2.058 ± 0.049	3.223 ± 0.555	1.938 ± 0.090
Specific Xylitol formation rate (g · g CDW ⁻¹ · L ⁻¹ · h ⁻¹)	0.173 ± 0.001	0.237 ± 0.016	0.361 ± 0.070	0.229 ± 0.006
Specific Glycerol formation rate (g · g CDW ⁻¹ · L ⁻¹ · h ⁻¹)	0.021 ± 0.013	0.005 ± 0.007	0.069 ± 0.005	0.004 ± 0.006
Specific Acetate formation rate (g · g CDW ⁻¹ · L ⁻¹ · h ⁻¹)	0.022 ± 0.006	0.030 ± 0.004	0.053 ± 0.022	0.027 ± 0.006
Specific Ethanol formation rate (g · g CDW ⁻¹ · L ⁻¹ · h ⁻¹)	0.507 ± 0.090	0.739 ± 0.041	1.137 ± 0.221	0.697 ± 0.018
Yield Ethanol per Xylose (g/g)	0.322 ± 0.039	0.359 ± 0.012	0.352 ± 0.008	0.360 ± 0.007
Yield Xylitol per Xylose (g/g)	0.111 ± 0.007	0.115 ± 0.005	0.112 ± 0.002	0.118 ± 0.002
Yield Acetate per Xylose (g/g)	0.014 ± 0.003	0.015 ± 0.002	0.016 ± 0.004	0.014 ± 0.004
Yield Glycerol per Xylose (g/g)	0.013 ± 0.008	0.003 ± 0.004	0.022 ± 0.002	0.002 ± 0.003
Carbon balance closure	70.52%	71.29%	68.07%	72.30%
Degree of reduction closure	93.14%	96.15%	92.64%	97.25%
Compensated Carbon balance closure	75.09%	73.86%	72.97%	74.13%
Compensated Degree of reduction closure	100.00%	100.00%	100.00%	100.00%

Table S2. Rates, yields and carbon balance data from the **anaerobic** shake flasks with **YNBX** (0-70h), performed in two biological replicates.

	TMB3755 (background strain)	TMB3765 (Δ ira2)	TMB3795 (Δ ira2 Δ isul)	TMB3865 (Δ ira2 Δ isul Δ hog1)
Volumetric Xylose consumption rate ($\text{g} \cdot \text{L}^{-1} \cdot \text{h}^{-1}$)	7.810 \pm 0.319	7.657 \pm 0.069	3.162 \pm 0.635	7.489 \pm 0.322
Volumetric Xylitol formation rate ($\text{g} \cdot \text{L}^{-1} \cdot \text{h}^{-1}$)	0.869 \pm 0.054	0.825 \pm 0.024	0.181 \pm 0.032	1.037 \pm 0.053
Volumetric Glycerol formation rate ($\text{g} \cdot \text{L}^{-1} \cdot \text{h}^{-1}$)	0.076 \pm 0.011	0.051 \pm 0.015	0.079 \pm 0.025	0.025 \pm 0.001
Volumetric Acetate formation rate ($\text{g} \cdot \text{L}^{-1} \cdot \text{h}^{-1}$)	0.096 \pm 0.026	0.060 \pm 0.029	0.066 \pm 0.011	0.081 \pm 0.029
Volumetric Ethanol formation rate ($\text{g} \cdot \text{L}^{-1} \cdot \text{h}^{-1}$)	2.496 \pm 0.100	2.623 \pm 0.105	1.118 \pm 0.115	2.128 \pm 0.288
Specific Xylose consumption rate ($\text{g} \cdot \text{g CDW}^{-1} \cdot \text{L}^{-1} \cdot \text{h}^{-1}$)	1.414 \pm 0.144	2.190 \pm 0.086	4.225 \pm 0.926	2.116 \pm 0.010
Specific Xylitol formation rate ($\text{g} \cdot \text{g CDW}^{-1} \cdot \text{L}^{-1} \cdot \text{h}^{-1}$)	0.158 \pm 0.019	0.236 \pm 0.005	0.242 \pm 0.047	0.293 \pm 0.001
Specific Glycerol formation rate ($\text{g} \cdot \text{g CDW}^{-1} \cdot \text{L}^{-1} \cdot \text{h}^{-1}$)	0.014 \pm 0.003	0.014 \pm 0.004	0.105 \pm 0.035	0.007 \pm 0.001
Specific Acetate formation rate ($\text{g} \cdot \text{g CDW}^{-1} \cdot \text{L}^{-1} \cdot \text{h}^{-1}$)	0.008 \pm 0.002	0.019 \pm 0.004	0.022 \pm 0.031	0.017 \pm 0.004
Specific Ethanol formation rate ($\text{g} \cdot \text{g CDW}^{-1} \cdot \text{L}^{-1} \cdot \text{h}^{-1}$)	0.451 \pm 0.010	0.751 \pm 0.066	1.492 \pm 0.181	0.600 \pm 0.053
Yield Ethanol per Xylose (g/g)	0.320 \pm 0.026	0.343 \pm 0.017	0.357 \pm 0.035	0.284 \pm 0.026
Yield Xylitol per Xylose (g/g)	0.111 \pm 0.002	0.108 \pm 0.002	0.058 \pm 0.002	0.138 \pm 0.001
Yield Acetate per Xylose (g/g)	0.012 \pm 0.003	0.008 \pm 0.004	0.022 \pm 0.008	0.011 \pm 0.004
Yield Glycerol per Xylose (g/g)	0.010 \pm 0.001	0.007 \pm 0.002	0.025 \pm 0.003	0.003 \pm 0.000
Carbon balance closure	70.41%	67.05%	61.48%	66.63%
Degree of reduction closure	94.10%	92.13%	86.53%	90.24%
Compensated Carbon balance closure	74.35%	72.30%	70.47%	73.14%
Compensated Degree of reduction closure	100.00%	100.00%	100.00%	100.00%

Table S3. Rates, yields and carbon balance data from the aerobic shake flasks with YNBX (0-120h), performed in two biological replicates.

	TMB3755 (Background strain)	TMB3765 (Aira2)	TMB3775 (Δ isul)	TMB3785 (Δ hog1)	TMB3795 (Aira2 Δ isul)	TMB3855 (Δ isul Δ hog1)	TMB3865 (Aira2 Δ isul Δ hog1)
Volumetric Xylose consumption rate ($\text{g} \cdot \text{L}^{-1} \cdot \text{h}^{-1}$)	3.748 \pm 0.262	1.503 \pm 0.551	2.743 \pm 0.185	2.858 \pm 0.052	0.625 \pm 0.121	1.800 \pm 0.427	0.654 \pm 0.026
Volumetric Xylitol formation rate ($\text{g} \cdot \text{L}^{-1} \cdot \text{h}^{-1}$)	0.065 \pm 0.024	0.174 \pm 0.074	0.029 \pm 0.007	0.171 \pm 0.040	0.026 \pm 0.021	0.074 \pm 0.013	0.085 \pm 0.025
Volumetric Glycerol formation rate ($\text{g} \cdot \text{L}^{-1} \cdot \text{h}^{-1}$)	0.006 \pm 0.007	0.000 \pm 0.000	0.003 \pm 0.004	0.001 \pm 0.002	0.000 \pm 0.000	0.000 \pm 0.000	0.000 \pm 0.000
Volumetric Acetate formation rate ($\text{g} \cdot \text{L}^{-1} \cdot \text{h}^{-1}$)	0.012 \pm 0.016	0.015 \pm 0.021	0.202 \pm 0.004	0.132 \pm 0.043	0.060 \pm 0.085	0.250 \pm 0.017	0.022 \pm 0.031
Volumetric Ethanol formation rate ($\text{g} \cdot \text{L}^{-1} \cdot \text{h}^{-1}$)	0.237 \pm 0.056	0.000 \pm 0.000	0.243 \pm 0.016	0.104 \pm 0.130	0.000 \pm 0.000	0.000 \pm 0.000	0.000 \pm 0.000
Specific Xylose consumption rate ($\text{g} \cdot \text{g CDW}^{-1} \cdot \text{L}^{-1} \cdot \text{h}^{-1}$)	0.319 \pm 0.028	0.233 \pm 0.054	0.435 \pm 0.038	0.372 \pm 0.028	0.202 \pm 0.061	0.382 \pm 0.089	0.244 \pm 0.042
Specific Xylitol formation rate ($\text{g} \cdot \text{g CDW}^{-1} \cdot \text{L}^{-1} \cdot \text{h}^{-1}$)	0.005 \pm 0.002	0.027 \pm 0.008	0.005 \pm 0.001	0.022 \pm 0.004	0.009 \pm 0.008	0.016 \pm 0.003	0.033 \pm 0.016
Specific Glycerol formation rate ($\text{g} \cdot \text{g CDW}^{-1} \cdot \text{L}^{-1} \cdot \text{h}^{-1}$)	0.000 \pm 0.001	0.000 \pm 0.000	0.000 \pm 0.001	0.000 \pm 0.000	0.000 \pm 0.000	0.000 \pm 0.000	0.000 \pm 0.000
Specific Acetate formation rate ($\text{g} \cdot \text{g CDW}^{-1} \cdot \text{L}^{-1} \cdot \text{h}^{-1}$)	0.001 \pm 0.001	0.002 \pm 0.003	0.032 \pm 0.000	0.017 \pm 0.007	0.021 \pm 0.029	0.053 \pm 0.004	0.009 \pm 0.013
Specific Ethanol formation rate ($\text{g} \cdot \text{g CDW}^{-1} \cdot \text{L}^{-1} \cdot \text{h}^{-1}$)	0.020 \pm 0.004	0.000 \pm 0.000	0.038 \pm 0.002	0.013 \pm 0.016	0.000 \pm 0.000	0.000 \pm 0.000	0.000 \pm 0.000
Yield Ethanol per Xylose (g/g)	0.064 \pm 0.019	0.000 \pm 0.000	0.089 \pm 0.012	0.037 \pm 0.046	0.000 \pm 0.000	0.000 \pm 0.000	0.000 \pm 0.000
Yield Xylitol per Xylose (g/g)	0.018 \pm 0.008	0.114 \pm 0.007	0.011 \pm 0.003	0.060 \pm 0.015	0.039 \pm 0.026	0.043 \pm 0.017	0.131 \pm 0.043
Yield Acetate per Xylose (g/g)	0.003 \pm 0.004	0.008 \pm 0.011	0.074 \pm 0.007	0.046 \pm 0.014	0.085 \pm 0.120	0.144 \pm 0.043	0.035 \pm 0.049
Yield Glycerol per Xylose (g/g)	0.002 \pm 0.002	0.000 \pm 0.000	0.001 \pm 0.002	0.001 \pm 0.001	0.000 \pm 0.000	0.000 \pm 0.000	0.000 \pm 0.000
Carbon balance closure	40.07%	52.34%	41.88%	40.88%	61.595%	42.90%	55.69%
Degree of reduction closure	45.20%	54.57%	48.36%	44.55%	63.320%	43.99%	58.05%
Compensated Carbon balance closure	76.60%	82.62%	76.31%	77.85%	86.048%	80.24%	83.65%
Compensated Degree of reduction closure	100.00%	100.00%	100.00%	100.00%	100.000%	100.00%	100.00%

Table S4. List of the primers that were used in this study. Lowercase underlined sequences indicate gRNA sequences.

Primer	Sequence 5'-3'	Description	Reference
LW105 + gRNA	<u>gaaacggtgtc</u> gagtagtaGTTT TAGAGCTA GAAATAGCAAG	gRNA for <i>IRA2</i>	This study
LW105 + gRNA	<u>attggtacaggg</u> gatgacctGTTT TAGAGCTA GAAATAGCAAG	gRNA for <i>ISU2</i>	This study
LW105 + gRNA	<u>agccgaataagg</u> atgagccaGTTT TAGAGCTA GAAATAGCAAG	gRNA for <i>HOG1</i>	This study
LWA103	GATCATTTATCTTTCACTGC	Reverse primer for gRNA	This study
IRA2_S1_ amdSYM_ f	GATATCAACTAACTGTATACATTA TCTTTCTTCAGGGAGAAGCA	HR tail 50bp for <i>IRA2</i> donor DNA	This study
IRA2_S2_ amdSYM_ r	TACAGATAGATATTGATATTTCTTT CATTAGTTTATGTAACACCT	HR tail 50bp for <i>IRA2</i> donor DNA	This study
IRA2_S1_ amdSYM_ f	TGAAGCTTCGTACGCTGCAG	Primer for <i>IRA2</i> donor DNA amplification	This study
IRA2_S2_ amdSYM_ r	GCATAGGCCACTAGTGGATCTG	Primer for <i>IRA2</i> donor DNA amplification	This study
IRA2_f	GACCGATTCCAAGTCATCCC	Verification of internal <i>IRA2</i>	This study
IRA2_r	TGACACAAAGAGAAGGGCAC	Verification of internal <i>IRA2</i>	This study
IRA2_Del_Verif_f	TGACTTGGGTTGGGACTTGG	Verification of <i>IRA2</i> deletion	This study
6_5' amdSYMup_r	CGAGGAGCCGTAATTTTGC	Verification of <i>IRA2</i> deletion	This study
5_3' amdSYMdown_f	CCAGATGCGAAGTTAAGTGC	Verification of <i>IRA2</i> deletion	This study
IRA2_Del_Verif_r	ACAGAAACACTTTCAACTAAGACG G	Verification of <i>IRA2</i> deletion	This study
Amp_ISU1_r	TGCATGAGAAGAGGGAGAGAAAGG AAATGCTAGATTAAGGGAAAGAAA TA	HR tail 50bp for <i>ISU1</i> donor DNA	This study
Amp_ISU1_f	TGCACGCTCATGGGTATCAATTGGC TAGGTCTAATATTGTTATTGTTGG	HR tail 50bp for <i>ISU1</i> donor DNA	This study
Amp_ISU1_r	TCAGCGATCTGTCTATTTCTG	Primer for <i>ISU1</i> donor DNA amplification	This study
Amp_ISU1_f	GAATGAAGCCATACCAAACG	Primer for <i>ISU1</i> donor DNA amplification	This study
ISU1_Del_Verif_f	ACAACCAATCTACGGGCACA	Verification of <i>ISU1</i> deletion	This study

Table S4 (cont'd)

Primer	Sequence 5'-3'	Description	Reference
ISU1_f	CATCAGACCTGTGAATGCCA	Verification of internal <i>ISU1</i>	This study
ISU1_r	CTTGATCGCATCTCCGCTA	Verification of internal <i>ISU1</i>	This study
Amp_HOG1_r	CGGTTAAAACAGAAAAAATCATG ATCGAAATACGTCCACTTTACTTTG T	HR tail 50bp for <i>HOG1</i> donor DNA	This study
Amp_HOG1_f	CAAAATATTATCTATCGTCGAAATTA TCATACTATCTTACAATAAGAGTAG	HR tail 50bp for <i>HOG1</i> donor DNA	This study
HOG1_US_f	CAGCGTTAGTGAGGTGAGGG	Verification of <i>HOG1</i> deletion	This study
Amp_Verif_r	CTACAGGCATCGTGGTGTC	Verification of deletion	This study
Amp_Verif_f	ATCTACACGACGGGGAGTCA	Verification of deletion	This study
HOG1_DS_r	TGCATTCCACATCCACGAA	Verification of <i>HOG1</i> deletion	This study
HOG1_f	GCATTTGGGTTGGTTTGCTC	Verification of internal <i>HOG1</i>	This study
HOG1_r	CCATCACTGCCACCAATCTT	Verification of internal <i>HOG1</i>	This study
LW11	GAACCTCACCTTAGAGC	<i>ALD6</i> amplification (Positive control of DNA)	[2]
LW12	TAGCACCTTGAAGTTAGCC	<i>ALD6</i> amplification (Positive control of DNA)	[2]
IRA2_Del_Verif_f	TGACTTGGGTTGGGACTTGG	Verification of amdSYM recycling	This study
IRA2_Del_Verif_r	ACAGAAACACTTTCAACTAAGACG G	Verification of amdSYM recycling	This study
5_3'amdSYMdown_f	CCAGATGCGAAGTTAAGTGC	Verification of amdSYM recycling	This study

Table S6. List of the plasmids used in this study.

Plasmid	Relevant Genotype	Reference
pLWA26	<i>gRNA-VAC17/MRC1 ; natMX</i>	[2]
pCfB2312	<i>TEF1p-Cas9-CYC1t; kanMX</i>	[3]
pCfB3496	<i>SNR52p-gRNA; ADE2-SUP4t; hphMX</i>	Supplied by Vratislav Stovicek (Technical University of Denmark, DTU)
pUG6- amdSYM2	<i>AmpR ; AnTEF2p-amdSYM-anTEF2t (from Aspergillus nidulans)</i>	[4]
gRNA_HOG1	<i>SNR52p; gRNA-HOG1-CYC1t; natMX</i>	This study
gRNA_ISU1	<i>SNR52p; gRNA_ISU1-CYC1t; hphMX</i>	This study
gRNA_IRA2	<i>SNR52p; gRNA-IRA2-CYC1t; natMX</i>	This study

References

1. Costenoble R, Adler L, Niklasson C, Lidén G: **Engineering of the metabolism of *Saccharomyces cerevisiae* for anaerobic production of mannitol.** *FEMS yeast research* 2003, **3**:17-25.
2. Osiro KO, Brink DP, Borgström C, Wasserstrom L, Carlquist M, Gorwa-Grauslund MF: **Assessing the effect of d-xylose on the sugar signaling pathways of *Saccharomyces cerevisiae* in strains engineered for xylose transport and assimilation.** *FEMS yeast research* 2018.
3. Stovicek V, Borodina I, Forster J: **CRISPR–Cas system enables fast and simple genome editing of industrial *Saccharomyces cerevisiae* strains.** *Metabolic Engineering Communications* 2015, **2**:13-22.
4. Solis-Escalante D, Kuijpers NG, Nadine B, Bolat I, Bosman L, Pronk JT, Daran J-M, Daran-Lapujade P: ***amdSYM*, a new dominant recyclable marker cassette for *Saccharomyces cerevisiae*.** *FEMS yeast research* 2013, **13**:126-139.

I love the symbolism found in art. Renaissance still lifes (or “stilleben”) are carefully composed and every item displayed symbolizes a higher concept. Books, owls and apples are symbols of knowledge. The (bumble)bee is industrious. Headgear reminds us of those who wore them. Although powerful on their own, symbols can also be combined, with interesting results. The evergreen spruce is a symbol for eternity, but a burning candle represents the passage of time and the futility in chasing temporary pleasures. Coffee in a porcelain cup symbolizes international relationships and trade while the milk you might add to that coffee represents local pride.

The symbolism and language of still lifes described above were developed around 500 years ago. By following tradition, the painter can convey a clear message in each piece of art. In an analogous manner, the yeast *Saccharomyces cerevisiae* has evolved for thousands of years to recognize signals in the environment. These signals symbolize the overall state of the surroundings, and need to be interpreted for the yeast to be able to form a cohesive picture. The symbols can include nutrients, temperature and intracellular metabolic state, and their astute interpretation and rapid response can grant advantages in a competitive environment., *S. cerevisiae* colonizes sweet but rapidly decaying fruit, such as apples, producing ethanol and a flowery smell. This aroma attracts bees, whose furry legs are optimized for transporting both pollen and hitchhiking yeast spores towards new places to colonize.

Does the woman in the painting represent us, mankind? Since we can't see her face she could be anyone. She is looking at a potted plant, a piece of nature that she has tamed and domesticated, all while surrounded by greenery. Replacing fossil resources with biobased raw materials, such as that from lignocellulose from forestry, requires microbial cell factories, and *S. cerevisiae* is one of them. In the present thesis work, I have been working alongside *S. cerevisiae* to decode the signals found in lignocellulose, and determining the best response. My work also included finding new routes for utilizing the lignocellulose, routes to enable formation of compounds that currently require fossil resources. In short, I have been trying to turn the yeast away from the fruit and towards the tree, with the hopes of it producing important items such as plastic LEGO®.

The items making up this still life are also of personal importance. The books consist of the lab journal of one of my students, a comic book with only 16 words, and the only fictional book found at my department, TMB: Toxin by Robin Cook. Bombus dahlbomii is an orange bumblebee native to Patagonia, where I was fortunate to spend five weeks traveling in 2018. The shiny owl is a gift from my nieces and nephew, the apples of my eye. The tiny scientist represents me, and the crocheted plushie is my closest coworker: *S. cerevisiae*. The spruce reminds me of home in the forests of Småland, and the lit candle is a symbol of hope for me. The cup represents two of the things most important for the completion of this thesis: coffee and the amazing friendships I have formed at TMB. The watercolor painting is a self-portrait painted by my grandmother. The absence of eye contact amazes me, because I can still tell that it is her, but it can also be anyone. And that's why I love art.